

NIST NCSTAR 1-6

**Federal Building and Fire Safety Investigation of the
World Trade Center Disaster**

Structural Fire Response and Probable Collapse Sequence of the World Trade Center Towers

John L. Gross
Therese P. McAllister

NIST NCSTAR 1-6

**Federal Building and Fire Safety Investigation of the
World Trade Center Disaster**

**Structural Fire Response and
Probable Collapse Sequence of the
World Trade Center Towers**

John L. Gross
Therese P. McAllister
*Building and Fire Research Laboratory
National Institute of Standards and Technology*

September 2005



U.S. Department of Commerce
Carlos M. Gutierrez, Secretary

Technology Administration
Michelle O'Neill, Acting Under Secretary for Technology

National Institute of Standards and Technology
William Jeffrey, Director

Disclaimer No. 1

Certain commercial entities, equipment, products, or materials are identified in this document in order to describe a procedure or concept adequately or to trace the history of the procedures and practices used. Such identification is not intended to imply recommendation, endorsement, or implication that the entities, products, materials, or equipment are necessarily the best available for the purpose. Nor does such identification imply a finding of fault or negligence by the National Institute of Standards and Technology.

Disclaimer No. 2

The policy of NIST is to use the International System of Units (metric units) in all publications. In this document, however, units are presented in metric units or the inch-pound system, whichever is prevalent in the discipline.

Disclaimer No. 3

Pursuant to section 7 of the National Construction Safety Team Act, the NIST Director has determined that certain evidence received by NIST in the course of this Investigation is “voluntarily provided safety-related information” that is “not directly related to the building failure being investigated” and that “disclosure of that information would inhibit the voluntary provision of that type of information” (15 USC 7306c).

In addition, a substantial portion of the evidence collected by NIST in the course of the Investigation has been provided to NIST under nondisclosure agreements.

Disclaimer No. 4

NIST takes no position as to whether the design or construction of a WTC building was compliant with any code since, due to the destruction of the WTC buildings, NIST could not verify the actual (or as-built) construction, the properties and condition of the materials used, or changes to the original construction made over the life of the buildings. In addition, NIST could not verify the interpretations of codes used by applicable authorities in determining compliance when implementing building codes. Where an Investigation report states whether a system was designed or installed as required by a code *provision*, NIST has documentary or anecdotal evidence indicating whether the requirement was met, or NIST has independently conducted tests or analyses indicating whether the requirement was met.

Use in Legal Proceedings

No part of any report resulting from a NIST investigation into a structural failure or from an investigation under the National Construction Safety Team Act may be used in any suit or action for damages arising out of any matter mentioned in such report (15 USC 281a; as amended by P.L. 107-231).

**National Institute of Standards and Technology National Construction Safety Team Act Report 1-6
Natl. Inst. Stand. Technol. Natl. Constr. Sfty. Tm. Act Rpt. 1-6, 425 pages (September 2005)
CODEN: NSPUE2**

U.S. GOVERNMENT PRINTING OFFICE
WASHINGTON: 2005

For sale by the Superintendent of Documents, U.S. Government Printing Office
Internet: bookstore.gpo.gov — Phone: (202) 512-1800 — Fax: (202) 512-2250
Mail: Stop SSOP, Washington, DC 20402-0001

ABSTRACT

One of the four main objectives of the National Institute of Standards and Technology (NIST) investigation of the collapse of the World Trade Center (WTC) towers was to determine why and how the two towers collapsed. Events that played a significant role in the structural performance of the towers were the aircraft impact, the rapid ignition of fires on multiple floors, the growth and spread of fires and the structural weakening resulting from effects of high temperatures. The passive fire protection applied to the steel structural components in the WTC towers was investigated to provide information on the in-place condition of the fire protection before and after aircraft impact. Standard fire resistance tests were conducted to establish the appropriate classification (fire resistance rating) of the original design of the WTC floor system and to develop insight into the structural performance of the composite steel and concrete floor system under exposure to a standard fire. Results of simulations of the aircraft impacts were used to predict damage to the structure, fire protection, and partition walls in the path of the debris field. Characterization of the temperatures of the structural components, determined from simulated WTC fires, allowed the calculation of the performance of major subsystems constituting the structural system of the towers including the core framing, the exterior wall (columns and spandrels), and full tenant floors. Insights gained from these analyses were used, in turn, to formulate and execute nonlinear, temperature-dependent finite element analyses of global structural systems to predict the collapse sequence of each tower. The structural analyses were guided, and where possible validated, by observations made from the review of thousands of photographs and video recordings. This report covers the characterization of the conditions of the WTC towers before the attacks, their weakening due to the aircraft impacts, the response of the structural systems to the subsequent growth and spread of fires, and the progression of local failures that led ultimately to the total collapse of both towers.

Keywords: Buildings, collapse, fire, large deflections, stability, structural analysis, structural damage, structural response to fire, World Trade Center.

This page intentionally left blank.

TABLE OF CONTENTS

| | |
|---|-----------|
| Abstract | iii |
| List of Figures | xi |
| List of Tables | xxi |
| List of Acronyms and Abbreviations | xxiii |
| Preface | xxv |
| Acknowledgments | xxxv |
| Executive Summary | xxxvii |
| | |
| Chapter 1 | |
| Introduction | 1 |
| 1.1 Project Objectives | 1 |
| 1.2 Technical Approach and Tasks | 2 |
| 1.2.1 Task A – Finite Element Reference Models | 4 |
| 1.2.2 Task B – Material Properties | 5 |
| 1.2.3 Task C – Passive Fire Protection | 5 |
| 1.2.4 Task D – Standard Fire Resistance Tests | 5 |
| 1.2.5 Task E – Aircraft Impact Damage | 6 |
| 1.2.6 Task F – Observations and Timeline | 6 |
| 1.2.7 Task G – Temperatures of Structural Components | 6 |
| 1.2.8 Task H – Component and Subsystem Analyses | 7 |
| 1.2.9 Task I – Major Subsystem Analyses | 7 |
| 1.2.10 Task J – Global Structural Analyses | 7 |
| 1.2.11 Task K – Probable Collapse Sequence | 8 |
| 1.3 Challenges | 9 |
| 1.4 Report Organization | 10 |
| | |
| Chapter 2 | |
| Passive Fire Protection | 13 |
| 2.1 Fire Resistance of Structural Elements | 13 |
| 2.2 Historical Review Related To Passive Fire Protection | 14 |
| 2.2.1 Building Code Requirements for the Design of the WTC Towers | 14 |
| 2.2.2 New York City Building Code Requirements | 14 |
| 2.2.3 Classification of WTC Towers | 15 |

| | | |
|------------------------------------|---|-----------|
| 2.2.4 | Response to Local Law 5/1973 | 16 |
| 2.2.5 | Selection of Fire Resistive Materials..... | 16 |
| 2.2.6 | Specified Thickness of Fire Resistive Material | 18 |
| 2.2.7 | Upgrading SFRM on Floor Trusses..... | 20 |
| 2.2.8 | Need for Fire Resistance Tests | 21 |
| 2.2.9 | Maintenance of SFRM in Elevator Shafts..... | 22 |
| 2.3 | As-Applied Thickness of SFRM..... | 22 |
| 2.3.1 | 1994 Measurements from WTC 1 Floors 23 and 24 | 22 |
| 2.3.2 | Analysis of Photographs..... | 23 |
| 2.3.3 | Port Authority Data on Upgraded SFRM on Trusses..... | 25 |
| 2.4 | Effect of the Variability of SFRM Thickness on Thermal Response | 25 |
| 2.4.1 | Effects of Thickness Variability and Gaps in SFRM | 25 |
| 2.4.2 | Thermally equivalent thickness of SFRM | 27 |
| 2.4.3 | Thickness of SFRM Used for Thermal Analyses | 28 |
| 2.5 | Summary of SFRM Thickness..... | 29 |
| 2.6 | Thermophysical Properties | 30 |
| 2.6.1 | Thermal Conductivity..... | 31 |
| 2.6.2 | Specific Heat Capacity | 31 |
| 2.6.3 | Density..... | 32 |
| 2.6.4 | Thermophysical Properties of Gypsum Panels..... | 32 |
| 2.7 | Estimation of SFRM Dislodged By to Aircraft Impact | 33 |
| 2.7.1 | In-place Density and Bond Strength..... | 33 |
| 2.7.2 | Specimen Preparation and Test Procedures..... | 34 |
| 2.7.3 | Test Results | 35 |
| 2.8 | References..... | 36 |
| | | |
| Chapter 3 | | |
| Fire Resistance Tests | | 37 |
| 3.1 | Background..... | 37 |
| 3.1.1 | Motivation for Conducting Standard Fire Tests..... | 37 |
| 3.1.2 | Purpose of the Standard Fire Tests | 37 |
| 3.2 | Description of WTC Floor System | 38 |
| 3.2.1 | Structural System..... | 38 |
| 3.2.2 | Fireproofing Thickness..... | 39 |
| 3.3 | Fire Resistance Testing..... | 39 |

| | | |
|--|---|-----------|
| 3.3.1 | General Description..... | 39 |
| 3.3.2 | Test Restraint Conditions and Ratings | 39 |
| 3.3.3 | Scale of Tests..... | 40 |
| 3.3.4 | Test Variables..... | 40 |
| 3.4 | Preparation of Test Assemblies | 41 |
| 3.5 | Description of Tests and Loading | 43 |
| 3.5.1 | Full-scale Tests (35 ft span) | 43 |
| 3.5.2 | Reduced-scale Tests (17 ft span) | 44 |
| 3.6 | Test Results..... | 44 |
| 3.6.1 | General Discussion of Tests | 44 |
| 3.6.2 | Fire Resistance Ratings | 48 |
| 3.6.3 | General Observations | 49 |
| 3.6.4 | Floor Deflections and Temperatures | 51 |
| 3.6.5 | Observations and Comparisons | 54 |
| 3.7 | Summary | 55 |
| | | |
| Chapter 4 | | |
| Structural Response of Components, Connections and Subsystems | | 57 |
| 4.1 | Mechanical Properties of Concrete and Steel | 57 |
| 4.1.1 | Concrete Properties and Failure Criteria | 58 |
| 4.1.2 | Steel Properties and Failure Criteria..... | 60 |
| 4.2 | Floor Subsystem Analysis..... | 65 |
| 4.2.1 | Description of Floor Subsystem | 66 |
| 4.2.2 | Truss Seats..... | 69 |
| 4.2.3 | Knuckles | 79 |
| 4.2.4 | Single Truss and Concrete Slab Section..... | 84 |
| 4.2.5 | Floor Subsystem Analysis | 89 |
| 4.3 | Exterior Wall Subsystem | 96 |
| 4.3.1 | Exterior Wall Subsystem Description | 97 |
| 4.3.2 | One, Two, and Three-Story High Columns..... | 100 |
| 4.3.3 | Exterior Wall Section Analysis | 103 |
| 4.3.4 | Summary | 119 |
| 4.4 | References..... | 119 |

| | |
|--|------------|
| Chapter 5 | |
| Aircraft Impact Damage..... | 121 |
| 5.1 Introduction..... | 121 |
| 5.2 Methodology and Criteria for Developing Input Data From Aircraft Impact Analysis Results.. | 122 |
| 5.2.1 Core Column Damage..... | 123 |
| 5.2.2 Structural Damage to Floor Slabs, Core Beams, and Floor Trusses | 126 |
| 5.2.3 Fireproofing Damage..... | 129 |
| 5.2.4 Summary of Aircraft Impact Damage | 133 |
| 5.3 Structural and Fireproofing Damage to WTC 1..... | 134 |
| 5.4 Structural and Fireproofing Damage to WTC 2..... | 141 |
| 5.5 Observations of Aircraft Impact Damage to the Pentagon | 147 |
| 5.6 Summary | 150 |
| 5.7 References..... | 151 |
| | |
| Chapter 6 | |
| Observations and Timeline of Structural Events | 153 |
| 6.1 Introduction..... | 153 |
| 6.2 Observations of Structural Events | 154 |
| 6.2.1 WTC 1 Structural Response Observations | 155 |
| 6.2.2 WTC 2 Structural Response Observations | 167 |
| | |
| Chapter 7 | |
| Structural Response of Major Tower Subsystems to Aircraft Impact Damage and Fire . | 185 |
| 7.1 Introduction..... | 185 |
| 7.2 Core Subsystem | 185 |
| 7.2.1 Model and Method of Analysis | 186 |
| 7.2.2 WTC 1 Core Analysis Results..... | 188 |
| 7.2.3 WTC 2 Analysis Results | 192 |
| 7.3 Full Floor Subsystem..... | 194 |
| 7.3.1 Model and Method of Analysis | 194 |
| 7.3.2 WTC 1 Analysis Results | 200 |
| 7.3.3 WTC 2 Analysis Results | 205 |
| 7.4 Exterior Wall Subsystem | 212 |
| 7.4.1 Finite Element Model and Methods of Analysis | 213 |
| 7.4.2 WTC 1 Analysis Results | 215 |
| 7.5 Summary of Subsystem Analyses..... | 224 |

Chapter 8

Structural Response of the WTC Towers to Aircraft Impact Damage and Fire..... 229

| | | |
|-------|--|-----|
| 8.1 | Introduction..... | 229 |
| 8.2 | Global Model of Towers..... | 230 |
| 8.2.1 | Model Description..... | 230 |
| 8.2.2 | Model Modifications..... | 233 |
| 8.3 | Analysis Methodology..... | 235 |
| 8.4 | Results of WTC 1 Analysis..... | 237 |
| 8.4.1 | WTC 1 Structural Response to Aircraft Impact Damage..... | 237 |
| 8.4.2 | WTC 1 Structural Response to Elevated Temperatures..... | 243 |
| 8.4.3 | WTC 1 Hat Truss Members and Connections..... | 251 |
| 8.5 | Results of WTC 2 Analysis..... | 253 |
| 8.5.1 | WTC 2 Structural Response to Aircraft Impact Damage..... | 254 |
| 8.5.2 | WTC 2 Structural Response to Elevated Temperatures..... | 260 |
| 8.5.3 | WTC 2 Hat Truss Members and Connections..... | 273 |
| 8.6 | Structural Response of the WTC Towers Without Impact Damage and Subjected to the Same Fires..... | 279 |
| 8.7 | Summary of Structural Response of the WTC Towers..... | 281 |

Chapter 9

Probable Collapse Sequences..... 285

| | | |
|-------|--|-----|
| 9.1 | Introduction..... | 285 |
| 9.2 | Methodology..... | 285 |
| 9.2.1 | Key Observed Events and Conditions..... | 286 |
| 9.2.2 | Collapse Hypotheses..... | 286 |
| 9.2.3 | Mathematical Modeling – Analysis Interdependencies..... | 288 |
| 9.2.4 | Sensitivity Studies to Identify Influential Variables..... | 290 |
| 9.2.5 | Evaluation of Collapse Hypotheses..... | 294 |
| 9.3 | Probable Collapse Sequences..... | 296 |
| 9.3.1 | Probable Collapse Sequence of WTC 1..... | 297 |
| 9.3.2 | Probable Collapse Sequence of WTC 2..... | 306 |
| 9.4 | Discussion and Summary..... | 319 |
| 9.4.1 | Structural Response to Impact Damage and Fire..... | 320 |
| 9.4.2 | Structural Response to Fire Without Impact Damage..... | 321 |
| 9.4.3 | Time to Collapse..... | 322 |
| 9.4.4 | Factors that Affected Performance..... | 322 |

Chapter 10

Findings 329

 10.1 Passive Fire Protection..... 329

 10.2 Building Code Requirements for Structural Fire Resistance 329

 10.2.1 Selection of Fire Resistive Materials..... 330

 10.2.2 Equivalent Thickness of SFRM..... 330

 10.3 Fire Resistance Tests..... 330

 10.3.1 Structural Performance..... 331

 10.3.2 Fire Resistance Ratings 331

 10.4 Structural Response of Components..... 332

 10.4.1 Floor System..... 332

 10.4.2 Exterior Wall System 332

 10.5 Fireproofing and Partition Damage Due to Aircraft Impact 332

 10.6 Observations and Timeline 333

 10.6.1 WTC 1 333

 10.6.2 WTC 2 334

 10.7 Structural Response of Major Tower Subsystems 335

 10.7.1 Isolated Core Subsystem 335

 10.7.2 Full Floor Subsystem..... 335

 10.7.3 Isolated Exterior Wall Subsystem 335

 10.8 Structural Response to Aircraft Impact Damage and Fire 336

 10.8.1 General Findings 336

 10.8.2 Performance with Intact fireproofing 337

 10.9 Probable Collapse Sequences 337

 10.9.1 Role of the Building Core..... 337

 10.9.2 Role of the Building Floors 337

 10.9.3 Role of Exterior Frame-Tube 338

 10.9.4 Probable Collapse Sequences..... 338

LIST OF FIGURES

| | | |
|--------------|--|-------------------------------------|
| Figure P-1. | The eight projects in the federal building and fire safety investigation of the WTC disaster. | Error! Bookmark not defined. |
| Figure 1-1. | Structural Analysis Sequence..... | 4 |
| Figure 2-1. | Mock up of floor truss system..... | 17 |
| Figure 2-2. | Demonstration of application of Monokote sprayed fire-resistive material to floor trusses..... | 18 |
| Figure 2-3. | Example of measurement procedure used to estimate SFRM thickness from photographs..... | 24 |
| Figure 2-4. | Example of “gap” in fire-resistive material on diagonal member of a bridging floor truss..... | 26 |
| Figure 2-5. | Thermo-mechanical response of 1 in. bar compared with uniform thickness SFRM..... | 28 |
| Figure 3-1. | Floor system of the WTC towers..... | 38 |
| Figure 3-2. | Schematic of floor system viewed along the main steel trusses. (not to scale)..... | 39 |
| Figure 3-3. | Drawing of 35 ft truss and end detail..... | 42 |
| Figure 3-4. | Trusses being fit-up in test frame of 35 ft test assembly..... | 43 |
| Figure 3-5. | 35 ft span test assembly loaded with concrete blocks and water-filled containers..... | 43 |
| Figure 3-6. | 17 ft span test assembly loaded with concrete blocks, water-filled containers and hydraulic actuators..... | 44 |
| Figure 3-7. | Unexposed surface of Assembly No. 1 after loading equipment was removed..... | 45 |
| Figure 3-8. | Unexposed surface of Assembly No. 2 after loading equipment was removed..... | 46 |
| Figure 3-9. | Unexposed surface of Assembly No. 3 after loading equipment was removed..... | 47 |
| Figure 3-10. | Unexposed surface of Assembly No. 4 after loading equipment was removed..... | 48 |
| Figure 3-11. | Fire exposure side of the 35 ft restrained test assembly after almost 2 hours of fire exposure..... | 49 |
| Figure 3-12. | Sections cut through concrete slab to confirm extent and depth of spalling..... | 50 |
| Figure 3-13. | Measurement of remaining slab thickness after spalling..... | 50 |
| Figure 3-14. | Detail of spalling concrete at east end of Assembly No. 1..... | 51 |
| Figure 3-15. | Deflection measured at the center of each assembly..... | 52 |
| Figure 3-16. | Deflection measured at the center of each assembly divided by the span..... | 52 |
| Figure 3-17. | Average temperature of the unexposed surface for all four tests..... | 53 |

| | |
|--|----|
| Figure 3–18. Average temperatures of the bottom chord for Test Nos. 1, 2 and 3 (3/4 in. thick SFRM)..... | 54 |
| Figure 4–1. Temperature–dependent concrete properties. | 59 |
| Figure 4–2. Concrete stress-strain curves..... | 60 |
| Figure 4–3. Temperature-dependent properties for all steels..... | 63 |
| Figure 4–4. Stress-strain relationships for Material ID 1 steel..... | 64 |
| Figure 4–5. Strain behaviors at elevated temperatures for Material ID 1 steel..... | 65 |
| Figure 4–6. Maximum plastic strain from the finite element analysis and limiting plastic strain..... | 65 |
| Figure 4–7. Floor structural subsystem (WTC 1, Floor 96)..... | 67 |
| Figure 4–8. Primary truss components..... | 68 |
| Figure 4–9. Plan view of truss seat connection, straps, and horizontal studs..... | 69 |
| Figure 4–10. Truss seat detail location on northeast quadrant of Floor 96 of WTC 1. Reproduced with permission of The Port Authority of New York and New Jersey..... | 70 |
| Figure 4–11. Finite element model of exterior seat..... | 71 |
| Figure 4–12. Failure sequence of the exterior seats against tensile force..... | 72 |
| Figure 4–13. Capacity of exterior seat against tensile force (Detail 1411 in Fig. 4–10)..... | 73 |
| Figure 4–14. Capacity of interior seat against vertical and horizontal force (Detail 22 in Fig. 4–10)..... | 73 |
| Figure 4–15. Truss seat capacity against vertical force. Reproduced with permission of The Port Authority of New York and New Jersey. Enhancements by NIST..... | 77 |
| Figure 4–16. Truss seat capacity against horizontal force. Reproduced with permission of The Port Authority of New York and New Jersey. Enhancements by NIST..... | 78 |
| Figure 4–17. Results of interior truss seat model at 500 °C..... | 80 |
| Figure 4–18. Laclede Steel Company shear tests of a knuckle..... | 81 |
| Figure 4–19. Compressive stresses in longitudinal shear finite element model (4,100 psi concrete)..... | 82 |
| Figure 4–20. Shear force versus displacement from finite element model for longitudinal shear of two knuckles (4,100 psi concrete)..... | 82 |
| Figure 4–21. Compressive stresses in transverse shear finite element model (2,500 psi concrete)..... | 83 |
| Figure 4–22. Shear force versus displacement from finite element model for transverse shear of two knuckles (2,500 psi concrete)..... | 83 |
| Figure 4–23. Composite truss and concrete slab model..... | 85 |
| Figure 4–24. Vertical displacement at 700 °C..... | 87 |
| Figure 4–25. Displacement versus temperature..... | 87 |
| Figure 4–26. Comparison of detailed and reduced truss models..... | 88 |
| Figure 4–27. Converted ANSYS model for Floor 96 of WTC 1..... | 90 |
| Figure 4–28. Long span trusses of converted ANSYS model for Floor 96 of WTC 1..... | 91 |

| | |
|---|-----|
| Figure 4–29. Core floor beams and columns of converted ANSYS model for Floor 96 of WTC 1. | 91 |
| Figure 4–30. Full floor model before impact damage is included (without concrete floor slab). | 94 |
| Figure 4–31. Break element locations in the floor model (Floor 96, WTC1). | 96 |
| Figure 4–32. Exterior wall section model. | 98 |
| Figure 4–33. Schematic of exterior column cross-section. | 98 |
| Figure 4–34. One-story exterior column model. | 101 |
| Figure 4–35. Load-deflection of column at room temperature (RT) and 700 °C. | 101 |
| Figure 4–36. Local buckling of column at room temperature. | 102 |
| Figure 4–37. Plastic hinge in column at room temperature. | 102 |
| Figure 4–38. Deformed shape of column at maximum axial load at 700 °C. | 103 |
| Figure 4–39. SAP2000 shell model of prefabricated panel. | 105 |
| Figure 4–40. ANSYS model of prefabricated panel showing finite element mesh. | 106 |
| Figure 4–41. ANSYS model of prefabricated panel showing boundary conditions and loading. | 106 |
| Figure 4–42. Deflection of prefabricated panel under 100 kip lateral load. | 107 |
| Figure 4–43. Typical spandrel splice layout for exterior wall section model. | 108 |
| Figure 4–44. Modeling of a typical interior spandrel splice in the exterior wall section model. | 108 |
| Figure 4–45. Column Splice Model used in Exterior Wall Model. | 109 |
| Figure 4–46. Exterior wall subsystem model with boundary conditions. | 110 |
| Figure 4–47. Typical meshing of exterior wall model components. | 110 |
| Figure 4–48. Exterior wall model temperature time-histories. | 112 |
| Figure 4–49. Spandrel plate deformations. | 114 |
| Figure 4–50. Lateral deflections for Case 6 and Case 7. | 114 |
| Figure 4–51. Structural response (out-of-plane deformations) for temperature time history DBARE and pulled-in at three disconnected floors for Case 8. (10X displacement magnification). | 115 |
| Figure 4–52. Column splice contact element status for temperature time history and DBARE and pulled at three disconnected floors for Case 8. | 116 |
| Figure 4–53. Column splice bolt stresses for temperature time history and DBARE and pulled at three disconnected floors for Case 8. | 116 |
| Figure 4–54. Structural response (out-of-plane deformations) for temperature time history DBARE and pushdown with three disconnected floors for Case 9 (10X displacement magnification). | 117 |
| Figure 4–55. Out-of-plane deformation as a function of pushdown displacement after application of temperature DBARE with three disconnected floors for Case 9. | 117 |
| Figure 4–56. Total reaction at column base resulting from pushdown with temperature DBARE and three disconnected floors for Case 9. | 118 |

| | | |
|--------------|--|-----|
| Figure 4–57. | Individual column reaction during pushdown with temperature DBARE and three disconnected floors for Case 9. | 118 |
| Figure 5–1. | Validation of Aircraft Impact Analysis Prediction With Observations for WTC 1 North Exterior Wall Damage. | 122 |
| Figure 5–2. | Validation of Aircraft Impact Analysis Prediction With Observations for WTC 2 South Exterior Wall Damage. | 123 |
| Figure 5–3. | Core column damage levels. | 124 |
| Figure 5–4. | Impact damage to WTC 1 Floor 95 for Case A (plan view). | 127 |
| Figure 5–5. | Damage to WTC 1 Floor 95 framing and slab for Case A. | 128 |
| Figure 5–6. | Debris and fuel field in WTC 1 Case B analysis of aircraft impact. | 131 |
| Figure 5–7. | WTC 1 Case B aircraft impact damage to framing, partitions, and furnishings on Floor 95. | 131 |
| Figure 5–8. | WTC 1 Case B Floor 95 partitions and furnishings layout prior to impact (layout provided in model only where interaction with aircraft was expected). | 132 |
| Figure 5–9. | WTC 1 Case B Floor 95 partitions and furnishings layout after impact with overlay showing extent of dislodged insulation from direct debris impact. | 132 |
| Figure 5–10. | Definition of structural floor and occupancy floor. | 133 |
| Figure 5-11. | Plan view of WTC 1 Case B insulation and column damage for Occupancy Floor 95. | 133 |
| Figure 5-12. | Plan view of WTC 1 Case B damage to Structural Floors 95. | 134 |
| Figure 5–13. | Plan view of WTC 1 Case A cumulative damage for Floors 93 to 98. | 135 |
| Figure 5–14. | Plan view of WTC 1 Case A insulation and column damage to Occupancy Floors 93 to 98. | 136 |
| Figure 5–15. | Plan view of WTC 1 Case A damage to Structural Floors 93 to 98. | 137 |
| Figure 5–16. | Plan view of WTC 1 Case B cumulative damage from Floors 93 to 98. | 138 |
| Figure 5–17. | Plan view of WTC 1 Case B insulation and column damage to Occupancy Floors 93 to 98. | 139 |
| Figure 5–18. | Plan view of WTC 1 Case B damage to Structural Floors 93 to 98. | 140 |
| Figure 5–19. | Plan view of WTC 2 Case C cumulative damage from Floors 78 to 83. | 141 |
| Figure 5–20. | Plan view of WTC 2 Case C insulation and column damage to Occupancy Floors 78 to 83. | 142 |
| Figure 5–21. | Plan view of WTC 2 Case C damage to Structural Floors 78 to 83. | 143 |
| Figure 5–22. | Plan view of WTC 2 Case D cumulative damage from Floors 78 to 83. | 144 |
| Figure 5–23. | Plan view of WTC 2 Case D insulation and column damage to Occupancy Floors 78 to 83. | 145 |
| Figure 5–24. | Plan view of WTC 2 Case D damage to Structural Floors 78 to 83. | 146 |
| Figure 5–25. | Overlay of WTC Footprint on Pentagon damage area from aircraft impact (original figure from ASCE, 2003). | 148 |

| | |
|--|-----|
| Figure 5–26. Typical damage to spirally reinforced columns in the Pentagon impacted and bent by large debris (ASCE, 2003). | 149 |
| Figure 5–27. Typical damage to spirally reinforced columns in the Pentagon not impacted or bent by large debris (ASCE, 2003). | 150 |
| Figure 6–1. Initial aircraft impact damage on WTC 1 north face. | 157 |
| Figure 6–2. Initial aircraft impact damage on WTC 1 west and south faces minutes after impact (exact time of image is unknown). | 158 |
| Figure 6–3. SFRM knocked off north exterior columns. Arrows show where fireproofing was damaged or missing. | 159 |
| Figure 6–4. South face of WTC 1 with fire visible only on the west side at 9:25. Arrow shows region where debris pile under missing panel was observed. | 159 |
| Figure 6–5. Fires on WTC 1 south face at 9:40 a.m. Note lack of inward bowing. | 160 |
| Figure 6–6. WTC 1 exterior columns bowing inward across most of the south face between Floors 95 to 97 (or 98) at 10:23 a.m. Note buckled panel at SW corner. | 161 |
| Figure 6–7. Expulsion of smoke and debris at WTC 1 Floor 98 on the east, north, and west faces. | 162 |
| Figure 6–8. Smoke expulsion at Floor 98 from north and west faces as collapse initiates. | 163 |
| Figure 6–9. Smoke expulsion at Floor 98 from north and east faces at collapse initiation. | 164 |
| Figure 6–10. Rotation of WTC 1 building section above the aircraft impact zone toward the south as viewed from due north. Note that there is no tilt in the east or west directions. | 165 |
| Figure 6–11. WTC 1 tilt to the south of approximately 8 degrees was measured before smoke and debris obscured view. Note view is from west and tilt is directly south. | 166 |
| Figure 6–12. Aircraft impact into WTC 2 and fireball, view from the east. | 171 |
| Figure 6–13. Hanging object (noted by arrows) in east windows of Floor 82 appears to be edge of Floor 83. | 172 |
| Figure 6–14. Debris piles at windows where fire are burning at the northeast corner. | 172 |
| Figure 6–15. Hanging object (noted by arrows) in north windows of Floor 79 appears to be edge of Floor 80. | 173 |
| Figure 6–16. Image showing damage to fireproofing on east face of WTC 2 due to internal impact. Red arrows highlight areas where fireproofing has been damaged. The blowup to the right shows a column where red Tnemec primer paint is visible. | 174 |
| Figure 6–17. WTC 2 exterior columns bowing inward across north side of the east face between Floors 77 to 83 at 9:21 a.m. | 175 |
| Figure 6–18. Inward Bowing of east Face of WTC 2 at 9:21 a.m. | 175 |
| Figure 6–19. Inward Bowing of east Face of WTC 2 at 9:53 a.m. | 176 |
| Figure 6–20. Inward Bowing of east Face of WTC 2 at 9:53 a.m. | 177 |
| Figure 6–21. WTC 2 exterior columns bowing inward across the east face between Floors 77 to 83 at 9:59 a.m. | 178 |

| | | |
|--------------|--|-----|
| Figure 6–22. | View of WTC 2 buckling of east wall near northeast corner as collapse initiates from northeast. | 179 |
| Figure 6–23. | View of east wall buckling and WTC 2 collapse from southeast. | 180 |
| Figure 6–24. | View of upper building section of WTC 2 tilting to the east. | 181 |
| Figure 6–25. | View of upper building section of WTC 2 tilting to the east from the northeast. | 182 |
| Figure 6–26. | Kink on southeast corner near Floor 106 formed after collapse initiation. | 183 |
| | | |
| Figure 7–1. | Isolated core models. | 188 |
| Figure 7–2. | Vertical displacement of WTC 1 isolated core model with impact damage and gravity loads. | 189 |
| Figure 7–3. | North side vertical displacement of the WTC 1 core model at 100 min for Case A temperatures. | 190 |
| Figure 7–4. | South side vertical displacement of the WTC 1 core model at 100 min for Case B temperatures. | 191 |
| Figure 7–5. | Vertical displacement of the WTC 2 isolated core model with impact damage and gravity loads (south and east faces). | 192 |
| Figure 7–6. | Vertical displacement of the WTC 2 core model at 60 min for Case C temperatures (south and east faces). | 193 |
| Figure 7–7. | South and east side vertical displacement of the WTC 2 core model at 60 min for Case D temperatures. | 194 |
| Figure 7–8. | Full floor model. | 195 |
| Figure 7–9. | Fireproofing damage to WTC 1 Floor 97 for Case A i and Case A. | 198 |
| Figure 7–10. | WTC 1 Floor 97 comparison of truss temperatures for Case A i and Case A. | 199 |
| Figure 7–11. | Vertical deflection of WTC 1 Floor 95 for Case Bi at 10 min. | 202 |
| Figure 7–12. | Vertical deflection of WTC 1 Floor 96 for Case Bi at 10 min. | 202 |
| Figure 7–13. | Vertical deflection of WTC 1 Floor 97 for Case Bi at 100 min. | 203 |
| Figure 7–14. | Vertical deflection of WTC 1 Floor 98 for Case Bi at 100 min. | 203 |
| Figure 7–15. | Vertical deflection of WTC 1 Floor 99 for Case Bi at 100 min. | 204 |
| Figure 7–16. | Loss of vertical supports in WTC 1 Floor 97 and Floor 98 for Case Bi. | 204 |
| Figure 7–17. | Vertical deflection of WTC 2 Floor 79 for Case Ci at 60 min. | 206 |
| Figure 7–18. | Vertical deflection of WTC 2 Floor 80 for Case Ci at 60 min. | 206 |
| Figure 7–19. | Vertical deflection of WTC 2 Floor 81 for Case Ci at 60 min. | 207 |
| Figure 7–20. | Vertical deflection of WTC 2 Floor 82 for Case Ci at 60 min. | 207 |
| Figure 7–21. | Vertical deflection of WTC 2 Floor 83 for Case Ci at 60 min. | 208 |
| Figure 7–22. | Loss of vertical supports in WTC 2 Floor 82 and Floor 83 for Case Ci. | 208 |
| Figure 7–23. | Vertical deflection of WTC 2 Floor 79 for Case Di. | 210 |
| Figure 7–24. | Vertical deflection of WTC 2 Floor 80 for Case Di. | 210 |

| | |
|---|-----|
| Figure 7–25. Vertical deflection of WTC 2 Floor 81 for Case Di..... | 211 |
| Figure 7–26. Vertical deflection of WTC 2 Floor 82 for Case Di..... | 211 |
| Figure 7–27. Vertical deflection of WTC 2 Floor 83 for Case Di..... | 212 |
| Figure 7–28. Isolated exterior wall segments from WTC 1 and WTC 2..... | 214 |
| Figure 7–29. Boundary conditions applied on the isolated exterior wall segment..... | 214 |
| Figure 7–30. Locations of WTC 1 disconnections and pull-in forces over five floors for Case B. | 216 |
| Figure 7–31. Inward displacement of the WTC 1 south wall at 80 min of the Case B temperatures with floor disconnections and 6 kip pull-in forces over five floors. | 217 |
| Figure 7–32. Inward displacement of the WTC 1 south wall at 100 min of the Case B temperatures with floor disconnections and 6 kip pull-in forces over five floors. | 218 |
| Figure 7–33. Out-of-plane displacements of the WTC 2 east wall calculated with 0.5 kip pull-in force with uniform magnitude distribution at 32 min. | 220 |
| Figure 7–34. Out-of-plane displacements of the WTC 2 east wall calculated with 5.0 kip pull-in force with uniform magnitude distribution at 18 min. | 221 |
| Figure 7–35. Out-of-plane displacements of east wall calculated with pull-in force of 1.0 kip on the south half and 4.0 kip on the north half of the WTC 2 east wall. | 222 |
| Figure 7–36. Out-of-plane displacements of east wall of WTC 2 calculated with pull-in forces of 1.5 kip on the south half and 5.0 kip on the north half. | 223 |
| | |
| Figure 8–1. Displaced shape of WTC 1 and WTC 2 at the end of gravity load analysis..... | 232 |
| Figure 8–2. Office area and core floors and core beams. | 233 |
| Figure 8–3. Hat truss with labeled outriggers. | 233 |
| Figure 8–4. Vertical displacement at Floor 99 of WTC 1. Total displacements are shown before aircraft impact and incremental displacements, with total displacements in parentheses, are shown after impact. | 238 |
| Figure 8–5. Vertical displacement of WTC 1 east and north exterior walls before aircraft impact..... | 238 |
| Figure 8–6. Vertical displacement of east and north exterior walls of WTC 1 after aircraft impact for Case B. | 239 |
| Figure 8–7. Vertical displacement of the east and north side of the WTC 1 core before aircraft impact..... | 239 |
| Figure 8–8. Vertical displacement of the east and north side of the WTC 1 core after aircraft impact for Case B..... | 240 |
| Figure 8–9. Maximum demand-to-capacity ratio for axial force in core columns between Floor 93 and Floor 99 of WTC 1 before aircraft impact. | 241 |
| Figure 8–10. Maximum demand-to-capacity ratio for axial force in core columns between Floor 93 and Floor 99 of WTC 1 after aircraft impact for Case B. | 241 |
| Figure 8–11. Out-of-plane displacement of south wall of WTC 1 at 80 min for Case B..... | 243 |
| Figure 8–12. Out-of-plane displacement of south wall of WTC 1 at 100 min for Case B conditions with 5 kip pull-in forces..... | 244 |

| | |
|---|-----|
| Figure 8–13. Time history of maximum out-of-plane displacement of WTC 1 south wall for Case B with 5 kip pull-in forces..... | 244 |
| Figure 8–14. Distribution of axial force in exterior columns at Floor 98 of WTC 1 south wall for Case B with 5 kip pull-in forces..... | 245 |
| Figure 8–15. Distribution of axial force in exterior columns at Floor 98 of WTC 1 east wall for Case B with 5 kip pull-in forces..... | 246 |
| Figure 8–16. Vertical displacement of west and south exterior walls of WTC 1 at 80 min for Case B..... | 246 |
| Figure 8–17. Vertical displacement of west and south exterior walls of WTC 1 at 100 min for Case B..... | 247 |
| Figure 8–18. Change in vertical displacement at Floor 99 of WTC 1 from the state before impact to 100 min for Case B..... | 247 |
| Figure 8–19. Maximum elastic-plus-plastic-plus-creep strain for columns between Floor 93 and Floor 99 of WTC 1 at 10 min for Case B (strain values are in percent)..... | 248 |
| Figure 8–20. Maximum elastic-plus-plastic-plus-creep strain for columns between Floor 93 and Floor 99 of WTC 1 at 40 min for Case B (strain values are in percent)..... | 249 |
| Figure 8–21. Maximum elastic-plus-plastic-plus-creep strain for columns between Floor 93 and Floor 99 of WTC 1 at 100 min for Case B with 5 kip pull-in forces (strain value are in percent)..... | 249 |
| Figure 8–22. Maximum demand-to-capacity ratio for axial force in core columns between Floor 93 and Floor 99 of WTC 1 at 80 min for Case B conditions..... | 250 |
| Figure 8–23. Maximum demand-to-capacity ratio for axial force in core columns between Floor 93 and Floor 99 of WTC 1 at 100 min for Case B with 5 kip pull-in forces..... | 251 |
| Figure 8–24. Tension demand-to-capacity ratio for core column splices at WTC 1 Floor 106 at 100 min for Case B with 5 kip pull-in forces..... | 252 |
| Figure 8–25. Location and label of outriggers and supporting columns for WTC 1..... | 253 |
| Figure 8–26. Vertical displacement before impact of WTC 2 exterior wall for Case D..... | 255 |
| Figure 8–27. Vertical displacement after impact of WTC 2 exterior wall for Case D..... | 256 |
| Figure 8–28. Vertical displacement before impact of WTC 2 core for Case D..... | 256 |
| Figure 8–29. Vertical displacement after impact of WTC 2 core for Case D..... | 257 |
| Figure 8–30. Lateral displacements after impact above WTC 2 Floor 86 in the x-direction (north-south) for Case D..... | 257 |
| Figure 8–31. Lateral displacements after impact above WTC 2 Floor 86 in the y-direction (east-west) for Case D..... | 258 |
| Figure 8–32. Core column loads (kip) before impact at WTC 2 Floor 83 for Case D (compression is positive)..... | 259 |
| Figure 8–33. Core column loads (kip) after impact at WTC 2 Floor 83 for Case D (compression is positive)..... | 260 |
| Figure 8–34. Vertical displacement of exterior wall of WTC 2 at 20 min for Case D..... | 262 |

| | |
|--|-----|
| Figure 8–35. Vertical displacement at Floor 83 of WTC 2 at 20 min for Case D (note the tilt toward east and south)..... | 262 |
| Figure 8–36. Vertical displacement of exterior wall of WTC 2 at 43 min for Case D..... | 263 |
| Figure 8–37. Vertical displacement at Floor 83 of WTC 2 at 43 min for Case D (note the tilt toward east and south)..... | 263 |
| Figure 8–38. Out-of-plane displacement of the east wall of WTC 2 at 20 min for Case D. | 264 |
| Figure 8–39. Out-of-plane displacement of the east wall of WTC 2 at 43 min for Case D. | 266 |
| Figure 8–40. Variation of maximum out-of-plane displacement on the east wall of WTC 2 over the time for Case D. | 266 |
| Figure 8–41. Vertical displacement of core of WTC 2 at 20 min for Case D. | 267 |
| Figure 8–42. Vertical displacement of core of WTC 2 at 43 min for Case D. | 267 |
| Figure 8–43. Core column loads (kip) at Floor 83 of WTC 2 at 20 min for Case D (compression is positive)..... | 268 |
| Figure 8–44. Core column loads (kip) at Floor 83 of WTC 2 at 43 min for Case D (compression is positive)..... | 268 |
| Figure 8–45. Total displacements of WTC 2 above Floor 86 at 43 min of Case D (deformed shape magnified 20 times). Note the tilt toward east and south..... | 269 |
| Figure 8–46. Axial force in the east wall columns at Floor 83 of WTC 2 for Case D (compression is positive)..... | 269 |
| Figure 8–47. Axial force in the west wall columns at Floor 83 of WTC 2 for Case D (compression is positive)..... | 270 |
| Figure 8–48. Axial force in the south wall columns at Floor 83 of WTC 2 for Case D (compression is positive)..... | 270 |
| Figure 8–49. Axial force in the north wall columns at Floor 83 of WTC 2 for Case D (compression is positive)..... | 271 |
| Figure 8–50. Axial force in Floor 83 columns of WTC 2 before impact for Case D (compression is positive)..... | 271 |
| Figure 8–51. Axial force in Floor 83 columns of WTC 2 at 43 min for Case D (compression is positive)..... | 272 |
| Figure 8–52. Maximum elastic-plus-plastic-plus-creep strains at 20 min for columns between Floor 78 and Floor 83 of WTC 2 for Case D (strain values are in percent)..... | 272 |
| Figure 8–53. Maximum elastic-plus-plastic-plus-creep strains at 43 min for columns between Floor 78 and Floor 83 of WTC 2 for Case D (strain values are in percent)..... | 273 |
| Figure 8–54. Axial force in core columns (kip) at WTC 2 Floor 105 (at hat-truss level) before impact for Case D (compression is positive). | 274 |
| Figure 8–55. Axial force in core columns (kip) at WTC 2 Floor 105 (at hat-truss level) after impact for Case D (compression is positive). | 275 |
| Figure 8–56. Axial force in core columns (kip) at Floor 105 (at hat-truss level) of WTC 2 for Case D conditions (compression is positive). | 276 |
| Figure 8–57. State of core column splices at Floor 105 of WTC 2..... | 277 |

| | |
|--|-----|
| Figure 8–58. Location and IDs of outriggers and supporting columns | 278 |
| Figure 8–59. Temperatures of two adjacent trusses (left) and two adjacent perimeter columns (right) exposed to simulated fires in WTC 1. Data plotted in blue are for structural steel components with fireproofing; data in red are for steel components without fireproofing (from NIST NCSTAR 1-5)..... | 281 |
| Figure 9–1. Critical analysis inter-dependencies..... | 289 |
| Figure 9–2. Full analysis tree for influential parameter effects..... | 291 |
| Figure 9–3. Pruned analysis tree for influential parameter effects..... | 292 |
| Figure 9–4. Data used for validating probable collapse sequences..... | 295 |
| Figure 9–5. Variability in global reserve capacity using model predictions and observables for sequential analyses with imperfect information..... | 296 |
| Figure 9–6. Vertical displacement contour of the detailed truss model under thermal loading. | 297 |
| Figure 9–7. Combined flexural and catenary action in the floor system..... | 297 |
| Figure 9–8. WTC 1 probable collapse sequence..... | 299 |
| Figure 9–9. Vertical displacement of Floors of WTC 1 for Case B' at 100 min..... | 302 |
| Figure 9–10. Loss of vertical supports observed in Floor 97 and Floor 98 of WTC 1 for Case B' (1x displacement magnification)..... | 302 |
| Figure 9–11. Inward bowing of the WTC 1 south wall of WTC 1 at 10:23 a.m..... | 303 |
| Figure 9–12. Inward bowing of south wall of WTC 1 global model with creep at 100 min for Case B with 5 kip pull-in forces (5x displacement magnification). | 304 |
| Figure 9–13. Expulsion of smoke and debris at WTC 1 Floor 98 on the east, north, and west faces. | 305 |
| Figure 9–14. WTC 2 probable collapse sequence..... | 307 |
| Figure 9–15. Vertical displacements of Floors 79 through Floor 88 of WTC 2 at 40 min (Case D). | 311 |
| Figure 9–16. Floor sagging observed on the east wall of WTC 2 at different stages..... | 312 |
| Figure 9–17. Out-of-plane displacements on the east wall of WTC 2 (Case D)..... | 313 |
| Figure 9–18. Out-of-plane displacement estimates of the east wall of WTC 2 from photographs. | 314 |
| Figure 9–19. Variation of maximum out-of-plane displacement on the east wall of WTC 2 (Case D). | 315 |
| Figure 9–20. Total column loads at Floor 83 of the east wall of WTC 2 at different stages (Case D). | 315 |
| Figure 9–21. Maximum elastic + plastic + creep strains for columns between Floor 78 and Floor 83 of WTC 2 at different stages (Case D) (strain values are in percent). | 316 |
| Figure 9–22. Inward bowing of the east wall of WTC 2 when buckled at 43 min for Case D (4x displacement magnification)..... | 317 |
| Figure 9–23. Inward bending of exterior columns of the west wall of WTC 2 just before collapse..... | 318 |
| Figure 9–24. Total displacements of WTC 2 above Floor 86 at 43 min for Case D. Note tilt toward east and south (20x displacement magnification). | 319 |

LIST OF TABLES

| | | |
|-------------|---|-------------------------------------|
| Table P-1. | Federal building and fire safety investigation of the WTC disaster. | Error! Bookmark not defined. |
| Table P-2. | Public meetings and briefings of the WTC Investigation. | Error! Bookmark not defined. |
| Table 2-1. | Average SFRM thickness from six measurements taken in 1994 on each of 16 random floor trusses on floors 23 and 24 of WTC 1..... | 23 |
| Table 2-2. | Summary of specified, in-place and thermally equivalent thickness of SFRM..... | 29 |
| Table 2-3. | Measured thermal conductivity as a function of temperature..... | 31 |
| Table 2-4. | Summary of physical characteristics of BLAZE-SHIELD DC/F specimens tested at NIST..... | 35 |
| Table 3-1. | Results of ASTM E119 Standard Fire Tests..... | 49 |
| Table 4-1. | Steel types used in WTC 1 and WTC 2..... | 61 |
| Table 4-2. | Interior seat capacity against vertical force..... | 74 |
| Table 4-3. | Exterior seat capacity against vertical force..... | 75 |
| Table 4-4. | Interior seat capacity against horizontal tensile force..... | 75 |
| Table 4-5. | Exterior seat capacity against horizontal tensile force..... | 76 |
| Table 4-6. | Knuckle shear capacity reduction for elevated temperatures..... | 84 |
| Table 4-7. | Comparison of SAP2000 and ANSYS results for gravity load case..... | 92 |
| Table 4-8. | Comparison of SAP2000 and ANSYS Modal Analysis Results..... | 92 |
| Table 4-9. | Types of break elements..... | 95 |
| Table 4-10. | Column section properties..... | 99 |
| Table 4-11. | Spandrel Splice Details..... | 99 |
| Table 4-12. | Column Splice Details..... | 99 |
| Table 4-13. | Prefabricated panel validation results..... | 107 |
| Table 4-14. | Thermal loading conditions used in the exterior wall model..... | 111 |
| Table 4-15. | Analysis cases for exterior wall section model..... | 113 |
| Table 5-1. | WTC 1 Case A core column damage..... | 124 |
| Table 5-2. | WTC 1 Case B core column damage..... | 125 |
| Table 5-3. | WTC 2 Case C core column damage..... | 125 |
| Table 5-4. | WTC 2 Case D core column damage..... | 126 |

| | | |
|-------------|--|-----|
| Table 6–1. | WTC1 Timeline of Observed Structural and Fire Events..... | 154 |
| Table 6–2. | WTC2 Timeline of Observed Structural and Fire Events..... | 167 |
| Table 6–3. | Possible floor damage observed in photos of WTC 2 windows. | 168 |
| Table 7–1. | Maximum vertical displacement of WTC 1 floors for Case Ai. | 199 |
| Table 7–2. | Maximum vertical displacement of WTC 1 floors for Case Bi. | 199 |
| Table 7–3. | Maximum vertical displacement of WTC 2 floors for Case Ci. | 203 |
| Table 7–4. | Maximum vertical displacement of WTC 2 floors for Case Di. | 207 |
| Table 8–1. | Total column loads at Floor 98 of WTC 1 for Case B conditions. | 240 |
| Table 8–2. | Total column loads at Floor 105 of WTC 1 for Case B conditions. | 240 |
| Table 8–3. | Demand-to-capacity ratio for axial force in outriggers of WTC 1 for Case B..... | 251 |
| Table 8–4. | Total column loads at WTC 2 Floor 83 for Case D (Compression is positive). | 256 |
| Table 8–5. | Total column loads at WTC 2 Floor 105 for Case D (Compression is positive). | 257 |
| Table 8–6. | Change in total column loads before and after aircraft impact. (Loads After Impact) – (Loads Before Impact) (Compression is positive). | 262 |
| Table 8–7. | Change in total column loads between 40 min and 43 min. (Loads at 43 min) – (Loads at 40 min) (Compression is positive). | 262 |
| Table 8–8. | Demand-to-capacity ratios for outriggers of WTC 2 for Case D conditions (outrigger IDs are shown in Fig. 8–3)..... | 276 |
| Table 9–1. | Aircraft impact analysis parameters..... | 290 |
| Table 9–2. | Fire dynamics analysis parameters. | 291 |
| Table 9–3. | Thermal analysis parameters..... | 291 |
| Table 9–4. | Structural response analysis parameters. | 292 |
| Table 9–5. | Observations for WTC 1..... | 296 |
| Table 9–6. | Total column loads at Floor 98 and Floor 105 of WTC 1 for Case B..... | 299 |
| Table 9–7. | Key observations on WTC 2..... | 304 |
| Table 9–8. | Total column loads at Floor 83 of WTC 2 for Case D. Compression is positive..... | 308 |
| Table 9–9. | Total column loads at Floor 105 of WTC 2 for Case D. Compression is positive..... | 308 |
| Table 9–10. | Change in total column loads when the east wall of WTC 2 buckles (Case D, compression is positive)..... | 317 |

LIST OF ACRONYMS AND ABBREVIATIONS

Acronyms

| | |
|--------|--|
| ASTM | ASTM International |
| BPS | Building Performance Study |
| FEMA | Federal Emergency Management Agency |
| MIG | Metal Inert Gas (welding) |
| NIST | National Institute of Standards and Technology |
| PANYNJ | Port Authority of New York and New Jersey |
| SEAoNY | Structural Engineers Association of New York |
| USC | United States Code |
| ULI | Underwriters Laboratories Inc. |
| WTC | World Trade Center |
| WTC 1 | World Trade Center 1 (North Tower) |
| WTC 2 | World Trade Center 2 (South Tower) |
| WTC 7 | World Trade Center 7 |

Abbreviations

| | |
|-----|--------------------|
| °C | degrees Celsius |
| °F | degrees Fahrenheit |
| ft | feet |
| in. | inch |
| L | liter |
| m | meter |
| µm | micrometer |
| min | minute |
| s | second |

This page intentionally left blank.

PREFACE

Genesis of This Investigation

Immediately following the terrorist attack on the World Trade Center (WTC) on September 11, 2001, the Federal Emergency Management Agency (FEMA) and the American Society of Civil Engineers began planning a building performance study of the disaster. The week of October 7, as soon as the rescue and search efforts ceased, the Building Performance Study Team went to the site and began its assessment. This was to be a brief effort, as the study team consisted of experts who largely volunteered their time away from their other professional commitments. The Building Performance Study Team issued its report in May 2002, fulfilling its goal “to determine probable failure mechanisms and to identify areas of future investigation that could lead to practical measures for improving the damage resistance of buildings against such unforeseen events.”

On August 21, 2002, with funding from the U.S. Congress through FEMA, the National Institute of Standards and Technology (NIST) announced its building and fire safety investigation of the WTC disaster. On October 1, 2002, the National Construction Safety Team Act (Public Law 107-231), was signed into law. The NIST WTC Investigation was conducted under the authority of the National Construction Safety Team Act.

The goals of the investigation of the WTC disaster were:

- To investigate the building construction, the materials used, and the technical conditions that contributed to the outcome of the WTC disaster.
- To serve as the basis for:
 - Improvements in the way buildings are designed, constructed, maintained, and used;
 - Improved tools and guidance for industry and safety officials;
 - Recommended revisions to current codes, standards, and practices; and
 - Improved public safety.

The specific objectives were:

1. Determine why and how WTC 1 and WTC 2 collapsed following the initial impacts of the aircraft and why and how WTC 7 collapsed;
2. Determine why the injuries and fatalities were so high or low depending on location, including all technical aspects of fire protection, occupant behavior, evacuation, and emergency response;
3. Determine what procedures and practices were used in the design, construction, operation, and maintenance of WTC 1, 2, and 7; and
4. Identify, as specifically as possible, areas in current building and fire codes, standards, and practices that warrant revision.

NIST is a nonregulatory agency of the U.S. Department of Commerce's Technology Administration. The purpose of NIST investigations is to improve the safety and structural integrity of buildings in the United States, and the focus is on fact finding. NIST investigative teams are authorized to assess building performance and emergency response and evacuation procedures in the wake of any building failure that has resulted in substantial loss of life or that posed significant potential of substantial loss of life. NIST does not have the statutory authority to make findings of fault nor negligence by individuals or organizations. Further, no part of any report resulting from a NIST investigation into a building failure or from an investigation under the National Construction Safety Team Act may be used in any suit or action for damages arising out of any matter mentioned in such report (15 USC 281a, as amended by Public Law 107-231).

Organization of the Investigation

The National Construction Safety Team for this Investigation, appointed by the then NIST Director, Dr. Arden L. Bement, Jr., was led by Dr. S. Shyam Sunder. Dr. William L. Grosshandler served as Associate Lead Investigator, Mr. Stephen A. Cauffman served as Program Manager for Administration, and Mr. Harold E. Nelson served on the team as a private sector expert. The Investigation included eight interdependent projects whose leaders comprised the remainder of the team. A detailed description of each of these eight projects is available at <http://wtc.nist.gov>. The purpose of each project is summarized in Table P-1, and the key interdependencies among the projects are illustrated in Fig. P-1.

Table P-1. Federal building and fire safety investigation of the WTC disaster.

| Technical Area and Project Leader | Project Purpose |
|--|---|
| Analysis of Building and Fire Codes and Practices; Project Leaders: Dr. H. S. Lew and Mr. Richard W. Bukowski | Document and analyze the code provisions, procedures, and practices used in the design, construction, operation, and maintenance of the structural, passive fire protection, and emergency access and evacuation systems of WTC 1, 2, and 7. |
| Baseline Structural Performance and Aircraft Impact Damage Analysis; Project Leader: Dr. Fahim H. Sadek | Analyze the baseline performance of WTC 1 and WTC 2 under design, service, and abnormal loads, and aircraft impact damage on the structural, fire protection, and egress systems. |
| Mechanical and Metallurgical Analysis of Structural Steel; Project Leader: Dr. Frank W. Gayle | Determine and analyze the mechanical and metallurgical properties and quality of steel, weldments, and connections from steel recovered from WTC 1, 2, and 7. |
| Investigation of Active Fire Protection Systems; Project Leader: Dr. David D. Evans; Dr. William Grosshandler | Investigate the performance of the active fire protection systems in WTC 1, 2, and 7 and their role in fire control, emergency response, and fate of occupants and responders. |
| Reconstruction of Thermal and Tenability Environment; Project Leader: Dr. Richard G. Gann | Reconstruct the time-evolving temperature, thermal environment, and smoke movement in WTC 1, 2, and 7 for use in evaluating the structural performance of the buildings and behavior and fate of occupants and responders. |
| Structural Fire Response and Collapse Analysis; Project Leaders: Dr. John L. Gross and Dr. Therese P. McAllister | Analyze the response of the WTC towers to fires with and without aircraft damage, the response of WTC 7 in fires, the performance of composite steel-trussed floor systems, and determine the most probable structural collapse sequence for WTC 1, 2, and 7. |
| Occupant Behavior, Egress, and Emergency Communications; Project Leader: Mr. Jason D. Averill | Analyze the behavior and fate of occupants and responders, both those who survived and those who did not, and the performance of the evacuation system. |
| Emergency Response Technologies and Guidelines; Project Leader: Mr. J. Randall Lawson | Document the activities of the emergency responders from the time of the terrorist attacks on WTC 1 and WTC 2 until the collapse of WTC 7, including practices followed and technologies used. |

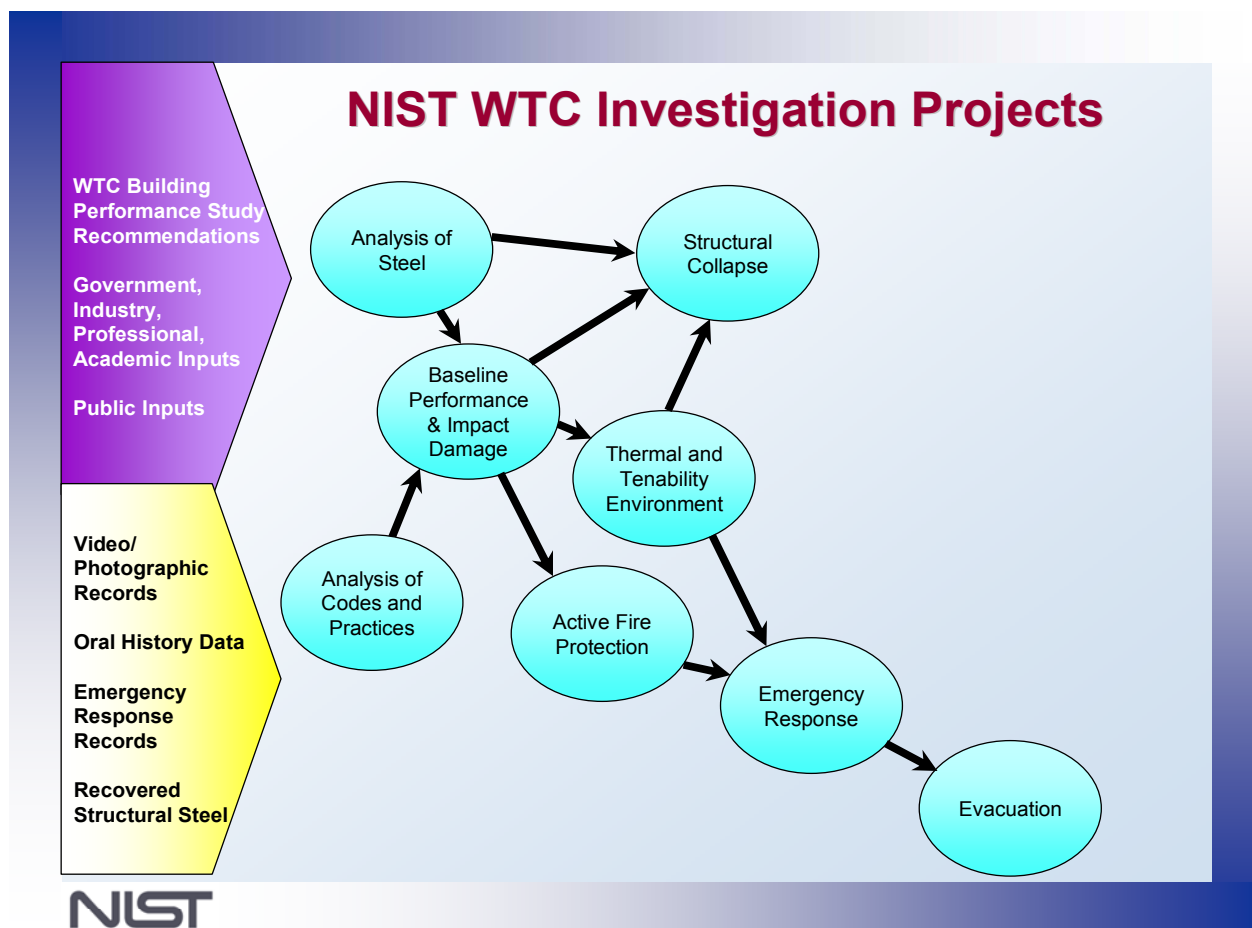


Figure P-1. The eight projects in the federal building and fire safety investigation of the WTC disaster.

National Construction Safety Team Advisory Committee

The NIST Director also established an advisory committee as mandated under the National Construction Safety Team Act. The initial members of the committee were appointed following a public solicitation. These were:

- Paul Fitzgerald, Executive Vice President (retired) FM Global, National Construction Safety Team Advisory Committee Chair
- John Barsom, President, Barsom Consulting, Ltd.
- John Bryan, Professor Emeritus, University of Maryland
- David Collins, President, The Preview Group, Inc.
- Glenn Corbett, Professor, John Jay College of Criminal Justice
- Philip DiNunno, President, Hughes Associates, Inc.

- Robert Hanson, Professor Emeritus, University of Michigan
- Charles Thornton, Co-Chairman and Managing Principal, The Thornton-Tomasetti Group, Inc.
- Kathleen Tierney, Director, Natural Hazards Research and Applications Information Center, University of Colorado at Boulder
- Forman Williams, Director, Center for Energy Research, University of California at San Diego

This National Construction Safety Team Advisory Committee provided technical advice during the Investigation and commentary on drafts of the Investigation reports prior to their public release. NIST has benefited from the work of many people in the preparation of these reports, including the National Construction Safety Team Advisory Committee. The content of the reports and recommendations, however, are solely the responsibility of NIST.

Public Outreach

During the course of this Investigation, NIST held public briefings and meetings (listed in Table P-2) to solicit input from the public, present preliminary findings, and obtain comments on the direction and progress of the Investigation from the public and the Advisory Committee.

NIST maintained a publicly accessible Web site during this Investigation at <http://wtc.nist.gov>. The site contained extensive information on the background and progress of the Investigation.

NIST's WTC Public-Private Response Plan

The collapse of the WTC buildings has led to broad reexamination of how tall buildings are designed, constructed, maintained, and used, especially with regard to major events such as fires, natural disasters, and terrorist attacks. Reflecting the enhanced interest in effecting necessary change, NIST, with support from Congress and the Administration, has put in place a program, the goal of which is to develop and implement the standards, technology, and practices needed for cost-effective improvements to the safety and security of buildings and building occupants, including evacuation, emergency response procedures, and threat mitigation.

The strategy to meet this goal is a three-part NIST-led public-private response program that includes:

- A federal building and fire safety investigation to study the most probable factors that contributed to post-aircraft impact collapse of the WTC towers and the 47-story WTC 7 building, and the associated evacuation and emergency response experience.
- A research and development (R&D) program to (a) facilitate the implementation of recommendations resulting from the WTC Investigation, and (b) provide the technical basis for cost-effective improvements to national building and fire codes, standards, and practices that enhance the safety of buildings, their occupants, and emergency responders.

Table P–2. Public meetings and briefings of the WTC Investigation.

| Date | Location | Principal Agenda |
|-----------------------|-------------------|--|
| June 24, 2002 | New York City, NY | Public meeting: Public comments on the <i>Draft Plan</i> for the pending WTC Investigation. |
| August 21, 2002 | Gaithersburg, MD | Media briefing announcing the formal start of the Investigation. |
| December 9, 2002 | Washington, DC | Media briefing on release of the <i>Public Update</i> and NIST request for photographs and videos. |
| April 8, 2003 | New York City, NY | Joint public forum with Columbia University on first-person interviews. |
| April 29–30, 2003 | Gaithersburg, MD | NCST Advisory Committee meeting on plan for and progress on WTC Investigation with a public comment session. |
| May 7, 2003 | New York City, NY | Media briefing on release of <i>May 2003 Progress Report</i> . |
| August 26–27, 2003 | Gaithersburg, MD | NCST Advisory Committee meeting on status of the WTC investigation with a public comment session. |
| September 17, 2003 | New York City, NY | Media and public briefing on initiation of first-person data collection projects. |
| December 2–3, 2003 | Gaithersburg, MD | NCST Advisory Committee meeting on status and initial results and release of the <i>Public Update</i> with a public comment session. |
| February 12, 2004 | New York City, NY | Public meeting on progress and preliminary findings with public comments on issues to be considered in formulating final recommendations. |
| June 18, 2004 | New York City, NY | Media/public briefing on release of <i>June 2004 Progress Report</i> . |
| June 22–23, 2004 | Gaithersburg, MD | NCST Advisory Committee meeting on the status of and preliminary findings from the WTC Investigation with a public comment session. |
| August 24, 2004 | Northbrook, IL | Public viewing of standard fire resistance test of WTC floor system at Underwriters Laboratories, Inc. |
| October 19–20, 2004 | Gaithersburg, MD | NCST Advisory Committee meeting on status and near complete set of preliminary findings with a public comment session. |
| November 22, 2004 | Gaithersburg, MD | NCST Advisory Committee discussion on draft annual report to Congress, a public comment session, and a closed session to discuss pre-draft recommendations for WTC Investigation. |
| April 5, 2005 | New York City, NY | Media and public briefing on release of the probable collapse sequence for the WTC towers and draft reports for the projects on codes and practices, evacuation, and emergency response. |
| June 23, 2005 | New York City, NY | Media and public briefing on release of all draft reports for the WTC towers and draft recommendations for public comment. |
| September 12–13, 2005 | Gaithersburg, MD | NCST Advisory Committee meeting on disposition of public comments and update to draft reports for the WTC towers. |
| September 13–15, 2005 | Gaithersburg, MD | WTC Technical Conference for stakeholders and technical community for dissemination of findings and recommendations and opportunity for public to make technical comments. |

- A dissemination and technical assistance program (DTAP) to (a) engage leaders of the construction and building community in ensuring timely adoption and widespread use of proposed changes to practices, standards, and codes resulting from the WTC Investigation and the R&D program, and (b) provide practical guidance and tools to better prepare facility owners, contractors, architects, engineers, emergency responders, and regulatory authorities to respond to future disasters.

The desired outcomes are to make buildings, occupants, and first responders safer in future disaster events.

National Construction Safety Team Reports on the WTC Investigation

A final report on the collapse of the WTC towers is being issued as NIST NCSTAR 1. A companion report on the collapse of WTC 7 is being issued as NIST NCSTAR 1A. The present report is one of a set that provides more detailed documentation of the Investigation findings and the means by which these technical results were achieved. As such, it is part of the archival record of this Investigation. The titles of the full set of Investigation publications are:

NIST (National Institute of Standards and Technology). 2005. *Federal Building and Fire Safety Investigation of the World Trade Center Disaster: Final Report on the Collapse of the World Trade Center Towers*. NIST NCSTAR 1. Gaithersburg, MD, September.

NIST (National Institute of Standards and Technology). 2008. *Federal Building and Fire Safety Investigation of the World Trade Center Disaster: Final Report on the Collapse of World Trade Center 7*. NIST NCSTAR 1A. Gaithersburg, MD, November.

Lew, H. S., R. W. Bukowski, and N. J. Carino. 2005. *Federal Building and Fire Safety Investigation of the World Trade Center Disaster: Design, Construction, and Maintenance of Structural and Life Safety Systems*. NIST NCSTAR 1-1. National Institute of Standards and Technology. Gaithersburg, MD, September.

Fanella, D. A., A. T. Derecho, and S. K. Ghosh. 2005. *Federal Building and Fire Safety Investigation of the World Trade Center Disaster: Design and Construction of Structural Systems*. NIST NCSTAR 1-1A. National Institute of Standards and Technology. Gaithersburg, MD, September.

Ghosh, S. K., and X. Liang. 2005. *Federal Building and Fire Safety Investigation of the World Trade Center Disaster: Comparison of Building Code Structural Requirements*. NIST NCSTAR 1-1B. National Institute of Standards and Technology. Gaithersburg, MD, September.

Fanella, D. A., A. T. Derecho, and S. K. Ghosh. 2005. *Federal Building and Fire Safety Investigation of the World Trade Center Disaster: Maintenance and Modifications to Structural Systems*. NIST NCSTAR 1-1C. National Institute of Standards and Technology. Gaithersburg, MD, September.

Grill, R. A., and D. A. Johnson. 2005. *Federal Building and Fire Safety Investigation of the World Trade Center Disaster: Fire Protection and Life Safety Provisions Applied to the Design and Construction of World Trade Center 1, 2, and 7 and Post-Construction Provisions Applied after Occupancy*. NIST NCSTAR 1-1D. National Institute of Standards and Technology. Gaithersburg, MD, September.

Razza, J. C., and R. A. Grill. 2005. *Federal Building and Fire Safety Investigation of the World Trade Center Disaster: Comparison of Codes, Standards, and Practices in Use at the Time of the Design and Construction of World Trade Center 1, 2, and 7*. NIST NCSTAR 1-1E. National Institute of Standards and Technology. Gaithersburg, MD, September.

Grill, R. A., D. A. Johnson, and D. A. Fanella. 2005. *Federal Building and Fire Safety Investigation of the World Trade Center Disaster: Comparison of the 1968 and Current (2003) New*

York City Building Code Provisions. NIST NCSTAR 1-1F. National Institute of Standards and Technology. Gaithersburg, MD, September.

Grill, R. A., and D. A. Johnson. 2005. *Federal Building and Fire Safety Investigation of the World Trade Center Disaster: Amendments to the Fire Protection and Life Safety Provisions of the New York City Building Code by Local Laws Adopted While World Trade Center 1, 2, and 7 Were in Use*. NIST NCSTAR 1-1G. National Institute of Standards and Technology. Gaithersburg, MD, September.

Grill, R. A., and D. A. Johnson. 2005. *Federal Building and Fire Safety Investigation of the World Trade Center Disaster: Post-Construction Modifications to Fire Protection and Life Safety Systems of World Trade Center 1 and 2*. NIST NCSTAR 1-1H. National Institute of Standards and Technology. Gaithersburg, MD, September.

Grill, R. A., D. A. Johnson, and D. A. Fanella. 2005. *Federal Building and Fire Safety Investigation of the World Trade Center Disaster: Post-Construction Modifications to Fire Protection, Life Safety, and Structural Systems of World Trade Center 7*. NIST NCSTAR 1-1I. National Institute of Standards and Technology. Gaithersburg, MD, September.

Grill, R. A., and D. A. Johnson. 2005. *Federal Building and Fire Safety Investigation of the World Trade Center Disaster: Design, Installation, and Operation of Fuel System for Emergency Power in World Trade Center 7*. NIST NCSTAR 1-1J. National Institute of Standards and Technology. Gaithersburg, MD, September.

Sadek, F. 2005. *Federal Building and Fire Safety Investigation of the World Trade Center Disaster: Baseline Structural Performance and Aircraft Impact Damage Analysis of the World Trade Center Towers*. NIST NCSTAR 1-2. National Institute of Standards and Technology. Gaithersburg, MD, September.

Faschan, W. J., and R. B. Garlock. 2005. *Federal Building and Fire Safety Investigation of the World Trade Center Disaster: Reference Structural Models and Baseline Performance Analysis of the World Trade Center Towers*. NIST NCSTAR 1-2A. National Institute of Standards and Technology. Gaithersburg, MD, September.

Kirkpatrick, S. W., R. T. Bocchieri, F. Sadek, R. A. MacNeill, S. Holmes, B. D. Peterson, R. W. Cilke, C. Navarro. 2005. *Federal Building and Fire Safety Investigation of the World Trade Center Disaster: Analysis of Aircraft Impacts into the World Trade Center Towers*, NIST NCSTAR 1-2B. National Institute of Standards and Technology. Gaithersburg, MD, September.

Gayle, F. W., R. J. Fields, W. E. Luecke, S. W. Banovic, T. Foecke, C. N. McCowan, T. A. Siewert, and J. D. McColskey. 2005. *Federal Building and Fire Safety Investigation of the World Trade Center Disaster: Mechanical and Metallurgical Analysis of Structural Steel*. NIST NCSTAR 1-3. National Institute of Standards and Technology. Gaithersburg, MD, September.

Luecke, W. E., T. A. Siewert, and F. W. Gayle. 2005. *Federal Building and Fire Safety Investigation of the World Trade Center Disaster: Contemporaneous Structural Steel Specifications*. NIST Special Publication 1-3A. National Institute of Standards and Technology. Gaithersburg, MD, September.

Banovic, S. W. 2005. *Federal Building and Fire Safety Investigation of the World Trade Center Disaster: Steel Inventory and Identification*. NIST NCSTAR 1-3B. National Institute of Standards and Technology. Gaithersburg, MD, September.

Banovic, S. W., and T. Foecke. 2005. *Federal Building and Fire Safety Investigation of the World Trade Center Disaster: Damage and Failure Modes of Structural Steel Components*. NIST NCSTAR 1-3C. National Institute of Standards and Technology. Gaithersburg, MD, September.

Luecke, W. E., J. D. McColskey, C. N. McCowan, S. W. Banovic, R. J. Fields, T. Foecke, T. A. Siewert, and F. W. Gayle. 2005. *Federal Building and Fire Safety Investigation of the World Trade Center Disaster: Mechanical Properties of Structural Steels*. NIST NCSTAR 1-3D. National Institute of Standards and Technology. Gaithersburg, MD, September.

Banovic, S. W., C. N. McCowan, and W. E. Luecke. 2005. *Federal Building and Fire Safety Investigation of the World Trade Center Disaster: Physical Properties of Structural Steels*. NIST NCSTAR 1-3E. National Institute of Standards and Technology. Gaithersburg, MD, September.

Evans, D. D., R. D. Peacock, E. D. Kuligowski, W. S. Dols, and W. L. Grosshandler. 2005. *Federal Building and Fire Safety Investigation of the World Trade Center Disaster: Active Fire Protection Systems*. NIST NCSTAR 1-4. National Institute of Standards and Technology. Gaithersburg, MD, September.

Kuligowski, E. D., D. D. Evans, and R. D. Peacock. 2005. *Federal Building and Fire Safety Investigation of the World Trade Center Disaster: Post-Construction Fires Prior to September 11, 2001*. NIST NCSTAR 1-4A. National Institute of Standards and Technology. Gaithersburg, MD, September.

Hopkins, M., J. Schoenrock, and E. Budnick. 2005. *Federal Building and Fire Safety Investigation of the World Trade Center Disaster: Fire Suppression Systems*. NIST NCSTAR 1-4B. National Institute of Standards and Technology. Gaithersburg, MD, September.

Keough, R. J., and R. A. Grill. 2005. *Federal Building and Fire Safety Investigation of the World Trade Center Disaster: Fire Alarm Systems*. NIST NCSTAR 1-4C. National Institute of Standards and Technology. Gaithersburg, MD, September.

Ferreira, M. J., and S. M. Strege. 2005. *Federal Building and Fire Safety Investigation of the World Trade Center Disaster: Smoke Management Systems*. NIST NCSTAR 1-4D. National Institute of Standards and Technology. Gaithersburg, MD, September.

Gann, R. G., A. Hamins, K. B. McGrattan, G. W. Mulholland, H. E. Nelson, T. J. Ohlemiller, W. M. Pitts, and K. R. Prasad. 2005. *Federal Building and Fire Safety Investigation of the World Trade Center Disaster: Reconstruction of the Fires in the World Trade Center Towers*. NIST NCSTAR 1-5. National Institute of Standards and Technology. Gaithersburg, MD, September.

Pitts, W. M., K. M. Butler, and V. Junker. 2005. *Federal Building and Fire Safety Investigation of the World Trade Center Disaster: Visual Evidence, Damage Estimates, and Timeline Analysis*. NIST NCSTAR 1-5A. National Institute of Standards and Technology. Gaithersburg, MD, September.

- Hamins, A., A. Maranghides, K. B. McGrattan, E. Johnsson, T. J. Ohlemiller, M. Donnelly, J. Yang, G. Mulholland, K. R. Prasad, S. Kukuck, R. Anleitner and T. McAllister. 2005. *Federal Building and Fire Safety Investigation of the World Trade Center Disaster: Experiments and Modeling of Structural Steel Elements Exposed to Fire*. NIST NCSTAR 1-5B. National Institute of Standards and Technology. Gaithersburg, MD, September.
- Ohlemiller, T. J., G. W. Mulholland, A. Maranghides, J. J. Filliben, and R. G. Gann. 2005. *Federal Building and Fire Safety Investigation of the World Trade Center Disaster: Fire Tests of Single Office Workstations*. NIST NCSTAR 1-5C. National Institute of Standards and Technology. Gaithersburg, MD, September.
- Gann, R. G., M. A. Riley, J. M. Repp, A. S. Whittaker, A. M. Reinhorn, and P. A. Hough. 2005. *Federal Building and Fire Safety Investigation of the World Trade Center Disaster: Reaction of Ceiling Tile Systems to Shocks*. NIST NCSTAR 1-5D. National Institute of Standards and Technology. Gaithersburg, MD, September.
- Hamins, A., A. Maranghides, K. B. McGrattan, T. J. Ohlemiller, and R. Anleitner. 2005. *Federal Building and Fire Safety Investigation of the World Trade Center Disaster: Experiments and Modeling of Multiple Workstations Burning in a Compartment*. NIST NCSTAR 1-5E. National Institute of Standards and Technology. Gaithersburg, MD, September.
- McGrattan, K. B., C. Bouldin, and G. Forney. 2005. *Federal Building and Fire Safety Investigation of the World Trade Center Disaster: Computer Simulation of the Fires in the World Trade Center Towers*. NIST NCSTAR 1-5F. National Institute of Standards and Technology. Gaithersburg, MD, September.
- Prasad, K. R., and H. R. Baum. 2005. *Federal Building and Fire Safety Investigation of the World Trade Center Disaster: Fire Structure Interface and Thermal Response of the World Trade Center Towers*. NIST NCSTAR 1-5G. National Institute of Standards and Technology. Gaithersburg, MD, September.
- Gross, J. L., and T. McAllister. 2005. *Federal Building and Fire Safety Investigation of the World Trade Center Disaster: Structural Fire Response and Probable Collapse Sequence of the World Trade Center Towers*. NIST NCSTAR 1-6. National Institute of Standards and Technology. Gaithersburg, MD, September.
- Carino, N. J., M. A. Starnes, J. L. Gross, J. C. Yang, S. Kukuck, K. R. Prasad, and R. W. Bukowski. 2005. *Federal Building and Fire Safety Investigation of the World Trade Center Disaster: Passive Fire Protection*. NIST NCSTAR 1-6A. National Institute of Standards and Technology. Gaithersburg, MD, September.
- Gross, J., F. Hervey, M. Izydorek, J. Mammoser, and J. Treadway. 2005. *Federal Building and Fire Safety Investigation of the World Trade Center Disaster: Fire Resistance Tests of Floor Truss Systems*. NIST NCSTAR 1-6B. National Institute of Standards and Technology. Gaithersburg, MD, September.
- Zarghamee, M. S., S. Bolourchi, D. W. Eggers, Ö. O. Erbay, F. W. Kan, Y. Kitane, A. A. Liepins, M. Mudlock, W. I. Naguib, R. P. Ojdrovic, A. T. Sarawit, P. R. Barrett, J. L. Gross, and

T. P. McAllister. 2005. *Federal Building and Fire Safety Investigation of the World Trade Center Disaster: Component, Connection, and Subsystem Structural Analysis*. NIST NCSTAR 1-6C. National Institute of Standards and Technology. Gaithersburg, MD, September.

Zarghamee, M. S., Y. Kitane, Ö. O. Erbay, T. P. McAllister, and J. L. Gross. 2005. *Federal Building and Fire Safety Investigation of the World Trade Center Disaster: Global Structural Analysis of the Response of the World Trade Center Towers to Impact Damage and Fire*. NIST NCSTAR 1-6D. National Institute of Standards and Technology. Gaithersburg, MD, September.

Averill, J. D., D. S. Mileti, R. D. Peacock, E. D. Kuligowski, N. Groner, G. Proulx, P. A. Reneke, and H. E. Nelson. 2005. *Federal Building and Fire Safety Investigation of the World Trade Center Disaster: Occupant Behavior, Egress, and Emergency Communication*. NIST NCSTAR 1-7. National Institute of Standards and Technology. Gaithersburg, MD, September.

Fahy, R., and G. Proulx. 2005. *Federal Building and Fire Safety Investigation of the World Trade Center Disaster: Analysis of Published Accounts of the World Trade Center Evacuation*. NIST NCSTAR 1-7A. National Institute of Standards and Technology. Gaithersburg, MD, September.

Zmud, J. 2005. *Federal Building and Fire Safety Investigation of the World Trade Center Disaster: Technical Documentation for Survey Administration*. NIST NCSTAR 1-7B. National Institute of Standards and Technology. Gaithersburg, MD, September.

Lawson, J. R., and R. L. Vettori. 2005. *Federal Building and Fire Safety Investigation of the World Trade Center Disaster: The Emergency Response Operations*. NIST NCSTAR 1-8. National Institute of Standards and Technology. Gaithersburg, MD, September.

McAllister, T., R. G. Gann, J. D. Averill, J. L. Gross, W. L. Grosshandler, J. R. Lawson, K. B. McGrattan, H. E. Nelson, W. M. Pitts, K. R. Prasad, F. H. Sadek. 2008. *Federal Building and Fire Safety Investigation of the World Trade Center Disaster: Structural Fire Response and Probable Collapse Sequence of World Trade Center Building 7*. NIST NCSTAR 1-9. National Institute of Standards and Technology. Gaithersburg, MD, November.

MacNeill, R., S. Kirkpatrick, B. Peterson, and R. Bocchieri. 2008. *Federal Building and Fire Safety Investigation of the World Trade Center Disaster: Global Structural Analysis of the Response of World Trade Center Building 7 to Fires and Debris Impact Damage*. NIST NCSTAR 1-9A. National Institute of Standards and Technology. Gaithersburg, MD, November.

ACKNOWLEDGMENTS

The work reported herein was conducted with the assistance of several contractors and, in addition, many companies and individuals contributed in a substantial way.

The structural analyses presented in this report were conducted in collaboration with:

- Simpson Gumpertz & Heger Inc. (SGH), of Waltham, Massachusetts; Dr. Mehdi Zarghamee, Project Leader, whose work included the development of structural models and the conduct of the temperature-dependent analyses for the prediction of the structural performance of components and subsystems of the WTC towers and for the determination of collapse of each tower .
- Computer Aided Engineering Associates Inc. (CAEA), Woodbury, Connecticut; Dr. Peter Barrett, Project Leader, who provided technical assistance to SGH and to NIST on the complex computer analyses.
- Dr. R. Shankar Nair of Teng Associates, Prof. Daniele Veneziano of MIT, and Prof. Kaspar Willam of the University of Colorado, who provided expertise in the areas of computational mechanics, structural behavior of tall buildings and reliability.

The work in determining the fireproofing of the WTC towers during their construction and the upgrading of fireproofing on the steel trusses that took place in the 1990's involved many companies and individuals. Their cooperation and assistance in providing the needed information is gratefully acknowledged. The companies and key individuals included:

- Isolatek International, Paulette Kaminski
- Laclede Steel Co, David McGee
- Morse Zehnter Associates, Roger Morse
- Leslie E. Robertson Assoc. (LERA), William Faschen and Richard Garlock

In addition to providing information on the fireproofing, the Port Authority of New York and New Jersey (PANYNJ), and in particular Saroj Bohl, Joe Englot, and Frank Lombardi, researched and provided answers to specific questions at the request of NIST.

Investigative work into the fireproofing of the WTC was led by Dr. Monica Starnes. Data analysis and determination of fireproofing for the finite element calculations was made by Dr. Nicholas Carino. Concrete properties at elevated temperatures were established by Dr. Long Phan for component and subsystem finite element analyses.

Large-scale furnace tests of floor assemblies were conducted by Underwriters Laboratories Inc. (UL), Northbrook, Illinois, and the contribution of the many individuals who contributed to this effort, led by Joe Treadway and Frederick Hervey, is gratefully acknowledged. The cooperation and dedication of the project team are greatly appreciated.

In addition, the following WTC Investigation projects made significant contributions:

- Project 2: Baseline Structural Performance and Aircraft Impact Damage Prediction, led by Dr. Fahim Sadek, provided reference models and the aircraft impact simulations allowing the estimation of structural and fireproofing damage.
- Project 3: Mechanical and Metallurgical Analysis of Structural Steel, led by Dr. Frank W. Gayle, provided the mechanical characteristics of the tower steels that were used in the constitutive models for the finite element analyses. In addition, Dr. Tim Foecke conducted the photographic interpretation and estimation of bowing of the exterior walls of both towers.
- Project 5: Reconstruction of Thermal and Tenability Environment, led by Dr. Richard Gann, provided temperature histories for the structural components for use in the finite element analyses of components, subsystems and global systems. In addition, Dr. William M. Pitts provided assistance in the collection, cataloging and interpretation of the many videos and photographs relevant to this project.

NIST acknowledges the parties to the insurance litigation for voluntarily making their findings available to NIST.

EXECUTIVE SUMMARY

E.1 PURPOSE AND SCOPE

One of the four objectives of the National Institute of Standards and Technology (NIST) investigation of the collapse of the World Trade Center (WTC) towers was to determine why and how the two towers (WTC 1 and WTC 2) collapsed following the initial impacts of the aircraft. Both the north and south towers of the World Trade Center were severely damaged by the impact of Boeing 767 aircraft, yet they remained standing for some time. The ensuing fires were observed to move through both buildings and eventually, both buildings collapsed. The probable collapse sequence for each of the WTC towers as well as the extent and relative importance of the damage caused by the aircraft impact and subsequent weakening by fires were investigated under this project, *Structural Response and Collapse Analysis of WTC Towers to Aircraft Impact Damage and Fire Conditions*.

Events that played a significant role in the structural performance of the towers were the aircraft impact, rapid ignition of fire on multiple floors, and the growth and spread of fire in each tower. Detailed information was required on the condition of the structural system and its passive fire protection system (also referred to as fireproofing or thermal insulation), both before and after the aircraft impact, and during the ensuing fires that elevated temperatures in the structural members. The purpose of this project, then, was to analyze the response of the WTC towers to fires—both with and without aircraft damage—and to determine the probable sequence of structural collapse for each tower. Specifically, the *Structural Response and Collapse Analysis* project intended to:

- Determine the pre- and post-aircraft impact condition of the passive fire protection used to thermally insulate the structural members and provide resistance to fire damage,
- Conduct tests of structural components and systems under fire conditions to quantify their behavior,
- Evaluate the response of floor and column systems under impact and fire conditions to understand their response,
- Evaluate the response of the WTC towers under impact and fire conditions, with and without aircraft impact damage, and
- Develop and evaluate failure hypotheses, resulting in the probable sequence of structural events leading to collapse for each WTC tower.

The unprecedented complexity and sophistication of these analyses required the use of various strategies for managing the computational demands while adequately capturing the essential physics. The overall approach—from impact analysis to collapse initiation—combined mathematical modeling, statistical and probability-based analysis, laboratory testing, and analysis of photographic and videographic records.

Data were collected from a number of sources and included structural plans and specifications, thermal and mechanical (adhesion/cohesion) properties of sprayed fire-resistive material (SFRM), SFRM

thickness and condition in the towers, and recorded observations of structural events subsequent to aircraft impact and prior to collapse. Information about tower construction was obtained from original drawings, design and construction specifications, project documents including correspondence and reports, and records provided by The Port Authority of New York and New Jersey (PANYNJ or Port Authority), Leslie E. Robertson Associates (LERA), Silverstein Properties, and a number of contractors that had worked on the design, construction, or modifications of the towers. Information about the events that occurred in each tower on September 11, 2001, was obtained from analysis of available photographic and videographic records, eyewitness accounts, and mechanical and metallurgical analysis of recovered structural steel.

Computer simulations were used to model the complete sequence of events leading to the initiation of collapse of the WTC towers. The analyses simulated the damage to the towers resulting from aircraft impact, the spread of multi-floor fires, the heating and thermal weakening of structural components, and the progression of local structural failures that led to the collapse of the buildings. The structural response analyses relied upon the following information:

- Reference global structural models of the WTC 1 and WTC 2 towers, and typical floor and exterior wall subsystem models (NIST NCSTAR 1-2)
- Extent of damage to the structural systems and interior contents of the WTC 1 and WTC 2 towers resulting from aircraft impact (NIST NCSTAR 1-2)
- Temperature-dependent mechanical properties of the steels, welds, and bolts used in the construction of the towers, including elastic, plastic, and creep properties from 20 °C to 700 °C (NIST NCSTAR 1-3)
- Time-temperature histories for structural components and connections for standard fires (e.g., ASTM E 119) and actual fires based on fire dynamics simulations (NIST NCSTAR 1-5).
- Photographic and videographic records with time stamps that documented the observed sequence of events (NIST NCSTAR 1-5).

E.2 METHODOLOGY AND ANALYSIS RESULTS

E.2.1 Overview and Approach

The interdependence of the analyses of significant events is illustrated in Fig. E-1. Reference structural models were first developed and used to determine the baseline performance of each tower prior to September 11, 2001. The reference models were then used as a basis for the aircraft impact damage models and the structural response models to ensure consistency between structural models. The aircraft impact analysis determined damage to the interior of the building, including the structural system, passive fire protection, partition walls, and furnishings for each tower. The analysis also provided an estimate of the fuel dispersion in the towers. These results provided initial conditions to the fire dynamics analysis, thermal analysis, and structural analysis. The fire dynamics analysis simulated the growth and spread of fires and produced gas temperature histories for each floor involved in fire. The fire dynamics model accounted for window breakage and damage to interior partition walls and floors (both affecting ventilation conditions), and the distribution of debris and fuel. The thermal analysis used the heat transfer

model to determine temperature histories for the various structural components. The thermal analysis required input from the structural analysis model, fire dynamics analysis results, damage to fire protection, and temperature-dependent thermal material properties. The structural temperature histories, also referred to as thermal loads, were input to the structural analysis, along with the structural impact damage and temperature-dependent material properties, to determine the structural response of each tower.

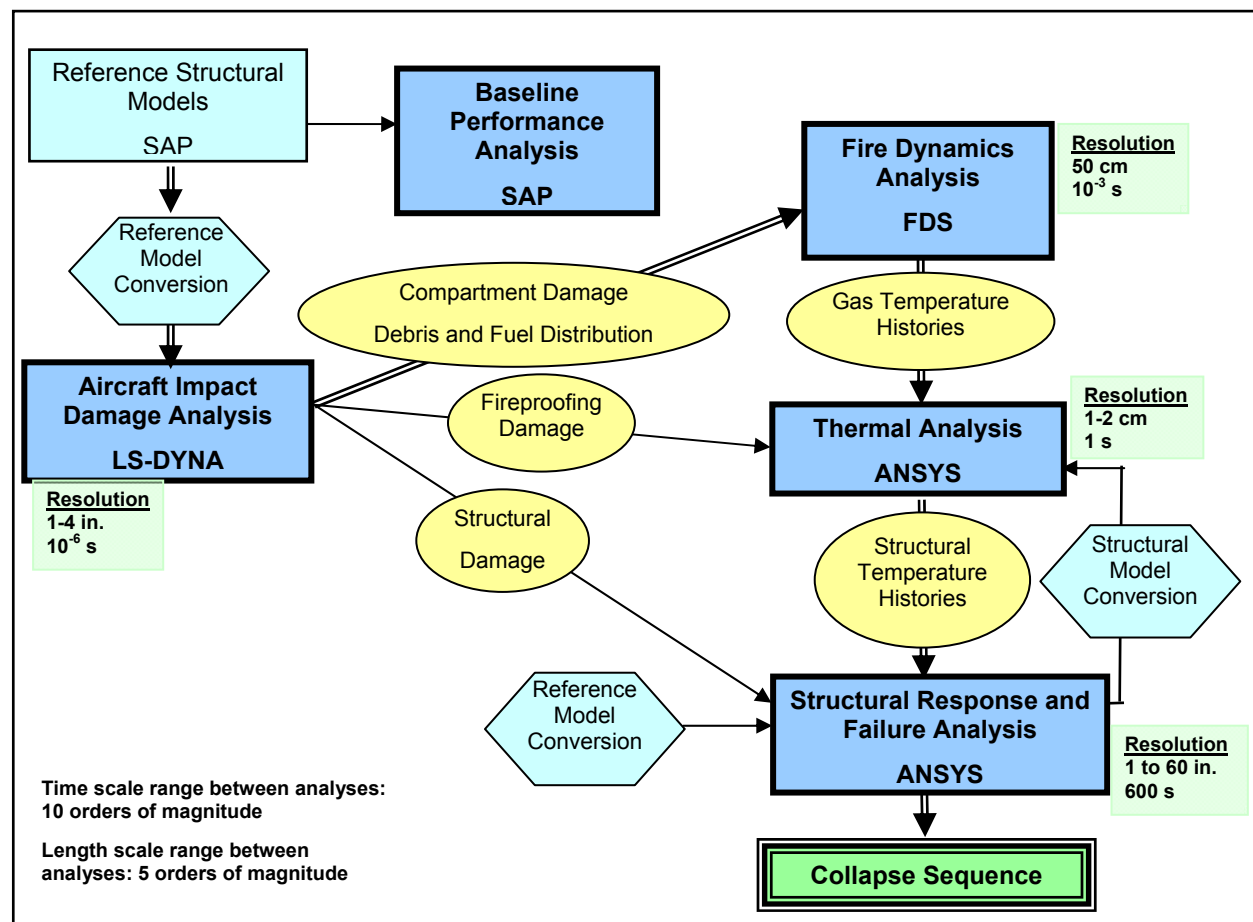


Figure E-1. Critical analysis inter-dependencies.

The WTC towers were large, complex structural systems. To include all of the structural components and connections and their associated behavior and failure mechanisms using refined finite element meshes would have been prohibitive. The analysis approach used was a variant of the well-established substructuring approach, adapted for the analysis of structures with highly nonlinear behavior that progressed from individual components to major subsystems to global systems, as shown in Fig. E-2. The component analyses were conducted to identify critical behavior and failure mechanisms that contributed to the global structural response of each tower. The subsystem analyses incorporated the behavior and failure mechanisms identified in the component studies, with modifications to reduce the model size and complexity, thereby enhancing computational performance, without adversely affecting the quality of the results. Whenever modeling modifications were used, they were validated against the detailed component model results. The global analyses incorporated critical behavior and failure mechanisms, determined from subsystem analyses, while making necessary modifications in the level of modeling detail.

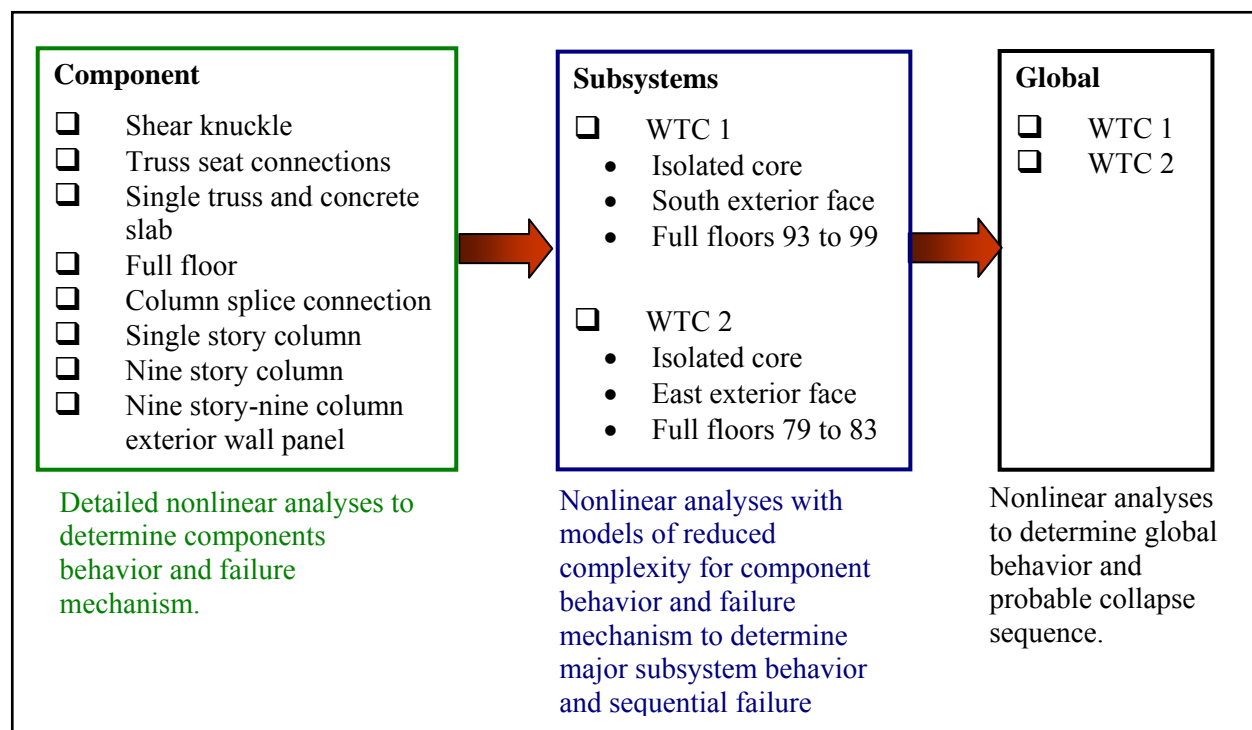


Figure E-2. Structural Analysis Sequence.

Analysis of the global behavior and determination of probable collapse sequences for both WTC 1 and WTC 2, which included work performed by other projects, was divided into the following tasks:

A. Develop finite element models based on reference models. Reference models faithfully represented the actual structures. These reference models became the basis for all subsequent finite element analyses.

B. Develop the constitutive relationships for the materials used in the construction of the towers. Mechanical and chemical properties were determined for steel specimens recovered from the WTC site to assure that the materials used were in conformance with properties specified in the original design. The mechanical properties at high loading rates for the aircraft impact analyses and at elevated temperatures (from room temperature to 800 °C) for the thermal and structural analyses were also determined from the steel specimens.

C. Characterize the passive fire protection applied to the structural steel. Neither the type of materials nor the required thicknesses of SFRM were identified in the contract documents or specifications. Estimates of the characteristics and condition of SFRM were needed for the thermal and structural modeling of the towers.

D. Conduct standard fire resistance tests of composite truss floor system. Tests were conducted to: (1) establish the baseline fire resistance rating of the composite truss floor system used in the WTC towers, (2) understand the influence of thermal restraint by testing the floor system under both thermally unrestrained and restrained conditions, and (3) provide experimental data to validate and provide guidance to the development of the floor models and to interpret the analyses results.

E. Establish the damage to the structure, passive fire protection, and partition walls as a result of aircraft impact. The aircraft impact resulted in significant damage to the exterior, floor, and core structures of the buildings. The jet fuel dispersed inside the towers ignited the building contents and furnishings as well as influenced the amount of oxygen reaching the fires. The fire protection of steel components was dislodged in areas of direct debris impact.

F. Document observations and data related to structural events. NIST validated analysis results with key observations obtained from its extensive collection of over 7,000 photographs and over 150 hours of videotape documenting the events at the World Trade Center on September 11, 2001. Key observations were used in the analyses in three ways: (1) to determine input parameters, (2) to impose time-related constraints upon an analysis, or (3) to validate analysis results.

G. Compute temperature histories for structural components subjected to fires. To determine how the towers were affected by the fires, estimates of the growth and spread of fires over time were developed using fire dynamics simulations. Temperature histories of the steel structural components and concrete floor slabs were predicted in thermal analyses.

H. Conduct component and subsystem analyses. These analyses provided understanding of the nonlinear behavior of structural components and subsystems under gravity and thermal loading and were used to develop reduced models for the global analyses. The components and subsystems considered included: (1) typical floor subsystem with (a) the shear knuckles, (b) truss seats, and (c) a single truss and concrete slab section; and (2) a nine-story by nine-column exterior wall subsystem with (a) bolted connection between exterior columns, (b) bolted connection between spandrels, (c) single exterior columns with spandrel sections, and (d) single exterior wall panel with three columns and three spandrels.

I. Conduct analyses of major subsystems. Analyses of three major subsystems - the isolated core framing subsystem, an exterior wall subsystem, and the composite floor subsystems - were analyzed to determine their ability to resist and redistribute loads after impact damage and response to elevated temperatures. The subsystem models used reduced models from the component analyses, which kept the analysis tractable while including nonlinear features and failure modes. These analyses were crucial for determining critical structural behaviors, including floor sagging under thermal loading, the resulting pull-in forces, and the inward bowing of the exterior walls.

J. Conduct a separate global analysis for each tower. These analyses determined the relative roles of impact damage and fires with respect to structural stability, sequential failures of components and subsystems, and probable collapse initiation sequences. Each global model was first evaluated for stability under gravity loads with structural impact damage. Temperature histories were applied in 10 min intervals and linearly ramped to the next temperature state. Pull-in forces from sagging floors were also applied during the appropriate 10 min intervals. The question of how the WTC towers would have responded to the same fires without the aircraft impact damage was considered to determine the vulnerability of the towers to collapse initiated by conventional large fires.

K. Determine the probable collapse sequence for each tower. A probable collapse sequence for each tower was determined. The collapse sequences were evaluated against key observables.

E.2.2 Structural Response

To conduct the global analysis of each tower, input data were collected from numerous sources, including fire dynamics, thermal, and impact analyses, as already described.

Thermal analyses to simulate the elevated temperatures of the structural components and consequent weakening required an assessment of the condition of the passive fire protection, including thermal properties and SFRM thicknesses. Additionally, tests of the WTC floor system under standard fire conditions provided insights into the dominant behavior of the floors at elevated temperatures and allowed validation of analytical results. Interpretation of the aircraft impact study results led to a determination of likely damage to load bearing structural elements and an estimation of damage to, and consequent loss of, passive fire protection of the floor trusses, core columns and beams, and exterior columns and spandrels. Properties of the materials of construction, including mechanical properties at room and elevated temperatures as well as thermal characteristics, were needed. The structural analyses of components, subsystems and, ultimately, the global systems could be accomplished with this information.

Passive Fire Protection for Structural Components

Passive fire protection delays the transfer of heat to structural components by providing an insulation barrier. Increasing thickness of passive fire protection materials, commonly referred to as fireproofing, correspondingly increases the time delay before the structural component temperature begins to rise. The amount of time delay for a given fire protection method, such as SFRM, is not predicted for design purposes because the actual fire conditions vary; instead, the relative performance is defined by comparative testing with the ASTM Standard Fire Test.

The structural steel in the WTC towers was sprayed with SFRM or protected with rigid fire-rated gypsum panels. SFRM is supplied as dry ingredients, and water is added at the time of application. The water mixes with the cementitious materials and allows the SFRM to adhere weakly to the steel. With time, the cementitious materials harden, and excess water evaporates resulting in a covering of insulation with some cohesive strength.

Three SFRM products that were used in the towers include:

- BLAZE-SHIELD DC/F for floor trusses, core columns, and the exterior surfaces of the exterior columns and spandrels
- BLAZE-SHIELD II for upgrades to floor trusses, which started in the 1990's
- W.R. Grace and Co., Monokote (sprayed cementitious vermiculite) for the interior surfaces of the exterior columns and spandrels

The gypsum panels were used to form fire resistant enclosures around steel core columns, stairwells, mechanical shafts, and the core area in the towers. The core column thermal insulation varied according to the column location and exposure to occupied spaces. Column surfaces in public access areas were protected with gypsum enclosures, while the remaining surfaces were protected with SFRM.

The following information was required to determine the in-place condition of the passive fire protection before and after aircraft impact and to conduct thermal analysis of structural components:

- Thermophysical properties of the passive fire protection materials,
- Effect of gaps in thermal insulation and variability of insulation thickness,
- Effective thickness of thermal insulation for use in thermal-structural analyses that accounts for thickness variability effects,
- Adhesive and cohesive strengths of BLAZE-SHIELD SFRM products (vermiculite product is no longer available).

Thermophysical properties were determined with ASTM standard tests for BLAZE-SHIELD DC/F, BLAZE-SHIELD II, and Monokote MK-5 SFRM products and for gypsum board. The specific heat, thermal conductivity, and density of each material were determined for temperatures ranging from 25 °C to 1200 °C. The standard tests used for SFRM products were ASTM C 1113 (1999), ASTM E 1269 (2001), ASTM E 1131 (1998), and ASTM E 228 (1995). The standard tests used for the gypsum board products were ASTM D 5334 (2000b) and ASTM E 1269 (2001). Densities were calculated from the thermogravimetric analysis and linear thermal expansion measurements.

Analyses showed that when the SFRM thickness is variable, the isotherms in the steel depend upon the shape of the SFRM surface contour. Thus, the temperature history at any point in the steel depends on the local thickness of the insulation. It was shown that an increase in thickness variability reduced the time to reach a certain temperature. In addition to the effect of variation in thickness, the effect of gaps in the SFRM coating was studied. As expected, thermal analysis results indicated that the exposed steel heated quickly and transmitted heat to the adjacent interior steel. However, the temperature rise quickly dissipated as the distance from the gap increased. Review of available photographs showed that gaps were a relatively infrequent occurrence in most floor truss areas. Because there was insufficient information to determine the frequency of occurrence of these gaps or their typical locations, insulation gaps were not considered in the thermal modeling.

SFRM thickness measurements were determined from analysis and interpretation of photographs showing the condition of the originally applied material. Finite element simulations were used to determine a thermally equivalent uniform thickness of SFRM for the original variable-thickness applied to the floor trusses. These values were used in the thermal analyses for determining temperature histories of structural components.

No information was available about the condition of thermal insulation for the exterior columns and spandrel beams, and little information was available for the core beams and columns. For thermal analyses of the towers, the SFRM on these elements was taken to have uniform thicknesses equal to the specified thickness.

The adhesive strength of BLAZE-SHIELD DC/F to steel coated with primer paint (average value of 171 psf to 185 psf) was found to be a third to a half of the adhesive strength to steel that had not been primed (average values of 450 psf to 666 psf). The SFRM products used in the WTC towers were applied

to steel components with primer paint. Cohesive strengths varied from average values of 367 psf to 610 psf.

Tests of Truss Floor Components and Subsystem

Review of available documents indicated that the fire performance of the composite floor system of the WTC towers was an issue of concern to the Port Authority and its contractors during the original design and throughout the service life of the buildings. NIST conducted a series of four standard fire tests to establish the baseline performance of the floor system of the WTC towers as they were originally built, to differentiate the factors that most influenced the response of the floors, and to study the procedures and practices used to accept an innovative structural and fire protection system. The ASTM E 119 furnace tests were performed on representative floor sections with SFRM for the as-specified thickness of 0.5 in. given in the design documents and the average as-built thickness of 0.75 in. that was applied before a program was established in the 1990's to upgrade the truss SFRM thickness to 1.5 in. The conditions in the standard test specified a prescribed temperature rise and duration until failure criteria were met; the estimated fire conditions in the WTC towers imposed varied heating and cooling conditions as the fires grew and spread.

The tested floor assemblies were similar, though not identical, to steel-joist-supported concrete floors that are widely used in low rise construction. The test results provided valuable insight into the behavior of these widely used assemblies and also identified issues that require further study for other types of structural components such as beams, girders, columns, trusses, etc.

The tests showed that the floors were capable of considerable sagging without collapse. The tests also showed thermal damage to the bridging trusses and buckling of compression diagonals and the vertical strut near the supports. No evidence of knuckle failures was seen in the tests.

The NIST tests have identified areas where further study related to the standard test method is warranted. Among the issues related to the test method that NIST identified as requiring further study are:

- the scale of the test for prototype assemblies that are larger than the tested assemblies,
- the effect of restraint conditions on test results,
- the repeatability of test results (e.g., do multiple fire resistance tests conducted under the same conditions yield the same results?),
- effects of test scale, end restraint, and test repeatability on other types of structural components (beams, girders, columns, trusses, etc.), and
- the acceptance criteria to evaluate the load carrying capacity of the tested assemblies (currently tests are stopped before the load carrying capacity of the assembly is reached because other acceptance criteria are met or if the deflection becomes excessive and assembly failure could damage the furnace).

Structural Response of Components and Detailed Subsystems to Assumed Damage and Fire

Material Properties and Failure Criteria

The WTC towers were designed and constructed using 14 grades of steel and two types of concrete. Nominal properties for these materials were provided in the design documents. Additional information was required about the mechanical properties at room and elevated temperature for analysis of the towers' response to the impact and elevated temperature conditions.

The collapse analyses of the WTC towers concentrated on modeling failure mechanisms in steel rather than concrete components, since the WTC towers were essentially steel structures; concrete was used only for the floor slabs.

The two general types of steel that were used in the towers are typically described as carbon steels and high strength steels. Carbon steels generally have lower strengths but are more ductile. The core columns, floor trusses, and beams and spandrel plates in the exterior wall were constructed with carbon steels, ranging from 36 ksi to 50 ksi specified yield strengths. The exterior columns were designed with various grades of high strength steels, ranging from 55 ksi to 100 ksi yield strength.

Normal weight concrete (150 pcf) was used in the core and mechanical floors, and lightweight concrete (110 pcf) was used in the floor system for the tenant spaces between the building core and exterior.

The mechanical properties of both steel and concrete are significantly affected by elevated temperatures. Steel and concrete properties that are temperature sensitive include modulus of elasticity, instantaneous coefficient of thermal expansion, tensile strength, and compressive strength. Additionally, creep strain rates for steel are also temperature dependent.

Mechanical properties of the various grades of steel used and normal and lightweight concrete, both at room temperature and throughout the expected temperature range, were determined. This information provided the bases for describing the material models used in the finite element analyses. In addition to material models, failure criteria were also developed for concrete and steel components. Failure criteria defined the necessary conditions to characterize and quantify the expected failure modes or mechanisms, including elastic or plastic buckling, yielding, or fracture. The state of component loads, material properties, and temperature also affected the mode of failure.

In addition, the following observations can be made:

- Modulus of elasticity is reduced by 25 percent at 600 °C for steel and by 50 percent to 75 percent for concrete.
- Steel yield strength reduces to 20 percent of its initial (room temperature) value and ultimate tensile strength is reduced to 40 percent of its initial value at 600 °C. Concrete compressive strength is reduced to between 30 percent and 50 percent of its initial value. Concrete tensile strength, which is already low, is also reduced to 30 percent.
- The instantaneous coefficient of thermal expansion for steel lies between that of lightweight and normal weight concrete for a given temperature. If steel truss and lightweight concrete

components are at the same temperature, the steel components will thermally expand more than the lightweight concrete. For steel beams and normal weight concrete in the core area, the normal weight concrete will expand more than the steel beams.

Floor Subsystem Analysis

The floors supported the occupants and furnishings and transferred these loads to the columns, acted as diaphragms to transfer loads between exterior faces when under wind loads, and provided lateral stability for columns. With damage to the SFRM on the floor trusses, fires caused thermal expansion and sagging of the floors in the impact damage areas.

The analysis of floors progressed from individual components to major subsystems to global systems. Three truss components were studied with detailed models using ANSYS, a general purpose finite element software package, before developing a model of a full floor subsystem:

- Shear connector between the truss and concrete slab,
- Truss seat connection to the columns,
- Composite section of a single floor truss and concrete slab that included the truss seats, knuckles, and section of the supporting exterior and core channel beam.

Shear connector tests conducted by the truss manufacturer, Laclede Steel, in the early 1960s were reviewed and modeled. The shear connector between the truss and the concrete slab was referred to as a knuckle, due to the bent bar configuration that extended past the top chord of the truss, instead of the studs that are typically welded to the top chord. Detailed ANSYS models of the knuckle and concrete slab were analyzed and compared to the measured transverse and longitudinal shear capacities of a knuckle. A reduced model of the knuckle for use in the single truss and full floor models was developed that captured the dominant temperature-dependent behavior and failure modes.

Truss seats connected the trusses to the core and exterior columns. Truss seats were constructed with standoff plates, seat angles, bolts, and welded gusset plates; details varied for each truss seat depending upon its location within the floor plan. Truss seats were designed to carry floor gravity loads and small horizontal loads, typically a few percent of the column capacity to which it was attached. Typical truss seats were analyzed to determine their failure modes and associated loading and thermal conditions. A series of analyses were conducted to determine the truss seat response to thermal expansion of the floor slab, floor sagging or deformation, and heating of the truss seat. A model of reduced complexity was developed that captured the behavior and failure modes of the truss seats for use in the single truss and full floor models.

With reduced models of the knuckle and truss seat, a composite section of a full single truss and concrete slab was modeled to determine its behavior and failure modes for elevated temperatures and additional debris loads. Steel components with damaged fire resistant coatings heated and softened within 10 to 15 minutes. The bottom surface of the concrete slab heated quickly, but the rate of heating through the slab depth was slower, so that the slab response to fire lagged behind the steel response. Concrete spalling was not included in the model. Analysis was conducted using uniform temperatures across the truss and an imposed linear thermal gradient across the slab depth to study the floor section response.

These conditions were assumed prior to completion of the fire and heat transfer analyses used for the full floor subsystem analysis. Two failure modes of interest were (1) floor component failures leading to sagging (i.e. buckling of truss components or knuckle separation from the concrete slab) and the truss pulling inward on the columns and (2) failure of the truss seats. Analysis results were used to develop a model of reduced complexity with break elements that captured the behavior and failure modes of the floor section for use in the full floor model.

The full floor model included core columns and floor beams, exterior columns and spandrel beams, floor trusses and bridging trusses, and normal and lightweight concrete in the core and floor truss areas, respectively. The columns were extended one floor level above and below the floor subsystem and were required to include the interaction between the floor subsystem and the core and exterior columns. The full floor model contained a number of modifications from the model developed using the SAP2000 software of Floor 96 (NIST NSTAR 1-2) that reduced the number of finite elements and incorporated the features for analyzing the structural response to thermal conditions.

Results of the floor system analyses showed that:

- Knuckle failures did not occur under gravity loading and elevated temperatures anticipated.
- Truss web diagonals buckled at loads and temperatures expected and, as a consequence, the floor system sagged.
- Sagging of the floor system resulted in possible inward pull on the exterior columns, although the magnitude of the force depended on fire conditions on surrounding floors.
- Truss seat connections could fail under elevated temperature conditions, and their behavior was included to accurately capture the overall performance of the floor system to impact and fire conditions.
- Essential floor behavior, including buckling of web diagonals and connection failures, could be achieved with reduced models.

Core Column and Exterior Column and Panel Analysis

The primary function of the core columns was to carry the building gravity loads. The exterior columns resisted wind loads and, in addition, carried approximately half of the gravity loads.

Preliminary analysis of the core and exterior columns considered their individual buckling behavior and how it varied for uniform elevated temperatures. The columns were found to have sufficient capacity for tower gravity loads even under elevated temperatures and a loss of lateral support at several floors. This was also found in more detailed finite element models of the columns.

The core columns were studied to determine the most efficient way to reduce the complexity of the model while still capturing buckling behavior at room and elevated temperatures.

Four exterior wall components were studied with detailed ANSYS models before developing a model of a nine-story by nine-column wall area:

- Bolted connection for exterior columns
- Bolted connections for spandrels
- Single exterior columns with spandrel sections
- Single exterior wall panel, fabricated as a single unit for construction purposes with three columns and three spandrels

The column and spandrel connections were analyzed to determine their failure modes and associated loading and thermal conditions. A reduced model was developed that captured the connector behavior and failure modes for use in exterior wall models.

The single column model with spandrel sections was loaded axially to determine its buckling load and post-buckling behavior at room and elevated temperatures for one, two, three, and nine story column heights.

The computer model of a single wall panel was validated against the reference structural models for the towers. The models were subjected to vertical and horizontal forces in the plane of the wall, representing intended design behavior, and a horizontal force transverse to the wall, representing a possible floor load.

The exterior wall had three connections: the column splice, the spandrel splice, and the truss seat (for the floors). The column splice had four bolts that connected columns through their end plates. The spandrel connection had a splice plate to connect the two spandrel plates using high strength bolts. The spandrel and column splices were represented in the nine by nine wall subsystem model and captured the spandrel failure modes of bolt shear, tearing of the spandrel plate, and tearout of the spandrel plate at the bolt holes.

The nine by nine wall model had a coarser mesh that used beam elements for the columns, shell elements for the spandrels, and break elements for the connections. The wall model was subjected to axial loads from above, lateral out-of-plane loads at the floor levels, and elevated temperature representative of fire conditions. The effect of missing floor supports was also evaluated.

Several analyses were run for a variety of temperature load cases and for various combinations of axial load, disconnected floors simulating floor failure and loss of lateral column support, and inward pull applied at one or more floor levels modeling floor sag due to elevated temperatures. Results showed that:

- Although spandrel plates experienced large distortions and high strains, column buckling did not occur under the various temperature loadings applied when floors remained in place and able to provide lateral support to the columns.
- Column buckling did not occur when lateral support was lost at three floors under the expected gravity load that included dead plus service live loads.
- Column buckling did occur when lateral support was lost at three floors and the gravity load was increased to 150 percent of the expected gravity load simulating redistribution of load to the exterior wall.

- Column buckling was found to occur when an inward lateral load (pull-in) of approximately 12 kips was applied to three adjacent floor levels. The inward deflection of the exterior wall when it could no longer support the gravity load (i.e., at the buckling load) was approximately 10 in.

Aircraft Impact Damage

The aircraft impact of the WTC towers caused extensive damage to the buildings' exterior, penetrated into the interior causing further damage to the structural system, dislodged thermal insulation, and ignited multi-floor fires. The structural damage to each tower resulting from the aircraft impact was estimated using a transient finite element analysis. Results of this analysis were used to predict damage to the structure, insulation, and partition walls in the path of the debris field.

The fire dynamics, thermal, and structural analyses all required input data derived from the aircraft impact analyses. The fire dynamics analyses used estimates of damage to the floors and partition walls to describe ventilation paths and to identify the distribution of fuel and debris immediately following impact. The thermal analysis required estimation of the areas that had dislodged insulation on the structural components of the towers. For the structural analyses, elements that represented severed or heavily damaged floors and columns were removed from the structural models of the towers.

The aircraft impact analyses considered three cases for each tower, where each case had a different set of input parameter values, based upon sensitivity studies and detailed component analyses. The results for the three cases were compared to observations from photographs and videos. Damage to the exterior walls predicted by the impact simulations matched reasonably well the exterior damage in photographic and video records. The observed exterior damage was used in the structural analyses. The analysis results from two cases for each tower were found to match observations reasonably well and were selected for continued analysis by the fire dynamics, thermal, and structural analyses. The cases for each tower were referred to as Case A and Case B for WTC 1 and Case C and Case D for WTC 2. However, prior to determining the final aircraft impact analysis results, earlier aircraft impact analyses produced an initial set of aircraft impact cases for each tower. These initial cases, referred to as Case A_i and Case B_i for WTC 1 and Case C_i and Case D_i for WTC 2, were used to develop experience and gain understanding of the fire spread and growth, the rate of structural component heating, and the structural response to damage and elevated temperatures.

The final set of impact damage data for fire dynamics, thermal, and structural analyses was Cases A, B, C, and D, with the exception of the full floor subsystem analyses which used initial damage Cases A_i to D_i. The use of the aircraft impact data in the sequence of structural analyses was as follows:

1. Full floor subsystem models were analyzed for all initial damage Cases A_i to D_i before the final damage cases were available.
2. Full floor subsystem models were evaluated for changes in damage between final Cases A to D and initial Cases A_i to D_i. Changes in impact damage to the structural components and insulation reflected in the two sets of Cases (i.e., initial and final) were found to have little effect on the floor subsystem structural response. The full floor subsystem structural response for Cases A_i to D_i and Cases A to D were found to be equivalent.

3. Isolated core and exterior wall subsystem models were analyzed for Cases A, B, C, and D.
4. The global model of WTC 1 and WTC 2 were analyzed for Case B and D, respectively, based upon the results of the subsystem analyses.

Four classifications of core column structural damage were established: severed, heavy damage, moderate damage, and light damage. Classification criteria included plastic strain levels and lateral deformation from the column centerline. Columns that were severed or heavily damaged were removed to simulate impact damage in the global analysis of each tower. Two types of floor structural damage were identified from the impact analysis results: (1) missing floor areas and (2) severely damaged floor areas incapable of supporting loads.

Thermal insulation was assumed to be dislodged from core columns only if the columns were subject to direct debris impact that failed wall partitions in the immediate vicinity of the column¹. For exterior columns, the debris impact was required to be strong enough to damage or destroy room furnishings (modular office workstations) adjacent to the columns. For floor trusses, the debris impact was required to be strong enough to damage or destroy room furnishings (modular office workstations) in the same area of the affected floor.

The structural damage in WTC 1 extended from the north exterior wall into the north side of the core. An exterior panel was knocked out of the south wall by aircraft debris. Damage to the insulation from direct debris impact extended over a larger region and extended to central regions of the south floor areas. Case B predicted more damage to core columns and a larger extent of insulation damage to the south floor area than Case A, including damage to the south exterior wall insulation on the inside face, as shown in Fig. E-3.

The structural damage in WTC 2 extended from the south exterior wall to southeast region of the core. Exterior columns were severed by debris near the northeast corner. Damage to the insulation from direct debris impact extended over a larger region and extended over most of the east floor area to the north face. Case D predicted more damage to core columns than Case C, but the extent of the insulation damage was similar, as shown in Fig. E-4.

¹ The Pentagon was impacted by an aircraft of similar size and at a similar speed as the WTC towers. The observed stripping of the concrete cover from columns in similar circumstances provides an independent set of data that supports the criteria established for the removal of fireproofing materials subject to direct debris impact in the WTC towers.

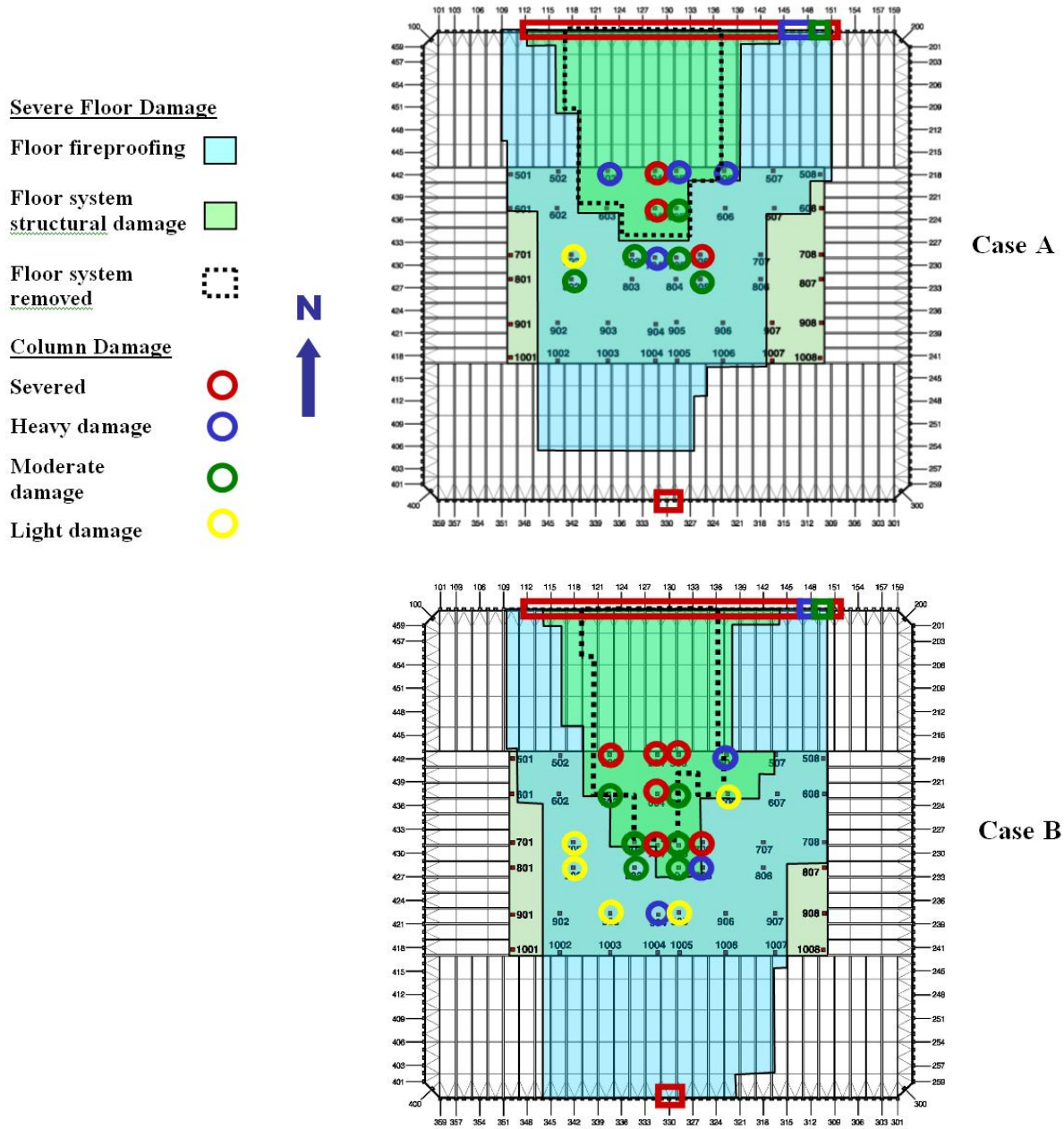


Figure E-3. Plan view of WTC 1 cumulative damage for Floors 93 to 99.

Severe Floor Damage

Floor fireproofing 

Floor system structural damage 

Floor system removed 

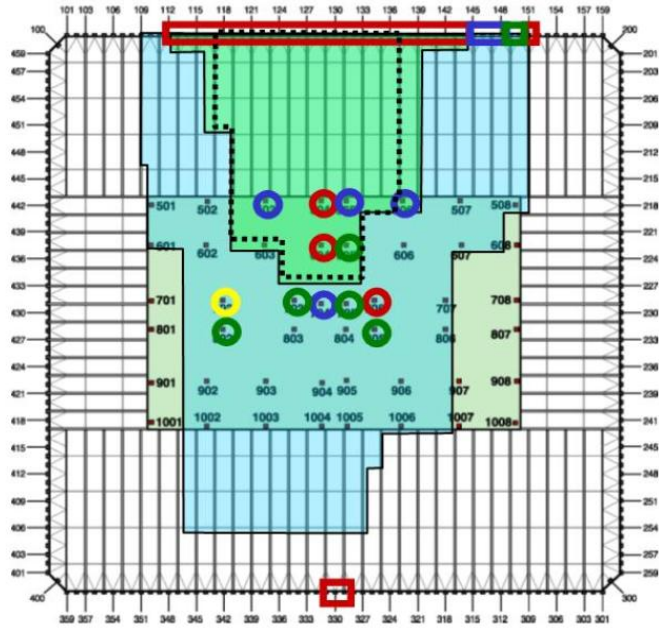
Column Damage

Severed 

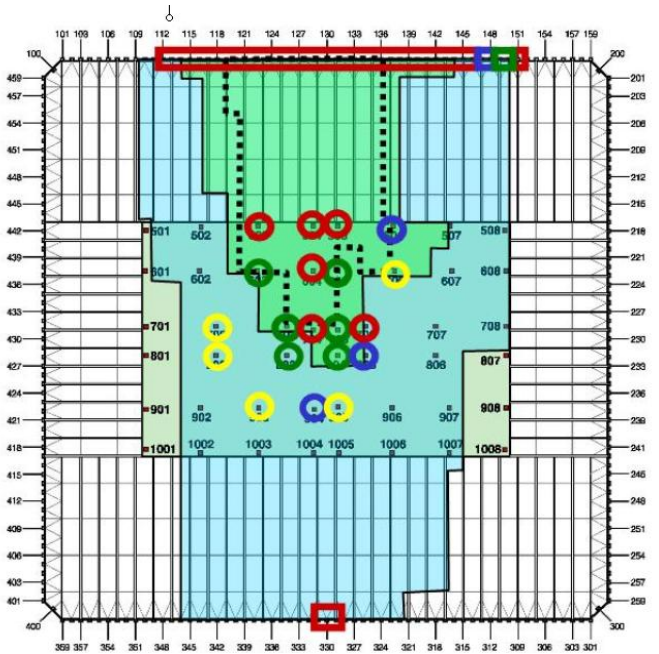
Heavy damage 

Moderate damage 

Light damage 



Case A



Case B

Figure E-4. Plan view of WTC 2 cumulative damage for Floors 78 to 84.

Observations and Timeline of Structural Events

NIST assembled a collection of nearly 150 hours of video footage and over 7,000 photographs, which were reviewed for insights into the structural performance of the towers. A timeline of significant events that characterized the weakening and eventual collapse of the WTC towers was developed with the photographs and videos that were time stamped. Quantitative information, such as the amount of inward bowing observed on the exterior walls of the buildings, was extracted from key photographs through image enhancement and scaled measurements. Key observations and the timelines were used to guide the global collapse analyses.

Development of the probable collapse sequence for each tower was shaped by evidence gathered in the investigation. Data about the events following the aircraft impact were primarily obtained from three sources:

- Photographic and videographic records that had been catalogued and time stamped for the NIST Investigation (NIST NCSTAR 1-5A)
- Interviews of individuals in the towers who survived and those who received telephone calls from individuals in the tower (NIST NCSTAR 1-7)
- Interviews of emergency response personnel and emergency communication records (NIST NCSTAR 1-8)

Photographs and videos provided knowledge about aircraft impact damage to the exterior walls, fire growth and spread at the building exterior, inward bowing of an exterior wall in each tower, and the direction of tilt for the building section above the impact and fire zone as the towers collapsed.

Changes in structural performance are generally difficult, if not impossible, to perceive until significant deformation has taken place relative to the dimensions of the structure and depend on the detail and resolution of the image being examined and the vantage point of the photographer. Observations of structural performance for the WTC towers included severed components, local deflections or buckling, possible sagging of floors, and relative alignment of columns or building sections.

Evidence was used in the analyses in three ways: (1) to determine input parameters, such as the aircraft speed and direction upon impact, (2) to impose time-related constraints upon an analysis, such as imposing observed broken windows over time to constrain the spread of fire, or (3) to validate analysis results, such as global stability after impact and during thermal loading.

Observations of structural behavior were broken into two groups: *key observations* and *noted observations*. Key observations were significant structural events that were explicitly addressed in or used to validate the structural analyses. Noted observations were events that may have been a structural response, but could not be conclusively identified as a structural response.

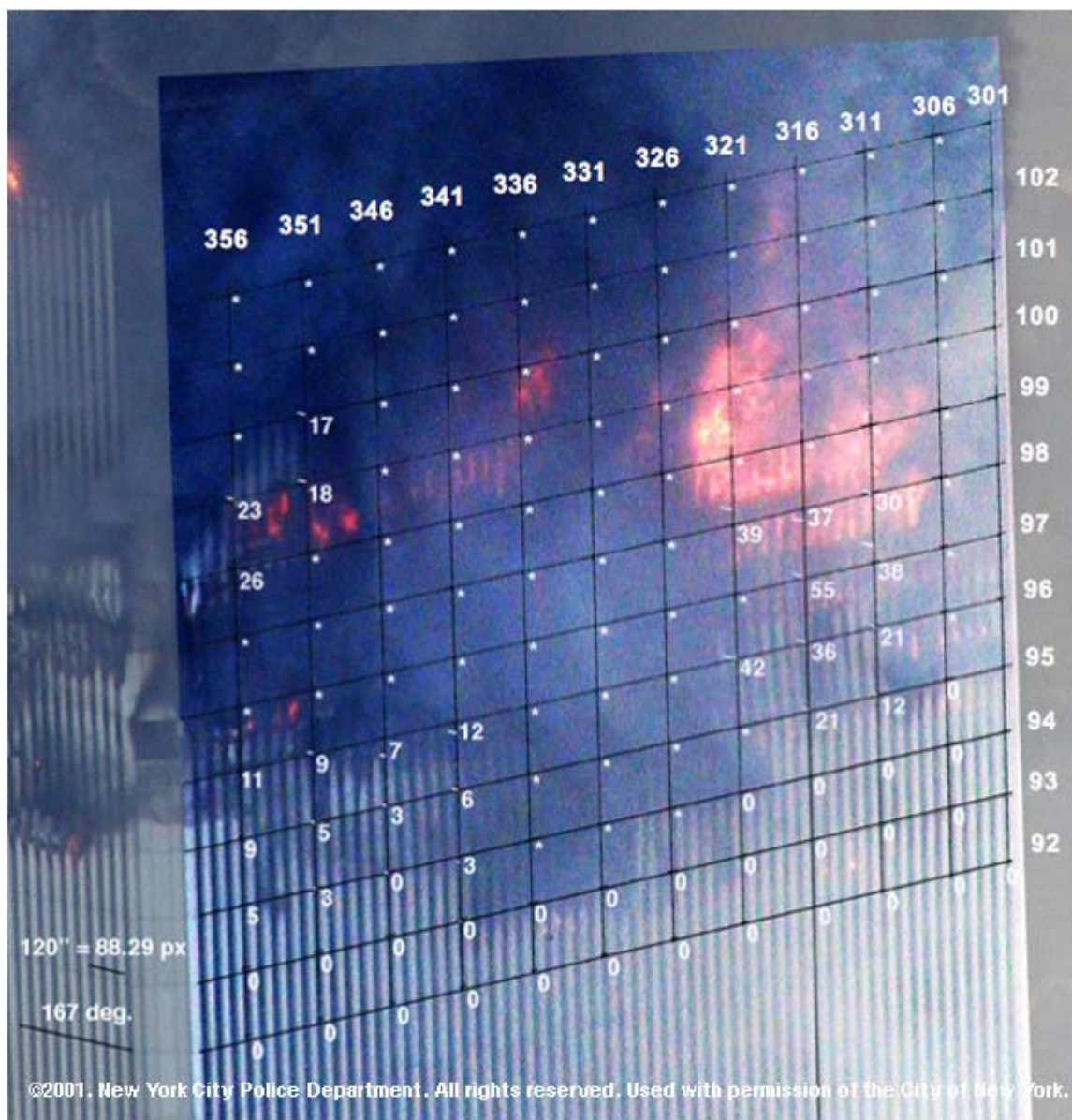
Key observations were used to develop a timeline of structural events for each tower. Structural analyses were used to support development of the collapse hypothesis for each tower and to develop and refine understanding of the probable sequence of events.

WTC 1 key observations were:

- Inward bowing of the south exterior wall was first observed at 10:23 a.m., as shown in Fig. E-5.
- The time to collapse initiation was 102 minutes from the aircraft impact (9:46:30 a.m. until 10:28:22 a.m.).
- From exterior observations, tilting of the building section appeared to take place near Floor 98. Column buckling was then observed to progress rapidly across the east and west faces.
- The WTC 1 building section above the impact and fire area tilted to the south as the structural collapse initiated, as shown in Fig. E-6. A tilt to the south of at least 8 degrees occurred before dust clouds obscured the view and the building section began to fall downward.

WTC 2 key observations were:

- Following the aircraft impact and fireballs, hanging objects were observed through the windows of the east and north faces. The hanging objects suggest that there was structural damage to WTC 2 Floor 83 along the east face and to Floors 81 to 83 of the north face near the northeast corner.
- Inward bowing of the east wall was first observed at 9:21 a.m. The inward bowing was approximately 10 in. at Floor 80.
- An increase of the inward bowing of the east wall was observed at 9:53 a.m. The greatest bowing was approximately 20 in.±1.0 in. at Floor 80 on the east face of WTC 1.
- Collapse initiated 56 minutes after the aircraft impact (9:02:59 a.m. to 9:58:59 a.m.).
- From a northeast viewpoint, initial downward motion was observed as columns moved inward on the north side of the east face, as shown in Fig. E-7. Tilt of the building section above the impact and fire area appeared to take place near Floor 82. Column buckling was then seen to progress across the north face.
- The building section above the impact and fire area tilted to the east and south as the structural collapse initiated as shown in Fig. E-8. There was approximately a 3 to 4 degree tilt to the south and a 7 to 8 degree tilt to the east prior to significant downward movement of the upper building section.



1. Measurements were based on calibration measures shown on the west face
2. Foreshortening into depth of field across the south face of 17% was included in the measurements
3. Measurement error was at least ± 6 inches

Figure E-5. WTC 1 exterior columns bowing inward across most of the south face between Floors 95 to 98 at 10:23 a.m.



Figure E-6. WTC 1 building section above impact damage zone tilts to the south.

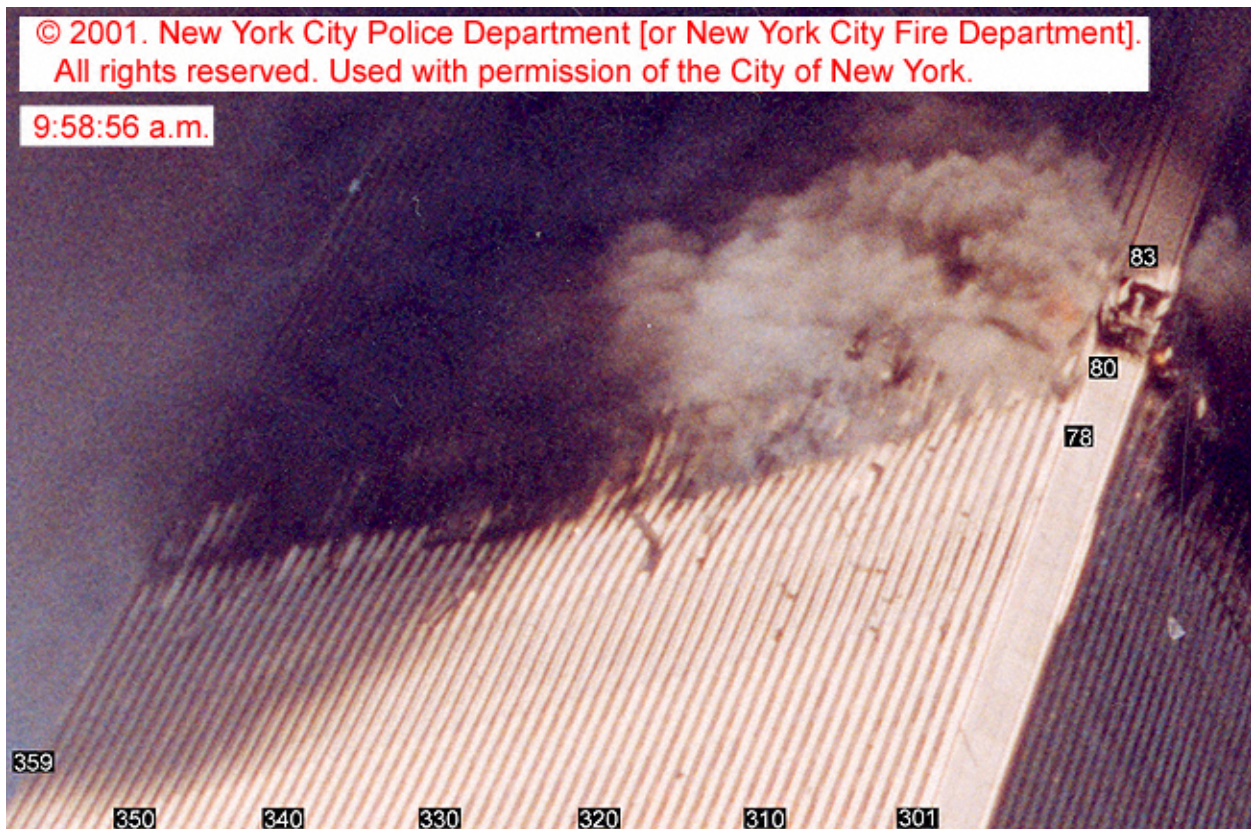


Figure E-7. View of WTC 2 buckling of east wall near northeast corner as collapse initiates from southeast.



Figure E–8. View of upper building section of WTC 2 tilting to the east.

Structural Response of Major Tower Subsystems

Prior to conducting the analysis of the global structural response of each tower, major structural subsystems were analyzed to provide insight into their behavior within the WTC global system. The three major structural subsystems, the core framing, a single exterior wall, and full tenant floors, were analyzed separately for their response to impact damage and fire. The hat truss was not analyzed separately as its structural behavior did not require significant reduction in the global analysis. The component analyses provided a foundation for these large, nonlinear analyses with highly redundant load paths by determining component behavior and failure modes and enabling a significant reduction in finite element model complexity and size. The major subsystem models used final estimates of impact damage and elevated temperatures determined from the aircraft impact analysis and the fire dynamics and thermal analyses.

The capacity of each subsystem to sustain loads for the imposed damage and elevated temperatures was evaluated. The isolated subsystem models lacked the restraint and load paths to other subsystems found in the global analysis. Even so, the isolated subsystem response was useful for refining the global models and interpreting subsystem behavior in the global system. For instance, when the column connections to the hat truss in WTC 2 failed at the southeast corner of the core, the only load path available to carry those column loads was the floor system within the core structure. However, in the global structure, the hat truss at the top of the core would transfer loads to other core columns or the exterior walls, assuming the connections between the core columns and hat truss remained intact.

The subsystem models used modeling reductions from the component analyses, which kept the analysis tractable while maintaining required nonlinear features. As previously noted, such reductions were necessary to maintain a careful balance between model size and complexity as the model size increased. Each of the major subsystem models used temperature histories for the towers. Elevated temperatures were applied to the models in 10 min intervals, where a temperature state was given for all structural components at a given time and linearly ramped to the next temperature state. Examination of structural

temperature histories indicated that no significant fluctuations between temperature states occurred for the 10 min intervals selected for analysis.

Core Subsystem

The core subsystem models included temperature-dependent plasticity, creep, and plastic buckling behavior in the core column elements. Core models extended from Floor 89 to Floor 106 for WTC 1 and from Floor 73 to Floor 106 for WTC 2, and did not include the hat truss. The models included core columns and floor beams and slabs. Floor slabs were modeled as membrane elements with a relatively coarse mesh, which resulted in approximate slab openings for elevators and mechanical shafts. The meshing did not affect the floor's ability to provide a load path between columns. For the purposes of the isolated core model, only the floor beams with partial moment connections were included, as simple shear connections were not capable of transferring significant loads between columns. Impact damage was modeled by removing severed core columns and damaged floor areas. The core subsystem was analyzed for stability under gravity loads. Temperature histories were then applied to the core structure.

By not including the hat truss, the primary load path for core column load redistribution was removed, leaving the core floors, which typically provided a secondary load path. The WTC 1 isolated core subsystem was stable with Case A aircraft impact damage and gravity loads. To reach a stable solution for Case C structural damage and gravity loads, the WTC 2 isolated core model required horizontal restraints to be added in the east and south directions at each floor, representing the lateral restraint provided by the office area floors. Without the horizontal restraints, the WTC 2 core model tilted significantly due to the severed columns in the southeast corner of the core. The isolated core models did not converge for WTC 1 Case B and WTC 2 Case D structural impact damage, which had more severed columns than Cases A and C. The core needed to redistribute loads to other areas in the global system for a stable solution with Cases B and D structural damage.

Full Floor Subsystem

The full floor subsystem models included large deflection and temperature-dependent material properties with plasticity for all steel components. Creep was not included in the full floor models, as this analysis feature did not work with beam elements in version 8.0 of ANSYS (the detailed truss model had 3D finite strain elements that were changed to beam elements in the full floor model). Creep was included for beam elements in ANSYS 8.1, and subsequent analyses of the core and exterior wall subsystems included creep deformation. The floor slab was modeled as lightweight concrete across the entire floor (tenant and core floor areas) with a bilinear stress-strain constitutive model that did not account for cracking, crushing, or spalling. The concrete material model used the compressive strength as the yield point, with the same yield strength in both tension and compression (the reinforcing steel was assumed to provide the tensile capacity in the composite floor). Separate floor models were created from the Floor 96 structural model by imposing the different damage and temperature conditions for WTC 1 Floors 93 to 99 and WTC 2 Floors 79 to 83. Structural components that were severed due to the aircraft impact were removed from each floor model, based upon the four initial damage cases, WTC 1 Case A_i and B_i and WTC 2 Case C_i and D_i. Each full floor model was analyzed for stability under floor gravity loads. No column loads were applied. Temperature histories were then applied to the floor structure.

The floor analysis results for Cases A_i to D_i were used for Cases A to D in the exterior wall subsystem and global analyses. Final damage Cases A, B, C, and D were completed after the initial set of floor

analyses were conducted with Cases A_i, B_i, C_i, and D_i. The full floor models were not rerun for Cases A through D as comparisons showed that the structural temperature histories of the floors were nearly identical for most floors and only slightly different for a few floors.

Exterior Wall Subsystem

The exterior wall subsystem models included temperature-dependent plasticity, creep strains, and plastic buckling behavior in the exterior wall components. The exterior wall analyses extended over approximately 20 floors and were centered around the areas of impact and fire zone. The south face of WTC 1 extended from Floor 89 to Floor 106 and the east face of WTC 2 extended from Floor 73 to Floor 90. The exterior panel that was severed during the aircraft impact and found south of the tower was removed from the south face of WTC 1. No structural damage to the panels was observed on the east wall of WTC 2. The analysis of a single exterior face provided insight into the conditions that would result in the inward bowing of the south wall of WTC 1 and the east wall of WTC 2 observed in photographs. Conditions examined included pull-in forces resulting from sagging floors, disconnected floors resulting from truss seat failure, additional vertical loads simulating load transfer to the exterior wall, and elevated temperatures.

The exterior wall models were used to estimate the pull-in force magnitude and locations for each tower that would produce the observed bowing of the exterior wall. The inward pull was caused by sagging of the floors. Heating of the inside face of the exterior columns also contributed to inward bowing. Thermal expansion occurred as soon as steel temperatures began to rise; column shortening occurred when creep and plastic strains overcame thermal expansion strains, typically at temperatures greater than 500 °C to 600 °C with accompanying high stresses and duration of temperatures and stress levels.

WTC 1 exterior wall analysis found that an inward pull force of 6 kips at each column at Floors 95 to 99, starting 80 min after the aircraft impact, caused a maximum inward bowing of 31 in., shown in Fig. E-9. This inward deflection was smaller than the observed maximum bowing of 55 in. ±6 in., and the wall was stable at 100 min. The magnitude of pull-in forces was expected to be less than 6 kip with the addition of gravity loads from the core subsystem as it also weakened; therefore, pull-in forces of 4 kip to 5 kip were used in the global model analyses.

WTC 2 exterior wall analysis found that an inward pull force of 1.0 kip to 1.5 kip and 4.0 kip to 5.0 kip on the south and north portions of the east wall, respectively, over Floors 79 to 83, caused a maximum inward bowing of 9.5 in. at 20 min and 37 in. at 50 min, as shown in Fig. E-10. The observed deflections were 10 in. and 20 in., respectively, at corresponding times. Considering the possible increase in column loads after impact for Case D conditions, a pull-in force of 1.0 kip on the south half and 4.0 kip on the north half of the east wall were selected for the initial estimate for the WTC 2 global model analysis.

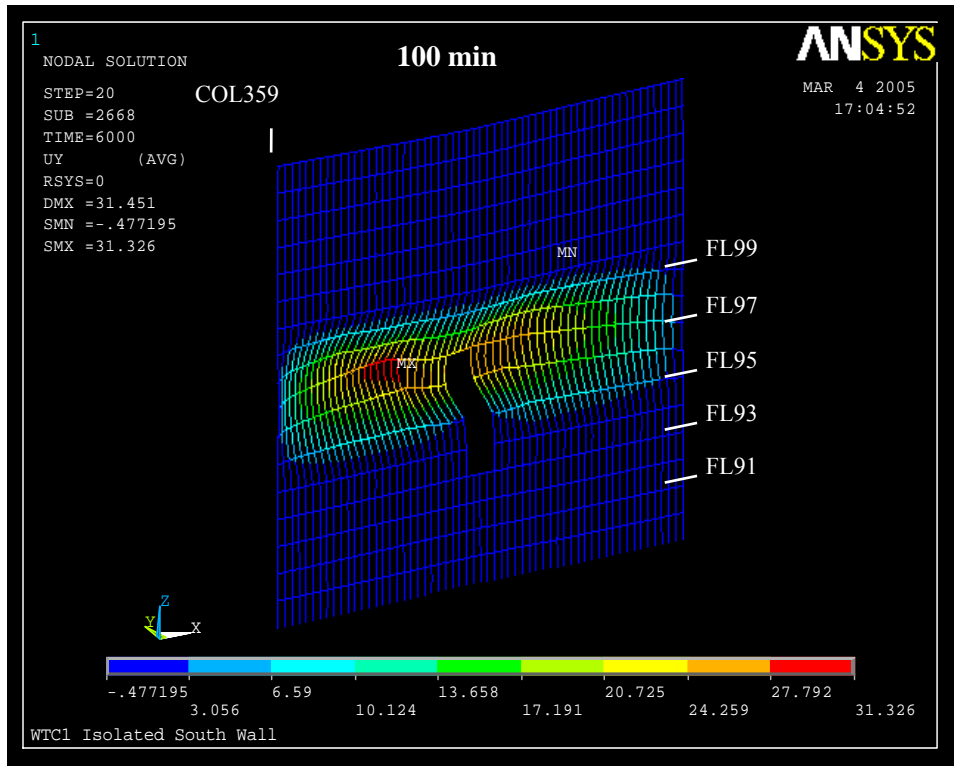
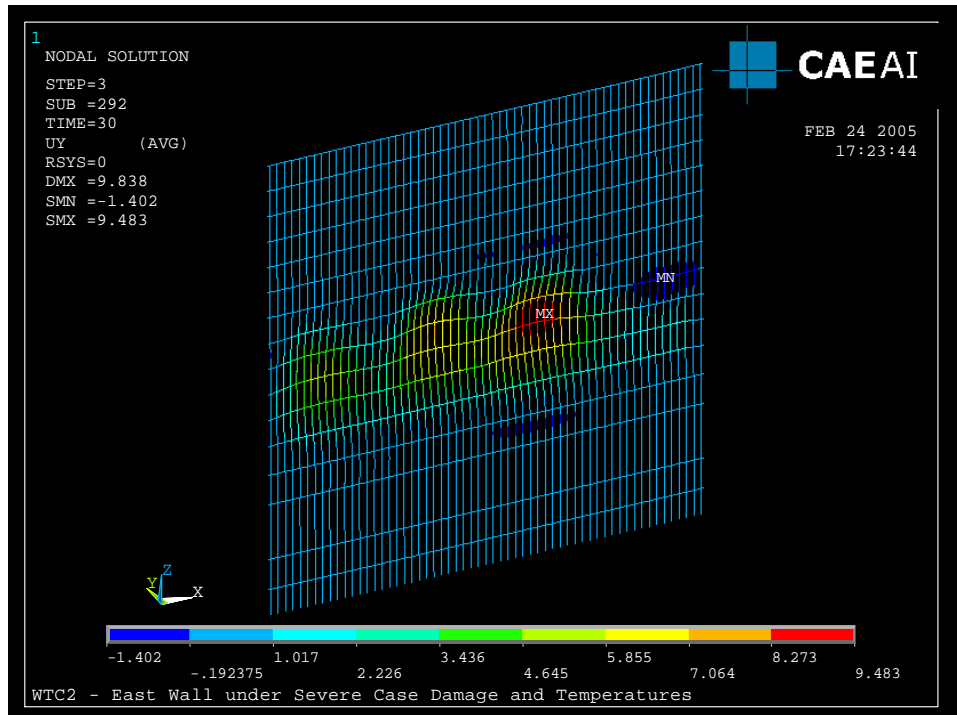
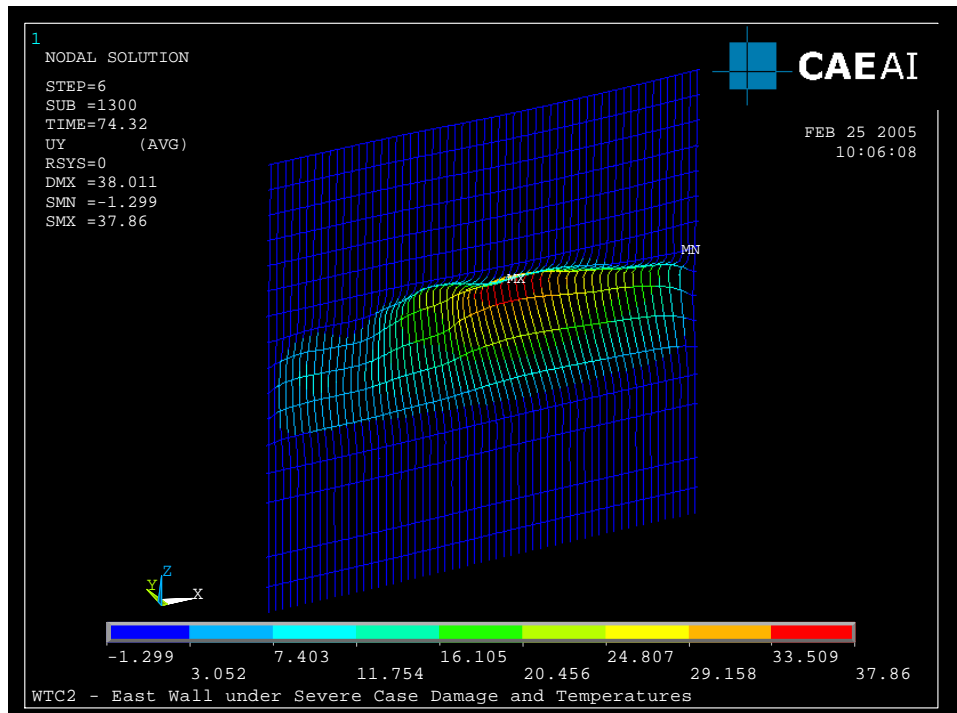


Figure E-9. Inward displacement of the WTC 1 south wall at 100 min of the Case B temperatures with floor disconnections and 6 kip pull-in forces over five floors.



At 20 min



At 50 min

Figure E-10. Out-of-plane displacements of east wall of WTC 2 calculated with pull-in forces of 1.5 kip on the south half and 5.0 kip on the north half.

Structural Response of the WTC Towers

A separate global analysis of each tower helped determine the relative roles of impact damage and fires with respect to structural stability and sequential failures of components and subsystems and was used to determine the probable collapse initiation sequence.

Results of the major subsystem analyses were incorporated into the global models, reducing the complexity of the modeling approach and/or level of detail where possible, while retaining sufficient detail for nonlinear structural responses. The global models of the towers extended from several stories below the impact area to the top of the structure. WTC 1 was truncated at Floor 91 and WTC 2 was truncated from Floor 77. The global models included the core subsystem, the exterior wall subsystem, the hat truss, and an equivalent plate representation of the floor system. The core columns and exterior columns and spandrels were modeled with elements and features similar to those used in the isolated core and exterior wall analyses. Column analysis features included the effects of thermal expansion, plastic, and creep strains on column behavior within the global structural system. The full floor model was not included in the global models, as it would have made the models computationally too large. Instead, office area and core floors were modeled with an equivalent floor slab thickness and modulus calculated to match the in-plane stiffness of the composite floor system, including the concrete slab, floor trusses, and the floor seats. Floor loads applied as concentrated loads at the column connections. These modeling simplifications of the floor system were able to capture the floor behaviors observed in the full floor subsystem analyses while keeping the analysis tractable.

Each global model was first evaluated for stability under gravity loads, with structural impact damage modeled by removing severed and heavily damaged columns and floor areas. Temperature histories were applied in 10 min intervals and linearly ramped to the next temperature state. Pull-in forces from sagging floors were also applied during the appropriate 10 min intervals. The global analysis results provided a sequence of component and subsystem failures that led to the onset of global instability and collapse initiation.

WTC 1 Global Analysis Results

After the aircraft impact, gravity loads that were previously carried by severed columns were redistributed to other columns. The north wall lost about 7 percent of its loads after impact. Most of the load was transferred by the hat truss, and the rest was redistributed to the adjacent exterior walls by spandrels. Due to the impact damage and the tilting of the building to the north after impact, the south wall also lost gravity loads, and about 7 percent was transferred by the hat truss. As a result, the east and west walls and the core gained the redistributed loads through the hat truss.

In the early stages of the fire, structural temperatures in the core rose, and the thermal expansion of the core was greater than the thermal expansion of the exterior walls. The difference in the thermal expansion increased the loads in the core columns at about 20 min. Thereafter, the core lost gravity loads due to its thermal weakening and shortening until the south wall started to bow inward. At about 100 min, approximately 20 percent of the core loads were transferred by the hat truss to the exterior walls due to thermal weakening of the core; the north and south walls each gained about 10 percent more loads, and the east and west walls each gained about 25 percent more loads. Since the hat truss outriggers to the east and west walls were stiffer than the outriggers to the north and south walls, they transferred more loads to the east and west exterior walls.

The inward bowing of the south wall caused failure of exterior column splices and spandrels, and induced column instability. The instability progressed horizontally across the entire south face. The south wall unloaded and redistributed its gravity loads to the thermally weakened core through the hat truss and to the east and west walls through the spandrels. The building section above the impact zone began tilting to the south as column instability progressed rapidly from the south wall along the adjacent east and west walls, and increased the gravity load on the core columns. The change in potential energy due to downward movement of building mass above the buckled columns exceeded the strain energy that could have been absorbed by the structure. Global collapse then ensued.

WTC 2 Global Analysis Results

Before aircraft impact, the load distribution across the exterior walls and core was symmetric with respect to the centerline of each exterior wall. After aircraft impact, the exterior column loads on the south side of the east and west walls and on the east side of south wall increased. This was due to the leaning of the building toward the southeast. After aircraft impact, the core carried 6 percent less loads. The north wall loads reduced by 6 percent, and the east face loads increased by 24 percent. The south and west walls carried 2 percent to 3 percent more load.

In contrast to the fires in WTC 1, which generally progressed from the north side to the south side over approximately an hour, the fires in WTC 2 were located on the east side of the core and floors for the entire duration, with the fires spreading from south to north. With insulation dislodged over much of the same area, the structural temperatures became elevated in the core, floors, and exterior walls at similar times. During early stages of the fires, columns with dislodged insulation elongated due to thermal expansion. As the structural temperatures continued to rise, the thermal expansion was overcome by plastic and creep deformations under compressive loads.

Vertical displacements of the south and east exterior columns were essentially constant after impact and remained around 7.5 in. (over the severed columns) on the south face and about 3.5 in. on the east face until the east wall became unstable at 43 min. The east wall, which had bowed inward to a total of approximately 62 in., suddenly unloaded. The west wall also unloaded. Loads increased on the core and on the north and south walls. The core had weakened on the east side and shortened by 3.0 in. at the southeast corner. At the same time, the northwest corner of the exterior wall displaced upward about 2.0 in., as the tower was tilting to the southeast around an axis passing through the southwest and northeast corners.

The inward bowing of the east wall caused failure of exterior column splices and spandrels, and induced column instability. The instability progressed horizontally across the entire east face. The east wall unloaded and redistributed its gravity loads to the thermally weakened core through the hat truss and to the north and south walls through the spandrels. The building section above the impact zone began tilting to the east as column instability progressed rapidly from the east wall along the adjacent north and south walls, and increased the gravity load on the weakened east core columns. The change in potential energy due to downward movement of building mass above the buckled columns exceeded the strain energy that could have been absorbed by the structure. Global collapse then ensued.

Structural Response of the WTC Towers to Fire Without Impact Damage

Whether the towers would have collapsed if subjected to the same fires with no aircraft impact damage was considered as part of understanding the relative roles of the impact damage and fires. It was found from the global analyses that both WTC 1 and WTC 2 were stable after the aircraft impact and that they had considerable reserve capacity with structural impact damage. The global analyses also found that the combined effect of structural and insulation impact damage with the ensuing fires caused both towers to collapse. The effect of the fires on the towers without structural or insulation damage was considered by examining the subsystem and global analysis results for portions of the structures with intact insulation that were subject to the fires.

The towers would likely not have collapsed under the combined effects of aircraft impact and the subsequent multi-floor fires if the insulation had not been dislodged or had been only minimally dislodged by aircraft impact. The existing condition of the insulation prior to aircraft impact and the SFRM thickness on the WTC floor system did not play a significant role in initiating collapse of the towers.

Probable Collapse Sequences

To determine the probable collapse sequence for each tower, NIST adopted an approach that combined mathematical modeling, statistical and probability based analysis methods, laboratory experiments, and analysis of photographs and videos. The approach accounted for variations in models, input parameters, analyses, and observed events. It included the evaluation and comparison of possible collapse hypotheses based on different damage states, fire paths, and structural responses to determine the following:

- The probable sequence of events from the moment of aircraft impact until the initiation of global building collapse;
- How and why WTC 1 stood nearly twice as long as WTC 2 before collapsing (102 min for WTC 1 versus 56 min for WTC 2), though they were hit by virtually identical aircraft (Boeing 767-200ER);
- What factors, if any, could have delayed or prevented the collapse of the WTC towers.

Collapse hypotheses were developed over the course of the NIST Investigation. The first hypotheses were published in the May 2003 NIST Progress Report, and were updated in the June 2004 NIST Progress Report and October 2004 Public Meeting at NIST. The Probable Collapse Sequence for each tower was presented at the April 2005 Public Meeting in New York City. The stages of hypothesis development are summarized as follows:

- **Possible Collapse Hypotheses** (May 2003) – not building specific; key events not identified
- **Working Collapse Hypothesis** (June 2004) – single hypothesis for both WTC towers; identified chronological sequence of major events

- **Leading Collapse Hypotheses** (October 2004) – separate hypothesis for each WTC tower; identified building-specific load redistribution paths and damage scenarios in addition to chronological sequence of major events
- **Probable Collapse Sequences** (April 2005) – refined building specific collapse sequences with chronological sequence of major events, load redistribution paths, and damage scenarios.

To determine the probable collapse sequence for each tower, the following steps were required:

- identification of key observables, primarily from photographs and videos
- development of collapse hypotheses, which were updated periodically through the course of the investigation with the acquisition of new data and analysis results
- sensitivity studies to identify influential parameters, through the application of a formal statistical approach, orthogonal factorial design (OFD)
- development and refinement of mathematical modeling –fire dynamics simulation with computational fluid dynamics and structural response to aircraft impact and fire with finite element analyses
- evaluation of analysis results against observed and expected structural behavior, with adoption of the event tree concept, and pruning and updating branches based upon comparisons with observed data

These steps were applied to the degree needed for the sequence of analyses, from aircraft impact to structural response.

E.3 Probable Collapse Sequence of WTC 1 and WTC 2

The specific factors in the collapse sequences relevant to both towers (the sequences vary in detail for WTC 1 and WTC 2) are:

- Each aircraft severed exterior columns, damaged interior core columns, and knocked off insulation from steel as the planes penetrated the buildings. The weight carried by the severed columns was distributed to other columns.
- Subsequently, fires began that were initiated by the aircraft's jet fuel but were fed for the most part by the building contents and the air supply resulting from breached walls and fire-induced window breakage.

- These fires, in combination with the dislodged insulation, were responsible for a chain of events in which the building core weakened and began losing its ability to carry loads.
- The floors weakened and sagged from the fires, pulling inward on the exterior columns.
- Floor sagging and exposure to high temperatures caused the exterior columns to bow inward and buckle—a process that spread across the faces of the buildings.
- Collapse then ensued.

The sequences are supported by extensive computer modeling and the evidence held by NIST. The probable collapse sequences for WTC 1 and WTC 2 are presented in Figs. E-11 and E-12, respectively.

1. Aircraft Impact Damage

- Aircraft impact severed a number of exterior columns on the north wall from Floors 93 to 98, and the wall section above the impact zone moved downward.
- After breaching the building's exterior, the aircraft continued to penetrate into the building, severing floor framing and core columns at the north side of the core. Core columns were also damaged toward the center of the core and, to a limited extent, on the south side of the core. Fireproofing was damaged from the impact area to the south exterior wall, primarily through the center of WTC 1 and at least over a third to a half of the core width.
- Aircraft impact severed a single exterior panel at the center of the south wall between Floors 94 and 96.
- The impact damage to the exterior walls and to the core resulted in redistribution of severed column loads, mostly to the columns adjacent to the impact zones. The hat truss resisted the downward movement of the north wall, and rotated about the east-west axis.
- As a result of the aircraft impact damage, the north and south walls each carried about 7 percent less gravity loads after impact, and the east and west walls each carried about 7 percent more loads. The core carried about 1 percent more gravity loads after impact.

2. Effects of Subsequent Fires and Impact Damaged Fireproofing

A. Thermal Weakening of the Core:

- The undamaged core columns developed high plastic and creep strains over the duration the building stood, since both temperatures and stresses were high in the core area. The plastic and creep strains exceeded thermal expansion in the core columns.
- The shortening of the core columns (due to plasticity and creep) was resisted by the hat truss, which unloaded the core over time and redistributed loads to exterior walls.
- As a result of the thermal weakening (subsequent to impact and prior to inward bowing of the south wall), the north and south walls each carried about 10 percent more gravity loads, and the east and west walls each carried about 25 percent more loads. The core carried about 20 percent less gravity loads after thermal weakening.

B. Thermal Weakening of the Floors:

- Floors 95 to 99 weakened, with increasing temperatures over time on the long-span floors, and sagged. The floors sagged first and then contracted due to cooling on the north side; fires reached the south side later, the floors sagged, and the seat connections weakened.
- Floor sagging induced inward pull forces on the south wall columns.
- About 20 percent of the connections to the south exterior wall on Floors 97 and 98 failed due to thermal weakening of the vertical supports.

C. Thermal Weakening of the South Wall:

- South wall columns bowed inward as they were subjected to high temperatures and inward pull forces in addition to axial loads.
- Inward bowing of the south wall columns increased with time.

Figure E–11. WTC 1 probable collapse sequence.

3. Collapse Initiation

- The inward bowing of the south wall induced column instability, which progressed rapidly horizontally across the entire south face.
- The south wall unloaded and tried to redistribute the loads via the hat truss to the thermally weakened core and via the spandrels to the adjacent east and west walls.
- The entire section of the building above the impact zone began tilting as a rigid block (all four faces, not only the bowed and buckled south face) to the south (at least about 8°) as column instability progressed rapidly from the south wall along the adjacent east and west walls.
- The change in potential energy due to downward movement of building mass above the buckled columns exceeded the strain energy that could be absorbed by the structure. Global collapse then ensued.

Figure E–11. WTC 1 probable collapse sequence (cont).

1. Aircraft Impact Damage

- Aircraft impact severed a number of exterior columns on the south wall from Floors 78 to 84, and the wall section above the impact zone moved downward.
- After breaching the building's exterior, the aircraft continued to penetrate into the building, severing floor framing and core columns at the southeast corner of the core. Fireproofing was damaged from the impact area through the east half of the core up to the north and east exterior walls. The floor truss seat connections over about one quarter to one half of the east side of the core were severed on Floors 80 and 81 and over about one third of the east exterior wall on Floor 83.
- Aircraft impact severed a few columns near the east corner of the north wall between Floors 80 and 82.
- The impact damage to the exterior walls resulted in redistribution of severed column loads, mostly to the columns adjacent to the impact zones. The impact damage to the core columns resulted in redistribution of severed column loads mostly to other intact core columns and the east exterior wall. The hat truss resisted the downward movement of the south wall, and rotated about the east-west axis.
- As a result of the aircraft impact damage, the core carried 6 percent less gravity loads after impact and the north face carried 10 percent less loads. The east face carried 24 percent more gravity load, while the west face and the south face carried 3 percent and 2 percent more gravity load, respectively.
- After impact, the core was leaning toward the east and south exterior walls. The exterior walls acted to restrain the core structure.

Figure E–12. WTC 2 probable collapse sequence.

2. Effects of Subsequent Fires and Impact Damaged Fireproofing

A. Thermal Weakening of the Core:

- Several of the undamaged core columns near the damaged and severed core columns developed high plastic and creep strains over the duration the building stood, since both temperatures and stresses were high in the core area. The plastic and creep strains exceeded thermal expansion in the core columns.
- The core continued to tilt toward the east and south due to the combination of column shortening (due to plasticity, creep, and buckling) and the failure of column splices at the hat truss in the southeast corner.
- As a result of thermal weakening (subsequent to impact), the east wall carried about 5 percent more gravity loads, and the core carried about 2 percent less loads. The other three walls carried between 0 and 3 percent less loads.

B. Thermal Weakening of the Floors:

- Floors 79 to 83 weakened, with increasing temperatures over time on the long-span floors on the east side, and sagged.
- Floor sagging induced inward pull forces on the east wall columns.
- About an additional one third of the connections to the east exterior wall on Floor 83 failed due to thermal weakening of the vertical supports.

C. Thermal weakening of the east wall:

- East wall columns bowed inward as they were subjected to high temperatures and inward pull forces in addition to axial loads.
- Inward bowing of the east wall columns increased with time.

3. Collapse Initiation

- The inward bowing of the east wall induced column instability, which progressed rapidly horizontally across the entire east face.
- The east wall unloaded and tried to redistribute the loads via the hat truss to the weakened core and via the spandrels to the adjacent north and south walls.
- The entire section of the building above the impact zone began tilting as a rigid block (all four faces, not only the bowed and buckled east face) to the east (about 7° to 8°) and south (about 3° to 4°) as column instability progressed rapidly from the east wall along the adjacent north and south walls. The building section above impact continued to rotate to the east as it began to fall downward, and rotated to at least 20 to 25 degrees.
- The change in potential energy due to downward movement of building mass above the buckled columns exceeded the strain energy that could be absorbed by the structure. Global collapse then ensued.

Figure E-12. WTC 2 probable collapse sequence (cont).

E.4 FACTORS THAT AFFECTED PERFORMANCE

- From the collective knowledge and insights gained through the Investigation of the collapse of the WTC towers, the following factors were identified that enhanced the performance of both towers on September 11, 2001: The closely spaced columns, along with deep short spandrels, allowed a redistribution of loads as a result of aircraft impact damage to the exterior wall.
- Because there was effectively no wind on the morning of September 11, 2001, the capacity of the exterior wall provided to accommodate design wind loads was available to carry redistributed gravity loads.
- The large dimensional size of the WTC towers helped the buildings withstand the aircraft impact.
- The composite floor system with primary and bridging trusses forming a 2-way grid, and the two layers of welded wire fabric in the slab, acted to bridge over damaged areas without propagation of collapse from areas of aircraft impact damage to other locations, thereby avoiding larger scale floor collapse upon impact.
- The hat truss played a major role in the post-impact performance of the building. This was accomplished through redistribution of the loads from the significant weakening of the core, due to aircraft impact damage and subsequent thermal effects, by redistributing loads from the damaged core columns to adjacent intact columns and, ultimately, by redistributing loads to the exterior walls from the thermally weakened core columns that lost their ability to support the buildings' weight.
- The buildings would likely not have collapsed under the combined effects of aircraft impact and the subsequent jet-fuel ignited multi-floor fires, if the insulation had not been dislodged or had been only minimally dislodged by aircraft impact. The existing condition of the insulation prior to aircraft impact and the SFRM thickness on the WTC floor system did not play a significant role in initiating collapse on September 11, 2001.

E.5 FINDINGS

E.5.1 PASSIVE FIRE PROTECTION

The passive fire protection applied to the steel structural components in the WTC towers was investigated to provide information on the in-place condition of the thermal insulation before and after aircraft impact. The specified and “as applied” thicknesses, the variability in thickness, the condition of the insulation over a 30-year service life, and the effects that the variability and condition have on the structural behavior of insulated steel members were studied. The rationale behind the selection of the effective thickness of thermal insulation for use in thermal analyses was presented. Additionally, the procedures and practices used to provide the passive fire protection for the floor system of the WTC tower structures was documented.

Building Code Requirements for Structural Fire Resistance

Finding 1: The WTC towers were classified as Class 1B, as defined by the 1968 New York City Building Code. This classification required a 3 h fire rating for columns and 2 h for floors. The towers could have been classified as Class 1A since both Class 1A and 1B permitted buildings of unlimited height. Class 1A required a 4 h fire resistance rating for columns and a 3 h rating for floors. In 1969, the Port Authority specified the 0.5 in. SFRM for all beams, spandrels, and trusses, to maintain the Class 1A Fire Rating of the New York City Building Code. A condition assessment conducted in 2000 reported that the WTC towers were classified as Class 1B—noncombustible, fire-protected, and retrofitted with sprinklers in accordance with Local Law 5/1973.

Selection of Fire-Resistive Materials

Finding 2: The passive fire protection for the floor trusses was specified to be 0.5 in. of BLAZE-SHIELD Type D, although the technical basis for the selection of this product and required thickness value is not known. After applying the Type D sprayed fire-resistive material to the lower 40 floors of WTC 1, the BLAZE-SHIELD insulating material was switched to Type D/CF (reported to meet or exceed the insulating properties of Type D), which did not contain asbestos. In 1995, the Port Authority conducted a study to establish the SFRM requirements for the floor trusses in areas undergoing major tenant renovation. The thickness required to achieve a 2 h fire rating was determined to be 1.5 in. using the BLAZE-SHIELD II product. At the time of the WTC disaster, SFRM had been upgraded on a number of floors in the WTC towers: 18 floors in WTC 1, including all of the floors affected by the aircraft impact and fires, and 13 floors in WTC 2, although none were directly affected by the aircraft impact and fires.

Equivalent thickness of SFRM

Finding 3: Based on analyses of SFRM thickness measurements and interpretation of photographs showing the condition of the originally applied material, the average thickness of the original thermal insulation on the floor trusses was estimated to be 0.75 in. with a standard deviation of 0.3 in. (coefficient of variation of 0.40). The average thickness of the upgraded thermal insulation was estimated to be 2.5 in. with a standard deviation of 0.6 in. (coefficient of variation of 0.24). Based on finite-element simulations, it was concluded that the original passive fire protection on the floor trusses was thermally equivalent to a uniform thickness of 0.6 in., and the upgraded insulation was thermally equivalent to a uniform thickness of 2.2 in. These values were used in the thermal analyses for determining temperature histories of structural components.

Finding 4: No information was available on in-place conditions of the thermal protection on the exterior columns and spandrel beams, and little information was available on the conditions of fire-resistive material on core beams and columns. For thermal analyses of the towers, the SFRM on these elements was taken to have uniform thicknesses equal to the specified thickness. This assumption was supported by the observation that measured average thickness tended to be *greater* than the specified thickness while, due to variability, the effective thickness tended to be *less* than the average uniform thickness. The specified thickness values were 0.5 in. for beams and spandrels, 2.06 in. (2 1/16 in.) for columns lighter than 14WF228, and 1.19 in. (1 3/16 in.) for columns equal to or heavier than 14WF228.

Finding 5: The adhesive strength of BLAZE-SHIELD DC/F to primed steel was found to be a third to a half of the adhesive strength to steel that had not been coated with primer paint. The SFRM products used in the WTC towers were applied to steel components with primer paint.

E.5.2 FIRE RESISTANCE TESTS

Four Standard Fire Tests (ASTM E 119) were conducted on floor assemblies constructed to duplicate, as closely as practical, the floor system used in the WTC towers. Full scale tests with a 35 ft span, and having $\frac{3}{4}$ in. thick SFRM were tested; one in the restrained test condition and the other in the unrestrained test condition. Tests of half-scale specimens, which spanned approximately 17 ft, were conducted using SFRM conditions simulating the “as specified” condition (0.5 in. thick) and the “as-applied” condition (0.75 in. thick). The following findings are based on this series of four tests and a comparison of their results.

Structural Performance

Finding 6: Test assemblies, representative of the WTC floor system, exposed to the Standard Fire Test (ASTM E 119) conditions resulted in extensive spalling on the underside of the floor slab, thermal damage to the bridging trusses, and buckling of compression diagonals and vertical struts of the main trusses.

Finding 7: All four tests demonstrated that the floor assemblies were capable of sagging without failure. The unrestrained test, which had two 0.875 in. bolts fastening the main truss to the truss seats, did not sag sufficiently to bear on the bolts. In the three restrained tests, the main truss ends were welded to the truss seats to provide the required restraint. The magnitude of the sagging observed in the tests was consistent with that computed from finite element structural analyses. No evidence of knuckle failures was seen in the tests.

Finding 8: All four test assemblies supported their full design load under standard fire conditions for two hours without collapse.

Fire Resistance Ratings

Finding 9: The 1968 New York City (NYC) Building Code—the code that the WTC towers were intended but not required to meet when they were built—required a 2 h fire rating for the floor system.

Finding 10: The restrained floor system obtained a fire resistance rating of 1.5 h while the unrestrained floor system achieved a 2 h rating. This finding was unexpected since the unrestrained rating is typically less than the restrained rating.

Finding 11: The test of the 17 ft specimen with as-applied SFRM did not produce the same rating as the 35 ft test specimen, giving 2 h and 1.5 h, respectively. In both cases, the rating was established on the basis of temperatures of the unexposed surface (top of concrete slab) and not on the ability of the specimen to support the load.

Finding 12: The 45 min rating for the standard 17 ft test with the specified 0.5 in. SFRM did not meet the 2 h requirement of the 1968 NYC Building Code. This test had no SFRM on the bridging trusses nor on the underside of the metal deck.

Finding 13: The 2 h rating for the standard 17 ft test with the as-applied average 0.75 in. SFRM met the 2 h requirement of the 1968 NYC Building Code. This test had half the SFRM thickness on the bridging trusses (0.375 in.) and overspray on the underside of the metal deck.

Finding 14: The difference in test results for the two 17 ft specimens is due primarily to the concrete slab performance (spalling and cracking) and the presence or lack of SFRM overspray on the metal deck and not due to the SFRM thickness on the trusses. Differences in the degree of concrete spalling were possibly due to differences in moisture content and the slab cracking.

E.5.3 RESPONSE OF STRUCTURAL COMPONENTS

The response of the structural components and their connections for the tenant floors and exterior walls was examined with detailed structural models. Results of the floor and exterior wall component and connection analyses identified structural behaviors and failure modes that were required for inclusion in the global analyses.

Floor System

Finding 15: The interior truss seats had a greater vertical shear capacity than the exterior truss seats. The controlling failure mode for vertical shear was weld fracture. However, the vertical load at the truss connection of approximately 16 kip had to increase by a factor of two to six to reach failure (weld fracture) for temperatures near 600 °C to 700 °C.

Finding 16: Detailed structural analysis of a single truss section of the composite floor system subjected to elevated uniform temperatures was found to initially push out on the exterior columns as a result of the concrete slab thermal expansion and then pull inward as the web diagonals buckled and the truss sag increased. The magnitude of the pull-in force was found to depend highly on the stiffness of the exterior box column which, in turn, depended on expansion of floors above and below.

Finding 17: Detailed analysis of the knuckles (shear connectors in the floor system for composite action) through test simulation and detailed truss analysis found that failure of the knuckles in the floor system was unlikely. This finding was also supported by the lack of any knuckle failures in the four standard fire resistance tests (ASTM E119) of the floor truss assemblies with twice the floor load that was on the WTC floors.

Exterior Wall System

Finding 18: Large inelastic deformations and buckling of the spandrels at elevated temperatures were predicted, but were found not to significantly affect the stability of the exterior columns. Partial separations of the spandrel splices were also predicted at elevated temperatures, but were found not to significantly affect the stability of the exterior columns.

Finding 19: Analyses of bolted splices in the exterior columns found that the splice may slide or open when the exterior columns are bowing and subject to large lateral deflections. No column splice bolts were predicted to have failed.

Finding 20: An exterior wall section (9 columns wide and 9 floors high) was found to bow inward when the floor connections applied an inward pull force. For the condition where three sequential floors were disconnected, there was no bowing of the columns for five different elevated temperature conditions. When the column section with three disconnected floors was subjected to increased axial column loads, the wall section bowed outward over the unsupported column length.

E.5.4 FIRE PROTECTION AND PARTITION DAMAGE DUE TO AIRCRAFT IMPACT

The aircraft impacts into the WTC towers caused extensive damage to the buildings' exterior, penetrated into the interior causing further damage to the structural system, dislodged insulation, and ignited multi-floor fires. The structural damage to each tower resulting from the aircraft impact was estimated using a transient finite element analysis. Results of this analysis were used to predict damage to the structure, insulation, and partition walls in the path of the debris field.

Finding 21: For WTC 1, partitions were damaged and insulation was dislodged by direct debris impact over five floors (Floors 94, 95, 96, 97, and 98) and included most of the north floor areas between the north face and the core, the core, and central regions of the south floor areas, and on some floors, extended to the south wall. For WTC 2, partitions were damaged and insulation was dislodged by direct debris impact over six floors (Floors 78, 79, 80, 81, 82, and 83) and included the south floor area between the north face and the core, the central and east regions of the core, and most of the east floor area, and extended to the north wall.

Finding 22: The insulation damage estimates were conservative as they ignored possibly damaged and dislodged insulation in a much larger region that was not in the direct path of the debris but was subject to strong vibrations during and after the aircraft impact. Robust criteria to generate a coherent pattern of vibration-induced dislodging could not be established to estimate the larger region of damaged insulation.

E.5.5 OBSERVATIONS AND TIMELINE

Thousands of photographs and hours of video records were reviewed for insights into the structural performance of the towers. A timeline of significant events that characterized the weakening and eventual collapse of the WTC towers was developed with the photographs and videos that were time-stamped. Quantitative information, such as the amount of inward bowing observed on the exterior walls of the buildings, was extracted from key photographs through image enhancement and scaled measurements. Key observations and the timelines were used to guide the global collapse analyses.

WTC 1

Finding 23: Inward bowing of the south exterior wall was first observed at 10:23 a.m. The bowing appeared to extend between Floors 94 and 100 and Columns 305 and 359. The maximum bowing was estimated from images to be 55 in.±6 in. at Floor 97 on the east side of the south face of WTC 1. The central area in available images was obscured by smoke. The extent of fires observed on all faces of

WTC 1 was similar, although somewhat more extensive on the east and west faces (where short span floors were located) and similarly extensive on the north and south faces (where long span floors were located). Inward bowing was observed only on the south face. The north face had extensive aircraft impact damage, and the damaged floors were not capable of imposing inward pull forces on the north face.

Finding 24: The time to collapse initiation was 102 minutes from the aircraft impact (8:46:30 a.m. until 10:28:22 a.m.).

Finding 25: From exterior observations, tilting of the building section appeared to take place near Floor 98. Column buckling was then observed to progress rapidly across the east and west faces.

Finding 26: The WTC 1 building section above the impact and fire area tilted to the south as the structural collapse initiated. The tilt was toward the side of the building that had long span floors. Video records taken from east and west viewpoints showed that the upper building section tilted to the south. Video records taken from a north viewpoint showed no discernable east or west component in the tilt. A tilt to the south of at least 8 degrees occurred before dust clouds obscured the view and the building section began to fall downward.

WTC 2

Finding 27: On the east face and north face of WTC 2, draped objects were observed through the windows of Floor 82 on the east face and Floors 81 to 83 on the north face near the northeast corner. The draped objects appeared to be hanging floors. The drape of these objects was observed to increase with time and extend across approximately half of the east face.

Finding 28: Inward bowing of the east wall was first observed at 9:21 a.m. The inward bowing was approximately 10 in.±1 in. at Floor 80 and extended between Floors 78 and 83 and Columns 304 and 344. The remaining portion of the face to the south of Column 344 was not included in the image. The bowing appeared to extend over a large fraction of the east face and to be greatest near the center of the face. Fires were more extensive along the east face (where long span floors were located) and at the east side of the north and south faces (where short span floors were located). Fires were not observed on the west face (where long span floors were located). Inward bowing was observed only on the east face. The south face had extensive aircraft impact damage, and the damaged floors were not capable of imposing inward pull forces on the south face. There was no impact damage or fire on the west floors to cause pull-in forces on the west face.

Finding 29: An increase of the inward bowing of the east wall was observed at 9:53 a.m. The inward bowing appeared to extend between Floors 78 and 84 and Columns 305 and 341. The remaining portion of the face to the south of Column 344 was not included in the image. The maximum bowing was estimated from images to be 20 in.±1 in. at Floor 80 on the east face of WTC 1.

Finding 30: The time to collapse initiation was 56 minutes after aircraft impact (9:02:59 a.m. to 9:58:59 a.m.).

Finding 31: From exterior observations, tilt of the building section above the impact and fire area appeared to take place near Floor 82. Column buckling was then seen to progress across the north face.

Finding 32: The building section above the impact and fire area tilted to the east and south at the onset of structural collapse. The tilt occurred toward the east side with the long span floors. Estimates made from photographs indicate that there was approximately a 3 degree to 4 degree tilt to the south and a 7 degree to 8 degree tilt to the east, prior to significant downward movement of the upper portion of the building. The tilt to the south did not increase any further as the upper building section began to fall, but the tilt to the east continued, reaching 20 degrees to 25 degrees before dust clouds obscured the view.

E.5.6 STRUCTURAL RESPONSE OF MAJOR TOWER SUBSYSTEMS

Prior to conducting the analysis of the global structural response of each tower, major structural subsystems were analyzed to provide insight into their behavior within the WTC global system. The three major structural subsystems, the core framing, a single exterior wall, and full tenant floors, were analyzed separately for their response to impact damage and fire. The hat truss was not analyzed separately as its structural behavior did not require significant simplification in the global analysis. The component analyses provided a foundation for these large, nonlinear analyses with highly redundant load paths, and they enabled a significant reduction in finite element model complexity and size. The major subsystem models used final estimates of impact damage and elevated temperatures determined from the aircraft impact analysis and the fire dynamics and thermal analyses.

Isolated Core Subsystem

Finding 33: The WTC 1 isolated core subsystem analysis found that the core structure was most weakened from impact and thermal effects at the center of the south side of the core. Smaller displacements occurred in the global model due to the constraints of the hat truss and floors.

Finding 34: The WTC 2 isolated core subsystem analysis found that the core structure was unstable for the estimated structural damage to core columns. The core was most weakened from impact and thermal effects at the southeast corner and along the east side of the core. Larger displacements occurred in the global model as the isolated core model had lateral restraints imposed that were somewhat stiffer than in the global model.

Full Floor Subsystem

Finding 35: Floor sagging was caused primarily by either buckling of truss web diagonals or disconnection of truss seats at the exterior wall or the core perimeter. Except for the truss seat failures near the southeast corner of the core in WTC 2 following the aircraft impact, web buckling or truss seat failure was caused primarily by elevated temperatures of the structural components.

Finding 36: Analysis results from both the detailed truss model and the full floor models found that the floors began to exert inward pull forces when floor sagging exceeded approximately 25 in. for the 60 ft floor span.

Finding 37: Sagging at the floor edge was due to loss of vertical support at the truss seats. The loss of vertical support was caused in most cases by the reduction in vertical shear capacity of the truss seats due to elevated steel temperatures.

Isolated Exterior Wall Subsystem

Finding 38: Inward pull forces were required to produce inward bowing that was consistent with displacements measured from photographs. The inward pull was caused by sagging of the floors. Heating of the inside face of the exterior columns also contributed to inward bowing.

Finding 39: The observed inward bowing of the exterior wall indicated that most of the floor connections were intact to cause the observed bowing.

Finding 40: The floors that were identified through analysis to be affected by the fires and the dislodged insulation matched well with the floors that were observed to have participated in the inward bowing of the exterior walls.

Finding 41: The extent of floor sagging required at each floor was greater than that predicted by the full floor models. The estimates of the extent of sagging at each floor were governed by the combined effects of insulation damage and fire; insulation damage estimates were limited to areas subject to direct debris impact. Other sources of floor and insulation damage from the aircraft impact and fires (e.g., insulation damage due to shock and subsequent vibrations as a result of aircraft impact or concrete slab cracking and spalling as a result of thermal effects) were not included in the floor models.

E.5.7 STRUCTURAL RESPONSE TO AIRCRAFT IMPACT DAMAGE AND FIRE

Global analysis of WTC 1 and WTC 2 used final estimates of impact damage and elevated temperatures to determine the structural response and sequence of component and subsystem failures that led to collapse initiation.

General Findings

Finding 42: The structural analyses of WTC 1 and WTC 2 found that the collapse of the towers was due to the combined effects of structural and insulation damage from aircraft impact and the subsequent fires on the core, floor systems and exterior walls. The towers collapsed when the weakened core and exterior columns could no longer redistribute or support the building loads with their reduced load carrying capacity.

Finding 43: Impact damage alone did not cause collapse of the towers, as they were stable after the aircraft impact. Global analyses showed that both towers had substantial reserve capacity after the aircraft impact.

Finding 44: The multi-floor fires alone did not cause collapse of the towers. Without impact damage to the insulation, the structural steel temperatures would have been generally less than 200 °C to 300 °C, with a few isolated locations of structural steel temperatures exceeding 400 °C in WTC 1 floors and 500 °C in WTC 2 floors. The core would not have weakened, the floor sag would have been insufficient to pull inward on the exterior columns, and the exterior walls would not have bowed inward.

Finding 45: The towers would likely not have collapsed under the combined effects of aircraft impact and the subsequent multi-floor fires if the insulation had not been dislodged or had been only minimally dislodged by aircraft impact. Had insulation not been dislodged by the debris field, temperature rise of

structural components would likely have been insufficient to induce global collapse. Structural components that became thermally weakened were generally determined by impact of the debris field. The existing condition of the insulation prior to aircraft impact and the insulation thickness on the WTC floor system did not play a role in initiating collapse of the towers.

Finding 46: Creep strain was significant in the core and exterior columns over the 56 min to 102 min period of fire exposure in columns with temperatures greater than 500 °C to 600 °C and high stress. Columns with creep strains of sufficient magnitude to cause column shortening played a significant role in the collapse initiation.

Finding 47: The faces of the buildings that exhibited inward bowing were associated with the long span direction of the floor system. The primary direction of tilting at collapse initiation for WTC 1 and WTC 2 was in the direction of the bowed faces.

Performance with Intact Fire Protection

Finding 48: A detailed thermal-structural analysis, which did not include slab delamination/spalling effects, showed that a full collapse of the WTC floor system would not occur even with a number of failed trusses or connections.

Finding 49: Most of the horizontal and vertical capacity of the floor connections to the exterior and core columns significantly exceeded the demand under design load conditions.

E.5.8 PROBABLE COLLAPSE SEQUENCES

The results of structural analyses conducted in this study on components, subsystems, isolated exterior walls, cores, and global models of WTC 1 and WTC 2 showed that the collapses of the towers were initiated due to the combined effects of the structural and insulation damage from aircraft impact and the subsequent intense fires. The probable collapse sequence for WTC 1 and WTC 2 are based upon the collective consideration of structural analyses, statistical based methods, observations, and laboratory testing.

Role of the Building Core

Finding 50: The core columns were weakened significantly by the aircraft impact damage and thermal effects. Thermal effects dominated the weakening of WTC 1. As the fires moved from the north to the south side of the core, following the debris damage path, the core was weakened over time by significant creep strains on the south side of the core. Aircraft impact damage dominated the weakening of WTC 2. Immediately after impact, the vertical displacement at the southeast corner of the core increased 6 in. (from 4 in. to 10 in.). With the impact damage, the core subsystem leaned to the southeast and was supported by the south and east floors and exterior walls.

Finding 51: As the core was weakened from aircraft impact and thermal effects, it redistributed loads to the exterior walls primarily through the hat truss. Additional axial loads redistributed to the exterior columns from the core were not significant (only about 20 percent to 25 percent on average) as the exterior columns were loaded to approximately 20 percent of their capacity before the aircraft impact.

Role of the Building Floors

Finding 52: The primary role of the floors in the collapse of the towers was to provide inward pull forces that induced inward bowing of exterior columns (south face of WTC 1; east face of WTC 2).

Finding 53: Sagging floors continued to support floor loads as they pulled inward on the exterior columns. There would have been no inward pull forces if many of the floor truss seats had failed and disconnected.

Role of Exterior Frame-Tube

Finding 54: Column instability over an extended region of the exterior face ultimately triggered the global system failure as the loads could not be redistributed through the hat truss to the already weakened building core. In the area of exterior column buckling, load transferred through the spandrels to adjacent columns and adjacent exterior walls. As the exterior wall buckled (south face for WTC 1 and east face for WTC 2), the column instability propagated to adjacent faces and caused the initiation of the building collapse.

Finding 55: The exterior wall instability was induced by a combination of thermal weakening of the columns, inward pull forces from sagging floors, and to a lesser degree, additional axial loads redistributed from the core.

Probable Collapse Sequences

Finding 56: Although the north face of WTC 1 had extensive impact damage, thermal weakening of the core columns on the south side of the core and inward bowing of the south face caused the building to tilt to the south at collapse initiation. The extent of fires observed on all faces of WTC 1 was similar, although somewhat more extensive on the east and west faces (where short span floors were located) and somewhat less extensive on the north and south faces (where long span floors were located). Thermal weakening of exterior columns with floor sagging (which induced inward pull and occurred on the south side) caused inward bowing of the south face and tilting in the south direction.

Finding 57: Although the south face of WTC 2 had extensive impact damage, thermal weakening of the core columns on the east side of the core and inward bowing of the east face caused the building to tilt more to the east and less to the south at collapse initiation. Fires were more extensive along the east face and at the east side of the north and south faces. Thermal weakening of exterior columns with floor sagging (which induced inward pull and occurred on the east side) caused inward bowing of the east face and primary tilting in that direction (with additional southward tilting due to the aircraft impact damage).

Finding 58: The time it took for each WTC tower to collapse was due primarily to the differences in structural damage, the time it took the fires to travel from the impact area across the floors and core to critical locations, and the time it took to weaken the core and exterior columns. WTC 2 had asymmetric structural damage to the core, including the severing of a corner core column, and WTC 1 had more symmetrical damage. The fires in WTC 2 reached the east side of the building more quickly, within 10 to 20 minutes, than the 50 min to 60 min it took the fires in WTC 1 to reach the south side.

Finding 59: NIST found no corroborating evidence for alternative hypotheses suggesting that the WTC towers were brought down by controlled demolition using explosives planted prior to September 11, 2001. NIST also did not find any evidence that missiles were fired at or hit the towers. Instead, photographs and videos from several angles clearly showed that the collapse initiated at the fire and impact floors and that the collapse progressed from the initiating floors downward, until the dust clouds obscured the view.

Chapter 1

INTRODUCTION

1.1 PROJECT OBJECTIVES

The National Institute of Standards and Technology (NIST) investigation into the collapse of the World Trade Center (WTC) towers had eight interdependent projects. The purpose of each project is summarized in Table P-1, and the key interdependencies among the projects are illustrated in Fig. P-1, found in the Preface to this report.

One of the four objectives of the technical investigation was to determine why and how the WTC towers (WTC 1 and WTC 2) collapsed following the initial impacts of the aircraft. This objective is addressed in this report. Both the north and south towers of the World Trade Center were severely damaged by the impact of Boeing 767 aircraft, yet they remained standing for some time. The ensuing fires were observed to move through both buildings and eventually, both buildings collapsed. The extent and relative importance of the damage caused by the aircraft impact and subsequent weakening by fires were investigated under this project, *Structural Fire Response and Collapse Analysis*. This report presents the technical approach, modeling and testing methodologies, summary of results, and findings of the structural response of the WTC towers to aircraft impact damage and ensuing fires.

In addition, this project contributes to another investigation objective by determining the procedures and practices that were used in establishing the fire resistance ratings and providing passive fire protection to the components that made up the WTC tower structures.

The purpose of the project was to analyze the response of the WTC towers to fires – both with and without aircraft damage – and to determine the probable sequence of structural collapse for each tower. Specifically, this project attempted to:

- Determine the pre- and post-aircraft impact condition of the passive fire protection used to thermally insulate the structural members and provide resistance to fire damage,
- Conduct tests of structural components and systems under fire conditions to quantify their behavior,
- Evaluate the response of floor and column components and subsystems under fire conditions to understand their response,
- Evaluate the response of the WTC towers under fire conditions, with and without aircraft impact damage, and
- Determine the probable sequence of structural collapse for each WTC tower.

The project relied primarily on a series of computer simulations to model the complete sequence of events leading to the initiation of collapse of the WTC towers. The analyses included the damage to the towers

resulting from aircraft impact, the spread of multi-floor fires ignited by jet-fuel, the heating and thermal weakening of structural components, and the progression of local structural failures that led to the collapse of the buildings. Each of these models advanced the current state of the art and tested the limits of computational capabilities. The unprecedented complexity and sophistication of these analyses required the use of various strategies for managing the computational demands while adequately capturing the essential physics. The overall approach -- from impact analysis to collapse initiation -- combined mathematical modeling, statistical and probability-based analysis, laboratory testing, and analysis of photographic and videographic records.

1.2 TECHNICAL APPROACH AND TASKS

Events that played a significant role in the structural performance of the towers on September 11, 2001, were the aircraft impact, the fireballs immediately following the aircraft impact, and the ensuing fires across multiple floors in each tower. To estimate the structural response, detailed information was required on the condition of the structural system and its passive fire protection system, both before and after the aircraft impact. During the ensuing fires that resulted in elevated structural temperatures, information on the degradation of the stiffness and strength of the structural system was also required.

Data was collected and reviewed from a number of sources. Such data included structural geometry, details, and connections; thermal and mechanical (adhesion/cohesion) properties of fire resistant materials; the thickness and condition of the passive fire protection in the towers; and recorded observations of structural events subsequent to aircraft impact and prior to collapse. Information about tower construction was obtained from original drawings and specifications, reports, and available records from The Port Authority of New York and New Jersey (PANYNJ or Port Authority), Leslie E. Robertson Associates (LERA), Silverstein Properties, and a number of contractors that had worked on the design, construction, or modifications to the towers. Information about the events that occurred in each tower on September 11, 2001, was obtained from analysis of available photographic and videographic records, eyewitness accounts, and metallurgical analysis of recovered structural steel.

The analyses performed to determine the probable collapse sequence for each tower considered the as-built structural systems and their response to aircraft impact damage, temperature-dependent properties of steel and concrete, growth and spread of the fires, and heating of structural components. The structural response analyses relied upon the following information:

- Reference global structural models of the WTC 1 and WTC 2 towers, and typical floor and exterior wall subsystem models (NIST NCSTAR 1-2)²
- Extent of damage to the structural systems and interior contents of the WTC 1 and WTC 2 towers resulting from aircraft impact (NIST NCSTAR 1-2)
- Temperature-dependent mechanical properties of the steels, welds, and bolts used in the construction of the towers, including elastic, plastic, and creep properties from 20 °C to 700 °C (NIST NCSTAR 1-3)

² This reference is to one of the companion documents from this Investigation. A list of these documents appears in the Preface to this report.

- Time-temperature histories for structural components and connections for both standard fires (e.g., ASTM E 119) and actual fires based on fire dynamics simulations (NIST NCSTAR 1-6B).
- Photographic and videographic records with time stamps that documented the observed sequence of events (NIST NCSTAR 1-5).

To simulate the effects of aircraft impact into the towers, the growth and spread of fires, and the subsequent weakening of the structural system that ultimately led to collapse, a series of sophisticated computer analyses was conducted. The results of any computer analysis depend on the fidelity of the input data and the ability of the computer software to capture the fundamental physics that produce the output response.

The WTC towers were large, complex structural systems. To include all of the structural components and connections and their associated behavior and failure mechanisms using refined finite element meshes would have been prohibitive. The analysis approach used was a variant of the well-established sub-structuring approach, adapted for the analysis of structures with highly nonlinear behavior, that progressed from individual components to major subsystems to global systems, as shown in Fig. 1–1. Extensive component analyses were conducted to identify critical behavior and failure mechanisms that contributed to the global structural response of each tower. Similarly, extensive subsystem analyses were then performed. These analyses incorporated the behavior and failure mechanisms identified in the component studies, with modifications to reduce the model size and complexity, thereby enhancing computational performance, without adversely affecting the quality of the results. Whenever modeling modifications were used, they were validated against the detailed component model results. The global analyses incorporated critical behavior and failure mechanisms, determined from subsystem analyses, while making necessary modifications in the level of modeling detail.

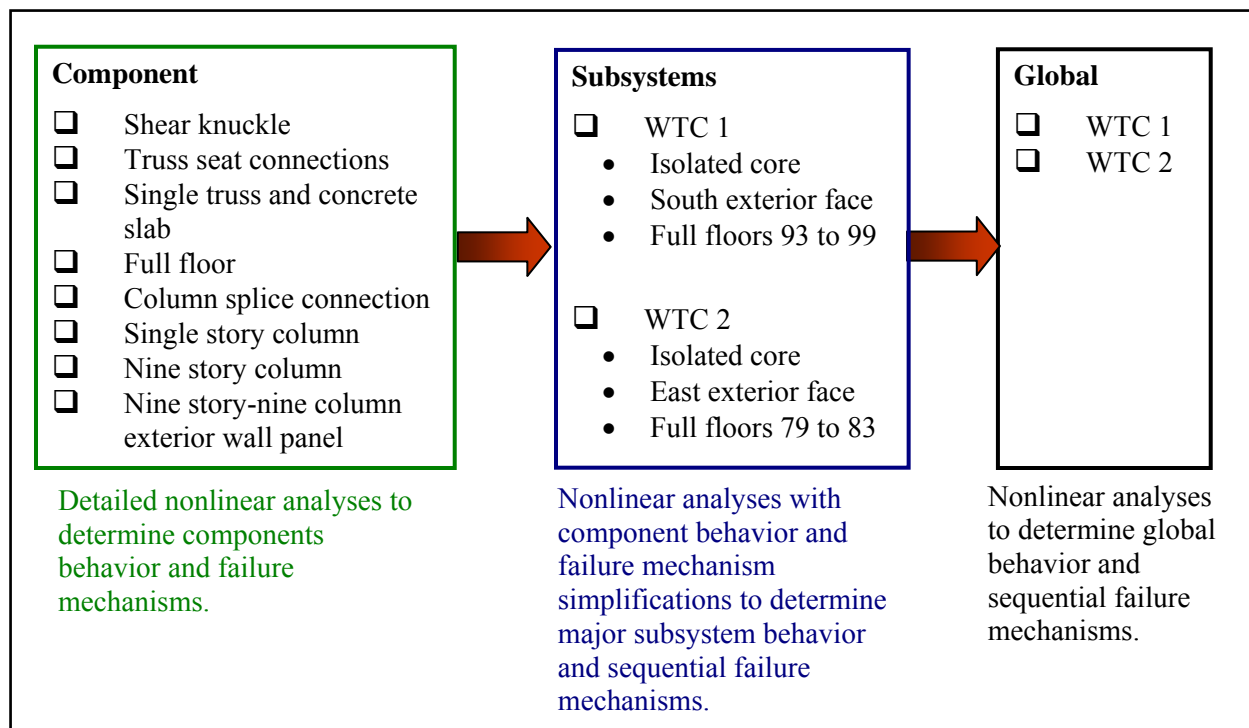


Figure 1-1. Structural Analysis Sequence.

As shown in Fig. 1-1, the structural response analyses began with the analysis of components, connections, and subsystems to develop an understanding of their structural behavior at elevated temperatures and associated failure mechanisms. Components, used herein, included single structural elements, such as a column or a truss web member. Subsystems were groups of components that had a major structural function, such as a floor system. Connections, such as a column splice or a floor truss seat, transfer loads between components or subsystems. Results of the component and subsystem analyses were used to develop the global models that were used to determine the global behavior and sequential failure mechanisms.

The response of WTC 1 and WTC 2 global systems was estimated by (1) evaluating the response of floor and column components, connections, and subsystems under thermal loading, (2) evaluating the response of the WTC towers with and without aircraft impact damage under actual fire conditions, (3) conducting tests of structural components and systems under fire conditions, and (4) developing and evaluating collapse hypotheses for the WTC towers. The effort, including work performed outside the scope of this project, was divided into the following tasks:

1.2.1 Task A – Finite Element Reference Models

Develop finite element models based on reference models: Modeling the structure of the towers, whether for the assessment of aircraft impact, the growth and spread of fires, or the structural response to those fires, necessitated that the geometry, cross-sectional properties, and the material properties of the structural components be a faithful representation of the actual structures. To that end, reference finite element models of both towers (since they were not identical) were developed. This was done under a contract to Leslie E. Robertson Associates (LERA), the designers of the WTC towers, within the

framework of Project 2 of the Investigation. The models underwent a thorough review process, including an in-house NIST review and a third-party review by the firm of Skidmore, Owings & Merrill LLP (SOM), also under contract to NIST, to test the accuracy of the models. The reviews included checking the consistency of the models with the original design documents, verification and validation of the models (including assumptions and level of detail), and testing the accuracy of the models under various loading conditions. The development of the reference models is described in NIST NCSTAR 1-2. These reference models became the basis for all subsequent finite element analyses.

1.2.2 Task B – Material Properties

Develop the constitutive relationships for the materials used in the construction of the towers: Properties of the structural steels used in the construction of the towers were part of the fundamental data needed for the development of models. Mechanical and chemical properties were determined for steel specimens recovered from the WTC site to assure that the materials used were in conformance with those specified in the original design. Further, the behavior of the structural steels used was characterized to determine the mechanical properties at high loading rates for the aircraft impact analyses and at elevated temperatures (from room temperature to 800 °C) for the thermal-structural response analyses. Properties of structural materials are given in NIST NCSTAR 1-3 and summarized in Chapter 4 of this report.

1.2.3 Task C – Passive Fire Protection

Characterize the passive fire protection applied to the structural steel: The type of SFRM materials and required thickness were specified in correspondence between the Port Authority and SFRM contractor. Estimates of the characteristics of SFRM materials were deemed essential for the thermal-structural modeling of the towers. Of primary importance was the condition of the sprayed fire-resistive material (SFRM) used since the type of material (hence its thermal insulating properties), its average applied thickness, and variation in application thickness all had an effect on the temperatures developed in the structural elements as a result of exposure to fire. Since upgrading of the SFRM was begun in the 1990s, and the upgraded thickness was greater than that originally applied, it was important to determine: (1) the areas in the buildings where upgrading had been completed, and (2) the average thickness and its associated variability. Chapter 2 of this report addresses the passive fire protection and its application, the determination of thermal properties, and calculation of an equivalent uniform thickness of material used for the thermal and structural finite element analyses. Detailed information and a complete description of the procedures and practices used in the selection of fire protection for the WTC project is covered in NIST NCSTAR 1-6A.

1.2.4 Task D – Standard Fire Resistance Tests

Conduct standard fire resistance tests of composite truss floor system: Tests were conducted to: (1) establish the baseline fire resistance rating of the composite truss floor system used in the WTC towers, (2) understand the influence of thermal restraint by testing the floor system under both thermally unrestrained and fully restrained conditions, and (3) provide experimental data to validate and provide guidance to the development of the floor models and to the interpretation of analyses results. The standard ASTM E 119 fire test was selected since it represents a fairly severe condition both in the fire exposure and specimen loading and provides a frame of reference with respect to the historical performance of alternative floor systems. Four tests, representing both full-scale and reduced-scale

specimens, are covered in Chapter 3 of this report and are reported in more detail in NIST NCSTAR 1-6B.

1.2.5 Task E – Aircraft Impact Damage

Establish the damage to the structure, insulation, and partition walls as a result of aircraft impact: The damage induced by the impact of a Boeing 767 aircraft into each tower had significant influence on many facets of the analytical investigation into how and why the towers collapsed. First, the aircraft impact resulted in significant damage not only to the exterior of the buildings, but also to the floors and core structures inside the buildings and as a consequence, weakened the structures to some degree. Second, the jet fuel dispersed inside the towers ignited the building contents and furnishings, and the damage to the buildings' facades as well as damage to the interiors influenced the amount of oxygen reaching the fires and, therefore, the speed at which the fires grew and moved throughout the affected floors. Third, the impacts of the jet aircraft were of sufficient force to dislodge significant portions of the all-important SFRM in the impact and fire-affected regions. The finite element analyses required to predict the extent of damage due to aircraft impact are presented in NIST NCSTAR 1-2. This information was then used to estimate the extent of the SFRM damage based on the results of impact simulations, including the paths of the debris field and damage to interior partitions and furnishings. Chapter 5 summarizes the results of the impact damage and the approach used to estimate the extent of insulation damage.

1.2.6 Task F – Observations and Timeline

Document observations and data for structural events: NIST has made concerted efforts to validate analysis results with key observations obtained from its extensive collection of over 7,000 photographs and over 150 hours of videotape (NIST NCSTAR 1-5A) documenting the events at the World Trade Center on September 11, 2001. Development of the probable collapse sequence for each tower was shaped by evidence gathered from these photographs and videos, along with eyewitness accounts. The photographs and videos provided knowledge about aircraft impact damage to the exterior walls, fire growth and spread at the building exterior, inward bowing of an exterior wall in each tower, and the direction of tilt for the building section above the impact and fire zone as the towers collapsed. Evidence was used in the analyses in three ways: (1) to determine input parameters, such as the aircraft speed and trajectory upon impact, (2) to impose time-related constraints upon an analysis, such as imposing observed broken windows over time thereby affecting the spread of fire, or (3) to validate analysis results, such as global stability after impact and during thermal loading. A timeline of impact, fire, and structural events was developed for each tower, primarily from photographs and videos. Analyses were used to develop and refine the probable sequence of events between timeline observations. The quality of the results compared to the visual and physical evidence supports NIST's view that the significant phenomena relevant to the probable collapse sequence have been adequately captured. Details of this task are provided in Chapter 6 of this report.

1.2.7 Task G – Temperatures of Structural Components

Compute temperature histories for structural components subjected to fires: After the aircraft impacted each building, fires started on multiple floors, ignited by the rapid spread of burning jet fuel. To determine how the towers were affected by the high temperatures resulting from the fires, estimates of the growth and spread of fires over time were developed using fire dynamics simulations. These were based

on sophisticated computational fluid dynamics (CFD) modeling as described in NIST NCSTAR 1-5. These computations relied on: (1) the fire loads on each floor, (2) estimated ventilation as determined from the aircraft impact analyses (**Task E**), and (3) window breakage resulting from the fires as determined from photographic interpretation (**Task F**). Temperatures of the steel structural components and concrete floor slabs were predicted using accurate models of the structures (**Task A**), thermal properties of the steel and concrete (**Task B**), thermal properties of the insulation applied to protect the steel and its equivalent uniform thickness (**Task C**), and the time and spatially varying temperature fields predicted from the fire dynamics calculations as described above. The thermal analyses conducted to estimate realistic temperatures in the steel and concrete are covered in NIST NCSTAR 1-5.

1.2.8 Task H – Component and Subsystem Analyses

Conduct component and subsystem analyses: The purpose of these analyses was to provide a basic understanding of the behavior of the various structural components and subsystems of the towers under gravity and thermal loading and to develop reduced models that could be reliably used in the global models. The subsystems considered in this phase of the study included: (1) typical floor subsystem with its associated components: (a) the shear knuckles, (b) truss seats, and (c) a single truss and concrete slab; and (2) a nine-story by nine-column exterior wall subsystem with its associated components (a) bolted connection between exterior columns, (b) bolted connection between spandrels, (c) single exterior column with spandrel sections, and (d) single exterior wall panel with three columns and three spandrels. The floor and exterior wall subsystems included modeling reductions as developed from the component models. The models were based on the reference models developed in **Task A**, material properties estimated in **Task B**, and SFRM thickness and properties determined from **Task C**. The floor components and subsystem models were verified using the standard fire test results (**Task D**). Chapter 4 of this report describes the development of the component and subsystem models

1.2.9 Task I – Major Subsystem Analyses

Conduct analyses of major subsystems: Analyses of three major subsystems - the isolated core framing subsystem, an exterior wall subsystem, and the composite floor subsystems - were analyzed to determine their ability to resist and redistribute loads after impact damage and elevated temperatures. These major subsystem models used final estimates of impact damage and elevated temperatures determined from the aircraft impact analysis (**Task E**) and the fire dynamics and thermal analyses (**Task G**). The subsystem models used modifications from the component analyses, which kept the analysis solution times reasonable while maintaining required nonlinear features and failure modes. These analyses were crucial for determining critical structural behaviors of the towers, including floor sagging under thermal loading, the resulting pull-in forces, and the inward bowing of the exterior walls. The subsystem analyses used the reference models (**Task A**), material properties (**Task B**), SFRM properties (**Task C**), and results and simplifications from component analyses (**Task I**). The major subsystem analyses were verified using photographs and videos (**Task F**). Details of these analyses are described in Chapter 7 of this report.

1.2.10 Task J – Global Structural Analyses

Conduct a separate global analysis for each tower: The purpose of these analyses was to determine the relative roles of impact damage and fires with respect to structural stability and sequential failures of components and subsystems and to determine the probable collapse initiation sequence. Results of the

major subsystem analyses were incorporated into the global models, simplifying the modeling approach and/or level of detail where possible, while retaining sufficient detail for the nonlinear structural responses, including creep and buckling effects on columns. Each global model was first evaluated for stability under gravity loads with structural impact damage modeled by removing severed core and exterior columns, failed spandrels, and damaged floor areas. Temperature time-histories based upon the fire dynamics and thermal analyses were applied in 10 min intervals and linearly ramped to the next temperature state. Pull-in forces from sagging floors were also applied during the appropriate 10 min intervals. The global analysis results provided a sequence of component and subsystem failures that led to the onset of global instability and collapse initiation. The global analyses used the output from various tasks (**A**, **B**, **C**, **E**, **G**, and **I**) and were verified using photos and the timeline (**Task F**). The global tower analyses are described in Chapter 8 of this report.

The question of how the WTC towers would have responded to the same fires without the aircraft impact damage was considered to determine the general vulnerability of the towers to fire-initiated collapse. The structural response of the WTC towers to large fires without impact damage considered if collapse was possible, or under what conditions collapse may have occurred, without the aircraft impact damage. The analyses of the major subsystems (**Task I**) and each global analysis (**Task J**) provided sufficient data for addressing this issue. This analysis considered the role of fire in the towers with respect to structural stability, sequential failures of components and subsystems, and collapse initiation for the towers without impact damage. This analysis is presented in Chapter 8 of this report.

1.2.11 Task K – Probable Collapse Sequence

Determine the probable collapse sequence for each tower: The following steps were taken:

- Identify key observed events,
- Refine collapse hypotheses,
- Conduct sensitivity studies to identify influential parameters,
- Conduct analyses with these parameters, and
- Evaluate the collapse hypotheses and analysis results against key observables.

Sensitivity analyses were performed to determine most influential parameters that affect the response of components, subsystems, and connections for the aircraft impact, fire dynamics, and thermal analyses. Three sets of values for the parameters most influential to the aircraft damage and the progress of the fires were determined from the sensitivity studies. The three sets of parameters represented a range of severity levels, including a base case, a more severe case, and a less severe case. Three aircraft impact (**Task E**) and fire dynamics (**Task F**) analyses were performed for correlated sets of expected aircraft and fire parameters that provided different levels of damage. The analysis results were compared to the key observables. Thermal and structural subsystem analyses (**Task I**) were conducted for the selected cases that reasonably matched observed impact damage and fire progression. The cases that reasonably matched the evidence were identified for global structural response analyses (**Task J**). The probable collapse sequence is presented in Chapter 9 of this report.

Task D was conducted in collaboration with experts from Underwriter's Laboratories (UL), under contract to NIST. Further details are provided in NIST NCSTAR 1-6B.

Tasks H, I and J were conducted in collaboration with experts from Simpson Gumpertz & Heger Inc. (SGH), under contract to NIST. Further details are provided in NIST NCSTAR 1-6C and NIST NCSTAR 1-6D.

1.3 CHALLENGES

Estimating the structural response of the WTC towers to impact damage and the ensuing fires presented a number of significant challenges:

- The towers had steel and concrete materials that exhibited nonlinear, temperature-dependent behavior. The structural behavior and failure mechanisms required for the analyses included mechanical properties (stress-strain) at room temperature and at elevated temperatures, thermal expansion, plasticity, creep, large deformations, and plastic buckling. The constitutive relationships for the materials included in the models were based on tests conducted by NIST on steels recovered from the collapse site, certified mill test reports found in historical project records, and data available in the technical literature.
- The WTC towers were large, complex structural systems. To include all of the structural components and connections and their associated behavior and failure mechanisms using refined finite element meshes would have been prohibitive. As a result, increasingly coarser meshes were used in the subsystem and global analyses. The models, thus, used a reduced number of elements while still capturing the nonlinear, complex behavior of the tower components. A number of component and connection analyses were conducted separately to develop a basis for the reduced models used in the global analyses that captured essential temperature-dependent behavior and failure mechanisms.
- This investigation required analyses of the structural response of components and subsystems of the WTC towers, such as temperature-dependent properties, creep and post-buckling strength of columns, that required software tools not typically employed in structural analysis or design. This study necessitated the use of sophisticated analysis methodologies at the limits of structural engineering experience and training.
- The thermal loadings (temperature histories) used in the analyses of the various components and subsystems, were derived from thermal analyses which, in turn, were derived from fire dynamics simulations. The mapping of the output from the fire dynamics simulations to the thermal models, and the mapping of the temperatures derived from the thermal analyses to the structural models, were complex and challenging tasks due to the vastly different dimensional scales, time increments, element types, and software used in the various analyses.
- For the subsystem and global models, with thousands of degrees of freedom, numerical convergence of the structural analyses that encountered local failures (such as connection failure), large deflections, plastic (inelastic) buckling, creep effects, etc., presented many problems that resulted in prematurely halting the simulation. Overcoming the convergence

issues and successive failures of thousands of elements, required considerable effort and innovative approaches. Some convergence problems were solved through the use of dynamic analysis with appropriate damping, and in some instances explicit dynamics formulation solvers were required to capture, for example, concrete crushing.

- The structural response analyses were subject to uncertainties in the input parameters, such as the extent of impact damage to the structure, the temperature histories of structural components (based upon the post-impact insulation condition and the fire growth and spread), and material properties at elevated temperatures. The aircraft impact damage and component temperature histories provided a range of inputs for the subsystem and global analyses that captured the uncertainty in these inputs. With the uncertainty of the aircraft impact and fires captured in the input data files, the primary parameters required for the structural response analyses were related to structural behavior and failure mechanisms. The uncertainty in the temperature-dependent material properties increased with increasing temperature. However, the effect of increasing temperature on the structural behavior and failure mechanisms influenced the results more than variability of the material properties.
- Testing of structural components under static or dynamic (time-varying) loadings is challenging at best. Testing of loaded structural components under fire conditions, particularly at the scale that it was done, was of even greater difficulty and pushed the limits of fire testing capabilities in the United States.

1.4 REPORT ORGANIZATION

Chapter 2 describes the as-built properties of the passive fire protection systems used for the structural components of the towers. The two types of passive fire protection systems used in the WTC towers were SFRM products and gypsum enclosures and partitions. The tests and data used to determine the thermal and mechanical properties of these systems as a function of temperature are presented. Also presented is the average thickness of the SFRM along with the variation in the thickness.

Chapter 3 describes the fire resistance tests of the composite floor truss components and subsystem under standard fire conditions. A series of four tests was conducted to establish the baseline performance of the WTC floor system under thermal loading as it was originally designed, differentiate factors that most influenced the response of the floors to fires, and study the procedures and practices used to accept an innovative structural and fire protection system.

Chapter 4 describes the component and detailed subsystem analyses. The chapter outlines the structural material properties and failure criteria used for the concrete, steel, welds, and bolts used in the WTC towers. The series of analyses conducted included detailed models of knuckle and truss seat connections, a single truss section of the floor, and a model of an entire floor subsystem. The analyses also included a nine-story by nine-column exterior wall subsystem along with its associated components, such as the bolted connection between exterior columns and between spandrels, a single exterior column, and a single exterior wall panel with three columns and three spandrels. Each analysis description includes details of the model, applied loads, and structural results. Modifications to models to reduce the model size and detail while retaining essential behaviors are described, and comparisons are made of the response of the modified model relative to the original detailed model.

Chapter 5 summarizes the results of the analysis of aircraft impact damage to the WTC towers. The chapter describes how the structural damage due to impact was imposed on the subsystem and global models used in this study and outlines the methodology used to estimate the damage to insulation as a result of aircraft impact.

Chapter 6 describes the observations and timeline of structural events. The observations and timeline are based primarily on photographic and videographic records. Key observations were used to help validate the probable collapse sequence for each tower.

Chapter 7 describes the analyses conducted for three major tower subsystems to aircraft impact damage and fire. These analyses included full floors, core columns, and exterior walls of WTC 1 and WTC 2 in the impact and fire zones. These analyses were conducted prior to the global analysis for each tower. Each analysis description includes details of the model, applied loads, and structural results.

Chapter 8 describes the global structural response of each WTC tower to aircraft impact damage and fire conditions. The model for each tower is described, including aircraft impact damage and temperature-histories for the observed fires. Modeling simplifications based on the previous analyses are described, and the results of the analyses are presented. The chapter also evaluates the structural response of the WTC towers to fire conditions without aircraft impact damage. A separate global analysis was not conducted for this analysis. Instead, the results from the analyses conducted in previous chapters are used as the basis for evaluating this hypothetical condition.

Chapter 9 presents the probable collapse sequence for each tower, based on the analysis results presented in Chapter 8 and the key observations presented in Chapter 6.

Chapter 10 presents the findings of the study.

This page intentionally left blank.

Chapter 2

PASSIVE FIRE PROTECTION

Many structural materials are adversely affected by high temperatures resulting from an uncontrolled building fire where compartment temperatures can reach 1,100 °C (2,000 °F). Generally, some means of protecting, or insulating, the structural components is required to provide an acceptable level of performance in fire. Steel, for example, loses both its strength and stiffness at the elevated temperatures associated with building fires, and an insulating barrier is required to slow or prevent damage to structural steel components.

The structural steel in the World Trade Center (WTC) towers was protected with sprayed fire-resistive material (SFRM) or rigid fire-rated gypsum panels. SFRMs are a combination of fibrous material and cementitious binder that, when mixed with water, can be spray-applied to the steel (Gewain et al. 2003). With time, the cementitious materials harden and the excess water evaporates, and when dry, SFRMs provide an insulation barrier to limit excessive temperature rise in the steel during a fire. Similarly, fire-rated gypsum wallboard was used to enclose some structural steel core columns to provide the required level of fire protection.

The structural analysis of the WTC towers focused on the response of the two towers damaged by the aircraft impact and exposed to the subsequent fires. To reduce the uncertainties in the calculated temperature histories of various structural elements, the thermal properties and condition of the passive fire protection as it existed on September 11, 2001, was estimated as accurately as possible. In addition, reasonable estimates of the extent of SFRM dislodged by the aircraft impact and flying debris were made (see Chapter 5).

NIST NCSTAR 1-6A reports on many aspects of the passive fire protection in the WTC towers, beginning with an overview of U. S. building regulations that are intended to provide structural fire resistance. The report continues with a chronicle of the procedures and practices used in the selection and application of the SFRMs used in the construction of the WTC towers. The variability of SFRM application on the uncertainty in estimating the steel temperatures is covered. Finally, the thermal and mechanical properties of the SFRM materials are reported. This chapter summarizes the salient material covered in NIST NCSTAR 1-6A.

2.1 FIRE RESISTANCE OF STRUCTURAL ELEMENTS

Building codes require that elements that support loads are to be protected to achieve a specified fire resistance rating³, expressed in hours. The fire rating of structural materials and assemblies is generally determined through testing, and in the United States, such testing is frequently conducted in accordance with the ASTM International standard, ASTM E 119, “Standard Test Methods for Fire Tests of Building Construction and Materials” (ASTM 2000).

³ The term “fire resistance rating” (or simply “fire rating”) is variously called in the ASTM E 119 Standard, “period of resistance,” “performance,” “exposure” or classification.”

Building codes generally require the highest fire resistance rating for columns and other elements supporting multiple floors, and a somewhat lower resistance rating for columns and other elements supporting single floors, and for floors. The required fire resistance ratings have been reduced in recent years when fire sprinklers are installed in high-rise and other commercial buildings. In the past, high-rise buildings generally required a 4 h rating for columns; this has been reduced to 3 h in recent model codes, and can be as low as 2 h in current model codes, based on the additional mandatory requirement for sprinklers. Some codes allow a reduction in fire-resistance rating for high-rise buildings that have been retrofitted with sprinklers.

2.2 HISTORICAL REVIEW RELATED TO PASSIVE FIRE PROTECTION

2.2.1 Building Code Requirements for the Design of the WTC Towers

As an interstate compact, The Port Authority of New York and New Jersey (Port Authority or PANYNJ) was not required to comply with the New York City Building Code (NYCBC 1968), or any other building code, for the design and construction of the WTC towers. The Port Authority, however, made explicit statements that it would comply with the New York City Building Code. In a letter dated May 15, 1963⁴, the Port Authority instructed its consulting engineers and architects to comply with the New York City Building Code. In areas where the Code was not explicit or where technological advances made portions of the Code obsolete, it directed that design could be based on acceptable engineering practice. At that time, the 1938 edition of the New York City Building Code was in effect, and a revised code was being drafted. In a directive dated September 29, 1965⁵, the Port Authority instructed its consultants to revise the WTC design plans to comply with the second and third drafts of the Code revision. The revised New York City Building Code became effective in December 1968.

2.2.2 New York City Building Code Requirements

Application of the 1968 New York City Building Code (NYCBC) provisions affected the assigned building classification and, thus, the required fire rating of the WTC towers and their structural members. The WTC towers were classified as Occupancy Group E—Business. The 1968 NYCBC identified two construction groups: Noncombustible Construction (Group 1) and Combustible Construction (Group 2). The WTC towers were classified as Construction Group 1 because their walls, exit ways, shafts, structural members, floors, and roofs were constructed of noncombustible materials. At the time of design and construction, the towers were not sprinklered.

The 1968 New York City Building Code defined five Classes within Construction Group 1. For Business occupancy, each Class required a fire endurance rating as follows:

- Class 1A: 4-hour protected
- Class 1B: 3-hour protected

⁴ Letter dated May 15, 1963 from Malcolm P. Levy (Chief, Planning Division, World Trade Department) to Minoru Yamasaki (Minoru Yamasaki & Associates) - see NIST NCSTAR 1-6A, Appendix Figure A-1.

⁵ Letter dated September 29, 1965 from Malcolm P. Levy (Chief, Planning Division, World Trade Department) to Minoru Yamasaki (Minoru Yamasaki & Associates) - see NIST NCSTAR 1-6A, Appendix Figure A-2.

- Class 1C: 2-hour protected
- Class 1D: 1-hour protected
- Class 1E: unprotected

Construction Classes 1A and 1B permitted buildings of unlimited height. Thus, the WTC towers could have been designed to meet either Class 1A or Class 1B requirements.

2.2.3 Classification of WTC Towers

It was the practice at the time, and continues to be the practice, for the architect to establish the building classification, fire rating of members and systems, and thermal protection requirements. The review of documents uncovered during the investigation indicated a discrepancy in the classification, and therefore the fire ratings, to be used in the design of the towers. Documents issued in the early stages of the design appear to indicate that the towers were classified as Class 1A⁶. With the directive in 1965 to comply with the 1968 New York City Building Code, it appears that the towers were classified ultimately as Class 1B⁷.

According to the 1968 New York City Building Code, construction classification 1B provided, in part, the following fire protection requirements:

- Columns, girders, trusses, other than roof trusses, and framing supporting more than one floor shall have 3-hour fire endurance;
- Columns, girders, trusses, other than roof trusses, and framing supporting one floor shall have 2-hour fire endurance
- Floor construction including beams shall have 2-hour fire endurance.
- Enclosure of vertical shafts, exits, passage-ways, and hoistways shall have 2-hour fire endurance; and
- Roof construction including beams, trusses, and framing including arches, domes, shells, cable supported roofs, and roof decks (for buildings over one story in height) shall have 2-hour fire endurance.

Thus, the columns were required to have a 3-hour fire endurance rating and the floor system was required to have a 2-hour rating when tested in accordance with ASTM E 119 (ASTM 1961).

⁶ Letter dated October 30, 1969 from Robert J. Linn (Manager, Project Planning, The World Trade Center) to Mr. Louis Di Bono, Mario & Di Bono Plastering Co., Inc. – see NIST NCSTAR 1-6A, Appendix Figure A-23.

⁷ Memorandum dated January 15, 1987 from Lester S. Field (Chief Structural Engineer, World Trade Department) to Robert J. Linn (Deputy Director for Physical Facilities, World Trade Department) – see NIST NCSTAR 1-6A, Appendix Figure A-7.

2.2.4 Response to Local Law 5/1973

In 1973, New York City Local Law No. 5 amended the New York City Building Code (effective January 18, 1973). Local Law No. 5 required, in part, the retrofit of existing unsprinklered office buildings 100 ft or higher. The New York City Department of Buildings permitted either:

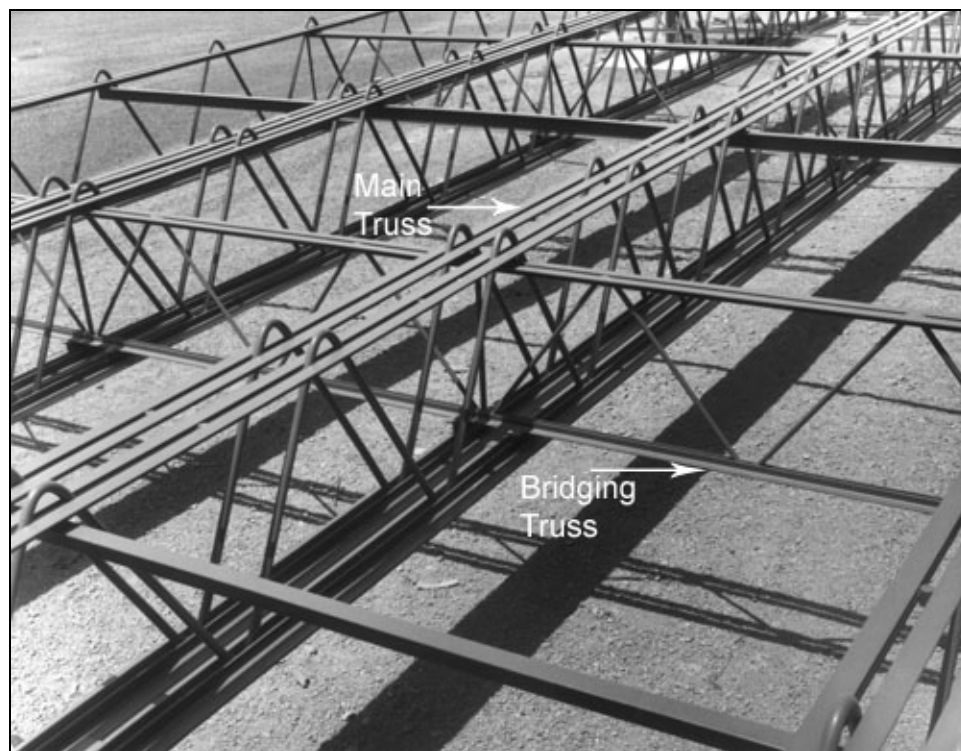
- Subdividing the floor area into compartments of specified square footage by fire separations (1-h or 2-h fire rated depending on the size of the compartment), or
- Providing sprinkler protection.

A code compliance evaluation of the towers, conducted in 1997, indicated that that all tenant floors in the two towers had been retrofitted with sprinklers (sprinklered) with the exception of four floors in WTC 1. In a 1999 update by the Port Authority, it was noted that all tenant floors had been sprinklered, and work was underway to complete sprinklering of the sky lobbies. In 2000, a property condition assessment report⁸ stated that the WTC towers were classified as “Class 1B – noncombustible, fire-protected, retrofitted with sprinklers in accordance with New York City Local Law 5/1973.”

2.2.5 Selection of Fire-Resistive Materials

Classification of a building leads to its overall fire endurance rating and ratings of the various structural components. The New York City Building Code, however, does not prescribe how the required fire resistance rating is to be achieved. The Port Authority chose to protect main structural components such as columns, spandrel beams, and floor trusses with sprayed fire-resistive material. This thermal protection technique was an established method for protecting columns, beams, and walls. In the 1960s, however, composite steel truss floor systems were usually protected using “lath and plaster” enclosures or fire-rated ceiling tiles. Figure 2–1 shows a mock-up of the steel truss system that supported the concrete floors in the World Trade Center towers, illustrating the thin steel rods that form the truss diagonals.

⁸ Property Condition Assessment of World Trade Center Portfolio, prepared for the Port Authority by Merritt & Harris, Inc., December 2000 – see NIST NCSTAR 1-6A, Appendix Figure A-41.



Source: (Photograph from about 1967) provided by Laclede Steel Co.

Figure 2-1. Mock up of floor truss system.

Since application of sprayed fire-resistive material to floor trusses was an innovative fire protection method, the Port Authority arranged for demonstrations to establish its feasibility for the World Trade Center (see Fig. 2-2). The demonstrations were successful, and in November 1968, the Port Authority awarded the contract for “spray fireproofing” of the interior portions (floor system and core) of the WTC towers to Mario & Di Bono Plastering Co., Inc. The fire protection of the exterior columns was included in the contract for the exterior aluminum cladding.



Source: Photograph provided by Laclede Steel Co.

Figure 2–2. Demonstration of application of Monokote sprayed fire-resistive material to floor trusses.

Several materials were considered for the sprayed thermal insulation. The exterior columns required insulation not only for fire protection but also to control column temperatures under service conditions. Alcoa recommended for the exterior columns the use of a sprayed material produced by U.S. Mineral Products, Co. known as BLAZE-SHIELD D. The same material was also selected for the floor trusses and core beams and columns. This product, however, contained asbestos fibers. On April 13, 1970, New York City issued restrictions on the application of sprayed thermal insulation containing asbestos. The use of BLAZE-SHIELD D was discontinued in 1970 at the 38th floor⁹ of WTC 1. The asbestos-containing material was subsequently encapsulated with a sprayed material that provided a hard coating. A green dye was added to the encapsulating material so that the asbestos-containing SFRM could be identified. Thermal protection of the remaining floors of WTC 1 and all of WTC 2 was carried out using BLAZE-SHIELD DC/F, a product that contained mineral wool (glassy fibers) in place of the crystalline asbestos fibers. On the basis of tests, it was reported that the thermal properties of BLAZE-SHIELD DC/F were equal to or “slightly better” than those of BLAZE-SHIELD D¹⁰.

2.2.6 Specified Thickness of Fire-Resistive Material

The thickness of fire-resistive material necessary to achieve the required fire endurance was being assessed in 1965, more than three years before the award of the thermal protection contract. At that time,

⁹ Various floor levels at which the asbestos-containing SFRM was reported to have been discontinued have been found in the documents reviewed for the investigation. Floor 38 is reported here but the exact floor is of no consequence in the investigation into the response of the towers to impact and fire.

¹⁰ Letter dated April 24, 1970 from S.W. Bell (Assistant Engineer, Fire Protection Department, Underwriters’ Laboratories, Inc.) to R. Monti (Construction Manager, World Trade Center, Port of New York Authority) – see NIST NCSTAR 1-6A, Appendix Figure A-29.

Emory Roth & Sons (ER&S), the Architect-of-Record, recommended 1 in. of thermal protection for the top and bottom chords of the floor trusses and 2 in. for other members of the trusses¹¹. WTC project specifications for sprayed fire-resistive material did not provide required material thickness or hourly ratings. In October 1969, the manager of project planning of WTC provided the following instructions to the contractor applying the sprayed insulation¹²:

“...Tower ‘A’ columns that are less than 14WF228 will require 2 3/16” thick of ‘Cafco Glaze [sic]-Shield ‘Type D’ spray-on fireproofing. All Tower columns equal to or greater than 14WF228 will require 1 3/16” of fireproofing...

All Tower beams, spandrels and bar joists requiring spray-on fireproofing are to have a 1/2” covering of ‘Cafco.’

The above requirements must be adhered to in order to maintain the Class 1-A Fire Rating of the New York City Building Code”

NIST’s review of available documents has not uncovered the reasons for selecting BLAZE-SHIELD fire-resistive material or the technical basis for specifying ½ in. thickness of thermal insulation for the floor trusses. The last sentence in the above excerpt indicates that, in October 1969, the towers were considered a Class 1A construction.

In February 1975, a fire broke out in WTC 1, spreading from the 9th to the 19th floor. After the fire, the Port Authority contracted Skilling, Helle, Christiansen, Robertson (SHCR), the Structural Engineer of Record for the design of the WTC towers, to assess the resulting structural damage and to report, in general, on the fire resistivity of the floor system. In its report to the Port Authority dated April 1, 1975¹³, SHCR stated,

“The fire of February, while reported in the press to have been very hot, did not damage a single primary, fireproofed element. Some top chord members (not needed for structural integrity [sic], some bridging members (used to reduce floor tremor and the like) and some deck support angles (used only as construction devices) were buckled an the fire – all were unfireproofed steel.”

The 1975 post-fire report by SCHR stated further that thermal protection of the top chords of the floor trusses was not necessary, except for the corners of the buildings where the floor acted as a two-way system in bending. Additionally, it was stated that protection of the bridging trusses was not required because the bridging trusses were “not required as a part of the structural system.” This information was used to guide the selection of the passive protection for the fire resistance tests conducted under Project 6 and discussed in Chapter 3.

¹¹ Letter dated December 23, 1965 from Julian Roth (ER&S) to Malcolm P. Levy (The Port of New York Authority) - see NIST NCSTAR 1-6A, Appendix Figure A-21.

¹² Letter dated October 30, 1969 from Robert J. Linn (Manager, Project Planning, The World Trade Center) to Mr. Louis DiBono (Mario & Di Bono Plastering Co., Inc.) - see NIST NCSTAR 1-6A, Appendix Figure A-23.

¹³ Report on WTC Fire dated April 1, 1975 from Skilling Helle Christiansen Robertson (SHCR) to the Port Authority – see NIST NCSTAR 1-6A, Appendix Figure A-30.

2.2.7 Upgrading SFRM on Floor Trusses

In 1995, the Port Authority performed a study¹⁴ to establish requirements for retrofit of SFRM to the floor trusses during major new construction or renovations when tenants vacated spaces in the towers. The study estimated the thermal protection requirements based on “the fireproofing requirements” for Design No. G805 contained in the Fire Resistance Directory published by Underwriters Laboratories (Underwriters Laboratories 2002). The study concluded that “a two hour fire rating for the steel floor joist trusses can be achieved by applying a 1 ½ inch thickness of spray-on mineral fiber fire protection material directly to the steel truss chords and webs.” In the years between 1995 and 2001, thermal protection was upgraded on a number of floors and some of these were affected by the fires on September 11, 2001. In WTC 1, floors 92 through 100 and 102 had been upgraded, and in WTC 2, floors 77, 78, 88, 89, 92, 96 and 97 had been upgraded.

In 1999, the Port Authority established “guidelines regarding fireproofing repairs, replacement, and upgrades” for the towers¹⁵. The guidelines for tenant spaces may be summarized as follows:

- For full floors undergoing new construction or renovation, the floor trusses should be protected with 1 ½ in. of sprayed mineral fiber fire-resistive material. Retrofit of thermal protection requires removal of existing material and controlled inspection.
- For “tenant spaces less than a full floor undergoing either new construction or renovation,” the floor trusses “need only meet the original construction standard. Fireproofing shall be inspected and patched as required to the greater of ¾ in. or to match existing” if it has already been upgraded to 1 ½ in.

In July 2000, Buro Happold, an engineering consultant, commissioned by the Port Authority to conduct a fire-engineering assessment of the insulation of the floor trusses, issued a report on the requirements of the fire resistance of the floor system of the towers¹⁶. This report stated that BLAZE-SHIELD DC/F was used on the majority of the floor trusses. Based on calculations and a risk assessment, the consultant concluded that:

- “The structural design has sufficient inherent fire performance to ensure that the fire condition is never the critical condition with respect to loading allowances.
- A single coat application is possible.
- Significant savings are possible.

¹⁴ White paper titled “Fireproofing Requirements for World Trade Center Tenant Floor Joist Construction that Requires Installation Due to Asbestos Removal or Local Removal to Facilitate Construction” transmitted by way of memorandum from Joseph Englot (Chief Structural Engineer, Port Authority) to Peter Sweeney (Engineering Program Manager, Port Authority) on August 18, 1995 – see NIST NCSTAR 1-6A, Appendix Figure A-34.

¹⁵ Memorandum dated March 24, 1999 from Alan L. Reiss (Director, World Trade Department) to John Castaldo and Kent Piatt (Port Authority) – see NIST NCSTAR 1-6A, Appendix Fig. A-36.

¹⁶ World Trade Center: Fire Engineering of Steelwork – Phase 1 Report, Buro Happold Consulting Engineers PC, February 2000 – see NIST NCSTAR Appendix Figure A-40.

- The target reduction of fiber content and increased long term durability can be achieved.
- Alternative materials should be considered.”

As quoted, the report states that significant savings were possible by reducing the fiber content and considering alternative materials. The report suggested that the thickness of the SFRM could be reduced to ½ in. if the material properties at ambient temperature are applicable at higher temperature. The report recognized the lack of available temperature-dependent material data for BLAZE-SHIELD DC/F. Thus, considering the uncertainties in the material properties and having the understanding of material degradation with temperature and time, it was recommended that 1.3 in. of fire-resistive material be used for the floor trusses.

Later, in December 2000, the final draft of a report on *Property Condition Assessment of World Trade Center Portfolio*¹⁷ stated that, based on existing conditions “The rating of the structural fireproofing in the Towers and subgrade has been judged to be an adequate 1-hour rating considering the fact that all Tower floors are now sprinklered.” The report also noted the ongoing Port Authority program to upgrade the fire-resistive material thickness to 1 ½ in. in order to achieve a 2-hour fire rating.

2.2.8 Need for Fire Resistance Tests

The fire protection of a truss-supported floor system by directly applying sprayed fire-resistive material to the trusses was innovative at the time the WTC towers were designed and constructed. While the benefits of conducting fire endurance tests were realized by individuals involved in the 1967 demonstrations of the application of SFRM, apparently no tests were conducted on the floor system used in the WTC towers. The Architect-of-Record, in a letter to the Port Authority¹⁸ addressing issues that “...might not conform to the New York City Building Code...”, dated July 25, 1966, stated,

“Obviously, with so many penetrations of the floor system the fire rating of the floor construction is of an indeterminate value unless tested. It is doubtful if it will meet a 3-hour test.”

In the 1975 post-fire report to the Port Authority¹⁹, the Structural Engineer-of-Record stated,

“These special floor assemblies would best be fire tested—since actual testing is the only known, reliable method known [sic] to assure compliance with fire testing requirements.”

Communication from the Port Authority in 2003²⁰ confirms that there is no record of fire endurance testing of assemblies representing the thermally protected floor system.

¹⁷ Property Condition Assessment of World Trade Center Portfolio, prepared for the Port Authority by Merritt & Harris, Inc., December 2000 – see NIST NCSTAR 1-6A, Appendix Figure A-41.

¹⁸ Letter dated July 25, 1966 from Harry J. Harman (ER&S) to Malcolm P. Levy (Port of New York Authority) - See NIST NCSTAR 1-6A, Appendix Figure A-26.

¹⁹ Report on WTC Fire dated April 1, 1975 from Skilling Helle Christiansen Robertson (SHCR) to the Port Authority – see NIST NCSTAR 1-6A, Appendix Figure A-30 - see NIST NCSTAR 1-6A, Figure A-43.

²⁰ See NIST NCSTAR 1-6A, Appendix Figure A-31.

To address some of these open issues, standard fire resistance tests of the floor system used in the WTC towers were conducted as part of this investigation. Results of four tests and the fire resistance ratings determined from these tests are presented in Chapter 3 of this report and in NIST NCSTAR 1-6B.

2.2.9 Maintenance of SFRM in Elevator Shafts

Throughout the life of the WTC towers, the structural members that required the largest amount of inspection and maintenance within the core were the exposed columns and beams within the elevator shafts. Except for the floors, these columns and beams were the only accessible fire-protected elements in the buildings. Adhesion failures were common, likely because of the exposed conditions of the columns and the inherently low bond strength of the SFRM.

Inspections of the shafts and accessible columns were reported as early as 1971. Problems were noted in the form of fallen insulation or with the over-spray material used to provide a harder surface. In 1993, the Port Authority commissioned Leslie E. Robertson Associates (LERA) to carry out a continuing Structural Integrity Inspection Program to appraise the condition of the accessible columns located in the core of the towers (see NIST NCSTAR 1-1C). The columns were inspected visually for signs of rusting, cracking, bowing, and loss of thermal insulation. During the first inspection, carried out in 1993, particular shafts were chosen based on the quantity and types of accessible columns, and the convenience to the Port Authority. Subsequent inspections involved sampling of the structural components and assemblies, which were more important to the structural integrity of the towers, and at locations with a relatively higher potential for defects and problems. The Structural Integrity Inspection Report²¹ stated that the accessible columns in selected elevator shafts in WTC 1 and WTC 2 were “generally in good condition, no structural deficiencies such as cracking or bowing were found, the most common irregularities observed were missing fireproofing and light surface rusting of the exposed steel.” Based on the inspections, LERA recommended “that remedial action to be taken where spray fireproofing is damaged, deteriorated or missing and where there is corrosion of the column base due to water leaks at elevator pits.”

2.3 AS-APPLIED THICKNESS OF SFRM

2.3.1 1994 Measurements from WTC 1 Floors 23 and 24

In its search of documents, NIST found no information related to measurements of the thickness of thermal insulation taken during construction. Reviewed documents, however, indicate that thickness appears to have been checked during construction. Recorded information on the in-place condition of the sprayed thermal insulation for the floor system first appeared in 1990 in the form of “Sample Area Data Sheets,” which provided qualitative comments on the state of the in-place SFRM. Information regarding quantitative inspection of existing fire-resistive material appeared in documentation from 1994. That year, the Port Authority performed a series of thickness measurements of the existing SFRM on floors 23 and 24 of WTC 1 (see NIST NCSTAR Appendix A Figure A-58). Six measurements were taken from “both flanges and web” of each of 16 randomly chosen trusses on each floor (see Table 2-1). Measured average thickness varied between 0.52 in. and 1.17 in. For the 32 measurements (16 on each floor), the overall average was 0.74 in., and the standard deviation of these averages was 0.16 in. Four of

²¹ Structural Integrity Inspection Report dated 14 April 1995 by LERA - see NIST NCSTAR 1-6A, Appendix Figure A-57.

the 32 floor trusses had average thicknesses between 0.52 in. and 0.56 in. These measurements suggest that the minimum average thickness exceeded ½ in. Analysis of the reported mean thicknesses data indicated that a lognormal distribution gave a better representation of the distribution than did a normal distribution.

Table 2–1. Average SFRM thickness from six measurements taken in 1994 on each of 16 random floor trusses on floors 23 and 24 of WTC 1.

| SFRM Thickness (in.) | |
|----------------------|----------|
| Floor 23 | Floor 24 |
| 0.60 | 0.76 |
| 0.53 | 0.60 |
| 0.70 | 0.90 |
| 0.76 | 0.72 |
| 0.88 | 0.64 |
| 0.89 | 0.80 |
| 0.83 | 0.68 |
| 1.17 | 0.65 |
| 0.88 | 0.67 |
| 0.71 | 0.77 |
| 0.82 | 0.96 |
| 0.52 | 0.66 |
| 0.69 | 0.65 |
| 0.52 | 1.11 |
| 0.64 | 0.95 |
| 0.52 | 0.56 |

Source: Data provided by The Port Authority of New York and New Jersey.

2.3.2 Analysis of Photographs

Additional SFRM thickness data were developed by evaluating photographs of floor trusses taken during inspections. Two groups of photographs were used. The first group included images of floor trusses from WTC 1 (floors 22, 23, and 27). These photographs were taken in the mid-1990s and illustrated conditions prior to the upgrade carried out by the Port Authority. Thus, SFRM thickness on the photographed trusses would be expected to be at least ½ in. The second group of photographs, taken in 1998, illustrated conditions after initiation of the upgrade program that began in 1995. These photographs were of trusses for floor 31 and below in WTC 1. Selection of the photographs to be used to estimate thickness of SFRM was based on clarity of SFRM edges and the presence of a feature of known dimension to provide a reference measurement. Figure 2–3 shows one such photograph used for the estimation of SFRM thickness. “Reference” points to a known dimension of the steel member which connects the damper to the bottom chord of the truss.

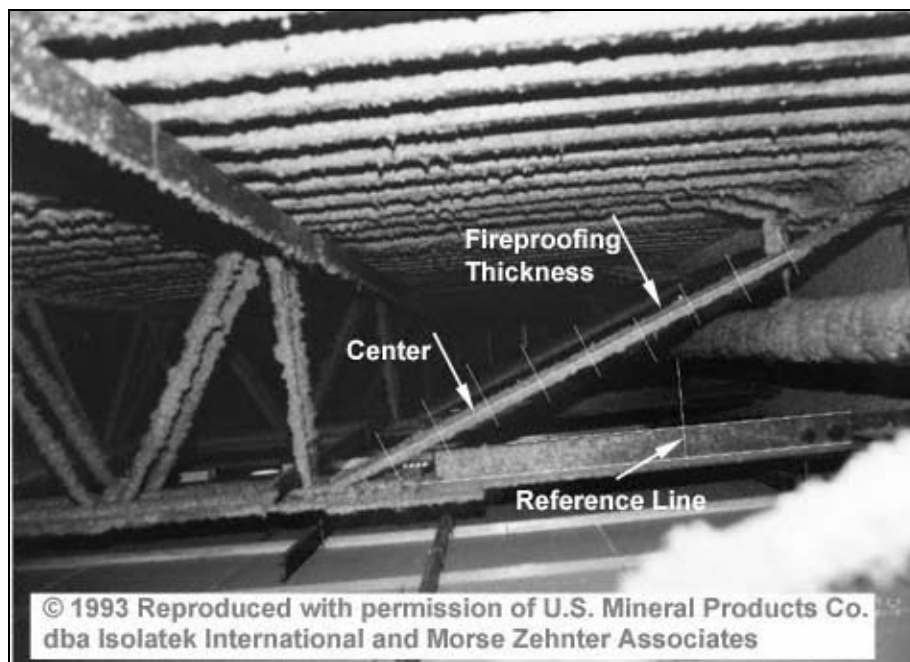


Figure 2–3. Example of measurement procedure used to estimate SFRM thickness from photographs.

For the floors that had not been upgraded, it was observed that the estimated thickness of SFRM on the webs of the main trusses tended to be greater than that on either the diagonal struts or on the webs of the bridging trusses. Hence, estimates of SFRM thickness for non-upgraded floors were divided into three groups: webs of main trusses, webs of bridging trusses, and diagonal struts at the exterior wall end of the truss.

It was not possible to estimate the thickness of the SFRM on any truss element except the round bars. Consequently, for the upgraded floors in WTC 1 that were included in the second group of photographs, only estimates of the thickness on the webs of the main trusses were made. The average, standard deviation, and coefficient of variation were computed for the total number of measurements in each of these groups. The results are summarized as follows:

- Main trusses before upgrade (85 measurements): Average thickness 0.6 in., standard deviation = 0.3 in., and coefficient of variation = 0.5.
- Bridging trusses before upgrade (52 measurements): Average thickness 0.4 in., standard deviation = 0.25 in., and coefficient of variation = 0.6.
- Diagonal struts before upgrade (26 measurements): Average thickness 0.4 in., standard deviation = 0.2 in., and coefficient of variation = 0.5.
- Main trusses after upgrade (52 measurements): Average thickness 1.7 in., standard deviation = 0.4 in., and coefficient of variation = 0.2.

2.3.3 Port Authority Data on Upgraded SFRM on Trusses

In the 1990s, the thermal protection for some floor trusses was upgraded to a specified thickness of 1 ½ in. as tenants vacated their spaces. According to the Port Authority²², 18 floors of WTC 1 and 13 floors of WTC 2 were upgraded. The Port Authority also stated that: “The entire impact zone for Tower 1 (92-99) was upgraded with 1 ½" spray-on fireproofing. Only the 78th floor was upgraded with the 1 ½" spray-on fireproofing within the impact zone in Tower 2 (78-84).” The Port Authority provided Construction Audit Reports to the NIST Investigation that included the density, average thickness, and strength characteristics of the upgraded SFRM (BLAZE-SHIELD II) as of 2000. In 2004, the Port Authority provided NIST reports of the individual measurements for many of the average thicknesses recorded in the Construction Audit Reports. These individual measurements permitted analysis of the variation of thickness at a cross section of a truss member and the variation in average thickness from truss to truss. A total of 18 data sets for WTC 1 (including floors 93, 95, 98, 99, and 100) and 14 data sets for WTC 2 (including floors 77, 78, 88, 89, and 92) were analyzed.

Data analysis indicated that the thickness measurements from the two towers represented similar distributions, and so the data were combined. It was also found that the distribution of thickness values could be approximated by a lognormal distribution.

The overall average thickness determined from the 256 individual measurements was found to be 2.5 in. with a standard deviation of 0.6 in. Thus, the average SFRM thickness on the upgraded upper floors appears to be greater than that estimated from photographs taken on the upgraded lower floors.

The overall standard deviation of 0.6 in. includes two contributions: (1) the variation of thickness at a cross section (within-truss variability), and (2) the variation of average thickness between trusses (between-truss variability). From analysis of variance, it was found that the within-truss standard deviation was 0.4 in., and the between-truss standard deviation was also 0.4 in. The within-truss standard deviation of 0.4 in. is similar to the standard deviation of the estimated individual thicknesses obtained from analysis of the photographs of upgraded main trusses.

2.4 EFFECT OF THE VARIABILITY OF SFRM THICKNESS ON THERMAL RESPONSE

As would be expected, and as confirmed by analyses of available data, the thickness of thermal insulation can have high variability. The effects of thickness variation on thermal response of a member are not well known. A sensitivity study using finite element analyses to simulate heat transfer was conducted to investigate the sensitivity of steel temperature rise to the variability in SFRM thickness.

2.4.1 Effects of Thickness Variability and Gaps in SFRM

A finite element model for thermal analysis was developed for a plate protected on both faces with SFRM of variable thickness. A random number generator was used to assign a lognormally distributed random thicknesses of insulation along the length of the plate, and the plate was subjected to a thermal flux representative of a 1,100 °C fire. A parametric study was conducted with average thickness of fire-

²² Structural Integrity Inspection Report dated 14 April 1995 by LERA - see NIST NCSTAR 1-6A, Appendix Figure A-57.

resistive material varying from 0 in. to 2 in. in increments of 1/4 in. and a standard deviation varying from 0 in. to 1 in. Steel temperatures at five locations in the plate were recorded at 30 min, 60 min, 90 min, and 120 min of exposure to the thermal flux. For more details, refer to NIST NCSTAR 1-6A

The simulations showed that when the SFRM thickness is variable, the isotherms in the steel follow the shape of the SFRM surface contour. Thus, the temperature history at any point in the steel depends on the local thickness of the insulation. It was shown that an increase in thickness variability reduced the time to reach a critical temperature. Conversely, for a given time to reach a specific temperature, the required average thickness of thermal insulation increased with increasing variability in thickness of SFRM.

In addition to the effect of variation in thickness, the effect of missing SFRM over a portion of a member was studied. Figure 2–4 shows an example of a “gap” in fire-resistive material on a diagonal member of a bridging truss. As expected, thermal analysis results indicated that the bare steel where the insulation was missing reached the gas temperature quickly, which led to a transmission of heat into the interior steel.

The combined effects of variation in insulation thickness and extent of missing material were examined by a full factorial design study with the following factors:

- Average thickness of insulation varying from 0 in. to 2.0 in. in 1/4 in. increments;
- Standard deviation of insulation thickness of 0 in., 0.25 in., 0.5 in., 0.75 in., and 1.0 in.; and
- Length of missing insulation varying from 0 in. to 30 in., in 6 in. increments.

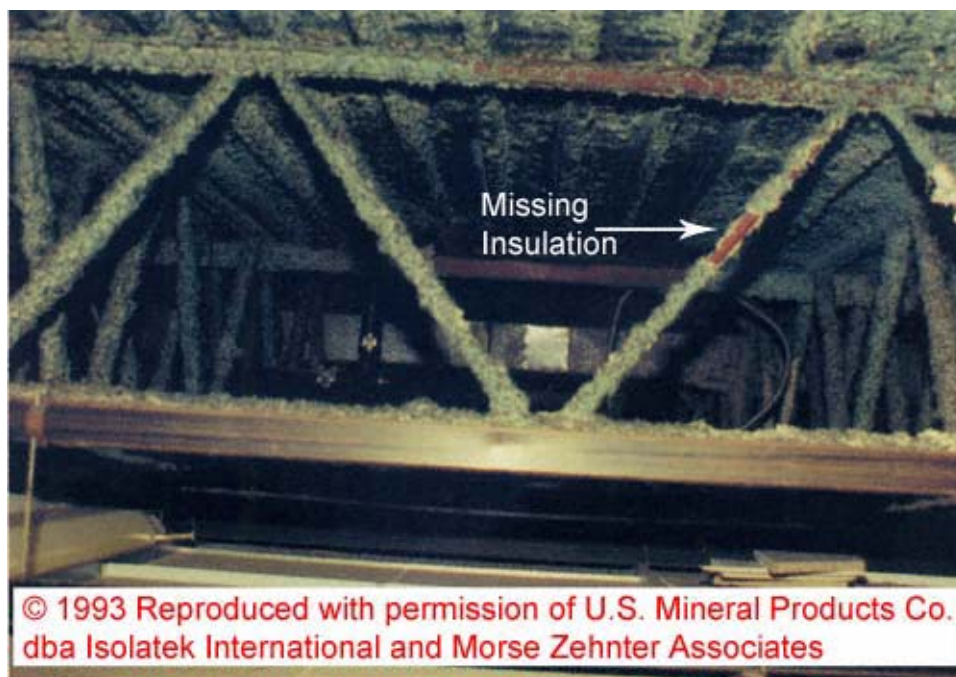


Figure 2–4. Example of “gap” in fire-resistive material on diagonal member of a bridging floor truss.

The results were summarized by a series of temperature-time plots representing the response for different combinations of the three factors (see NIST NCSTAR 1-6A). As expected, increasing the variability of insulation thickness or gap length reduced the time to reach a given critical temperature. Because there was not sufficient information to determine the frequency of occurrence of these gaps or their typical locations, gaps in insulation were not considered in the thermal modeling.

2.4.2 Thermally equivalent thickness of SFRM

A sensitivity study, reported in NIST NCSTAR 1-6A, indicated that increased variation in thickness reduced the “effective thickness” of the SFRM. It would be impractical to attempt to account for the variation in SFRM thickness in the thermal modeling of the WTC towers by introducing variable thickness insulation material in the finite-element models. As an alternative, a “thermally equivalent uniform thickness” was determined that would result in the same thermo-mechanical response of a member as the variable thickness thermal protection. In the analyses, an insulated 1 in. diameter by 60 in. long steel bar was subjected to the heat flux arising from a 1,100 °C fire. The temperature history along the length of the bar was computed and was used to calculate the length change of the unrestrained bar under a tensile stress of 12,500 psi. The bar was assumed to be similar to the steel used in the WTC floor trusses, and the temperature dependence of the coefficient of thermal expansion and the modulus of elasticity was based on NIST measurements.

The average SFRM thickness and variability in thickness used in the models were based on the measurements (summarized in NIST NCSTAR 1-6A) for the web bars of the main trusses with both the original insulation and the upgraded insulation. The following values were investigated:

- Original conditions: Average thickness = 0.75 in., standard deviation = 0.3 in., lognormal distribution.
- Upgraded conditions: Average thickness = 2.5 in., standard deviation = 0.6 in., lognormal distribution.

Three sets of random data were generated for each condition. When the randomly selected thicknesses of each element were applied to the bar, abrupt changes in insulation thickness along the length of the bar resulted. This “rough” surface texture was not representative of actual conditions. As an alternative, five-point averaging was used to reduce the roughness of the insulation profile and produce a profile that was consistent with photographic evidence. Care was taken to ensure the “smoothed” profiles maintained the required variability (i.e., mean and standard deviation).

The calculated temperature histories of the bar elements were used to calculate the unrestrained length changes of the bar due to thermal expansion and the applied stress. For comparison, elongations of the bar with different uniform thicknesses of thermal insulation were calculated. The “thermally equivalent thickness” was taken as the uniform thickness that resulted in approximately the same elongation of the bar as produced with the variable thickness insulation. Figure 2–5 shows a plot of the thermo-mechanical response of 1 in. diameter bar with both rough and smooth random thickness SFRM and thermally equivalent uniform thickness SFRM.

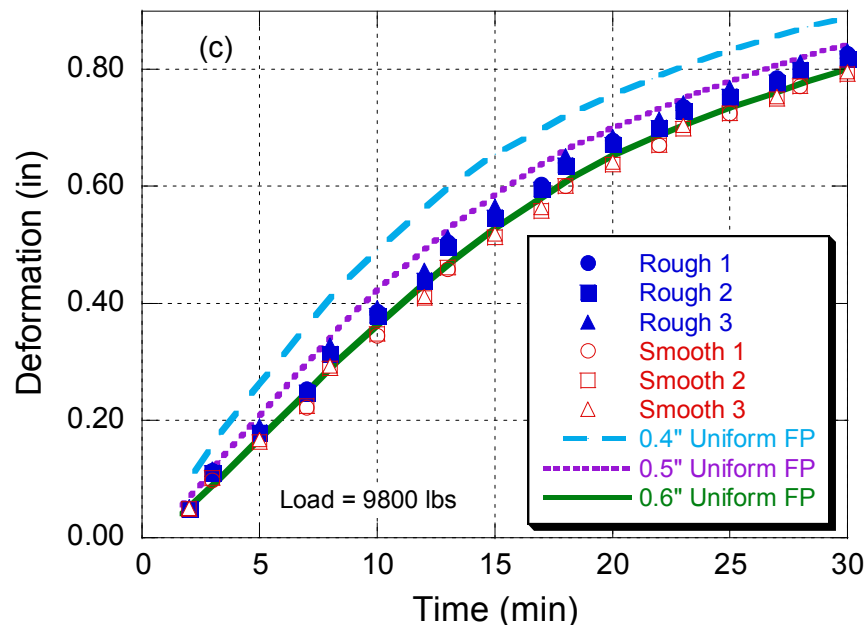


Figure 2–5. Thermo-mechanical response of 1 in. bar compared with uniform thickness SFRM.

On the basis of these analyses, it was concluded that SFRM with a uniform thickness of 0.6 in. provides thermally equivalent protection to an average thickness of 0.75 in. and a standard deviation of 0.3 in. (see the solid green line in Fig. 2–5). Similarly, 2.2 in. of uniform thickness insulation is thermally equivalent to an average SFRM thickness of 2.5 in. with a standard deviation of 0.6 in.

2.4.3 Thickness of SFRM Used for Thermal Analyses

Analyses of available data on SFRM thickness and thermal modeling revealed the following:

- From measurements of SFRM thickness, the average values exceeded the specified thickness.
- SFRM thickness was variable, and the distribution of thickness in the floor trusses was best described by a lognormal distribution.
- The standard deviation of SFRM thickness on the trusses varied between about 0.3 in. and 0.6 in.
- The standard deviation of SFRM thickness on columns and beams from the core tended to be lower, with a value of 0.2 in. obtained from the available data.
- No information was available on the SFRM thickness on the exterior columns and spandrel beams.
- Variation in thickness reduces the effectiveness of SFRM, and the thermally equivalent uniform thickness, based on thickness measurements, exceeded the specified thickness.

Based on the findings given above, the following uniform thicknesses for the undamaged SFRM were used in the thermal analyses to determine temperature histories of the WTC towers under various fire scenarios:

- Original SFRM thickness on all floor trusses (primary and bridging): 0.6 in.
- Upgraded SFRM thickness on all floor trusses (primary and bridging): 2.2 in.
- Thermal protection on other elements: the specified thickness.

The choice of specified thickness for those members lacking data is justified by the following offsetting factors: (1) measured average thicknesses were found to exceed specified values, and (2) variation in thickness reduces the effectiveness of the SFRM.

2.5 SUMMARY OF SFRM THICKNESS

Establishing the specified SFRM material and thickness for the protection of the steel trusses, columns and beams in the WTC towers required the review of documents, correspondence, photographs, and videos that chronicled the decisions made in selection of the passive fire protection in the towers. Since the towers were destroyed completely when they collapsed on September 11, 2001, establishing the in-place thicknesses and condition of the SFRM required analysis of available thickness measurement data and interpretation of available photographs. Lastly, the determination of appropriate thickness of the SFRM for use in thermal calculations required finite element thermal analyses to establish a thermally equivalent uniform thickness. Table 2–2 summarizes the specified thickness, in-place (or as-applied) thickness, and thermally equivalent thickness for the structural elements that were fire-protected using SFRM.

Table 2–2. Summary of specified, in-place and thermally equivalent thickness of SFRM

| Building Component | Material | Thickness (in.) | | |
|----------------------------|-------------------|--------------------------|---------------------|----------------------|
| | | Specified ⁽¹⁾ | In-place | Thermally Equivalent |
| FLOOR SYSTEM | | | | |
| Original | | | | |
| Main trusses | BLAZE-SHIELD DC/F | 1/2 | 0.75 | 0.6 |
| Main truss diagonal Strut | BLAZE-SHIELD DC/F | 1/2 | 0.75 ⁽²⁾ | 0.6 |
| Bridging trusses – One-Way | BLAZE-SHIELD DC/F | 1/2 ⁽³⁾ | 0.38 ⁽⁴⁾ | (5) |
| Bridging trusses – Two-Way | BLAZE-SHIELD DC/F | 1/2 ⁽³⁾ | 0.75 ⁽⁴⁾ | 0.6 ⁽⁶⁾ |
| Metal deck | | (7) | (8) | (9) |
| Upgraded | | | | |
| Main trusses | BLAZE-SHIELD II | 1 1/2 | 2.5 | 2.2 |
| Main truss diagonal Strut | BLAZE-SHIELD II | 1 1/2 | 2.5 | 2.2 |
| Bridging trusses | BLAZE-SHIELD II | 1 1/2 | 2.5 | 2.2 |
| Metal deck | | (7) | (8) | (9) |

| Building Component | Material | Thickness (in.) | | |
|-------------------------------|---------------------|--------------------------|----------|----------------------|
| | | Specified ⁽¹⁾ | In-place | Thermally Equivalent |
| EXTERIOR WALL PANEL | | | | |
| Box columns | | | | |
| Exterior faces (plates 1 & 2) | BLAZE-SHIELD DC/F | 1 3/16 | (8) | 1.2 |
| Interior face (plate 3) | Vermiculite plaster | 7/8 | (8) | 0.8 |
| Spandrels (plate 4) | | | | |
| Exterior face | BLAZE-SHIELD DC/F | 1/2 | (8) | 0.5 |
| Interior face | Vermiculite plaster | 1/2 | (8) | 0.5 |
| CORE COLUMNS | | | | |
| Wide flange columns | | | | |
| < WF14x228 | BLAZE-SHIELD DC/F | 2 3/16 | (8) | 2.2 |
| ≥ WF14x228 | BLAZE-SHIELD DC/F | 1 3/16 | (8) | 1.2 |
| Box columns | | | | |
| < 228 lb/ft | BLAZE-SHIELD DC/F | (6) | (8) | 1.2 ⁽¹⁰⁾ |
| ≥ 228 lb/ft | BLAZE-SHIELD DC/F | (6) | (8) | 2.2 ⁽¹⁰⁾ |
| CORE BEAMS | | | | |
| All | BLAZE-SHIELD DC/F | 1/2 | (8) | 0.5 |

- (1) In no case was a specified SFRM material or thickness found on contract documents. Rather, the term “specified” means material and thicknesses determined from correspondence among various parties.
- (2) Anecdotal and photographic evidence suggests that there may have been, in general, less than 0.75 in. thick SFRM on the diagonal struts, but there is insufficient evidence to estimate what that value should be.
- (3) Thickness of SFRM on bridging trusses was not expressly specified (only “trusses” were mentioned), and anecdotal and photographic evidence as well as written documentation, suggests that the one-way and two-way floor areas were treated differently; specifically SFRM was required for the two-way floor areas and, while not required, was also applied in the one-way areas.
- (4) Analysis of photographs of originally applied SFRM indicates that the thickness on the bridging trusses was approximately one half that on the main trusses.
- (5) A thermally equivalent thickness was not calculated for this condition and a value of 0.6 in. was used for the thermal analyses.
- (6) 1975 report by LERA indicates bridging trusses in two-way areas were fire protected.
- (7) Not specified.
- (8) Unknown or not able to be determined.
- (9) Not included in analyses.
- (10) Since no information regarding specified thickness was found and installed thickness could not be determined, the same thickness specified for the wide flange columns (based on weight of section per foot) was used for thermal analyses.

2.6 THERMOPHYSICAL PROPERTIES

To provide thermophysical property data for modeling the fire-structure interaction of the towers, the thermal conductivity, specific heat capacity, and density of the SFRMs used in the WTC towers were determined as a function of temperature up to 1,200 °C (2,190 °F). Since there are no ASTM test methods for characterizing the thermophysical properties of SFRMs as a function of temperature, ASTM test methods developed for other materials were used. Samples were prepared by the manufacturers of the fire-resistive materials, which included BLAZE-SHIELD DC/F, which was originally applied, BLAZE-SHIELD II, used in the recent upgrade, and Monokote MK-5, assumed to be similar to the

vermiculite plaster applied to the inside surface of the exterior columns. Since Monokote MK-5 is no longer produced, the samples were manufactured specially for this study according to the original MK-5 formulation.

2.6.1 Thermal Conductivity

The thermal conductivity measurements were performed according to ASTM C 1113, Standard Test Method for Thermal Conductivity of Refractories by Hot Wire (Platinum Resistance Thermometer Technique) (ASTM 1999). The room temperature values were in general agreement with the manufacturer's published values for BLAZE-SHIELD DC/F and BLAZE-SHIELD II. No published values were available for Monokote MK-5. The thermal conductivities increased with temperature as shown in Table 2–3.

Table 2–3. Measured thermal conductivity as a function of temperature.

| Temperature (°C) | Thermal Conductivity (W/(m · K))* | | |
|------------------|-----------------------------------|-----------------|---------------|
| | BLAZE-SHIELD DC/F | BLAZE-SHIELD II | Monokote MK-5 |
| 25 | 0.0460 | 0.0534 | 0.0954 |
| 50 | 0.0687 | 0.0745 | 0.0926 |
| 100 | 0.0628 | 0.0921 | 0.1252 |
| 200 | 0.0810 | 0.0895 | 0.0919 |
| 300 | 0.1106 | 0.1057 | 0.1214 |
| 400 | 0.1286 | 0.1362 | 0.1352 |
| 500 | 0.1651 | 0.1689 | 0.1504 |
| 600 | 0.2142 | 0.2156 | 0.1622 |
| 800 | 0.3380 | 0.2763 | 0.1895 |
| 1000 | 0.5010 | 0.3708 | 0.2618 |
| 1200 | 0.5329 | 0.4081 | ----- |

* Results are presented in SI units because this system was used to make the measurements. To convert to BTU · in / (h · ft² · °F) divide by 0.1442279.

2.6.2 Specific Heat Capacity

Specific heat capacity determinations were made with the same instrument as for thermal conductivity with a slight modification. A thermocouple was added to the system, which permitted determination of the thermal diffusivity of the material. Knowing the thermal conductivity, the thermal diffusivity, and the density obtained from other tests, the specific heat capacity was calculated. The inherently indirect nature of the technique used precluded the direct measurements of specific heat capacity peaks associated with chemical reactions.

To examine the chemical reactions associated with heating of SFRMs, differential scanning calorimetry (DSC) measurements were made in accordance with ASTM E 1269, Standard Test Method for Determining Specific Heat Capacity by Differential Scanning Calorimetry (ASTM 2001). Differential thermal analysis (DTA) which is a "fingerprinting" technique that provides information on the chemical reactions, phase transformations, and structural changes that occur in a specimen during a heating or

cooling cycle. These tests revealed large peaks in the specific heat capacities in the range of 125 °C to 140 °C, which were accounted for in the thermal analyses conducted in the course of this investigation.

2.6.3 Density

Bulk densities of the SFRMs were not measured directly (except at room temperature) but were calculated from thermal gravimetric analysis (TGA) and thermal expansion measurements. The TGA tests to measure mass loss were performed according to ASTM E 1131, Standard Test Method for Compositional Analysis by Thermogravimetry (ASTM 1998). Thermal expansion measurements were performed according to ASTM E 228, Standard Test Method for Linear Thermal Expansion of Solid Materials (ASTM 1995). Since the materials were not isotropic, separate measurements were performed in the plane of the SFRM sample and perpendicular to the free surface of the sample. Consequently, measurements were performed both in the plane of deposition and perpendicular to the plane of deposition. The density values were calculated from the results of the thermal gravimetric analysis and thermal expansion. The room temperature densities were found to be 15.7 pcf for BLAZE-SHIELD DC/F, 20.8 pcf for BLAZE-SHIELD II, and 19.4 pcf for Monokote MK-5.

2.6.4 Thermophysical Properties of Gypsum Panels

Thermophysical properties of four representative types of commercially available gypsum panels were examined. The materials were:

- 5/8 in. thick gypsum panel A,
- ½ in. thick gypsum panel,
- 5/8 in. thick gypsum panel B, and
- 1 in. thick gypsum liner panel.

Thermal conductivity was measured using the heated probe technique described in ASTM D 5334, Standard Test Method for Determination of Thermal Conductivity of Soil and Soft Rock by Thermal Needle Probe Procedure (ASTM 2000b). In general, the thermal conductivity initially decreased as the temperature increased to 200 °C and then increased with increasing temperature above 300 °C.

Specific heat capacities of the cores of the four gypsum panel samples were measured using a differential scanning calorimeter according to ASTM E 1269, Standard Test Method for Determining Specific Heat Capacity by Differential Scanning Calorimetry (ASTM 2001). The four panels had similar specific heat capacities as a function of temperature, with a high peak at about 150 °C and a smaller peak at about 250 °C.

Densities were calculated from the thermogravimetric analysis and linear thermal expansion measurements. All four materials showed the same trend as a function of temperature. The variation in density with temperature is associated with the mass loss and the change in volume of the gypsum material.

2.7 ESTIMATION OF SFRM DISLODGED BY AIRCRAFT IMPACT

To analyze the thermo-structural response of the WTC towers during the fires after the aircraft impacts, it was necessary to estimate the extent of dislodged thermal insulation on structural members.

Dislodgement could occur as a result of direct impact by debris or due to inertial forces resulting from aircraft impact. The dislodgement due to flying debris was estimated from results of the aircraft impact analyses that predicted damage to the structure (columns, beams and floors), partitions, and furnishings. In addition, a study was conducted to estimate dislodgement due to inertial forces. NIST established conservative estimates for the extent of dislodged SFRM. However, since NIST was not able to establish robust criteria to predict the extent of vibration-induced dislodgement, insulation dislodged by inertial effects other than that dislodged by direct debris impact was ignored and not included in the analyses. The methodology and criteria for estimating the extent of damage and dislodgement of SFRM from results of the aircraft impact analysis are presented in Chapter 5.

2.7.1 In-place Density and Bond Strength

The magnitude of the inertial forces resulting from shock and vibration is dependent on the density and thickness of the thermal insulation. The insulation would dislodge if the stresses resulting from inertial forces exceed the bonding, or adhesive/cohesive strength of the insulation.

The Port Authority provided data on in-place density and bond strength characteristics of the thermal insulation (BLAZE-SHIELD II) applied to the floor trusses during tenant alterations. According to the manufacturer, BLAZE-SHIELD II is about 20 percent denser and has about 20 percent greater adhesive/cohesive strength than BLAZE-SHIELD DC/F. The Port Authority test reports indicate that bond strength was determined in accordance with ASTM E 736, Standard Test Method for Cohesion/Adhesion of Sprayed Fire-Resistive Materials Applied to Structural Members (ASTM 2000a). The method involves gluing a jar screw cap to the surface of the thermal insulation, and after the glue has cured, pulling on the cap until failure of the SFRM occurs. The force required to pull off the cap is divided by the area of the cap, and reported as the “cohesive/adhesive strength.” Failure is described as “cohesive” if it occurs within the insulation and is defined as “adhesive” if it occurs at the interface with the substrate.

Analysis of the reported density values indicated no statistically significant differences between the average SFRM densities in the two towers. The overall average density was 18.9 pcf with a standard deviation of 3.2 pcf, giving a coefficient of variation of 16 percent.

Analysis of the bond strength values indicated that there were statistically significant differences between the average bond strengths for the different floors, but there was no statistically significant difference between the average bond strengths for the two towers. The overall average bond strength was 302 psf, with a standard deviation of 91 psf, giving a coefficient of variation of 30 percent. This average value is less than the “tested performance” value of 360 psf indicated in the manufacturer’s catalogs, but this published value is for tests under controlled conditions and may not be representative of field strengths. The manufacturer’s product literature dated February 2002 refers to average bond strength of 150 psf as “standard performance,” and the same value is used in its guide specification for BLAZE-SHIELD II.

2.7.2 Specimen Preparation and Test Procedures

While the in-place bond strength data of BLAZE-SHIELD II reported by the Port Authority appear to indicate acceptable performance, ASTM E 736 tests do not provide sufficient information for predicting whether insulation would be dislodged from structural members under various impact conditions. The standard test does not provide unambiguous values of cohesive and adhesive strengths, and it does not provide tensile strength in a direction parallel to the surface, that is, the in-plane cohesive strength. Thus, tests were conducted by NIST to determine different tensile strength properties of sprayed thermal insulation. BLAZE-SHIELD DC/F was used because the Port Authority data did not include tests of this material.

Test specimens were made by applying the SFRM to $\frac{1}{4}$ in. steel plates measuring 8 in. by 16 in. One half of the plates were coated with primer paint. Nominal SFRM thicknesses of $\frac{3}{4}$ in. and 1 $\frac{1}{2}$ in. were applied. Thickness was built up in several passes of the spray nozzle. Gentle hand rubbing was used to remove local high spots and produce reasonably uniform thicknesses. The plate specimens were allowed to dry for over five months in the laboratory before testing. Companion specimens were weighed periodically to determine loss of water, and it was found that the 1 $\frac{1}{2}$ in. thick specimen reached equilibrium in about one month.

Tests were devised to determine adhesive strength, cohesive strength normal to the surface, and cohesive strength parallel to the surface of the SFRM. The first two properties were determined by adapting the pull-off test method described in ASTM C 1583, Standard Test Method for Tensile Strength of Concrete Surfaces and the Bond Strength or Tensile Strength of Concrete Repair and Overlay Materials by Direct Tension (Pull-off Method) (ASTM 2004). The SFRM layer was cut carefully in two orthogonal directions to create a prismatic test specimen, and a $\frac{3}{8}$ in. by 2.7 in. by 2.7 in. aluminum plate was glued to the surface. The advantages of this approach over the ASTM 736 technique are that the resisting area is easily determined and it offers the ability to measure both adhesive and cohesive strengths.

From each plate, three specimens were prepared for measuring both density and in-plane cohesive strength, and two specimens were prepared for measuring adhesive strength and cohesive strength normal to the surface. Prismatic specimens were prepared by carefully removing strips of SFRM from the steel plates and sanding them to obtain uniform thickness. These specimens were weighed to determine their densities. Then the specimens were glued to a steel plate, and a small plate was glued to the other end for applying a tensile load.

The adhesive strength and cohesive strength normal to the surface were obtained using the modified pull-off procedure. An aluminum plate was bonded to the top surface of the SFRM using a fast curing, two-component urethane foam adhesive. After the adhesive had cured, the SFRM layer was cut to produce a prismatic test specimen. A hook was screwed into the aluminum plate, and a load was applied by hand using a 50-lb. digital force gauge. The average length and width of the failure area were measured and used to compute the adhesive or cohesive strength. After the first test, the specimen was repaired with the same polyurethane adhesive, and the test was repeated. If the first test resulted in an adhesive failure, the second test of the repaired specimen measured cohesive strength of the bulk SFRM. If the first test resulted in cohesive failure, specimens were repaired and retested until an adhesive failure was obtained.

2.7.3 Test Results

Table 2–4 summarizes the results of the test described in the previous section.

Table 2–4. Summary of physical characteristics of BLAZE-SHIELD DC/F specimens tested at NIST

| Property | Bare Steel | | Primed Steel | |
|---|------------|-----------|--------------|------------------------|
| | ¾ in. | 1 ½ in. | ¾ in. | 1 ½ in. |
| Density (pcf) | | | 27.2 (0.8)* | 29.7 (1.3) |
| In-plane cohesive strength (psf) | | | 1120 (390) | 1740 (540) |
| Adhesive strength (psf) | 450 (63) | 666 (151) | 185 (96) | 171 ⁺ (196) |
| Cohesive strength normal to surface (psf) | 433 (99) | 610 (142) | 367 (79) | 595 (163) |

* First number is the average and the number in parentheses is the standard deviation.

⁺ Based on testing selected samples.

The densities of the BLAZE-SHIELD DC/F measured in this study were higher than published values in the manufacturer’s catalogs and higher than the in-place average density of 18.9 pcf reported in Port Authority test reports for BLAZE-SHIELD II. The difference in average densities of the two thicknesses was statistically significant. The higher values in this study are attributed to the specimen preparation procedures, which tended to result in denser test specimens than would be representative of field application.

The difference in average adhesive strength for the two SFRM thicknesses is statistically significant. The relative strengths are consistent with the difference in density for the two thicknesses.

The presence of primer reduced the adhesive strength, especially for the 1 ½ in. thick specimens. Two-thirds of the specimens with the thicker SFRM had no adhesion to the coated steel plates.

Analysis of the cohesive strength normal to the surface indicated that there was no statistically significant effect due to the presence or absence of primer. This is logical because the condition of the steel surface is not expected to influence the properties of the bulk SFRM. There was a statistically significant difference in the average strengths for the two thicknesses, with the 1 ½ in. SFRM having higher strength.

For comparison with the measured cohesive strength normal to the surface, two tests were conducted in accordance with ASTM E 736. The results of the two tests were in agreement with those obtained by the pull-off technique. This suggests that the ASTM E 736 procedure probably provides a measure of cohesive strength.

A comparison was made of the adhesive strength and cohesive strength normal to the surface for the plates made with bare steel. An analysis of variance indicated that there is an 8 percent probability that the difference could be the result of randomness. Generally, if this probability is greater than 5 percent, it can be concluded that the difference is not statistically significant. Thus, for the case of good adhesion, the test results do not contradict the assumption that the adhesive strength and cohesive strength normal to the surface are equal. If this assumption is accepted, the average of the adhesive and cohesive strengths was found to be 409 psf for the ¾ in. SFRM, and the average is 622 psf for the 1 ½ in. SFRM. These values are considerably greater than the manufacturer’s published strength of 295 psf, obtained using the ASTM E 736 method under laboratory conditions.

2.8 REFERENCES

- ASTM 1961. Standard Test Methods for Fire Tests of Building Construction and Materials. ASTM E 119-61, ASTM International, West Conshohocken, PA.
- ASTM 1995. Standard Test Method for Linear Thermal Expansion of Solid Materials With a Vitreous Silica Dilatometer, ASTM E 228-95, ASTM International, West Conshohocken, PA.
- ASTM 1998. Standard Test Method for Compositional Analysis by Thermogravimetry, ASTM E 1131-98, ASTM International, West Conshohocken, PA.
- ASTM 1999. Standard Test Method for Thermal Conductivity of Refractories by Hot Wire (Platinum Resistance Thermometer Technique), ASTM C 1113-99. ASTM International, West Conshohocken, PA.
- ASTM 2000. Standard Test Methods for Fire Tests of Building Construction and Materials, ASTM E 119-00a. ASTM International, West Conshohocken, PA.
- ASTM 2000a. Standard Test Method for Cohesion/Adhesion of Sprayed Fire-Resistive Materials Applied to Structural Members, ASTM E 736-00, ASTM International, West Conshohocken, PA.
- ASTM 2000b. Standard Test Method for Determination of Thermal Conductivity of Soil and Soft Rock by Thermal Needle Probe Procedure, ASTM D 5334-00, ASTM International, West Conshohocken, PA.
- ASTM 2001. Standard Test Method for Determining Specific Heat Capacity by Differential Scanning Calorimetry, ASTM E 1269-01, ASTM International, West Conshohocken, PA.
- ASTM 2004. Standard Test Method for Tensile Strength of Concrete Surfaces and the Bond Strength or Tensile Strength of Concrete Repair and Overlay Materials by Direct Tension (Pull-off Method), ASTM C 1583-04. ASTM International, West Conshohocken, PA.
- Gewain, R.G., Iwankiw, N.R. and Alfawakhiri, F. 2003. *Facts for Steel Buildings—Fire*, American Institute of Steel Construction, Chicago, IL, October 2003. 51 pp.
- NYCBC 1968. Building Code—Local Law No. 76 of the City of New York. New York, NY.
- Underwriters Laboratories Inc. (2002). Fire Resistance Directory – Volume 1, Northbrook, IL.

Chapter 3

FIRE RESISTANCE TESTS

3.1 BACKGROUND

3.1.1 Motivation for Conducting Standard Fire Tests

National Institute of Standards and Technology (NIST) review of available documents indicated that the fire performance of the composite floor system of the World Trade Center (WTC) towers was an issue of concern to the building owners and designers from the original design and throughout the service life of the buildings (NIST NCSTAR 1-6A). NIST found no evidence regarding the technical basis for the selection of the SFRM for the WTC floor trusses and for the SFRM thickness to achieve a 2 h rating. Further, NIST no evidence was found that fire resistance tests of the WTC floor system were conducted. Review of the documents did not identify a similar concern for other structural components of the WTC towers.

NIST NCSTAR 1-6B reports on the motivation for testing full- and reduced-scale assemblies representing the floor system used in the World Trade Center towers, and the purpose of the Standard Fire Test. The test variables are given and the construction of the floor test assemblies, test set-up, and loading are described. Results (fire resistance ratings) of the four tests are presented and discussed. This chapter summarizes the salient material covered in NIST NCSTAR 1-6B.

3.1.2 Purpose of the Standard Fire Tests

NIST conducted a series of four standard fire tests of the WTC floor system:

- to establish the baseline performance of the floor system of the WTC towers under thermal loading as they were originally designed,
- to differentiate the factors that most influenced the response of the WTC floors to fires as they may relate to normal building and fire safety considerations and those unique to the events of September 11, 2001,
- to determine whether there was an adequate technical basis for the original SFRM specification, and
- to study the procedures and practices used to accept an innovative structural and fire protection system.

3.2 DESCRIPTION OF WTC FLOOR SYSTEM

3.2.1 Structural System

The floor system design for the World Trade Center consisted of a lightweight concrete floor slab supported by steel trusses bridging between the core and exterior wall²³. The main composite trusses, which were used in pairs, were spaced at 6 ft 8 in. on center (o.c.) and had a nominal clear span of either 60 ft or 35 ft. The trusses were fabricated using double-angles for the top and bottom chords and round bars for the webs. The web members protruded above the top chord in the form of a “knuckle,” which was embedded in the concrete slab to develop composite action. Additionally, the floor system included bridging trusses (perpendicular to main trusses) spaced 13 ft 4 in o.c. In the corners of the towers, the bridging trusses acted with the main trusses to provide “two-way” slab action, i.e., bending moments existed in both principal directions. Figure 3–1 is a cut-away of the floor system showing the main trusses, bridging trusses, metal deck, and concrete floor slab. Figure 3–2 shows a cross-sectional view of the basic configuration of the floor system.

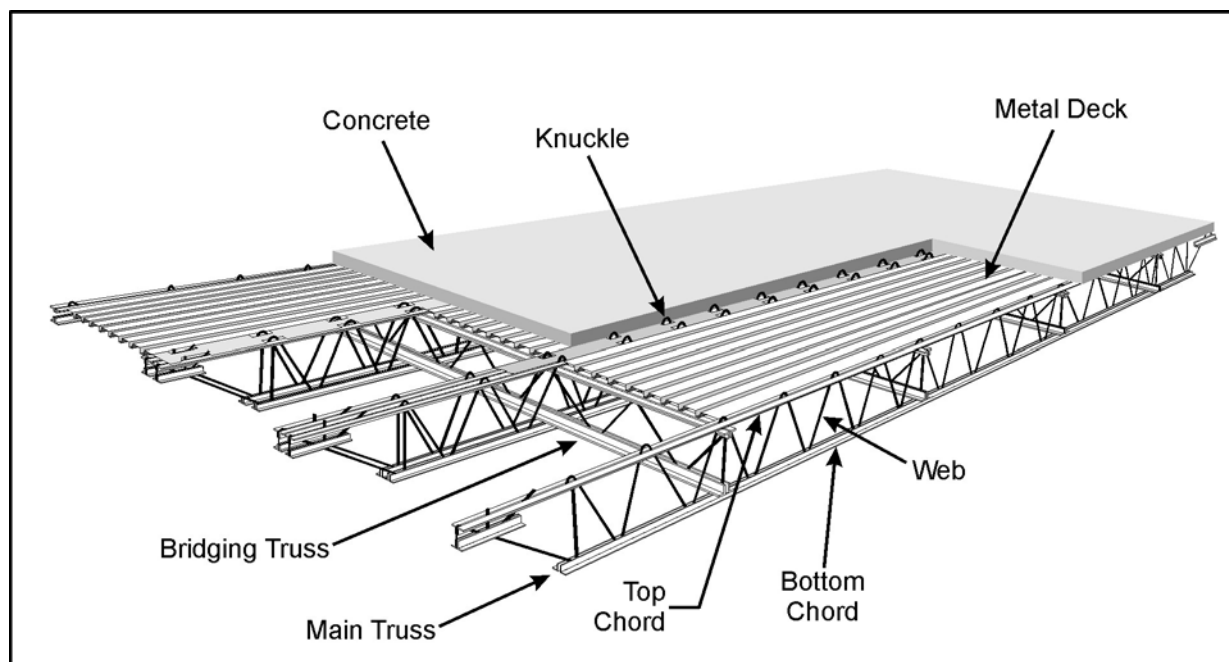


Figure 3–1. Floor system of the WTC towers.

²³ All information and data related to the design and construction of the WTC floor system were obtained from contract drawings provided to NIST by The Port Authority of New York and New Jersey. Refer to NIST NCSTAR 1-2A for a complete description of the WTC structural system and index of all structural drawings.

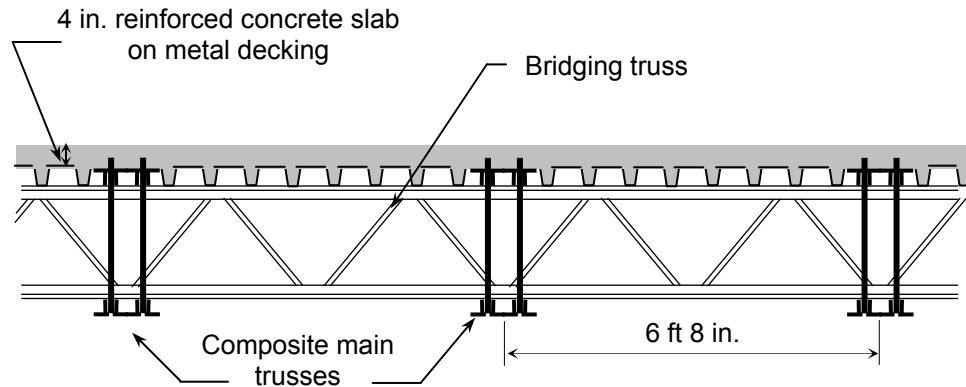


Figure 3–2. Schematic of floor system viewed along the main steel trusses. (not to scale)

3.2.2 Sprayed Fire-Resistive Material (SFRM) Thickness

As noted in Chapter 2, the average thickness of SFRM as originally installed was approximately $\frac{3}{4}$ in. The thicknesses of $\frac{1}{2}$ in. representing the specified thickness, and $\frac{3}{4}$ in. representing average applied thickness, were used in the standard fire resistance tests described here.

3.3 FIRE RESISTANCE TESTING

3.3.1 General Description

The fire rating of structural materials and assemblies is generally determined through testing, and in the United States, such testing is frequently conducted in accordance with the ASTM International standard, ASTM E 119, “Standard Test Methods for Fire Tests of Building Construction and Materials.” This standard was first published in 1917 as a tentative standard, ASTM C 19, and was first adopted as ASTM E 119 in 1933. Since its introduction, the test method has been modified and updated, although its essential character has remained unchanged. ASTM E 119 prescribes a standard fire exposure for comparing the test results of building construction assemblies. For the tests of floors and roofs, a test assembly is structurally loaded, and the standard fire exposure is applied to the underside of the specimen. The assembly is evaluated for its ability to contain a fire by limiting passage of flame or hot gases, and limiting heating of the unexposed surface, while maintaining the applied load. The assembly is given a rating, expressed in hours, based on these acceptance, or end-point, criteria.

3.3.2 Test Restraint Conditions and Ratings

ASTM E 119 Standard in 1971 introduced the concept of fire endurance classifications based on two conditions of support: restrained and unrestrained. A restrained condition²⁴ is “one in which expansion at the support of a load carrying element resulting from the effects of fire is resisted by forces external to the element.” In an unrestrained condition, the element is free to expand and rotate at its supports.

²⁴ According to Appendix A4 of ASTM E 119-73.

The current standard describes a means to establish both restrained and unrestrained ratings from assemblies tested in the restrained condition. The conditions of acceptance are based on limiting passage of flame or hot gases, limiting temperatures on the unexposed surface of the slab, and failure to support the applied load. In addition, temperature limitations are placed on the main structural members. The location of temperature measurements on the structural members is specified in the Standard.

In addition, the Standard describes a means to establish unrestrained ratings from unrestrained test conditions. For tests of assemblies not restrained against thermal expansion, the fire resistance rating is based on limiting passage of flame and hot gases, exceeding temperatures on the unexposed surface of the slab, and failure to sustain the applied load; however, there are no limiting temperatures for the steel structural members.

Prior to 1970, restrained and unrestrained ratings were not defined in ASTM E 119. Ratings were determined based upon the requirements for restrained assemblies except that no temperature limitations were placed on the structural steel members.

In practice, a floor assembly such as that used in the WTC towers is neither restrained nor unrestrained against thermal expansion, but is likely somewhere in between. Testing under both restraint conditions bounds expected performance under standard fire exposure.

3.3.3 Scale of Tests

For floor and roof assemblies, ASTM E 119 requires that the area exposed to fire be a minimum of 180 ft² with neither dimension of the furnace less than 12 ft. Furnaces available in 2002 in the United States for conducting standardized fire resistance tests of floor and roof assemblies had a maximum span less than 18 ft (NIST GCR 02-843). Traditionally, relatively small scale assemblies have been tested, and results have been scaled to practical floor system spans.

The Underwriters Laboratories (UL) fire testing facility in Toronto, Canada has a furnace with nominal dimensions of 35 ft by 14 ft. Thus, full- or large-scale floor assemblies could be tested in this furnace. Availability of the 35 ft furnace in UL's Toronto facility, in addition to the 17 ft furnace at its Northbrook, Illinois, facility allowed NIST to conduct tests to compare the effect of scale.

3.3.4 Test Variables

To limit the number of tests and obtain information of greatest value to meet the investigation objectives discussed above, NIST studied three factors: SFRM thickness, scale of the test, and test restraint conditions. To this end, four tests were conducted as follows:

- Test #1: Full-scale (35 ft span), restrained test condition, ¾ in. thick SFRM.
- Test #2: Full-scale (35 ft span), unrestrained test condition, ¾ in. thick SFRM.
- Test #3: Reduced-scale (17 ft span), restrained conditions, ¾ in. thick SFRM.
- Test #4: Reduced-scale (17 ft span), restrained conditions, ½ in. thick SFRM.

The objective of the full-scale restrained test with $\frac{3}{4}$ in. thick SFRM, Test 1, was to determine the baseline fire resistance of the floor system with average as-applied SFRM thickness. This test also demonstrated whether the fire resistance of such a system was significantly different from that of a system with the specified SFRM thickness of $\frac{1}{2}$ in.

The test conditions for Test 2, full-scale unrestrained test with $\frac{3}{4}$ in. thick SFRM, were the same as those for Test 1 except that the specimen was supported to allow thermal expansion and, therefore, represented the unrestrained test condition. Results of this test allowed a determination of the unrestrained rating by test and, by comparing with the results of Test 1, a comparison of unrestrained ratings from both a restrained and unrestrained assembly test.

Test 3 was a reduced-scale test which, other than scale, was the same as Test 1. Thus, a comparison of the results of these two tests allowed an examination of whether test results are independent of test assembly scale.

Test assemblies for Tests 1, 2 and 3 were fire protected in the same manner, with $\frac{3}{4}$ in. thick SFRM representing the average SFRM thickness in the impact and fire affected floors of WTC 2. Measurements taken from photographs of the originally applied SFRM indicated that, while the SFRM thickness on main the trusses was approximately $\frac{3}{4}$ in., the thickness on the bridging trusses was approximately half that value (see NIST NCSTAR 1-6A). Also, photographs indicated that the metal deck was sometimes sprayed and sometimes not. For these three tests (Tests 1, 2, and 3), then, the main trusses were protected with $\frac{3}{4}$ in. thick SFRM, the bridging trusses with $\frac{3}{8}$ in. thick SFRM, and the metal deck was not intentionally sprayed but was also not masked from overspray and thereby had, in most instances, at least a light covering of SFRM. These conditions best represented the thickness of the SFRM as it was originally applied in the one-way slab areas.

The objective of the test with the $\frac{1}{2}$ in. SFRM (Test 4) was to determine whether or not there was adequate technical basis for the original SFRM specification. As explained by the designer, it was not necessary to fire protect the bridging trusses in the one-way areas nor was it necessary to spray the metal deck (see NIST NCSTAR 1-6A). Consequently, the Test 4 specimen had $\frac{1}{2}$ in. thick SFRM applied to the main trusses and no SFRM applied to either the bridging trusses or the underside of the metal deck. Both the bridging trusses and metal deck were masked to prevent overspray as well. These conditions best represented the SFRM that was necessary, in the opinion of the designer, to provide the required level of passive fire protection.

3.4 PREPARATION OF TEST ASSEMBLIES

Original shop drawings by Laclede Steel were used for the design of the 35 ft 0 in. span and 17 ft 5½ in. span test assemblies. Figure 3–3 shows a drawing for the trusses used in the 35 ft span assemblies. The steel trusses faithfully duplicated the geometry of the original design. Since equipment for making the resistance welds is not available in the United States, metal inert gas (MIG) welding was used, and the welds were designed per the American Institute of Steel Construction (AISC) weld criteria to develop the web capacities in tension or compression. This strength requirement was based on test data from Laclede's files indicating that weld capacities exceeded design loads by a factor of 2.

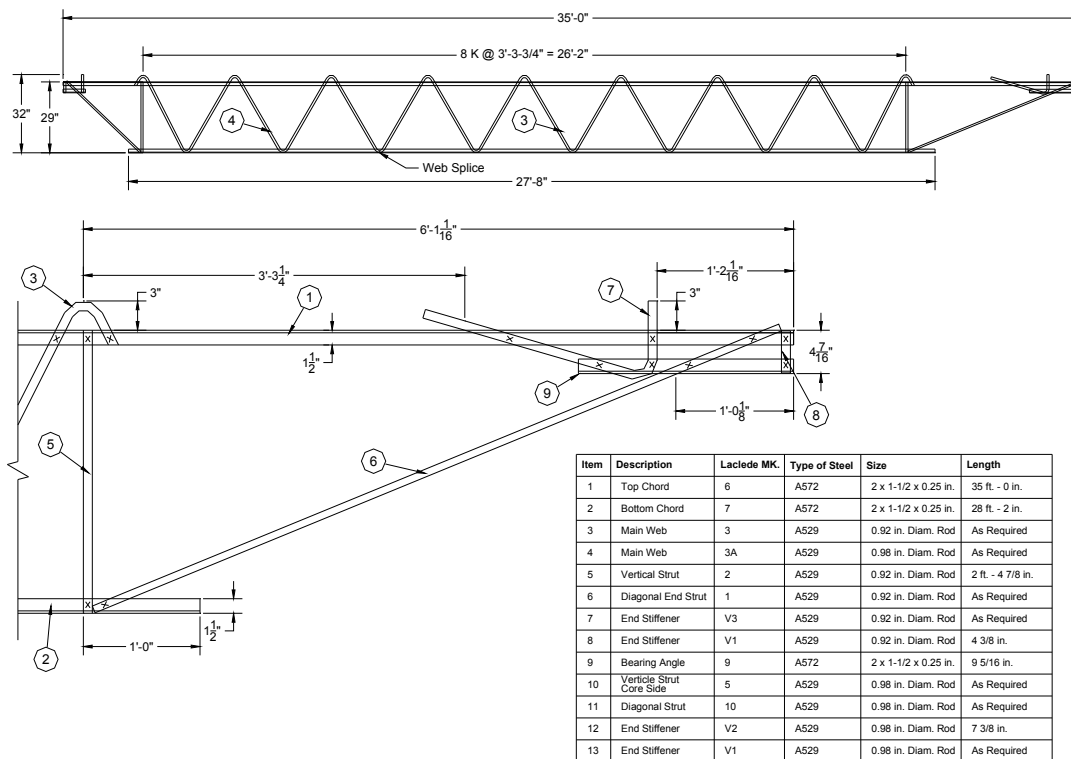


Figure 3–3. Drawing of 35 ft truss and end detail.

In addition, the steel angles, round bars, reinforcing steel, welded wire fabric (WWF), metal deck, lightweight concrete, and primer paint were all matched as closely as practical. Figure 3–4 shows the steel trusses being fit-up and welded in the test frame for one of the 35 ft span test assemblies. NIST NCSTAR 1-6B provides a complete description of the construction of the test assemblies, including materials used, sprayed fire-resistive material, and instrumentation.



Source: NIST.

Figure 3–4. Trusses being fit-up in test frame of 35 ft test assembly.

3.5 DESCRIPTION OF TESTS AND LOADING

3.5.1 Full-scale Tests (35 ft span)

Full-scale (35 ft span) tests were conducted at the UL furnace facility in Toronto, Canada. Loading of the floor slab, to “simulate a maximum load condition” as required by ASTM E 119, was accomplished through a combination of concrete block and steel containers filled with water. The water containers were restrained using steel cables to prevent them from falling into the furnace and causing damage to the fire brick and instrumentation in the event of a catastrophic failure of the floor system. Figure 3–5 shows the water containers being placed on the concrete slab.



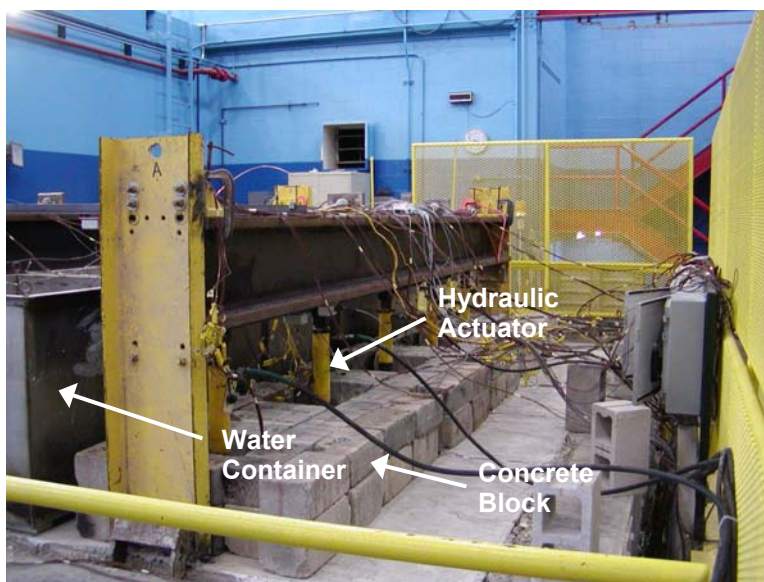
Source: NIST.

Figure 3–5. 35 ft span test assembly loaded with concrete blocks and water-filled containers.

3.5.2 Reduced-scale Tests (17 ft span)

The reduced-scale tests were designed to extract as much information as practicably possible considering that the purpose of the Standard Fire Resistance Test is to measure the ability of the test assembly to contain a fire and is, therefore, based on integrity (passage of hot gases), thermal insulation (heating of the unexposed surface) and load bearing capacity (support of the applied load). For the reduced-scale tests, the sizes of the steel members and the slab thickness were the same as in the full-scale tests. Otherwise, the length and depth of the trusses were scaled by one half. The spacing between the trusses was the same as in the full-scale test. The scaled length and depth, coupled with the original member sizes, slab thickness, and truss spacing, required an increase in the loading to produce the same stress levels as in the full-scale specimen. The loading represented the maximum calculated load condition as required by the ASTM E119 Standard.

The superimposed uniform load was applied through a combination of concrete blocks, water-filled containers, and hydraulic actuators located along the trusses. Figure 3–6 shows the assembly of blocks, water containers, and hydraulic actuators.



Source: NIST.

Figure 3–6. 17 ft span test assembly loaded with concrete blocks, water-filled containers and hydraulic actuators.

3.6 TEST RESULTS

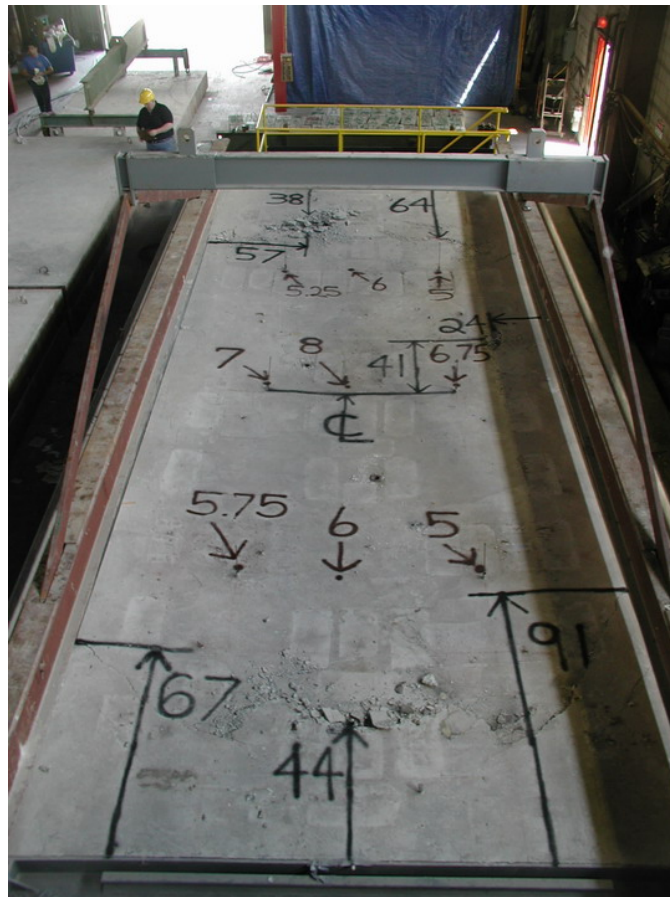
3.6.1 General Discussion of Tests

Specimen No. 1: 35 ft span restrained specimen with 3/4in. SFRM

In the test of Specimen No. 1, loud noises (reports) were heard beginning roughly fifteen minutes after the start of the test. These loud, but somewhat muffled, reports continued and were often accompanied by noticeable bulging of the metal deck and the dislodging of deck SFRM. It is believed that these loud

noises were associated with spalling of the concrete on the underside of the slab. The slab was later sectioned to determine the depth of delamination resulting from the spalling.

At about 50 min, a very loud report was heard, associated with a noticeable sudden downward deflection of the specimen. When access to the top of the slab was possible after completion of the test, it was found that significant cracking and dislocation of the slab had occurred near the corners of the slab. Several of these events were recorded, and post-test inspection revealed that concrete failure had occurred in all four corners of the slab as shown in Fig. 3–7. It is believed that the very loud report and abrupt deflection was a result of the sudden concrete cracking. The test was stopped at 116 min when, after another sudden drop, the center span deflection reached about 15 in.



Source: NIST.

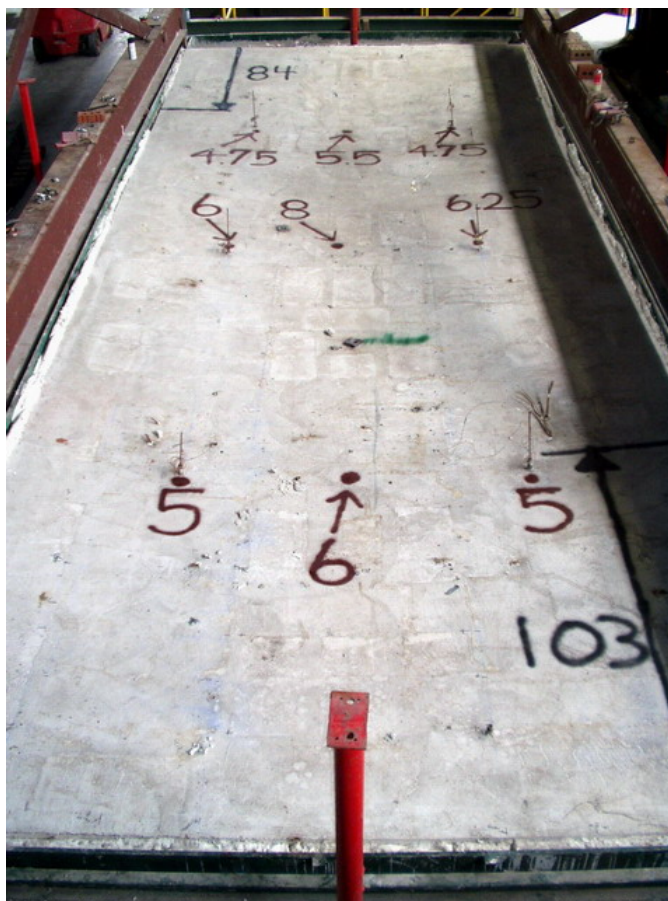
Figure 3–7. Unexposed surface of Assembly No. 1 after loading equipment was removed.

The specimen supported the applied load for the duration of the test. Post-test inspection showed that the corners of the slab had not deflected; rather, all of the slab deflection occurred beginning roughly 5 ft from the ends as seen in Fig. 3–7. It is believed that the thermal expansion of the concrete and the resistance provided by the test frame, put the slab in compression and “wedged” the slab so that no deflections could occur at the ends of the slab. The high compressive stresses that developed likely contributed to the failures noted above.

The test was conducted beyond the E119 end point criteria to obtain as much information as possible. This test, as well as the other three, were continued as long as practical. The tests were stopped, in general, when there was a risk of imminent failure or when deflections were so large as to affect instrumentation readings and, as a consequence, safe conduct of the test. The restrained and unrestrained ratings obtained from this test are given in Section 3.6.2.

Specimen No. 2: 35 ft span unrestrained specimen with 3/4in. SFRM

Reports were heard during the test of the 35 ft unrestrained Specimen No. 2 but were not as loud as those observed during the previous test. A significant difference was that no loud reports or attendant sudden increase in downward deflection were observed for the entire test period, which was 146 minutes, almost two and a half hours, and post-test inspection of the top of the concrete slab showed very little cracking as seen in Fig. 3–8. Since there was a gap between the concrete slab and test frame, thermal expansion of the slab did not produce a state of stress that resulted in significant and sudden cracking and crushing similar to that observed in Specimen No. 1. Additionally, the slab in this test was not wedged at the ends and, unlike Specimen No. 1, the slab deflected over its entire length.



Source: NIST.

Figure 3–8. Unexposed surface of Assembly No. 2 after loading equipment was removed.

The center-of-slab deflection at the end of the test was more than 13 in. The test had to be stopped when the slab deflections affected the instrumentation, and readings could not be obtained. The unrestrained rating for Specimen 2 obtained from this test is given in Section 3.6.1.

Specimen No. 3: 17 ft span restrained specimen with 3/4in. SFRM

As in the first two tests, the metal deck began bulging due to spalling of concrete on the underside of the slab within the first 15 min. At 82 min into the test, a very loud report was heard, and pieces of concrete flew in the air signifying explosive spalling at the north end of the slab as shown in Fig. 3–9. A slight increase in downward deflection at the center of the slab was recorded at 82 min. The test was continued for 210 min and was stopped when the deflections were so large as to affect instrumentation.

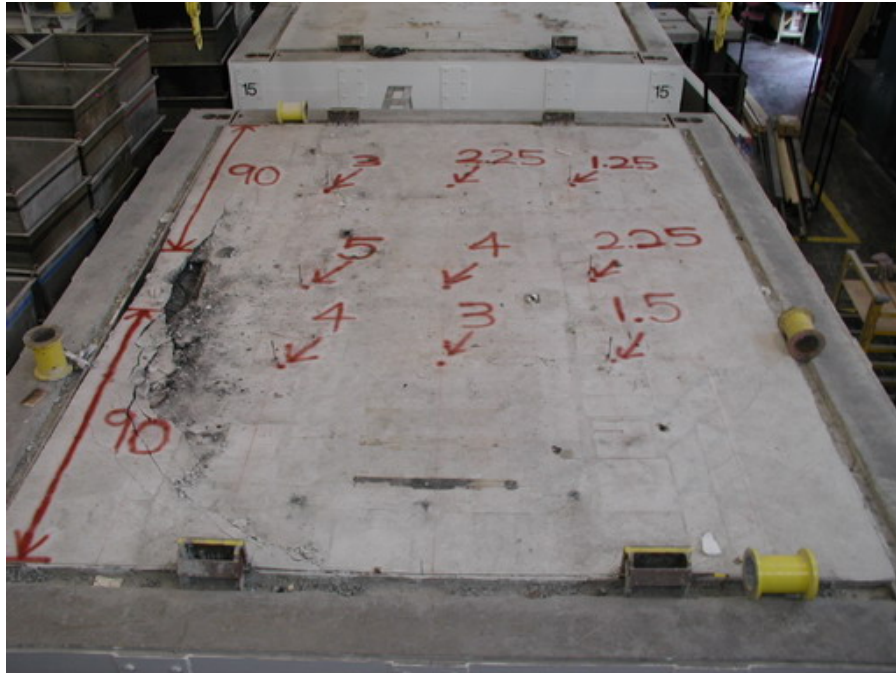


Source: NIST.

Figure 3–9. Unexposed surface of Assembly No. 3 after loading equipment was removed.

Specimen No. 4: 17 ft span restrained specimen with 1/2 in. SFRM

Specimen No. 4 behaved similarly to the other three specimens with regard to bulging of the metal deck on the underside of the slab beginning in the early stages of the test. At 55 minutes, a very loud report was heard, and a significant section of the slab spalled explosively, sending concrete fragments high in the air. As seen in Fig. 3–10, the resulting hole in the slab (left side of the photograph) measured over 2 ft in length and had to be covered with insulating material to safely continue the test as hot gases were coming through the hole.



Source: NIST.

Figure 3–10. Unexposed surface of Assembly No. 4 after loading equipment was removed.

3.6.2 Fire Resistance Ratings

As noted above, prior to 1971, the ASTM E 119 Standard did not differentiate between testing and classifying thermally restrained and unrestrained floor assemblies. The 1961 revision of ASTM E 119, the revision referenced in the 1968 New York City Building Code, is used for reporting the Standard Fire Test rating (no distinction was made for an unrestrained rating). The year 2000 revision of the Standard is used for reporting restrained and unrestrained ratings.

Table 3–1 shows results for all four tests giving the times (in minutes) to reach the acceptance, or end-point, criteria and the Standard Fire Test rating (in hours) for both the 1961 and 2000 revisions of ASTM E 119. Note that in none of the tests did the floor assembly fail to support the superimposed load.

Table 3–1. Results of ASTM E119 Standard Fire Tests.

| Test | Description | Times to Reach End-Point Criteria (min) | | | | | Test Terminated (min) | Standard Fire Test Rating (hr) | | |
|------|----------------------------------|---|--------------------------|--------------------|------------------|-------------------------|-----------------------|--------------------------------|-------------------|---------------------|
| | | Temperature on Unexposed Surface | | Steel Temperatures | | Failure to Support Load | | ASTM E 119-61 | ASTM E119-00 | |
| | | Average (Ambient +250°F) | Maximum (Ambient+ 325°F) | Average (1100°F) | Maximum (1300°F) | | | Rating | Restrained Rating | Unrestrained Rating |
| 1 | 35 ft, restrained, 3/4 in SFRM | --- | 111 | 66 | 62 | (3) | 116(1) | 1 ½ | 1 ½ | 1 |
| 2 | 35 ft, unrestrained, 3/4 in SFRM | --- | --- | 76 | 62 | (3) | 146(2) | 2 | --- | 2 |
| 3 | 17 ft, restrained, 3/4 in SFRM | 180 | 157 | 86 | 76 | (3) | 210(2) | 2 | 2 | 1 |
| 4 | 17 ft, restrained, 1/2 in SFRM | --- | 58 | 66 | 58 | (3) | 120(1) | ¾ | ¾ | ¾ |

- (1) Imminent collapse
- (2) Vertical displacement exceeded capability to measure accurately
- (3) Did not occur

3.6.3 General Observations

Buckling of Trusses

A photograph of the underside of the 35 ft, restrained test specimen after almost two hours of fire exposure is shown in Fig. 3–11. Buckling of the compression diagonals can be seen as well as sagging of the metal deck between supports. Note that, upon cooling, the test specimen recovered at least half of the deflection achieved during the test so deflections seen in Fig. 3–11 are considerably less than the deflections at the end of the test.



Source: NIST.

Figure 3–11. Fire exposure side of the 35 ft restrained test assembly after almost 2 hours of fire exposure

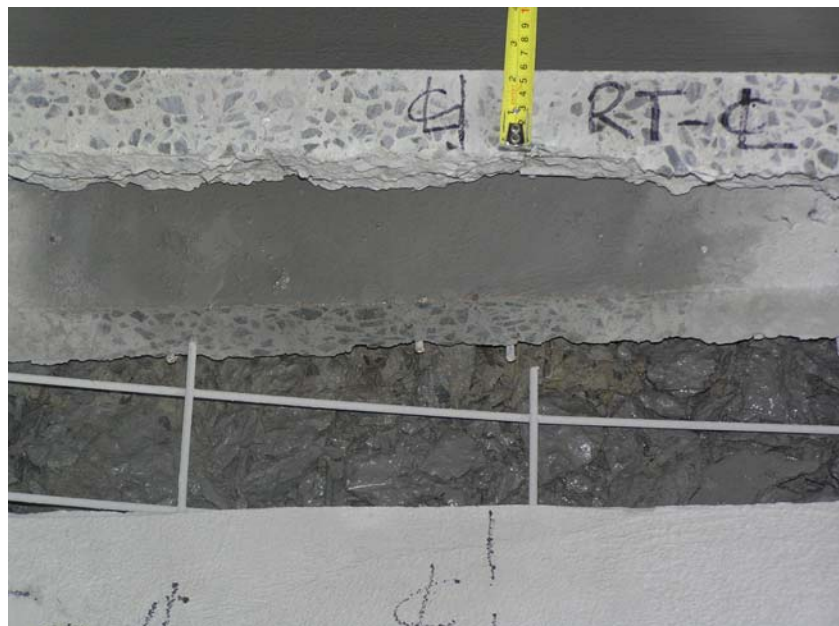
Spalling of Concrete

The sagging of the metal deck was assumed to be a result of spalling of the underside of the concrete slab. This was confirmed when, after the tests, concrete cores were removed and sections cut to determine the condition of the concrete as shown in Fig. 3–12. The depth of the delamination varied but the depth of the remaining slab was on the order of 2 in. to 3 in., essentially up to the double layer of welded wire fabric as seen in Fig. 3–13.



Source: NIST.

Figure 3–12. Sections cut through concrete slab to confirm extent and depth of spalling.



Source: NIST.

Figure 3–13. Measurement of remaining slab thickness after spalling.

Concrete Slab Failure

The three specimens that were restrained showed significant cracking and explosive spalling at the top surface of the concrete slab. The 35 ft restrained specimen had significant cracking and crushing of concrete near the ends and the corners as seen in Fig. 3–7 and Fig. 3–14. These major concrete failures were accompanied by sudden increases in deflection of the floor as seen in Fig. 3–15. The unrestrained 35 ft specimen showed little cracking and no crushing or explosive spalling at the top surface of the slab unlike the restrained specimen. The restrained 17 ft specimen with ½ in. of SFRM exhibited significant explosive spalling in which concrete fragments flew in the air and left a hole in the slab about 2 ft long through which hot gases escaped.



Source: NIST.

Figure 3–14. Detail of spalling concrete at east end of Assembly No. 1.

3.6.4 Floor Deflections and Temperatures

Deflections of floor assembly

The following plots show the vertical deflection measured at the center of each floor assembly. Figure 3–15 shows the deflection while Fig. 3–16 is a plot of the deflection normalized by the span length. It is seen that Specimen No.1 experienced a significant increase in vertical deflection at 49 min which corresponded directly to a loud report and visible increase in deflection noted during the test. A small increase in vertical deflection for Specimen No. 3 was seen to occur at 82 min, the time when the slab spalled explosively at one end.

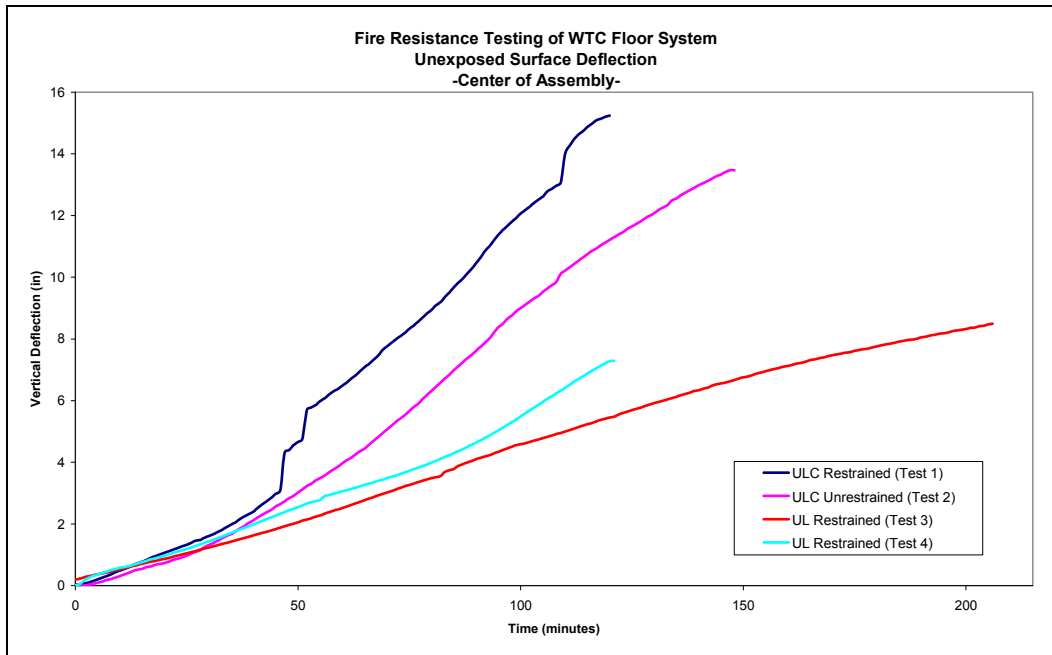


Figure 3-15. Deflection measured at the center of each assembly.

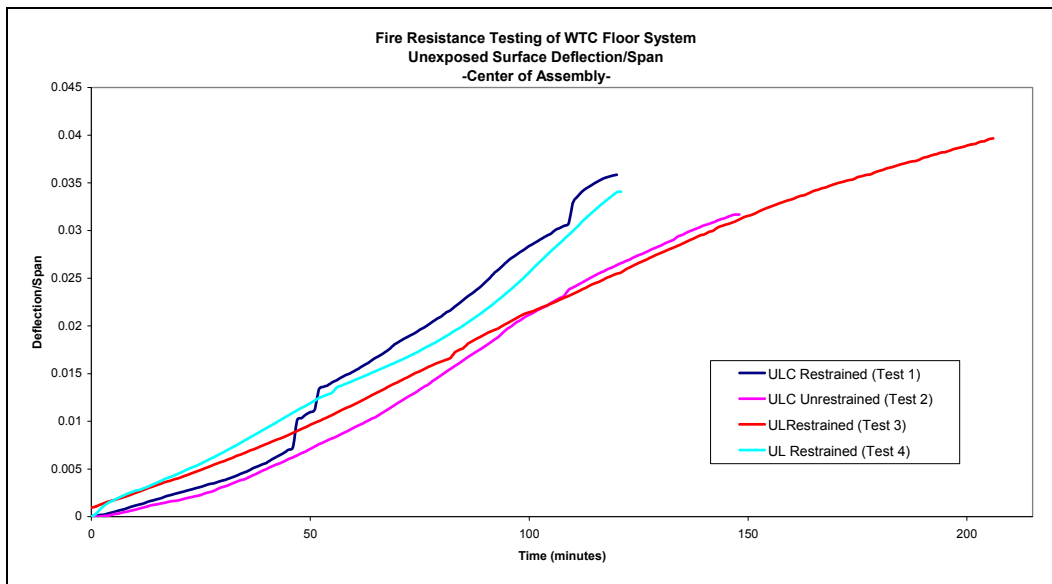


Figure 3-16. Deflection measured at the center of each assembly divided by the span.

Unexposed surface temperatures

The temperature of the top (unexposed) surface of the floor assemblies is plotted in Fig 3–17. It is observed that the unexposed surface temperatures of all four test assemblies were similar prior to the onset of significant concrete crushing and spalling at around 50 min. In Test 4, the surface-mounted thermocouple on the west edge near the center of the span was affected by the explosive failure of the slab and recorded hot gas temperatures.

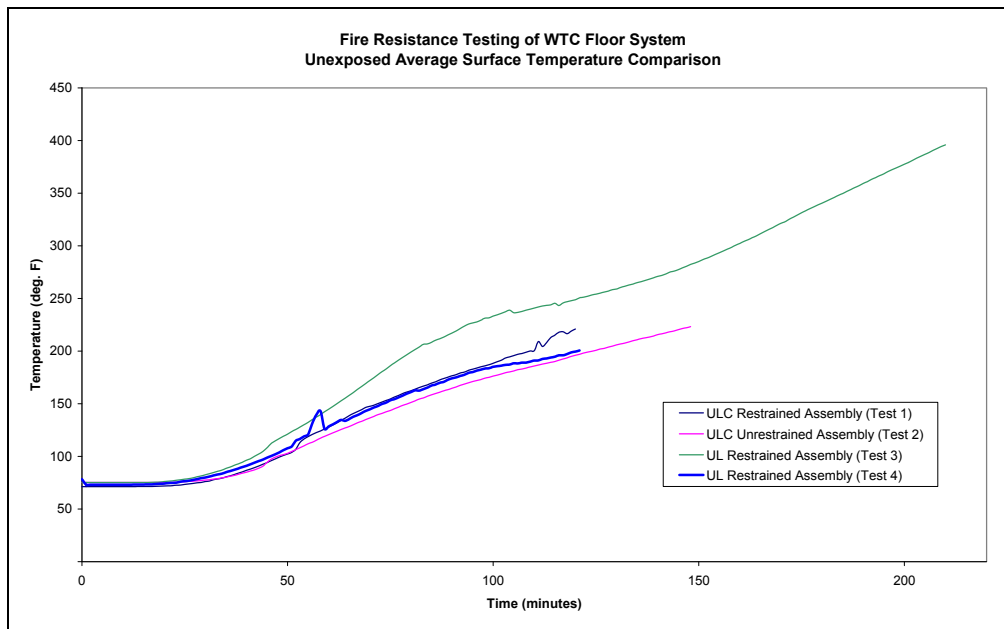


Figure 3–17. Average temperature of the unexposed surface for all four tests.

Steel temperatures

Steel temperatures were recorded at several locations on the main and bridging trusses. Figure 3–18 shows a comparison of the average temperature of the bottom chord for the three tests in which the thickness of the SFRM was $\frac{3}{4}$ in. Temperatures were seen to be very comparable up to about 75 min, which was around the time when SFRM began to dislodge. The location and extent of dislodged SFRM could not be ascertained through visual observation during the tests.

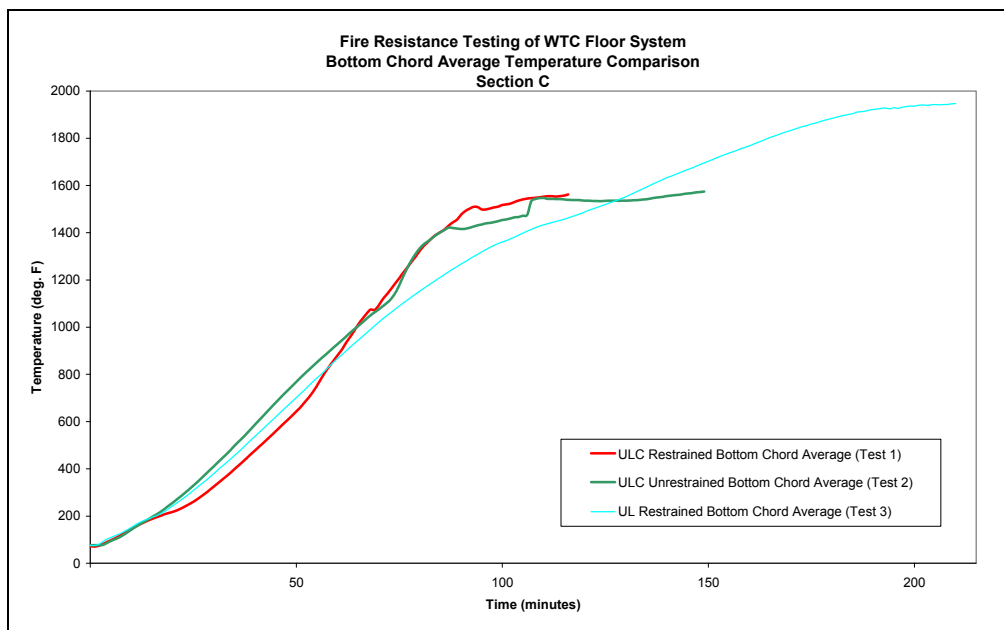


Figure 3–18. Average temperatures of the bottom chord for Test Nos. 1, 2 and 3 (3/4 in. thick SFRM).

3.6.5 Observations and Comparisons

Several observations can be made from the results presented and the summary table of hourly ratings (Table 3–1). The reader is referred to NIST NCSTAR 1-6B for a complete description of the fire resistance tests and the results obtained.

- The test assemblies were able to withstand standard fire conditions for between $\frac{3}{4}$ h and 2 h without exceeding the limits prescribed by ASTM E 119.
- Test specimens protected with $\frac{3}{4}$ in. thick spray applied fire-resistive material were able to sustain the maximum design load for approximately two hours (the minimum was 116 min) with no structural failure; in the 35 ft, unrestrained test, the load was maintained for $3\frac{1}{2}$ h (210 min).
- The restrained 35 ft floor system obtained a fire resistance rating of $1\frac{1}{2}$ h while the unrestrained 35 ft floor system achieved a 2 h rating. Past experience with the ASTM E 119 test method would lead investigators to expect that the unrestrained floor assembly would not perform as well as the restrained assembly, and therefore, would receive a lower fire rating.
- A fire rating of 2 h was determined from the 17 ft restrained test with the average applied SFRM thickness of $\frac{3}{4}$ in. while a fire rating of $1\frac{1}{2}$ h was determined from the 35 ft restrained test with the same SFRM thickness.
- A fire rating of $\frac{3}{4}$ h was determined from the 17 ft restrained test with the specified SFRM thickness of $\frac{1}{2}$ in.

3.7 SUMMARY

The tested floor assemblies were similar, though not identical, to steel-joist-supported concrete floors that are widely used in low rise construction. The test results provided valuable insight into the behavior of these widely used assemblies and also identified issues that require further study.

The fire resistance tests showed that the floors were capable of considerable sagging without collapse. The tests also showed fire damage to the bridging trusses and buckling of compression diagonals and the vertical strut near the supports. No evidence of knuckle failures was seen in the tests.

The standard test method has been used for many decades and has for the most part served its intended purpose well when taken together with the fire rating requirements. This is supported by historical fire loss data for more than half a century for different high-rise building occupancies. In addition, there is extensive data and experience that has been developed using the test method.

The NIST tests have identified areas where further study related to the standard test method may be warranted. Among the issues related to the test method that NIST identified as requiring further study are:

- Criteria for determining structural limit states, including failure, and means for measurement,
- Scale of test assembly versus prototype application,
- Effect of end restraint conditions (restrained and unrestrained) on test results, including the influence of stiffness,
- Structural connections (not currently addressed in ASTM E 119),
- Combination of loading and exposure (temperature profile) adequately represent expected conditions,
- Procedures to analyze and evaluate data from fire resistance tests of other building components and assemblies to qualify an untested building element,
- Repeatability of test results (single test currently defines rating for system),
- Reproducibility of heat flux environment between different furnaces and laboratories, and
- Relationships between prescriptive ratings and performance of the assembly in realistic building fires.

This page intentionally left blank.

Chapter 4

STRUCTURAL RESPONSE OF COMPONENTS, CONNECTIONS AND SUBSYSTEMS

In this chapter, the structural analysis of components, connections, and detailed analysis for the development of two subsystems -- a floor subsystem and an exterior wall subsystem -- are covered²⁵. The subsystem response to impact damage and fire is addressed in Chapter 7. This work was conducted to provide guidance for the development of the global finite element models with respect to element types and sizes, appropriate constitutive models, and failure criteria for any given structural component. The subsystem models were also used to correlate the results of the fine mesh component analyses with the coarser mesh global analyses.

Work reported herein includes the following:

- Evaluation of the structural response of components, connections and subsystems to service loads due to gravity (dead and live loads) and elevated structural temperatures.
- Identification of the failure modes and failure sequences, the associated temperatures at failure, and where temperature histories were used, times to failure.
- Identification of the changes in mechanical properties or geometry at initiation of component and subsystems failure.
- Identification of modifications for the global structural models to reduce complexity and size while maintaining the quality of analysis results.

This chapter covers the mechanical properties of concrete and steel at elevated temperatures, analysis of components and connections for the floors and exterior wall, and the development of models for a full floor and portion of an exterior wall. The reader is referred to NIST NCSTAR 1-6C for a complete description of component, connection, and subsystem structural analyses.

4.1 MECHANICAL PROPERTIES OF CONCRETE AND STEEL

The mechanical properties of both steel and concrete are affected significantly by temperature. In the following sections, the material properties used in this study are specified as a function of temperature. For finite element analysis (FEA) of components, subsystems, and global models of the World Trade Center (WTC) towers, a material properties catalog was developed. Each material model was identified with a number in ANSYS²⁶; steels were Material ID 1 through Material ID 29, and concretes were

²⁵ All information and data related to the design and construction of the WTC floors and exterior walls were obtained from contract drawings provided to NIST by The Port Authority of New York and New Jersey. Refer to NIST NCSTAR 1-2A for a complete description of the WTC structural system and an index of all structural drawings.

²⁶ ANSYS (ANSYS, Inc., Cannonsburg, PA) is the structural analysis software used for nonlinear finite element analyses.

Material ID 51 through Material ID 83. The details of concrete and steel materials are discussed separately in this section.

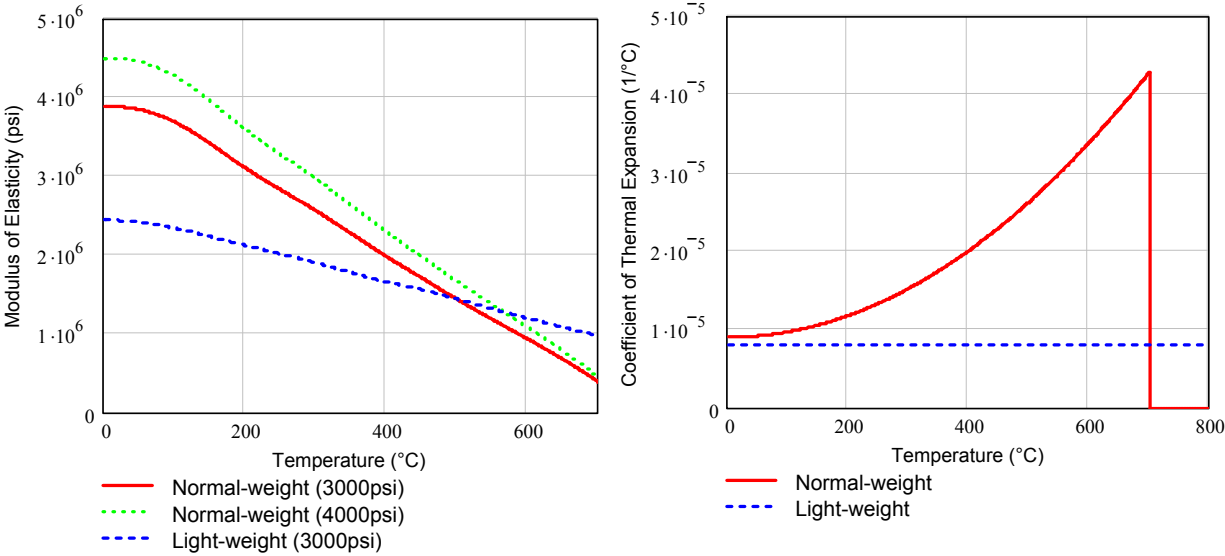
4.1.1 Concrete Properties and Failure Criteria

Two types of concrete were used for the floors of the World Trade Center towers: lightweight concrete in the tenant office areas and normal-weight concrete in the core area. Thermal properties of normal-weight concrete depend on the type of aggregate. Petrographic inspection of several samples of lightweight concrete taken from the debris showed siliceous sand in the lightweight concrete. Because coarse and fine aggregates are usually from the same source for a construction site, it was assumed that the normal-weight concrete had siliceous aggregate.

The specified design strength for lightweight concrete was 3,000 psi and either 3,000 psi or 4,000 psi for normal-weight concrete, depending upon the floor location within the buildings. The actual strength of concrete at room temperature is greater than that measured from cylinders poured for testing during construction, referred to as 28-day cylinder strength, as concrete continues to strengthen with age. Methods for estimating changes in concrete strength with age are specified by the American Concrete Institute (ACI) 209. The actual compressive strength of WTC concrete slabs was estimated to be 38 percent greater than the specified design strengths: 5,500 psi for 4,000 psi normal-weight concrete and 4,100 psi for 3,000 psi normal-weight and lightweight concretes (see NIST NCSTAR 1-6C).

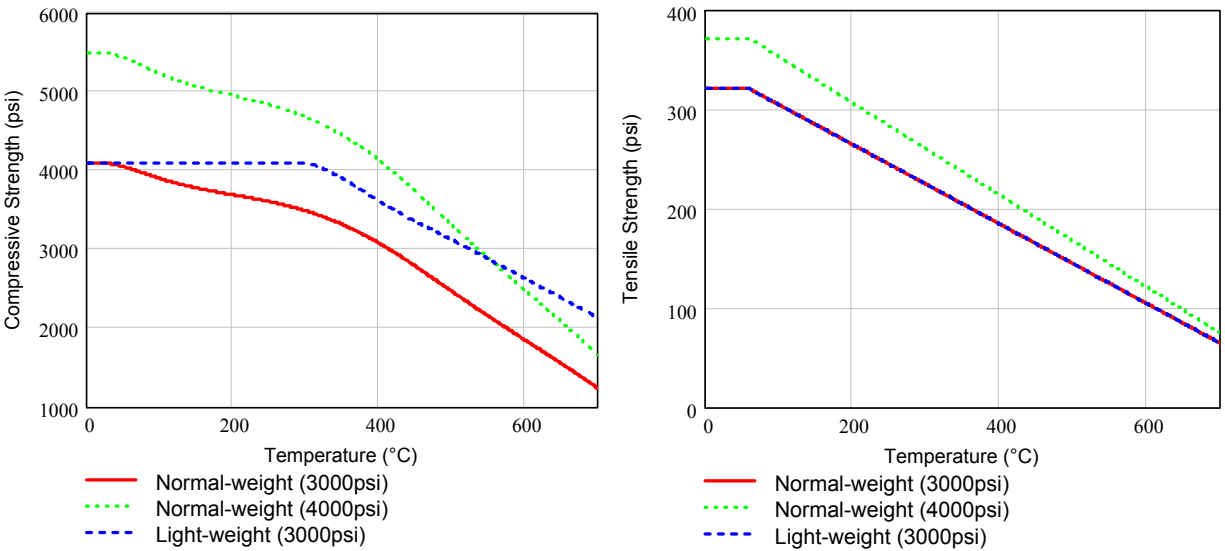
Normal-weight and lightweight concrete had similar design strengths of 3,000 psi to 4,000 psi, but respond differently to elevated temperatures. Temperature dependent properties of concrete are modulus of elasticity, instantaneous coefficient of thermal expansion, compressive strength, and tensile strength.

The effects of elevated temperature on concrete mechanical properties, plotted in Fig. 4–1, are based upon Phan (1996) and Phan and Carino (2003). Lightweight concrete shows less degradation in modulus of elasticity and a constant instantaneous coefficient of thermal expansion as temperatures increase. Lightweight concrete heats more slowly than does normal weight concrete. Tensile strength is identical for lightweight and normal weight concretes with the same compressive strength, since tensile strength depends upon the formation of cracks. Compressive strength for lightweight concrete shows no degradation until 300 °C, whereas normal weight concretes begin degrading as temperatures exceed room temperature.



(a) Modulus of elasticity

(b) Instantaneous coefficient of thermal expansion



(c) Compressive strength

(d) Tensile strength

Figure 4–1. Temperature–dependent concrete properties.

Figure 4–2 shows concrete stress-strain curves at room and elevated temperatures, where compressive stresses and strains are negative and tensile stresses and strains are positive. Tensile stress in concrete increases linearly up to the tensile strength. When strained beyond this point, the concrete begins to crack and the stress across the section will drop. However, this drop in the stress-strain relationship caused significant numerical instability problems during structural analysis. Numerical instabilities were avoided by assuming that the reinforced concrete slab became plastic in tension as the reinforcement carried the tensile load.

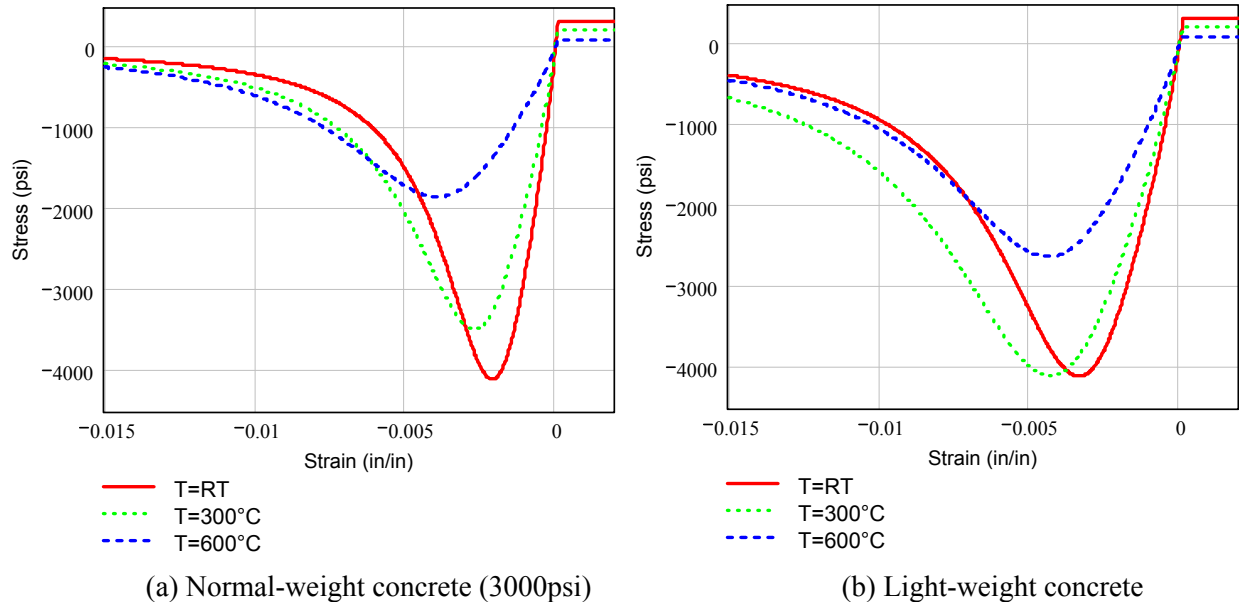


Figure 4–2. Concrete stress-strain curves.

The assumption of concrete plasticity after the onset of cracking is valid for balanced reinforcement in concrete. Although the reinforcement ratio in the WTC concrete slabs was smaller than the balanced reinforcement ratio, the inaccuracy was not significant.

Compressive failure of the concrete slabs was modeled with the von Mises yield criterion.

4.1.2 Steel Properties and Failure Criteria

Steels used in WTC 1 and WTC 2 are listed in Table 4–1. For each steel, described by its design strength, the table lists the estimated yield and ultimate strengths, σ_{yRT} and σ_{uRT} , respectively. Figure 4–3 shows the mechanical properties of steel that are affected by elevated temperatures: (a) modulus of elasticity; (b) Poisson’s ratio; (c) yield strength reduction factor; (d) tensile strength reduction factor; and (e) instantaneous coefficient of thermal expansion. A single line is plotted for the properties of all steels in Table 4–1, since the reduction factors for elevated temperature effects on steel mechanical properties were assumed to be the same for all steels, except for the yield and tensile strength reduction factors for bolt steels. See NIST NSTAR 1-3C for a complete description of the development of the steel properties at elevated temperatures.

When compared to concrete properties, the following observations can be made:

- Modulus of elasticity is reduced by 25 percent at 600 °C for steel and by 50 percent to 75 percent for concrete.
- Poisson’s ratio increases for steel but remains constant for concrete at 0.17. However, the values for steel up to 600 °C are close to the rounded value of 0.3 that is often assumed for design purposes at room temperature.

Table 4–1. Steel types used in WTC 1 and WTC 2.

| Material ID | Description | σ_{yRT} (psi) | σ_{uRT} (psi) |
|-------------|---|-------------------------|-------------------------|
| 1 | All 36 ksi core box columns, plates, straps ^a | 36,720 | 64,470 |
| 2 | All 36 ksi core WF, channels, and tubes 36 ksi large area and large inertia “rigid” beams in SAP2000 model ^a | 37,000 | 63,450 |
| 3 | All 42 ksi box columns ($1 \leq t \leq 0.75$ in.) | 51,400 | 79,200 |
| 4 | All 42 ksi box columns (0.75 in. $< t \leq 1.5$ in.) | 47,000 | 74,800 |
| 5 | All 42 ksi box columns ($t > 1.5$ in.) | 42,600 | 70,400 |
| 6 | 42 ksi or 45 ksi Group 3 WF core columns | 53,800 | 74,400 |
| 7 | 42 ksi or 45 ksi Group 3 WF core columns | 49,000 | 71,040 |
| 8 | 42 ksi Group 4&5 WF core columns | 44,200 | 66,640 |
| 9 | 45 ksi Group 4&5 WF core columns | 47,800 | 71,074 |
| 10 | All 36 ksi Plates 1, 2, and 4 in perimeter columns | 35,630 | 61,170 |
| 11 | All (42, 45, or 46) ksi Plates 1, 2, and 4 in. perimeter columns | 53,051 | 74,864 |
| 12 | All 50 ksi Plates 1, 2, and 4 in. perimeter columns. All 50 ksi channels and plates ^a | 53,991 | 75,618 |
| 13 | All 55 ksi Plates 1, 2, and 4 with $t \leq 1.5$ in. in perimeter columns | 60,817 | 82,558 |
| 14 | All 60 ksi Plates 1, 2, and 4 with $t \leq 1.25$ in. in perimeter columns | 62,027 | 87,250 |
| 15 | All 65 ksi Plates 1, 2, and 4 with $t \leq 0.5$ in. in perimeter columns ^b | 69,642 | 90,442 |
| 16 | All 70 ksi Plates 1, 2, and 4 in. perimeter columns | 76,735 | 91,951 |
| 17 | All 75 ksi Plates 1, 2, and 4 in perimeter columns | 82,469 | 96,821 |
| 18 | All 80 ksi perimeter columns steels, regardless of plate | 91,517 | 99,442 |
| 19 | All (85, 90, 100) ksi perimeter column steels, regardless of plate | 104,783 | 115,983 |
| 20 | Laclede truss web bar rounds specified as A36 | 38,067 | 59,567 |
| 21 | Laclede truss chord angels (regardless of ASTM Spec) and all rounds specified as A242 | 55,332 | 74,050 |
| 22 | A325 bolts ^c | 104,783 | 115,983 |
| 23 | All 42 ksi Plate 3 in perimeter columns | 42,600 | 67,216 |
| 24 | All 45 ksi Plate 3 in perimeter columns | 45,900 | 69,831 |
| 25 | All 50 ksi Plate 3 in perimeter columns | 51,400 | 74,188 |
| 26 | All 55 ksi Plate 3 in perimeter columns | 56,900 | 78,546 |
| 27 | All 60 ksi Plate 3 in perimeter columns | 62,400 | 83,903 |
| 28 | All 65 ksi Plate 3 in perimeter columns | 67,900 | 87,261 |
| 29 | All 70 ksi and 75 ksi Plate 3 in perimeter columns | 78,900 | 95,976 |

a. Steels in the following members are assumed to have the properties shown in the table:

- 36 ksi plates and straps (Material 1).
- 36 ksi channels, tubes, and “rigid” beams (Material 2).
- 50 ksi channels and plates (Material 12).

b. 65 ksi steels in perimeter columns with $t > 0.5$ in. are assumed to have the same properties as those in Material 15.

c. In the column model, stress-strain relationships of bolts are used.

Note: Bolt properties are assumed to be the same as those in Material 19.

- Steel yield strength reduces to 20 percent of its initial value and its ultimate tensile strength is reduced to 40 percent at 600 °C. Concrete compressive strength is reduced to 30 percent to 50 percent of its initial value. Concrete tensile strength, which is already low, is also reduced to 30 percent.

- The instantaneous coefficient of thermal expansion for steel lies between the curves for lightweight and normal weight concrete. If steel truss and lightweight concrete components are at the same temperature, the steel components will thermally expand more than the lightweight concrete. For steel beams and normal weight concrete in the core area, the normal weight concrete will expand more than the steel beams.

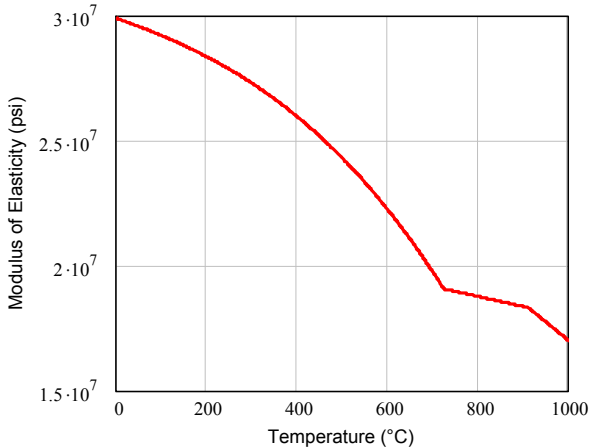
To illustrate the effect of elevated temperature reduction factors on steel strength, Fig. 4–4 shows stress-strain curves for Material ID 1 (see Table 4–1) at room and elevated temperatures. Figure 4–4 (a) shows the low strain range and Fig. 4–4 (b) shows strain levels up to 0.3. These figures show elastic and plastic strains, but for temperatures above 350 °C, the stress-strain curve beyond the elastic limit may also include creep strains. The presence of significant creep strains relative to plastic strains depends upon the combination of three factors: temperature, stress level, and time duration at the temperature and stress level. Creep strain behavior for steel was based upon the creep model by Fields and Fields (1991). The creep model was validated against experimental data (NIST NCSTAR 1-3D). Figure 4–5 illustrates behavior of steel elastic, plastic, and creep strains at elevated temperatures for Material ID 1. Figure 4–5 (a) shows the effect of creep strain rate for various temperatures, and Fig. 4–5 (b) compares elastic, plastic, creep, elastic plus plastic, and total strains at $T = 400$ °C and constant loading for an 1,800 s duration.

The elastic-plastic behavior of steels was modeled with ANSYS “Multi-linear isotropic hardening von Mises plasticity” material model. Creep behavior was modeled using the ANSYS time hardening implicit creep model for nonlinear beam elements (BEAM 188 and BEAM 189) in the full floor model. For BEAM 24 in the global models, an explicit primary creep model was used. BEAM 188 and BEAM 189 elements include thermal expansion, creep, and temperature-dependent material properties. When the elements were used in the global model, numerical difficulties occurred for creep and post-buckling behaviors which were resolved by using BEAM 24 elements.

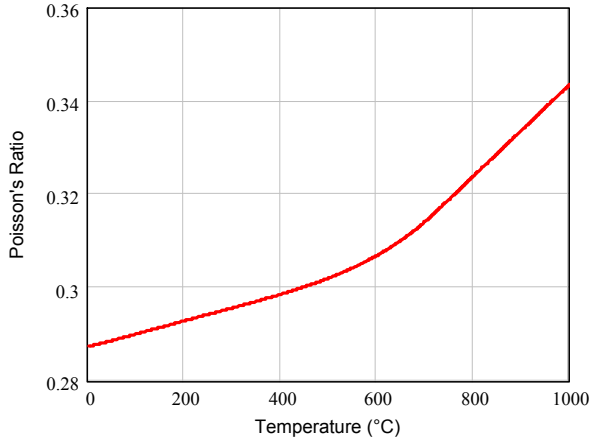
The failure criteria for steel were defined in terms of plastic strains. The multiaxial fracture strain criterion for true stress and true strain was evaluated under a uniaxial stress condition. For element sizes ranging from 0.025 in. to 0.75 in., a relationship between element size and equivalent uniaxial fracture plastic strain was established. The process was repeated for steel at temperatures 20 °C, 100 °C, 300 °C, 500 °C, and 700 °C leading to a fracture criteria for various mesh sizes of components. Figure 4–6 (a) shows the ratio of the maximum plastic strain in the direction of applied displacement-to-uniaxial plastic strain vs. element size at various temperatures. The finite element analysis results were extrapolated to an element size of 50 in. based on the linear curve fit to the analysis results shown in Fig. 4–6 (a). Plastic strain shown in Fig. 4–6 (b) was used as the fracture criterion for the corresponding element size in subsequent finite element analyses.

Weld properties at all temperatures were assumed to have essentially the same material properties as the base metal of the same ultimate tensile strength (see NIST NCSTAR 1-3). High temperature properties of weld metals were not found in the literature, however, most observed fractures in the exterior columns were in the base metal and not the welds.

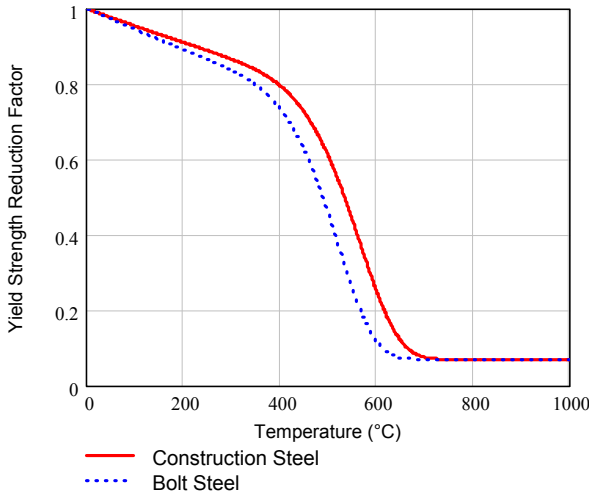
ASTM A325 bolts were used in the perimeter column, spandrel, and floor truss connections. In addition to accounting for shear strength, the analyses included load elongation curves developed for tensile loading of bolts.



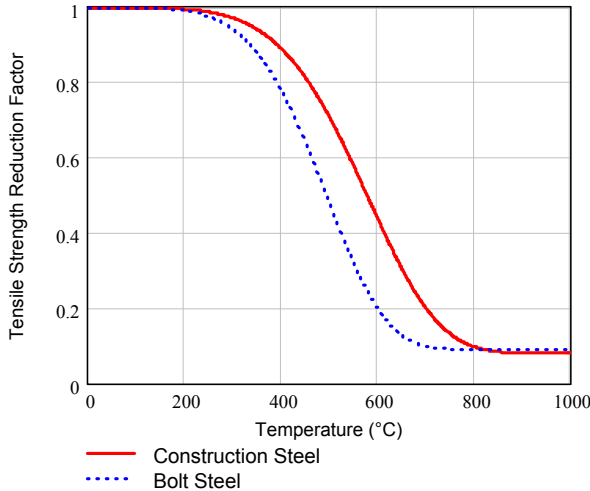
(a) Modulus of elasticity



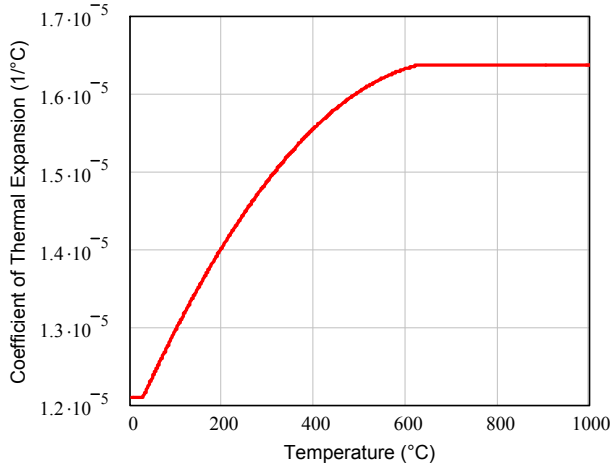
(b) Poisson's ratio



(c) Yield strength reduction factor

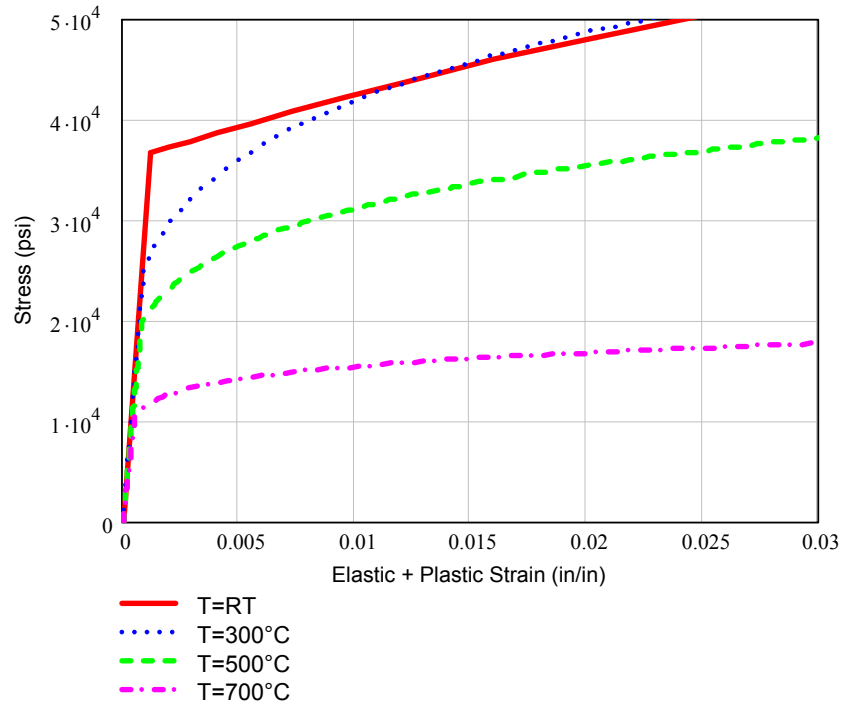


(d) Tensile strength reduction factor

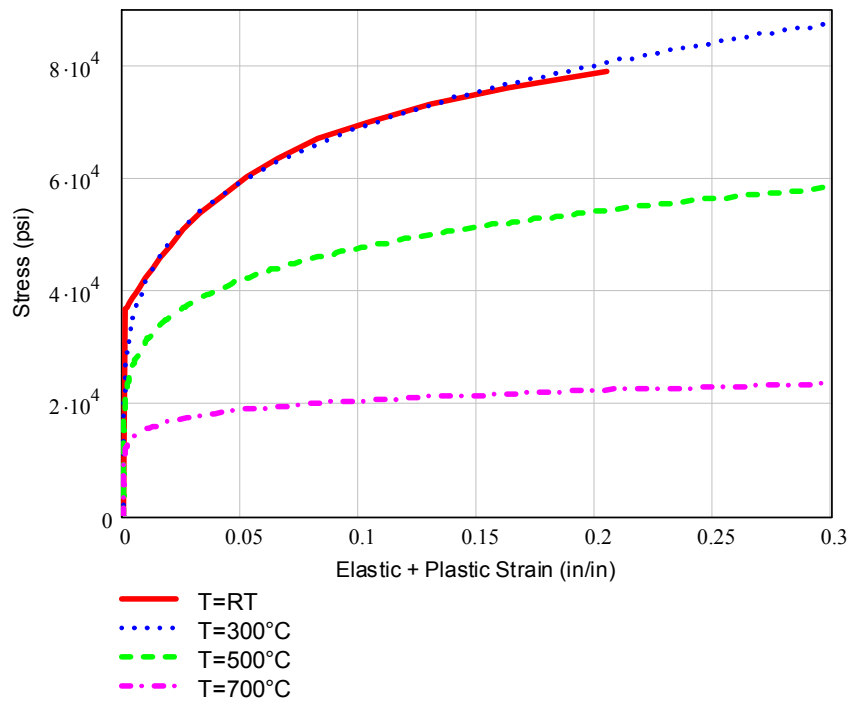


(e) Instantaneous coefficient of thermal expansion

Figure 4-3. Temperature-dependent properties for all steels.



(a) Strain < 0.03



(b) Strain < 0.30

Figure 4-4. Stress-strain relationships for Material ID 1 steel.

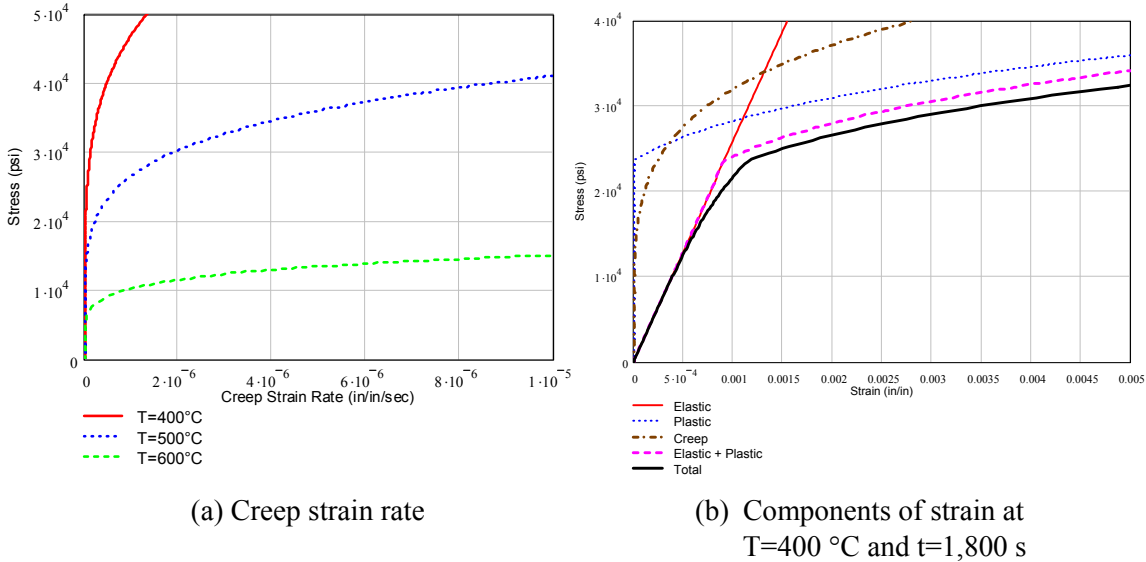


Figure 4–5. Strain behaviors at elevated temperatures for Material ID 1 steel.

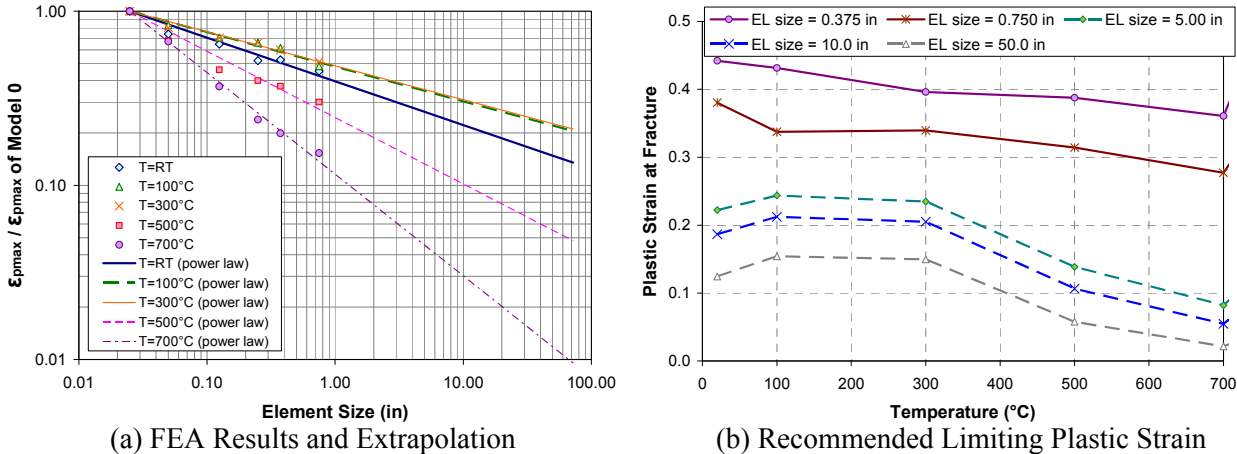


Figure 4–6. Maximum plastic strain from the finite element analysis and limiting plastic strain.

4.2 FLOOR SUBSYSTEM ANALYSIS

The floors played an important role in the structural response of the World Trade Center towers to the aircraft impact and ensuing fires, and were identified as a critical subsystem requiring study prior to the development of global models for each tower. The floor system in the office area, outside the core, was a composite system consisting of a lightweight concrete slab supported by steel trusses. Within the core area, a composite steel beam and normal weight concrete slab floor system was used.

The floor subsystem analysis included: (1) the translation, validation, and modification of ANSYS models to incorporate nonlinear behavior, (2) evaluation of structural response under dead and live loads and elevated structural temperatures, (3) identification of failure modes and associated temperatures and times to failure, and (4) reduction in complexity of detailed component models for inclusion in the floor model.

Component analyses included the truss seat connections, shear connectors between the truss and lightweight concrete slab (referred to as knuckles), and a single truss and concrete slab section.

The failure modes and the failure loads for different components of the full floor subsystem were evaluated through analysis of detailed models of those components, using either hand calculations or finite element analyses. Models with a reduced size and/or complexity that captured the failure loads and failure modes were then developed for each component. These modified models of component behavior were incorporated in the full floor subsystem model.

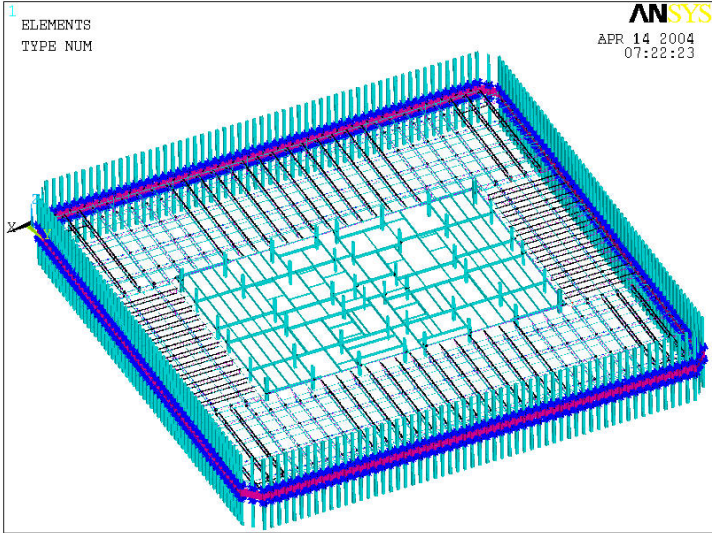
4.2.1 Description of Floor Subsystem

The WTC towers had two types of floors above the plaza and mezzanine areas, tenant floors and mechanical floors. The structural layout and features of the tenant floors were similar throughout the towers, with minor differences in component dimensions and core framing layouts. Core framing changes were made to accommodate stairs, vents, and other features that varied in their locations between floors. Most of the floors in the towers were tenant floors. Mechanical floors were located at the skylobby levels and near the roof level of the towers (floors 7, 9, 41, 43, 75, 77, 107, 108, and 110). The aircraft impact and ensuing fires did not directly affect any mechanical floors.

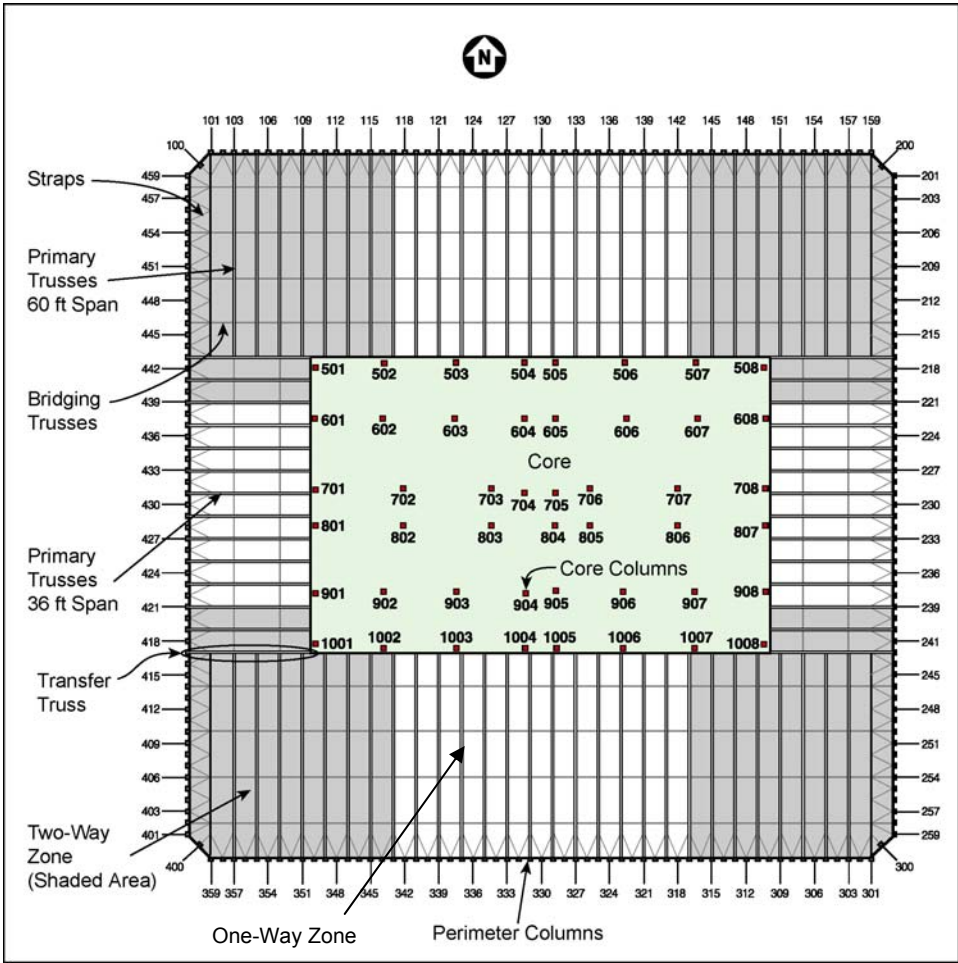
Figures 4–7 (a) and (b) illustrate the structural layout and features of Floor 96 in WTC 1. The core area contained the elevators, stairways, mechanical shafts, restrooms, and storage areas. Office space was generally located outside the core where the floors were supported by truss framing. Above the 77th floor, a portion of the core was used for office space since there were fewer elevator shafts and the additional floor space could be used for tenant occupancy.

The floor system for WTC 1 and WTC 2 consisted of a lightweight concrete floor slab supported by steel trusses that spanned between the core and perimeter walls and a normal weight concrete floor slab supported by steel beams in the core area. There were three “types” of trusses comprising the floor system as illustrated in Fig. 4–7 (b). The trusses that spanned from the core to the exterior wall were referred to simply as “trusses” or were sometimes called “primary” or “main” trusses, or on some contract drawings, “C32” trusses. Trusses which ran perpendicular to the primary trusses were called “bridging trusses.” At the corners of the floor areas, special trusses referred to as “transfer trusses” supported the end reactions of several primary trusses. This section will focus on the load-carrying trusses which will be referred to as “primary trusses.”

Figures 4–8 and 4–9 illustrate a primary truss section and connection details. The primary trusses, which were installed in pairs, were spaced 6 ft-8 in. on center and had a nominal clear span of either 60 ft for the long span direction or 35 ft for the short span. The trusses, commonly referred to as steel bar joists, were fabricated using double-angles for the top and bottom chords, and round bars for the webs. The web members protruded above the top chord in the form of a “knuckle” which was embedded in the concrete slab and provided composite action between the trusses and the slab. Additionally, the floor system included bridging trusses (perpendicular to the primary trusses) spaced 13 ft-4 in. on center. In the corners of the towers, the bridging trusses acted with the primary trusses to provide two-way floor action, where loads were transferred to both perimeter walls near the corners and the transfer truss that ran between the core corner and the exterior wall.



(a) Single floor structural system (without slab)



(b) Floor plan

Figure 4-7. Floor structural subsystem (WTC 1, Floor 96).

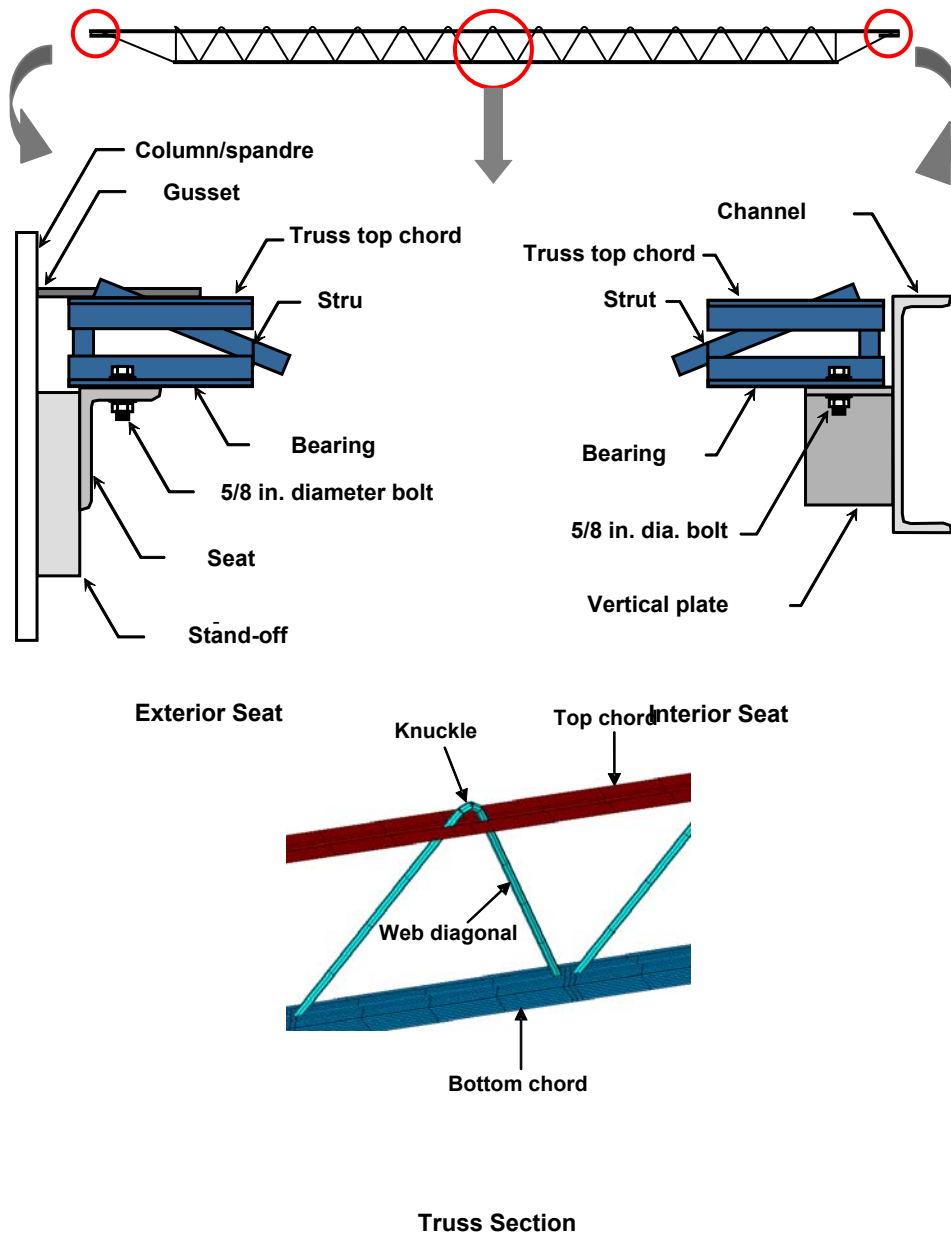


Figure 4–8. Primary truss components.

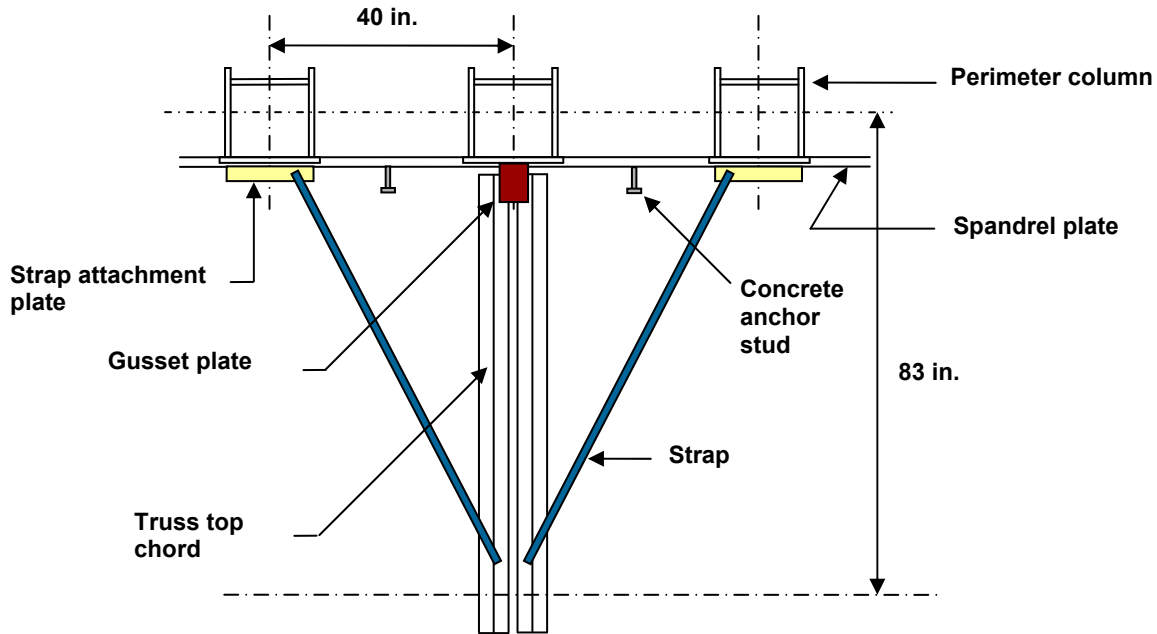


Figure 4–9. Plan view of truss seat connection, straps, and horizontal studs.

The primary trusses were supported by a seat angle at the exterior wall and a stiffened seat at the interior ends. The trusses framed into every other perimeter column (the odd numbered columns). The interior stiffened seat was welded to a steel channel that ran continuously around the core area. The steel channel was supported by the perimeter core columns through stub beam members. Each truss was attached to the seat with a 5/8 in. bolt through a truss bearing angle. The exterior seat angles and interior stiffened seat had 1 3/4 in. slotted holes. At the exterior wall connection, there were three additional components that tied the floor subsystem to the perimeter columns. A gusset plate was welded to the spandrel with a complete penetration groove weld and to the top chord of the two primary trusses with a fillet weld. Additionally, a pair of straps with shear studs tied the primary trusses to the intermediate columns and a shear stud, welded to the spandrels between each column, anchored the concrete slab.

The lightweight concrete slab was supported by a 22 gauge, 1 1/2 in. deep “Type B” steel deck. The steel deck was supported by the top chord of the bridging trusses (which were 1 1/2 in. below the primary truss top chord) and by deck support angles. The concrete slab had two layers of welded wire fabric reinforcement, and steel reinforcing bars at the perimeter of the floor, perpendicular to the primary trusses at the knuckles, over the trench headers (conduits for electrical wiring in the floor) and at the interface between the lightweight and normal weight concrete slabs to maintain slab continuity.

4.2.2 Truss Seats

The truss seat connections transferred floor gravity loads to the exterior and core columns and provided lateral bracing for the columns. All seat connections were similar in design, but varied in their dimensions and weld sizes. For Floor 96 of WTC 1, there were seven types of interior truss seats and eight types of exterior truss seats. The different types of interior truss seats were identified with Detail Numbers 15, 17, 20, 21, 22, 23, and 226A; and the exterior truss seats with Detail Numbers 1013, 1111, 1212, 1311, 1313, 1411, 1511, and 1611, as shown in Fig. 4–10.

stand off plates (see Fig. 4–8). The seat restrained the moment until the horizontal force in the connection caused slip between the seat angle and bearing angle. Fillet welds, connecting the stand-off plates to the spandrel, resist shear, bending, and compression, and controlled the seat capacity. The controlling failure mode was fracture of the fillet welds at this connection, which resulted in loss of vertical support.

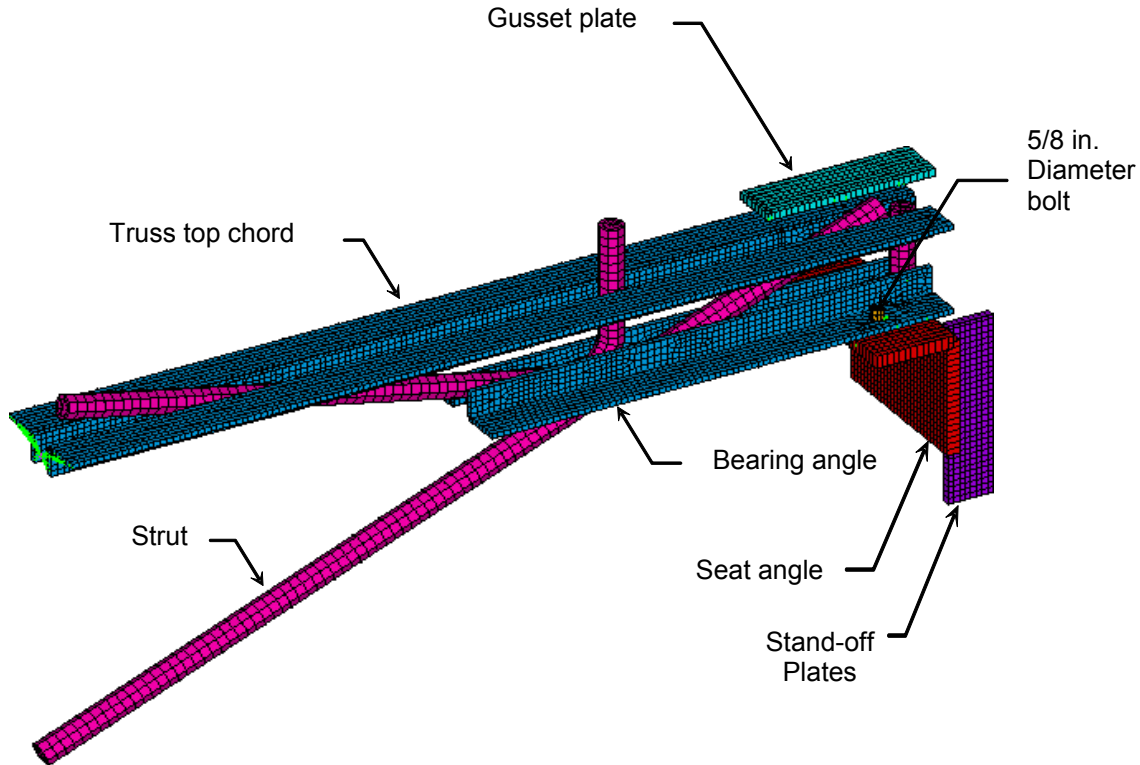
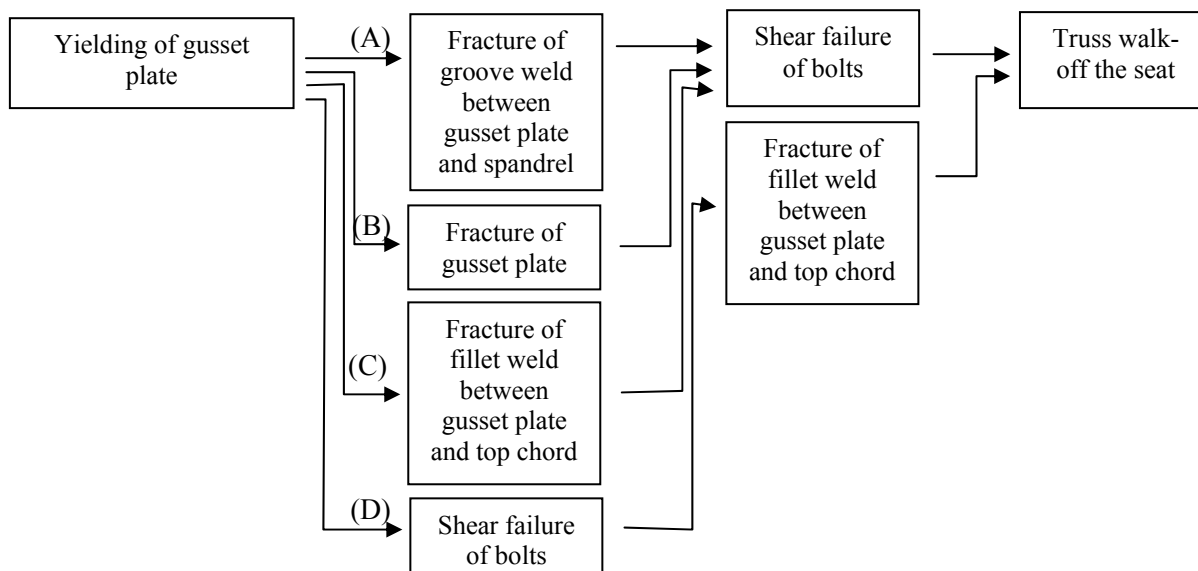


Figure 4–11. Finite element model of exterior seat.

The failure modes for the truss seats were identified for vertical force (shear), horizontal tensile force, horizontal compressive force, and combined vertical and horizontal force. Failure modes and sequences of failure were computed for each truss seat type. The capacity of, for example, an exterior seat due to horizontal tensile (pull-in) force was determined by considering: (1) fracture of the groove weld between the gusset plate and spandrel, (2) fracture of the fillet weld between the gusset plate and the truss top chord, (3) tensile fracture of the gusset plate, and (4) shear failure of the bolted connection by bolt shear, bolt bearing, tear-out, and block shear. For calculation purposes, the bolts were assumed to be centered in the slotted holes. The typical failure sequence of the truss seat was determined to be: yield failure of the gusset plate, yielding followed by fracture of the gusset plate groove weld, truss deformation leading to bolt bearing against the slotted hole, bolt shear failure, and finally the truss slipping or “walking off” the seat. The travel distance for the truss to walk off the seat was computed to be 4 5/8 in. This failure sequence is illustrated in Fig. 4–12 as path (A) and shown in Fig. 4–13, where the relationship between the tensile force resistance from the seat connection and the truss travel distance is plotted. In this plot, frictional resistance between the seat angle and bearing angle was not included.

Under combined vertical and horizontal forces, the failure modes were a combination of the individual failure modes for vertical and horizontal forces.

A typical interaction relationship for the capacity of an interior seat against combined vertical and horizontal tensile forces is shown in Fig. 4–14.



(A) Seat details 1311, 1411, 1511, and 1611 at all temperatures.

(B) Seat detail 1111 at all temperatures.

(C) Seat detail 1013 at temperatures below 100°C.

(D) Seat details 1212 and 1313 at all temperatures, and detail 1013 at temperatures more than or equal to 100°C.

Figure 4–12. Failure sequence of the exterior seats against tensile force.

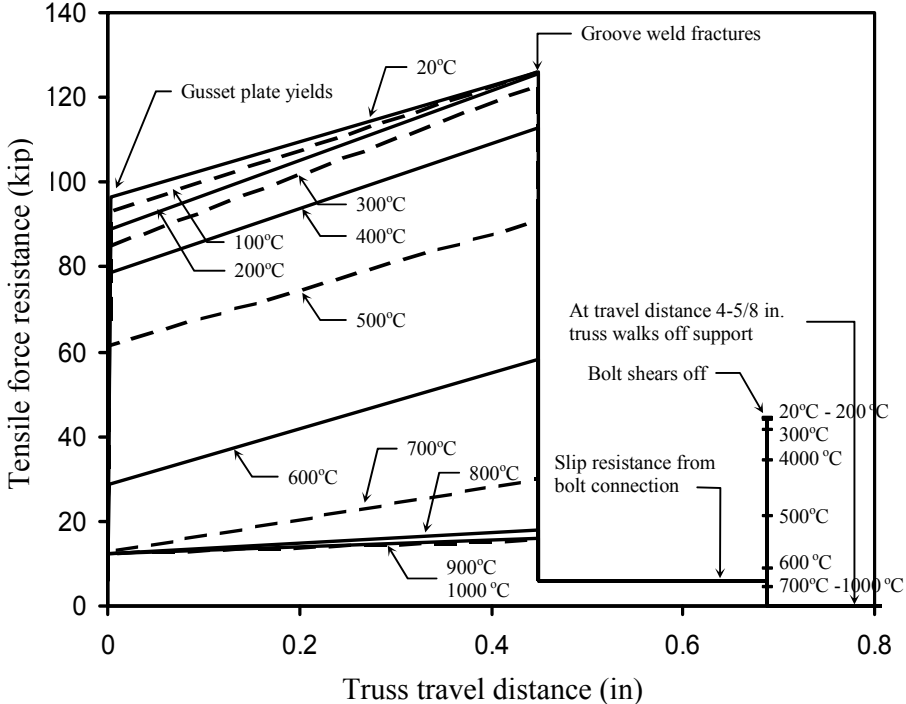


Figure 4-13. Capacity of exterior seat against tensile force (Detail 1411 in Fig. 4-10).

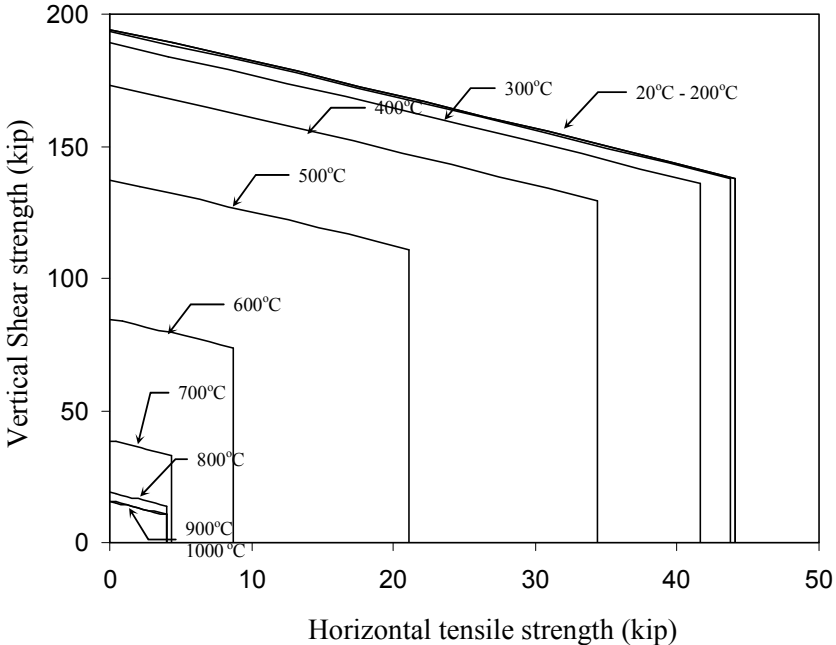


Figure 4-14. Capacity of interior seat against vertical and horizontal force (Detail 22 in Fig. 4-10).

Loads

Truss seat failures were analyzed for vertical and horizontal loads. The floor system gravity loads were approximately 80 psf for dead load and service live load. The dead load is the weight of the floor system and the service live loads are the loads due to occupancy that are supported by the floor, which are generally on the order of 25 percent of the design live loads. The load from the pair of trusses that each truss seat connection supported was approximately 16 kips for the 80 psf service gravity loads (where 16 kips = $\frac{1}{2} \times 60$ ft span \times 6.67 ft width \times 80 psf).

Computation Results

Tables 4–2 through 4–5 show the computed capacity of each truss seat detail as a function of steel temperature and loading direction. Truss seat capacities against vertical and horizontal force are presented graphically in Figs. 4–15 and 4–16, respectively. In general, the exterior seat had a greater horizontal tensile capacity, and the interior seat had a greater vertical shear capacity. Even though the controlling failure mode for vertical shear was weld fracture, truss seat connection failure from vertical loads was less likely, given the capacities listed in Tables 4–2 and 4–3. The vertical load at the truss connection of approximately 16 kips would have had to increase by a factor of 2 to 6 to reach failure (weld fracture) for temperatures near 600 °C to 700 °C.

Table 4–2. Interior seat capacity against vertical force.

| Temp. (°C) | Connection Capacity Against Vertical Force (kip) | | | | | | |
|---------------|--|-----|-----|-----|-----|-----|-------|
| | #15 | #17 | #20 | #21 | #22 | #23 | #226A |
| 20 | 233 | 233 | 274 | 229 | 194 | 194 | 395 |
| 100 | 233 | 233 | 274 | 229 | 194 | 194 | 395 |
| 200 | 232 | 232 | 273 | 228 | 194 | 194 | 393 |
| 300 | 226 | 226 | 267 | 223 | 189 | 189 | 384 |
| 400 | 207 | 207 | 244 | 204 | 173 | 173 | 352 |
| 500 | 164 | 164 | 194 | 162 | 137 | 137 | 279 |
| 600 | 101 | 101 | 119 | 100 | 85 | 85 | 172 |
| 700 | 46 | 46 | 54 | 45 | 39 | 39 | 78 |
| 800 | 23 | 23 | 27 | 22 | 19 | 19 | 38 |
| 900 | 19 | 19 | 22 | 18 | 16 | 16 | 32 |
| 1000 | 19 | 19 | 22 | 18 | 16 | 16 | 32 |

Table 4–3. Exterior seat capacity against vertical force.

| Temp. (°C) | Connection Capacity against Vertical Force (kip) | | | | | | | |
|---------------|--|-------|-------|-------|-------|-------|-------|-------|
| | #1013 | #1111 | #1212 | #1311 | #1313 | #1411 | #1511 | #1611 |
| 20 | 94 | 94 | 111 | 94 | 94 | 140 | 193 | 207 |
| 100 | 94 | 94 | 111 | 94 | 94 | 140 | 193 | 207 |
| 200 | 93 | 93 | 110 | 93 | 93 | 139 | 192 | 206 |
| 300 | 91 | 91 | 108 | 91 | 91 | 136 | 187 | 201 |
| 400 | 84 | 84 | 100 | 84 | 84 | 126 | 172 | 184 |
| 500 | 69 | 69 | 81 | 69 | 69 | 102 | 136 | 146 |
| 600 | 45 | 58 | 53 | 60 | 45 | 78 | 84 | 90 |
| 700 | 29 | 26 | 34 | 27 | 29 | 35 | 38 | 41 |
| 800 | 14 | 13 | 17 | 13 | 14 | 17 | 19 | 20 |
| 900 | 12 | 11 | 14 | 11 | 12 | 14 | 16 | 17 |
| 1000 | 12 | 11 | 14 | 11 | 12 | 14 | 15 | 17 |

Table 4–4. Interior seat capacity against horizontal tensile force.

| Temp. (°C) | Capacity (kip) |
|---------------|------------------------|
| | Shear Failure of Bolts |
| 20 | 44 |
| 100 | 44 |
| 200 | 44 |
| 300 | 42 |
| 400 | 34 |
| 500 | 21 |
| 600 | 9 |
| 700 | 4 |
| 800 | 4 |
| 900 | 4 |
| 1000 | 4 |

Table 4–5. Exterior seat capacity against horizontal tensile force.

| Temp (°C) | Connection Detail Capacity for Horizontal Tensile Force (kip) | | | | | | | |
|--------------|--|--------------------------------|------------------------------|-------------------------------|------------------------------|-------------------------------|-------------------------------|-------------------------------|
| | #1013 | #1111 | #1212 | #1311 | #1313 | #1411 | #1511 | #1611 |
| | Fracture of Fillet Weld/ Shear Failure of Bolts | Fracture of Gusset Plate | Shear Failure of Bolts | Fracture of Groove Weld | Shear Failure of Bolts | Fracture of Groove Weld | Fracture of Groove Weld | Fracture of Groove Weld |
| 20 | 100 | 104 | 182 | 126 | 182 | 126 | 126 | 126 |
| 100 | 138 | 104 | 181 | 126 | 181 | 126 | 126 | 126 |
| 200 | 135 | 103 | 180 | 126 | 180 | 126 | 126 | 126 |
| 300 | 130 | 101 | 174 | 123 | 174 | 123 | 123 | 123 |
| 400 | 115 | 93 | 156 | 113 | 156 | 113 | 113 | 113 |
| 500 | 84 | 75 | 117 | 91 | 117 | 91 | 91 | 91 |
| 600 | 42 | 49 | 67 | 58 | 67 | 58 | 58 | 58 |
| 700 | 20 | 25 | 32 | 30 | 32 | 30 | 30 | 30 |
| 800 | 14 | 16 | 19 | 18 | 19 | 18 | 18 | 18 |
| 900 | 13 | 14 | 17 | 16 | 17 | 16 | 16 | 16 |
| 1000 | 13 | 14 | 17 | 16 | 17 | 16 | 16 | 16 |

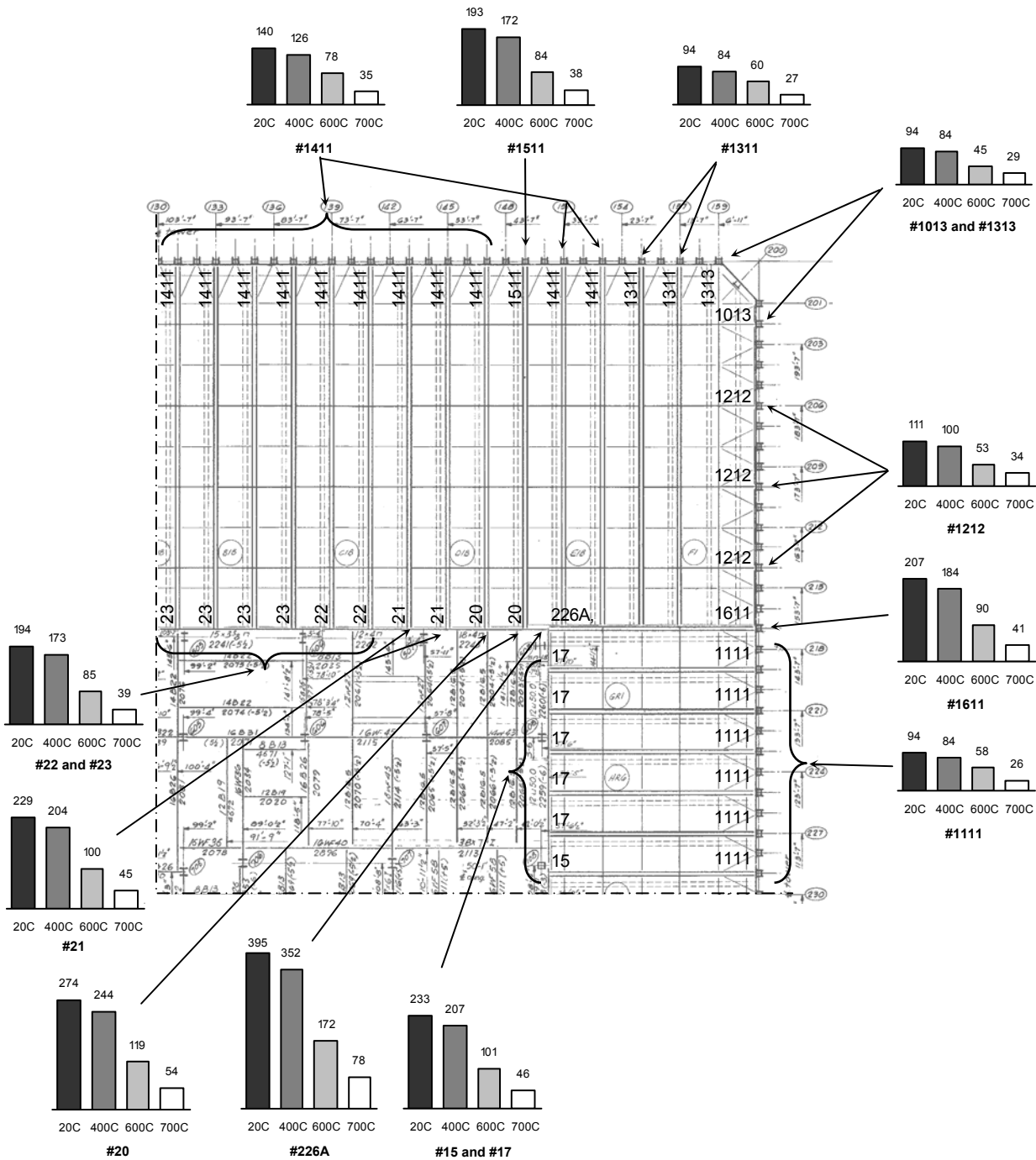


Figure 4-15. Truss seat capacity against vertical force. Reproduced with permission of The Port Authority of New York and New Jersey. Enhancements by NIST.

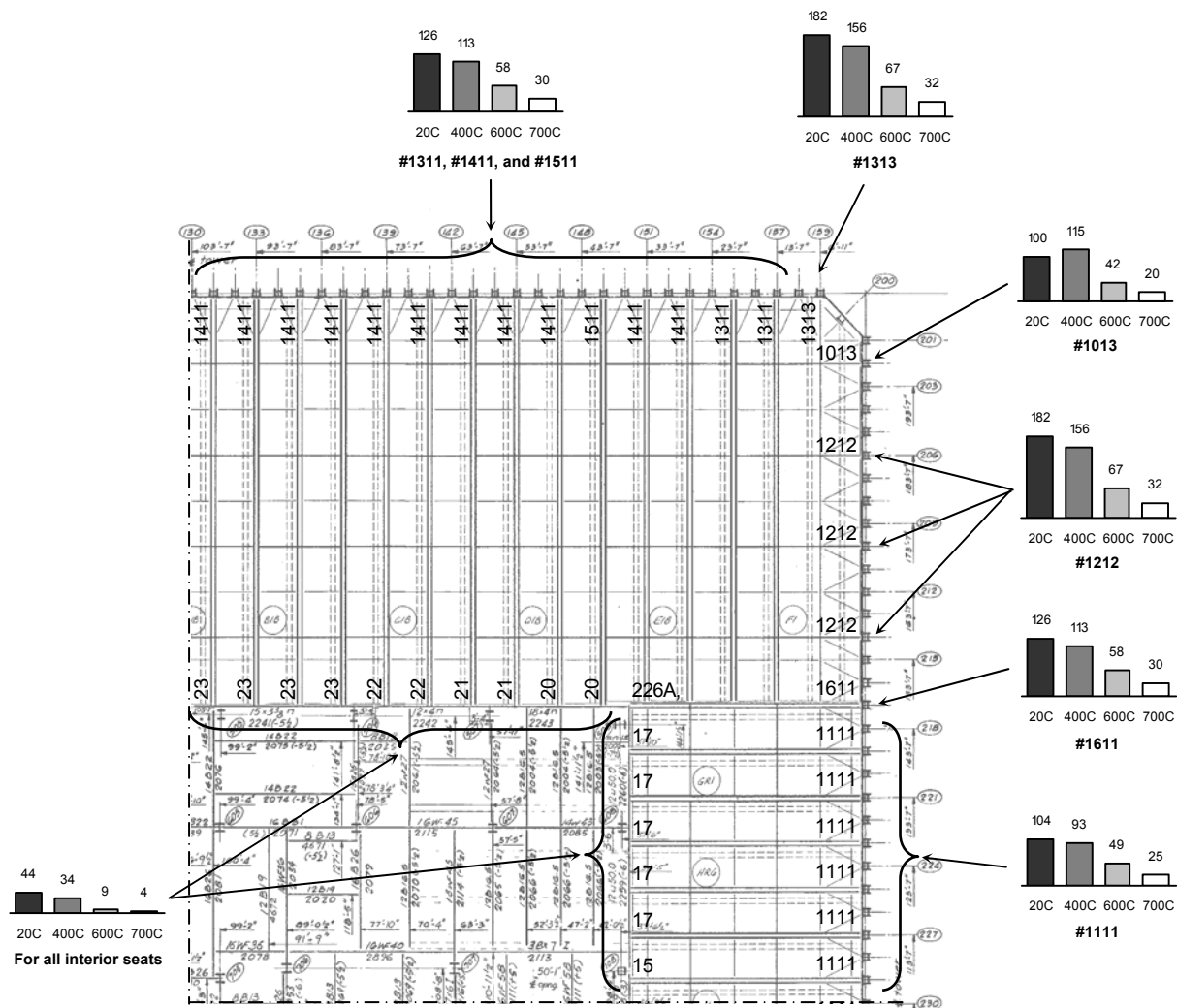


Figure 4–16. Truss seat capacity against horizontal force. Reproduced with permission of The Port Authority of New York and New Jersey. Enhancements by NIST.

Reduced Complexity Model

Break elements (ANSYS user-defined element) were developed for use in the full floor model that captured the temperature-dependent failure modes of the truss seat connections, strap anchors, and spandrel studs. These elements replaced the detailed 3-D solid finite element model used for the truss connection analysis, allowing a reduction in model size.

A break element is a unidirectional spring element that can simulate connection failure by disconnecting two “active nodes” when the relative displacement between two “control nodes” exceeds a specified threshold. Temperature dependence was achieved by coupling the active nodes to a beam element with specified thermal expansion characteristics. Failure modes that required multiple connection failures

were created with break elements using parallel and series constructs. For example, Fig. 4–17 illustrates the sequence of events that occurs for an interior truss seat under a) horizontal tensile loading and b) vertical shear loading.

Figure 4–17 a) shows the results from analysis where the interior truss seat was subjected to a constant vertical load and horizontal displacement increments at 500 °C. Failure of a truss seat subjected to a large horizontal tension and small vertical shear was by bolt shearing off followed by truss walking off the seat. The shear strength of the bolts controlled the truss seat horizontal tension capacity. The bolt shear by itself did not cause the truss to lose its vertical support, but was the prerequisite for truss walking off the seat. The travel distance for a truss to walk off a truss seat was 4 in. for an interior seat.

Figure 4–17 b) shows the results from analysis where the interior truss seat was subjected to a constant horizontal load and vertical displacement increments at 500 °C. In this case, seat failure was governed by fracture of the fillet welds between the vertical plate stiffeners and the channel beam resulting in loss of both vertical and horizontal support.

4.2.3 Knuckles

The “knuckle” is formed by the extension of the truss diagonals into the concrete slab and provides for composite action of the steel truss and concrete slab. The composite action is due to the shear transfer between the knuckle and the concrete slab both in the truss transverse and longitudinal directions. The purpose of this analysis was to predict the knuckle capacity when the truss and concrete slab act compositely and to develop a reduced model of the knuckle behavior for the full floor model.

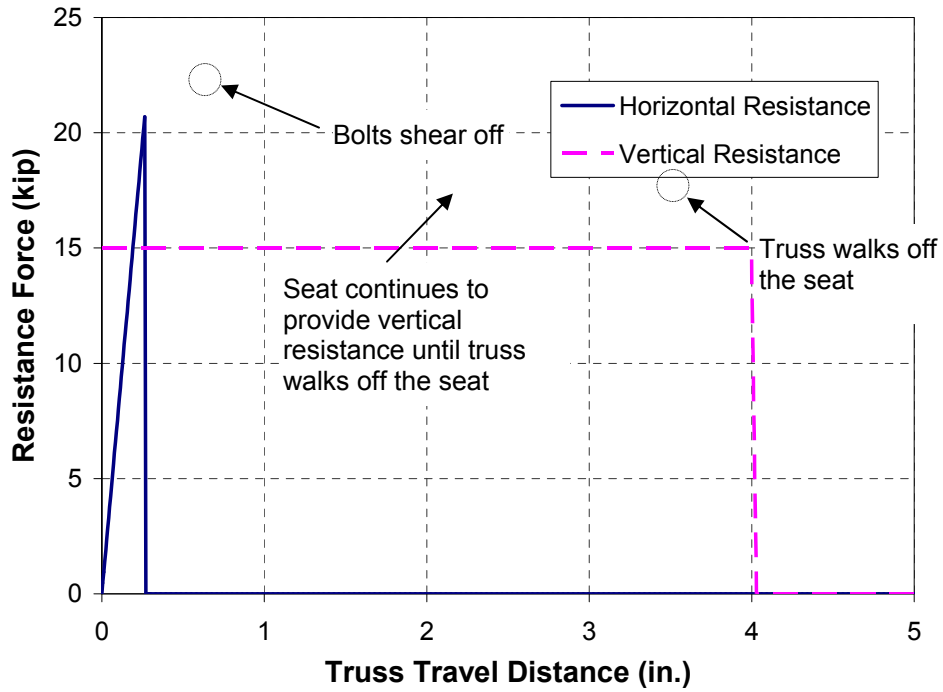
Failure Modes

Failure modes for the knuckles included: (1) horizontal shear failure by crushing of concrete over a small region adjacent to the knuckle and (2) vertical tensile failure where the knuckle pulls a conical section of concrete out of the slab.

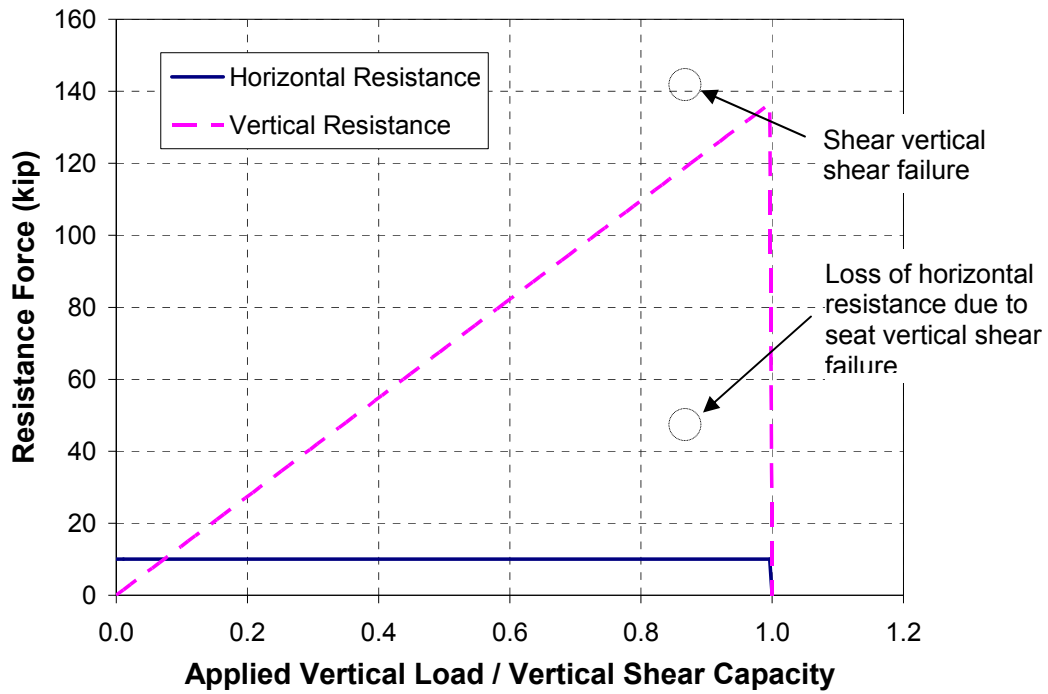
Experimental Data

As part of the original truss design, Laclede Steel Company in Saint Louis, Missouri, conducted experiments in 1967 to determine the transverse and longitudinal shear capacities of the knuckle. Knuckles were cast into two reinforced concrete blocks confined at the corners by angles, as shown in Figure 4–18, and loaded to determine the knuckle shear capacity in both the transverse and longitudinal directions.

The transverse tests were conducted when the lightweight concrete was 6 and 27 days old. The average shear capacity measured was 16.9 kips per knuckle when concrete shear failure occurred. A comparable value of 35 kips per knuckle for the WTC floor system was determined after adjusting for the strength of in-place, mature, lightweight concrete.



a) failure from horizontal force



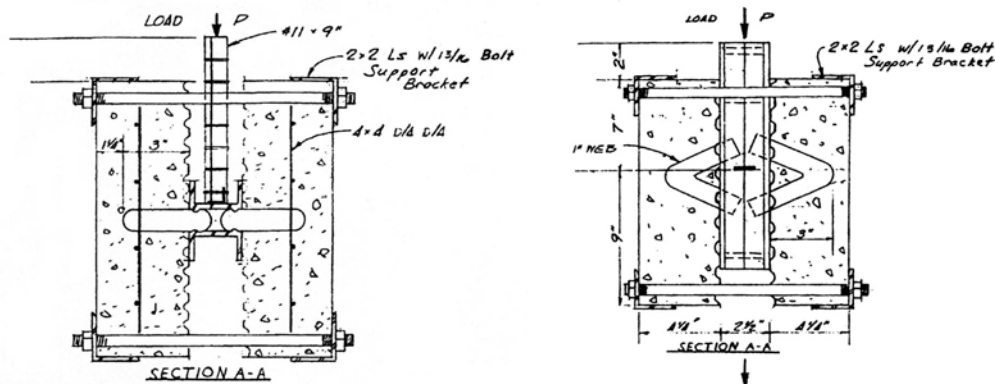
b) failure from vertical shear force

Figure 4-17. Results of interior truss seat model at 500 °C.

The longitudinal tests, which used normal weight concrete, were conducted when the concrete was 28 and 96 days old. Of the five tests conducted, three reported a weld failure in the rebar loading the knuckles, and two reported a failure in the concrete. The average shear capacity measured was 28.3 kips per knuckle. A value of 31 kips per knuckle for the WTC floor system was determined after adjusting for the strength of in-place, mature, lightweight concrete.

Analysis and Results

Finite element analyses of the Laclede knuckle test set-up were conducted to compare analysis results to the measured transverse and longitudinal shear capacities. The bond between the concrete and steel was varied in the analysis; the bars were assumed to be either full bonded or frictionless, which had a significant effect on the results.



Reproduced with permission of Laclede Steel.
(a) Transverse shear test.

Reproduced with permission of Laclede Steel.
(b) Longitudinal shear test.

Figure 4–18. Laclede Steel Company shear tests of a knuckle.

Finite Element Analysis of Tests

The results of the finite element analyses modeling the Laclede tests are shown in Figs. 4–19 through 4–21. Analyses were conducted to establish both the longitudinal capacity and the transverse capacity of the knuckle. The results showed significant dependence on the interface characteristics between the steel and concrete. A plot of compressive stresses for the longitudinal shear model is shown in Fig. 4–19. Results of the analyses for longitudinal shear, with steel-to-concrete interface either fully bonded or completely unbonded (frictionless), are shown in Fig. 4–20. Results showed that each knuckle had strength in the range of 15 kip to 35 kip, depending on the interface condition. When the analysis results were compared to the test results, the fully bonded case showed better agreement.

Compressive stresses for the transverse shear model are plotted in Fig. 4–21. The small crushed regions indicate that a pair of knuckles can be expected to behave nearly independently of each other, and, therefore, have nearly double the capacity of a single knuckle. The transverse shear results (Fig. 4–22) showed that transverse knuckle strength was about 24 kip for the frictionless condition with 2,500 psi concrete, which corresponds to 39 kip for 4,100 psi concrete. For the full bonded case, the analysis was terminated at 20 kip per knuckle before reaching the ultimate strength.

Although the analysis showed the sensitivity of the results to the steel-concrete interface assumptions, it supported the shear capacities determined from test results.

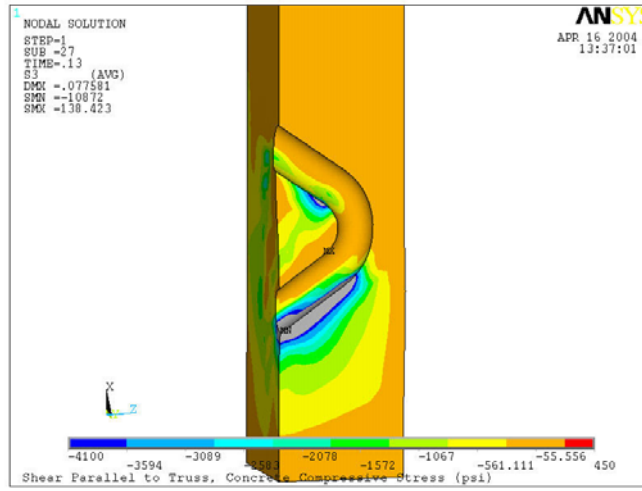


Figure 4–19. Compressive stresses in longitudinal shear finite element model (4,100 psi concrete).

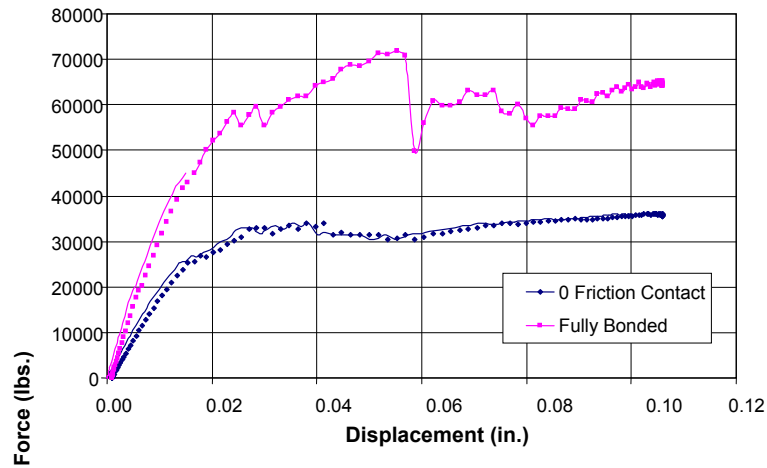


Figure 4–20. Shear force versus displacement from finite element model for longitudinal shear of two knuckles (4,100 psi concrete).

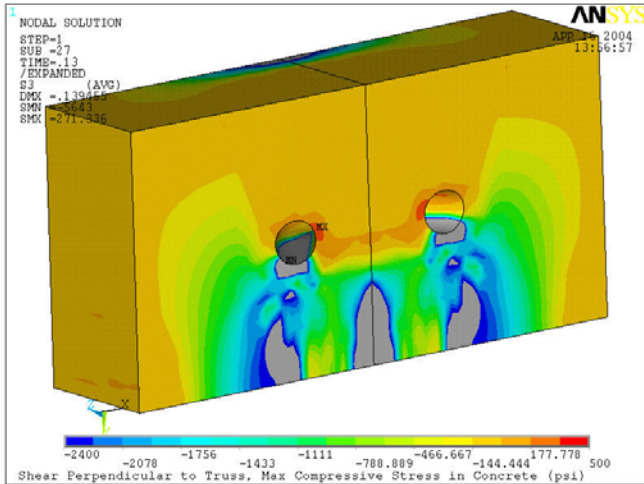


Figure 4–21. Compressive stresses in transverse shear finite element model (2,500 psi concrete).

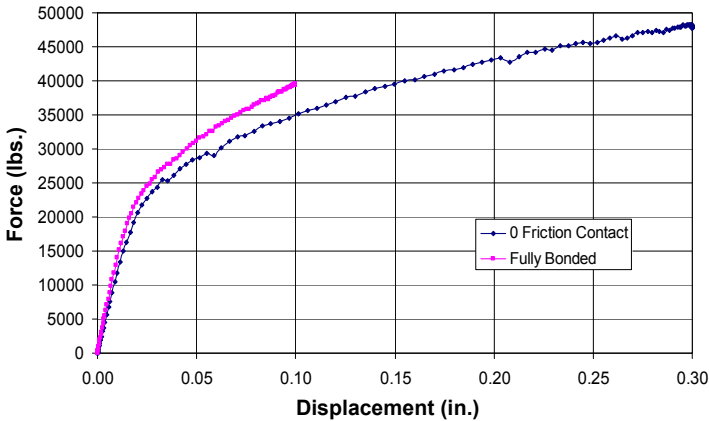


Figure 4–22. Shear force versus displacement from finite element model for transverse shear of two knuckles (2,500 psi concrete).

Reduced Model

Based upon the analysis results, a reduced model with beam and break elements was developed for the composite floor section with a single truss and the full floor models. The temperature-dependent knuckle behavior was represented with 15 break elements and five beam elements.

Based on the results of the Laclede tests and the finite element analyses, the knuckle capacity for the reduced model was estimated and is shown in Table 4–6. Steel temperatures in Table 4–6 were assumed with a corresponding reduction in concrete temperature immediately around the knuckle of 75 °C to 150 °C. Concrete has a lower coefficient of conductivity and does not respond as rapidly to rising temperatures as steel.

Table 4–6. Knuckle shear capacity reduction for elevated temperatures.

| Steel temperature (°C) | Concrete temperature (°C) | Knuckle shear capacity (kip) |
|---------------------------|------------------------------|---------------------------------|
| 20 - 375 | 20 - 300 | 30 |
| 550 | 450 | 24 |
| 725 | 600 | 19 |
| 900 | 750 | 15 |

4.2.4 Single Truss and Concrete Slab Section

A single composite truss with concrete slab was modeled to study failure modes and sequences of failures under gravity and thermal loads. The thermal loading approximated a uniform heating condition, not a fire exposure from the WTC towers. The purpose of these analyses was to determine the relative importance of the truss and slab components and their failure modes. These results were used to develop a reduced truss model for the full floor model that captured essential behaviors while reducing the level of model complexity.

Failure Modes

Two possible deformation/failure modes were identified for the floor-truss section:

- Sagging of the floor section due to yielding or buckling of truss components or failures of the knuckle/concrete interface,
- Loss of truss seat support due to combinations of vertical and horizontal loads and thermal weakening that result in bolt shear and truss walk-off or stand-off plate weld failure at the spandrel.

Truss weld failures were not included as a failure mode. From data gathered from the truss manufacturer, the resistance welds between the web and chord members were found to have a greater capacity than the members they connected.

Finite Element Model

Figure 4–23 illustrates the composite truss and concrete slab model. Symmetry allowed modeling one of the two trusses and one half of the 80 in. composite concrete slab. The model included two perimeter columns, the spandrel, the truss seat, and strap attachments. Each column extended one floor above and one floor below the floor section to account for interaction between the exterior wall and the floor section. Each column was attributed with half of its area and bending properties to account for the symmetry reduction of the floor section. The interior and exterior truss seat connections were also included. The truss was restrained at bridging truss locations to simulate the lateral bracing that would be provided at the bottom chord.

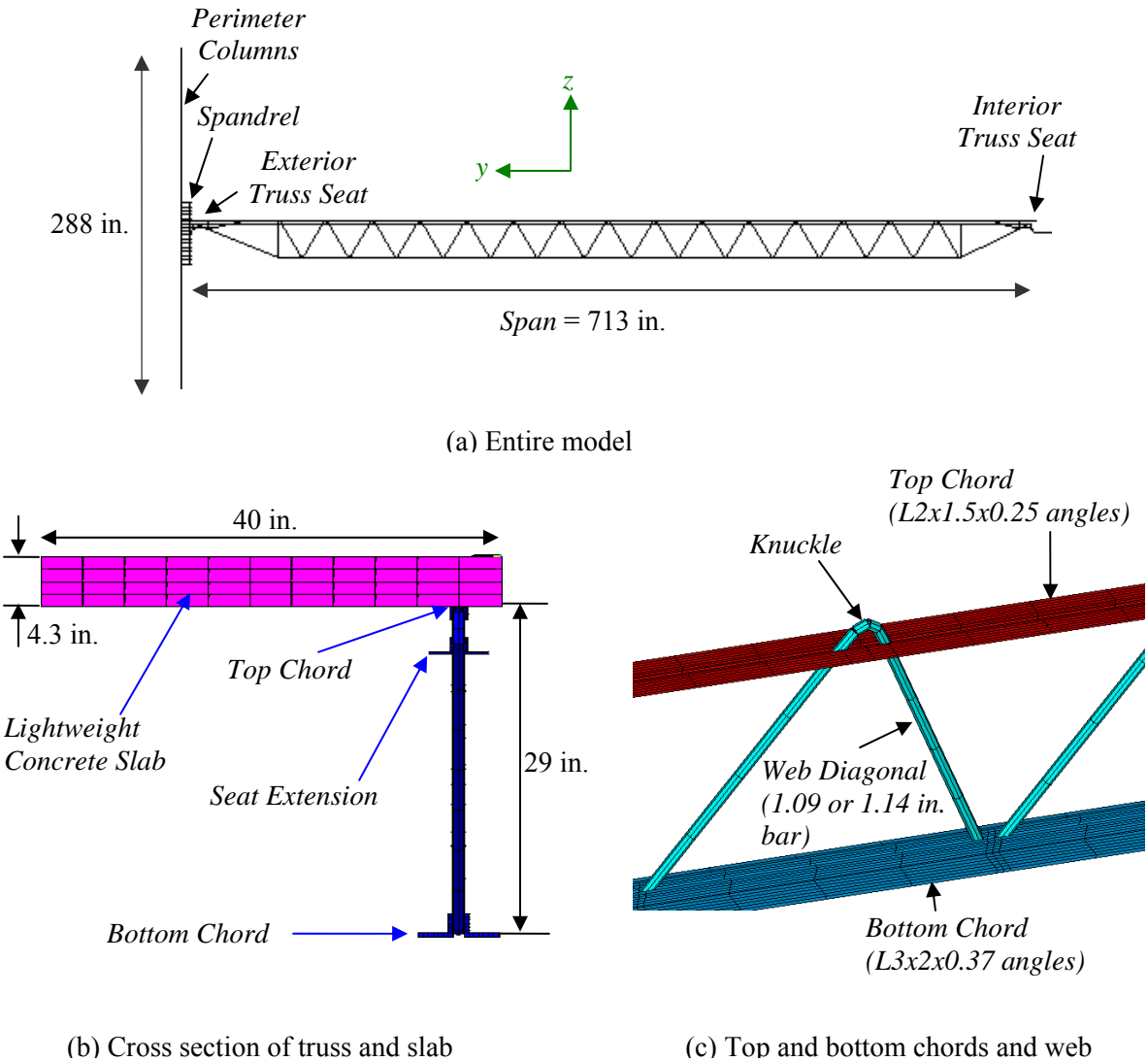


Figure 4-23. Composite truss and concrete slab model.

The concrete slab was modeled as an isotropic plate with a thickness of 4.3 in. (the average thickness of a 4 in. slab on 1 1/2 in. metal deck) using eight-node solid elements. The Hjeltn plasticity model was used with the solid elements to allow different yield strengths in tension and compression. Slab cracking was simulated by assuming tensile plasticity after the onset of cracking, where the reinforcement carried the tensile load.

The top and bottom chords of the truss were modeled with quadratic finite strain beam elements with temperature dependent elastic, plastic, and creep material properties. The chords had four elements between panel points (a panel point is the intersection of the web diagonal and chord).

Loading

Loading of the truss model consisted of gravity dead and live loads and temperature histories for the truss, truss seats, and concrete slab. The gravity loads included the weight of the structure, 8 psf superimposed dead load (including nonstructural dead loads due to architectural items and fixed service equipment), and 13.75 psf of live load equal to 25 percent of design live load of 55 psf. The temperature was ramped from 20 °C to 700 °C in the steel members; from 20 °C to 700 °C at the bottom surface of the slab and from 20 °C to 300 °C at the top surface of the slab over a period of 1,800 s. Thereafter, the truss and concrete temperatures were linearly increased by 200 °C at 2,400 s. A linear gradient through the thickness of the slab was assumed. Temperature loading was not applied to the columns.

Effects of construction sequence were included by applying the ANSYS “element birth and death” feature to the concrete slab. This feature allows elements to be treated as either acting or not acting, as defined by the user. In the first step, the self-weight of the truss members and concrete slab was applied to the truss without the concrete slab acting (i.e., fresh concrete has no strength). In the second step, the concrete slab was reactivated (i.e., cured concrete now able to carry load), and superimposed dead load and live load were applied.

To determine the effect of debris load on the truss behavior, the gravity load was increased until the analysis failed to converge, signaling collapse.

Analysis and Results

Under gravity load to simulate casting of the concrete slab, the maximum calculated vertical deflection was found to be 1.7 in. downward. Note that the design camber ranged from 1 in. to 2 in. to accommodate this deflection, resulting in a slab of uniform thickness. When the superimposed dead load and the live load were applied to the truss and concrete slab, the maximum calculated vertical deflection was 2.0 in. The maximum stress in the top chord, bottom chord, diagonal, and end diagonal strut were 14.8 ksi, 11.6 ksi, 6.7 ksi, and 15.7 ksi, respectively.

For gravity and thermal loading, the analysis was carried out statically until the solution failed to converge at which point the analysis was switched to dynamic mode with 5 percent Rayleigh damping to overcome convergence difficulties. The analysis proceeded to a temperature of 727 °C. Figure 4–24 shows the vertical displacement contour at 700 °C. Figure 4–25 presents plots of displacement versus temperature where Fig. 4–25 (a) is the horizontal displacement at Column 143, and Fig. 4–25 (b) is the vertical displacement at midspan after the self-weight is applied. A positive horizontal displacement indicates that the exterior columns were pushed out, and negative vertical displacement indicates that the truss deflected downward. For the assumed thermal loading, the analysis indicated that, at 445 °C, the horizontal displacement at the exterior column started to decrease, and at 565 °C, the exterior columns began to pull inward.

The plot of the deflected shape shown in Fig. 4–24, shows that compression diagonals at the core end of the truss have buckled, and the floor system has deflected approximately 42 in.

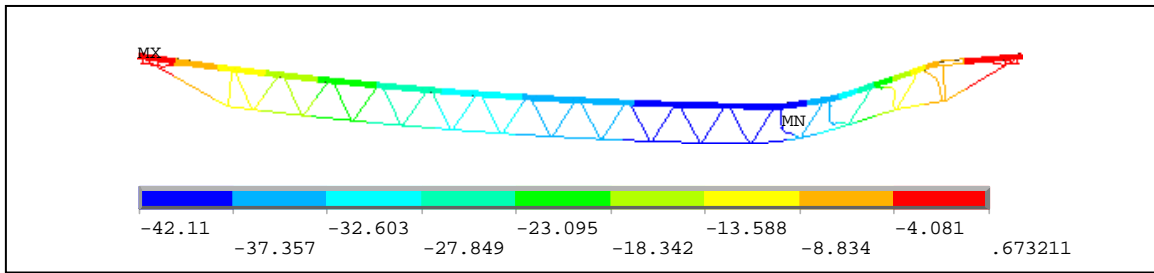
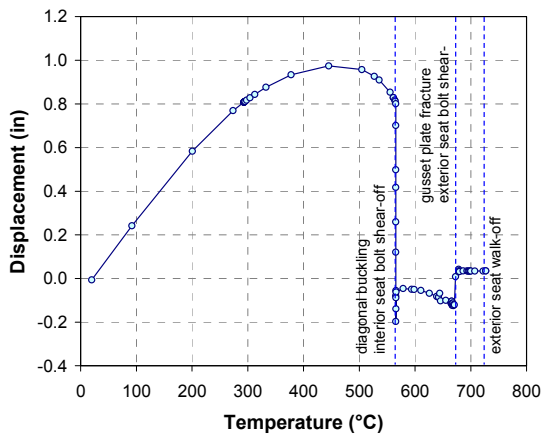
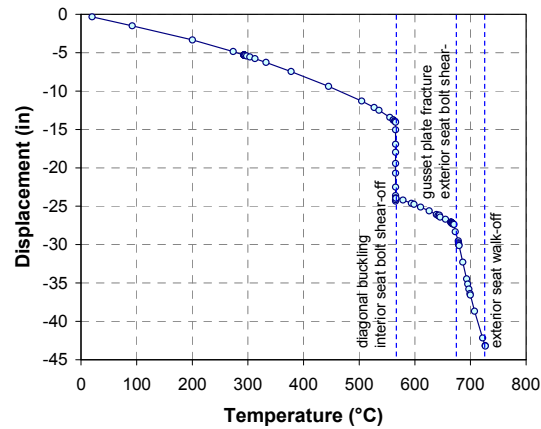


Figure 4-24. Vertical displacement at 700 °C.



(a) Horizontal displacement at column 143



(b) Vertical displacement at midspan

Figure 4-25. Displacement versus temperature.

The truss behavior under the gravity and uniform thermal loading where the temperature was ramped up to 727 °C can be summarized as follows:

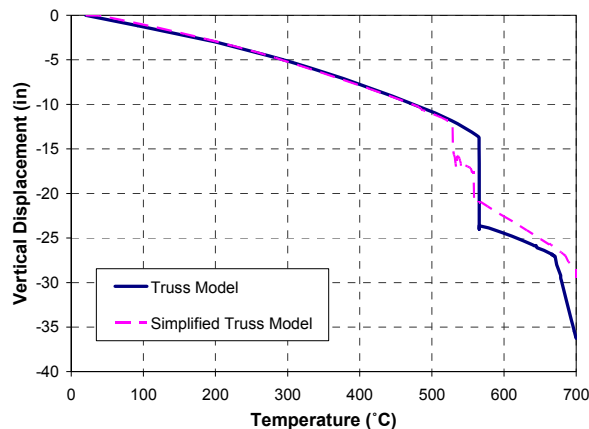
- The stud on the spandrel and studs on the strap anchor failed in shear below 275 °C.
- The first knuckle from the interior end failed in vertical tension at around 100 °C, and the second and third knuckles from the interior end failed in the horizontal shear at 566 °C.
- Top chords yielded above 300 °C due to the difference in coefficients of thermal expansion of steel and lightweight concrete.
- Four compression web diagonals buckled due to high axial compressive force at 565 °C.
- The interior truss seat bolts sheared off at 566 °C.
- The gusset plate fractured and the exterior truss seat bolts sheared off at around 680 °C.
- The truss walked off the exterior truss seat at 730 °C.

Reduced Model

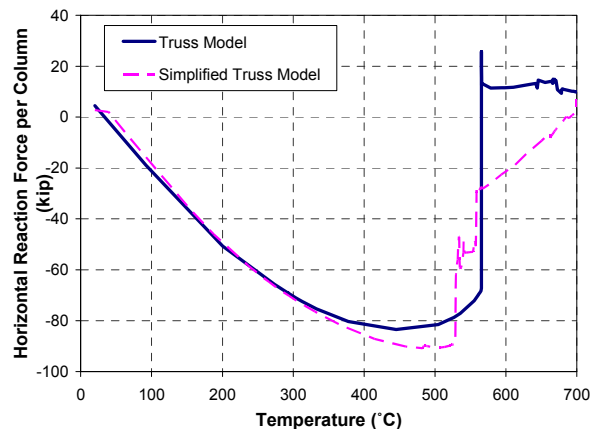
For the full floor subsystem model, the trusses were reduced in size. The reduced model captured essential behavior: (1) the same total horizontal reaction force under the thermal loading and (2) the same vertical deflection at midspan under the thermal loading. The reduced truss model had the following features:

- The geometry of the truss was preserved.
- A pair of trusses was merged into one truss. Areas of truss members were doubled.
- The top and bottom chords and diagonals were modeled by 3-D linear finite strain beam elements (BEAM 188). A member between two panel points was modeled by one element only.
- Break elements (ANSYS user-defined elements) were used to model the following failure modes: (a) seat bolt shear failure; (b) gusset plate fracture; (c) truss walk-off; (d) diagonal buckling/resistance weld failure; (e) failure of studs on the spandrel; and (f) weld failure between strap anchors and top chords.
- Steel had temperature-dependent elastic and plastic properties. Creep was not included.
- The concrete slab was modeled by SHELL 181 elements with temperature-dependent elastic properties.

Figure 4–26 shows the comparison between the detailed and reduced truss models. Figure 4–26 (a) compares the vertical deflection at midspan while Fig. 4–26 (b) compares the horizontal reaction at exterior columns. Although the reduced truss model predicted buckling of diagonals at roughly 530 °C, which is about 35 °C lower than the temperature at which diagonal buckling occurred in the detailed truss model, overall truss behavior under the uniform thermal loading was found to be in good agreement between the two models.



(a) Midspan vertical deflection



(b) Horizontal reaction force at exterior columns

Figure 4–26. Comparison of detailed and reduced truss models.

4.2.5 Floor Subsystem Analysis

Analysis of a full floor of the World Trade Center towers involved:

- the translation, validation, and modification of finite element models in ANSYS to incorporate nonlinear behavior,
- evaluation of structural response under dead and live loads and elevated structural temperatures,
- identification of failure modes and associated temperatures and times to failure, and
- reduction of detailed component models for inclusion in the floor model.

Failure Modes

Possible deformation/failure modes of the floor subsystem that were investigated are as follows:

- Floor sagging *between edge supports* resulting from:
 - loss of stiffness and weakening of steel truss and/or concrete slab at high temperature,
 - change in floor behavior from flexure to catenary action due to yielding or buckling of diagonal web members required for truss action, or
 - loss of composite action from floor slab-knuckle failures.

Note that floor sagging between supports may cause tensile failure of the truss seats, or development of tensile forces that pull columns inward.

- Floor sagging *at edge supports* resulting from failure of truss seat connections at either the interior or exterior supports.

Floor sagging at the exterior edge was observed in photographs of the east exterior wall of WTC 2, near the impact zone. Floor sagging along one edge would have a tendency to reduce the buckling strength of columns supported by that floor and would increase demand on other components of the floor.

- Abrupt failure of the floor truss supports due to:
 - vertical shear failure resulting from debris and/or impact load of the dropping floor above,
 - vertical and/or horizontal shear failure resulting from slab expansion acting on truss support seats, or
 - tension failure of column truss seats from inward pull forces

Finite Element Model

A review of floors in the impact zones of WTC 1 and WTC 2 found that floor 96 in WTC 1 was representative of the floors of interest (see NIST NCSTAR 1-2A), and it was used for the floor analysis. Reference structural models of Floor 96 were developed in SAP2000 for traceability to a verified data set (see NIST NCSTAR 1-2) and translated into ANSYS models (see NIST NCSTAR 1-6C). The ANSYS floor model was used for the structural response analyses. Figure 4–27 shows an overall view of the converted ANSYS model of Floor 96. Figure 4–28 and Fig. 4–29 show a close-up of the truss floor and core framing, respectively.

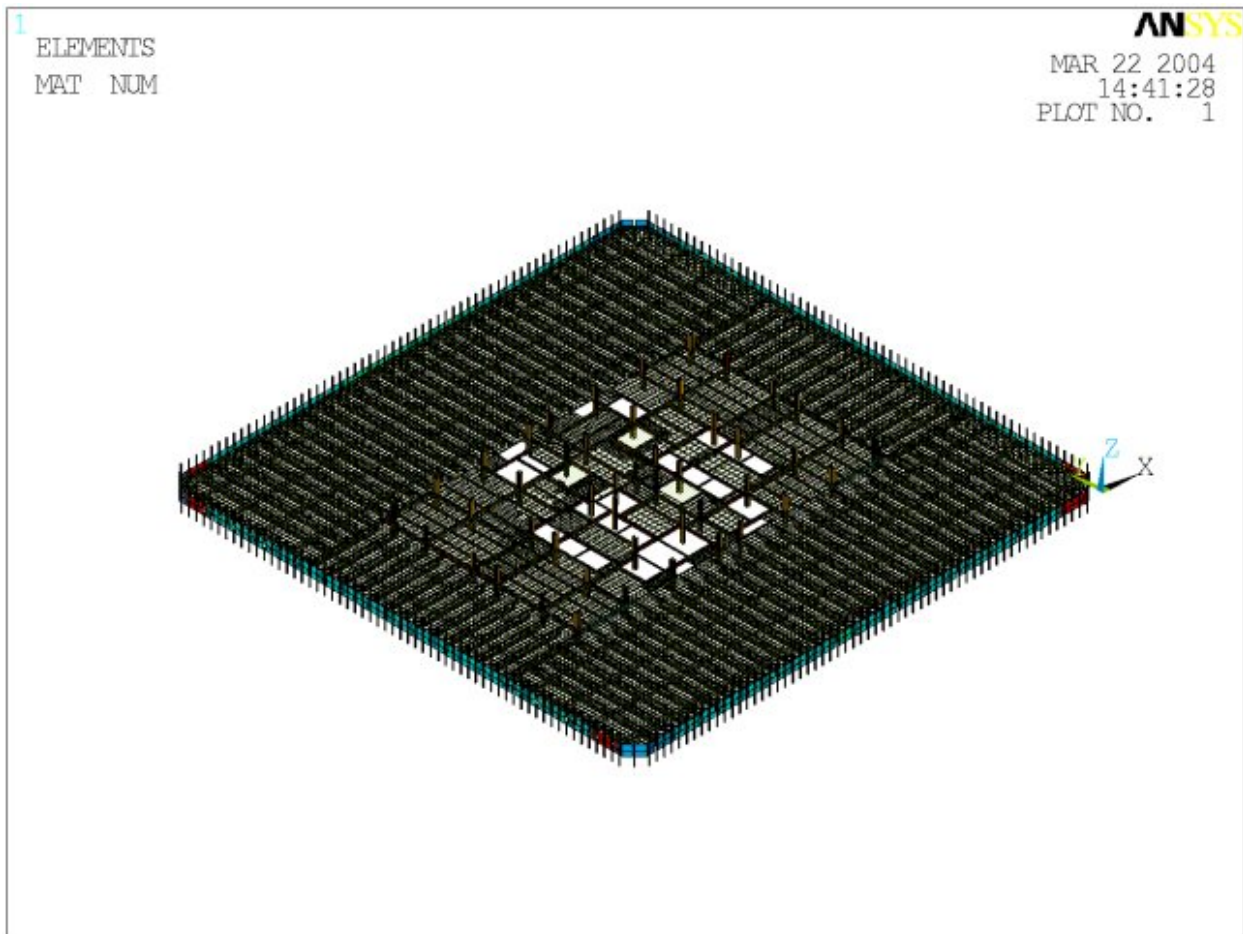


Figure 4–27. Converted ANSYS model for Floor 96 of WTC 1.

Analyses were conducted to validate the converted ANSYS floor model against the verified SAP2000 model as follows:

- Static analysis with gravity loads.
- Modal analysis using structural mass only.

Comparisons of the SAP2000 and ANSYS results for the gravity load case are given in Table 4–7. The total reactions for the SAP2000 and ANSYS models were within 0.1 percent of each other. The maximum slab displacement predicted by the ANSYS model was 3.2 percent smaller than that obtained from the SAP2000 model.

Table 4-7. Comparison of SAP2000 and ANSYS results for gravity load case.

| | SAP2000 | ANSYS (BEAM 188) |
|--------------------------------|----------|--------------------|
| Total reaction, kip | 2,212.81 | 2,210.85 (-0.09 %) |
| Maximum slab displacement, in. | 0.718 | 0.695 (-3.2 %) |

Table 4–8 summarizes the comparison of the SAP2000 and ANSYS results for the modal analysis. The total masses of the SAP2000 and ANSYS models were within 0.02 percent of each other. The dominant natural frequency of the floor predicted by the ANSYS model was 2.5 percent higher than that obtained from the SAP2000 model, which is consistent with the discrepancy observed for gravity displacement.

Table 4-8. Comparison of SAP2000 and ANSYS Modal Analysis Results.

| | SAP2000 | ANSYS (BEAM 188) |
|---|---------|-------------------|
| Total mass, lb-sec ² /in. | 5448.7 | 5447.7 (-0.018 %) |
| Dominant natural frequency of floor, Hz | 4.32 | 4.43 (+2.5 %) |

Reduced Model

The converted ANSYS model was modified to incorporate the nonlinear behaviors of the components and to reduce model complexity to achieve computation efficiency while retaining essential behaviors. The final model used for analyzing the floor response to gravity loads and elevated temperatures included the following modifications:

- Two adjacent trusses were combined into a single truss. The elements in the truss model had twice the areas and moments of inertia of elements in each single truss.
- Spandrels defined as beam sections in SAP2000 model were replaced with four-node finite strain shell (SHELL 181) elements (eight elements between two columns and four elements along the height). This modification eliminated the need for defining panel zone stiffness.
- Elastic column elements were changed to 3-D quadratic finite strain beam (BEAM 189) elements with user-defined composite sections and nonlinear material properties.

- Section offsets of exterior columns were removed, and nodes were placed at centroids of their cross sections.
- Spandrel plates were connected to exterior columns using rigid beam elements.
- The entire core was remeshed to produce a more uniform element size.
- Section offsets of core beams were removed to eliminate the end bending moment due to eccentricity. Core beams were placed at their centroids and connected to the slab by rigid beams.
- Beam elements of the top chord between panel points were merged into one element to prevent the top chord from buckling and penetrating the slab.
- Web diagonals were modeled by 3-D linear beam (BEAM 188) elements.
- Coincident nodes were provided for break elements.
- Break elements were incorporated into the model to represent:
 - buckling of diagonals;
 - truss seat failure;
 - failure of connections between primary and bridging trusses;
 - failure of connections between long-span and transfer trusses;
 - failure of studs connecting the slab and the spandrel;
 - failure of welds between strap anchors and top chords.

The full floor model as shown in Fig. 4–30 included the following structural members:

- Exterior and core columns extending from one floor below to one floor above
- Spandrels on the floor of interest
- Concrete floor slab
- Steel floor trusses including primary and bridging trusses
- Strap anchors
- Core beams
- Deck support angles

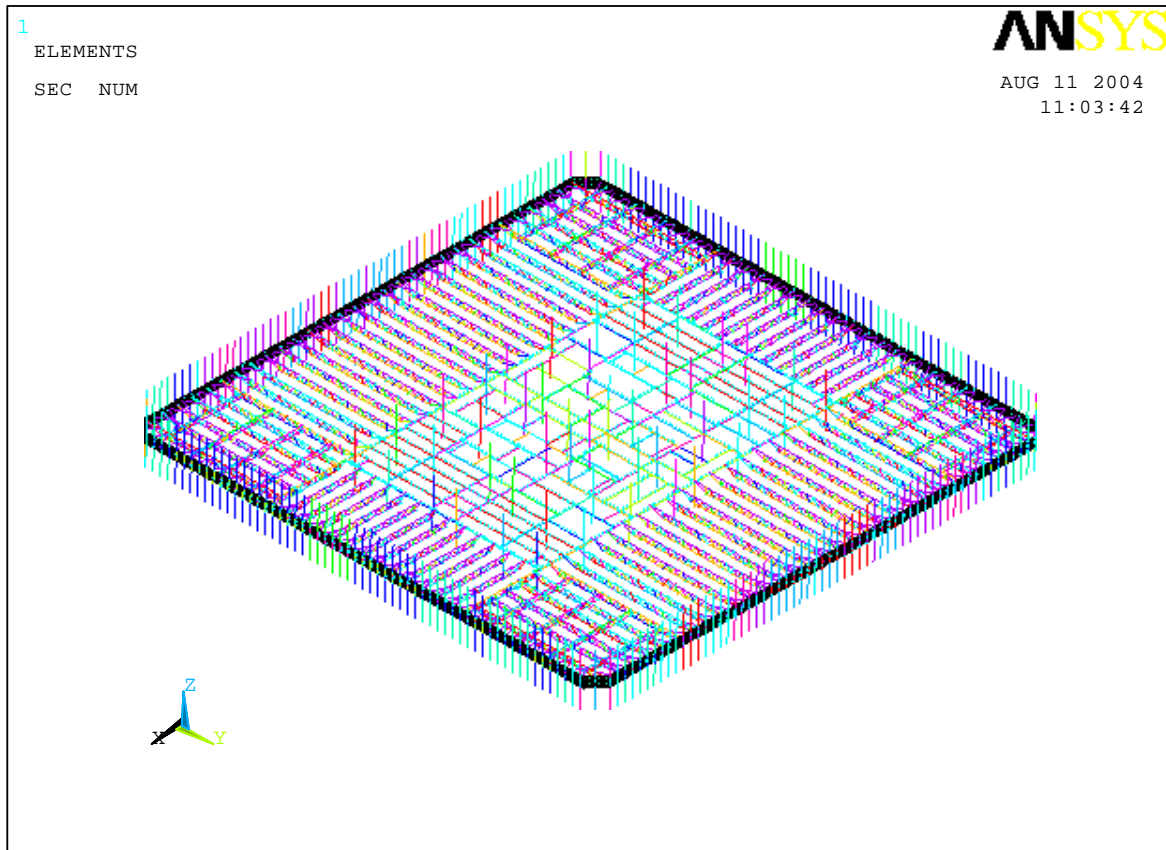


Figure 4–30. Full floor model before impact damage is included (without concrete floor slab).

Some components were found to fail in early stages of thermal loading, causing numerical solution difficulties, and were removed from the model. Removal of these components did not control the stability or failure mode of the full floor system under thermal loading. The removed members were:

- Deck support angles
- Shear studs on strap anchors and welds between strap anchors and truss top chords
- Bridging trusses in the one-way zone, and extending to the corner of the core
- Shear studs connecting the slab and the spandrel
- Strap anchors

The concrete slab was attached to the trusses at the knuckle nodes. Break elements were not used to represent knuckle failure as the detailed truss and slab analyses showed that web diagonal buckling, rather than knuckle failure, caused floors to sag. Concrete slab and trusses were always connected in the analysis.

Four different types of break elements were used in the full floor model. Their features are summarized in Table 4-9. There were a total of 2,028 break elements used to capture failure of the web diagonals, truss seats and truss-to-truss connections, welds, and studs. Figure 4-31 shows a summary of break element locations in the floor model.

Table 4-9. Types of break elements.

| Type | D.O.F. | Capacities to be defined | Stiffness to be defined | Description | Usage in the floor model |
|------|--|--|--|---|---|
| 102 | UX UY UZ ROTX ROTY ROTZ | Positive FX Negative FX Positive FY Negative FY Positive FZ Negative FZ MX MY MZ | Initial and post-failure stiffness for UX, UY, and UZ Initial and post-failure stiffness for ROTX, ROTY, and ROTZ | All force and moment components are checked with corresponding capacities. | Failure of seats. Fracture of gusset plates. Failure of connections between primary and bridging trusses. Failure of connections between long-span and transfer trusses. |
| 103 | UX UY UZ | Positive F Negative F | Initial and post-failure stiffness for UX, UY, and UZ | SRSS* of three force components is checked with the capacity. The sign of force is determined by the direction specified by the user. | Failure of strap anchor welds. |
| 104 | UX UY UZ | Positive FX Negative FX Positive FY Negative FY Positive FZ Negative FZ | Initial and post-failure stiffness for UX, UY, and UZ | All force components are checked with corresponding capacities. | Failure of studs connecting the spandrel and the slab. |
| 105 | UX UY UZ ROTX ROTZ ROTZ | Positive F Negative F | Initial and post-failure stiffness for UX, UY, and UZ Initial and post-failure stiffness for ROTX, ROTY, and ROTZ | SRSS of three force components is checked with the capacity. The sign of force is determined by the direction specified by the user. | Buckling of web diagonals. Failure of resistance weld between web diagonals and chords. |

*SRSS: square-root-of-sum-of-square

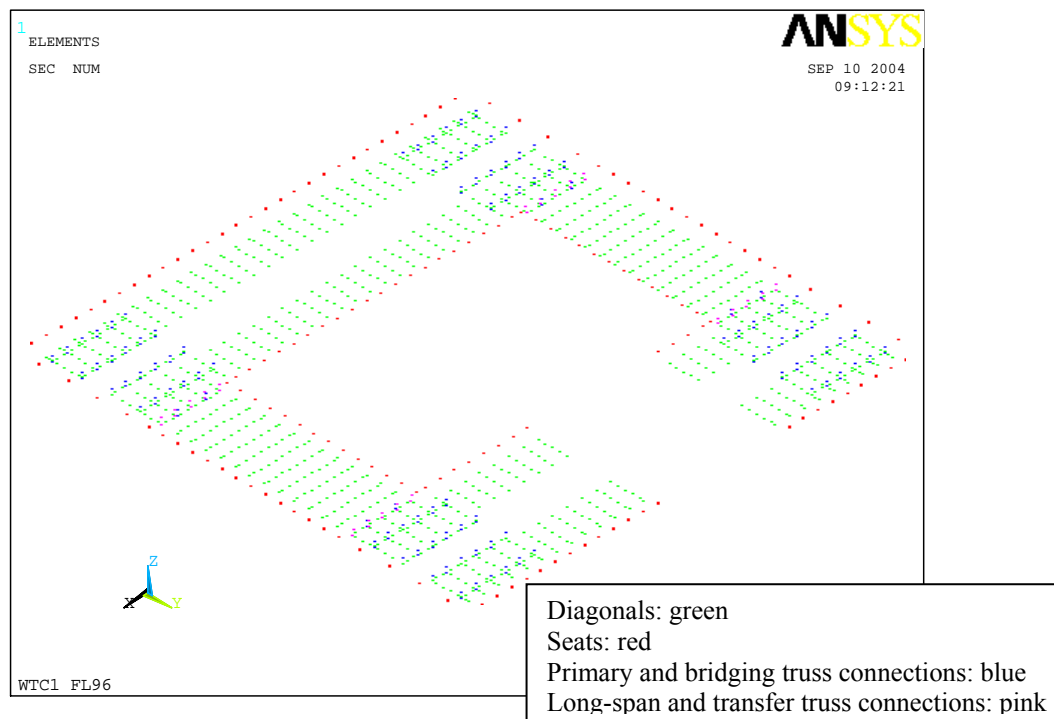


Figure 4–31. Break element locations in the floor model (Floor 96, WTC1).

Floor Analysis Results

The results of the full floor analyses are given in Chapter 7, Structural Response of Major Tower Subsystems. The floor models were analyzed for their response to impact damage and elevated temperatures from the fires for each floor in WTC 1 and WTC 2.

4.3 EXTERIOR WALL SUBSYSTEM

Just as the floors played an important role in the response of the World Trade Center towers to both aircraft impact and the ensuing fires, so did the exterior columns. Indeed, photographic and video evidence shows bowing of large sections and eventual buckling of an exterior wall of each tower at the time of collapse.

The exterior walls of the towers were made up of closely-spaced steel box columns and deep spandrel plates. For construction, three story high panels, consisting of three columns and three spandrels, were shop fabricated, lifted into position, and bolted together.

Component analyses were conducted to enable capturing all of the relevant failure modes for: (1) spandrel splices, (2) bolted column splices, and (3) a single column of one, two, or three stories.

A section of an exterior wall was analyzed that was three panels wide and three panels high and included the column and spandrel splices. Thus, the model had nine columns and nine spandrel plates. The objective of the exterior wall section model was to study the performance of the wall under the combined

effects of gravity and thermal loads for several conditions of lateral support. The wall section analyses included (1) the translation and validation of a single-panel ANSYS model, (2) development of the wall section model, and (3) evaluation of structural response under gravity loads and pull-in forces resulting from floor sag and elevated structural temperatures.

4.3.1 Exterior Wall Subsystem Description

The exterior wall of the towers was comprised of prefabricated wall panels, referred to hereafter as panels. Typical panels contained three-column segments spanning three stories with portions of the spandrels extending one half-span past the outer columns. The panels were typically arranged such that spandrel splices between panels aligned vertically and column splices between panels offset each other by one story.

The wall panel section selected for study was located on the north face of WTC 1 toward the east side and included nine columns, extending vertically from the column splice located below Floor 91 to the column splice above Floor 99, and nine spandrels, extending horizontally from the spandrel splice located at mid-span between Columns 149 and 150 to the spandrel splice at mid-span between Columns 158 and 159. This exterior wall subsystem model included seven full panels and portions of four other panels.

Figure 4–32 shows the exterior wall section, and Fig.4-33 is a schematic of an exterior box column showing the column plate notation. Tables 4–10 through 4–12 give the dimensions of the column and spandrel plates and their splice connections.

The odd-numbered columns supported floor trusses. Pairs of strap anchors extended diagonally from the top chords of truss pairs to the even-numbered columns. The trusses and the straps braced the exterior columns out-of-plane of the exterior wall.

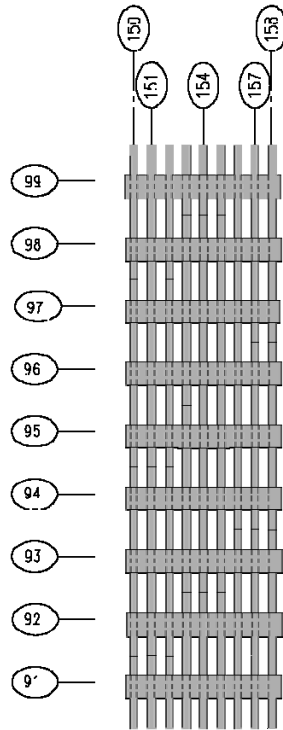


Figure 4–32. Exterior wall section model.

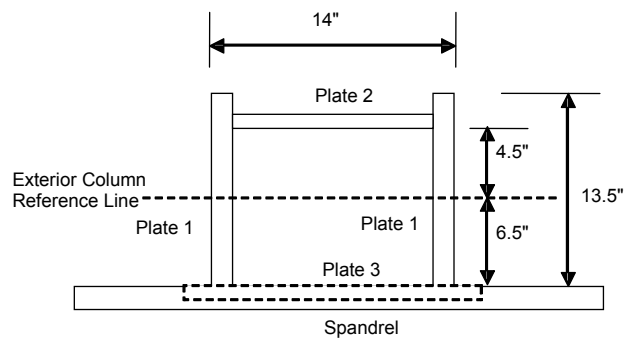


Figure 4–33. Schematic of exterior column cross-section.

Table 4-10. Column section properties.

| Column Type | Plate 1 length by thickness (in. x in.) | Plate 2 length by thickness (in. x in.) | Plate 3 length by thickness (in. x in.) |
|-------------|---|---|---|
| 120 | 13.5 x 0.25 | 13.5 x 0.25 | 15.75 x 0.25 |
| 121 | 13.5 x 0.3125 | 13.375 x 0.25 | 15.75 x 0.25 |
| 122 | 13.5 x 0.375 | 13.25 x 0.25 | 15.75 x 0.25 |
| 123 | 13.5 x 0.4375 | 13.125 x 0.25 | 15.75 x 0.25 |
| 124 | 13.5 x 0.5 | 13 x 0.25 | 15.75 x 0.25 |
| 125 | 13.5 x 0.5625 | 12.875 x 0.25 | 15.75 x 0.25 |

¹All spandrels in exterior wall subsystem model are 52 in. deep x 3/8 in. thick.

Table 4-11. Spandrel Splice Details.

| Spandrel Splice Type | Number of Bolts/Row | Total Number Of Rows | Bolt Spacing (No. of bolts@ spacing) (in.) | Gage (in.) | Overall Splice Plate Dimensions (in. x in. x in.) | Bolt to Centerline of Splice (in.) | Gap Between Spandrels (in.) | Spandrel Splice ID |
|----------------------|---------------------|----------------------|--|------------|---|------------------------------------|-----------------------------|--------------------|
| 101 | 6 | 2 | 5@9 | | 49x6.75x.25 | 1.875 | 0.75 | 101 |
| 102 | 8 | 2 | 3,6,3@9,6,3 | | 49x6.75x.25 | 1.875 | 0.75 | 102 |
| 111 | 6 | 4 | 5@9 | 3 | 49x12.75x.25 | 1.875 | 0.75 | 111 |
| 112 | 8 | 4 | 3,6,3@9,6,3 | 3 | 49x12.75x.25 | 1.875 | 0.75 | 112 |

¹All spandrel splices use 7/8 in. A325 bolts; specified spandrel plate yield strength is 36 ksi.

²Holes in spandrel are 1/4 in. larger than bolts; holes in plates are bolt + 1/16 in. or option to match spandrel holes.

Table 4-12. Column Splice Details.

| Column Splice Type | Butt Plate Thickness (in.) | Number of Bolts | Bolt Diameter (in.) | Gage (in.) | Bolt Spacing (in.) | Column Splice ID |
|--------------------|----------------------------|-----------------|---------------------|------------|--------------------|------------------|
| 411 | 1.375 | 4 | 0.875 | 3.5 | 6 | 411 |
| 421 | 1.625 | 4 | 0.875 | 3.5 | 6 | 421 |
| 431 | 1.875 | 4 | 1 | 3.5 | 6 | 431 |

¹Butt plates have specified yield strength of 50 ksi.

²Bolts are A325.

4.3.2 One, Two, and Three-Story High Columns

Figure 4–34 shows the finite element model of a one-story high exterior column representing Column 151 (see Fig. 4–32). Shell elements were used to model the plates comprising the box column and the spandrels. Rigid elements connected the center of gravity of the column to its component plates and the spandrel at both the top and the bottom of the model. The column was simply supported in three directions at the bottom and simply supported in the horizontal directions at the top. Increments of axial displacement were applied at the top of the model.

Figure 4–35 shows the variation of axial load with imposed axial displacement and resulting lateral deflection for two assumed uniform temperature conditions, room temperature and 700 °C. Figure 4–35 also presents results of standard handbook calculations at room temperature and at 700 °C for (1) local buckling of plates 2 and 3, (2) uniform yielding of the column, and (3) gravity load demand.

Figure 4–36 shows the local buckling deformation of Plate 2 and Plate 3 at the maximum load level (approximately 1,050 kip) at room temperature. Figure 4–37 shows a plastic hinge at mid-height of the column for an axial displacement of 2 in. Figure 4–38 shows the presence of local buckling in Plate 2 and Plate 3 at 700 °C and the maximum load (approximately 250 kip).

It can be seen from Fig. 4–35 that, at room temperature, local buckling occurs at a load that is less than the maximum column load, but that at 700°C the column yields before it buckles locally. This figure also shows that the column demand load of 175 kip is substantially lower than the local buckling load at room temperature and the column yield load at 700°C. At room temperature, the post-buckling strength decreased rapidly; however, the reduction in the strength was much more gradual in the post-buckling regime at 700 °C.

Axial load-displacement behaviors of two- and three-story models are also examined, and the results are shown in Fig. 4–35. As can be seen, for longer unsupported lengths and higher temperatures, the slope of the axial load-deflection curve in the post-buckling regime became less steep.



Figure 4-34. One-story exterior column model.

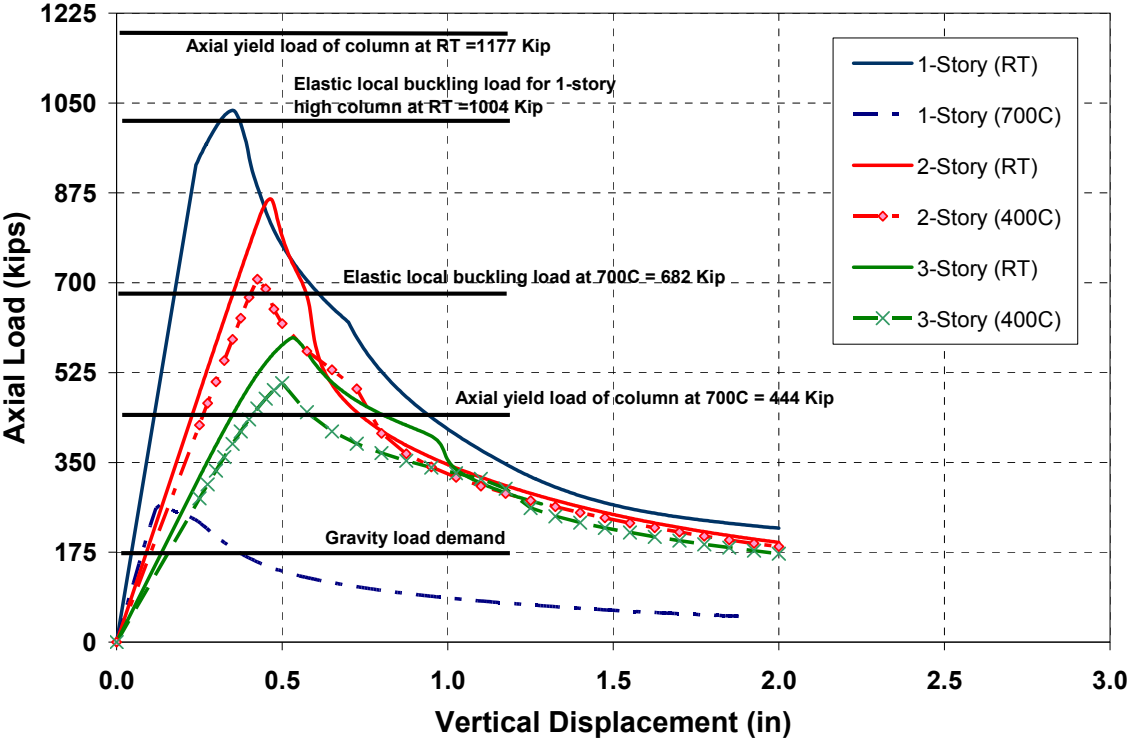


Figure 4-35. Load-deflection of column at room temperature (RT) and 700 °C.

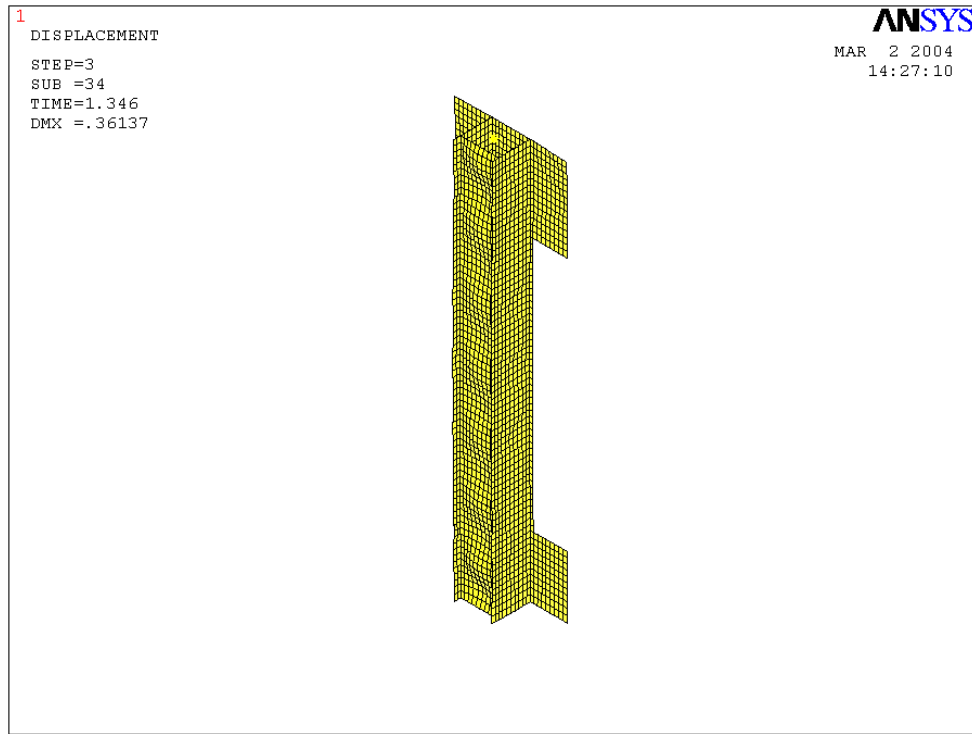


Figure 4–36. Local buckling of column at room temperature.

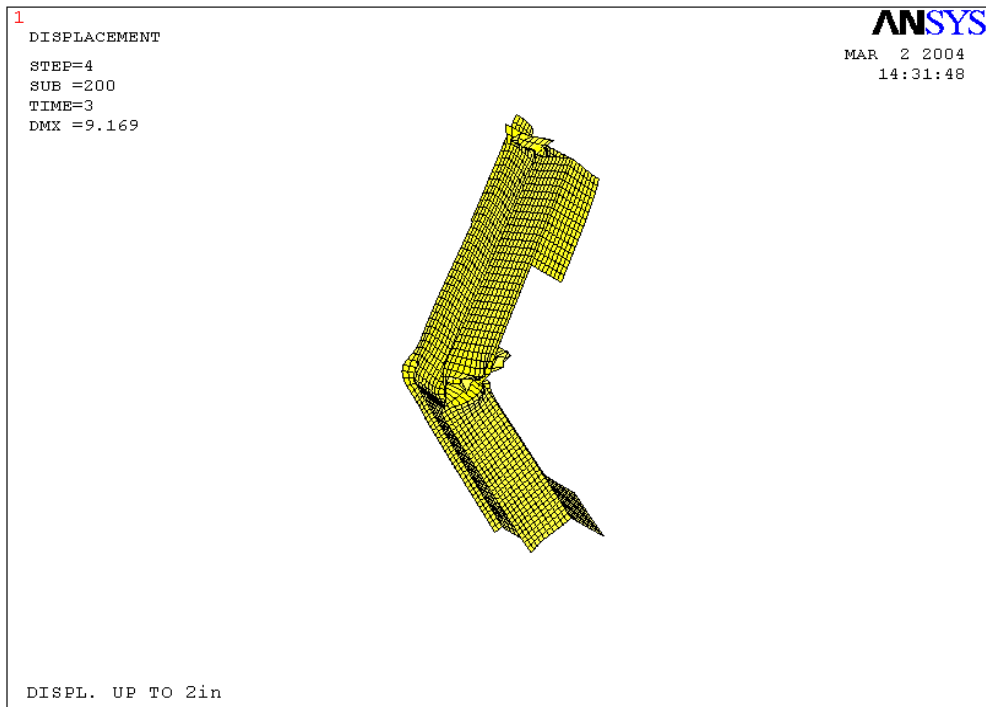


Figure 4–37. Plastic hinge in column at room temperature.

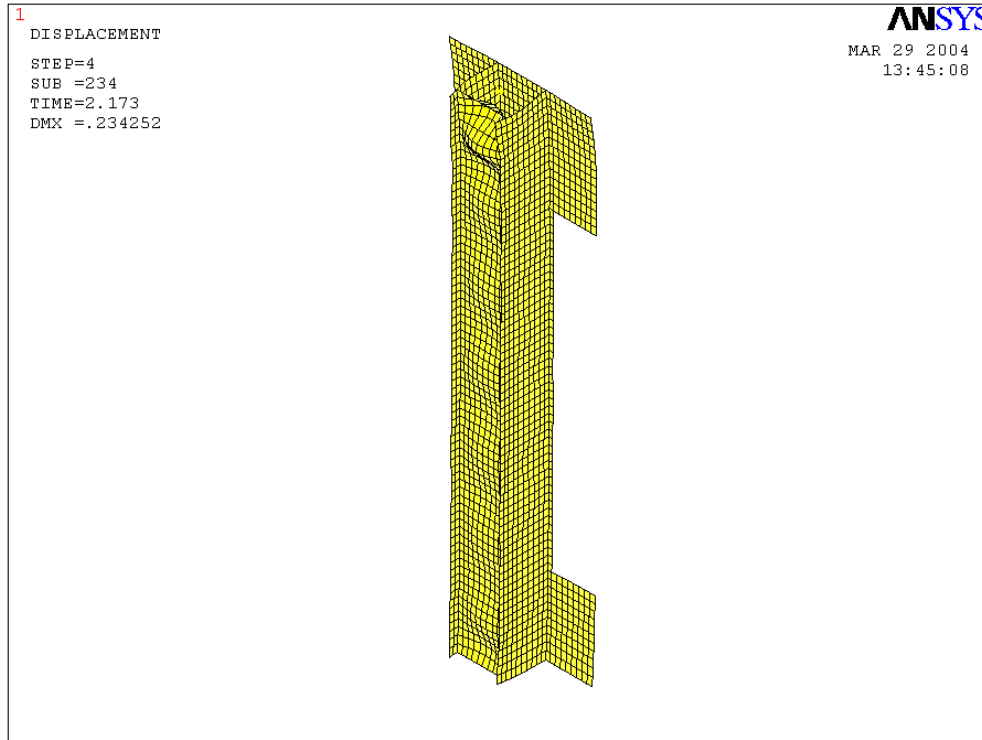


Figure 4–38. Deformed shape of column at maximum axial load at 700 °C.

4.3.3 Exterior Wall Section Analysis

Analysis of a section of the exterior wall of the World Trade Center towers involved:

- the translation and validation of a single panel finite element model to ANSYS and modification to include nonlinear behavior,
- development of the exterior wall section model,
- evaluation of structural response under dead and live loads and elevated structural temperatures, and
- determination of loads that cause buckling (instability).

Failure Modes

The exterior wall section model captured the following failure modes:

- Column buckling from large lateral deformations,
- Column buckling from loss of support at floor truss seats and diagonal straps,
- Failure of column splice bolts, and
- Failure of spandrel splice bolts or tearing of spandrel or splice plates at bolt holes.

Finite Element Model of Single Panel

A finite element model of a single exterior wall panel using both beam and shell elements was developed to reduce the model size. This model was validated against a finite element shell model of a single exterior wall panel developed by LERA (NIST NCSTAR 1-2A) by comparing the stiffnesses for a variety of loading conditions.

Figure 4–39 shows the SAP2000 shell model of a typical prefabricated panel at Floors 79 to 82, and Fig. 4–40 shows the reduced ANSYS model which had fewer degrees of freedom. In the ANSYS panel model, beam elements replaced shell elements to model the columns, while shell elements were used to model the spandrels, and beam elements attached the center of gravity of the columns to the mid-plane of its corresponding spandrel component at each shell element through the depth of the spandrel.

Each of the models was subjected to the following loads at room temperature as shown in Fig. 4–41:

- A vertical force (FZ) at the top of one of the outside columns.
- A horizontal force in the plane of the wall (FX) at the top of one of the outside columns. The stiff beam elements distributed this shear between the tops of all three columns.
- A transverse force (FY) on the middle column at Floor 81 (middle floor).

Figure 4–42 shows the deflected shape of the panel for both the SAP2000 and ANSYS models for the case of 100 kip lateral load at the top of the panel. Table 4–13 presents the results for this and the other two loading conditions.

Lateral and vertical displacements were found to be within 7 percent while the out-of-plane displacement for the ANSYS model was 13 percent less than that obtained from the SAP2000 model.

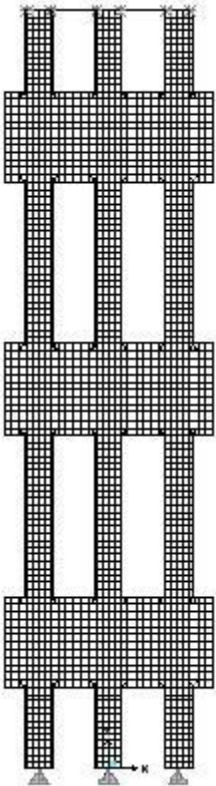


Figure 4–39. SAP2000 shell model of prefabricated panel.

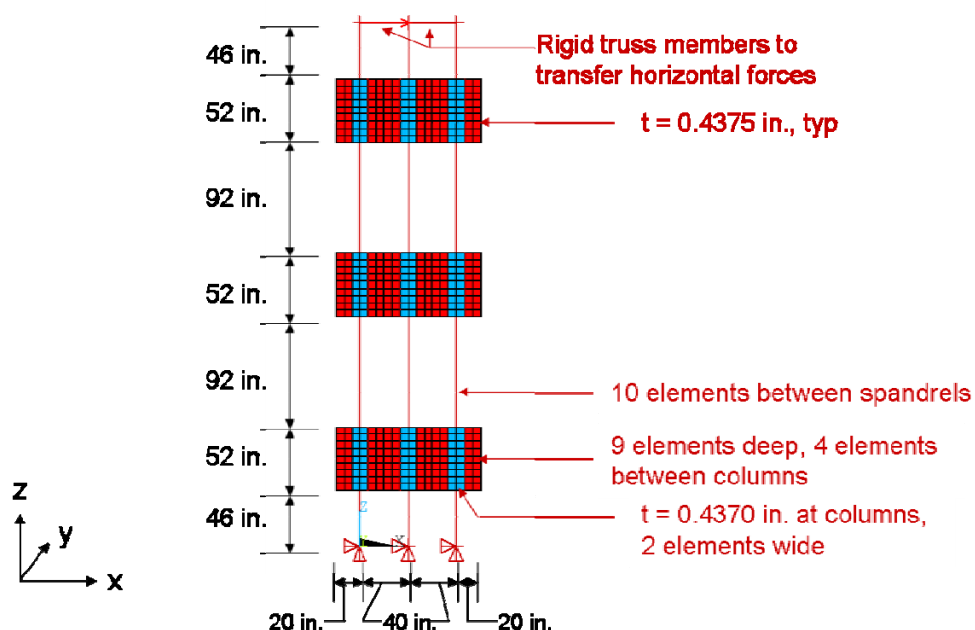


Figure 4–40. ANSYS model of prefabricated panel showing finite element mesh.

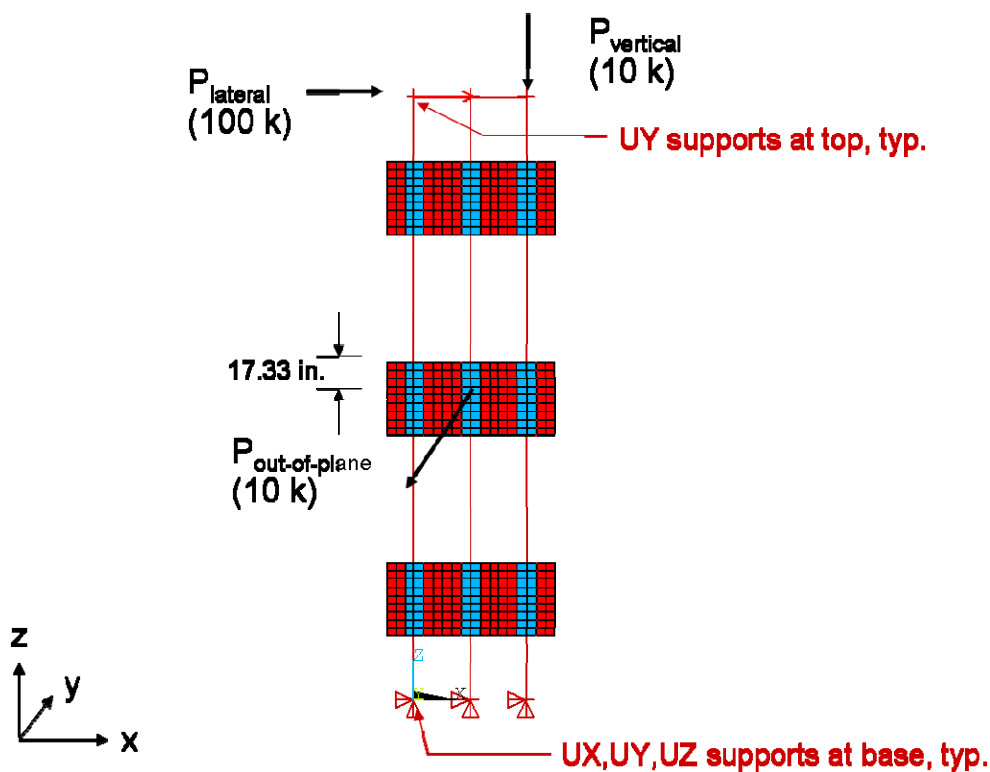


Figure 4–41. ANSYS model of prefabricated panel showing boundary conditions and loading.

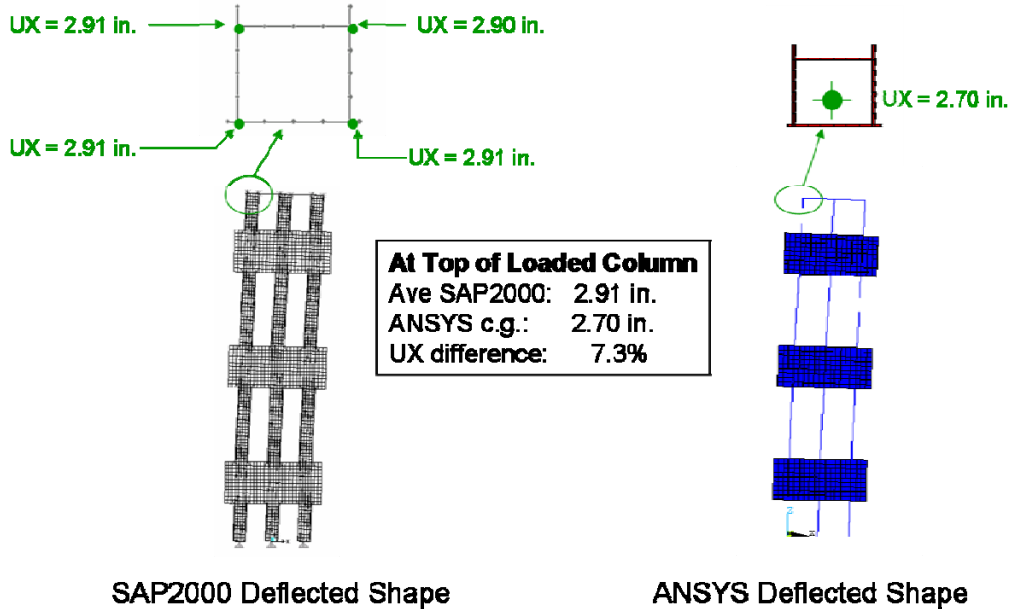


Figure 4-42. Deflection of prefabricated panel under 100 kip lateral load.

Table 4-13. Prefabricated panel validation results.

| Loading Condition | SAP2000/ANSYS Difference Range | |
|-------------------|--------------------------------|----------------------------|
| | Reaction | Displacements ¹ |
| Lateral FX | RX: -2% to +1% | UX: 7% |
| Transverse FY | RY: -6% to +7% | UY: -13% |
| Vertical FZ | RZ: -1% to +2% | UZ: -7% |

1. Displacements considered at tops of columns for FX and FZ, and at points of load application for FY.

Spandrel Splice Model

Figure 4–43 shows a typical layout of the spandrel splices in the model. User-defined break elements model the interior spandrel splice connections, and nodal couples model the exterior spandrel splice connections. Figure 4–44 shows the modeling of an interior spandrel splice. User-defined break elements at each node through the depth of a spandrel allow the model to capture connection failure modes including (1) bolt shear, (2) tearing of the spandrel plate, and (3) tearing of the splice plates at the bolt holes. The break elements transfer forces and moments between nodes according to the initial stiffness values until the element reaches capacity in one direction. Upon reaching one of the capacities, the stiffness of the element in all directions changes to the corresponding failure stiffness, and the element sheds load through other load paths.

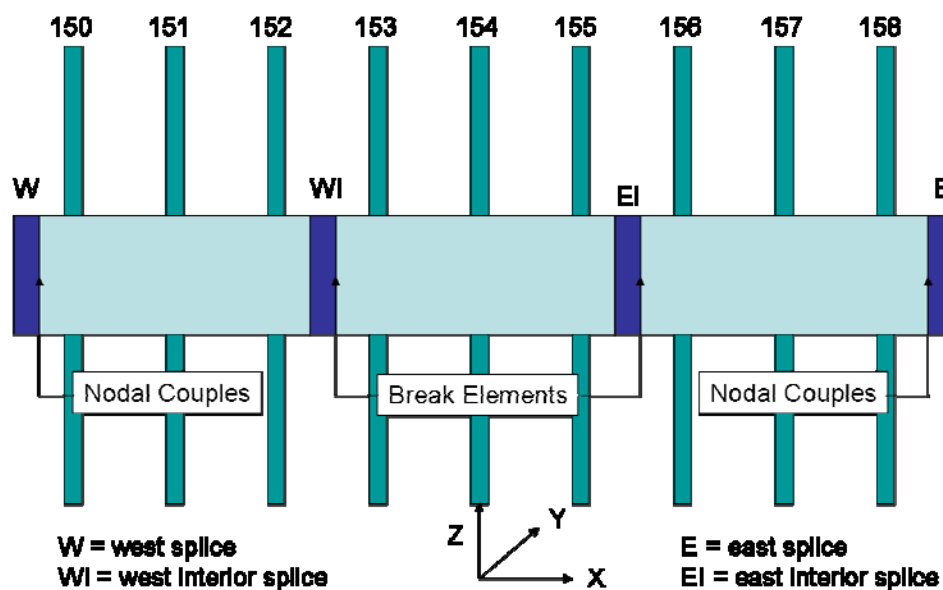


Figure 4–43. Typical spandrel splice layout for exterior wall section model.

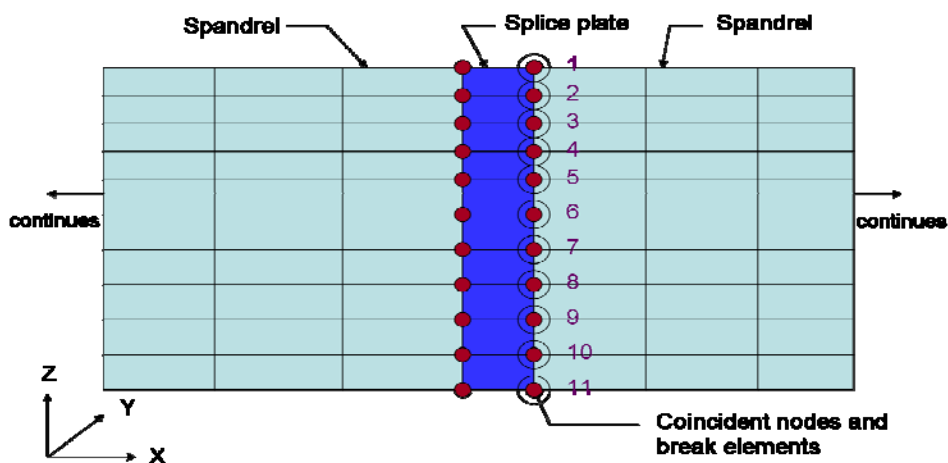


Figure 4–44. Modeling of a typical interior spandrel splice in the exterior wall section model.

Column Splice Model

Bolted column splices were modeled using beam elements for each of the four bolts, four pairs of contact elements at the faying (contact) surfaces between column ends (butt plates) and stiff beam elements connecting the tops of the bolts to the contact elements. Fracture of the column bolts was included and was based on test data (NIST NCSTAR 1-3). Figure 4–45 shows a schematic view of the column splice model. The contact elements use a coefficient of friction of 0.35. The 7/8 in. diameter column splice bolts are pretensioned to 36.05 kip at 20 °C (AISC 1964).

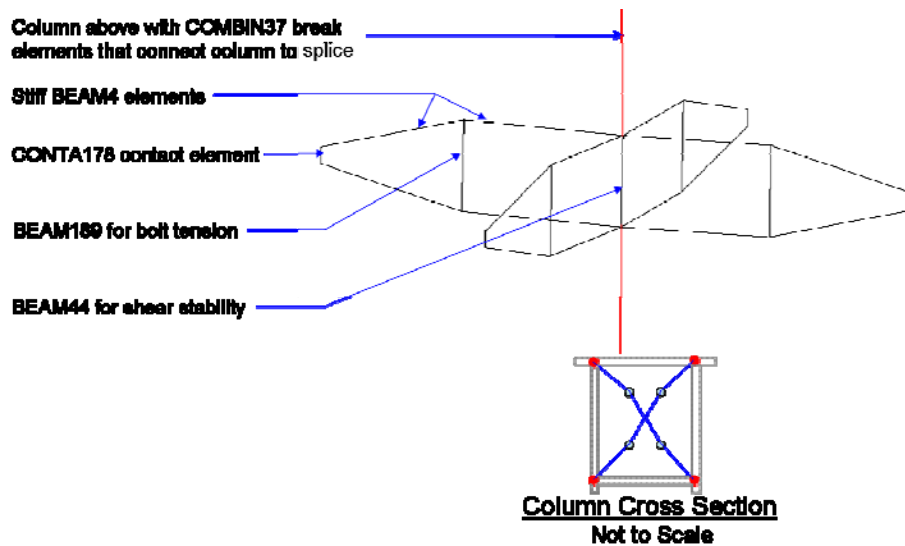


Figure 4–45. Column Splice Model used in Exterior Wall Model.

Finite Element Model of Exterior Wall Section

The single panel model was used to form a nine column by nine spandrel wall section model. Fig. 4–46 shows the model in elevation, and Fig. 4–47 shows a typical finite element mesh for a portion of the model. The colors of the elements illustrated in Fig. 4–47 represent the various element properties assigned. Element properties include large deflections, plastic deformation, and creep at elevated temperatures.

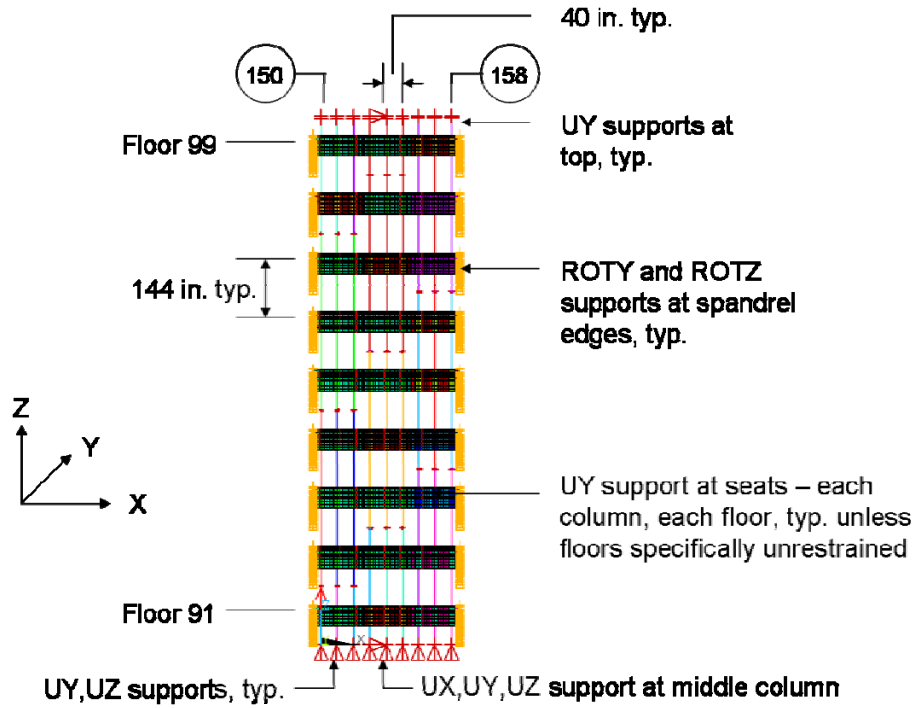


Figure 4-46. Exterior wall subsystem model with boundary conditions.

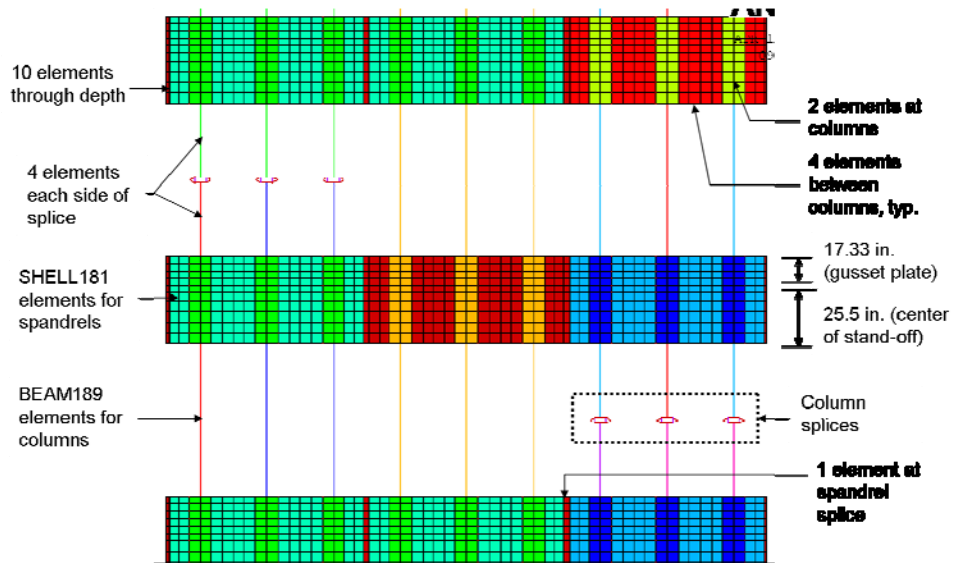


Figure 4-47. Typical meshing of exterior wall model components.

Loading

The exterior wall section was subjected to several loading conditions as described here. Gravity loads corresponding to dead load plus 25 percent of the design live load were applied to simulate the axial forces in the columns and floor loads applied to the truss seats. Five thermal load conditions were considered (see NIST NCSTAR 1-5G) that represented fire exposures and thermal insulation conditions at several locations in the towers. The most severe of these conditions was used for subsequent analyses. The five thermal loading conditions were labeled Cases D, E and F, DBARE (representing absence of insulation); and E119 (corresponding to the standard ASTM E 119 thermal loading). Table 4-14 presents the various thermal load conditions, and Fig. 4-48 shows how the maximum temperature anywhere in the model varied with time for each thermal loading condition. Thermal loading condition DBARE was selected as the most severe exposure from this group. (The designation of thermal load condition D used here should not be confused with Cases D introduced later on in this report.)

Table 4-14. Thermal loading conditions used in the exterior wall model.

| Thermal Loading Condition | Building and Location | Columns | Floors | Insulation | Time Duration | Maximum Temperature °C |
|---------------------------|------------------------------------|-----------|---------|--------------|---------------|------------------------|
| D | WTC1 South face towards West | 340 – 348 | 91 – 99 | as specified | 5400 s | 537 °C |
| DBARE | WTC1 Same as D | 340 – 348 | 91 – 99 | none | 5400 s | 598 °C |
| E | WTC1 East face towards North | 221 – 229 | 91 – 99 | as specified | 5400 s | 871 °C |
| E119 | WTC1 | | | as specified | 5400 s | 418 °C |
| F | WTC2 North face East corner | 250 – 258 | 76 – 84 | as specified | 3600 s | 382 °C |

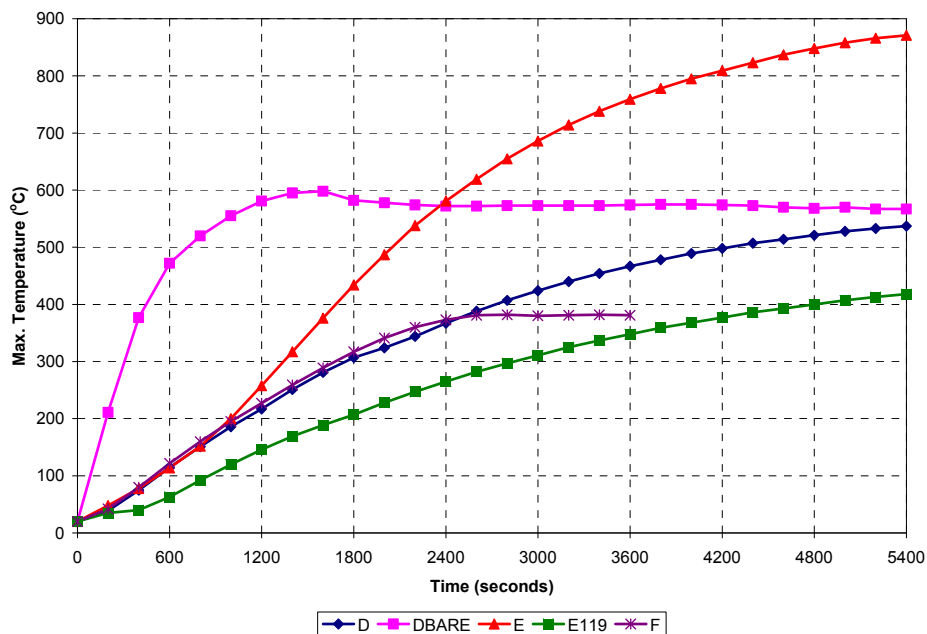


Figure 4–48. Exterior wall model temperature time-histories.

Table 4–15 shows the nine cases that were analyzed for the exterior wall model that included the thermal load cases, creep effects, and floor support conditions. Several combinations of disconnected floors were analyzed for the effects of loss of lateral support if a floor sagged or failed and the consequent increase in un-braced length of the columns.

Two cases were analyzed to investigate the stability of the exterior wall section. In one case, forces were applied to simulate pull-in from sagging floors to the point of instability. When trusses sag extensively, they pull the columns inward. Results of truss component analyses indicated approximately 14 kips of inward pull per truss. The strap anchors helped distribute this pull to the columns that did not support trusses. A 15 kip inward pull force was applied at each column that was laterally-unsupported, and in the second case, with three disconnected floors, a “push-down” analysis was conducted to simulate additional column loads being redistributed from the core. The top of the wall model was displaced downward until instability was reached.

The loads on the model were applied in stages in the following order:

- Self weight of the exterior wall components,
- Column splice bolt preload,
- Dead load of floor construction, including superimposed dead loads,
- 25 percent of floor design live loads,
- Temperatures of fire scenarios, and

- Transverse pull loading from sagging trusses, or
- Imposed vertical displacements at top of columns.

Table 4-15. Analysis cases for exterior wall section model.

| Analysis Case | Thermal Load Condition | Bolt Temperatures | Creep Effects | Floor Supports | Pull-in Force | Push-Down Force |
|---------------|------------------------|-------------------|---------------|------------------------|---------------|-----------------|
| 1 | D | No | Yes | All | | |
| 2 | DBARE | No | Yes | All | | |
| 3 | E | Yes | Yes | All | | |
| 4 | E119 | No | Yes | All | | |
| 5 | F | No | Yes | All | | |
| 6 | DBARE | Yes | Yes | All but 95 and 96 | | |
| 7 | DBARE | Yes | No | All but 95, 96, and 97 | | |
| 8 | DBARE | Yes | No | All but 95, 96, and 97 | X | |
| 9 | DBARE | Yes | No | All but 95, 96, and 97 | | X |

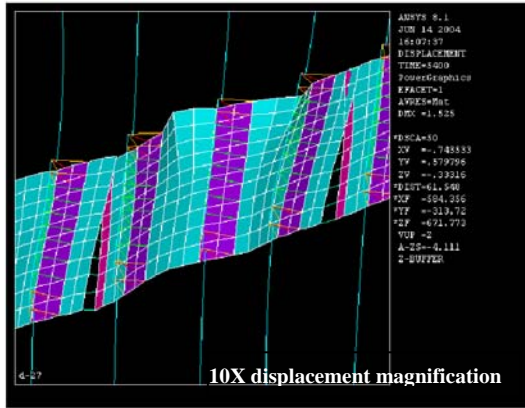
Exterior Wall Analysis Results

Columns Laterally Supported at All Floors (Case 1 - Case 5)

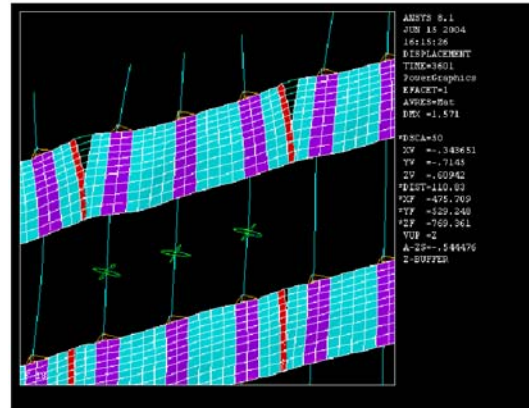
The analysis results for the five thermal load conditions in Cases 1 to 5 indicated the following:

- Spandrels had the maximum stress (strains are plastic)
- Spandrels experienced large lateral distortions and separated partially; no spandrel splice separated completely in any of the five Cases.
- Lateral (out-of-plane) deflections of the columns were less than 1.0 in. and were due primarily to differential thermal expansion between the columns and spandrels.
- Column and spandrel thermal expansion was unrestrained. The columns elongated between 1 and 3 in.
- General instability (buckling) of exterior wall columns did not occur.

Deformations observed in the spandrel plates are illustrated in Fig. 4-49.



Fire Scenario D (Case 1) - Floor 94



Fire scenario F (Case 5) - Floor 99

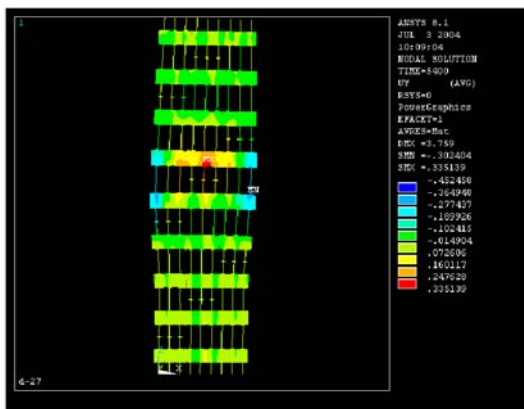
Figure 4–49. Spandrel plate deformations.

Columns Not Laterally Supported at Two or Three Consecutive Floors (Cases 6 and 7)

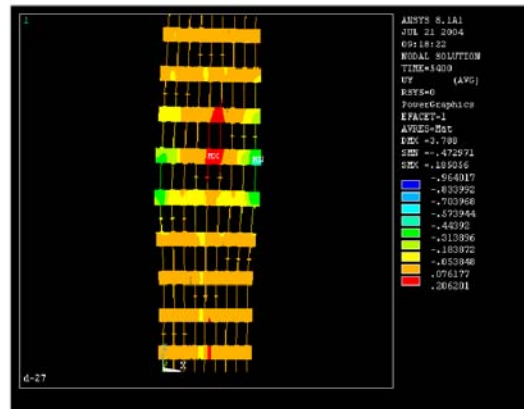
The analysis results for Case 6 and Case 7 are similar and the following observations can be made for both conditions:

- Lateral deflections of the columns were less than 1.0 in. for the thermal loads.
- No plastic strain in the columns and spandrels.
- All column splices remained in contact.
- Spandrel splices separated partially on several floors; no spandrel splice separated completely
- The structures remained stable.

The out-of-plane deformations for the two cases are show in Fig. 4–50. Deformations for the case with three floors removed were somewhat greater than for the case with two floors removed, although the maximum deformations in both cases was less than 1.0 in.



Two Floors Removed (Case 6)



Three Floors Removed (Case 7)

Figure 4–50. Lateral deflections for Case 6 and Case 7.

Columns Not Laterally Supported and Pulled-In at Three Floors (Case 8)

The analysis results for Case 8 indicated the following:

- Column instability (buckling) was reached with a transverse load of 12.6 kips per column
- For a lateral load of 12.6 kips, the inward deflection of the exterior wall section was 10.2 in.
- The maximum column tensile stress of 77.2 ksi was at Floor 94 where the lateral deflection was 10.2 in.
- Column splices experienced slip or opened up at several column locations; no column splice bolts fractured

Figure 4–51 shows the deflected shape of the exterior wall subsystem at the point of instability due to inward pull. The status of the column splice contact elements is shown in Fig. 4–52 and the column splice bolt stresses are shown in Fig. 4–53.

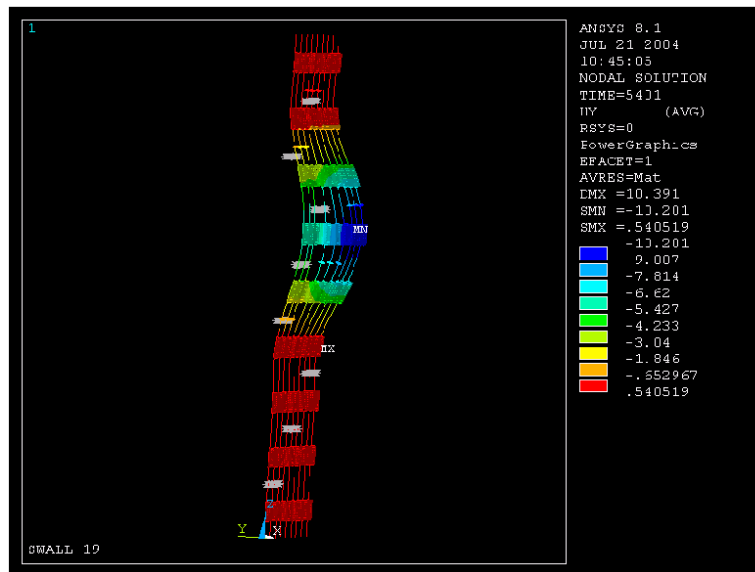


Figure 4–51. Structural response (out-of-plane deformations) for temperature time history DBARE and pulled-in at three disconnected floors for Case 8. (10X displacement magnification).

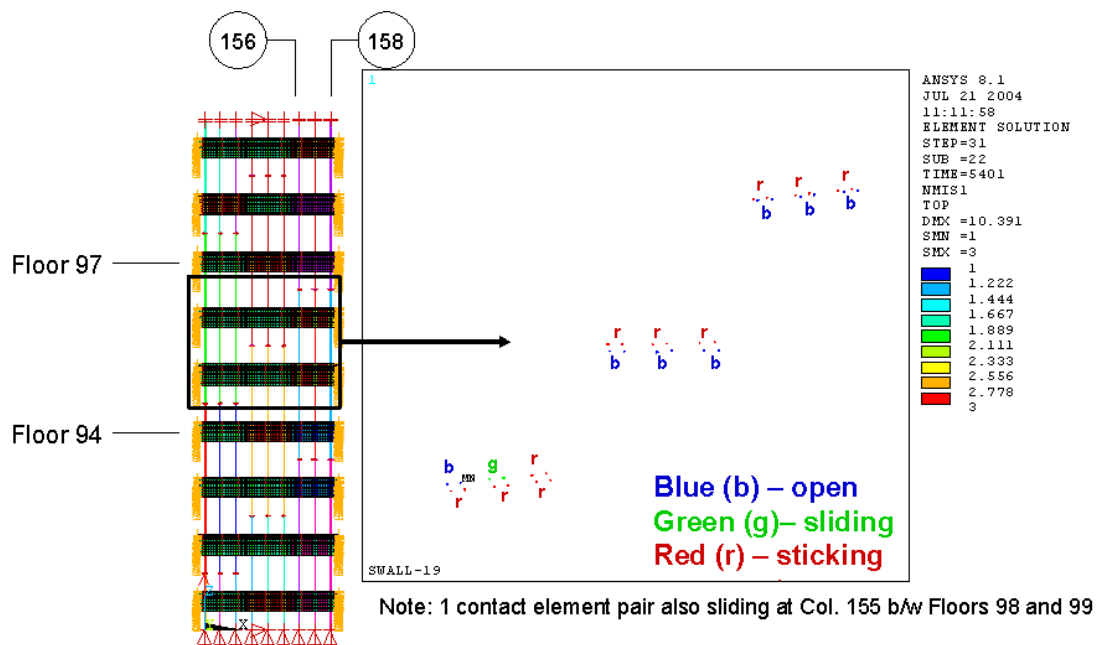


Figure 4–52. Column splice contact element status for temperature time history and DBARE and pulled at three disconnected floors for Case 8.

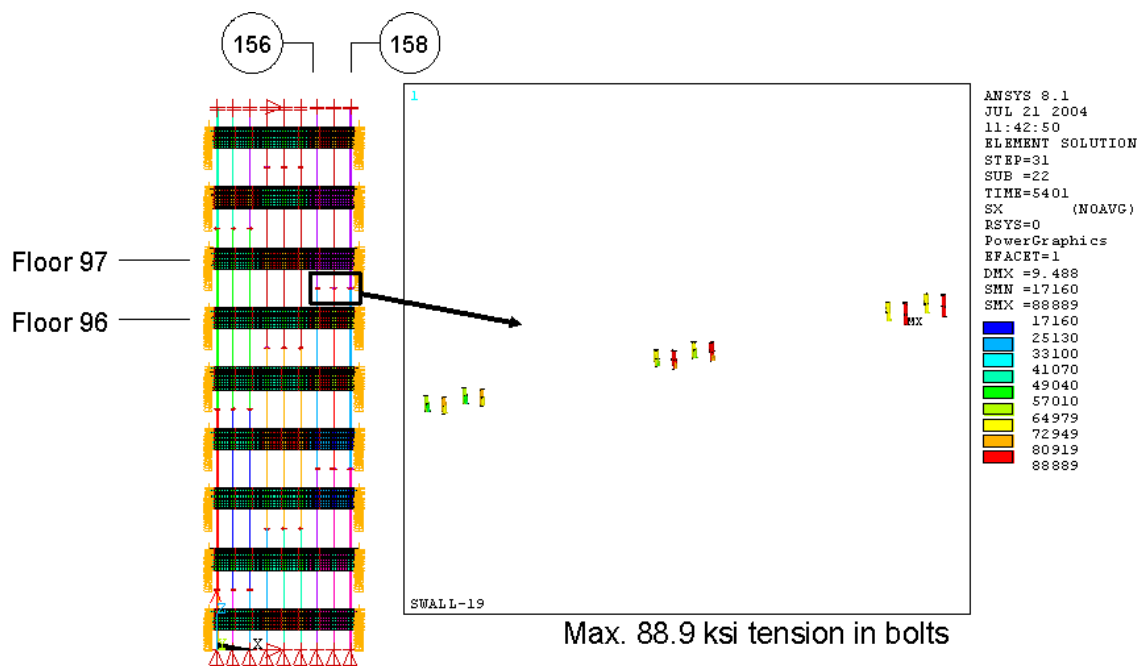


Figure 4–53. Column splice bolt stresses for temperature time history and DBARE and pulled at three disconnected floors for Case 8.

Columns Not Laterally Supported at Three Floors and Columns Pushed Down at Top (Case 9)

Figure 4–54 shows the deflected shape of the exterior wall subsystem due to push-down. The out-of-plane deformation as a function of push-down displacement is shown in Fig. 4–55.

The total vertical reaction (sum of the gravity and push-down loads) vs. imposed vertical displacement is plotted in Fig. 4-56. Plastic buckling was found to occur with a vertical applied displacement of approximately 1.2 in. which occurred, as can be seen in Fig. 4–56, at the point at which the total vertical reaction began to decrease. It is seen from Fig. 4–56 that, for the given thermal loading condition, the maximum total vertical reaction was approximately 2,700 kips, or an average of 300 kips on an individual column. Individual column forces are shown in Fig. 4–57 and are seen to range from approximately 250 kips to 350 kips. The gravity load on an individual column was approximately 200 kips.

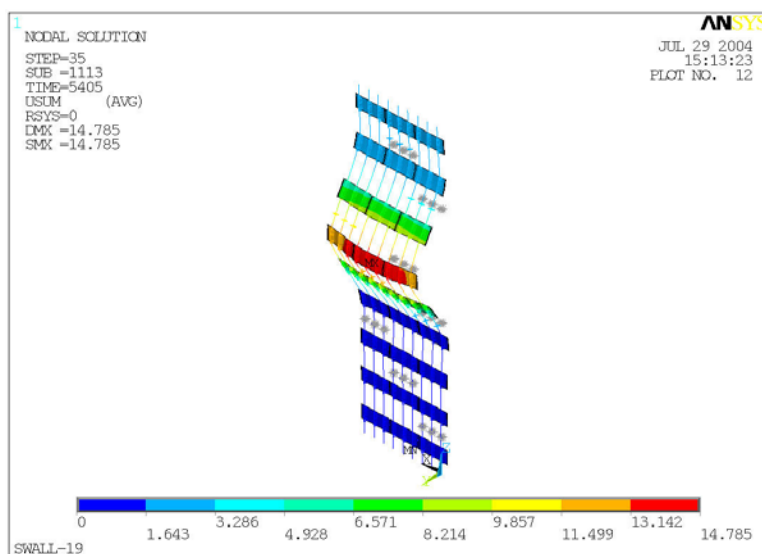


Figure 4–54. Structural response (out-of-plane deformations) for temperature time history DBARE and pushdown with three disconnected floors for Case 9 (10X displacement magnification).

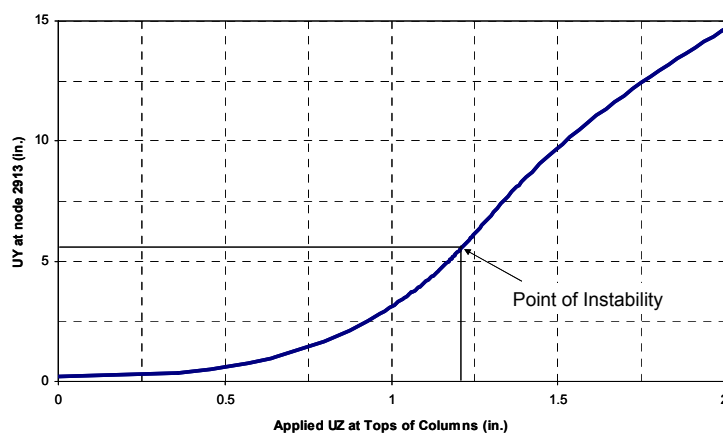


Figure 4–55. Out-of-plane deformation as a function of pushdown displacement after application of temperature DBARE with three disconnected floors for Case 9.

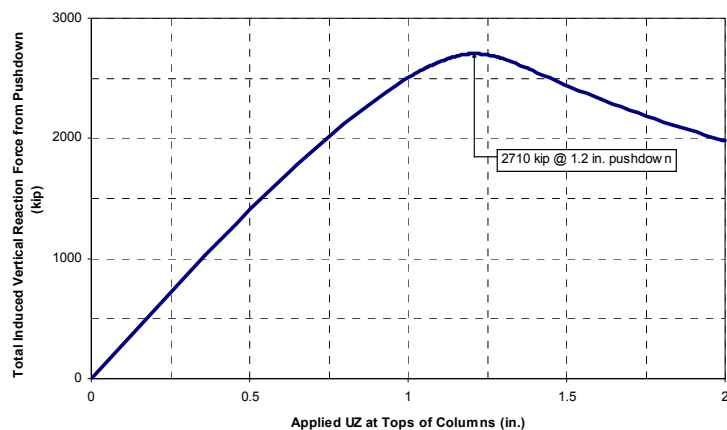


Figure 4–56. Total reaction at column base resulting from pushdown with temperature DBARE and three disconnected floors for Case 9.

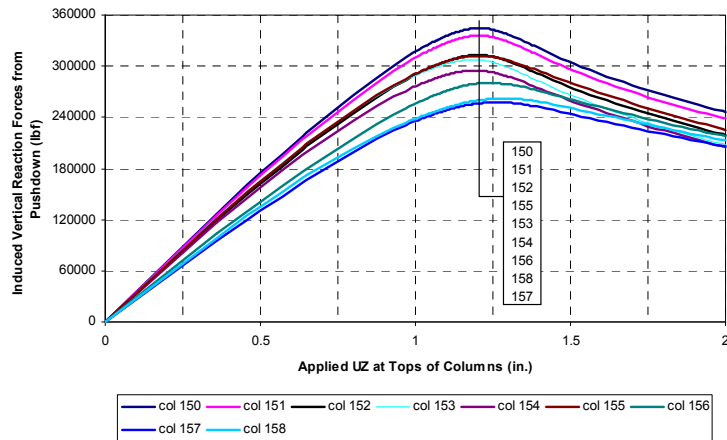


Figure 4–57. Individual column reaction during pushdown with temperature DBARE and three disconnected floors for Case 9.

The analysis results for Case 9 indicated the following:

- The maximum total reaction force resulting from self weight, column and floor loads, and pushdown force was 4,580 kip for nine columns; the maximum individual reaction force was approximately 570 kip.
- The maximum pushdown force was 2,710 kip; the maximum push-down force at a column was approximately 350 kip (Fig. 4–56).
- The push-down deflection was 1.2 in. for the maximum column forces (Fig. 4–56).
- The lateral deflection at a push-down deflection of 1.2 in. was 5.2 in. (Fig. 4–55).

- For a downward deflection of 2.0 in. (the maximum downward deflection analyzed) the push-down force decreased from 2,710 kips to approximately 2,000 kip (Fig. 4–56).
- At a downward deflection 2.0 in., the lateral deflection increased from 5.2 in. to 14.7 in. (Fig. 4–55).
- Plastic buckling occurred at a downward deflection of 1.2 in. when the pushdown force was about 150 percent of the column gravity loads.
- At lower temperatures, thermal expansion of the inside face was insufficient to result in inward bowing of the entire exterior column. At higher temperatures, outward bowing resulted from the combined effects of reduced steel strength on the heated inside face, which shortened first under column gravity loads, and the lack of lateral restraint from the floors.

4.3.4 Summary

The analyses of the exterior wall section model support the following modifications for modeling of the exterior walls:

1. Large inelastic deformations and buckling of the spandrels at elevated temperatures could be expected, but would not significantly affect the stability of the exterior columns and need not be accurately modeled in the global models, except at specific locations where large shear forces were expected to exist.
2. Partial separations of the spandrel splices could occur at elevated temperatures, but would not significantly affect the stability of the exterior columns and need not be accurately modeled in the global models, except at specific locations where large shear forces were expected to exist.
3. Exterior column splices could fail by sliding or opening when floors applied a pull-in force to the exterior wall that results in lateral deflection and had to be accurately modeled in the global models.
4. Instability of an exterior wall subsystem could occur when at least three floors were disconnected (i.e. the floor does not restrain the exterior wall subsystem) and the exterior wall subsystem was subjected to additional vertical or lateral loads.
5. Plastic buckling by kinking with rapid reduction of load in the post-buckling regime of columns could occur at high column loads and room temperatures.

4.4 REFERENCES

- Phan, L. T. (1996), Fire Performance of High-Strength Concrete: A Report of the State-of-the-Art, NISTIR 5934, National Institute of Standards and Technology, Gaithersburg, MD.
- Phan, L. T. and Carino, N. J. (2003), Code provisions for high strength concrete strength-temperature relationship at elevated temperatures, *Materials and Structures*, v 36, issue 256, p 91-98.

Voce, E. 1948. "The relationship between stress and strain for homogeneous deformation," J. Inst. Metals, v 74, p. 537.

Chapter 5

AIRCRAFT IMPACT DAMAGE

5.1 INTRODUCTION

The structural damage to each tower resulting from the aircraft impact was estimated using a transient finite element analysis of a Boeing 767 aircraft model crashing into a global model of the tower as described in NIST NCSTAR 1-2 and NIST NCSTAR 1-2B. Results of the impact damage analyses were used in the fire dynamics analysis and thermal analysis (NIST NCSTAR 1-5) and the structural response analysis (this report).

The analysis of aircraft impact was conducted using the LS-DYNA software. A range of damage estimates was produced for each tower by varying the values of input parameters that were found to strongly influence the analysis results. An experimental design approach, using the method of orthogonal factorial design, was used to determine the parameters that had the greatest effect on the estimated damage. The parameter ranges were selected on the basis of the uncertainty associated with 1) interpretation of photographs and videos of the impact events, 2) material properties that were obtained by testing or from the technical literature, and 3) live loads on the floors of the towers. Three global aircraft impact analyses were conducted for each tower, where the input parameters were selected to represent a *base case*, a *more severe case* and a *less severe case* of damage estimates. Analysis results were compared with observations of damage at the exterior walls and the location of debris that exited the buildings. Two of the three analyses, those associated with the base case and the severe case, were found to have a reasonable match to key observations. The less severe case was not used in the subsequent fire dynamics, thermal, and structural analyses as it did not reasonably match key observables. These analyses are fully described in NIST NCSTAR 1-2 and NIST NCSTAR 1-2B.

The fire dynamics analysis, thermal analysis, and structural response analysis all used the impact damage results associated with the base case and the more severe case for each tower to determine which case most closely matched key post-impact observations up to the time of collapse of each tower. For World Trade Center (WTC) 1, these cases are referred to as Case A and Case B for the base case and the more severe case, respectively, and for WTC 2, Case C and Case D for the base case and the more severe case, respectively.

Prior to producing the final aircraft impact analysis results, initial cases referred to as Case A_i and Case B_i for WTC 1 and Case C_i and Case D_i for WTC 2, were run to develop experience and gain understanding of the fire spread and growth, the rate of structural component heating, and the structural response to damage and elevated temperatures. These initial cases were used in the full floor subsystem analyses described in Chapter 7. The fires and floor slab temperatures were the same for an initial and final Case (i.e., such as A_i and A); the thermal insulation damage estimated for the columns and floor framing differed to a moderate degree. Floor 97 in WTC 1 had the largest change in insulation damage to the floor trusses, where the insulation damage over 11 trusses increased from just beyond the core to two thirds of the floor span. Structural analysis showed that the differences in the floor framing insulation damage would cause little difference in the floor temperatures or in the structural behavior.

This Chapter presents the methodology and criteria for developing input data from the aircraft impact analysis results for the fire dynamics, thermal, and structural analyses, and summarizes the aircraft impact damage data for Cases A, B, C, and D. A brief discussion of how aircraft impact affected the concrete columns in the Pentagon shows how direct debris impact dislodged the columns' concrete cover, which has a much higher bond strength than the SFRM and gypsum materials for thermal insulation of the structural steel. Data sets for structural analyses with Cases A_i, B_i, C_i, and D_i are presented in Appendix A and Cases A, B, C, and D are presented in Appendix B.

5.2 METHODOLOGY AND CRITERIA FOR DEVELOPING INPUT DATA FROM AIRCRAFT IMPACT ANALYSIS RESULTS

The fire dynamics, thermal, and structural analyses all required input data derived from the aircraft impact analyses. The fire dynamics analyses used estimates of damage to the floors and partition walls to describe ventilation paths and to identify the distribution of jet fuel and debris immediately following impact. The thermal analysis required estimation of the areas that had dislodged insulation on the structural components of the towers. For the structural analyses, elements that represented severed or heavily damaged floors and columns were removed from the structural models of the towers.

Damage to the exterior walls in the structural models was based on photographic and video records, which matched reasonably well the exterior damage predicted by the impact simulations (see NIST NCSTAR 1-2). Figures 5-1 and 5-2 show a comparison between the observed and predicted aircraft impact damage to the exterior walls for WTC 1 and WTC 2. The observed exterior damage was used in the structural analyses.

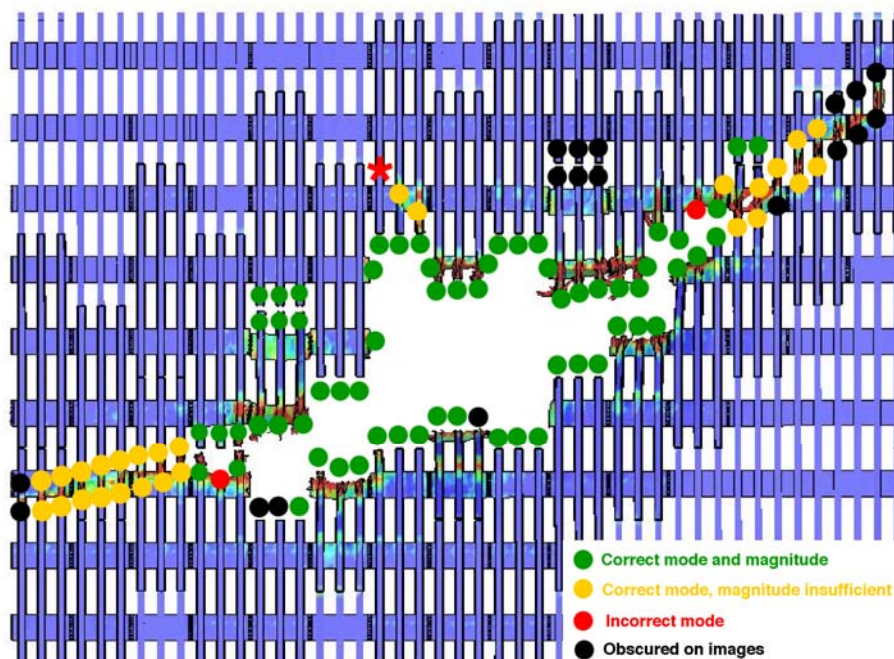


Figure 5-1. Validation of Aircraft Impact Analysis Prediction With Observations for WTC 1 North Exterior Wall Damage.

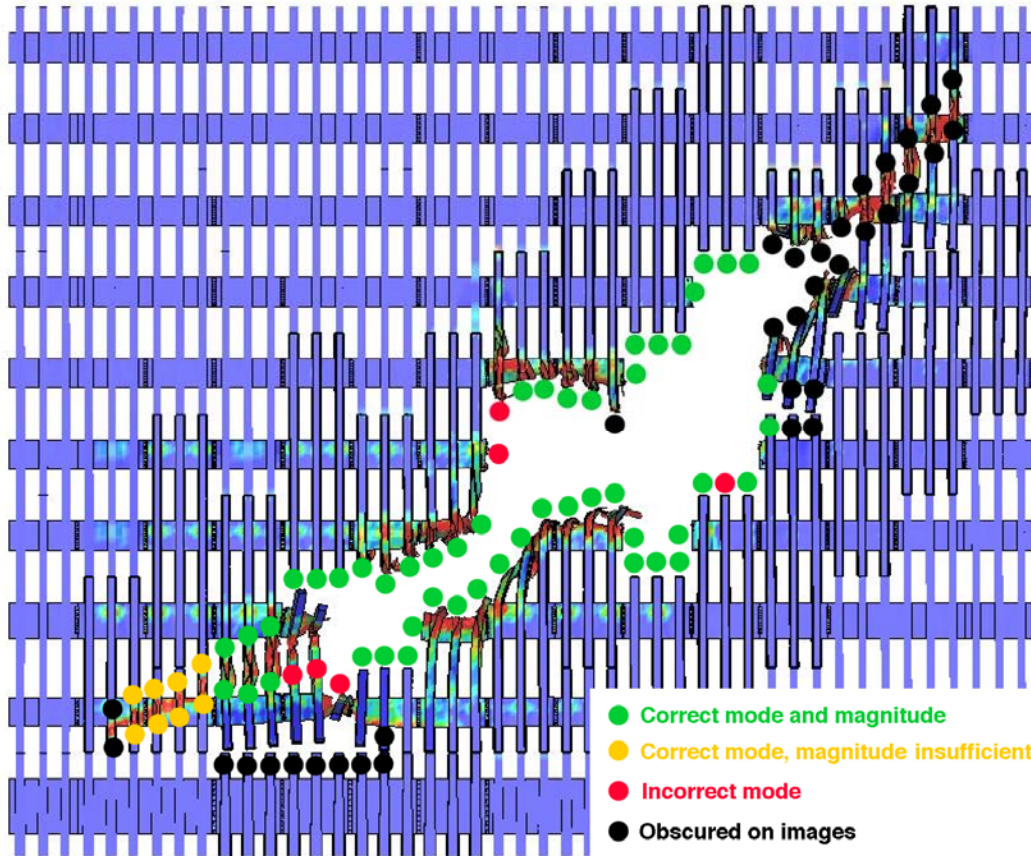


Figure 5–2. Validation of Aircraft Impact Analysis Prediction With Observations for WTC 2 South Exterior Wall Damage.

5.2.1 Core Column Damage

The damage predicted by the impact simulations was classified into four levels as shown graphically in Figure 5–3 (the colors represent plastic strain magnitude with undamaged sections in blue and strains at or above 5 percent shown in red). The classification levels were *light damage*, *moderate damage*, *heavy damage*, and *failed* (or severed). The light damage level had low level plastic strains but no significant structural deformations. The moderate damage level had visible local deformations of the column cross section (e.g. local flange bending) but without lateral displacements of the column centerline. The heavy damage level had significant global deformations that resulted in a permanent deflection of the column centerline. The failed columns were completely severed and could not carry any load. For details, refer to NIST NCSTAR 1-2.

The column damage criteria were applied to the aircraft impact analysis results. Tables 5–1 to 5–4 show the column damage classifications obtained from each analysis. Refer to Fig. 4–7 for core column numbering. Figure 4–7 shows the WTC 1 column layout with the 100 series exterior columns on the north side; WTC 2 column layout is the same except that the 200 series exterior columns face north. WTC 1 was estimated to have 3 severed core columns and 4 heavily damaged columns for Case A, and 6 severed core columns and 3 heavily damaged columns for Case B. The WTC 1 severed and heavily damaged columns were located at the center of the north side of the core. WTC 2 was estimated to have

5 severed core columns and 4 heavily damaged columns for Case C, and 10 severed core columns and a heavily damaged column for Case D. The WTC 2 severed and heavily damaged columns were located at the southeast corner of the core. The core column damage was used in the major subsystem and global analyses for each tower. The misalignment of the heavily damaged columns dramatically reduced their load carrying capacity. In the structural models described in this report, elements corresponding to the heavily damaged and severed columns were removed, while those corresponding to moderately or lightly damaged columns were retained without modifications.

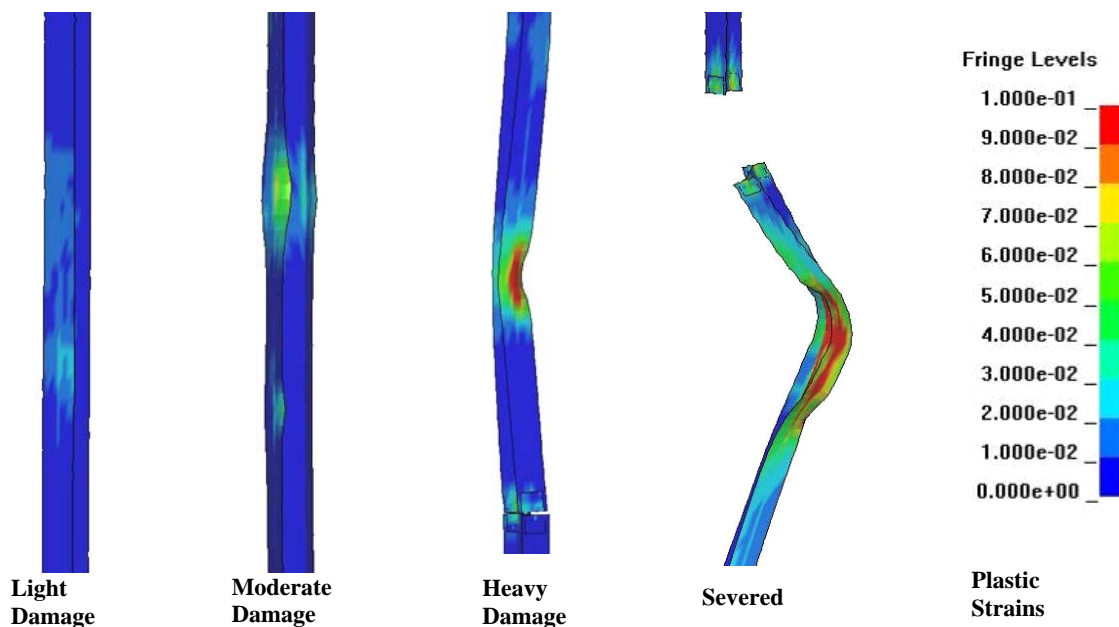


Figure 5-3. Core column damage levels.

Table 5-1. WTC 1 Case A core column damage.

| Column | Location | Damage Level | Lateral Deflection of Column Centerline (in.) |
|------------|--------------|--------------|---|
| Column 503 | Floor 96 | Heavy | 18 |
| Column 504 | Floors 92-96 | Severed | |
| Column 505 | Floors 93-96 | Heavy | 20 |
| Column 506 | Floors 93-94 | Heavy | 10 |
| Column 604 | Floors 92-96 | Severed | |
| Column 605 | Floors 94-95 | Moderate | |
| Column 702 | Floor 96 | Moderate | |
| Column 703 | Floor 96 | Moderate | |
| Column 704 | Floor 94 | Heavy | 18 |
| Column 705 | Floor 95 | Moderate | |
| Column 706 | Floors 93-95 | Severed | |
| Column 802 | Floor 96 | Moderate | |
| Column 805 | Floor 94 | Moderate | |

Table 5–2. WTC 1 Case B core column damage.

| Column | Location | Damage Level | Lateral Deflection of Column Centerline (in.) |
|---------------|-----------------|---------------------|--|
| Column 503 | Floor 95-96 | Severed | |
| Column 504 | Floors 92-96 | Severed | |
| Column 505 | Floors 93-96 | Severed | |
| Column 506 | Floors 93-95 | Heavy | 24 |
| Column 603 | Floors 96-97 | Moderate | |
| Column 604 | Floors 92-96 | Severed | |
| Column 605 | Floors 94-95 | Moderate | |
| Column 606 | Floors 94 | Light | |
| Column 702 | Floor 97 | Light | |
| Column 703 | Floor 96 | Moderate | |
| Column 704 | Floors 92-96 | Severed | |
| Column 705 | Floor 95 | Moderate | |
| Column 706 | Floors 93-95 | Severed | |
| Column 802 | Floor 96 | Light | |
| Column 803 | Floors 96-97 | Moderate | |
| Column 804 | Floor 94-96 | Moderate | |
| Column 805 | Floors 93-95 | Heavy | 20 |
| Column 903 | Floor 96 | Light | |
| Column 904 | Floors 95-96 | Heavy | 19 |
| Column 905 | Floor 95 | Light | |

Table 5–3. WTC 2 Case C core column damage.

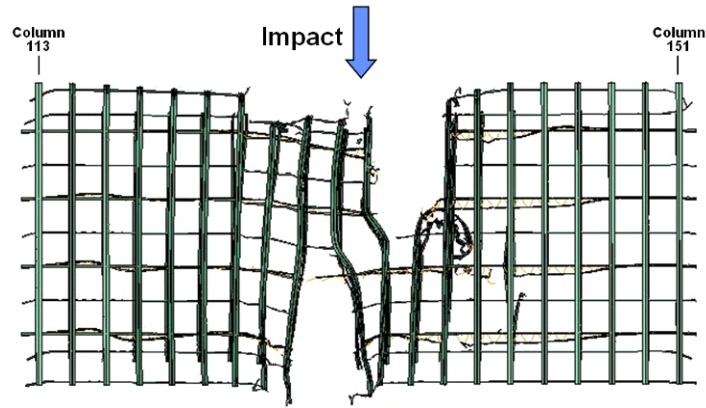
| Column | Location | Damage Level | Lateral Deflection of Column Centerline (in.) |
|---------------|-----------------|---------------------|--|
| Column 801 | Floor 79 | Heavy | 10 |
| Column 901 | Floors 79-82 | Severed | |
| Column 902 | Floor 79 | Heavy | 32 |
| Column 903 | Floors 77-83 | Severed | |
| Column 904 | Floor 79 | Moderate | |
| Column 905 | Floor 79 | Heavy | 18 |
| Column 1001 | Floors 77-83 | Severed | |
| Column 1002 | Floors 79-81 | Severed | |
| Column 1003 | Floor 80 | Severed | |
| Column 1004 | Floor 80 | Heavy | 18 |

Table 5–4. WTC 2 Case D core column damage.

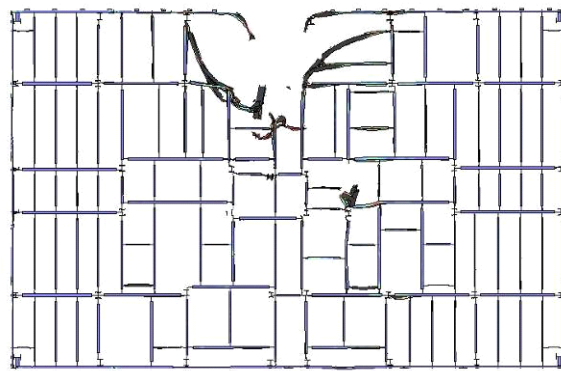
| Column | Location | Damage Level | Lateral Deflection of Column Centerline (in.) |
|---------------|-----------------|---------------------|--|
| Column 602 | Floor 79 | Moderate | |
| Column 605 | Floor 79 | Moderate | |
| Column 701 | Floors 79-80 | Severed | |
| Column 702 | Floor 79 | Heavy | 16 |
| Column 703 | Floor 79 | Moderate | |
| Column 704 | Floor 79 | Light | |
| Column 705 | Floors 78-79 | Light | |
| Column 705 | Floor 78 | Light | |
| Column 801 | Floors 79-80 | Severed | |
| Column 802 | Floors 77-80 | Severed | |
| Column 803 | Floors 77-80 | Severed | |
| Column 804 | Floor 79 | Light | |
| Column 901 | Floors 80-81 | Severed | |
| Column 902 | Floor 79 | Moderate | |
| Column 903 | Floors 77-83 | Severed | |
| Column 904 | Floors 79-81 | Moderate | |
| Column 905 | Floors 79 & 81 | Light | |
| Column 907 | Floor 81 | Light | |
| Column 1001 | Floors 77-83 | Severed | |
| Column 1002 | Floors 79-83 | Severed | |
| Column 1003 | Floors 79-83 | Severed | |
| Column 1004 | Floors 79-83 | Severed | |
| Column 1005 | Floors 79-81 | Moderate | |

5.2.2 Structural Damage to Floor Slabs, Core Beams, and Floor Trusses

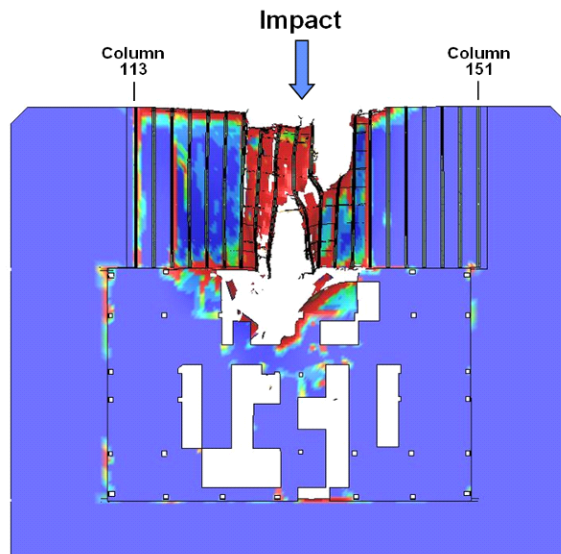
Two types of floor damage were identified from the impact analysis results: (1) missing floor areas and (2) severely damaged floor areas incapable of supporting loads. Figure 5–4 illustrates the floor damage computed by the aircraft impact analysis, with WTC 1 Structural Floor 95 Case A as an example. The damage to floor framing (i.e., trusses and beams) ranged from being severed and bent out of alignment to having localized damage to a component of the framing. Concrete slab damage ranged from crushed areas (failure of both concrete slab and metal decking) to permanent plastic strains (failure of concrete slab, but not metal decking). The concrete slab was failed in the red regions shown in Figure 5–4(c), which indicated a 2 percent plastic strain or greater. At these strain levels, the concrete slab was assumed to be severely damaged and likely exposed the supporting metal decking.



a. Floor trusses



b. Core floor beams



c. Floor slab

Figure 5–4. Impact damage to WTC 1 Floor 95 for Case A (plan view).

For the fire dynamics analysis, missing floor areas were important since they created new ventilation paths between floors. Ventilation is a critical parameter for fire growth and spread. For the structural analyses, floor areas were removed where the intended structural function of the floor was severely impaired or no longer available. For instance, if truss end connections were severed, the floor framing could not transfer its loads to the column at that point. The condition of the concrete slab was also important as the concrete slab and floor framing were designed to act compositely. Severe damage to the concrete over more than half of a truss or a beam length was considered to cause a severely impaired floor area.

Figure 5–5 shows an example of how the damage in Figure 5–4 was evaluated and summarized for the structural analysis. Areas with severed floor framing and crushed concrete (indicated by red zones) were outlined with a dashed line, indicating where floor areas were to be removed or considered missing. Areas with misaligned framing or loss of composite action with the slab (due to damaged concrete) over more than half the member length were marked with green shading as damaged floor areas. In this example, the dashed outline and green overlay cover nearly the same area, though this is not generally the case for all floors. For analysis purposes, only severe damage was considered; isolated member damage or small areas of concrete damage were ignored as they were considered localized damage. Damage ranges in Figure 5–5 were delineated by boxed areas as there was insufficient data to develop criteria for irregular boundaries.

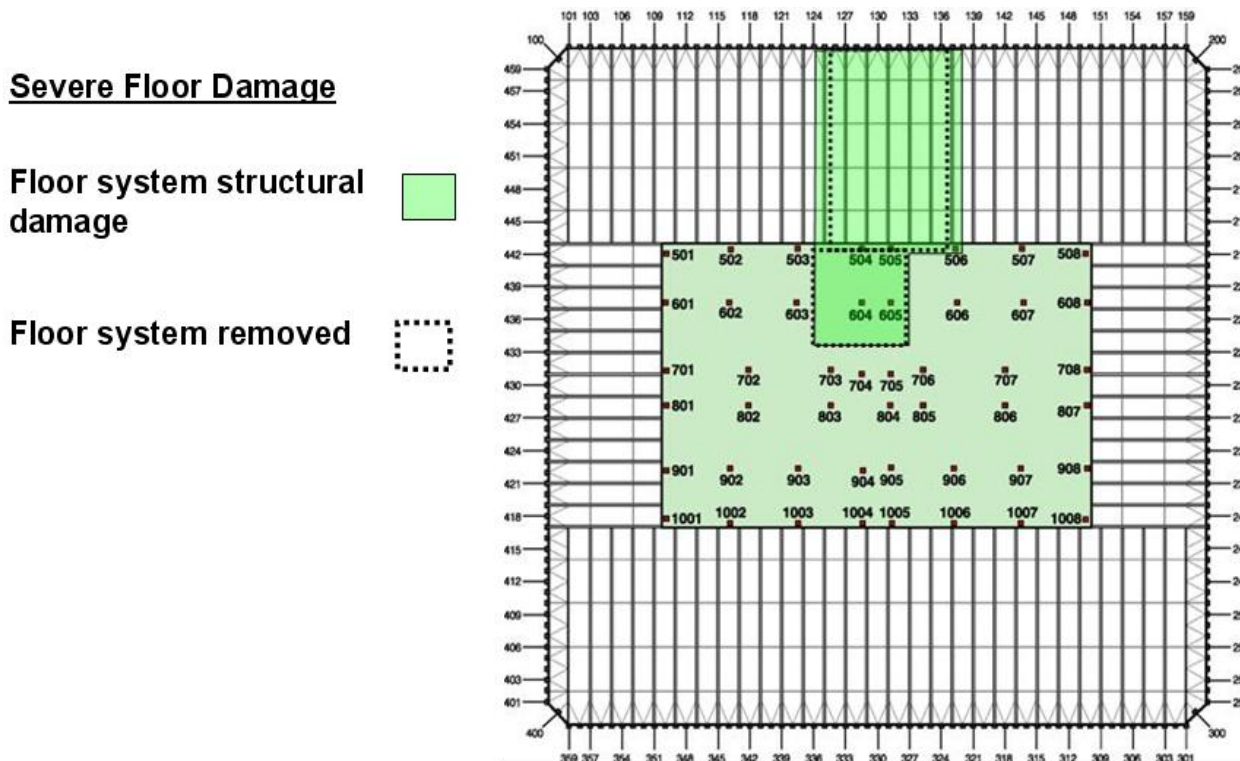


Figure 5–5. Damage to WTC 1 Floor 95 framing and slab for Case A.

5.2.3 Damage to Fire Protection for Structural Steel

The aircraft impact simulation models included not only the structural components of the towers and aircraft, but also representations of the partition walls and building contents and furnishings (modular office workstations). The results of the analyses included damage to the partition walls, workstations, and structural elements. Such damage estimates were crucial for the estimation of areas with dislodged insulation as explained in this section.

Estimates of the post-impact condition of the fire protection was based on criteria that considered damage to structural components, building partitions, and furnishings along with the debris field as calculated from the aircraft impact analyses. Estimates for the extent of dislodged insulation considered insulation damage to structural components only in the direct path of debris, as follows:

- Core columns had sprayed fire-resistant material (SFRM), gypsum wallboard enclosures, or a combination of both. Insulation was assumed to be dislodged from the columns if they were subject to direct debris impact that could fail wall partitions in the immediate vicinity. The representative bending strength of building partitions in the impact simulations was 500 psi (NIST NCSTAR 1-2), while the representative adhesive and cohesive strength of SFRM measured in the laboratory by NIST was generally less than 12 psi (NIST NCSTAR 1-6A). Gypsum column enclosures were also assumed to have a lesser representative strength than wall partitions.

To consider that insulation on core columns was damaged, the predicted debris impact had to be sufficient to fail building partitions immediately in front of the columns. If the wall partitions remained intact in the core area after interaction with the debris field, then the insulation on core columns behind these partitions was assumed to remain intact. If wall partitions were damaged or destroyed by the debris field, then insulation on core columns behind these partitions was assumed to be dislodged over that floor height.

- To consider that insulation on exterior columns was damaged, the debris impact had to damage or destroy office furnishings (modular office workstations) adjacent to the columns. If the office furnishings remained intact after interaction with the debris field, then the insulation on the inside face of the exterior columns behind these furnishings was assumed to remain intact. If the room furnishings were damaged or destroyed after interaction with the debris field, then the insulation on the inside face of the exterior columns in the same vicinity was assumed to be dislodged over that floor height. The other three faces of the exterior columns were protected by the windows and/or aluminum cladding and were assumed to have no insulation damage.
- To consider that SFRM on floor trusses was damaged, the debris impact had to be sufficient to damage or destroy room furnishings (modular office workstations) in the same area of the affected floor. If the room furnishings remained intact, then the insulation on the steel trusses above these furnishings was assumed to remain intact. If the room furnishings were damaged or destroyed by the debris field, then the insulation on the steel trusses above these furnishings was assumed to be dislodged.

The insulation damage estimates were conservative as they ignored possibly damaged and dislodged insulation in a much larger region that was not in the direct path of the debris but was subject to strong

vibrations during and after the aircraft impact. A robust criteria to generate a coherent pattern of vibration-induced dislodging could not be established due to (1) the numerical noise inherent in the acceleration time-histories on structural components obtained from the aircraft impact analyses, and (2) lack of data on the strength of insulation materials under such a high rate of loading with sharp peaks in a very short duration. However, there were indications that insulation damage occurred over a larger region than that estimated. Photographic evidence showed insulation dislodged from exterior columns not directly impacted by debris (NIST NCSTAR 1-3C). The towers underwent a period of strong impact loading for about 0.6 to 0.7 s. Further, video analysis showed that WTC 2 vibrated for over 4 minutes after aircraft impact with amplitudes in excess of 20 inches at the roof top (NIST NCSTAR 1-5A). First-person interviews of building occupants indicated that building vibrations due to aircraft impact were strong enough to dislodge ceiling tiles and collapse walls throughout the height of both WTC towers and to cause nearly all elevators to stop functioning (NIST NCSTAR 1-7). Due to lack of experimental data, estimates of insulation damage ignored the possibility that the impact of jet fuel might also result in dislodging insulation. The global structural analyses used to determine the probable collapse sequence included some variation in the extent of dislodged insulation.

Figure 5–6 shows an elevation view of WTC 1 during the aircraft impact for Case B. As impact debris traveled across multiple floors, it tended to fill the space between the two floor slabs. Figure 5–7 shows more detail with specific damage to framing, partitions, and furnishings on Floor 95. The floor-to-floor dispersal pattern led to the assumption that when the insulation was dislodged from direct debris impact, it was dislodged over the full floor height. This assumption was consistent with the level of modeling detail (i.e. insulation was not included in the aircraft impact model) and with expected thermal behavior of a steel component if substantial portions of the insulation were removed.

As an example, Figs. 5–8 and 5–9 show plan views of WTC 1 Floor 95 for Case B impact damage. Figure 5–8 shows the location of floor furnishings and partitions prior to impact. The extent of furnishings and partitions in the impact models was limited to areas where interaction with the aircraft was expected due to computational limits on the number of nodes and elements in the model. Figure 5–9 shows the extent of damage to Floor 95. The area of dislodged insulation for columns and floor framing between floor slabs 95 and 96 is indicated by the shaded overlay. Where partition walls and furnishings remained intact, the insulation was also assumed to remain intact. Where the debris extended to the exterior wall, the insulation on the inside surface of the exterior columns and spandrels was assumed to be dislodged over the full floor height.

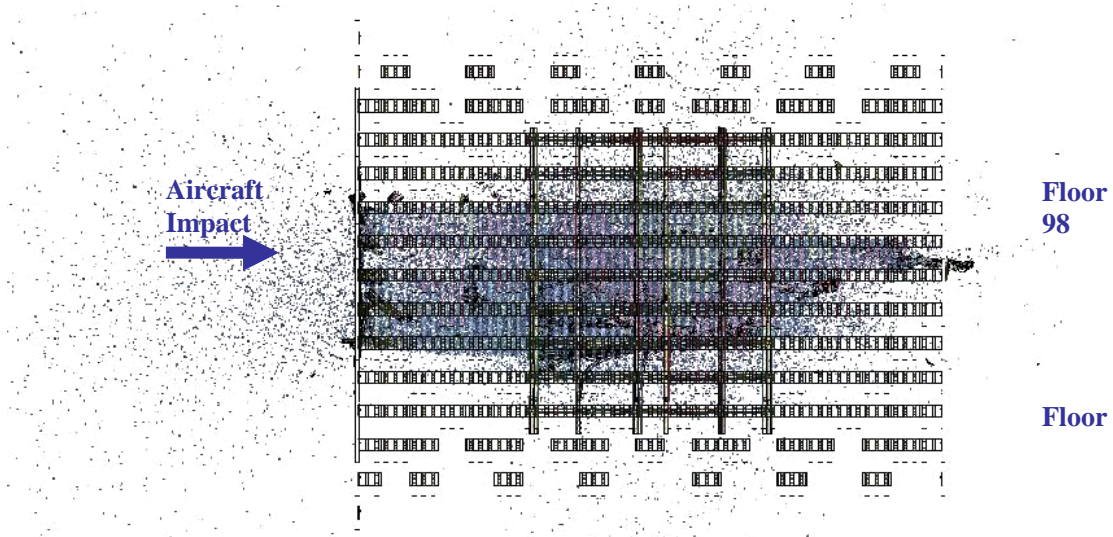


Figure 5–6. Debris and fuel field in WTC 1 Case B analysis of aircraft impact.

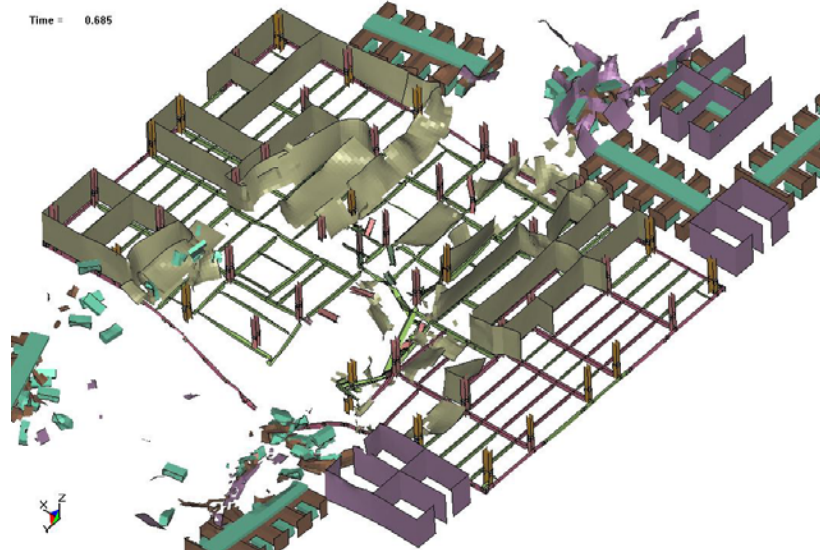


Figure 5–7. WTC 1 Case B aircraft impact damage to framing, partitions, and furnishings on Floor 95.

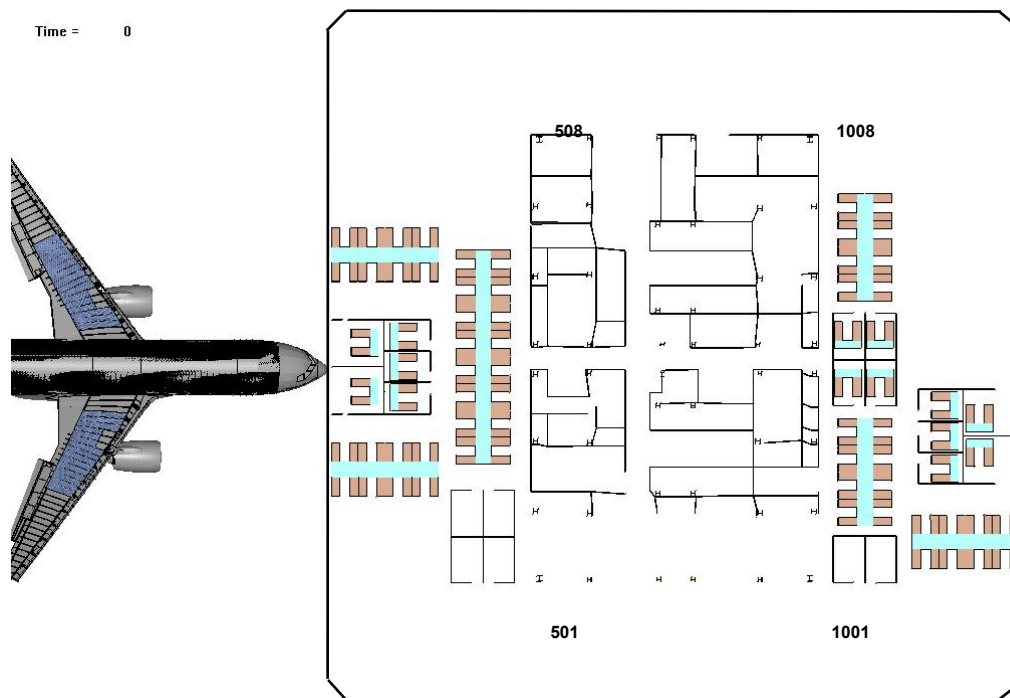


Figure 5–8. WTC 1 Case B Floor 95 partitions and furnishings layout prior to impact (layout provided in model only where interaction with aircraft was expected).

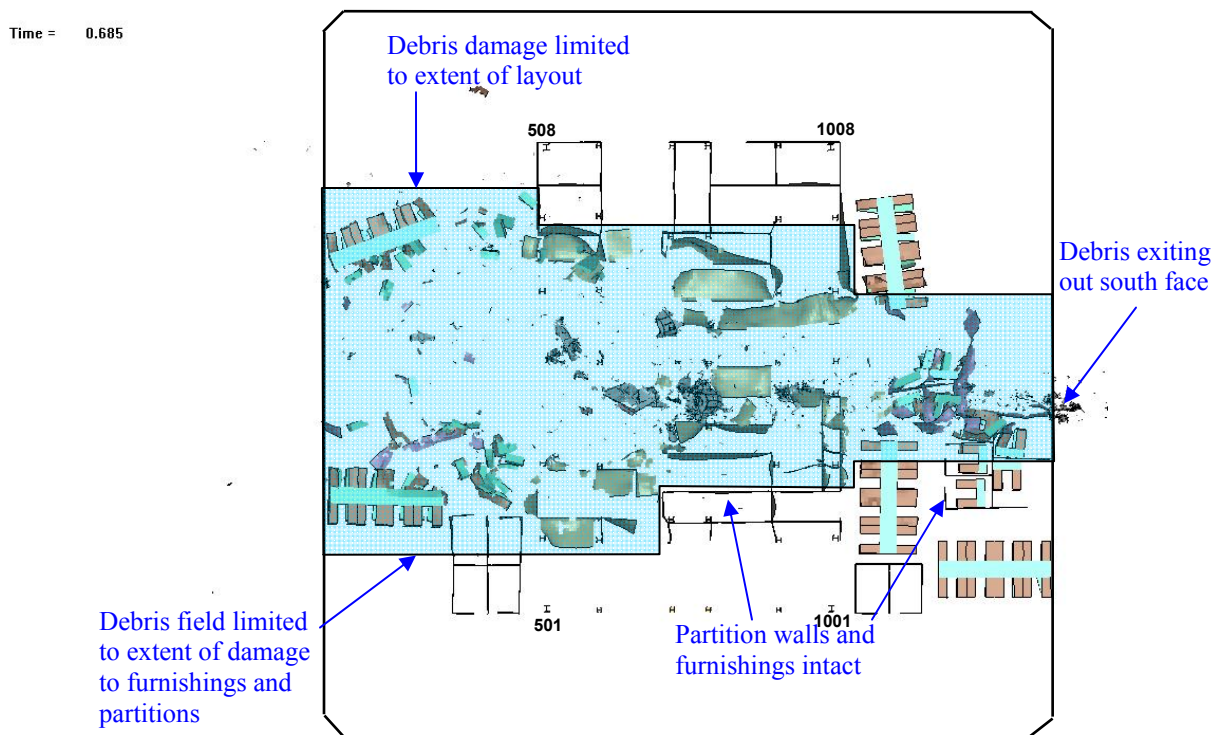


Figure 5–9. WTC 1 Case B Floor 95 partitions and furnishings layout after impact with overlay showing extent of dislodged insulation from direct debris impact.

5.2.4 Summary of Aircraft Impact Damage

The use of the aircraft impact results by the fire dynamics, thermal, and structural analyses required presentation of debris damage data in two formats, referred to here as ‘occupancy floor’ and ‘structural floor’ formats. Figure 5–10 illustrates the terms occupancy floor (e.g. the elevator floor number) and structural floor. Damage to columns, partitions, and insulation between floor slabs are presented in the occupancy floor format, as shown in Fig. 5–11. Structural damage to the composite floor (i.e. truss, beams, and floor slab) is presented in the structural floor format, as shown in Fig. 5–12. The aircraft impact, thermal, and structural analyses used both formats. The fire dynamics analyses used the occupancy floor format, as the floor slabs provided natural boundaries for fire.

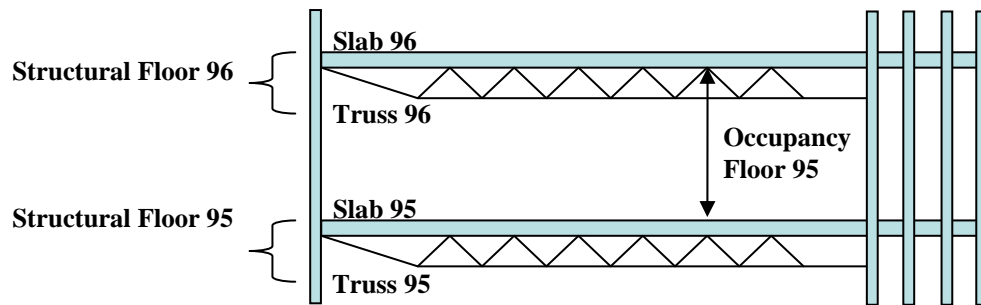


Figure 5–10. Definition of structural floor and occupancy floor.

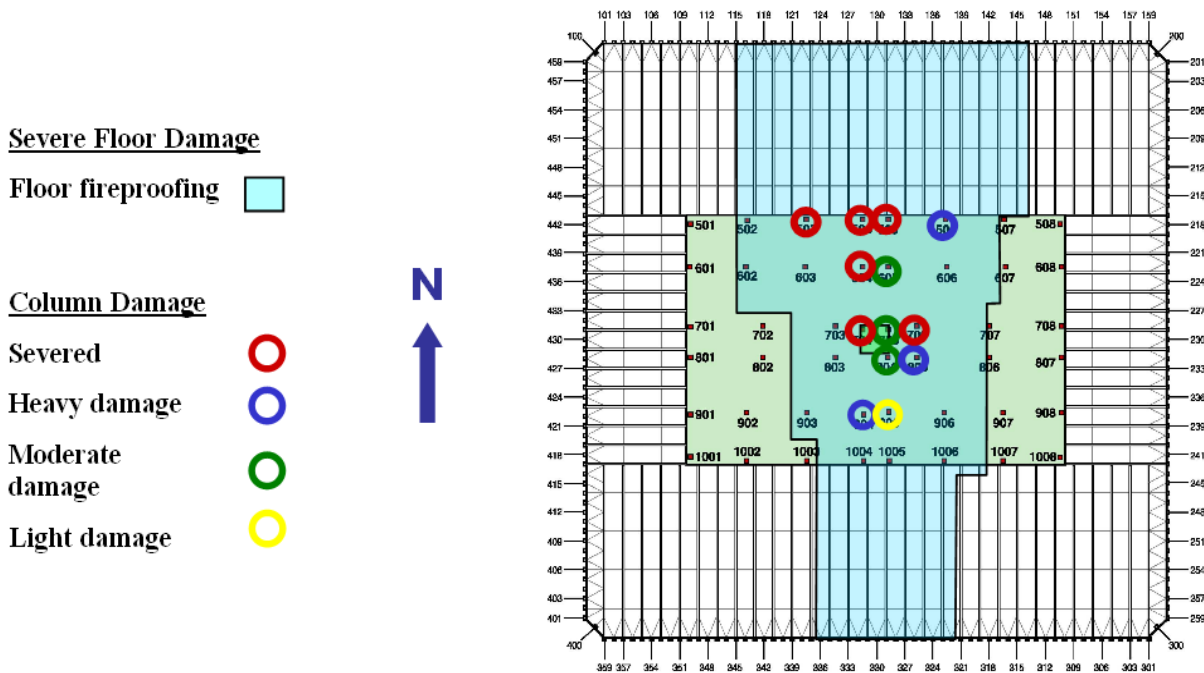


Figure 5-11. Plan view of WTC 1 Case B insulation and column damage for Occupancy Floor 95.

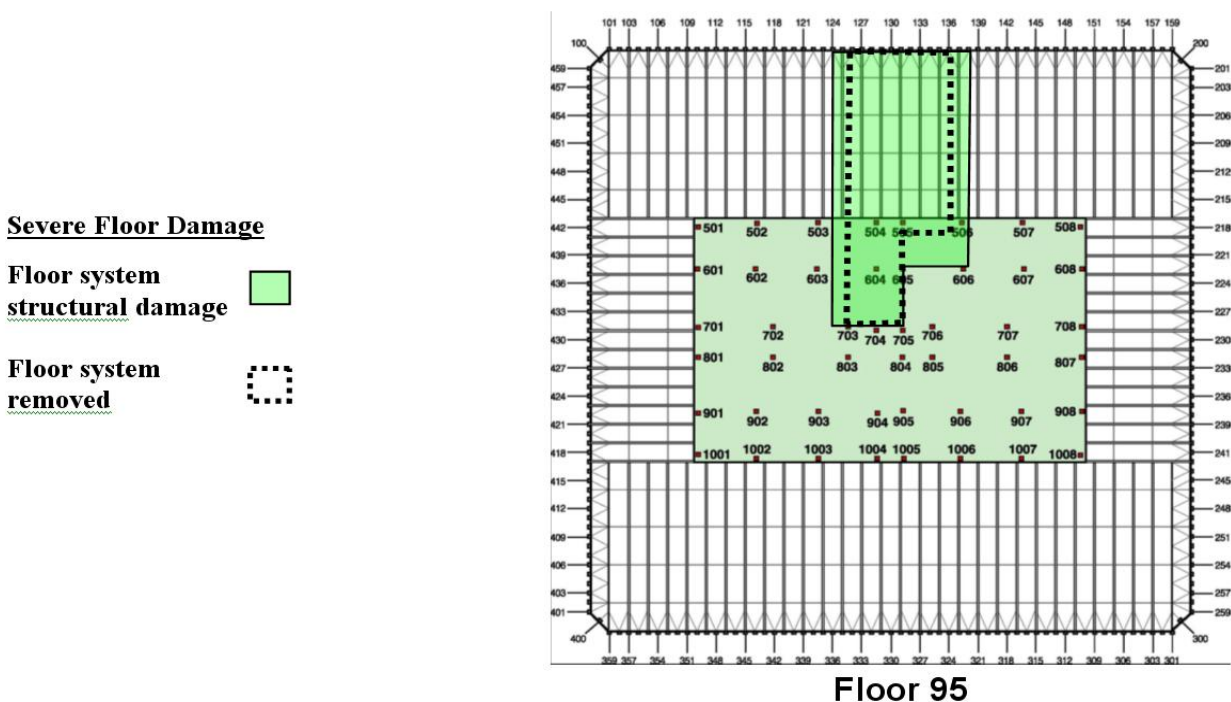


Figure 5-12. Plan view of WTC 1 Case B damage to Structural Floors 95.

5.3 STRUCTURAL AND FIRE PROTECTION DAMAGE TO WTC 1

This section presents summary graphics of structural and fire protection damage that were developed using results of the aircraft impact simulations. Figures 5–13 and 5–16 show plan views of the cumulative damage over Floors 93 to 99 for Case A and Case B, respectively. The impact damage at each floor level is shown in Figures 5–14 and 5–15 for Case A and 5–17 and 5–18 for Case B with occupancy and structural formats. The damage graphics for Cases A and B are also presented at a larger scale in Appendix B.

The structural damage in WTC 1 extended from the north exterior wall, through the central region of the north floor area and through to the south side of the core. An exterior panel was knocked out of the south wall by aircraft debris. Damage to the insulation from direct debris impact extended over a larger region and included most of the north floor areas, the core, and central regions of the south floor areas. Case B predicted more damage to core columns and a larger extent of insulation damage to the south floor area than Case A, including damage to the south exterior wall insulation on the inside face.

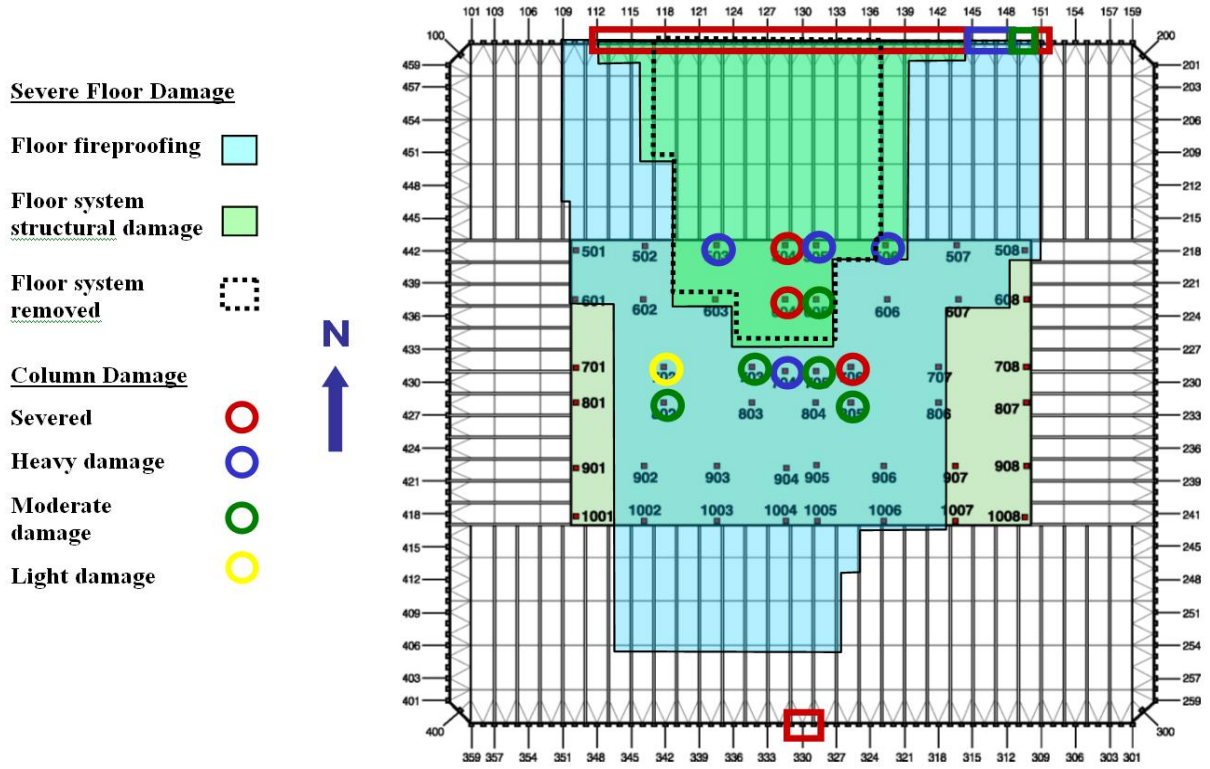


Figure 5–13. Plan view of WTC 1 Case A cumulative damage for Floors 93 to 98.

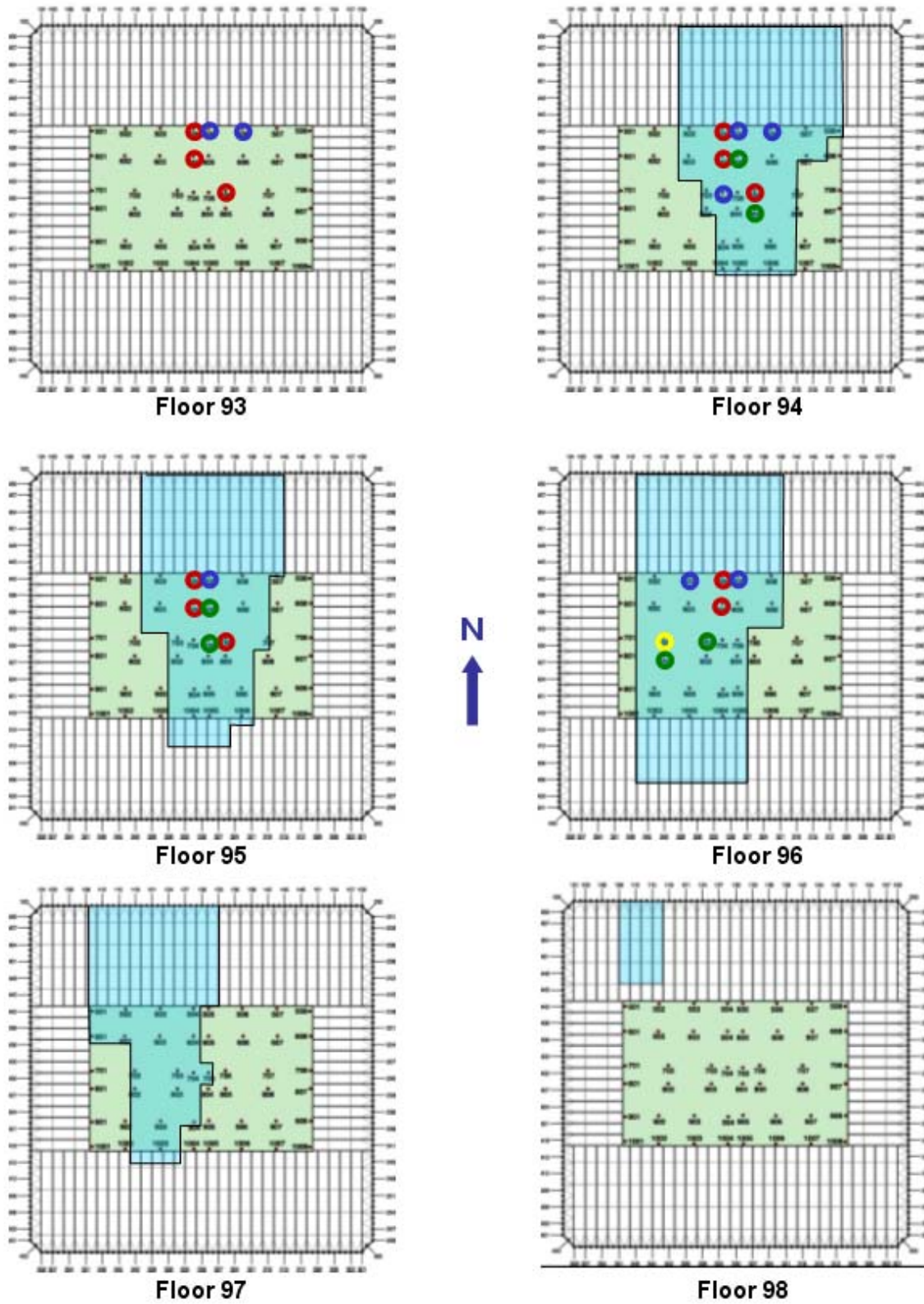


Figure 5-14. Plan view of WTC 1 Case A insulation and column damage to Occupancy Floors 93 to 98.

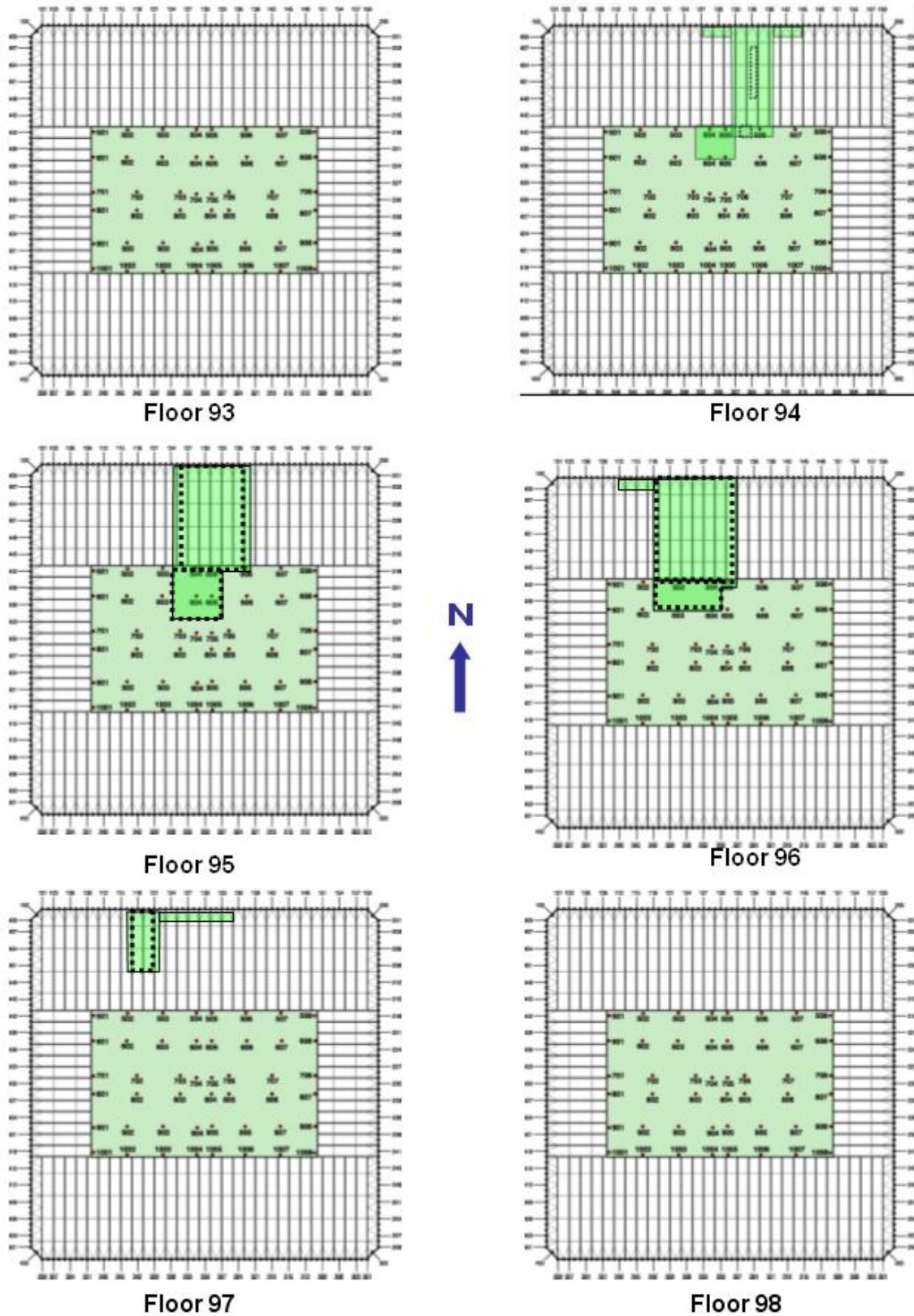


Figure 5–15. Plan view of WTC 1 Case A damage to Structural Floors 93 to 98.

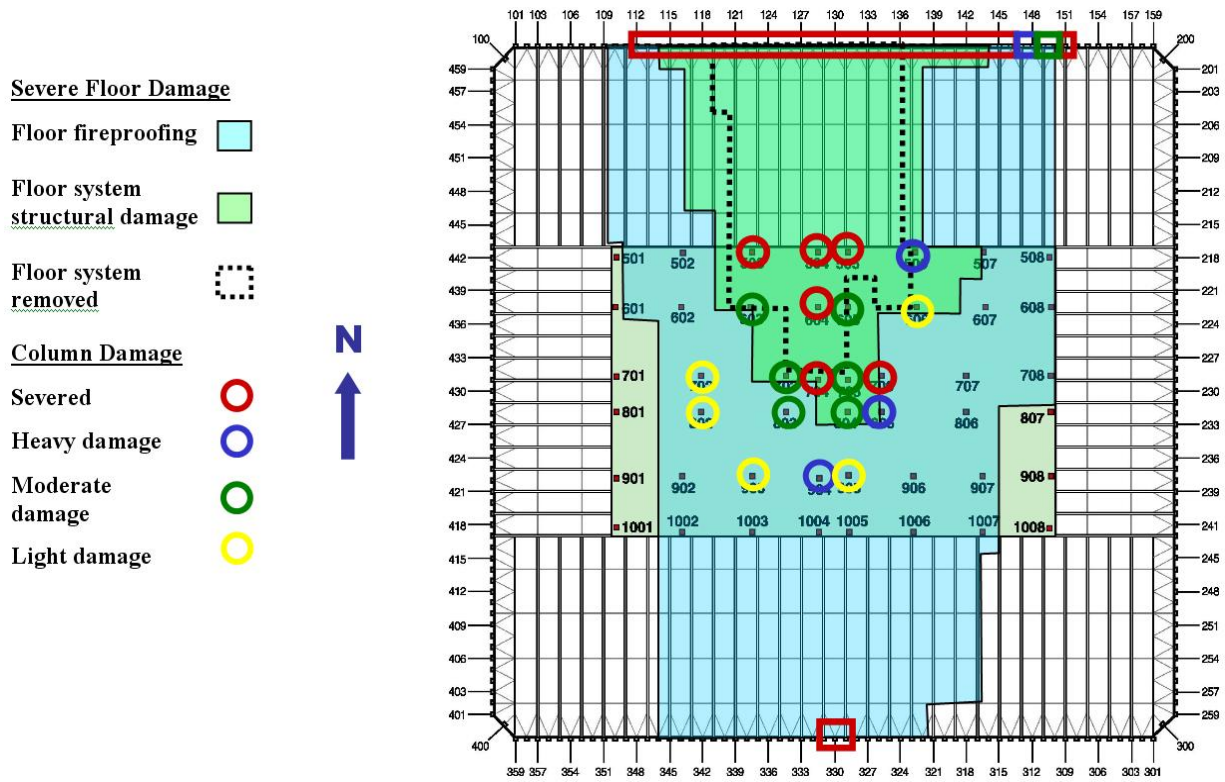


Figure 5–16. Plan view of WTC 1 Case B cumulative damage from Floors 93 to 98.

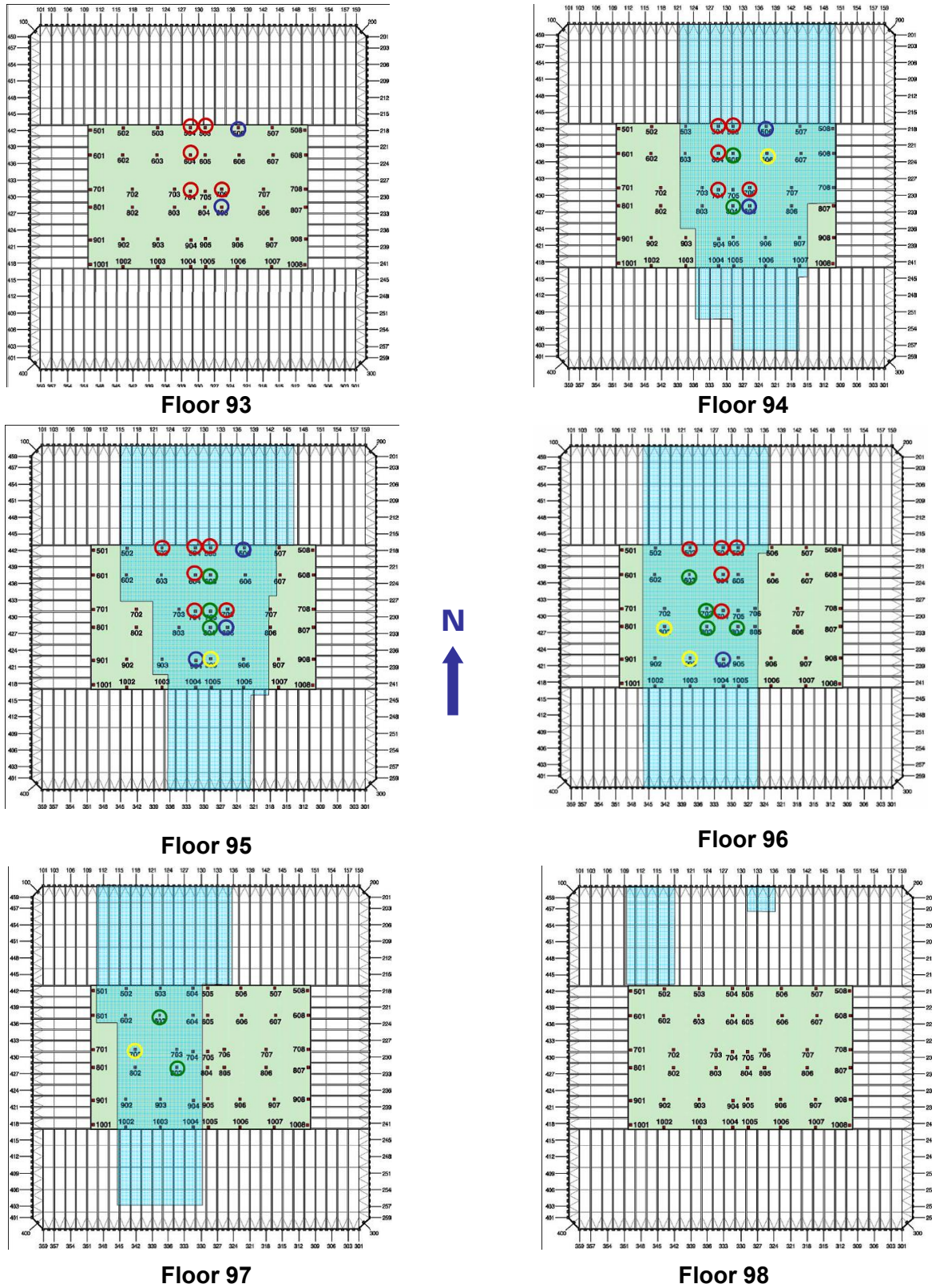


Figure 5–17. Plan view of WTC 1 Case B insulation and column damage to Occupancy Floors 93 to 98.

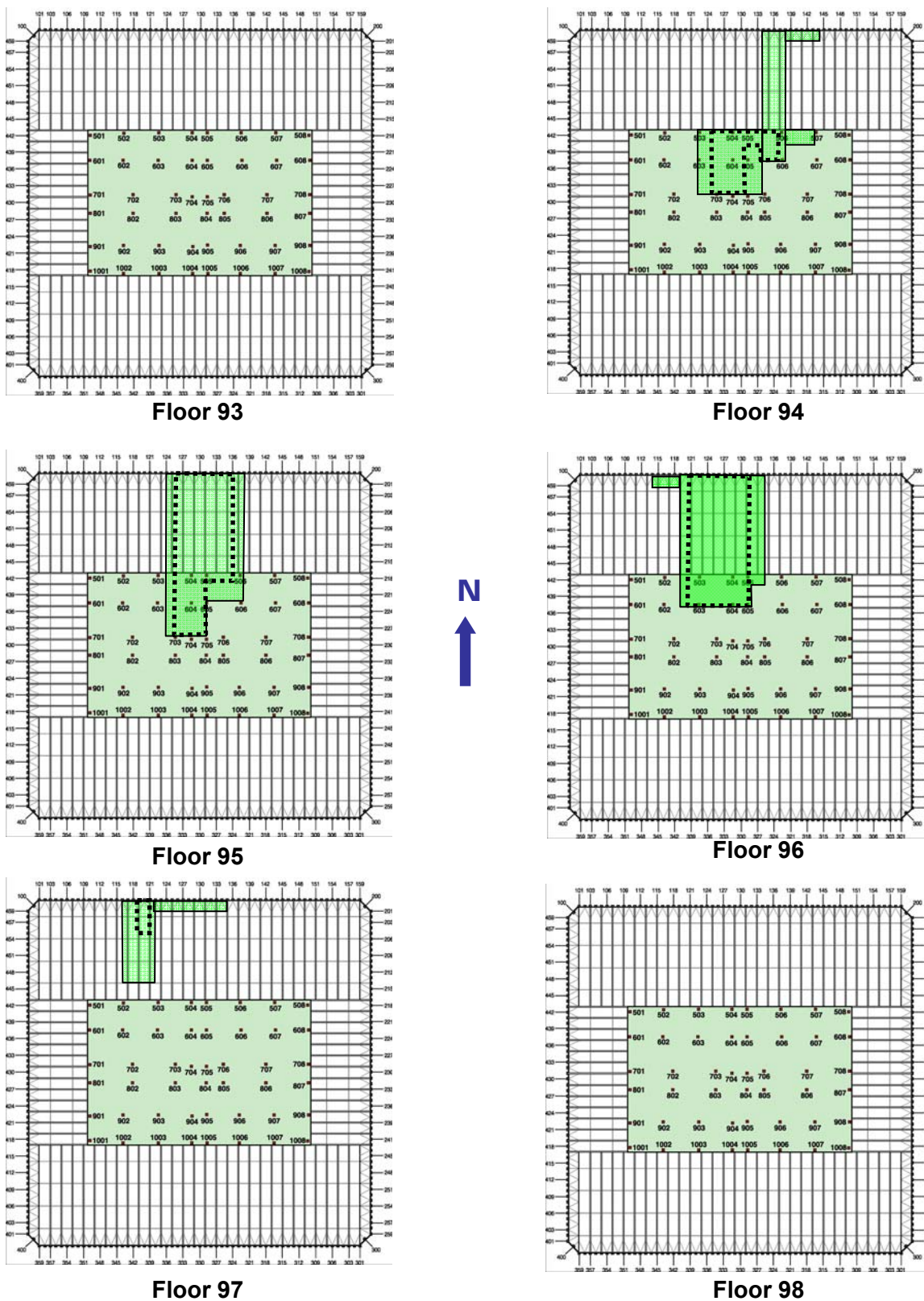


Figure 5–18. Plan view of WTC 1 Case B damage to Structural Floors 93 to 98.

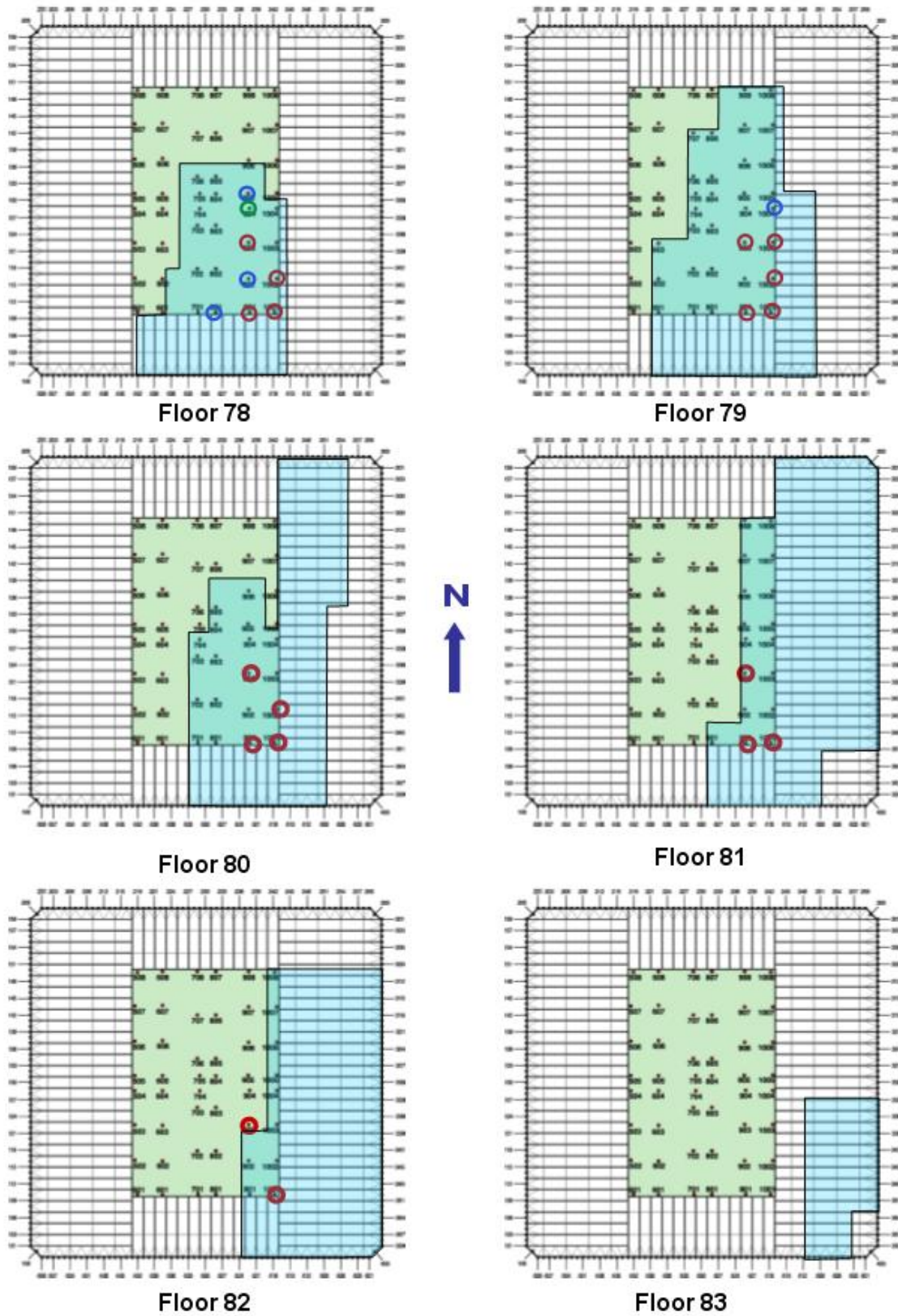


Figure 5–20. Plan view of WTC 2 Case C insulation and column damage to Occupancy Floors 78 to 83.

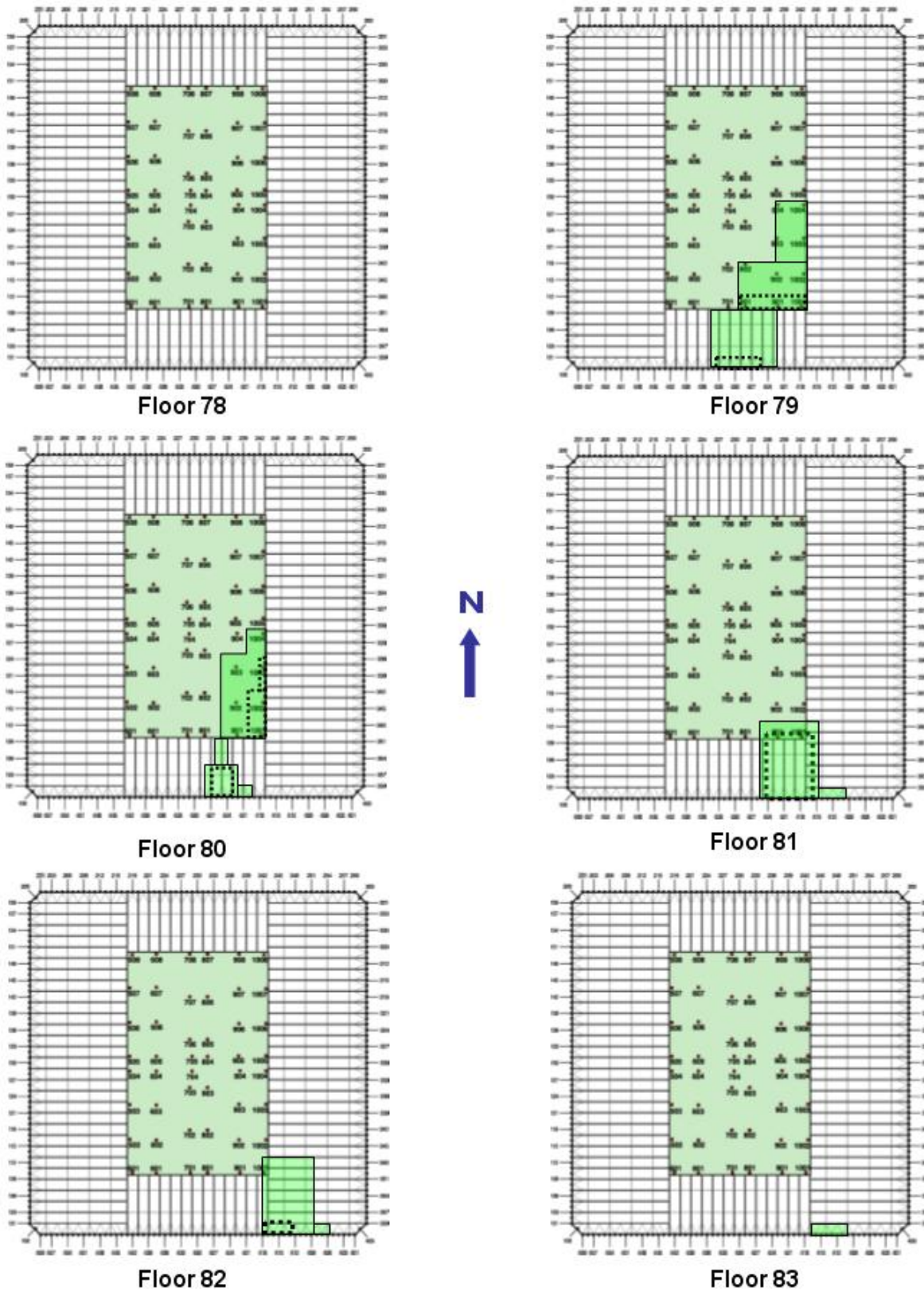


Figure 5–21. Plan view of WTC 2 Case C damage to Structural Floors 78 to 83.

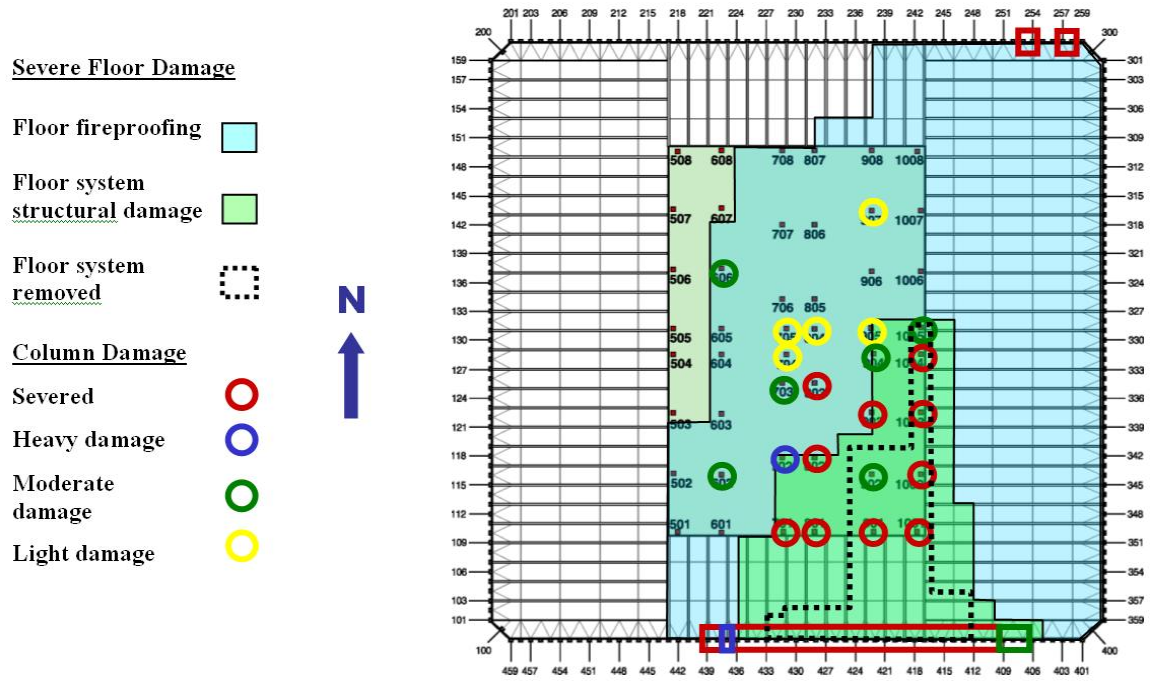


Figure 5–22. Plan view of WTC 2 Case D cumulative damage from Floors 78 to 83.

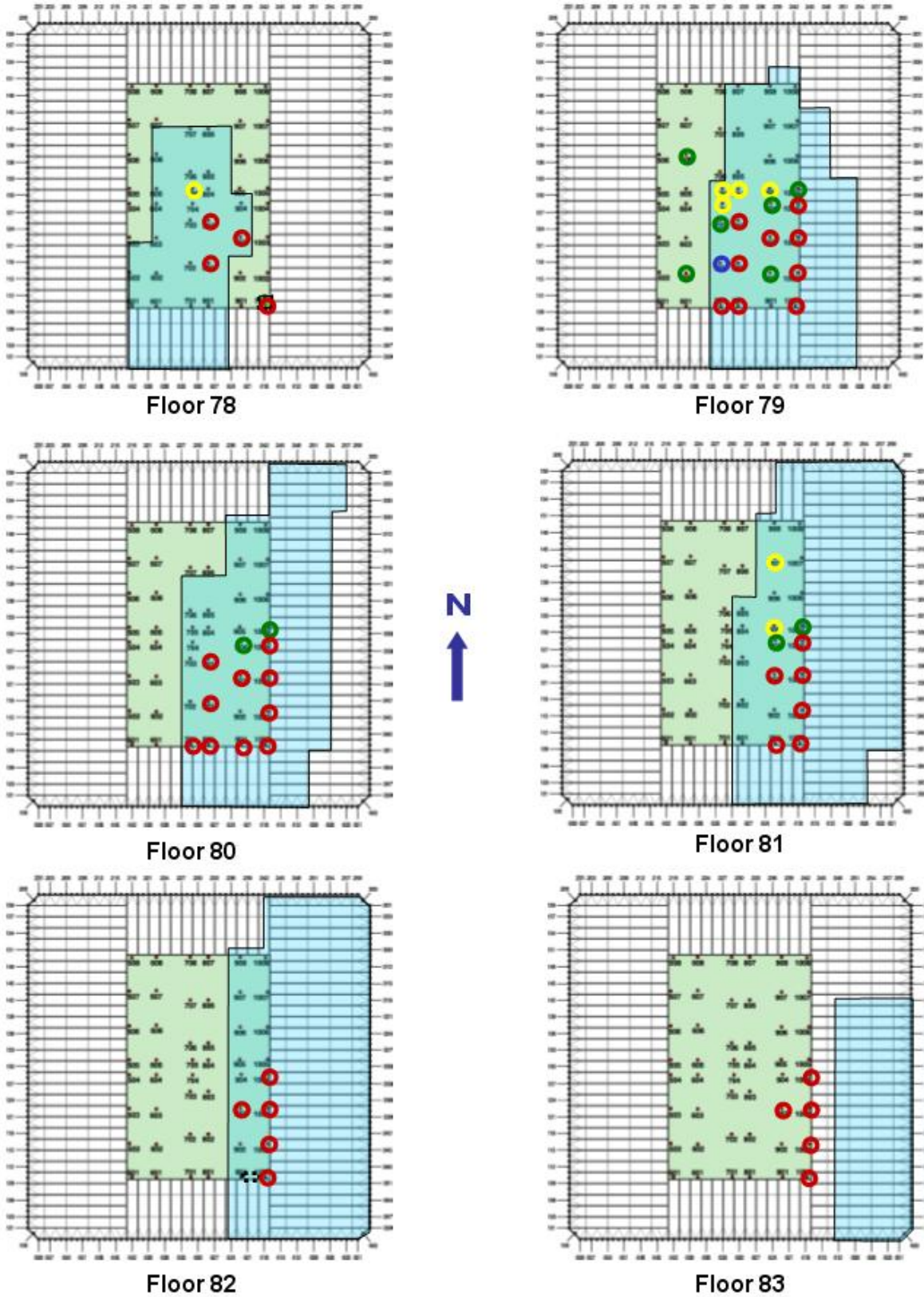


Figure 5–23. Plan view of WTC 2 Case D insulation and column damage to Occupancy Floors 78 to 83.

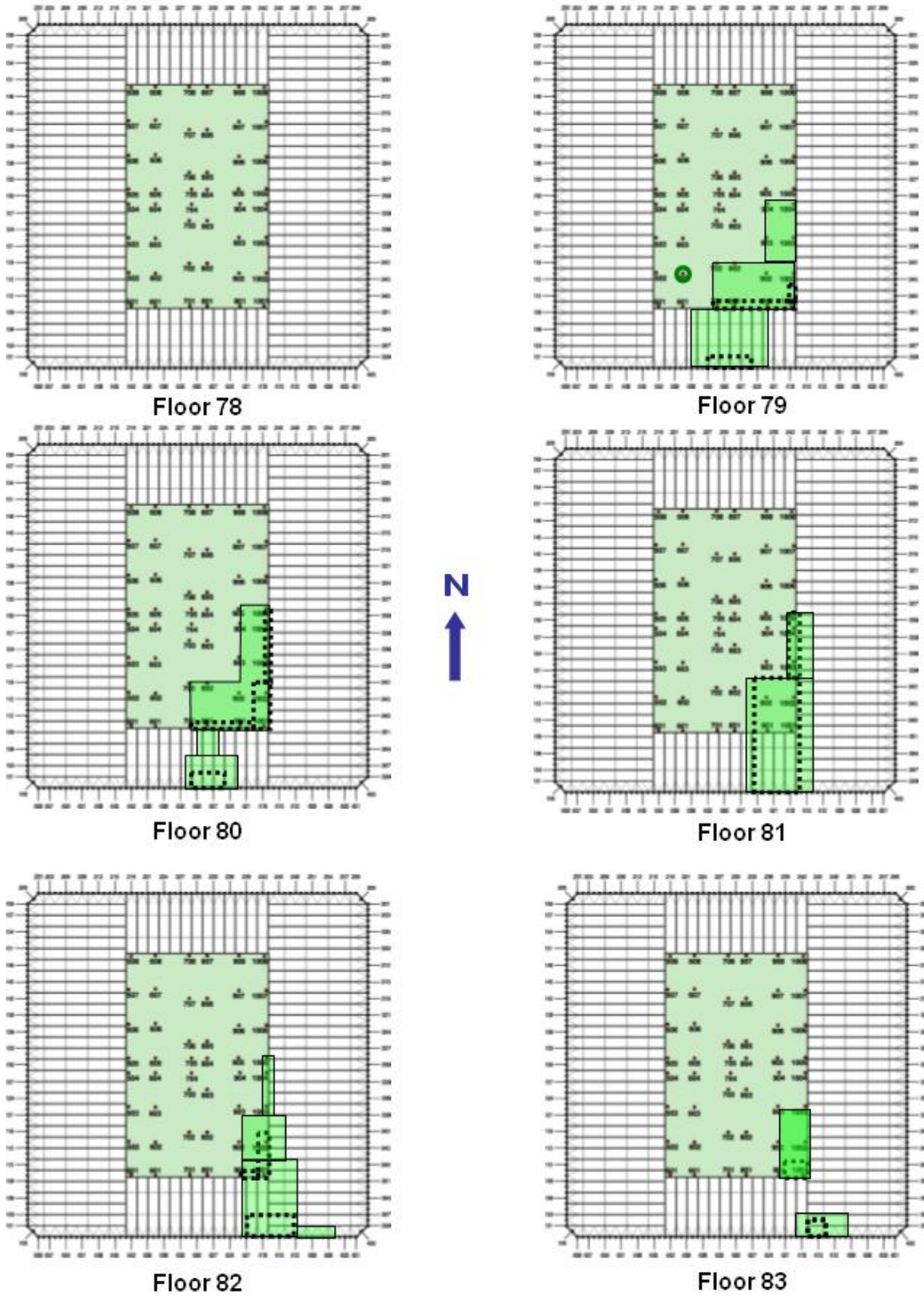
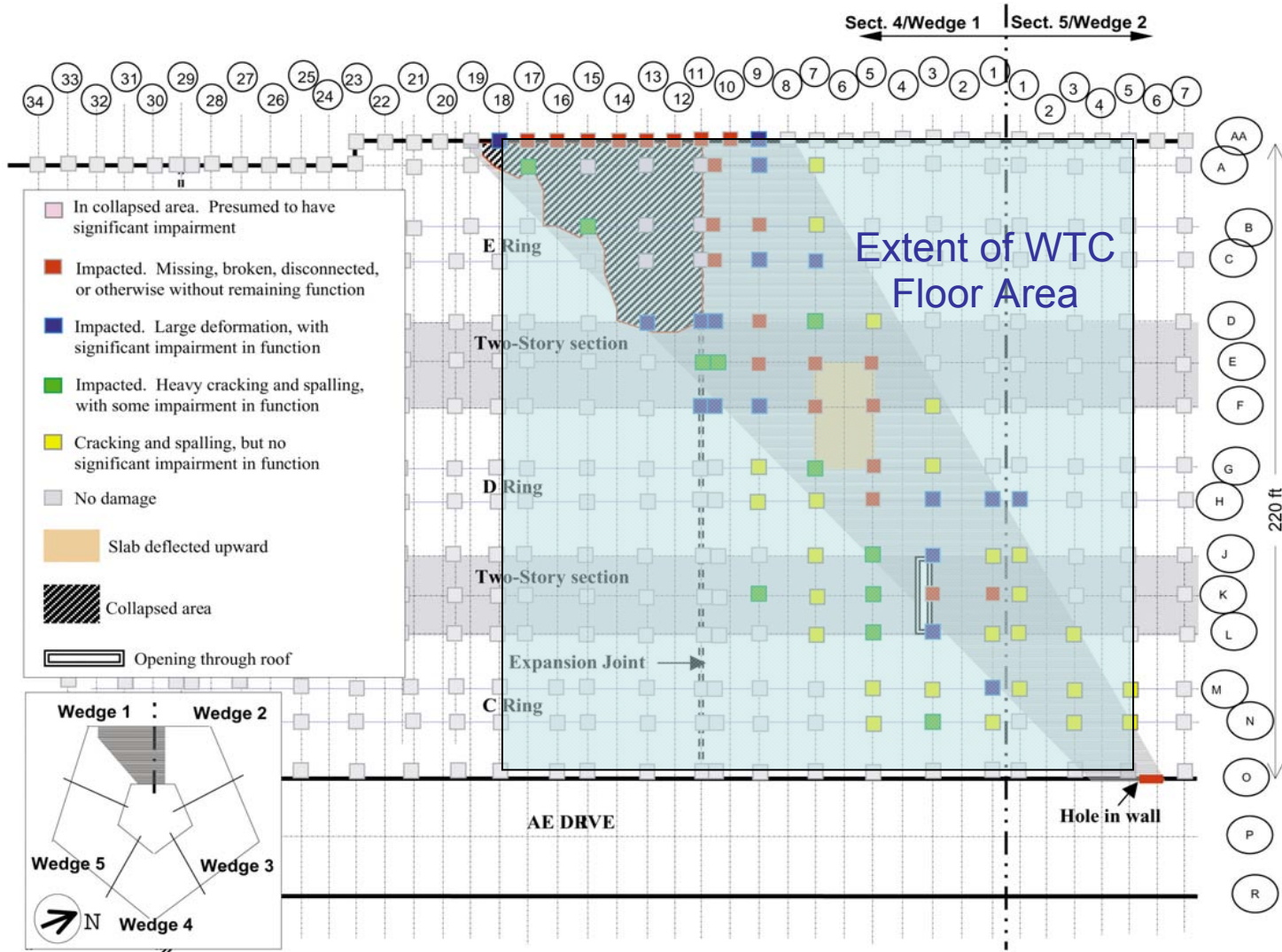


Figure 5–24. Plan view of WTC 2 Case D damage to Structural Floors 78 to 83.

5.5 OBSERVATIONS OF AIRCRAFT IMPACT DAMAGE TO THE PENTAGON

The Pentagon was impacted by an aircraft of similar size (Boeing 767) and at a speed similar to those of the WTC towers (ASCE 2003). The impact speed at the Pentagon was about 530 mph (460 knots or 780 fps), which is similar to the aircraft impact speeds of 443 mph and 542 mph for WTC 1 and WTC 2, respectively. The aircraft completely entered the lower floors of the Pentagon and traveled along a diagonal path for approximately 230 ft. The Pentagon was constructed with a reinforced concrete frame with columns spaced at regular intervals. Figure 5–25 shows a graphic depiction of the damage that was documented after the impact and subsequent fire. An overlay of the WTC tower footprint was added to the original graphic to provide a sense of scale between the two building footprints. Figure 5–25 shows column damage classifications similar to those described in Section 5.2.1—severed, heavy damage (permanently deformed laterally from the column centerline), moderate damage (some impairment of function), and light damage (concrete cracking and spalling but no impairment of function).

It is the light damage that is of interest relative to insulation damage from aircraft impact. Reinforced concrete columns have a concrete cover of at least one inch, and typically more, over the steel reinforcement. Figures 5–26 and 5–27 show two examples of columns with their concrete cover stripped by the debris field down to the spiral reinforcement over most of the column height. It was assumed that if the debris field could strip away concrete cover then a similar debris field would strip SFRM from steel components.



Source: Reproduced from "The Pentagon Building Performance Report" (2003) and use with permission of The American Society of Civil Engineers.

Figure 5-25. Overlay of WTC Footprint on Pentagon damage area from aircraft impact (original figure from ASCE, 2003).



Source: Reproduced from "The Pentagon Building Performance Report" (2003) and use with permission of The American Society of Civil Engineers.

Figure 5–26. Typical damage to spirally reinforced columns in the Pentagon impacted and bent by large debris (ASCE, 2003).



Source: Reproduced from "The Pentagon Building Performance Report" (2003) and use with permission of The American Society of Civil Engineers.

Figure 5–27. Typical damage to spirally reinforced columns in the Pentagon not impacted or bent by large debris (ASCE, 2003).

5.6 SUMMARY

The methodology and criteria for developing input data from the aircraft impact analysis results was summarized for Cases A, B, C, and D. The approach for identifying severe structural damage to columns and floors and insulation damage was described.

A four category classification of core column structural damage into four categories was established: severed, heavy damage, moderate damage, and light damage. Classification criteria included plastic strain levels and lateral deformation from the column centerline. Two types of floor structural damage were identified from the impact analysis results: (1) missing floor areas and (2) severely damaged floor areas incapable of supporting loads.

Insulation was assumed to be dislodged from core columns only if the columns were subject to direct debris impact that failed wall partitions in the immediate vicinity of the column. For exterior columns, the debris impact was required to be strong enough to damage or destroy room furnishings (modular office workstations) adjacent to the columns. For floor trusses, the debris impact was required to be strong enough to damage or destroy room furnishings (modular office workstations) in the same area of the affected floor.

The insulation damage estimates were conservative as they ignored possibly damaged and dislodged insulation in a much larger region that was not in the direct path of the debris but was subject to strong vibrations during and after the aircraft impact. A robust criteria to generate a coherent pattern of vibration-induced dislodging could not be established to estimate the larger region of damaged insulation.

The structural damage in WTC 1 extended from the north exterior wall, through the central region of the north floor area, into the north side of the core. An exterior panel was knocked out of the south wall by aircraft debris. Damage to the insulation from direct debris impact extended over a larger region, and included most of the north floor areas, the core, and central regions of the south floor areas. Case B predicted more damage to core columns and a larger extent of insulation damage to the south floor area than Case A, including damage to the south exterior wall insulation on the inside face.

The structural damage in WTC 2 extended from the south exterior wall, through the south and east floor areas and the southeast region of the core. Exterior columns were severed by debris near the northeast corner. Damage to the insulation from direct debris impact extended over a larger region and included the south floor area, the central and east regions of the core, and most of the east floor area. Case D predicted more damage to core columns than Case C, but the extent of the insulation damage was similar.

5.7 REFERENCES

ASCE (2003) “The Pentagon Building Performance Report”, American Society of Civil Engineers, Reston, VA, 20191.

This page intentionally left blank

Chapter 6

OBSERVATIONS AND TIMELINE OF STRUCTURAL EVENTS

6.1 INTRODUCTION

Development of the probable collapse sequence for each tower was shaped by evidence gathered in the investigation, from photographs and videos, design and maintenance documents, and eyewitness accounts. Data about the events following the aircraft impact were primarily obtained from three sources:

- Photographic and videographic records that had been catalogued and time stamped for the NIST Investigation (NIST NCSTAR 1-5A)
- Interviews of individuals in the towers who survived and individuals outside the towers who received telephone calls from individuals in the towers (NIST NCSTAR 1-7)
- Interviews of emergency response personnel and emergency communication records (NIST NCSTAR 1-8)

Changes in structural performance are generally difficult, if not impossible, to perceive until significant deformation has taken place relative to the dimensions of the structure. The ability to perceive structural changes depends on the detail and resolution of the image being examined and the vantage point of the photographer. Observations of structural performance for the WTC towers include severed components, local deflections or buckling, possible sagging of floors, and relative alignment of columns or building sections.

Photographic and videographic records were reviewed to identify structurally-related events. Where possible, all four faces of a building were examined for a given event or time period to provide complete understanding of the building response. Observations from a single vantage point can be misleading and may result in incorrect interpretation of events. For instance, photographic and videographic records taken from due north of the WTC 1 collapse appeared to indicate that the antenna was sinking into the roof (McAllister 2002). When records from east and west vantage points were viewed, it was apparent that the building section above the impact area tilted to the south as the building collapsed.

Photographs and videos provided information about events at or near the exterior walls of the towers. Events that occurred in the building interior were predicted through analytical simulations validated by exterior observations of aircraft impact, fire dynamics, and structural response.

Evidence was used in the analyses in three ways: (1) to determine input parameters, such as the aircraft speed and direction upon impact or floor sagging at exterior windows, (2) to impose time-related constraints upon an analysis, such as imposing observed broken windows over time to constrain the spread of fire or the extent of inward bowing of an exterior wall, or (3) to validate analysis results, such as global stability after impact and during thermal loading.

Observations of structural behavior were broken into two groups: *key observations* and *noted observations*. Key observations were significant structural events that were explicitly addressed in or used to validate the structural analyses. Noted observations were events that may have been a structural response but could not be conclusively identified as to their significance to the structural response.

Key observations were used to develop a timeline of structural events for each tower. Structural analyses were used to support development of the probable collapse sequence for each tower and to develop and refine understanding of the probable collapse sequence of events between observations.

6.2 OBSERVATIONS OF STRUCTURAL EVENTS

The following key observations were obtained primarily from photographic and videographic records and are shown in the structural events timeline developed for each tower. Some of the observations may not have directly reflected the structural condition of the towers, but they contributed to a determination of the extent of damage or the duration of fires in damaged areas. Other observations reported here were derived from testing of materials recovered from the collapse site.

Aircraft Impact:

- Aircraft impact conditions – aircraft velocity, location, orientation to building
- Structural damage to the exterior columns and spandrels
- Structural stability of each tower after the aircraft impact
- Areas of debris accumulation near the exterior walls
- Locations where debris exited the buildings
- Stairwell damage
- Damage to WTC 2 east and north face floor systems (observed as draped, hanging objects in windows)
- Damage to fireproofing on the exterior sides of the exterior columns

Fire and Thermal Analysis:

- Duration and location of fires and smoke near the perimeter of the floors
- Locations and times of window breakage

Structural Materials:

- Mechanical properties of all steel types from recovered steel
- Concrete composition from concrete samples

- Damage and fracture patterns in recovered steel

Structural Response:

- Additional damage to floor systems on the east and north sides of WTC 2 (observed as draped, hanging objects in windows)
- Inward bowing of an exterior wall on the south face of WTC 1 and the east face of WTC 2
- Tilting of the building section above the impact areas as the structural collapse initiated (WTC 1 tilted to the south, WTC 2 tilted primarily to the east and somewhat to the south)
- Time to collapse initiation
- Observed component and subsystem failures and building movements at collapse initiation

The specific events and timelines for each tower are given in the following sections.

6.2.1 WTC 1 Structural Response Observations

Table 6–1 summarizes the timeline of structural events for WTC 1. Column 6 of the table refers to the figure (Figs. 6–1 through 6–11) that illustrates the described event.

Key Observations

- Inward bowing of the south exterior wall was first observed at 10:23 a.m., as shown in Fig. 6–6. The bowing appeared to extend between Floors 94 to 100 and columns 305 to 359. The maximum bowing was estimated from images to be 55 in.±6 in. at Floor 97 on the east side of the south face of WTC 1. The central area in available images was obscured by smoke. The extent of fires observed on all faces of WTC 1 was similar, although somewhat more extensive on the east and west faces (where short span floors were located) and similar in extent on the north and south faces (where long span floors were located). Inward bowing was observed only on the south face.
- The time to collapse initiation was 102 minutes from the aircraft impact (9:46:30 a.m. until 10:28:22 a.m.)
- From exterior observations, tilting of the building section appeared to take place near Floor 98. Column buckling was then observed to progress rapidly across the east and west faces
- The WTC 1 building section above the impact and fire area tilted to the south as the structural collapse initiated, as shown in Fig. 6–7. The tilt was toward the side of the building that had long span floors. Video records taken from east and west viewpoints showed that the upper building section tilted to the south. Video records taken from a north viewpoint showed no discernable east or west component in the tilt. A tilt to the south of at least 8 degrees occurred before dust clouds obscured the view and the building section began to fall downwards.

Noted Observations

At 10:18 a.m., smoke was observed to be suddenly expelled on the north and west faces:

- North face - Floor 92, Floor 94 on the east side, and Floors 95 to 98 on west side
- West face - Floors 95 and 98 on north side; a lower floor on south side
- Smoke puffs were observed, but they occurred less frequently than in WTC 2.
- The first exterior sign of collapse (downward movement of building) was observed at Floor 98. From a northwest viewpoint (there were no useful south views), large amounts of smoke and dust were first expelled from Floor 98 across the north and west faces. Smoke and dust were also observed being expelled from the east face.

Table 6–1. WTC 1 Timeline of Observed Structural and Fire Events.

| | Start Time | Floors | Face | Columns | Figures | Event Description |
|---|------------|--------|------|----------|----------------------------------|---|
| 1 | 8:46:26 | 93-99 | N | 109-152 | Fig. 6–1 | WTC 1 was impacted by a Boeing 767 between Floors 93 to 99 and Columns 109 to 152. Fig. 6–1 (taken nearly an hour after impact) shows Columns 120 to 159. |
| 2 | | 94-96 | S | 329 | Fig. 6–2 | A perimeter wall panel face was knocked out by the aircraft nose or landing gear at the center of the south between Floors 94 to 96 |
| 3 | | 92-95 | N | 130-151 | Fig. 6–3 | SFRM was knocked off the exterior sides of perimeter columns; the pattern of damage was irregular |
| 4 | 9:25:28 | | | | Fig. 6–4 | Fire was observed only on the west side of the south face (note debris under missing panel) |
| 5 | 9:40 | | S | 301-323 | Fig. 6–5 | No inward bowing of perimeter columns was visible |
| 6 | 10:22:59 | 95-99 | S | 308-326+ | Fig. 6–6 | Inward bowing of the south perimeter wall was visible from Floor 95 to about Floor 99, with a maximum inward bowing of ~ 55 in. at Column 315 and Floor 97 |
| 7 | 10:28:18 | | | | Fig. 6–7 Fig. 6–8 Fig. 6–9 | Pressure pulses of smoke were pushed out the west face at its north edge and center; Smoke and debris clouds were pushed out the north, east, west faces at Floor 98; Fire came out windows on the north, east, west, and south faces between Floors 92 to 98 and Floor 104 |
| | 10:28:20 | | | | Fig. 6–10 Fig. 6–11 | WTC 1 began to collapse. The first exterior movement was at Floor 98. Rotation of the building section above the impact and fire zone to at least 8 degrees to the south occurred before the building section began to fall vertically. |



Figure 6–1. Initial aircraft impact damage on WTC 1 north face.



Figure 6–2. Initial aircraft impact damage on WTC 1 west and south faces minutes after impact (exact time of image is unknown).

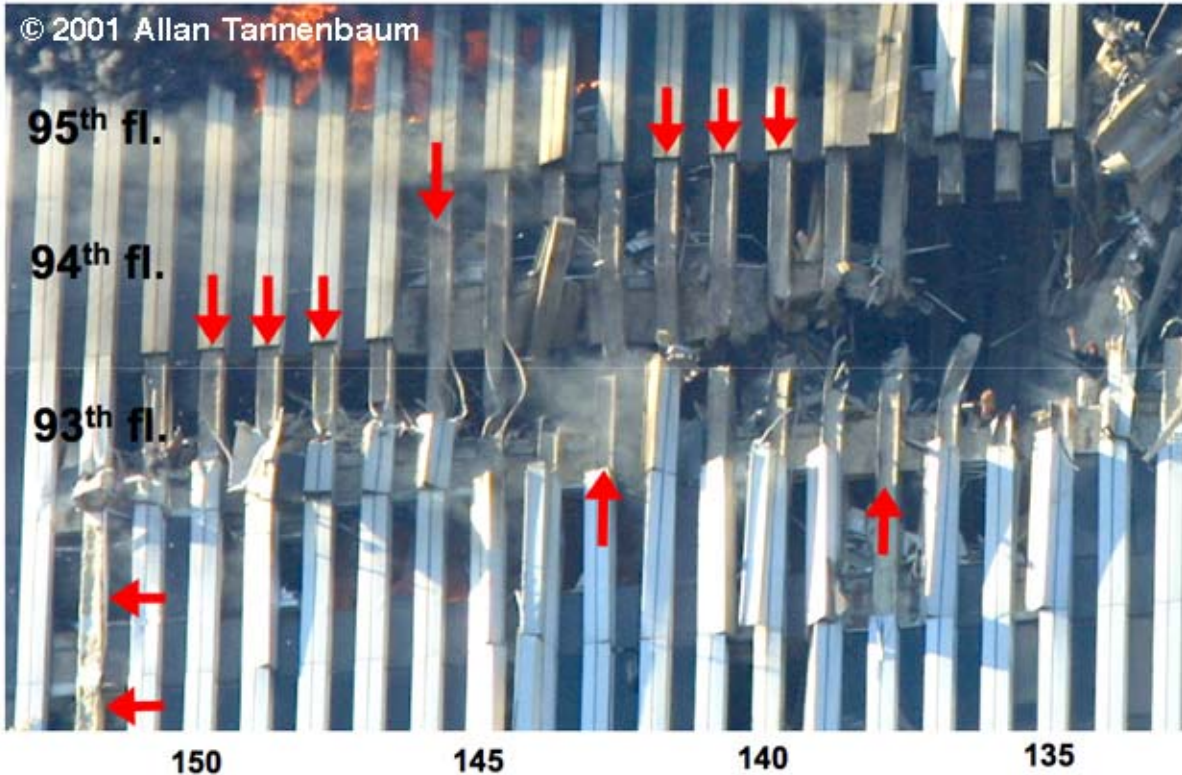


Figure 6–3. SFRM knocked off north exterior columns. Arrows show where fireproofing was damaged or missing.

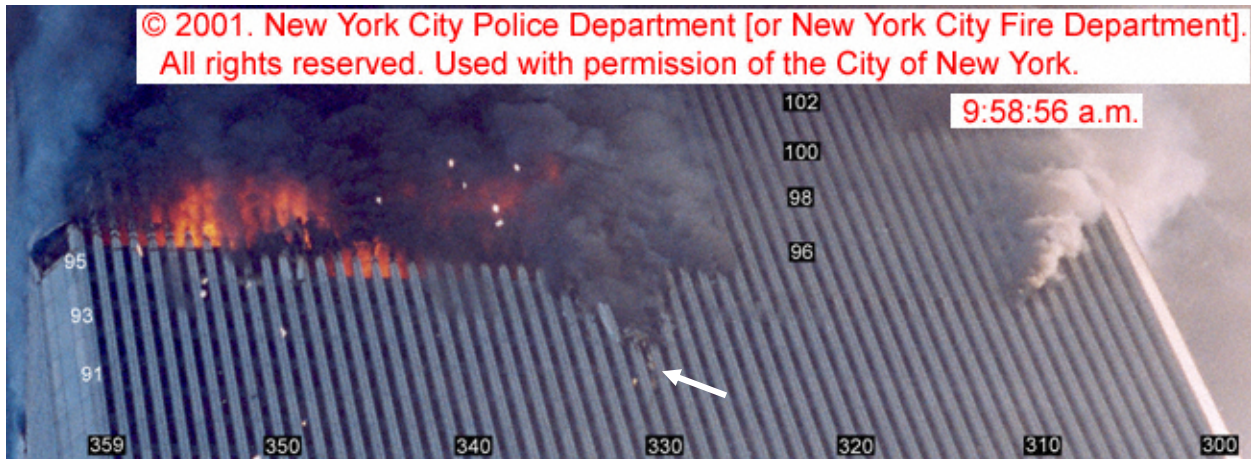
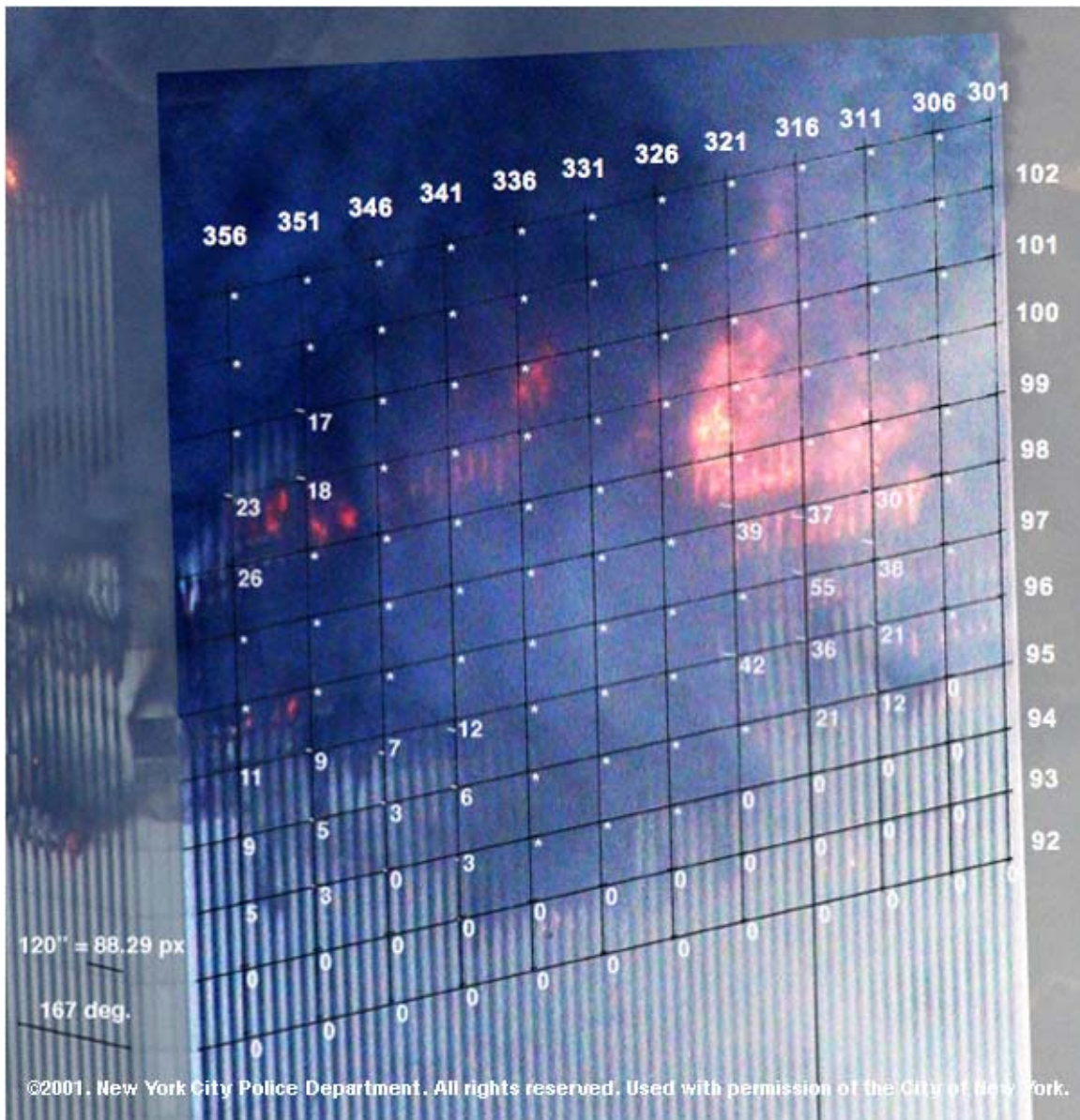


Figure 6–4. South face of WTC 1 with fire visible only on the west side at 9:25. Arrow shows region where debris pile under missing panel was observed.



Figure 6–5. Fires on WTC 1 south face at 9:40 a.m. Note lack of inward bowing.



Measurements were based on calibration measures shown on the west face
 Foreshortening into depth of field across the south face of 17% was included in the measurements
 Measurement error was at least +/- 6 inches

Figure 6–6. WTC 1 exterior columns bowing inward across most of the south face between Floors 95 to 97 (or 98) at 10:22:59 a.m. Note buckled panel at SW corner.



Fire expelled on east face

Smoke and debris expelled on north face at Floor 98



Tim Main / Mike Ballou © 2001

WTC 1 building section above impact damage zone tilts to the south



Tim Main / Mike Ballou © 2001

Figure 6–7. Expulsion of smoke and debris at WTC 1 Floor 98 on the east, north, and west faces.



Smoke is ejected from Floor 98 at the north face

Smoke is ejected from Floor 98 across the north and west faces



Upper building section moves downward

Figure 6–8. Smoke expulsion at Floor 98 from north and west faces as collapse initiates.



Figure 6–9. Smoke expulsion at Floor 98 from north and east faces at collapse initiation.

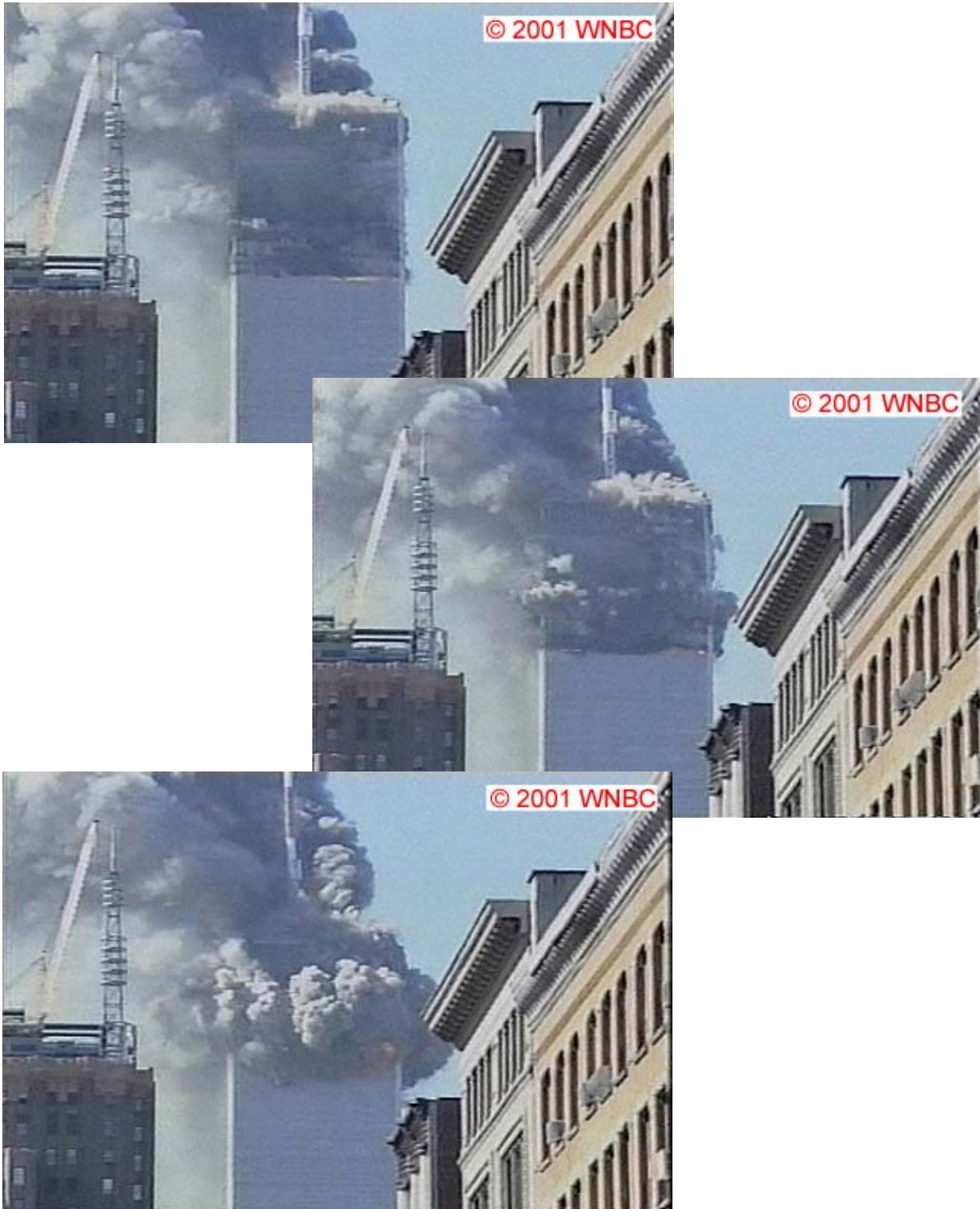


Figure 6–10. Rotation of WTC 1 building section above the aircraft impact zone toward the south as viewed from due north. Note that there is no tilt in the east or west directions.



Figure 6–11. WTC 1 tilt to the south of approximately 8 degrees was measured before smoke and debris obscured view. Note view is from west and tilt is directly south.

6.2.2 WTC 2 Structural Response Observations

Table 6–2 summarizes the timeline of structural events for WTC 1. Column 6 of the table refers to the figures and table (Figs. 6–12 through 6–26 and Table 6–3) that illustrate the described event.

Key Observations

- Following the aircraft impact and fireballs, hanging objects were observed through the windows of the east and north faces. These objects appeared to be floor slabs and were observed to change shape and/or length over time and extend across approximately half of the east face. The hanging objects suggest that there was structural damage to WTC 2 Floor 83 along the east face and to Floors 81 to 83 of the north face near the northeast corner.
- Inward bowing of the east wall was first observed at 9:21 a.m. The inward bowing was approximately 10 in. at Floor 80 and extended between Floors 78 and 83 and Columns 304 and 344. The remaining portion of the face to the south of Column 344 was not included in the image. The bowing appeared to extend over a large fraction of the east face and to be greatest near the center of the face. Fires were more extensive along the east face (where long span floors were located) and at the east side of the north and south faces (where short span floors were located). Fires were not observed on the west face (where long span floors were located). Inward bowing was observed only on the east face.
- An increase of the inward bowing of the east wall was observed at 9:53 a.m. The inward bowing appeared to extend between Floors 78 and 84 and Columns 305 and 341. The remaining portion of the face to the south of Column 344 was not included in the image. The greatest bowing was approximately 20 in.±1.0 in. at Floor 80 on the east face of WTC 1.
- Collapse initiated 56 minutes after the aircraft impact (9:02:59 a.m. to 9:58:59 a.m.).
- From a northeast viewpoint, initial downward motion was observed at several columns as they moved inward on the north side of the east face. From exterior observations, tilt of the building section above the impact and fire area appeared to take place near Floor 82. Column buckling was then seen to progress across the north face.
- The building section above the impact and fire area tilted to the east and south as the structural collapse initiated. Estimates from photographs indicated that there was approximately a 3 to 4 degree tilt to the south and a 7 to 8 degree tilt to the east prior to significant downward movement of the upper building section. The tilt to the south did not increase any further as the upper building section began to fall, but the tilt to the east continued up to 20 to 25 degrees before dust clouds obscured the view.

Noted Observations

- A fireball on the east face was observed coming from Floor 82. Fireballs on the north face were observed coming from Floors 79 to 82. The deflagration prior to the fireballs may have caused a pressure pulse to act on floors above and below.

- A ‘cold spot’ on the north face, where little or no fires were observed, may indicate that Floors 82 and 81 had disconnected and dropped over a 12 window span along the north face.
- Molten material pouring from the northeast corner indicated that Floor 81 on the east side of the north face may be shifting. If the substance was molten aluminum, that would have required temperatures on the order of 500 °C or higher.
- Numerous puffs of smoke may indicate internal changes in architectural or structural features.
- Outward bowing of the spandrel near the center of the north face on Floor 79 was observed near columns 237 and 238.
- As the portion of the building above the impact area tilted to the south and east:
 1. A kink formed at the southeast corner near Floor 106 as the upper building section tilted and collapse initiated.
 2. The southeast corner also kinked approximately midway between the impact and fire zone and the kink near Floor 106 as the upper building section tilted.

Hanging Objects

The hanging objects observed on the east face and north face of WTC 2 (listed in the Key Observations) appeared to be the exterior edges of the floor slabs.

The slab thickness was nominally 4 inches over a fluted deck with 1.5 in. ribbing. Scaling of the object in the windows found the depth to be approximately 4 in. to 6 in. The concrete slab was reinforced with two layers of welded wire fabric and had a flexural stiffness that was greater than other items that might have been draped in the windows, such as ductwork. The drape of the object was consistent with a floor flexural stiffness. There was ductwork between the damper at the lower chord of the truss and the floor slab at the exterior wall. However, for the ductwork to be draped in the windows, all the dampers would have had to fail while the floor slab would have had to remain in place. Such a sequence of events is unlikely. Also, such ductwork would be light and hang with a deeper drape. From these observations, it appears that the hanging objects were the exterior edges of floor slabs.

Table 6–2. WTC 2 Timeline of Observed Structural and Fire Events

| | Start Time | Floors | Face | Columns | Figures and Tables | Event Description |
|----|------------|--------|--------|----------|------------------------|--|
| 1 | 9:02:59 | 77-85 | S | 404-443 | Fig. 6–12 | WTC 2 was impacted by a Boeing 767 between Floors 77 and 85 and Columns 404 and 443. |
| 2 | 9:03:42 | 83 | E | 310-342 | Fig. 6–13 Tbl. 6–3 | The edge of Floor 83 appeared to be draped in Floor 82 windows between Columns 310 and 342. |
| 3 | 9:10:01 | 79-83 | N,E | | Fig. 6–15 | Hanging object in windows of Floor 79 that appears to be the edge of Floor 80. |
| 4 | 9:11:14 | 79-82 | N | | Fig. 6–14 Tbl. 6–3 | Debris piles were visible at windows where fires were burning at Floor 79, Columns 231 to 241, and Floors 81 to 82 at the northeast corner. Hanging objects noted with arrows. |
| 5 | 9:14:03 | 79-82 | N | 237-254 | Fig. 6–16 | Missing SFRM on several columns. |
| 6 | 9:21:29 | 78-82 | E | 302-342 | Fig. 6–17 Fig. 6–18 | Inward bowing of east face, maximum deflections of 10 in. at Floor 80. |
| 7 | 9:53:04 | ~78-82 | E | 318-334+ | Fig. 6–19 Fig. 6–20 | Bowing in of columns, maximum deflections of 20 in. at Floor 80. |
| 8 | 9:55:04 | 83 | E | 310-342 | Tbl. 6–3 | Floor edge is draped in Floor 82 windows between columns 310 and 342. |
| 9 | 9:58:55 | | E | | Fig. 6–21 | Perimeter columns bowing inward on east face. |
| 10 | 9:58:59 | | | | | WTC2 begins to collapse. |
| 11 | 9:58:59 | 78-83 | E | 324-359 | Fig. 6–22 Fig. 6–23 | Columns spring back from bowing as collapse initiates on east face near NE corner (every 3 rd panel). |
| | 9:58:59 | | E,N,W | | | Smoke and debris clouds are expelled from Floor 81 on E,N,W faces of the building. |
| | 9:58:59 | | S | | Fig. 6–24 Fig. 6–25 | Building section above the impact area tilted to the east and south. Tilting appears to take place around Floor 82. Rotation of approximately 4 to 5 deg to the south and 20 to 25 deg to the east occurred before the building section begins to fall vertically. |
| | 9:59:02 | ~ 106 | SE + E | | Fig. 6–26 | Kink (and offset) about Floor 106 which propagates across the east face where degrades into a gentle curve on the northeast corner; indicates that the kink did not precede the initiation of the global collapse. |

Table 6–3. Possible floor damage observed in photos of WTC 2 windows.

| East Face | | | | |
|-------------------|--|------------------------------------|-------------------------------------|---|
| <i>Floor</i> | <i>Estimated Left Intact Column Connection</i> | <i>Left Visible Floor Location</i> | <i>Right Visible Floor Location</i> | <i>Estimated Right Intact Column Connection</i> |
| 9:03:42 | | | | |
| 83 | 343 | 340 | 321 | 317 |
| 9:38:22 | | | | |
| 83 | 317 | 317 | 311 | 308 |
| 9:55:04 | | | | |
| 83 | 346 | 343 | 310 | 309 |
| North Face | | | | |
| <i>Floor</i> | <i>Estimated Left Intact Column Connection</i> | <i>Left Visible Floor Location</i> | <i>Right Visible Floor Location</i> | <i>Estimated Right Intact Column Connection</i> |
| 9:10:01 | | | | |
| 82 | | | | |
| 81 | 251 | 248 | 241 | 241 |
| 80 | | | | |
| 9:14 | | | | |
| 83 | | | | |
| 82 | 247 | 243 | 238 | 237 |
| 81 | 251 | 248 | 241 | 237 |
| | 255 | 254 | 252 | 251 |
| 80 | | | | |
| 9:58:37 | | | | |
| 83 | 259 | 259 | 250 | 248 |
| 82 | 254 | 251 | 247 | 235 |
| 81 | 251 | 249 | 245 | 235 |
| 80 | 234 | 234 | 229 | 226 |
| | 258 | 255 | 252 | 249 |

*Floor is not visible beyond this point, separation from wall was truncated at the closest intact point where there appeared to be no damage beyond the burning debris pile on Floor 79.

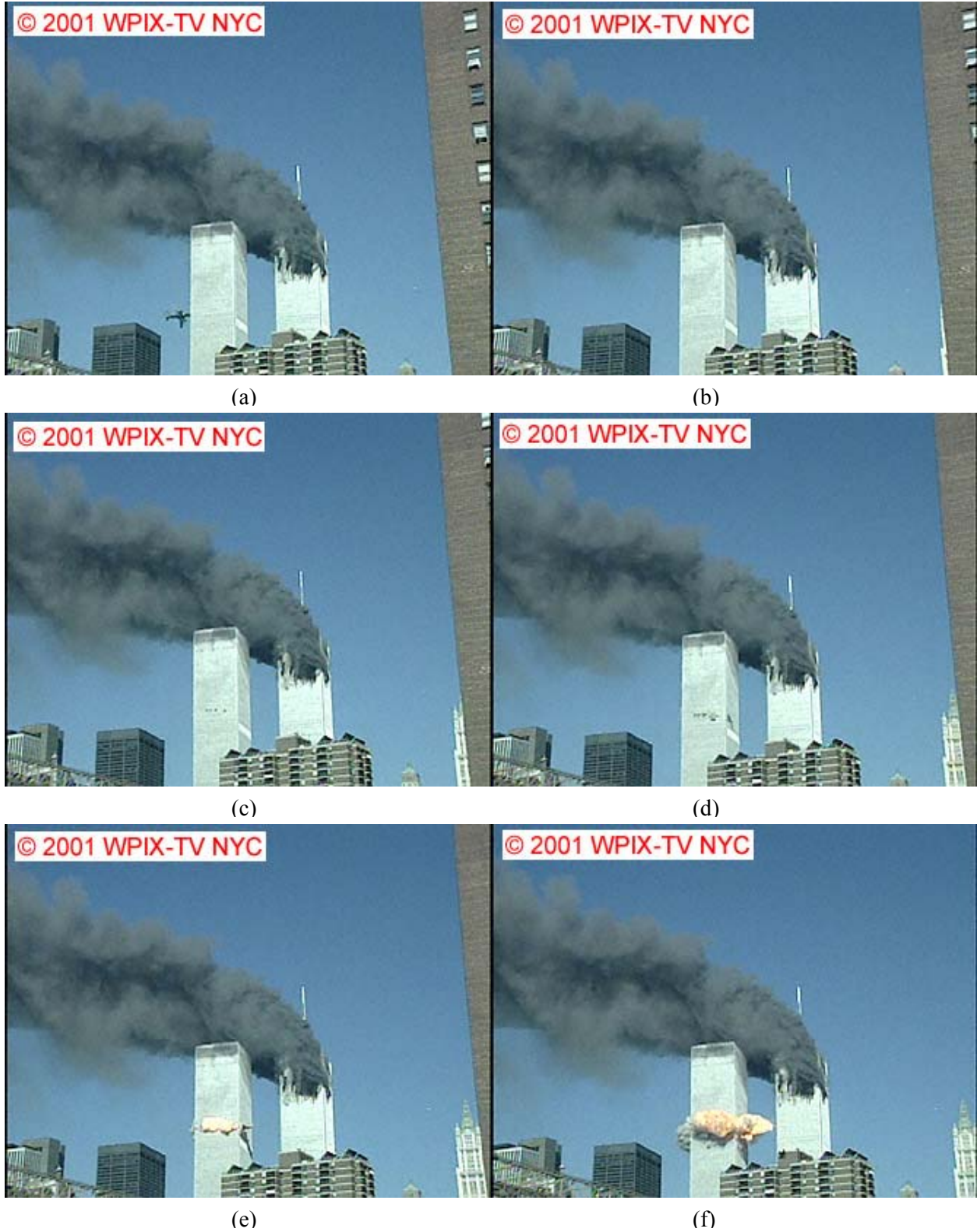


Figure 6–12. Aircraft impact into WTC 2 and fireball, view from the east.

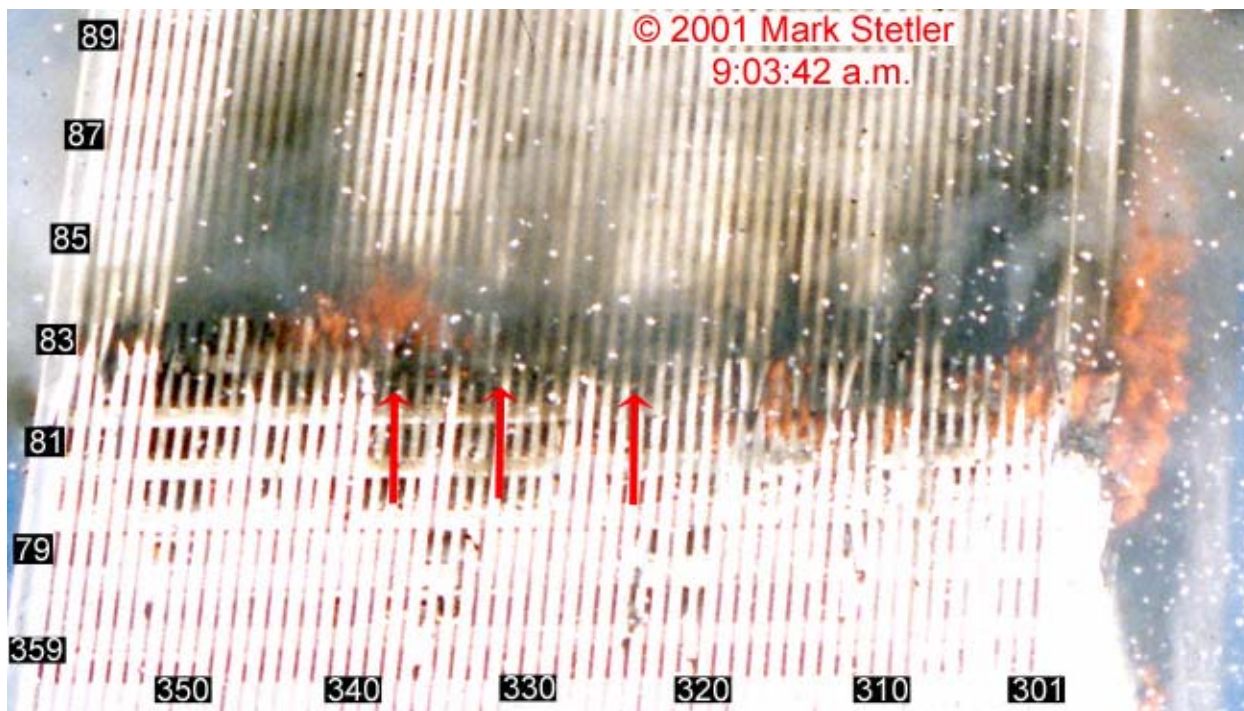


Figure 6–13. Hanging object (noted by arrows) in east windows of Floor 82 appears to be edge of Floor 83.



Figure 6–14. Debris piles at windows where fires are burning at the northeast corner.



Figure 6–15. Hanging object (noted by arrows) in north windows of Floor 79 appears to be edge of Floor 80.

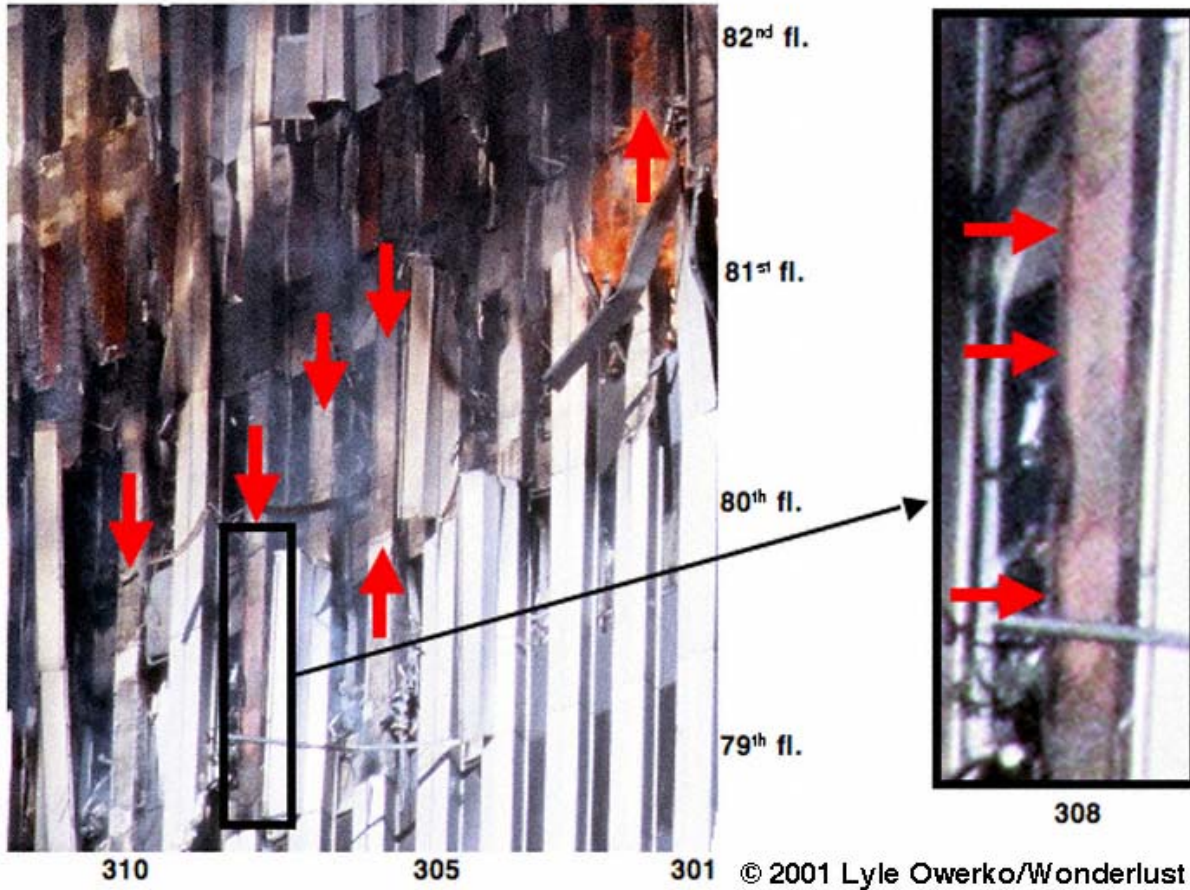


Figure 6–16. Image showing damage to fireproofing on east face of WTC 2 due to internal impact. Red arrows highlight areas where fireproofing has been damaged. The blowup to the right shows a column where red Tnemec primer paint is visible.



Figure 6–17. WTC 2 exterior columns bowing inward across north side of the east face between Floors 77 and 83 at 9:21 a.m.

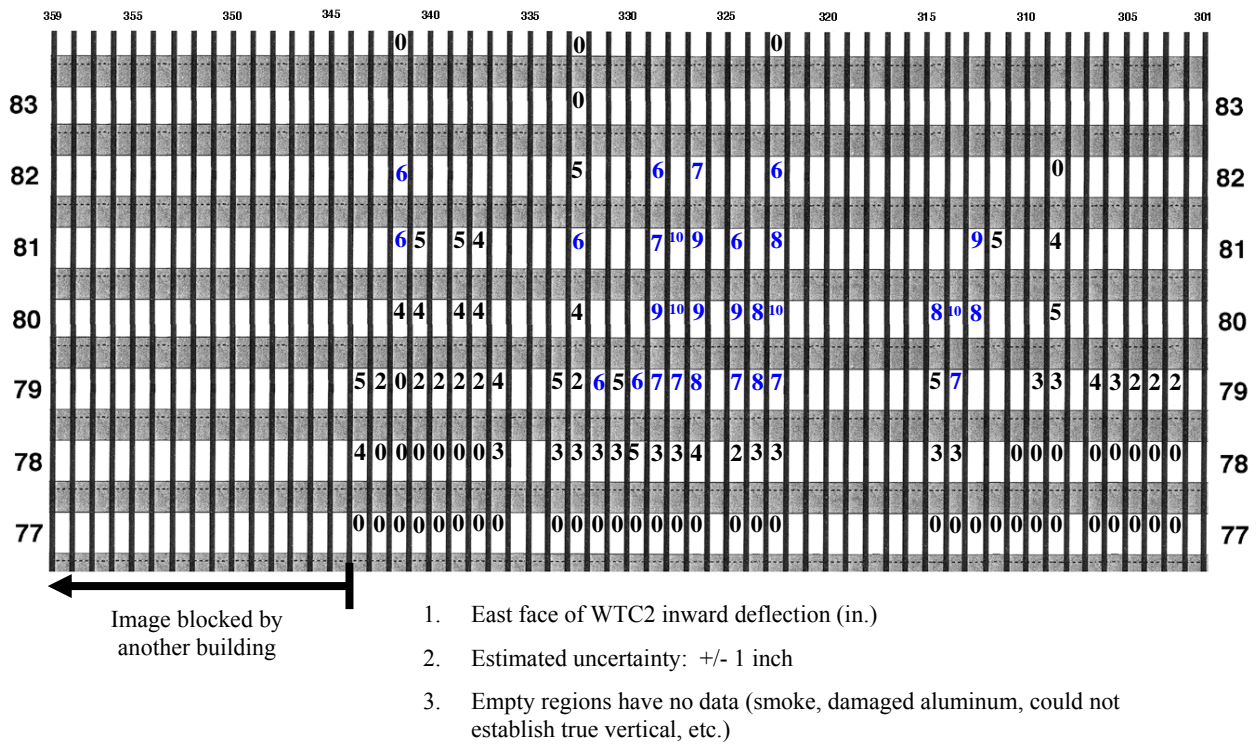


Figure 6–18. Inward Bowing of east Face of WTC 2 at 9:21 a.m.

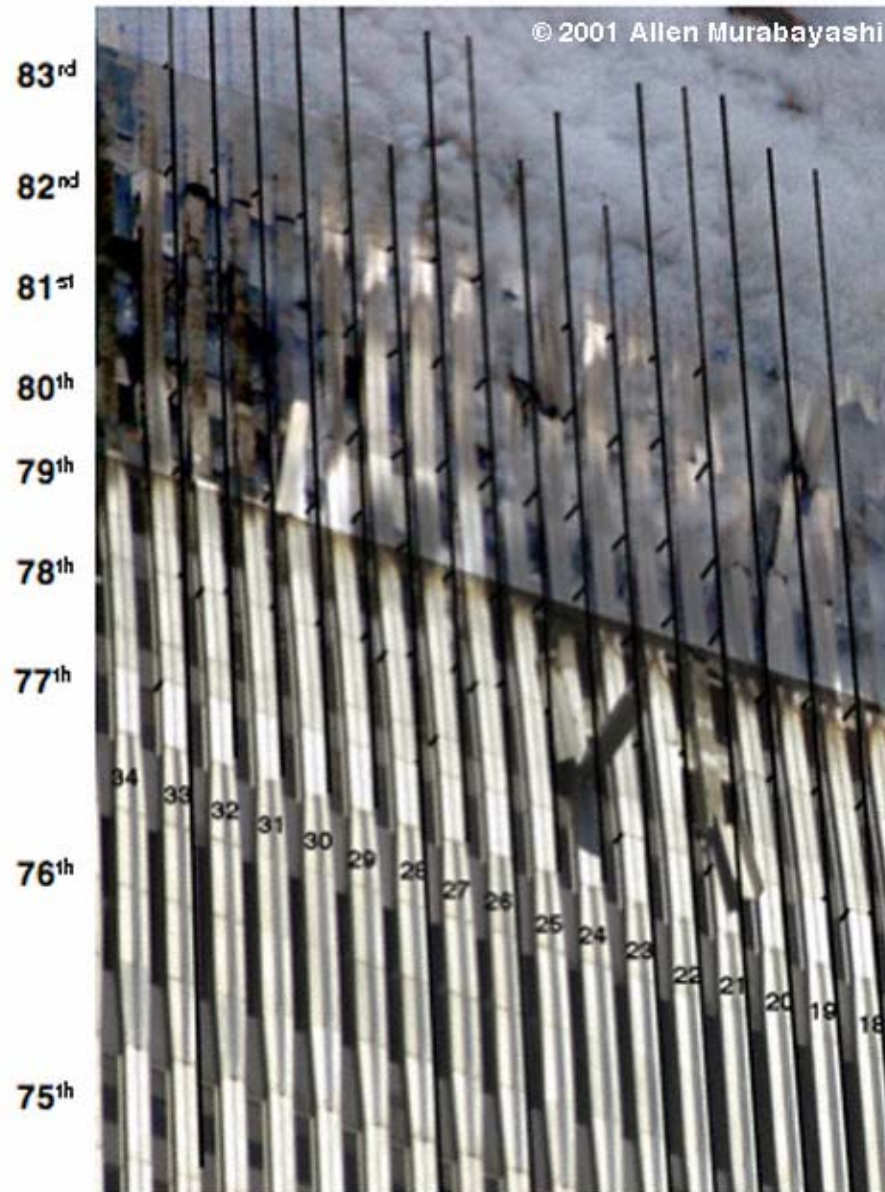


Figure 6–19. Inward Bowing of east Face of WTC 2 at 9:53 a.m.

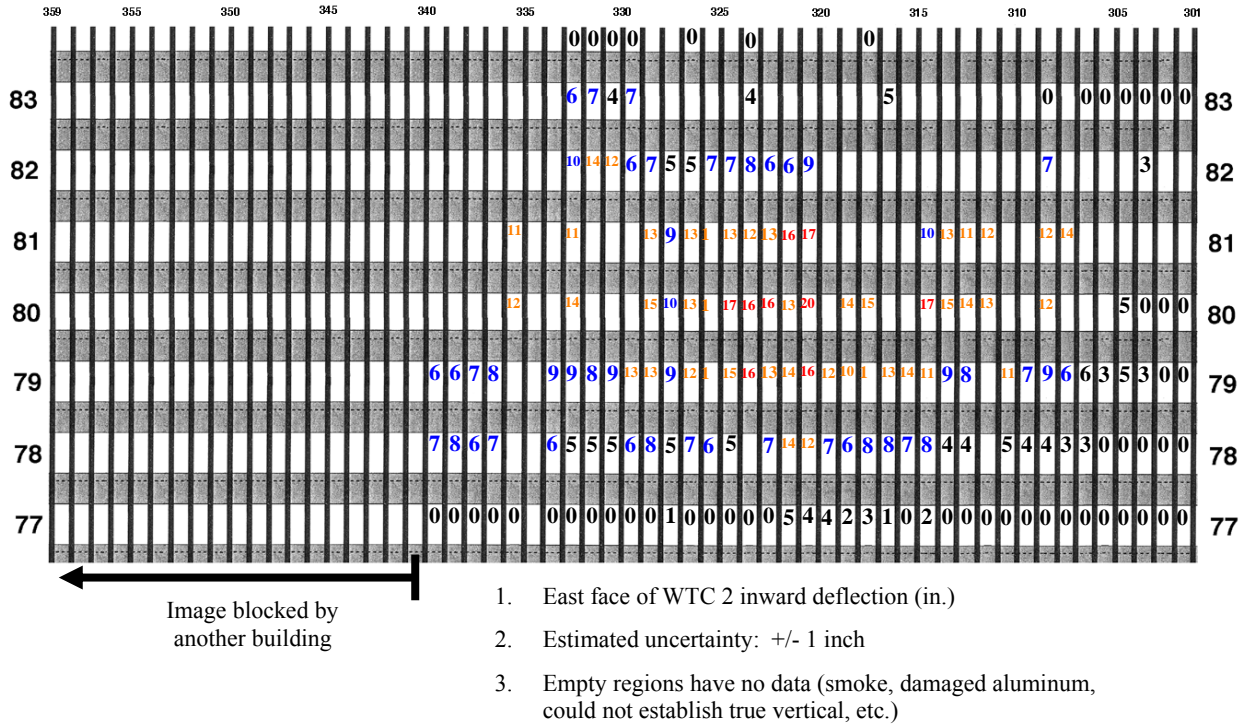


Figure 6–20. Inward Bowing of east Face of WTC 2 at 9:53 a.m.



Figure 6–21. WTC 2 exterior columns bowing inward across the east face between Floors 77 and 83 at 9:58:55 a.m.



Figure 6–22. View of WTC 2 buckling of east wall near northeast corner as collapse initiates from northeast.

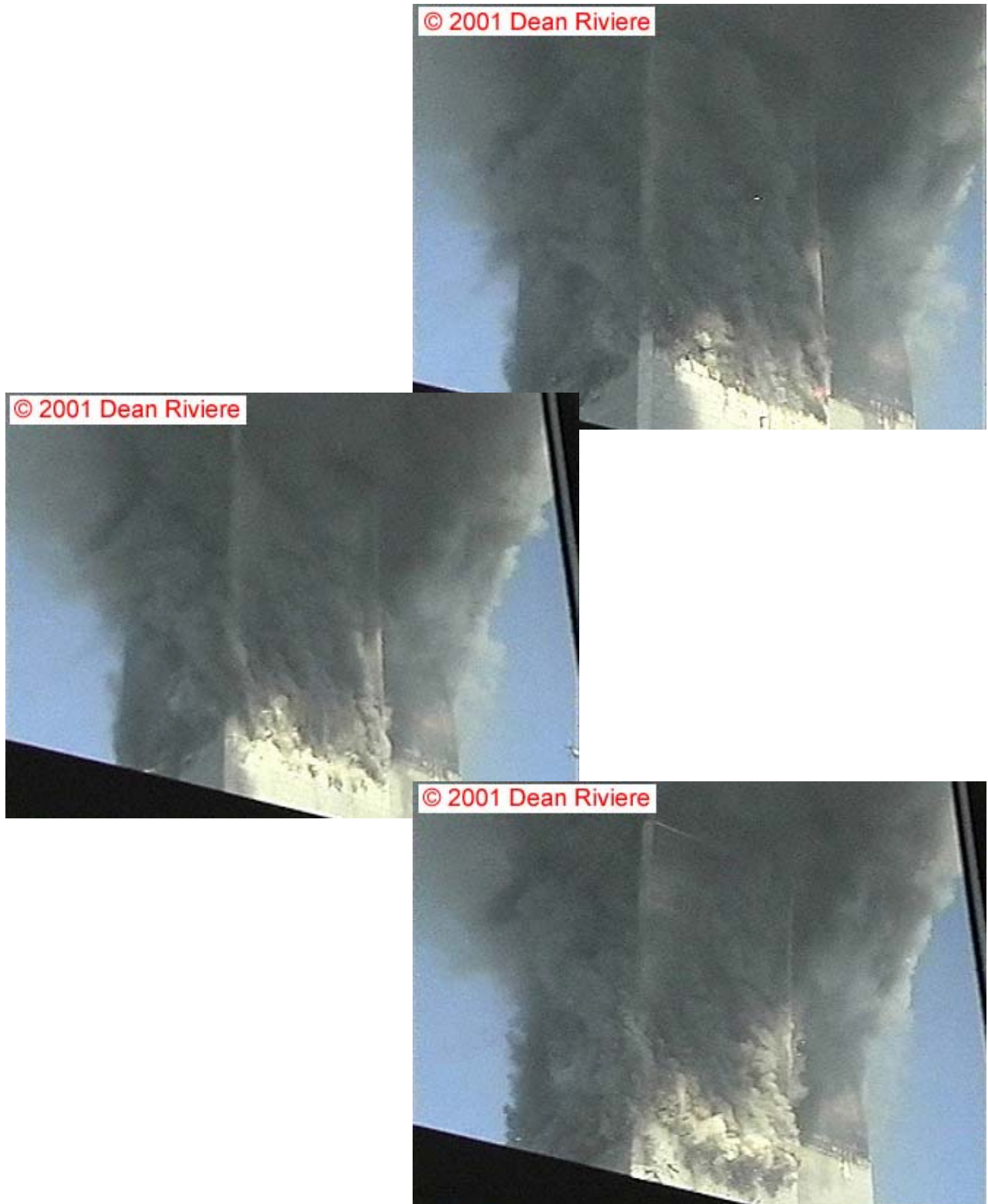


Figure 6–23. View of east wall buckling and WTC 2 collapse from southeast.

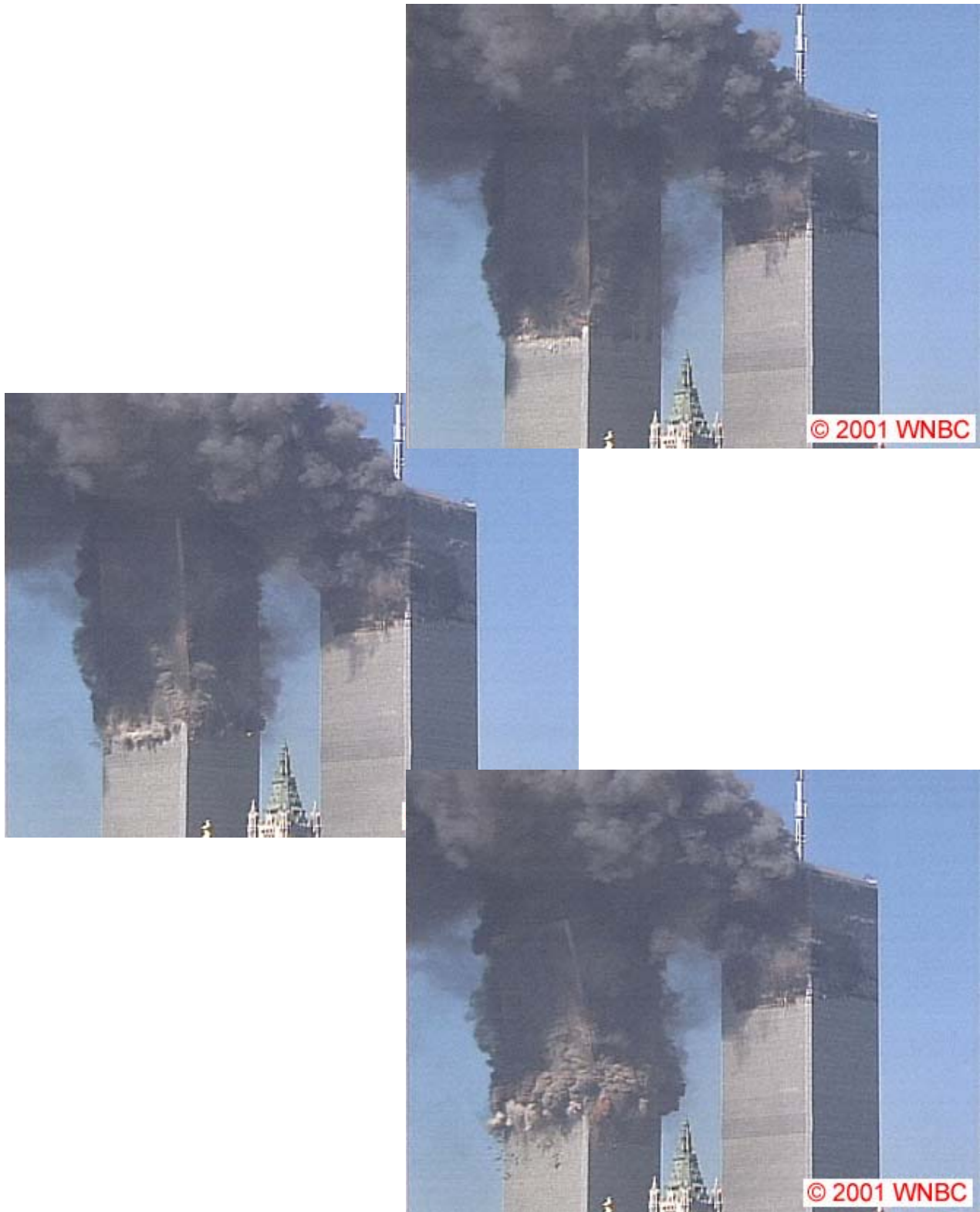


Figure 6–24. View of upper building section of WTC 2 tilting to the east.

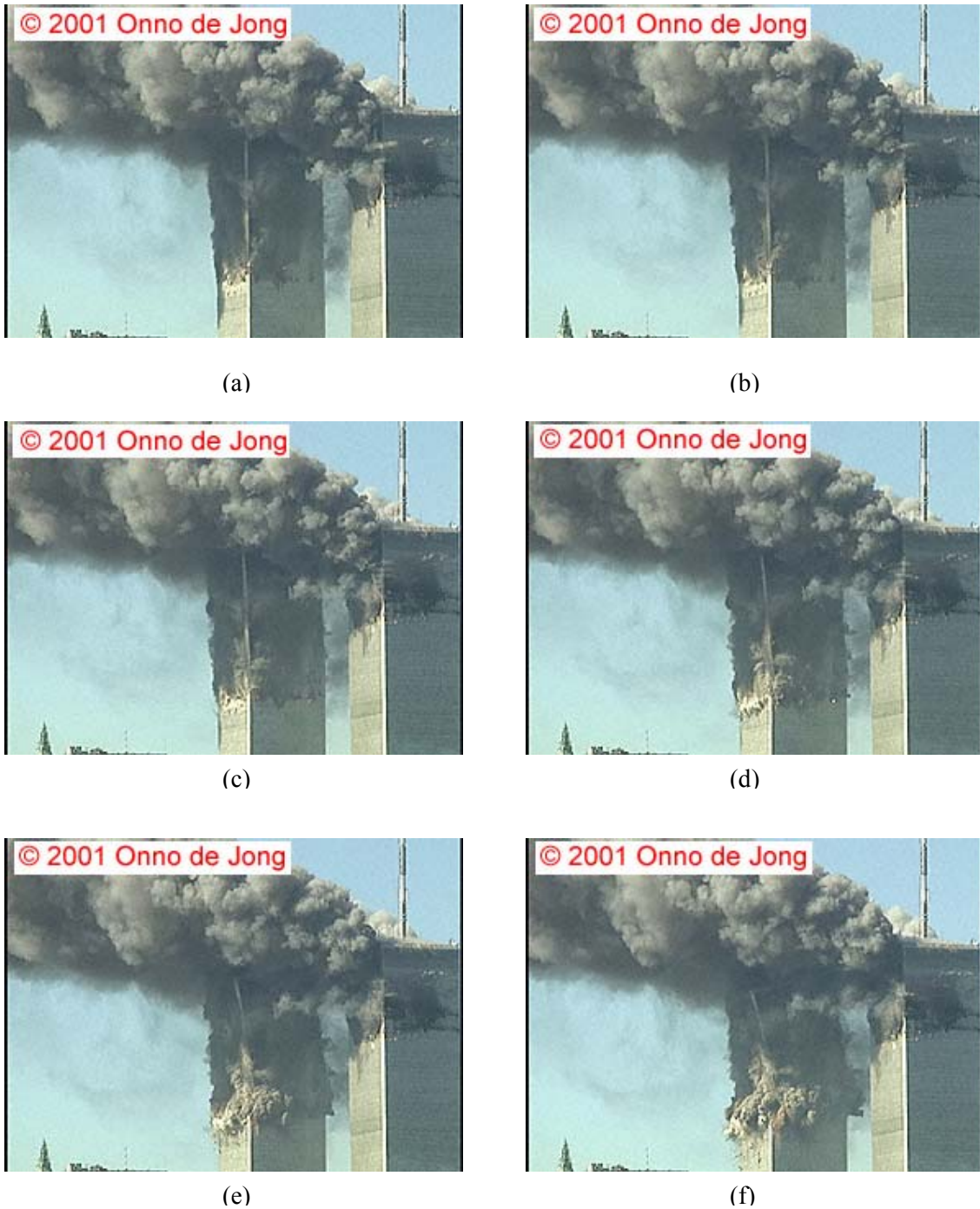


Figure 6–25. View of upper building section of WTC 2 tilting to the east from the northeast.



Figure 6–26. Kink on southeast corner near Floor 106 formed after collapse initiation.

This page intentionally left blank.

Chapter 7

STRUCTURAL RESPONSE OF MAJOR TOWER SUBSYSTEMS TO AIRCRAFT IMPACT DAMAGE AND FIRE

7.1 INTRODUCTION

Prior to conducting the analysis of the global structural response of each tower, major structural subsystems were analyzed to provide insight into their behavior within the WTC global system¹. The three major structural subsystems, the core framing, a single exterior wall, and full tenant floors, were analyzed separately for their response to impact damage and fire. The hat truss was not analyzed separately as its structural behavior did not require significant reductions in model complexity for the global analysis. The component analyses provided a foundation for these large, nonlinear analyses with highly redundant load paths by determining component behavior and failure modes and enabling a significant reduction in finite element model complexity and size. While the component models used preliminary estimates of elevated temperatures, the major subsystem models used final estimates of impact damage and elevated temperatures determined from the aircraft impact analysis and the fire dynamics and thermal analyses.

The capacity of each subsystem to sustain loads for the imposed damage and elevated temperatures was evaluated. The isolated subsystem models lacked the restraint and load paths to other subsystems found in the global analysis. Even so, the isolated subsystem response was useful for refining the global models and interpreting subsystem behavior in the global system. For instance, when a column buckled in the isolated core subsystem model, the only load path available to carry that column's load was the floor system within the core structure. However, in the global structure, the hat truss at the top of the core would transfer loads to other core columns or the exterior walls, assuming the connections between the core columns and hat truss remained intact.

7.2 CORE SUBSYSTEM

The core subsystem in the WTC towers was designed to carry gravity loads, which included the weight of the structure, equipment, furnishings, and occupants. The core system was not designed to carry lateral wind loads. The core columns were 3 stories in length (36 ft) and were either box columns or wide flange columns. At the aircraft impact floors, box columns transitioned to wide flange columns as loads and member sizes decreased with height. Column connections used either welded or bolted splice plates and were designed for compressive loads only; tensile, shear, or moment load transfer between columns was not intended. The core floor slab was typically 4.5 in. normal weight concrete that was composite with the floor beams through shear studs. The core floor was supported by wide flange beams with either a simple shear connection or a moment connection to the core columns.

¹ All information and data related to the design and construction of the WTC towers were obtained from contract drawings provided to NIST by The Port Authority of New York and New Jersey. Refer to NIST NCSTAR 1-2A for a complete description of the WTC structural system and an index of all structural drawings.

It is important to note that in the global structure, the core floors provided a secondary load path for load redistribution between the core columns. The primary load path for load redistribution was through the hat truss to adjacent columns. If columns were severed or a column or hat truss connection failed under tensile loads, the floors above the damage area provided the load redistribution between columns.

The isolated core models provided insight into expected behavior for situations where the hat truss was not able to redistribute loads. It also provided insight into the effects of impact damage and thermal weakening over time of affected areas of the core structure.

7.2.1 Model and Method of Analysis

Isolated core models extended from Floor 89 to Floor 106 for WTC 1 and from Floor 73 to Floor 106 for WTC 2, shown in Figs. 7–1(a) and (b), and did not include the hat truss, which extended from Floor 107 to the top of each building. The models included core columns and floor beams and slabs. Floor slabs were modeled as membrane elements with a relatively coarse mesh, which resulted in approximate slab openings for elevators and mechanical shafts. The meshing did not affect the floor's ability to provide a load path between columns. For the purposes of the isolated core model, only the floor beams with partial moment connections were included. It was assumed that simple shear connections were not capable of transferring significant loads between columns. At the base of the models, vertical springs were provided to represent the stiffness of columns below the model. The core subsystem model included large deflection, temperature-dependent material properties with plasticity and creep for all structural framing and plastic buckling behavior for columns.

The core subsystem was first analyzed for stability under gravity loads. The structural impact damage and gravity loads were applied to the core subsystem for all four damage cases, WTC 1 Cases A and B and WTC 2 Cases C and D (see Chapter 5). Impact damage was modeled by removing severed core columns and damaged floor areas. The gravity loads included dead load, superimposed dead load, and service live load (25 percent of design live load). The use of 25 percent of design live load as the service live load is discussed in NIST NCSTAR 1-2.

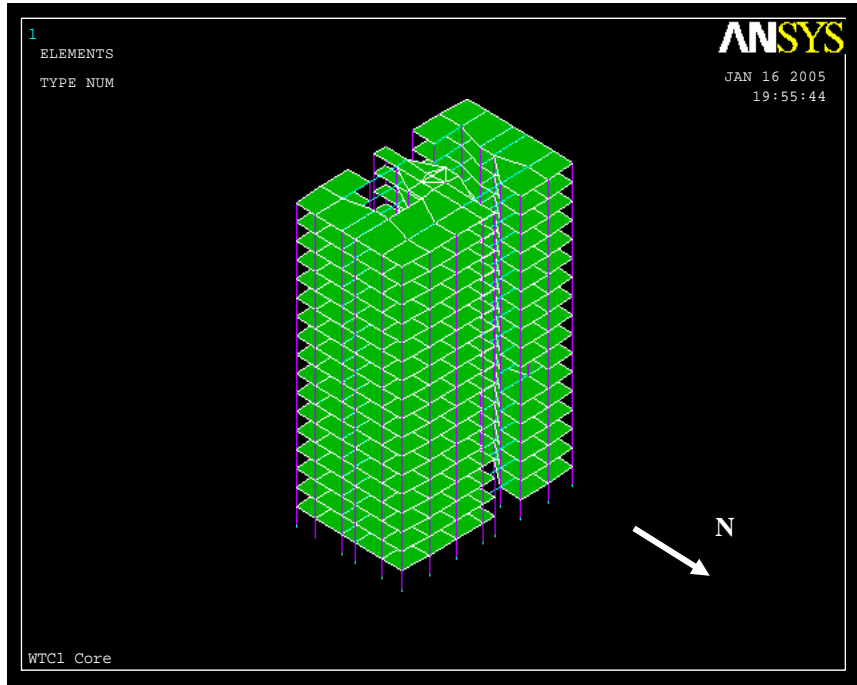
The WTC 1 isolated core model was stable for Case A structural damage and applied gravity loads. The isolated core model solution did not converge for WTC 1 Case B structural impact damage, which had more severed columns than Case A. The core structure was not able to tolerate the imposed damage without shedding some load to the exterior walls. For the WTC 2 isolated core model to reach a stable solution under Case C structural damage and gravity loads, horizontal restraints were required in the east and south directions at each floor to represent the lateral restraint provided by the office area floors and the exterior framed tube. Without the horizontal restraints, the WTC2 core model tilted significantly to the southeast due to the severed columns in that corner of the core. The isolated core model did not converge for WTC 2 Case D structural impact damage, which had more severed columns than Case C.

Each isolated core model was subjected to two temperature conditions as follows:

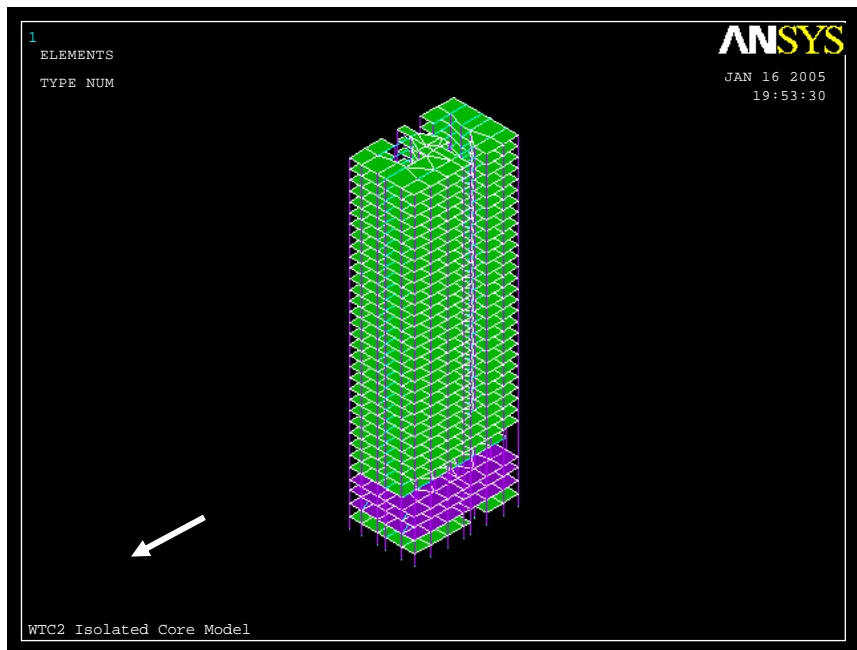
- WTC 1 (Case A impact damage) was subjected to Case A and Case B temperature histories
- WTC 2 (Case C impact damage) was subjected to Case C and Case D temperature histories

Case B and Case D impact damage could not be used for the isolated core models as no stable solution was obtained. Instead, for WTC 1, Case A impact damage was used for both Case A and Case B temperature histories and, for WTC 2, Case C impact damage was used for both Case C and Case D temperature histories. This approach allowed for comparison of the differences between Case thermal loads for the same impact damage for each tower.

Temperature histories were input as nodal temperatures at each node in the structural model that was subject to heating. The temperatures predicted in the structural members depended on the extent of insulation assumed to be in place and on the material properties and geometry of the structural members. In each tower, the temperature in the structural members varied through the length and cross section and changed with time. The temperature at every node in the global models was calculated by interpolation of temperatures from the thermal analysis, which had a much finer mesh than the global structural models. A linear temperature gradient was assumed across column cross sections and along the length of members. To reduce data handling, the continuous temperature time histories were replaced with piecewise linear time-histories without significant loss of accuracy. Elevated temperatures were applied to the damaged core structure in 10 min intervals, where a temperature state was given for all structural components at a given time and linearly ramped to the next temperature state. Examination of temperature histories indicated that no significant fluctuations between temperature states occurred for the 10 min intervals selected for analysis. Temperature data were provided at 10 min intervals up to 100 min for WTC 1 and up to 60 min for WTC 2 (see NIST NCSTAR 1-5G for more discussion of the 10 min intervals).



(a) WTC 1



(b) WTC 2

Figure 7–1. Isolated core models.

7.2.2 WTC 1 Core Analysis Results

Figure 7–2 shows the vertical displacement of the WTC 1 isolated core model with impact damage (prior to applying thermal loading) for Case A, where the colors represent the magnitude of vertical displacement. The maximum vertical displacement was approximately 5 in. along the north side of the

core where core columns were severed. Figures 7–3 and 7–4 show the WTC 1 core structural response to Case A and Case B temperature histories, respectively. Case A resulted in column buckling at the northwest corner and the center of the south side between Floors 94 and 97. There was a 21 in. vertical displacement at the northwest corner and a 12 in. vertical displacement at the center of the south side of the core. Case B resulted in column buckling between Floors 94 and 98 and a 44 in. vertical displacement at the center of the south side of the core.

For Case A temperatures, the core structure was first weakened on the northeast side as fires started in that area after the aircraft impact and then on the south side as the fires spread. For Case B temperatures, the core structure weakened at the center of the north side and then the south side. The core structural responses to these two temperature conditions illustrate the slight difference in core areas that were weakened by the elevated temperatures (northeast versus center of north side). When the results of each isolated core model were compared to the observed behavior of WTC 1, the weakening on the south side of the core was best matched by Case A impact damage and Case B temperatures (Case A impact damage and Case A temperatures showed core weakening at the northwest corner of the core).

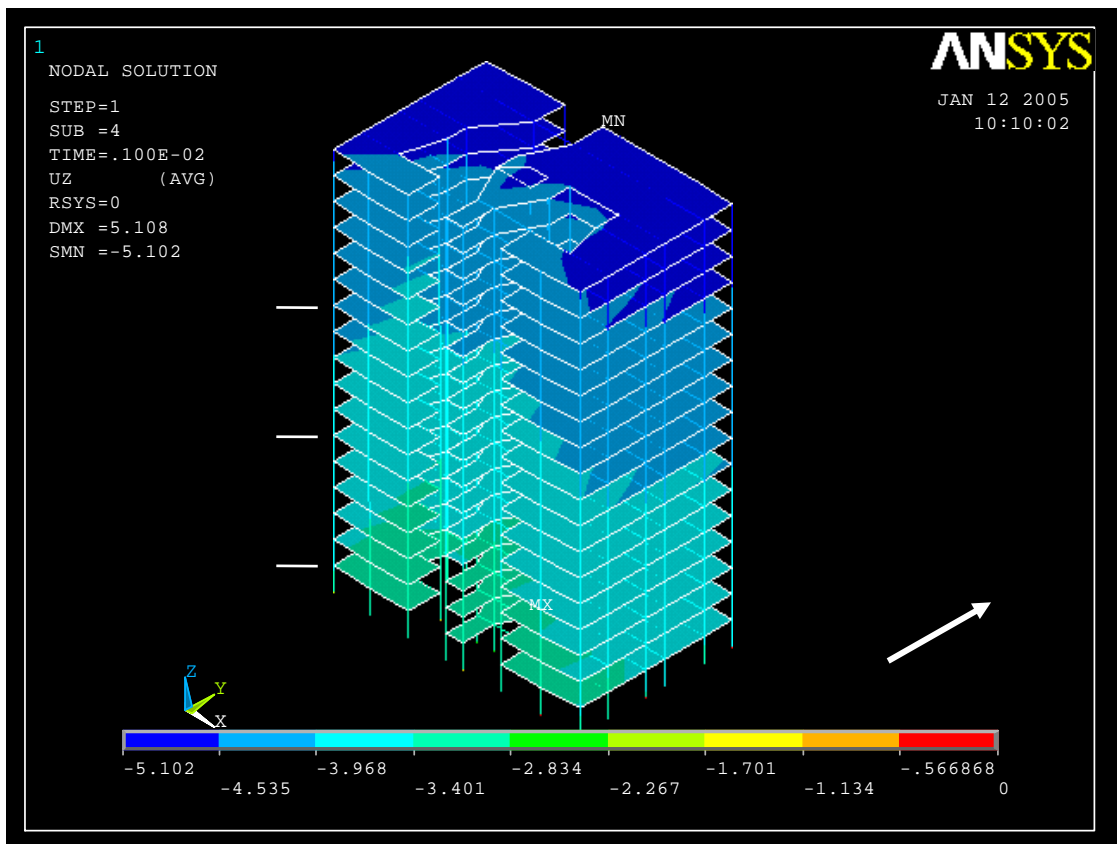
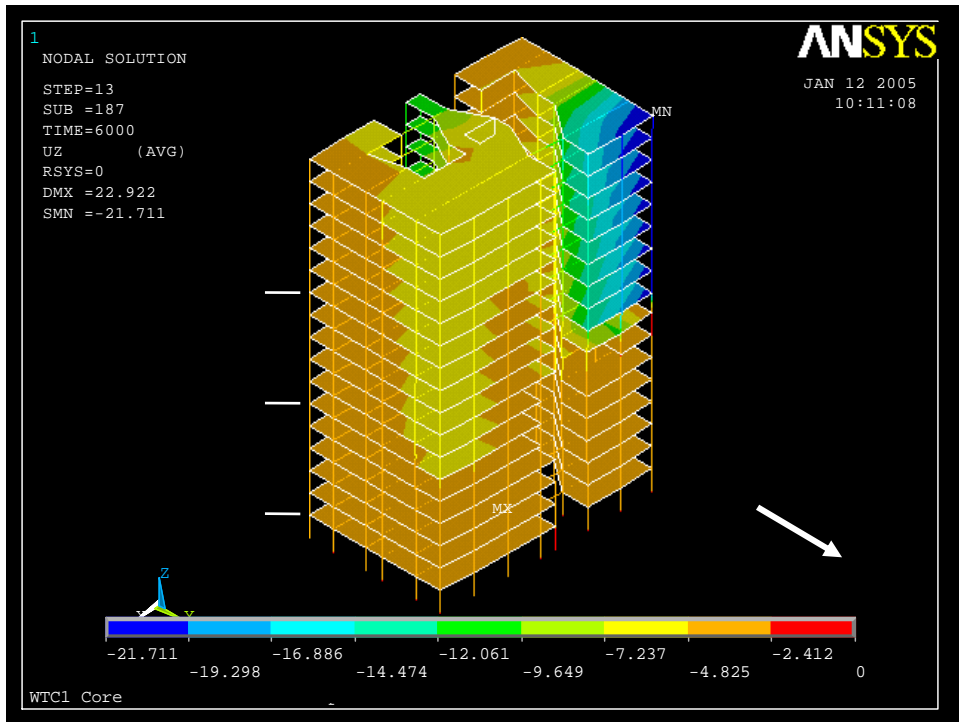
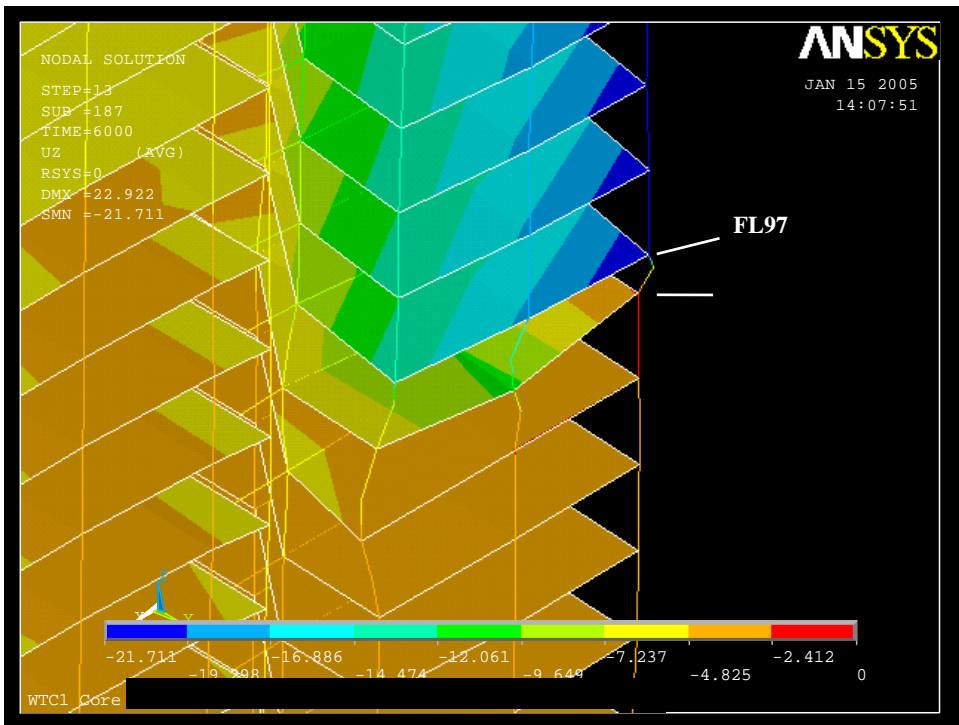


Figure 7–2. Vertical displacement of WTC 1 isolated core model with impact damage and gravity loads.

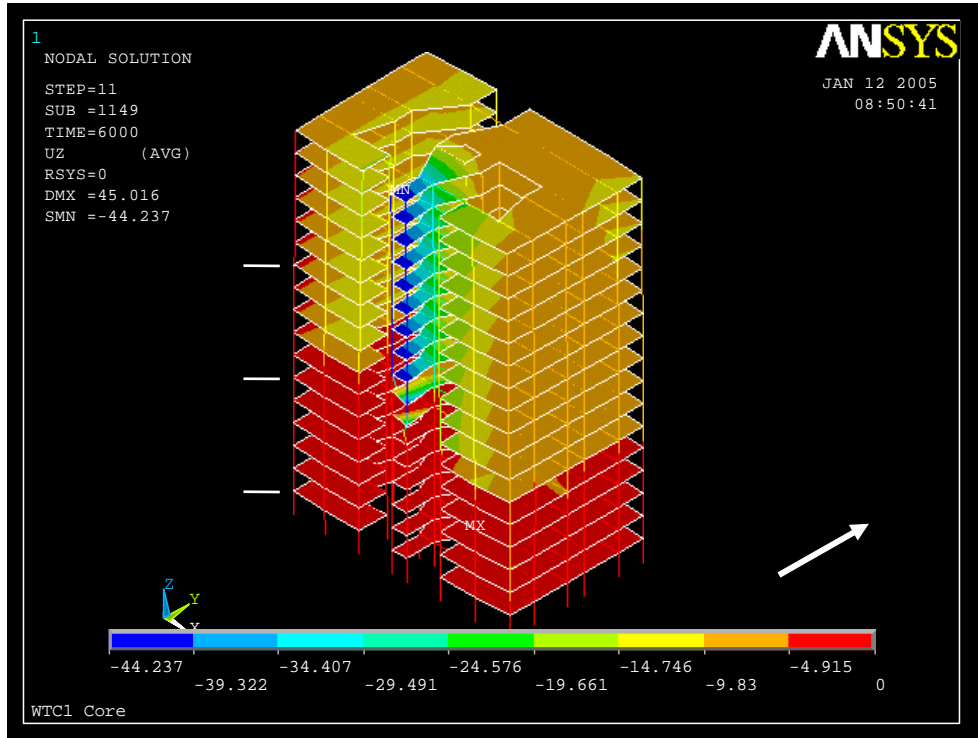


(a) North and east sides

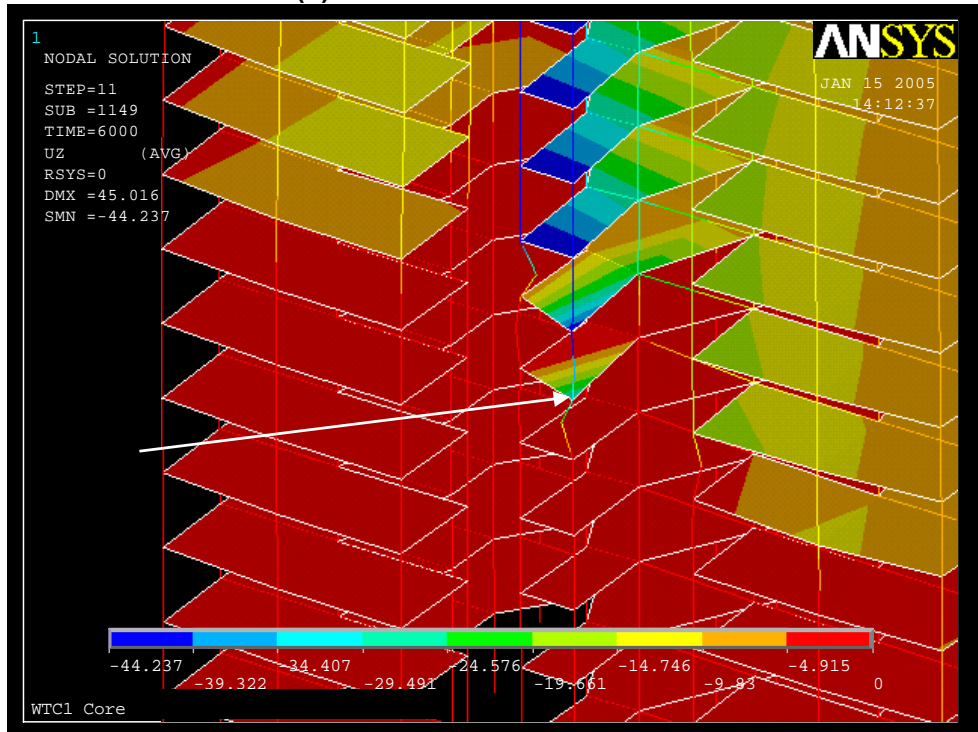


(b) Northwest corner (5X magnification)

Figure 7-3. North side vertical displacement of the WTC 1 core model at 100 min for Case A temperatures.



(a) South and east sides



(b) South side (10X magnification)

Figure 7-4. South side vertical displacement of the WTC 1 core model at 100 min for Case B temperatures.

7.2.3 WTC 2 Analysis Results

Figure 7–5 shows the vertical displacement of the WTC 2 isolated core model with impact damage for Case C. The maximum vertical displacement was approximately 5.6 in. at the southeast corner of the core where core columns were severed. Figures 7–6 and 7–7 show the response (vertical displacement) of the WTC 2 core model to Case C and Case D temperature histories, respectively. Case C resulted in a 6.1 in. vertical displacement at the southeast corner. Case D resulted in an 8.1 in. vertical displacement at the southeast corner. Without horizontal restraints, the core would have tilted more toward the southeast corner, and the vertical displacement would have been larger. No columns buckled in either Case C or Case D.

For both Case C and Case D temperatures, the core structure was weakened at the southeast corner and along the east side of the core. The core structural responses to these two temperature conditions illustrate the slight difference in core weakening by the larger deflection in the southeast corner for Case D, which had more column damage. The WTC 2 response for Case C and Case D temperatures was similar, with a 2 in. increase for Case D. When the results of each isolated core model were compared to the observed behavior of WTC 2, both Cases provided a reasonable match.

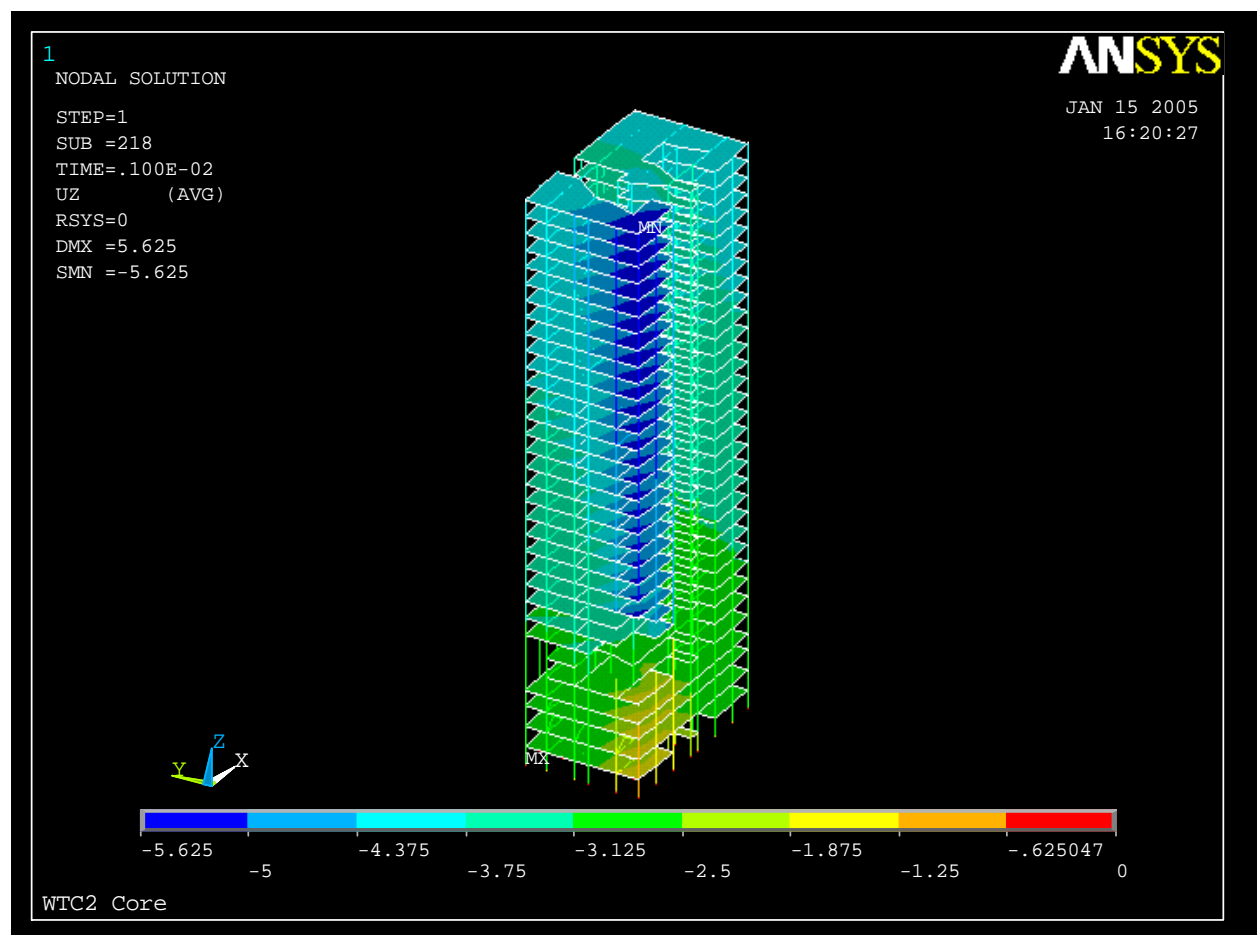


Figure 7–5. Vertical displacement of the WTC 2 isolated core model with impact damage and gravity loads (south and east faces).

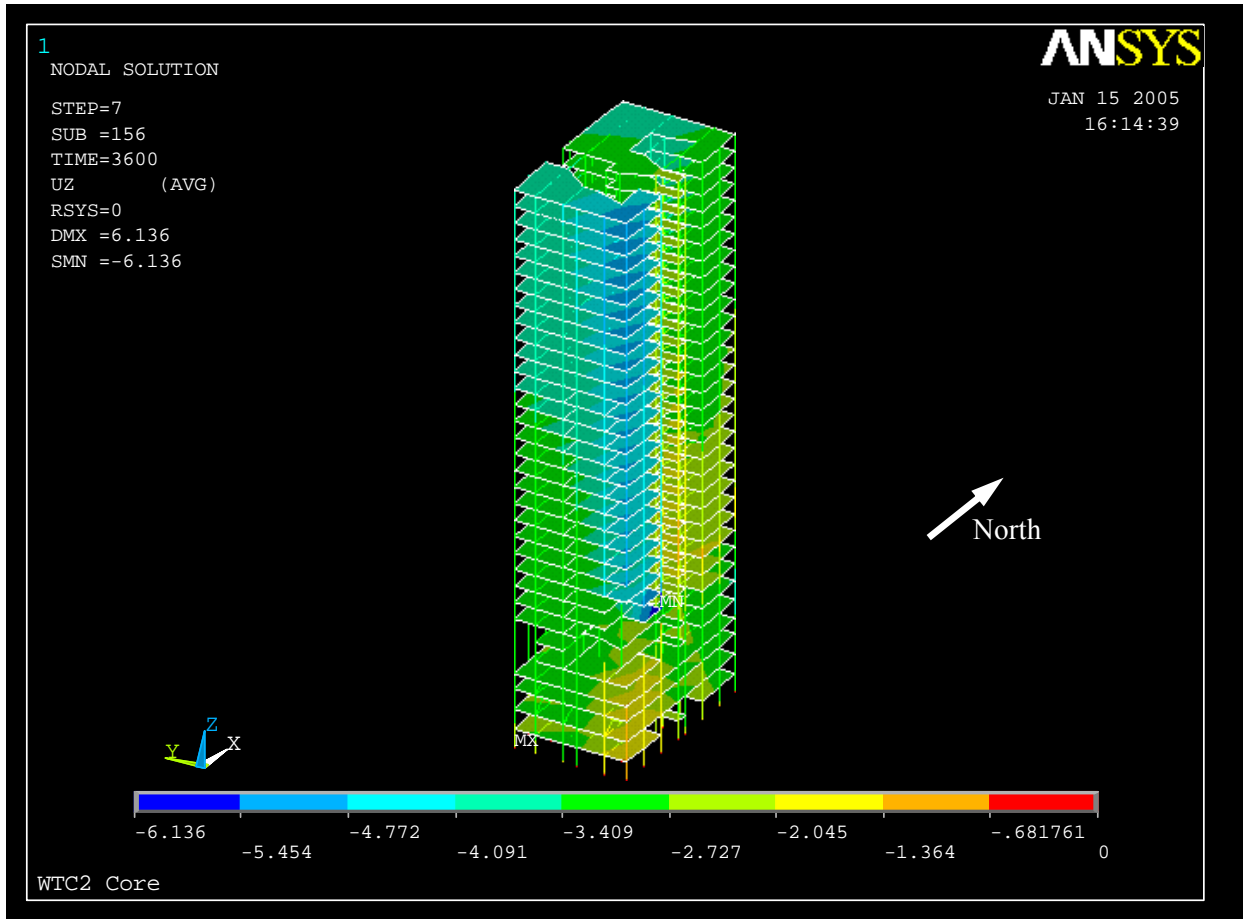


Figure 7–6. Vertical displacement of the WTC 2 core model at 60 min for Case C temperatures (south and east faces).

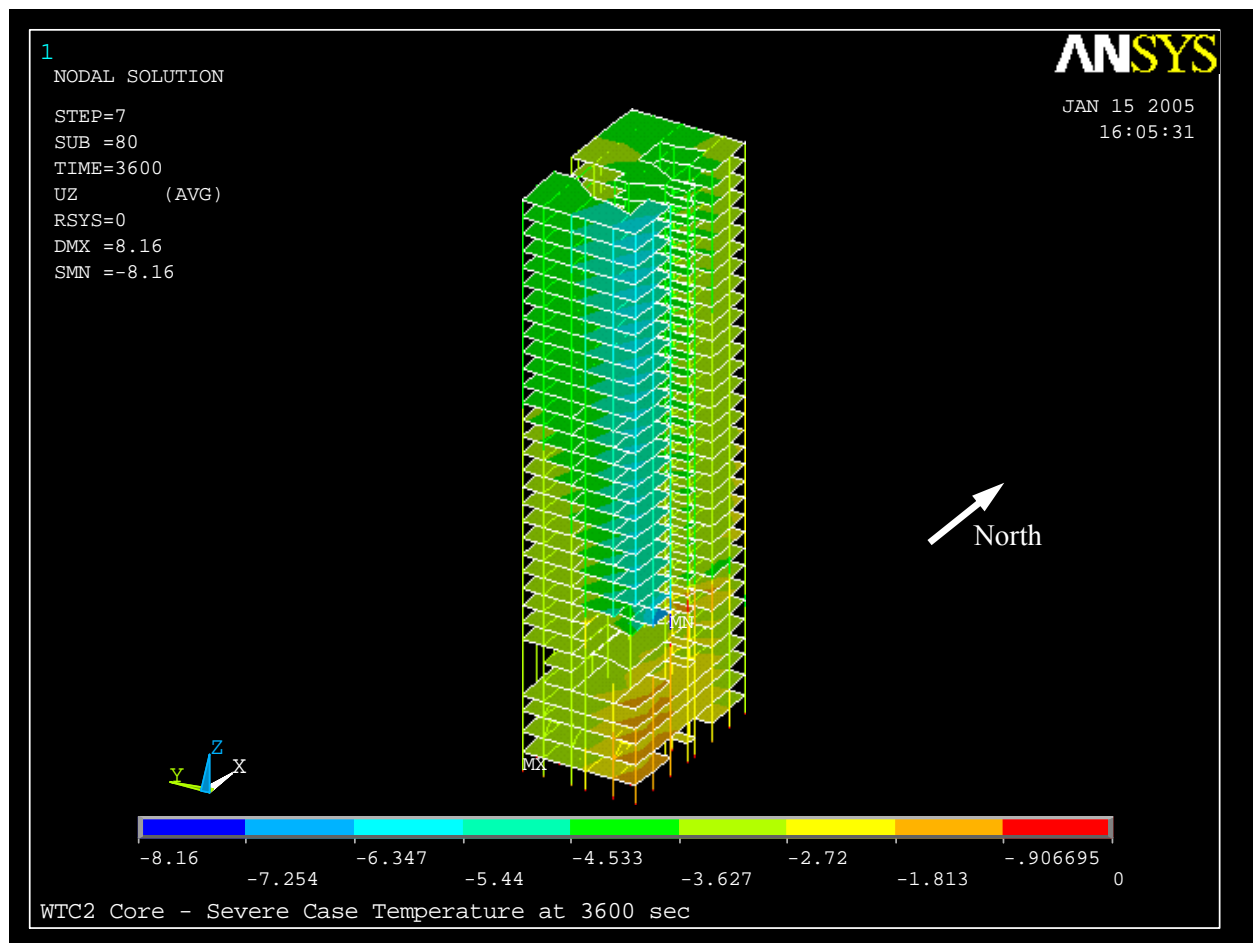


Figure 7–7. South and east side vertical displacement of the WTC 2 core model at 60 min for Case D temperatures.

7.3 FULL FLOOR SUBSYSTEM

7.3.1 Model and Method of Analysis

Figure 7–8 shows the full floor model (described in Chapter 4), which included 1) exterior and core columns extending one story below and one story above the floor model, 2) spandrels, 3) floor slab, 4) floor trusses (bridging trusses were retained only in the two-way floor areas), 5) strap anchors, 6) core beams, 7) deck support angles, and 8) break elements to capture failure modes. Both core and exterior columns were fixed against vertical movement at the lower ends and free to displace at the upper ends. Exterior columns were restrained from out of plane displacement and all three components of rotation at the both column ends. The core columns were free to displace horizontally. Note that the two-way zones shown in Fig. 7–8 extended only to the corners of the core rather than beyond the corners as shown in Fig. 4–7. The extent of two-way action shown in Fig. 7–8 was believed to better represent actual structural boundary conditions.

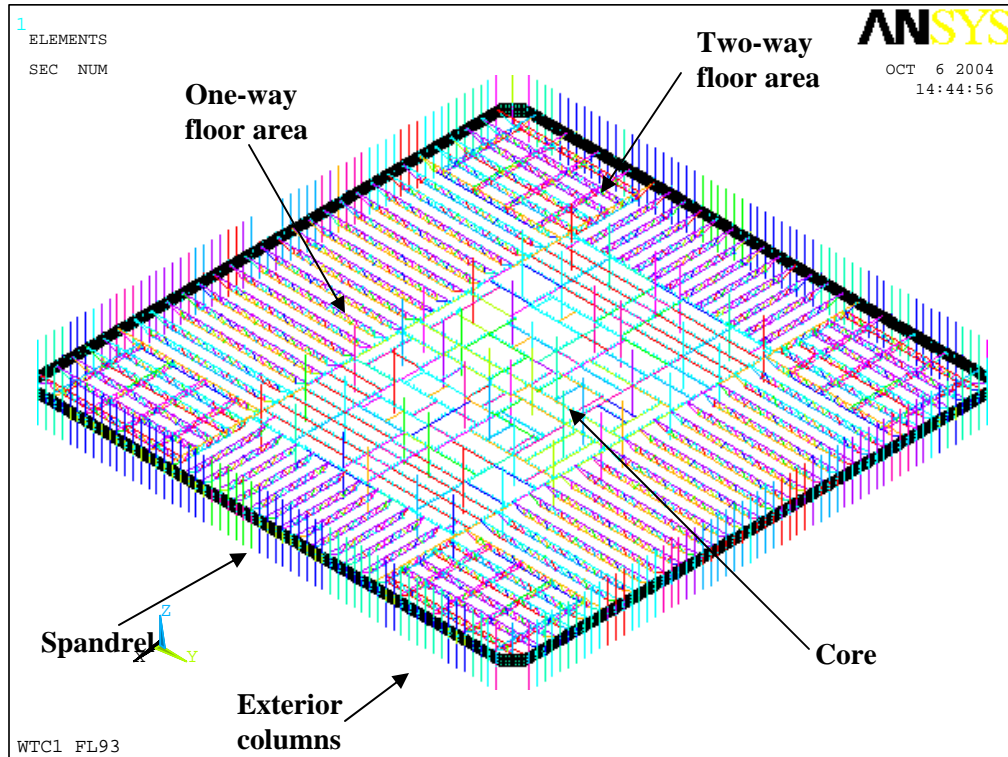


Figure 7–8. Full floor model.

The full floor subsystem models included large deflection and temperature-dependent material properties with plasticity for all steel components. The model was used to evaluate structural response under dead and live loads and elevated temperatures, identify failure modes and associated temperatures and times to failure, and identify reductions in modeling complexity for global models and analyses. The structural response included thermal expansion of steel and concrete members, temperature-dependent properties of steel and concrete that affected material stiffness and strength, and bowing or buckling of structural members. Creep was not included in the full floor models, as this analysis feature did not work with the BEAM 188/189 elements in version 8.0 of ANSYS (the detailed truss model had 3D finite strain elements that were changed to beam elements in the full floor model). Creep was included for beam elements in ANSYS 8.1, and subsequent analyses of the core and exterior wall subsystems included creep deformation.

The floor slab was modeled as lightweight concrete across the entire floor (tenant and core floor areas) with a bilinear stress-strain constitutive model that did not account for cracking or crushing. The concrete material model used the compressive strength as the yield point, with the same yield strength in both tension and compression (the reinforcing steel was assumed to provide the tensile capacity in the composite floor). With this material model, tensile strength of the concrete slab was not represented accurately, and the actual floor stiffness was overestimated. In the full floor models, bending stresses in the concrete slab that exceeded the actual tensile strength of concrete were found in few locations. This phenomenon was typically observed when the temperature of the top of the slab was higher than the temperature at the bottom of the slab, and the concrete slab still deflected down due to large thermal expansion of the truss. However, when the temperature is higher at the bottom, the simplified truss model

with this material model showed a very similar behavior to the detailed truss model, and the key failure modes of the floors were not significantly affected.

Failure modes of the full floor model included truss diagonal buckling and weld failure, exterior and interior truss seat failure, stud failure, strap anchor weld failure, connection failure between primary and bridging trusses, and connection failure between long-span and transfer trusses.

Separate floor models were created from the Floor 96 structural model by imposing the different damage and temperature conditions for WTC 1 Floors 93 to 99 and WTC 2 Floors 79 to 83. Structural components that were severed due to the aircraft impact were removed from each floor model, based upon four initial damage cases, WTC 1 Case A_i and Case B_i and WTC 2 Case C_i and Case D_i. Each full floor model was analyzed for stability under gravity loads consisting of dead load, superimposed dead load, and service live load (25 percent of design live load), which varied from 55 psf to 85 psf. No column loads were applied.

Each floor model was then subjected to the corresponding temperature conditions for each Case in 10 min intervals, as described previously. Temperatures were assigned at structural component nodes. A uniform distribution of temperatures through a cross section was assumed for truss members and spandrels. For columns, a linear gradient in two directions was assumed, and the slabs had temperatures defined at 5 nodes through the slab depth.

Some members were removed from the model to improve computational performance. They were found to fail in the early stages of thermal loading and caused convergence problems. Removal of the following members did not affect the stability and ultimate failure mode of the full floor system under fire:

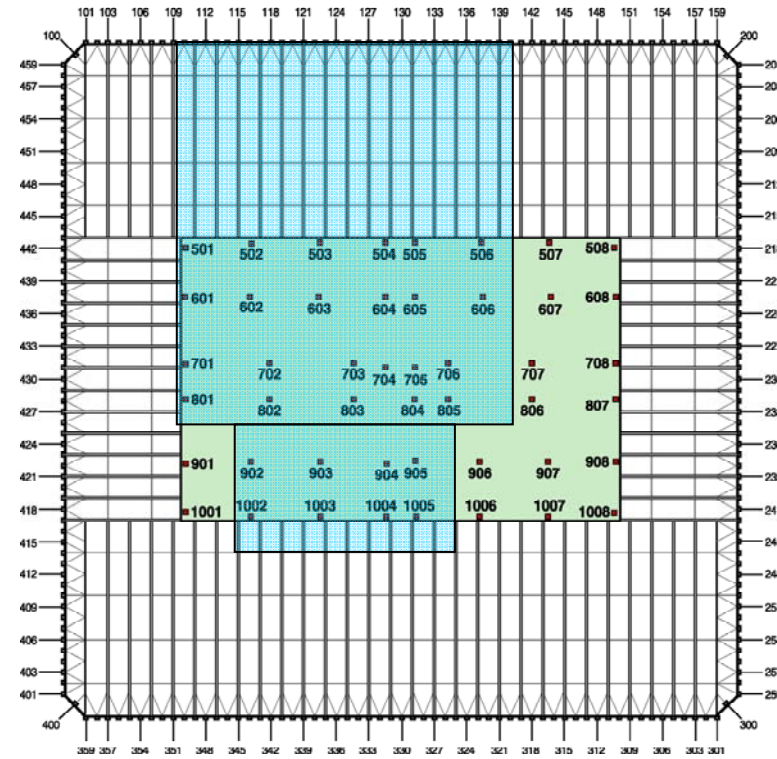
- Deck support angles and bridging trusses, which buckled due to thermal expansion.
- Shear studs and welds between strap anchors and truss top chords, which failed due to shear force caused by differential thermal expansion between the floor and the exterior wall.

Final damage Cases A, B, C, and D were completed after the initial set of floor analyses were conducted, as described above. The fire simulations did not change between initial Cases A_i to D_i and final Cases A to D, which resulted in the same concrete slab temperatures for the initial and final Cases. The truss temperatures differed as a result of the different estimates of dislodged fireproofing. The full floor models were not rerun for Cases A through D as comparisons showed that the structural temperature histories of the floors were nearly identical for most floors and only slightly different for a few floors. The floor analysis results for Cases A_i to D_i were used for Cases A to D in the exterior wall subsystem (Section 7.4) and global analyses (Chapter 8).

For WTC 1, only Floor 97 showed a significant increase in damage to truss fireproofing on the south side between Case A_i and Case A, where the fireproofing damage over 11 trusses increased from just beyond the core to two thirds of the floor span, as shown in Fig. 7–9. Figure 7–10 shows the temperature distributions for WTC 1 Floor 97 trusses for Case A_i and Case A. Analysis of Floor 97 for Case A damage and temperature histories showed little difference in the floor behavior. Case B_i and Case B structural and fireproofing damage were similar for all floors.

A review of WTC 2 Cases showed that the differences in truss fireproofing damage between Cases C_i and C and Cases D_i and D (mostly on the east side) would cause little difference in the floor temperatures or in the structural behavior. The exception was Floor 83 for Cases C_i and C, where the fireproofing damage increased from half to three quarters of the floor area. However, observations from photographs suggested that the floor was disconnected immediately after the aircraft impact and fireball in this area. Since Floor 83 was assumed to be disconnected at the exterior wall over the area that would be heated in Case C, the analysis was not rerun for this case.

Case A_i



Case A

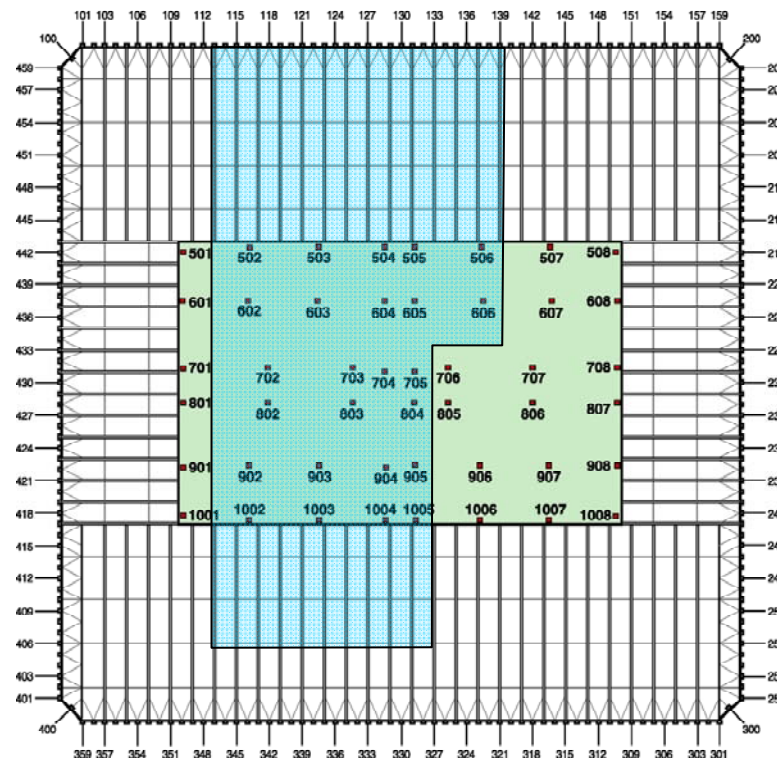
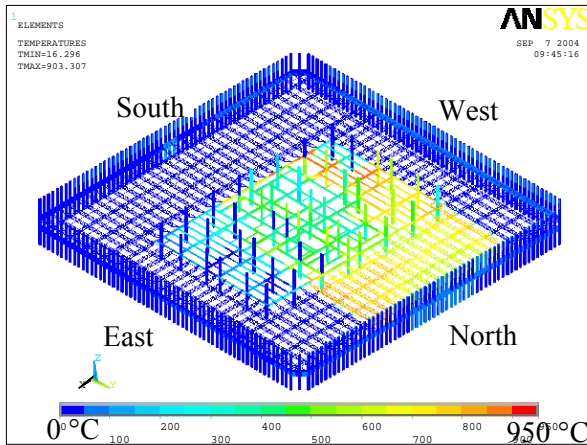
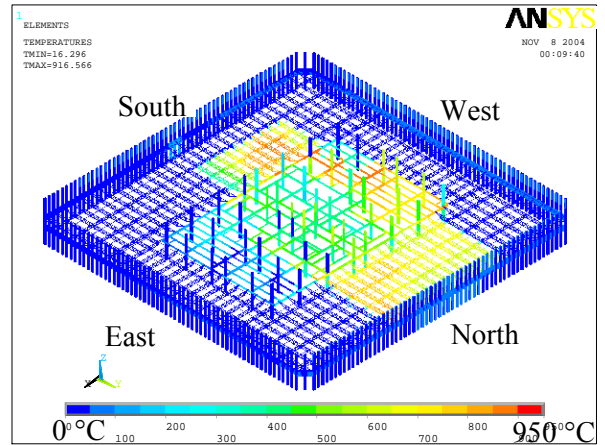


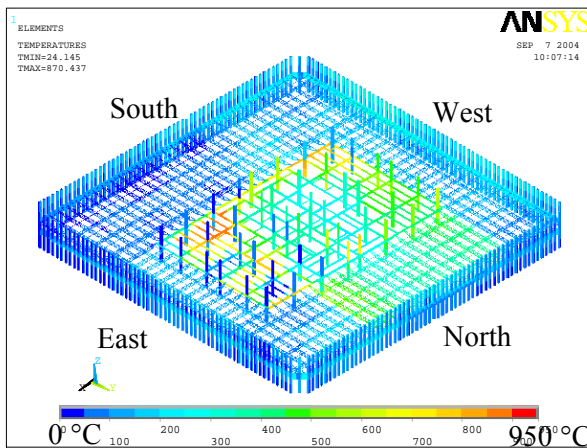
Figure 7-9. Fireproofing damage to WTC 1 Floor 97 for Case A_i and Case A.



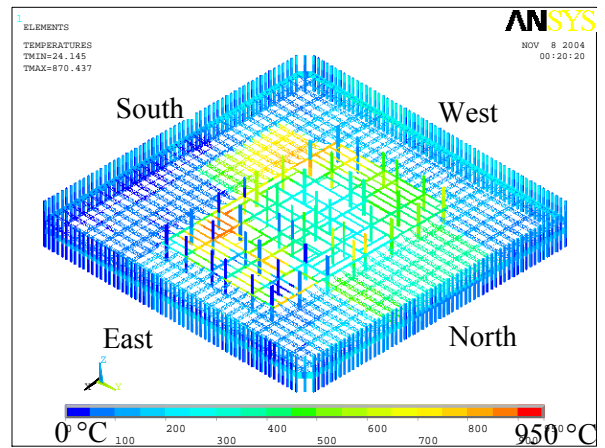
(a) Case A₁ top view at 10 min



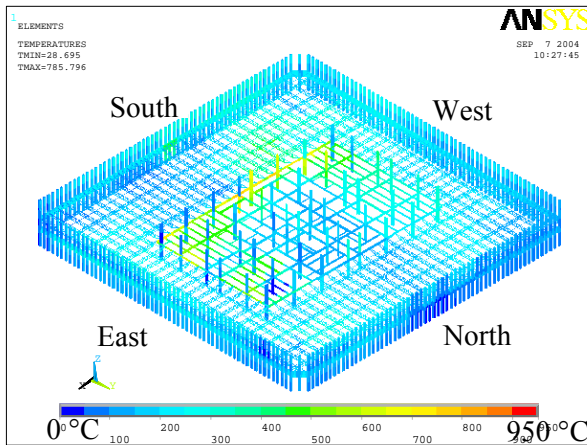
(b) Case A top view at 10 min



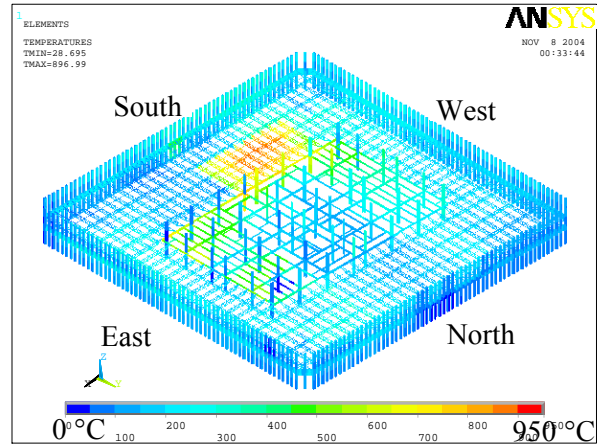
(c) Case A₁ top view at 50 min



(d) Case A top view at 50 min



(e) Case A₁ top view at 100 min



(f) Case A top view at 100 min

Figure 7–10. WTC 1 Floor 97 comparison of truss temperatures for Case A₁ and Case A.

7.3.2 WTC 1 Analysis Results

Areas of the floors that were subject to the combined effects of dislodged fireproofing and exposure to fire were found to have two primary failure mechanisms: buckling of diagonal web members and associated sagging of the floor or disconnection of exterior truss seat connections. When the vertical support of truss seat connections failed, the floor would hang or sag between the remaining intact supports. The following descriptions of floor responses to structural impact damage and temperature histories for Cases A_i, B_i, C_i, and D_i present the time, locations, and maximum vertical displacements of the sagging predicted in the floors.

Case A_i

As shown in Fig. 7–9, the intact fireproofing on the south floor trusses resulted in delayed heating of the trusses. The WTC 1 floors in the impact zone had upgraded fireproofing thickness of 2.5 in. (modeled as a thermally equivalent 2.2 in. to account for variability in thickness, Chapter 2). The maximum temperatures shown for Floor 97 trusses on the south side ranged from 300 °C to 400 °C at 100 min. At these temperatures, the steel expanded thermally but had only a modest reduction in stiffness and strength (see Chapter 4).

The maximum vertical displacements of WTC 1 floors are listed in Table 7–1. Floor 95 to Floor 98 showed a significant vertical deflection (sag) in the north office area near the impact damage. The vertical deflection in the south office area was found to be insignificant for all floors. Many diagonals of Floor 95 to Floor 98 buckled in the hottest zones of the north office area. Although gusset plates fractured at several locations, a complete disconnection of the floor from the exterior wall was not predicted. Slab thermal expansion at 100 min (across the entire floor) ranged between 4 in. and 8 in. Since the floors did not sag except in areas adjacent to the impact zone on the north side, almost all the exterior columns were pushed out by the floors. The high level of restraint imposed on the slab expansion by the exterior columns, due to their fixed boundary conditions at column ends, resulted in compressive forces developing in the slab. These compressive forces would likely have been smaller in the towers, as the exterior columns would have expanded outward over the four to five floors subject to fires and provided minimal restraint against thermal expansion of the slab.

Case B_i

Table 7–2 gives the maximum vertical displacement of WTC 1 floors for Case B_i, and Figs. 7–11 through 7–15 show the vertical displacement contours at time of maximum displacement for Floors 95 to 99. Floors 93 and 94 had no fireproofing damage to the south floor trusses. The maximum deflection of Floors 95 and 96 occurred just after the aircraft impact on the north side next to the damage area. Floors 97 and 98 maximum deflection occurred at 100 min on the south side. The time and location of maximum floor deflections illustrate the movement of the fires from the north side just after impact to the south and the effect of the truss fireproofing. The large deflections on the south side of Floors 97 and 98 were caused by the exterior seat failures that began at 90 min, due to reduction of vertical shear strength under the elevated temperatures. Figure 7–16 shows the extent of truss seat failures for Floor 97 and Floor 98, which was a loss of 18 percent to 25 percent of exterior connections for the two floors on the south face. The average slab expansion across the entire floor ranged from 5 in. to 8.5 in. The interaction of the floor slab and exterior columns was the same as described for Case A_i.

Table 7-1. Maximum vertical displacement of WTC 1 floors for Case A_i.

| Floor | Maximum Displacement (in.) | Location of Displacement on WTC 1 floor | Time after Aircraft Impact (min) |
|--------------|-----------------------------------|--|---|
| 93 | 5.4 | North side | 30 |
| 94 | 13.5 | North side | 100 |
| 95 | 30.9 | North side | 10 |
| 96 | 23.3 | North side | 10 |
| 97 | 31.5 | North side | 60 |
| 98 | 26.4 | North side | 30 |
| 99 | 7.0 | North side | 50 |

Table 7-2. Maximum vertical displacement of WTC 1 floors for Case B_i.

| Floor | Maximum Displacement (in.) | Location of Displacement on WTC 1 floor | Time after Aircraft Impact (min) |
|--------------|-----------------------------------|--|---|
| 93 | -5.8 | South side | 100 |
| 94 | 12.7 | South side | 100 |
| 95 | 29.2 | North side | 10 |
| 96 | 28.6 | North side | 10 |
| 97 | 37.4 | South side | 100 |
| 98 | 49.0 | South side | 100 |
| 99 | 6.8 | North side | 100 |

Note: Negative value represents upward displacement.

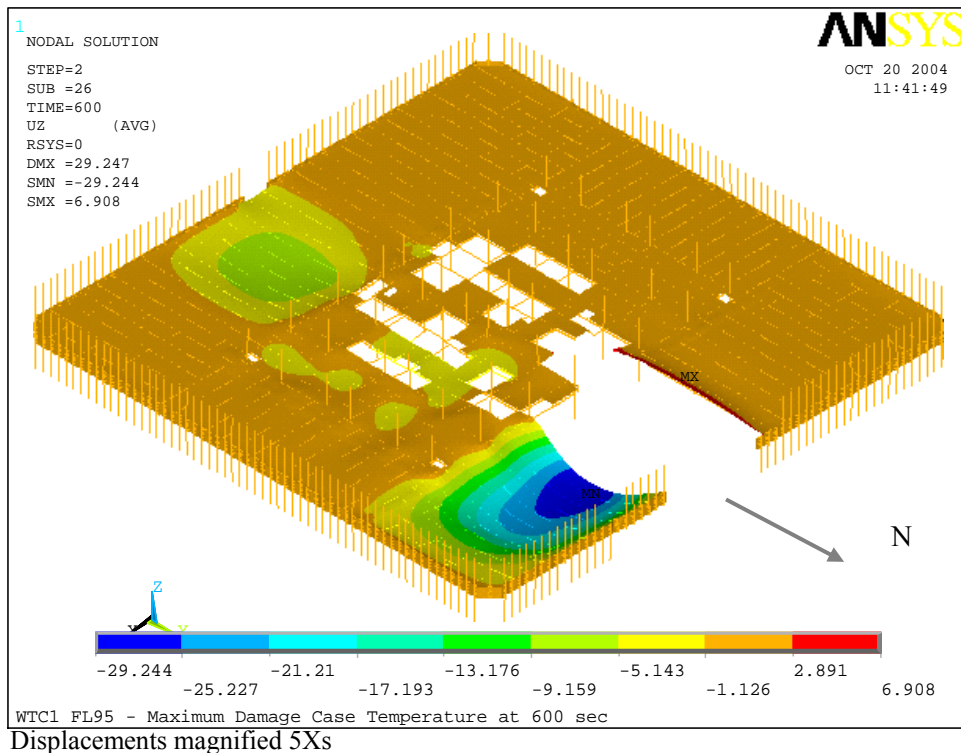


Figure 7-11. Vertical deflection of WTC 1 Floor 95 for Case B_i at 10 min.

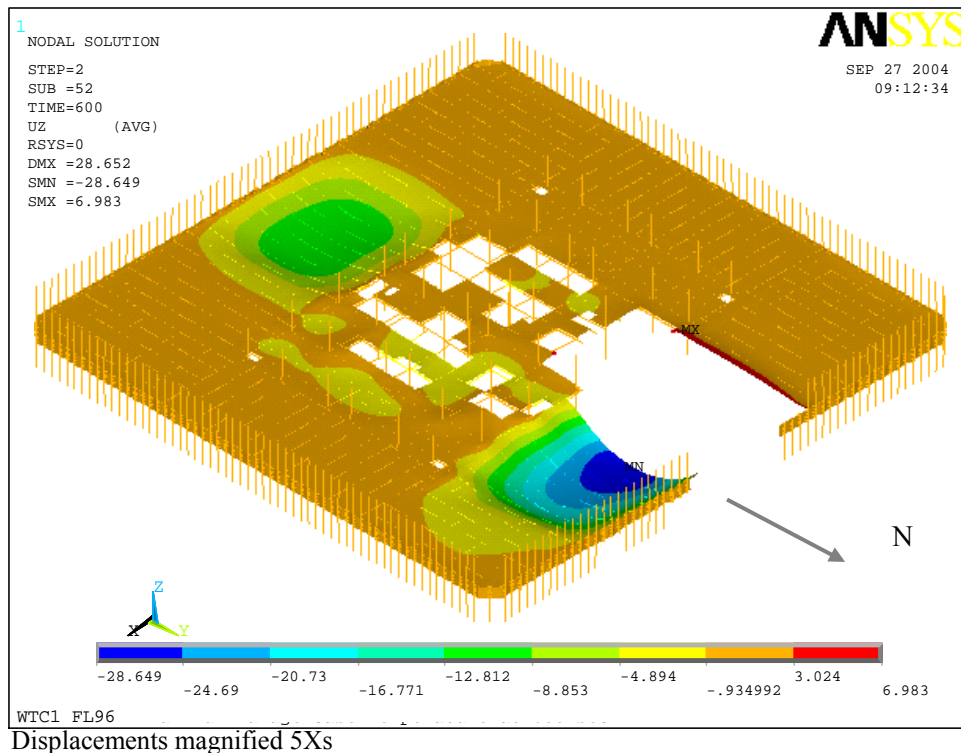


Figure 7-12. Vertical deflection of WTC 1 Floor 96 for Case B_i at 10 min.

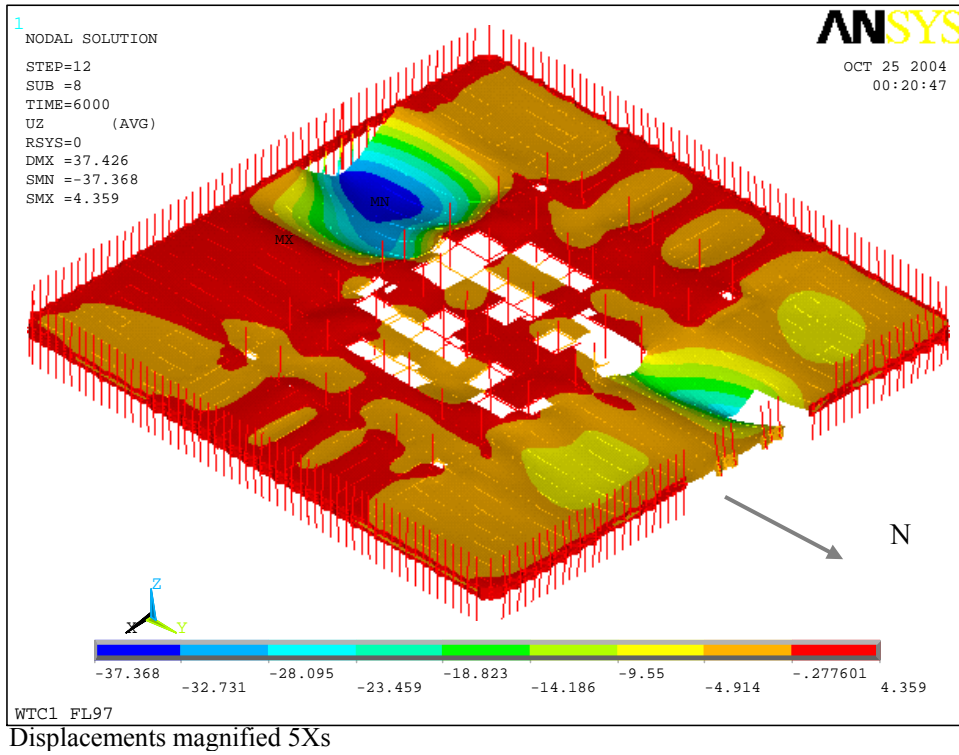


Figure 7–13. Vertical deflection of WTC 1 Floor 97 for Case B_i at 100 min.

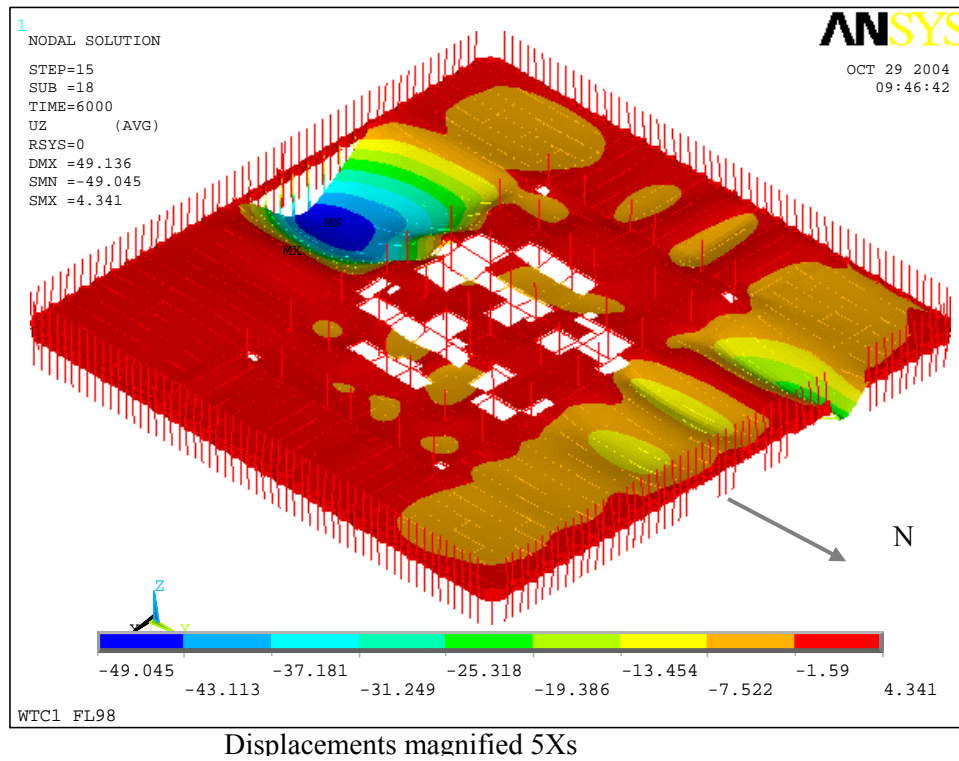


Figure 7–14. Vertical deflection of WTC 1 Floor 98 for Case B_i at 100 min.

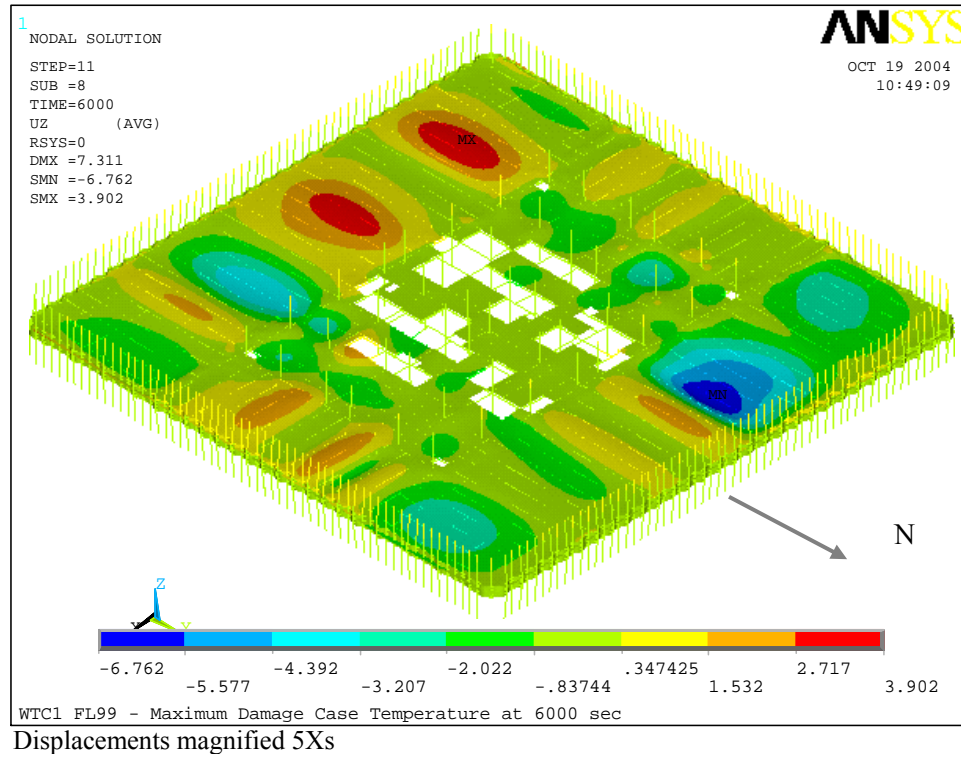


Figure 7–15. Vertical deflection of WTC 1 Floor 99 for Case B_i at 100 min.

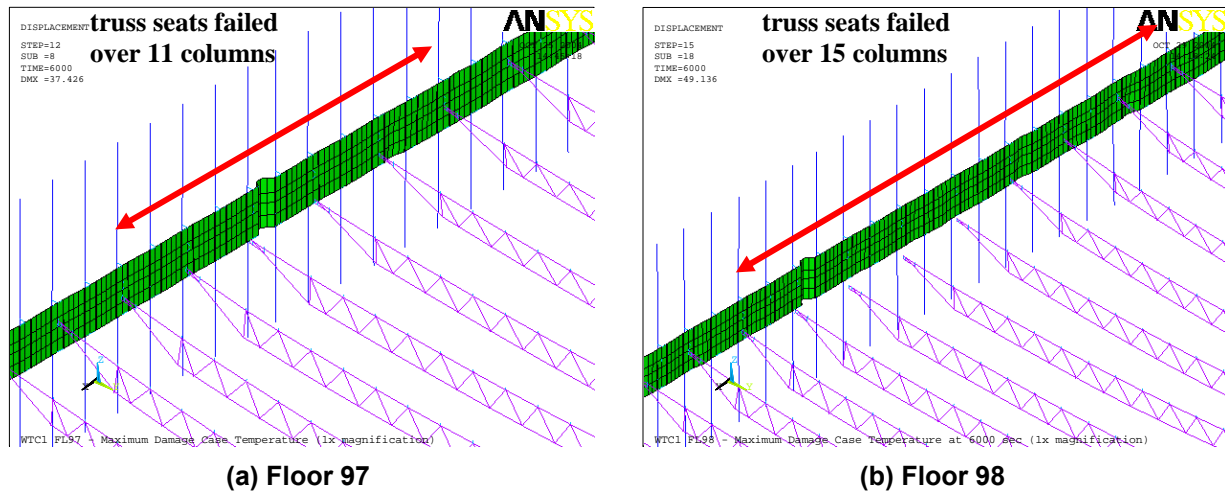


Figure 7–16. Loss of vertical supports in WTC 1 Floor 97 and Floor 98 for Case B_i.

7.3.3 WTC 2 Analysis Results

Case C_i

Table 7–3 lists the maximum vertical displacement of WTC 2 floors for Case C_i, and Figs. 7–17 through 7–21 show the vertical displacement contours at time of maximum displacement for Floors 79 to 83. Floors 79 to 83 had impact damage at the south side of the east floor area, but Floors 80 and 81 had many interior truss seats severed from the south exterior wall to the east side of the core perimeter. The maximum vertical deflection occurred in the southeast floor area near the impact damage for all floors, with the exception of Floor 82, which had a maximum deflection in the northeast floor area. The maximum deflection occurred at 60 min for all floors. The location of the maximum deflection was primarily due to the combined effects of impact damage and elevated temperatures. Floor 82 had a large span of unsupported floor along the exterior wall resulting from heat-induced truss seat failures, which led to floor sagging in the northeast corner (see Fig. 7–20).

The west office area of Floors 79 to 83 had vertical deflections ranging from 12 in. to 18 in. at 60 min, due to the combined effect of hot gases that spread throughout the floors and the 0.75 in. fireproofing on the trusses. The average thermal expansion of slabs across the entire floor ranged from 2.5 in. to 5.5 in. at 60 min.

A significant number of truss web diagonals buckled in the east floor area of Floor 81 to Floor 83. Truss seat failures were not observed on Floor 79 to Floor 81. Figure 7–22 shows the truss seat failures for Floor 82 and Floor 83, which extended over 15 percent to 30 percent of the exterior wall width.

Table 7–3. Maximum vertical displacement of WTC 2 floors for Case C_i.

| Floor | Max. Displacement (in) | Location of Displacement On East Floor | Time After Aircraft Impact (min) |
|-------|---------------------------|---|--|
| 79 | 19.0 | South side | 60 |
| 80 | 30.1 | South side | 60 |
| 81 | 31.0 | South side | 60 |
| 82 | 45.2 | North side | 60 |
| 83 | 38.9 | South side | 60 |

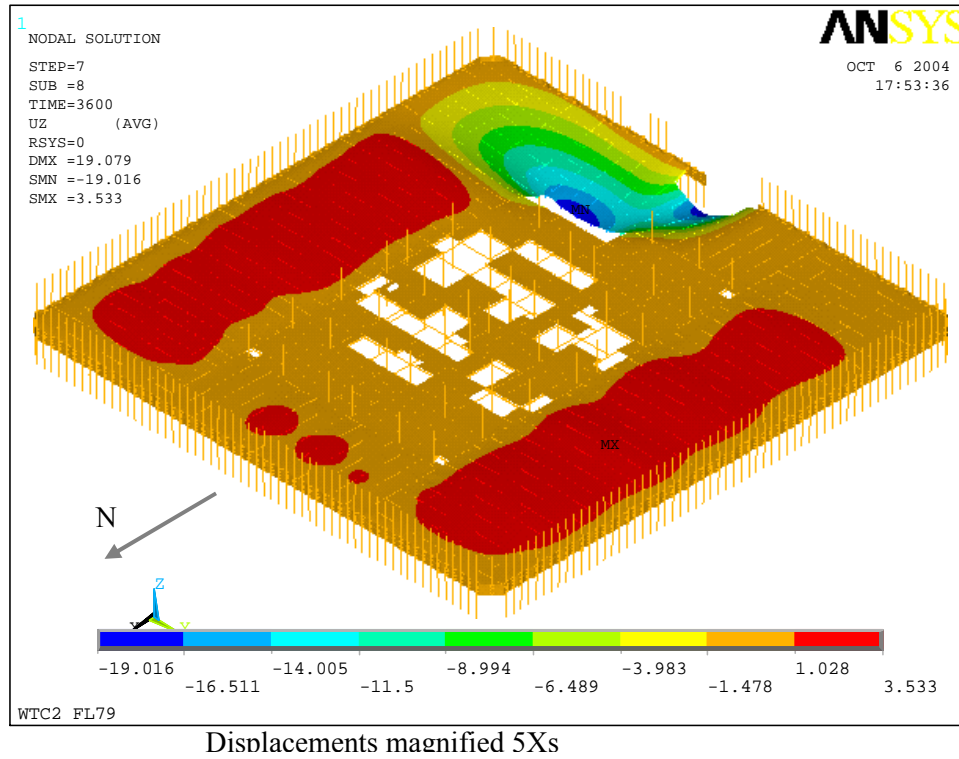


Figure 7–17. Vertical deflection of WTC 2 Floor 79 for Case C_i at 60 min.

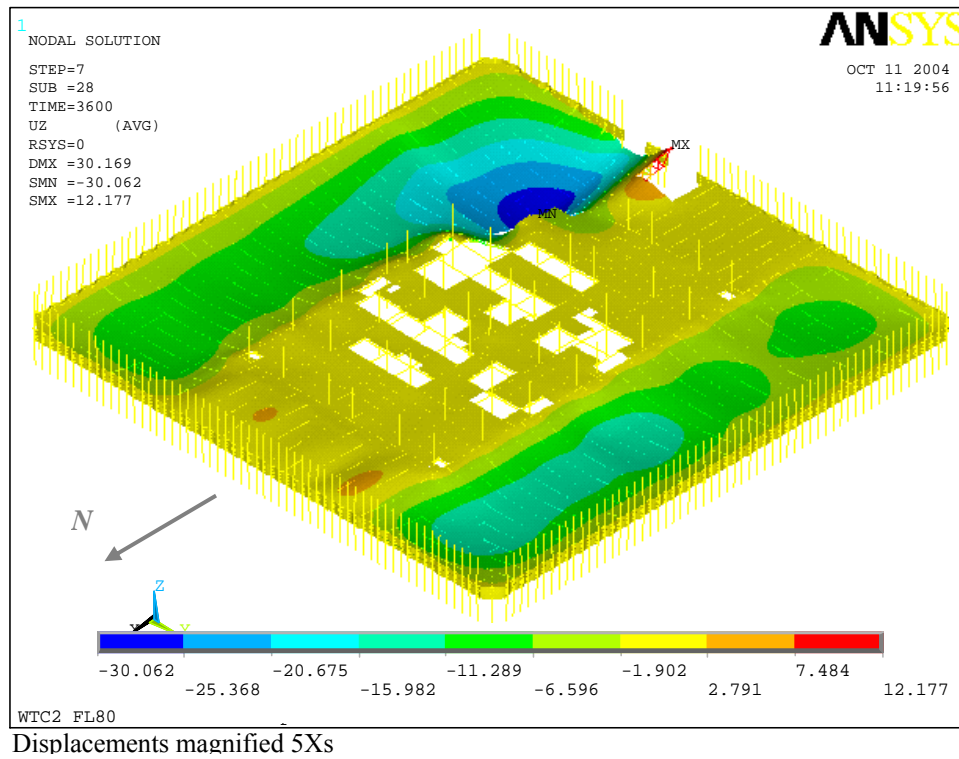


Figure 7–18. Vertical deflection of WTC 2 Floor 80 for Case C_i at 60 min.

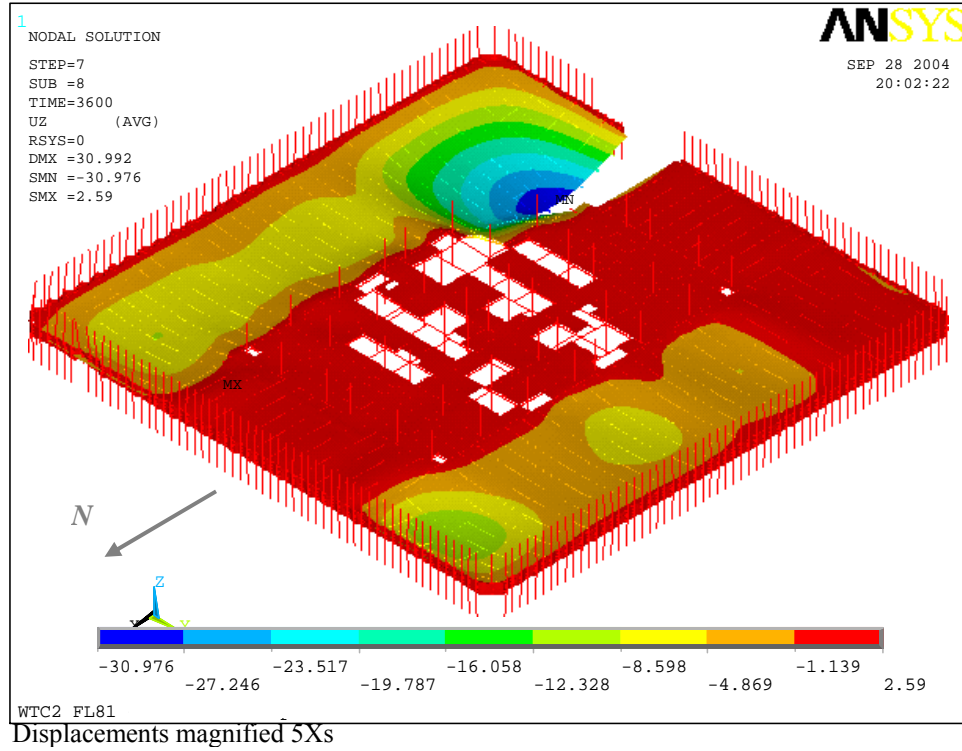


Figure 7–19. Vertical deflection of WTC 2 Floor 81 for Case C_i at 60 min.

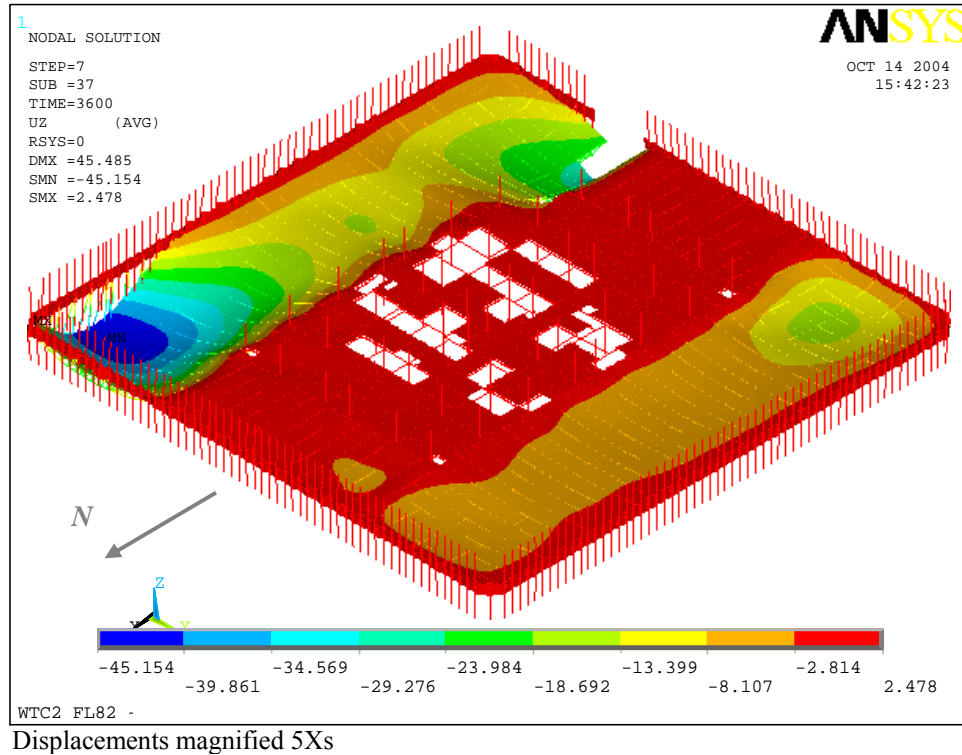


Figure 7–20. Vertical deflection of WTC 2 Floor 82 for Case C_i at 60 min.

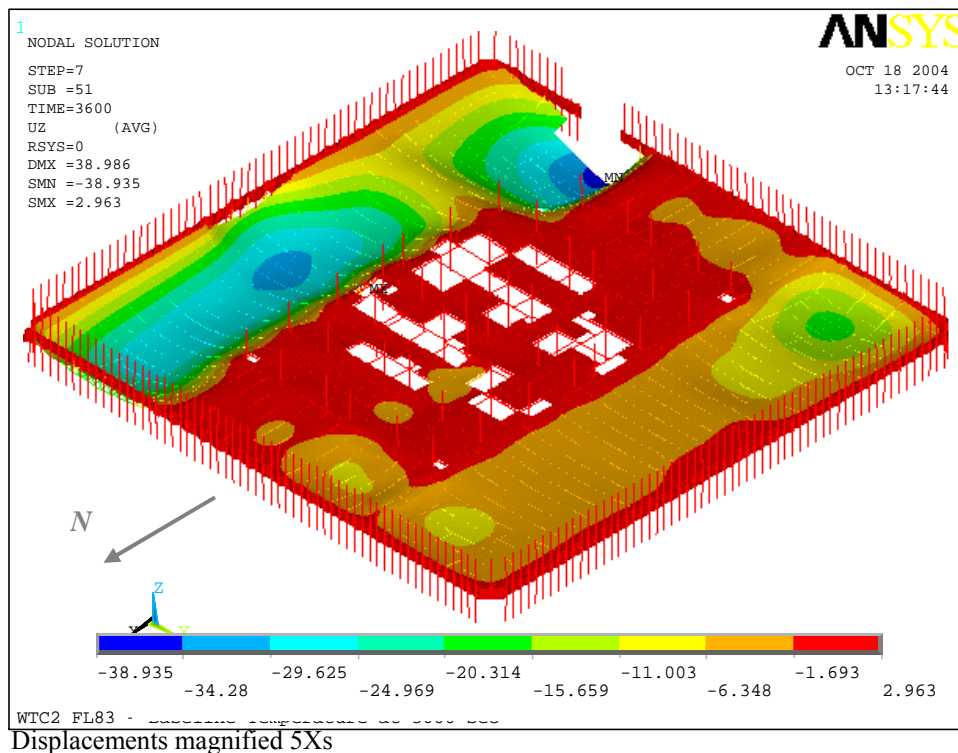
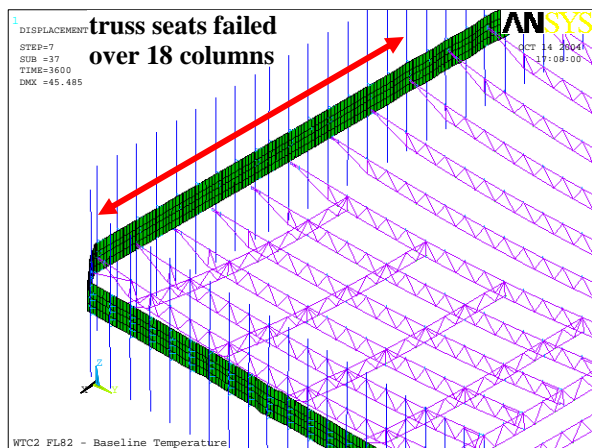
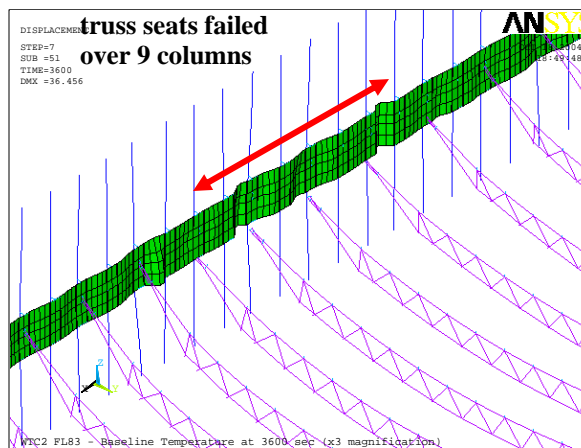


Figure 7–21. Vertical deflection of WTC 2 Floor 83 for Case C_i at 60 min.



(a) Floor 82



(b) Floor 83
(3X displacement magnification)

Figure 7–22. Loss of vertical supports in WTC 2 Floor 82 and Floor 83 for Case C_i.

Case D_i

Table 7–4 lists the maximum vertical displacement of WTC 2 floors for Case D_i, and Figs. 7–23 through 7–27 show the vertical displacement contours at time of maximum displacement for Floors 79 to 83. Floors 79 to 83 had impact damage at the southeast floor area, but Floors 80 and 81 had many interior truss seats severed from the south exterior wall to the east side of the core perimeter. As Case D_i had more impact damage near the southeast corner of the core than did Case C_i, Floors 80 and 81 had much greater vertical deflections. At 50 min they were 66 in. and 97 in., respectively, in the southeast floor area. The maximum temperatures were similar for Case C_i and Case D_i, but differences in times and locations of maximum temperatures led to differences in locations of maximum vertical displacements. Bridging trusses that had been removed in Case C_i were replaced in Floors 80 and 81 to provide support to the primary trusses in the single-span (one-way) floor area during greater vertical deflections.

The slab expansion across the entire floor ranged from 1 in. to 5 in. Gusset plates and bolts at more than 75 percent of all the exterior seats along the east face of Floors 82 and 83 failed. These connection failures were due to horizontal shear, parallel to the exterior wall, which was caused by differential thermal expansion between the floor framing, the floor slab, and the exterior wall. The truss at Column 357 of Floor 81 was the only one that lost its vertical support at the exterior seat among all the floors. This truss walked off the truss seat.

Several columns along the east and west sides of Floor 80 were pulled inward by the floor sagging in the southeast area. (The inward pull on the west face was due to the lack of horizontal restraint for the core columns in the floor model; in the global model, the inward pull would be resisted by the core. The west face inward pull was not applied in the global model). Floor 79 and Floor 81 showed similar behaviors to Floor 80 in terms of column horizontal reaction forces. Many columns of the west face of Floor 82 were pulled inward, while reaction forces at many columns of the east face were close to zero. As described above, gusset plates and seat bolts failed at a number trusses on the east face of Floor 82. Because columns at these locations were not supported in the horizontal direction by the floor, the reaction force became zero at these columns.

Table 7–4. Maximum vertical displacement of WTC 2 floors for Case D_i.

| Floor | Maximum Displacement (in) | Location of Displacement on East Floor | Time After Aircraft Impact (min) |
|-------|---------------------------|--|----------------------------------|
| 79 | 35.8 | South side | 60 |
| 80 | 65.6 | South side | 40 |
| 81 | 96.7 | South side | 50 |
| 82 | 49.4 | South side | 60 |
| 83 | 44.6 | South side | 60 |

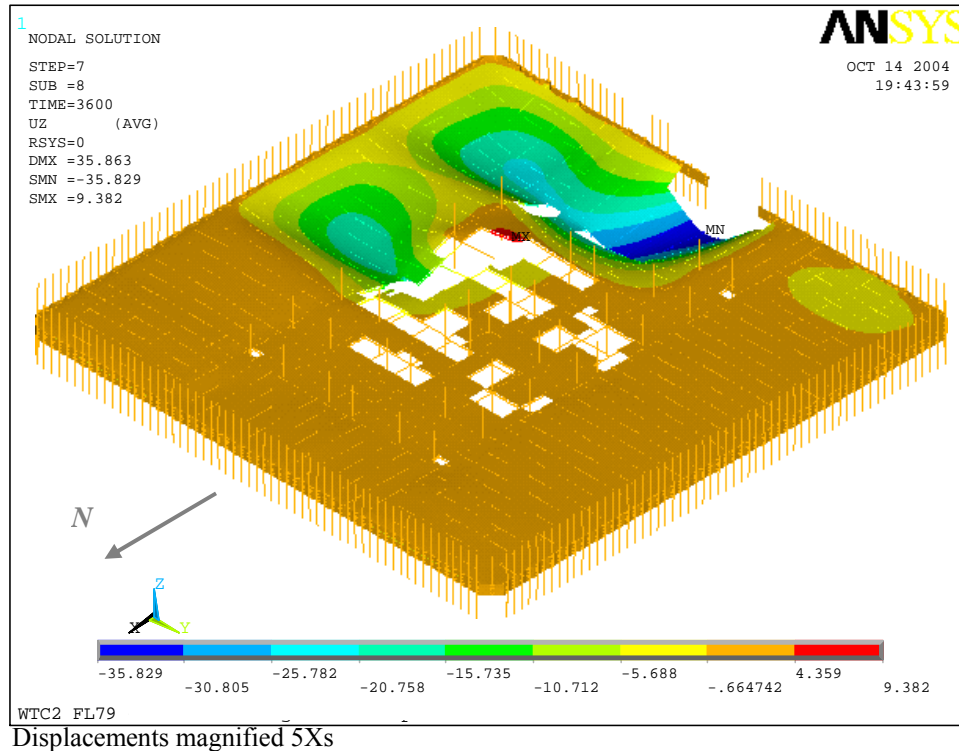


Figure 7–23. Vertical deflection of WTC 2 Floor 79 for Case D_i.

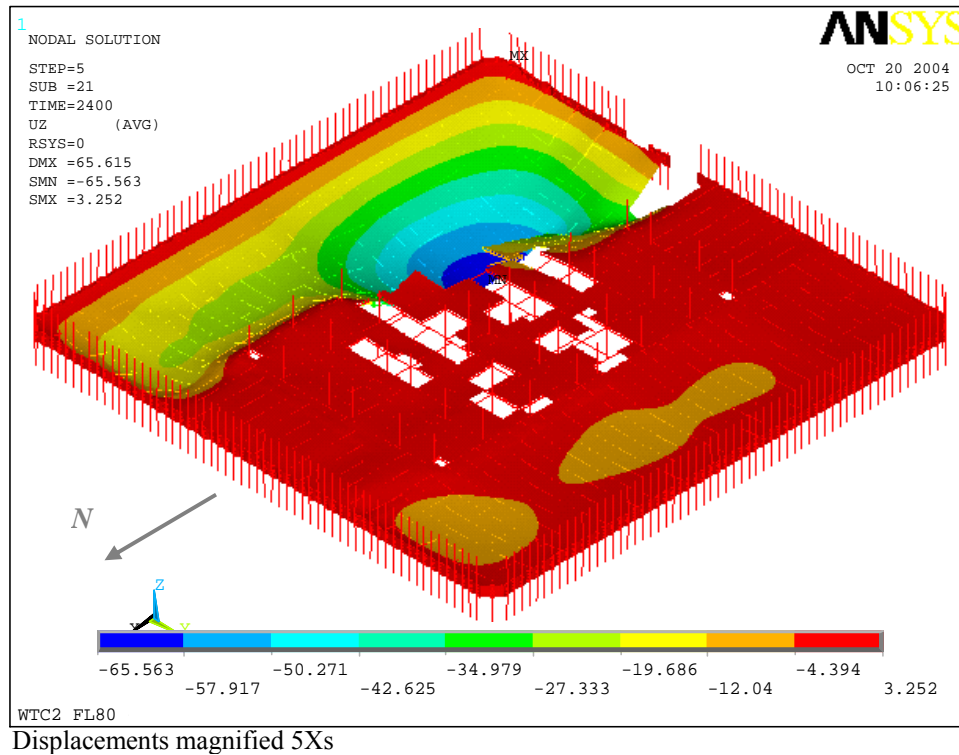


Figure 7–24. Vertical deflection of WTC 2 Floor 80 for Case D_i.

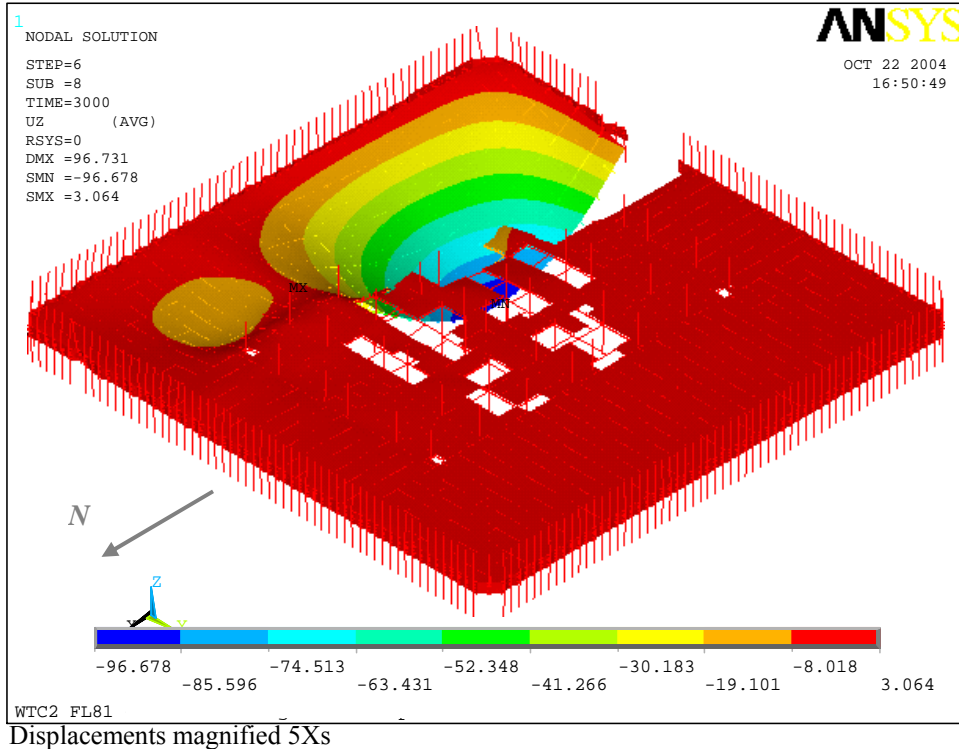


Figure 7–25. Vertical deflection of WTC 2 Floor 81 for Case D_i.

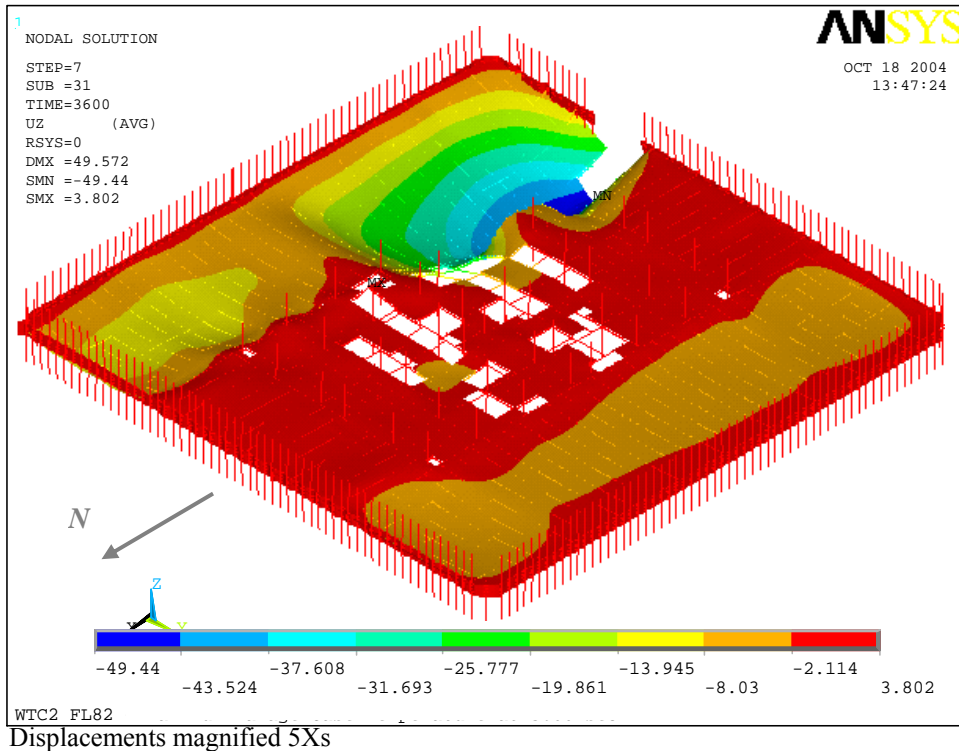


Figure 7–26. Vertical deflection of WTC 2 Floor 82 for Case D_i.

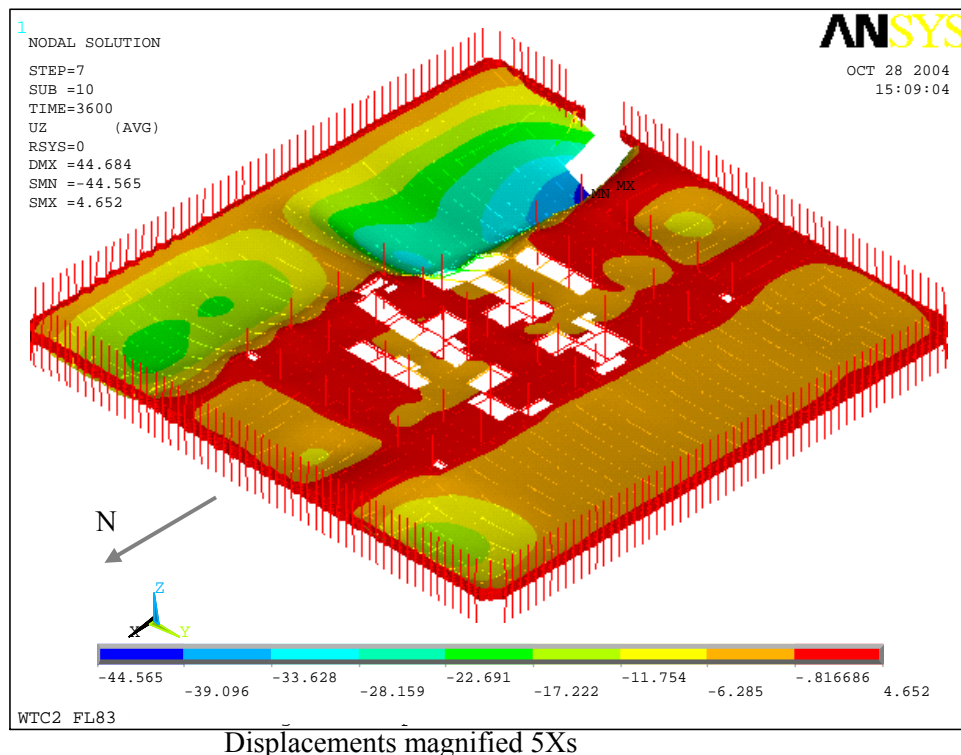


Figure 7–27. Vertical deflection of WTC 2 Floor 83 for Case D_i.

7.4 EXTERIOR WALL SUBSYSTEM

The primary function of the exterior walls of the WTC towers was to resist wind loads, but they also carried approximately 50 percent of the building gravity loads. For the WTC tower response to impact damage and ensuing fires, the performance of the exterior wall under gravity loads was of interest and is addressed in this section. NIST NCSTAR 1-2 addresses the performance of the exterior wall under gravity and wind loads.

The exterior wall was assembled with panels that were 3 stories high and 3 columns wide with spandrel beams at each floor level. Adjacent panels were staggered by one floor to avoid alignment of the bolted panel connections across a given floor level. Panel geometry was generally uniform at the upper stories of the towers, but the steel grade and plate thickness varied within and between panels, depending upon a panel's location in the tower face. Examination of structural drawings showed that the plates at the impact floors had the same yield strength. Therefore, in the translation process, all plates in the same column cross section were considered to be of the same material. Panel connections were designed for compressive and tensile loads.

Floor trusses were attached to every other column, with the same set of columns loaded at every floor. The exterior columns and deep spandrel beams resulted in a rigid frame that was efficient at redistributing loads in the plane of the wall. The columns redistributed their loads within three to four floors. The floors and spandrels provided lateral support to the exterior columns. Loss of lateral support through failed floor connections increases the possibility of column instability (buckling), depending upon a column's load and temperatures. The hat truss was connected to each exterior wall at Floor 108 with four

truss members extending from the core perimeter. The hat truss provided a load path between the core and exterior walls. As discussed previously, the hat truss was the primary load path between the core and exterior walls, and the floors provided a secondary load path.

The analysis of a single exterior face provided insight into the conditions that would result in the inward bowing of the south wall of WTC 1 and the east wall of WTC 2 observed in photographs (see Chapter 6). Conditions examined included pull-in forces resulting from sagging floors, disconnected floors resulting from truss seat failure, additional vertical loads simulating load transfer to the exterior wall, and elevated temperatures.

7.4.1 Finite Element Model and Methods of Analysis

The exterior wall models extended over 18 floors for the full width of a single face and were centered around the areas of impact and fire damage. The south face of WTC 1 extended from Floor 89 to Floor 106, and the east face of WTC 2 extended from Floor 73 to Floor 90, as shown in Fig. 7–28. The exterior panel that was severed during the aircraft impact and found south of the tower was removed from the south face of WTC 1. No structural damage to the panels was observed on the east wall of WTC 2. The same boundary conditions were applied for both exterior wall models, shown in Fig. 7–29. Springs were included at the base of the global models to represent the response of the exterior wall below the model. The exterior wall models included temperature-dependent plasticity, creep, and plastic buckling behavior.

The exterior wall models were first analyzed for gravity loads with aircraft impact damage. The loads in the columns right after aircraft impact included a set of axial forces at the top of the isolated wall model that accounted for the columns above the top of the model. These loads were taken from an initial global model that did not include creep or column buckling. This global model is further described in NIST NCSTAR 1-6C. Floor gravity loads were also applied at each column with a floor connection.

The exterior wall models were then subjected to two temperature conditions for each tower: Case A and Case B for WTC 1 and Case C and Case D for WTC 2. Elevated temperatures were applied to the wall structure in 10 min intervals, as described previously. At the beginning of each 10 min interval, floor connections were either (1) disconnected where observed in photographs and videos or computed in the full floor analyses, or (2) loaded with an inward force where inward bowing was observed during that time interval. At later stages of the WTC 2 analysis, where additional floor disconnection occurred, the inward pull at that connection was removed.

Temperatures of structural components were based upon the combined effects of member size, fireproofing damage, and fire size and duration. For the exterior columns and spandrels, the interior face was heated directly by fires through radiation and convection and the adjacent faces were heated through conduction and cooled by convection. Elevated temperatures caused thermal expansion of heated columns and modified the stresses in affected and adjacent structural members. Elevated temperatures above 400 °C to 500 °C resulted in a reduction of load-carrying capacity and an increase in plastic and creep deformations.

Inward pulling forces were estimated through a trial and error procedure. In each trial, a magnitude of inward pull force was assumed and the model results were checked. The magnitude was kept constant until the end of the analyses unless a floor connection became disconnected (see Section 7.3), at which point the inward pulling force was set to zero. The inward bowing displacements were compared to the

displacements measured from photographs at the same time points. The wall response was significantly affected by accumulated plastic and creep strains, which were themselves functions of temperature and inward pull over time.

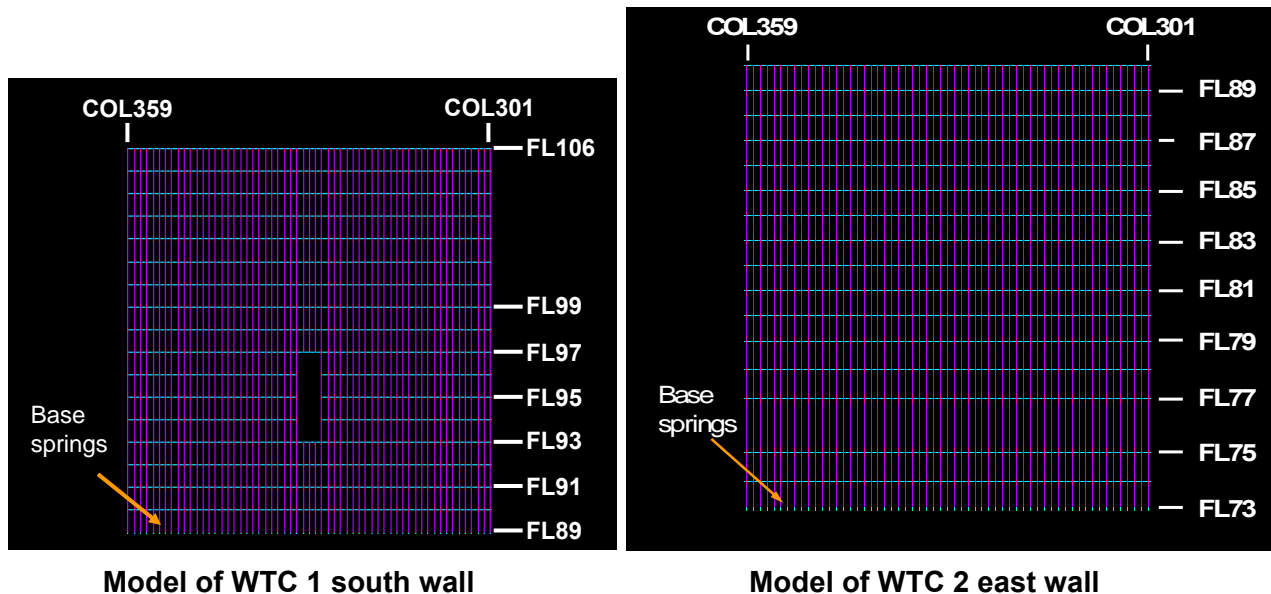


Figure 7–28. Isolated exterior wall segments from WTC 1 and WTC 2.

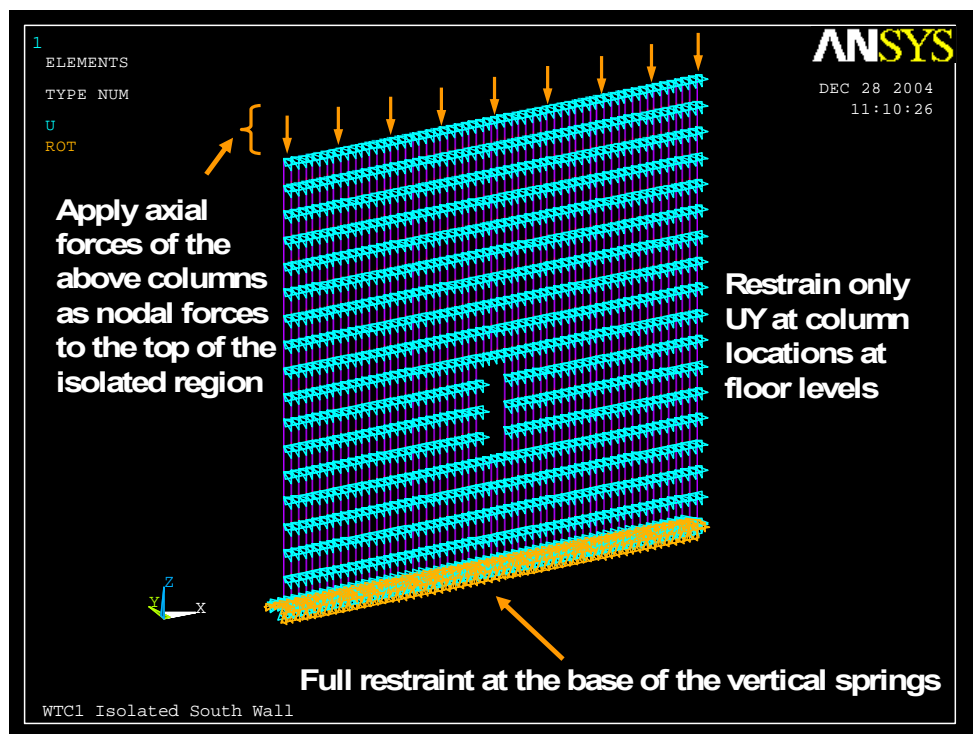


Figure 7–29. Boundary conditions applied on the isolated exterior wall segment.

7.4.2 WTC 1 Analysis Results

The magnitude and distribution of inward pull forces on the south wall, which resulted in inward bowing similar to that observed in photographs, were estimated from the WTC 1 exterior wall subsystem analyses. The final magnitude thus obtained was used in the WTC 1 global analysis.

Initial trials with Case A and Case B damage and temperatures limited pull-in forces to areas with floor sagging sufficient in the full floor models to cause pull-in forces. However, such limited areas of pull-in forces did not produce results that were consistent with the observed inward bowing. This was primarily due to the lack of fireproofing damage to the south exterior wall and floor truss on the south side in Case A impact damage estimates. With the thermally equivalent 2.2 in. of fireproofing intact on the south trusses, these trusses did not heat appreciably, and the floors did not sag.

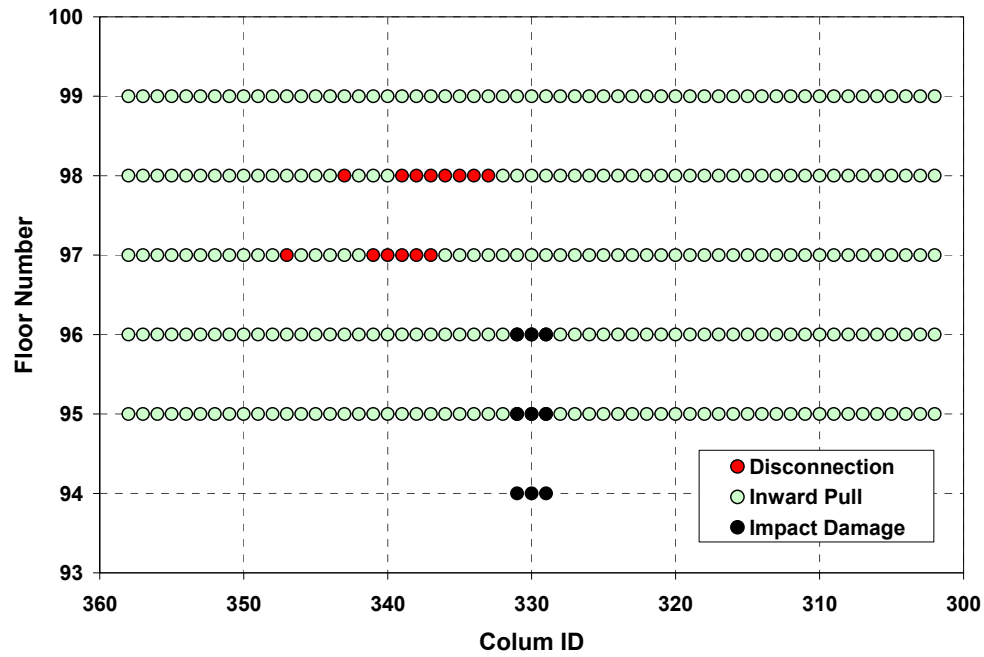
Case B had elevated temperatures for the south floor trusses and exterior columns where fireproofing was damaged between Floors 94 and 98. A second set of trials applied a pull-in force uniformly across Floors 95 to 99, except where the floor connections had failed. This extent of pull-in forces from floor sagging was greater than that shown by the full floor analyses, but produced a better estimate of the inward bowing as evidenced from the photographs. The smaller extent of floor sagging in Floors 95 to 99 that was predicted by the full floor analyses was likely due to the conservative estimates of fireproofing damage. This assumption produced a lower bound on the bare steel surface area, thereby making it more difficult to heat the steel to the point of failure. Greater fireproofing damage from structural accelerations caused by the aircraft impact and subsequent vibrations as well as possible damage to the concrete slab from high thermal gradients near the slab surface may have contributed to the more extensive inward bowing of the exterior wall that was observed.

In one trial, the magnitude of the pull-in force was increased over time until the the wall became unstable at 90 min. When the magnitude of the pull-in force reached 9.37 kip per column, the analysis stopped due to non-convergence. At the end of analysis, the maximum inward bowing was 24.7 in.

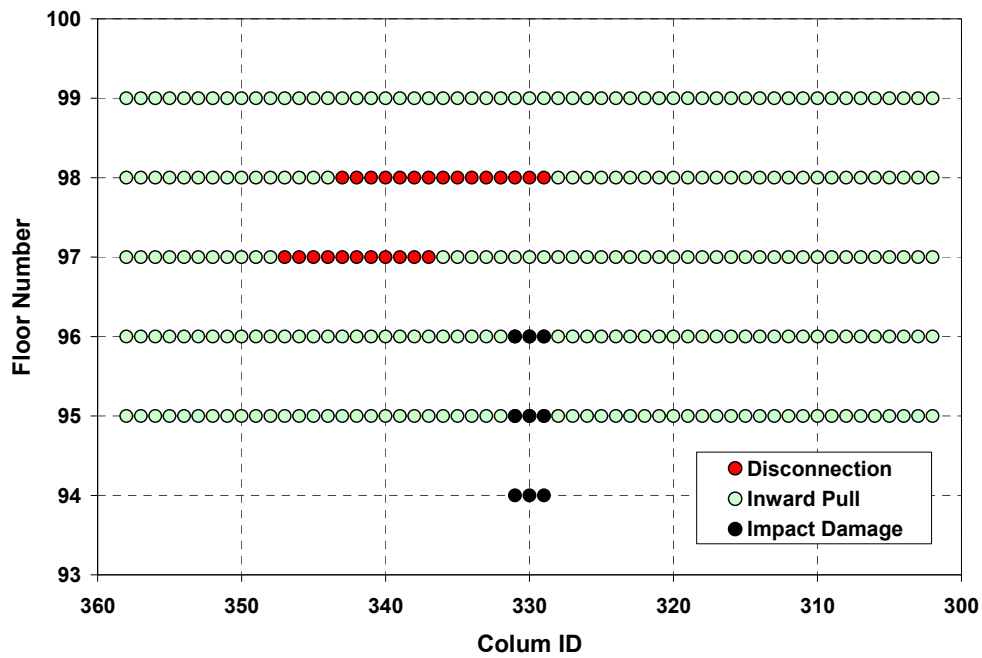
In another trial, the effect of thermal loading in combination with pull-in forces was examined. Pull-in forces were applied at 80 min, since temperatures on the south side began to increase around that time, and the thermal loading was continued to 100 min. In this analysis, the magnitude of the pull-in force was set to 6 kip per column so that the wall would not become unstable as a result of pull-in forces alone.

Figure 7–30 shows the locations of floor disconnections and pull-in forces. After applying a 6 kip pull-in force per column from 80 min to 100 min, the maximum inward bowing increased from 12.2 in. to 31.3 in., as shown in Figs. 7–31 and 7–32. This analysis demonstrated that the thermal softening increased existing inward bowing. Analysis results also showed that, at 100 min, Columns 320 to 346 had reached their load capacity for their plastically buckled shape and steel temperatures and were shedding their loads to adjacent columns.

The maximum inward bowing of 31 in. was smaller than the observed maximum bowing of 55 in., and the bowed wall was still stable in the analysis at 100 min. The magnitude of pull-in forces was expected to be less than 6 kip in the global analysis with the addition of gravity loads from the core subsystem as it also weakened; therefore, pull-in forces of 4 kip to 5 kip were used in the global model analyses.



(a) Between 80 min and 90 min



(b) Between 90 min and 100 min

Figure 7–30. Locations of WTC 1 disconnections and pull-in forces over five floors for Case B.

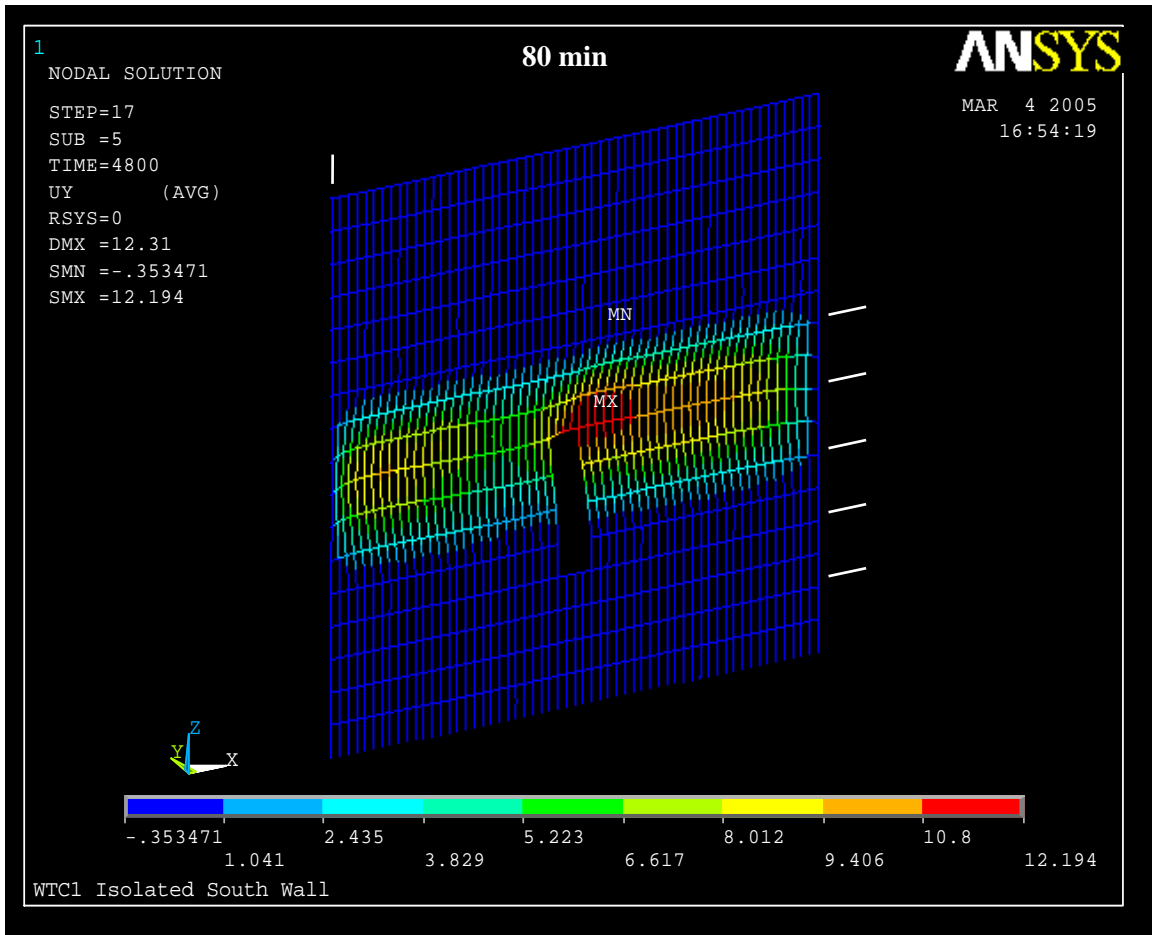


Figure 7–31. Inward displacement of the WTC 1 south wall at 80 min of the Case B temperatures with floor disconnections and 6 kip pull-in forces over five floors.

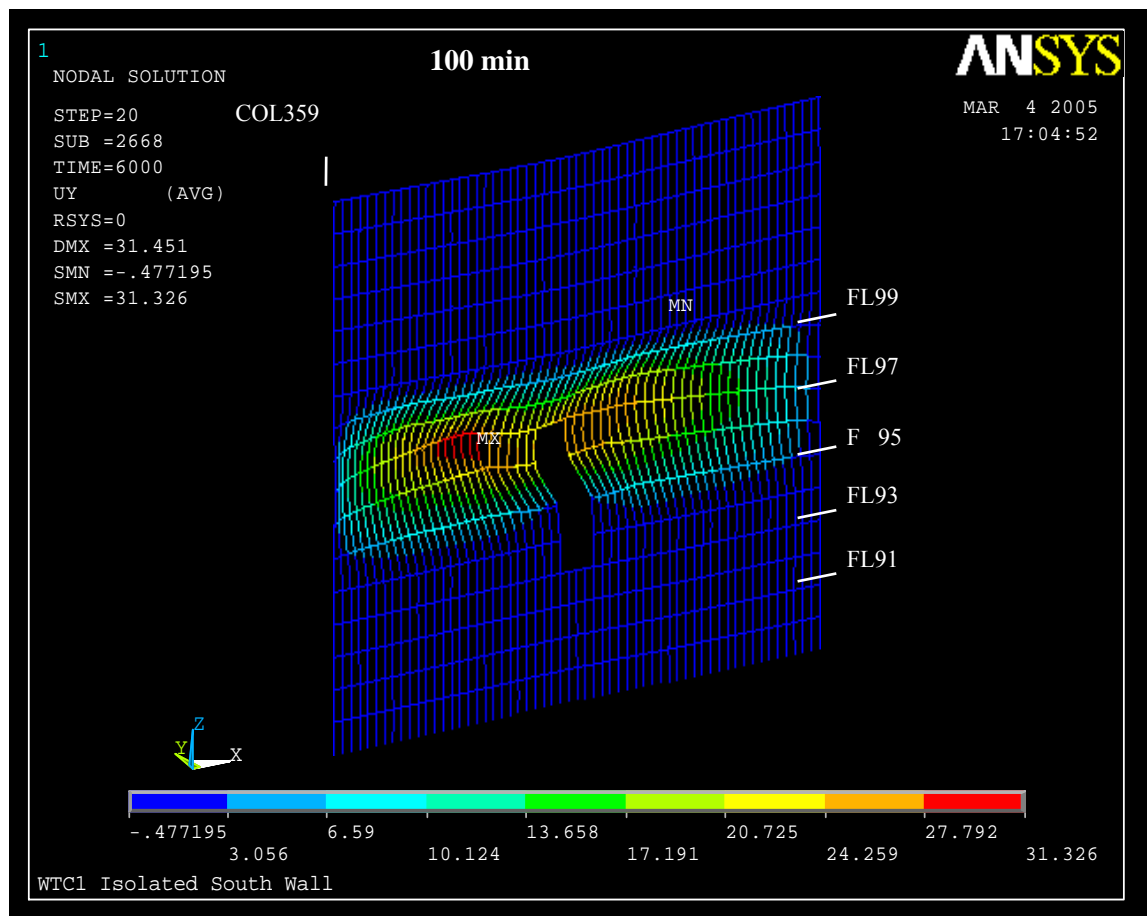


Figure 7–32. Inward displacement of the WTC 1 south wall at 100 min of the Case B temperatures with floor disconnections and 6 kip pull-in forces over five floors.

7.4.3 WTC 2 Analysis Results

The magnitude and distribution of inward pull forces on the east wall, which resulted in inward bowing similar to that observed in photographs at approximately 20 min and 50 min after the aircraft impact, were estimated with these analyses. The final estimated magnitude and distribution was used in the WTC 2 global analysis.

Initial trials with Case C and Case D damage and elevated temperatures limited pull-in forces to areas with floor sagging sufficient in the full floor models to cause pull-in forces. However, such limited areas of pull-in forces did not produce results that were compatible with the observed inward bowing. While damage to truss and exterior column fireproofing was similar for Cases C and D, the fire spread and growth was not the same and produced different temperature histories for structural elements. Case C full floor models sagged and had pull-in forces at the north side of the east wall, whereas Case D had floor sagging and pull-in forces at the south side of the east wall. Review of full floor model results showed that Case D temperature histories more closely matched the observed inward bowing of the east face. Case D was used for the global analyses.

A second set of trials with Case D elevated temperatures applied a pull-in force uniformly across Floors 79 to 83 of the east wall, except where the floor connections had failed. In two separate analyses, pull-in forces of 0.5 kip and 5 kip were held constant as the temperature histories were applied until the analysis failed to converge. The analysis with the 0.5 kip pull-in force failed to converge at 32 min. As shown in Fig. 7–33, the wall bowed primarily outward (positive displacement direction is inward) as the pull-in force was insufficient to cause inward bowing. The analysis with the 5.0 kip pull-in force failed to converge at 18 min. The inward bowing of the exterior wall had reached 31 in., as shown in Fig. 7–34. This value is about three times larger than the 10 in. displacement measured in photographs at this time, indicating that the assumed value of pull-in force was too large. Based on these two analyses, it was concluded that the magnitude of the pull-in force for a uniform distribution was bounded by 0.5 kip and 5.0 kip. This range for the pull-in force is of the same order of magnitude as the tension calculated from the detailed truss model (see Chapter 4).

The out-of-plane displacements shown in Fig. 7–33 at 20 min were inward on the south side and outward in the middle and north section of the wall. This difference in behavior was due to the combined effects of column temperatures and column loads across the east wall. Temperatures were higher at the middle and north half of the wall compared to the area near the southeast corner. The primary reasons for the outward bowing on the north side of the east wall are as follows: (1) the higher temperatures in the north side of the wall resulted in restrained thermal expansion and larger column loads; (2) the higher temperatures of the inside face of the columns, relative to the outside, caused higher plastic and creep strains and resulted in differential shortening of the inside relative to the outside; and (3) the plastic softening and creep of the inside caused an outward shift in the neutral axis, and a resulting outward bow of the columns.

This observation formed the basis for the next set of trials, where a step function was used to represent the distribution of pull-in forces along the east wall. In each trial, the magnitude of pull-in force for each half of the wall was assigned independently, with a higher magnitude on the north half of the east wall.

Two additional trials were analyzed. In the first trial, the magnitude of the pull-in forces was set to 1.0 kip and 4.0 kip for the south and north halves of the east wall, respectively. Figure 7–35 shows the out-of-plane displacements at 20 min and 50 min. As can be seen, the maximum inward bow calculated at 20 min was 7.5 in. and located near the middle of Floor 81. This agreed well with the measured displacements, which showed a maximum inward displacement of 10 in. near the middle of Floor 81.

The inward bowing started to decrease with time after 20 min and at around 40 min changed to outward bowing. The bowing at 50 min was mostly outward and did not agree with the measured displacements at this time. This indicated that the assumed magnitudes of the applied pull-in force were smaller than the actual pull-in force on the east wall.

In the second trial, the magnitude of the pull-in force was increased to 1.5 kip and 5.0 kip on the south and north portions of the east wall, respectively. Temperature histories were applied up to 50 min, at which point the analysis failed to converge. Figure 7–36 shows the magnitude of inward bowing at 20 min and at 50 min. The maximum inward bowing calculated at 20 min was 9.5 in. near the middle of Floor 81. This observation agreed well with the 10 in. measured displacements at that time. The inward bowing continued to increase with increasing time and reached a maximum of 37 in. at 50 min. As seen in Fig. 7–30, the location of the maximum displacements agreed well with the observations, but the calculated magnitude of 37 in. was twice as large as the measured inward displacement of 20 in.

This indicated that the magnitude of the applied pull-in force was close to the two sets of values assumed for the step function distribution, 1.0 kip to 1.5 kip and 4.0 kip to 5.0 kip on the south and north portions of the east wall, respectively. Considering the possible increase in column loads after impact for Case D conditions, a pull-in force of 1.0 kip on the south half and 4.0 kip on the north half of the east wall was selected as the initial estimate for the WTC 2 global model analysis.

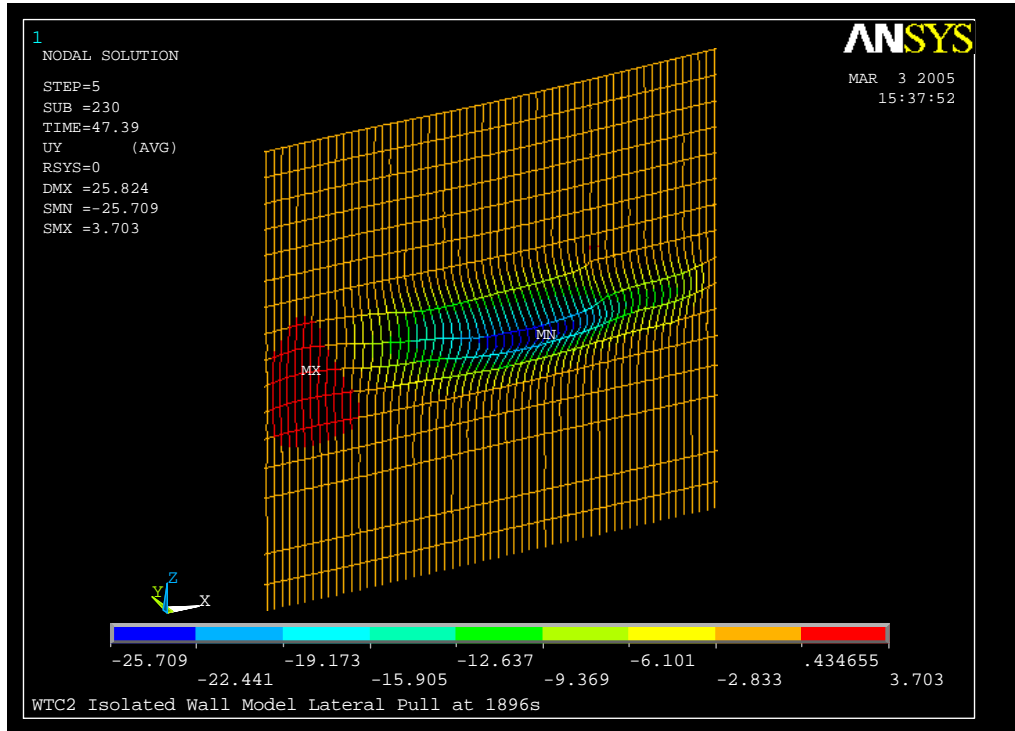


Figure 7–33. Out-of-plane displacements of the WTC 2 east wall calculated with 0.5 kip pull-in force with uniform magnitude distribution at 32 min.

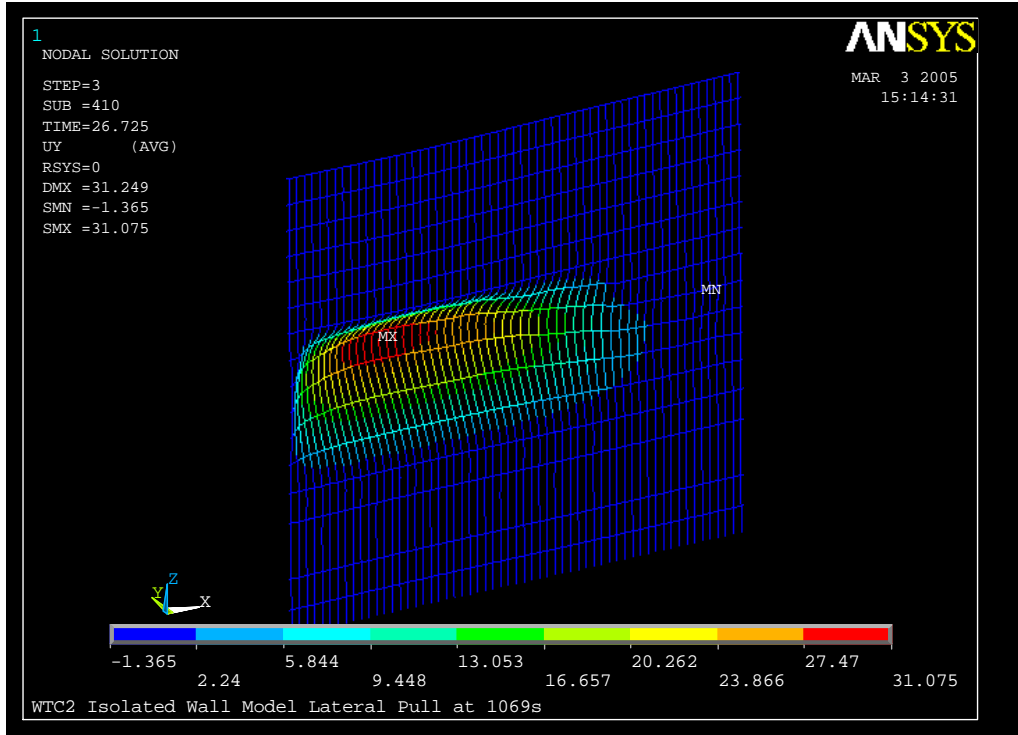
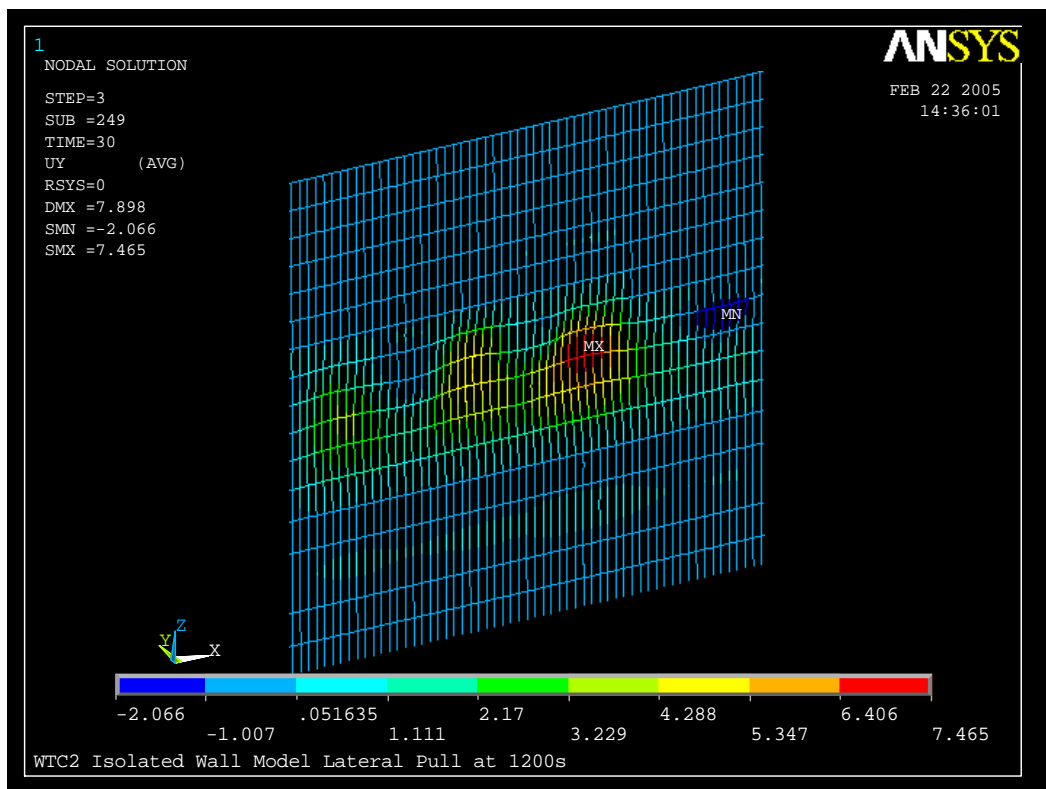
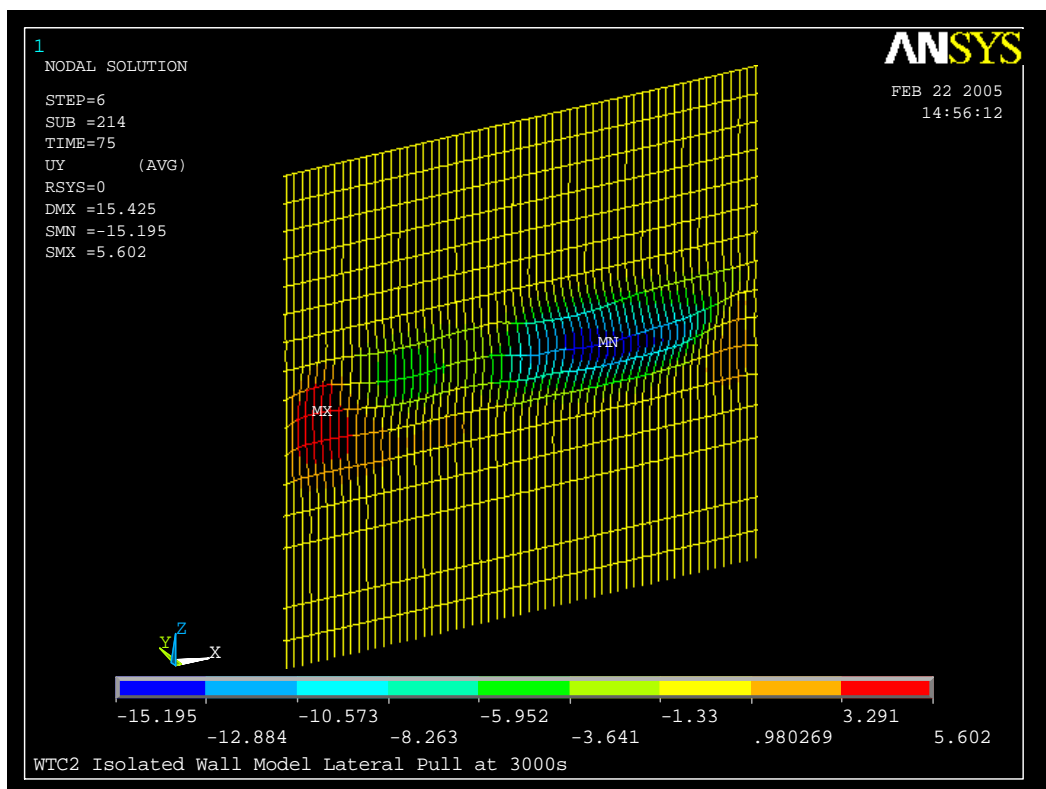


Figure 7–34. Out-of-plane displacements of the WTC 2 east wall calculated with 5.0 kip pull-in force with uniform magnitude distribution at 18 min.



At 20 min



At 50 min

Figure 7–35. Out-of-plane displacements of east wall calculated with pull-in force of 1.0 kip on the south half and 4.0 kip on the north half of the WTC 2 east wall.

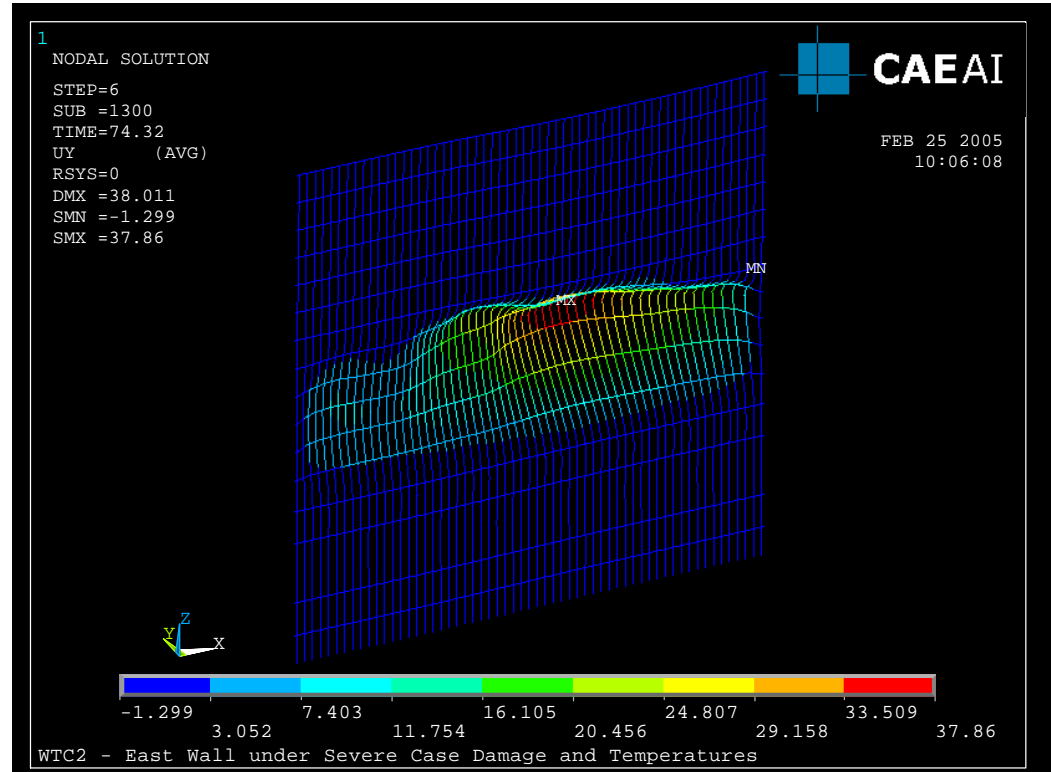
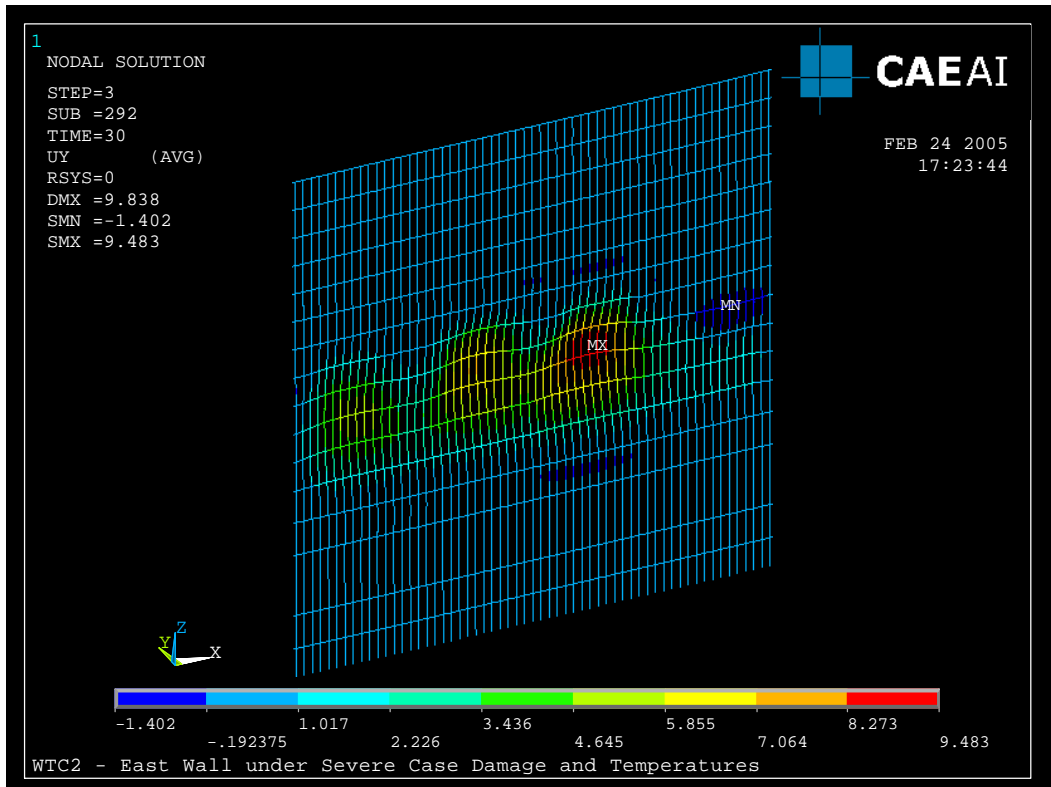


Figure 7-36. Out-of-plane displacements of east wall of WTC 2 calculated with pull-in forces of 1.5 kip on the south half and 5.0 kip on the north half.

7.5 SUMMARY OF SUBSYSTEM ANALYSES

The structural response of the isolated major subsystems (core, full floor, and exterior wall) to aircraft impact damage and fire are summarized here. These responses provided insight for the global model and results analysis.

Core Subsystem

- If core column connections to the hat truss failed, the core subsystem may have experienced large vertical deflections in the local area of the connection failure due to loss of the primary load path for the redistribution of loads and subsequent column plastic buckling and/or plastic and creep deformations.
- The WTC 1 isolated core subsystem was stable with Case A aircraft impact damage and gravity loads.
- To reach a stable solution for Case C structural damage and gravity loads, the WTC 2 isolated core model required horizontal restraints to be added in the east and south directions at each floor representing the lateral restraint provided by the office area floors. Without the horizontal restraints, the WTC 2 core model tilted significantly due to the severed columns in the southeast corner of the core.
- The isolated core models did not converge for WTC 1 Case B and WTC 2 Case D structural impact damage, which had more severed columns than Case A and Case C, respectively. The core needed to redistribute loads to other areas in the global system for a stable solution with Case B and Case D damage.
- The WTC 1 isolated core subsystem with Case A impact damage and Case B temperature histories resulted in column buckling between Floors 94 and 98 and a 44 in. vertical displacement at the center of the south side of the core. The core structure was most weakened from impact and thermal effects at the center of the south side of the core. Smaller displacements occurred in the global model due to the constraints of the hat truss and floors.
- The WTC 2 isolated core subsystem with Case C impact damage and Case D temperature histories resulted in an 8.1 in. vertical displacement at the southeast corner. Without the horizontal restraints, the core would have tilted more toward the southeast corner, and the vertical displacement would have been larger. No columns buckled. The core structure was weakened from impact and thermal effects at the southeast corner and along the east side of the core.

Full Floor Subsystem

- Final damage Cases A, B, C, and D were completed after the initial set of floor analyses were conducted with Cases A_i, B_i, C_i, and D_i. The fires did not change between initial Cases A_i to D_i and final Cases A to D. The concrete slab temperatures were the same for the initial and final Cases. The truss temperatures changed where the fireproofing damage changed. The full floor models were not rerun for Cases A through D as comparisons showed that the

structural temperature histories of the floors were nearly identical for most floors and only slightly different for a few floors. The floor analysis results for Cases A_i to D_i were used for Cases A to D in the exterior wall subsystem and global analyses.

- The full floor model boundary conditions for the exterior columns constrained thermal expansion of the concrete slab, which led to high compressive forces in the slabs, even with sagging of floors.
- At lower elevated temperatures (approximately 100 °C to 400 °C), the floors thermally expanded and displaced the exterior columns outward by a few inches; horizontal displacement of the core columns was insignificant. None of the floors buckled as they thermally expanded, even with the exterior columns restrained so that no horizontal movement was allowed at the floors above and below the heated floor, which maximized column resistance to floor expansion. Even with level of column restraint, the exterior columns did not develop a sufficient reaction force (push inward to resist the expansion outward) to buckle any of the floors.
- At higher elevated temperatures (above 400 °C), the floors began to sag as the floors' stiffness and strength were reduced with increasing temperature and the difference in thermal expansion between the trusses and the concrete slab became larger. As the floor sagging increased, the outward displacement of the exterior columns was overcome, and the floors exerted an inward pull force on the exterior columns.
- The floors began to exert inward pull forces when floor sagging exceeded approximately 25 in. for the 60 ft floor span. This is based upon analysis results of both the detailed truss model and the full floor models (which showed a reduction in compression instead of tension at the truss connections).
- Floor sagging was primarily caused by either buckling of truss web diagonals or disconnection of truss seats at the exterior wall or the core perimeter. Except for the truss seat failures near the southeast corner of the core in WTC 2 following the aircraft impact, web buckling or truss seat failure was caused primarily by elevated temperatures of the structural components.
- Sagging at the floor edge was due to loss of vertical support at the truss seats. The loss of vertical support was caused by the reduction in vertical shear capacity of the truss seats due to elevated steel temperatures in most cases.
- When the gusset plates and bolts of the truss seat failed in the floor models due to horizontal loads, it was rare that the truss also walked-off of the seats because the thermal expansion of the floor was restrained by the exterior columns. The straps and studs at the exterior wall had been removed from the floor models, which provided additional resistance to horizontal loads; if the floor slab expansion had not been restrained by the exterior columns, the horizontal loads between the slab and gusset plate and bolt would have been reduced.
- The high surface temperatures in the concrete slabs of fire affected floors could have resulted in delamination by spalling of the slab. This would possibly compromise knuckle strength,

crack the slab, or cause loss of integrity of the floor system, contributing to greater floor sagging.

- Case B impact damage and thermal loads for WTC 1 floors resulted in floor sagging on the south side of the tower over floors that reasonably matched the location of inward bowing observed on the south face. Case A impact damage and thermal loads did not result in sagging on the south side of the floors.
- Case C and Case D impact damage and thermal loads for WTC 2 both resulted in floor sagging on the east side of the tower over floors that reasonably matched the location of inward bowing observed on the east face. However, Case D provided a better match.

Exterior Wall Subsystem

- Inward forces were required to produce inward bowing that was consistent with displacements measured from photographs. The inward pull was caused by sagging of the floors. Heating of the inside face of the perimeter columns also contributed to inward bowing. Thermal expansion occurred as soon as steel temperatures began to rise; column shortening occurred when creep and plastic strains overcame thermal expansion strains, typically at temperatures greater than 500 °C to 600 °C with accompanying high stresses and duration of temperatures and stress levels.
- Models of exterior wall sections bowed outward in a pushdown analysis when several consecutive floors were disconnected, the interior face of the columns was heated, and column gravity loads increased (e.g., due to load redistribution from the core and hat truss). At lower temperatures, thermal expansion of the inside face was insufficient to result in inward bowing of the entire exterior column. At higher temperatures, outward bowing resulted from the combined effects of reduced steel strength on the heated inside face, which shortened first under column gravity loads, and the lack of lateral restraint from the floors.
- The observed inward bowing of the exterior wall indicated that most of the floor connections must be intact to cause the observed bowing.
- The floor levels predicted to have damaged fireproofing in the aircraft impact analysis matched well with the floors that were identified from photographic and video analysis to have participated in the inward bowing of the exterior walls.
- The extent of floor sagging required at each floor was greater than that predicted by the full floor models. The estimates of the extent of sagging at each floor were governed by the combined effects of fireproofing damage and fire; fireproofing damage was limited to areas subject to direct debris impact. Other sources of floor damage from the aircraft impact and fires (e.g., fireproofing damage from structural accelerations at impact and subsequent strong vibrations or floor damage from concrete cracking and spalling from thermal effects) were not included in the floor models.
- The exterior wall models were used to estimate the pull-in force magnitude and locations for each tower that would produce the observed bowing of the exterior wall.

- The WTC 1 isolated exterior wall analysis found that an inward pull force of 6 kip at each column at Floors 95 to 99, starting 80 min after the aircraft impact, caused a maximum inward bowing of 31 in. This inward deflection was smaller than the observed maximum bowing of 55 in., and the bowed wall was stable at 100 min. The magnitude of pull-in forces was expected to be less than 6 kip in the global analysis with the addition of gravity loads from the core subsystem as it also weakened; therefore, pull-in forces of 4 kip to 5 kip were used in the global model analyses.
- The WTC 2 isolated exterior wall analysis found that an inward pull force of 1.0 kip to 1.5 kip and 4.0 kip to 5.0 kip on the south and north portions of the east wall, respectively, over Floors 79 to 83, caused a maximum inward bowing of 9.5 in. at 20 min and 37 in. at 50 min. The observed deflections were 10 in. and 20 in., respectively. Considering the possible increase in column loads after impact for Case D conditions, a pull-in force of 1.0 kip on the south half and 4.0 kip on the north half of the east wall was selected for the initial estimate for the WTC 2 global model analysis.

This page intentionally left blank.

Chapter 8

STRUCTURAL RESPONSE OF THE WTC TOWERS TO AIRCRAFT IMPACT DAMAGE AND FIRE

8.1 INTRODUCTION

Prior to conducting global analysis of the structural response of each World Trade Center (WTC) tower, a tremendous amount of input data was obtained² and developed. Input data required for the structural response models included:

- Reference model of each WTC tower before the aircraft impact, based upon design and construction documents (NIST NCSTAR 1-2)
- Steel and concrete material properties for room and elevated temperatures (NIST NCSTAR 1-3 and Chapter 4)
- Structural damage to columns and floors from the aircraft impact (NIST NCSTAR 1-2 and Chapter 5)
- Passive fire protection conditions before and after impact (NIST NCSTAR 1-6A and Chapter 5)
- Temperature histories for all structural elements in the impact zone (NIST NCSTAR 1-5)
- Observed structural conditions and events from photographic and videographic records (NIST NCSTAR 1-5A and Chapter 6)

Input data was based on available records. For data that were not directly available, analytical and experimental results were used to develop the required information. The tower design and construction and the supplied structural materials were well documented. The passive fire protection conditions before impact were less well documented, but review of Port Authority of New York and New Jersey (PANYNJ) records and interpretation of photographs (from several sources throughout the life of the structure) provided a documented basis for determining the likely conditions that existed in both towers before September 11, 2001. Steel and concrete temperature-dependent properties were developed from available technical literature and from tests of samples recovered from the collapse site (steel tests were conducted at National Institute of Standards and Technology (NIST) and concrete tests were conducted at Simpson Gumpertz & Heger, Inc. (SGH) under contract to NIST) to assess conformance with specified properties. Temperature histories were developed from fire dynamics simulations and thermal analyses conducted at NIST. The observed structural conditions and events defined the known events that occurred that day. The structural response analyses helped determine the probable collapse sequence for each tower. These sequences were validated using the observed structural events.

² All information and data related to the design and construction of the WTC towers were obtained from contract drawings provided to NIST by The Port Authority of New York and New Jersey. Refer to NIST NCSTAR 1-2A for a complete description of the WTC structural system and an index of all structural drawings.

The global analyses of WTC 1 and WTC 2 used final estimates of impact damage and elevated temperatures to determine the structural response and sequence of component and subsystem failures that led to collapse initiation. Case B was used for WTC 1 and Case D was used for WTC 2 used, as described in previous chapters.

The global models and required input data are discussed in Section 8.2. The analysis methodology is presented in Section 8.3, and the results of the global analyses for WTC 1 and WTC 2 are presented in Sections 8.4 and 8.5, respectively. To better understand the relative contributions of impact damage and fire to each tower collapse initiation, the hypothetical condition of the towers subjected to the same fires without aircraft impact damage is discussed in Section 8.6.

8.2 GLOBAL MODEL OF TOWERS

8.2.1 Model Description

The global model of each tower, which was used to determine the structural collapse sequence, was based on the reference structural models developed for baseline structural analyses of the towers (NIST NCSTAR 1-2). The reference models were developed with SAP2000 and were used as a common basis for the aircraft impact analysis, using LS-DYNA, and the structural response analysis, using ANSYS.

The SAP2000 global models were more detailed than models typically used for structural design purposes. The models included exterior and core columns, the hat truss, and mechanical floors, but did not explicitly model the tenant floors due to model size limitations. The tenant floors were accounted for with constraint equations and concentrated floor loads at floor-to-column connection nodes.

The reference global models for WTC 1 and WTC 2 were translated into ANSYS models using an automated translator developed specifically for this effort by Computer Aided Engineering Associates, Inc. (CAEA), as a subcontractor under the NIST contract to SGH. The coordinates of the nodes, cross-sectional properties of members including orientation and offset of the cross-section, nodal loads, material properties, and member end releases were automatically converted from the SAP2000 format to the ANSYS format as described in NIST NCSTAR 1-6C.

The ANSYS models were truncated several floors below the impact floors, as previous analyses showed that the structural response below the impact area remained elastic. WTC 1 was truncated at Floor 91, and WTC 2 was truncated at Floor 77. The axial stiffness of the remaining structure below the line of truncation was replaced with equivalent elastic springs. The global models of the two towers are shown in Fig. 8-1.

The truncated ANSYS global models were validated against the SAP2000 baseline global analyses for gravity loads. The results from the translated ANSYS global models showed good agreement with the baseline analyses: displacements were within 1.4 percent for WTC 1 and 0.7 percent for WTC 2, and base reactions were within 1.2 percent for WTC 1 and 0.3 percent for WTC 2. Based on these comparisons, it was concluded that the translation of the global models from SAP2000 to ANSYS was correct, and the ANSYS models and their derivatives were used for the global analyses. Details of the translation and validation are found in NIST NCSTAR 1-6C.

The core columns and exterior columns and spandrels were modeled with elements and features similar to those used in the isolated core and exterior wall analyses. Column analysis features included the effects of thermal expansion, plastic, and creep strains on column behavior within the global structural system. When thermally-induced strains were sufficiently large, column loads increased if they were restrained. Columns shortened and shed loads if either plastic or creep strains were large enough or if they buckled plastically. Plastic (or inelastic) buckling describes the condition where a column becomes bowed (displaced laterally between its ends) by plastic or creep strains, but continues to support a reduced axial load. As the bowing becomes larger, the column's capacity to carry load diminishes further (see Fig. 435) until the column no longer participates in carrying load in the global structure.

Floors in the global model were modeled by shell elements, which have their membrane stiffness equal to that of the full floor system. Floors in the global model functioned as diaphragms and transferred loads between the exterior wall system and the core. Office area and core floors were modeled with an equivalent floor slab thickness and modulus calculated to match the in-plane stiffness of the composite floor system, including the concrete slab, floor trusses, and the floor seats. Bending stiffness of the floor system was not matched because the floor loads were applied at the columns. Both core and office area floor slabs were modeled with linear-elastic material properties for lightweight concrete.

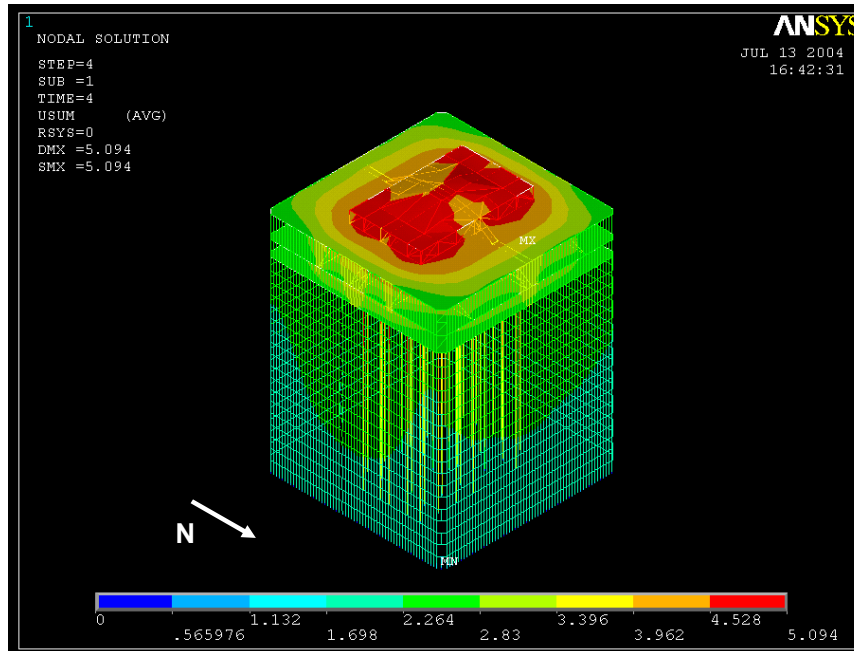
Figure 8–2 shows the model of the core and tenant floors and the core beams that had moment connections. Beams without moment connections cannot effectively transfer shear between columns without significant relative displacement and, thus, were not modeled individually. The stiffness of simply connected beams was smeared into that of the slab to capture the in-plane stiffness of the floor in the core. Inclusion of the core and office area floors was necessary for modeling force redistribution within the core and between the core and the exterior columns. The core was effective in redistributing loads from damaged core columns to adjacent core columns when the load path through the hat truss could not be developed due to either severed columns or column splices.

Floors in the global models were not intended to capture floor response and failure modes during fires. It was not practical, or in some cases not possible, to create computationally efficient global models that included all details of the floor system. The BEAM188/189 elements used in the full floor model caused severe convergence problems when creep was included and those elements experience thermally-induced buckling. Also, the extent of pull-in forces from sagging floors in the full floor models was less than estimated from the observed bowing of the exterior walls in photographs and videos because the aircraft impact damage to thermal insulation of the floors was conservatively estimated by limiting the dislodged thermal insulation to regions of direct debris impact.

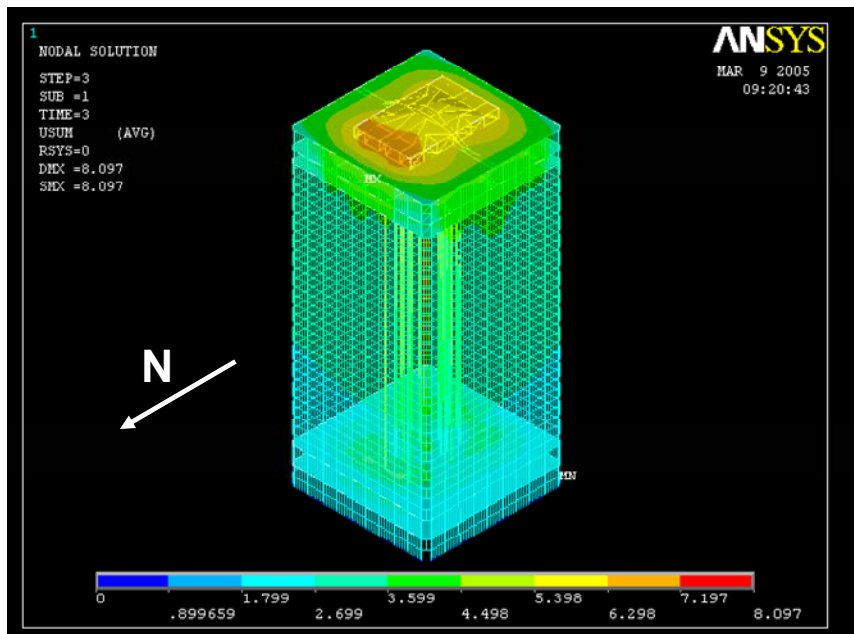
Important failure modes were identified in the truss and full floor analyses and incorporated into the global models as floor/wall disconnections and pull-in forces at appropriate time intervals. Since the full floor models did not accurately estimate the pull-in forces at floor/wall connections, the fire-induced damage obtained from the full floor model analyses were modified by observations obtained from the examination of photographs and videos performed by NIST (NIST NCSTAR 1-5A). See Chapter 7 in NIST NCSTAR 1-6C and Chapter 2 in NIST NCSTAR 1-6D for more details.

The global model included the hat truss at the top of each tower. The hat truss was designed to support an antenna on top of the towers and transmitted loads to both the core and exterior columns. The loads were distributed primarily to the core columns. There were four outriggers to each exterior wall that provided rotational restraint for the antenna under wind loads. In addition, the outriggers provided a secondary

load path between the core and exterior walls as determined from the structural response of the towers to impact damage and fires. Figure 8–3 shows the hat truss, with the outriggers labeled A through P. During the global structural response to impact and fire, the hat truss provided a primary path for transferring loads between the core columns and between the core and exterior walls.



(a) WTC 1 ANSYS Model Vertical Displacements



(b) WTC 2 ANSYS Model Vertical Displacements

Figure 8–1. Displaced shape of WTC 1 and WTC 2 at the end of gravity load analysis.

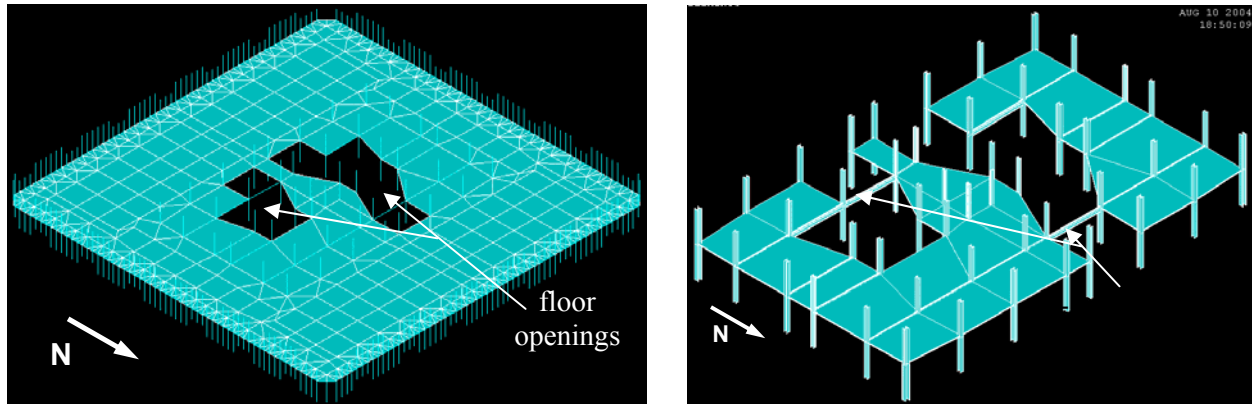


Figure 8-2. Office area and core floors and core beams.

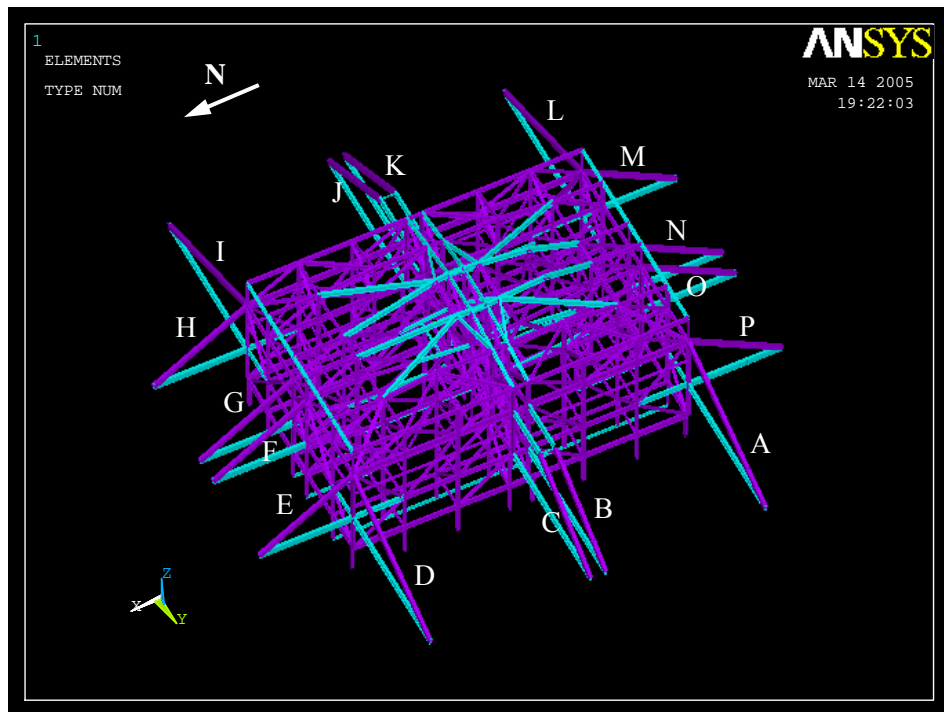


Figure 8-3. Hat truss with labeled outriggers.

8.2.2 Model Modifications

The validated ANSYS models were modified to incorporate nonlinear material and geometric behaviors required in areas subject to impact and fire. Modifications incorporated modeling enhancements and refined input data based on numerous component and subsystem analyses. Temperature-dependent modifications included material properties, coefficients of thermal expansion, plastic and creep strains. Nonlinear geometric behavior modifications included large displacements, plastic buckling and post-buckling of columns. Break elements were not included, based on the behaviors shown in the major subsystem analyses of the isolated core, exterior wall, and full floors. Break elements for knuckles, exterior wall bolted connections, and spandrel connections did not fail in the full floor and exterior wall

analyses. Truss seat connection failures were imposed during analyses according to the time they were calculated or observed to have occurred, rather than through use of break elements.

Preliminary global analyses had unacceptably slow rates of computation, due to the size of the models and the computational effects of temperature-dependent material properties, especially creep. To reduce the size of the global models and to increase the speed of the solution without adversely affecting the analysis results, modifications were made to the models to improve computational efficiency.

The spandrels were modeled with BEAM 188 elements which experienced convergence problems when thermal expansion caused them to buckle since there were not enough elements between two columns to capture the buckling detail. The buckling of spandrels did not compromise their ability to transfer shear and bending moment. Based on visual evidence, buckling of spandrels did not play an important role in the collapse sequence, and increasing the number of spandrel elements would have unnecessarily increased the model size. Therefore, the coefficient of thermal expansion for spandrels was set to zero, and the axial degree of freedom was released.

Since trusses were not modeled individually, the equivalent floor slab buckled easily when thermal expansion was restrained by the exterior wall. Buckling of the equivalent floor slab often caused convergence problems in the global analysis. The coefficient of thermal expansion of the floor in the office area was set to zero to eliminate the unrealistic buckling problem. Neglecting the thermal expansion of the office area floors introduced errors in bending of exterior columns between a heated floor and a cool floor. The effect of this modeling assumption was small for columns extending between two heated floors.

Neglecting the thermal expansion of the office area slabs did introduce small errors in the out-of-plane bending of columns extending between a hot floor and a cool floor, but such errors were small for columns extending between two hot floors. The error introduced by this modification was not expected to change failure modes or collapse sequence in the global analysis, because thermal expansion of floors was limited to less than a few inches (see Appendix A). The full floor models thermally expanded and pushed outward on the columns until the thermal expansion was overcome by the floor sagging and the floors pulled inward on the exterior columns.

Construction sequence was not included in the global models with creep. The effect of neglecting construction sequence was examined for both buildings. When construction sequence was not included in the analysis, the total axial loads in columns along the exterior walls increased by 7 percent to 15 percent. Similarly, the total column loads supported by the core columns decreased by about 10 percent.

The calculations showed that the outriggers in the WTC 1 simulations were more highly stressed when the construction sequence was not considered. Since it was believed that the hat truss played an important role in transferring loads in WTC 1, the yield strengths of the materials for these outriggers in WTC 1 were artificially increased to account for the incorrect increase in compressive stresses when construction sequence was not considered.

The term “super-element” in ANSYS is used for sub-structuring in an analysis, where a portion of the model with elastic behavior is condensed into a single element with a representative stiffness, damping and mass matrix. The WTC 2 model was suitable for such a simplification as the section of the building

above Floor 86 was expected to remain elastic, based on the results of the isolated core analyses and preliminary global analyses without creep strains or plastic buckling (see NIST NCTAR 1-6D).

The use of super-elements reduced the time to complete a single iteration by a factor of three. However, if at later stages of the analysis the hat truss members became inelastic, the nonlinearities associated with such inelastic behavior were not captured. A super-element cannot determine individual component behavior as the group of components is represented by a single ‘super’ element. Moreover, the effects of construction sequence on the load distribution between the core and wall elements could not be represented, since the birth and death option could not be used in a super-element. (Birth and death refer to the addition or removal, respectively, of an element during an analysis.) The effect of not including construction sequence was evaluated and found to introduce an error of less than 12 percent for vertical displacement. To evaluate whether the hat truss exceeded elastic limits, a separate model that included the components at and above Floor 86 in the super-element was created. The stresses in all the components were calculated at the end of each 10 min time interval and compared with their capacities.

As the use of a super-element in the WTC 2 global model precluded the application of construction sequence, construction sequence was not included in either the WTC 1 or WTC 2 global analysis. Construction sequence refers to an analysis method where the self-weight loads are applied to the structural model in steps to simulate the sequential loading that takes place as a building is constructed. When construction sequence was not included, the total column loads in each exterior wall increased by 7 percent to 15 percent, and the total core columns loads decreased by about 10 percent for both models. It was also found that the outriggers of the hat truss were more highly stressed in the WTC 1 model without construction sequence than in the translated ANSYS model which included construction sequence (see Section 8.2.1). Since the hat truss played an important role in transferring loads, the yield strengths of these outriggers in WTC 1 were increased to account for the artificially higher compressive stresses that resulted without consideration of construction sequence. The difference in the maximum displacement between the models with and without construction sequence was within 12 percent for both WTC 1 and WTC 2.

8.3 ANALYSIS METHODOLOGY

WTC 1 and WTC 2 global models were subjected to Case B and Case D aircraft damage and fires, respectively. The results of the isolated wall, core, and full floor analyses indicated that structural responses to Case B and Case D more closely matched observed structural behavior in photographs and videos than did Case A or Case C, respectively. Thus, Case B and Case D were chosen for the global analysis of WTC 1 and WTC 2, respectively.

The global analysis was conducted in steps. Severed and heavily damaged core columns, floors, and exterior columns and spandrels were removed from the model, and gravity loads were applied as concentrated loads at each column-floor node. Then, dead load and 25 percent of the design live loads were applied to the model without considering construction sequence. The solution for the first step, which determined the structural condition of the tower after aircraft impact, provided the initial condition for the application of temperature histories and thermally-induced structural damage.

Wind forces were not included in the global analysis of the WTC towers. Wind speeds were recorded at three nearby airports, and are shown in Table 8–1. The average wind speed on September 11, 2001,

ranged from 7 knots to 11 knots (10 mph to 13 mph). In comparison, the design wind speed was 98 mph averaged over 20 minutes at a height of 1,500 ft above ground (see Chapter 3 of NIST NCSTAR 1-2). This speed is equivalent to a 3 s peak gust wind speed of about 81 mph to 90 mph at 33 ft above ground in open terrain. Wind force is proportional to the wind velocity squared, therefore, the wind force on the towers from the 13 mph winds on September 11, 2001, were approximately two percent of the average design wind speed of 86 mph, which were negligible.

Table 8–1: Wind speeds recorded at airports near the WTC towers on September 11, 2001.

| Airport | Time (a.m.) | Direction | Speed ¹ (knots) | Speed ² (mph) |
|------------------------------|-------------|-----------|----------------------------|--------------------------|
| LaGuardia (NOAA 2001a) | 8:51 | 320 | 9 | 13 |
| | 9:51 | 340 | 9 | 13 |
| John F. Kennedy (NOAA 2001b) | 8:51 | 310 | 11 | 16 |
| | 9:51 | 350 | 7 | 10 |
| Newark, NJ (NOAA 2001c) | 8:51 | 330 | 8 | 12 |
| | 9:51 | No data | No data | No data |
| Average Wind Speed | | | 9 | 13 |

1. Wind speed recorded as a 20 min average at a 33 ft elevation.

2. Wind speed converted to a 3 s peak gust at 33 ft (knots (20min) * 1.4375 = mph (3 s))

Temperature data were provided for heated structural components at 10 min intervals up to 100 min for WTC 1 and up to 60 min for WTC 2. The temperature histories were based on the combined effects of impact damage to fireproofing and fire spread and growth. The structural analysis used time steps significantly less than 10 min, as a result the temperatures were linearly interpolated between the temperatures at 10 min intervals.

Column-floor disconnections and pull-in forces that occurred during a time step were imposed at the start of the time step. In the global models, nodal couplings tied the exterior columns to the floors. The nodal couplings were removed at locations of floor/wall disconnections. If disconnections were projected to occur or were observed in visual evidence at a time intermediate to the 10 min intervals used in the analyses, for example, between 10 min and 20 min, they were imposed starting at the earlier time point, in this example, at 10 min. Once a portion of a floor was disconnected from the exterior wall, it remained disconnected for the remainder of the analysis. Similarly, pull-in forces were also applied to the global models at the beginning of the 10 min time intervals in which they were predicted to occur or were observed, and they were maintained at a constant level for the 10 min time interval.

Thermal expansion of the floors was not included in the global models. Floor analyses showed that the floors initially pushed exterior column outward by a few inches. However, significant outward bowing was not observed and several inches of outward deflection of exterior columns would not affect the global stability of the towers.

8.4 RESULTS OF WTC 1 ANALYSIS

The global model of WTC 1 with creep, plastic buckling of columns, plasticity, and nonlinear geometry was analyzed with Case B structural damage and temperature histories.

8.4.1 WTC 1 Structural Response to Aircraft Impact Damage

Case B structural and passive fire protection damage after the aircraft impact was as follows:

- WTC 1 had 41 north exterior columns (Columns 112 to 151) severed, 9 core columns on the north central side of the core (Columns 503, 504, 505, 506, 604, 704, 706, 805, and 904), and one exterior panel of the south face (Columns 329 to 331 between Floors 93 and 96) severed or heavily damaged between Floors 93 and 98
- Floor slabs and framing were severed or heavily damaged in the north office floor area through to the central north region of the core on Floors 94 to 97
- WTC 1 fireproofing damage was centered primarily through the north face and floor area, the core, and into the south floor area between Floors 94 to 99.

Figure 8–4 shows the vertical displacements at Floor 99, just above the impact area, with total displacements before aircraft impact and incremental displacements after impact. Figures 8–5 through 8–8 show the vertical displacement contours of the exterior walls and the core area before and after the aircraft impact. Before the aircraft impact, the maximum vertical displacements of the exterior wall and the core at Floor 99 were 2.5 in. and 3.6 in., respectively. Due to severe impact damage on the north face and the north side of the core, WTC 1 tilted slightly to the north after the aircraft impact as can be seen in Fig. 8–4. The maximum displacement of the north wall increased from 2.5 in. to 5.7 in., and the maximum displacement of the south wall decreased from 2.5 in. to 2.4 in. The vertical displacement of the east and west wall slightly increased due to load redistribution.

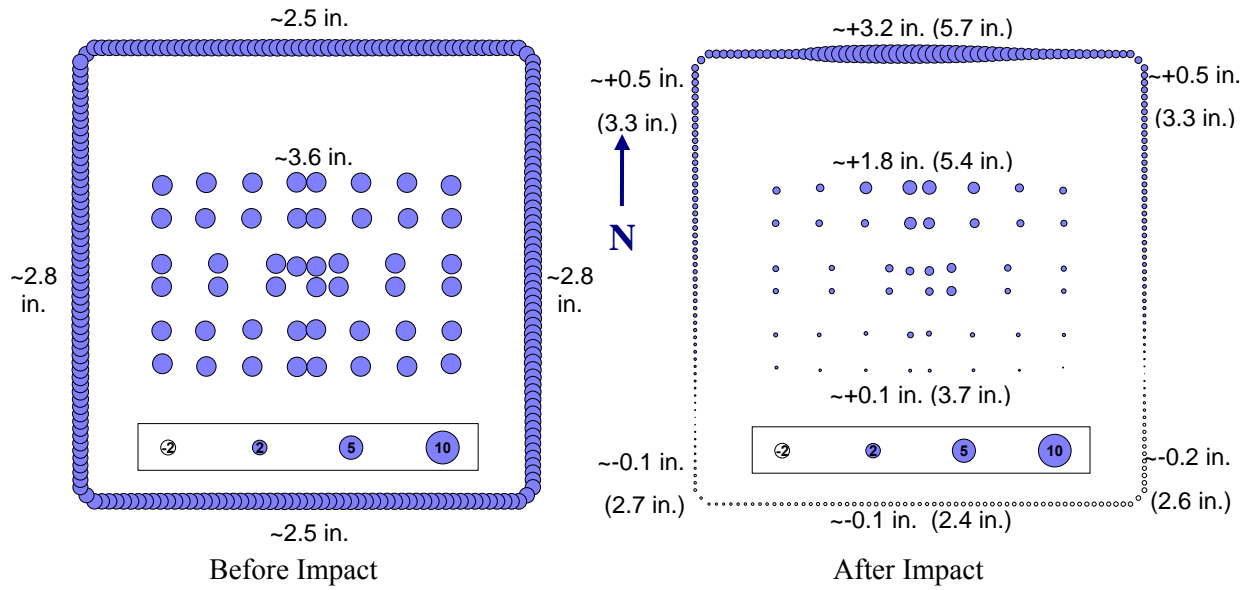


Figure 8-4. Vertical displacement at Floor 99 of WTC 1. Total displacements are shown before aircraft impact and incremental displacements, with total displacements in parentheses, are shown after impact.

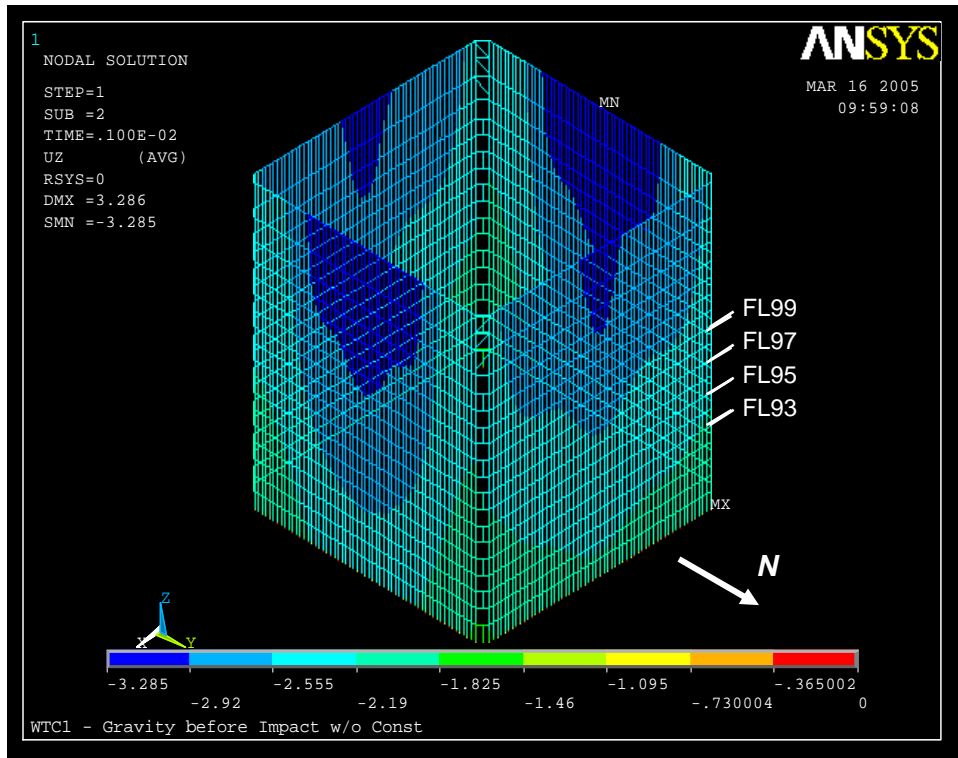


Figure 8-5. Vertical displacement of WTC 1 east and north exterior walls before aircraft impact.

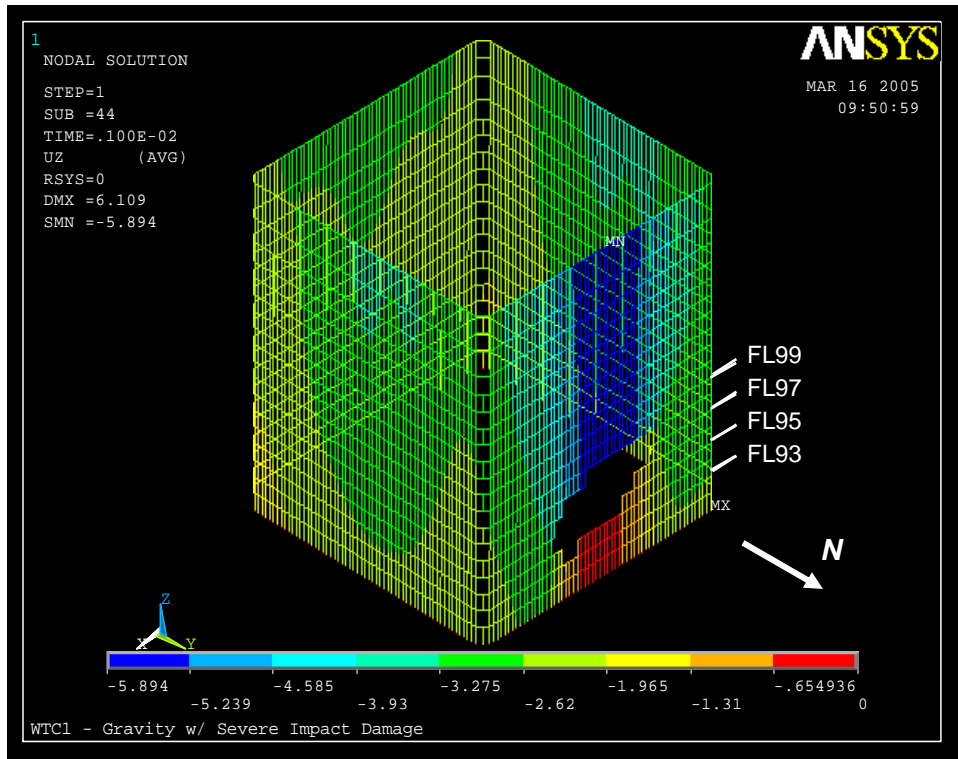


Figure 8–6. Vertical displacement of east and north exterior walls of WTC 1 after aircraft impact for Case B.

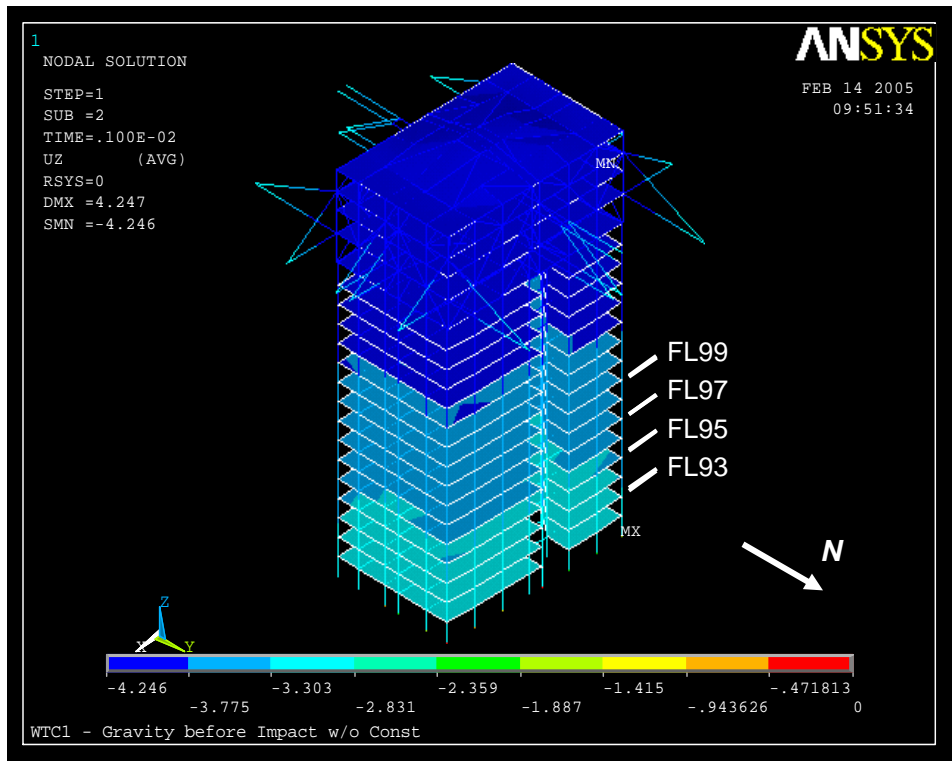


Figure 8–7. Vertical displacement of the east and north side of the WTC 1 core before aircraft impact.

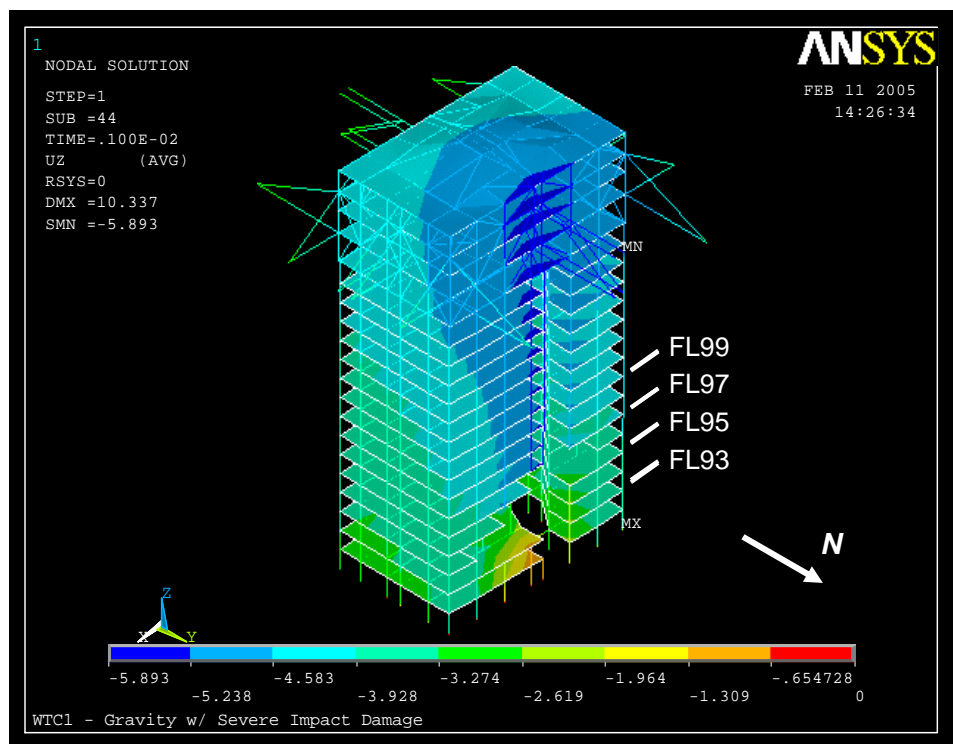


Figure 8–8. Vertical displacement of the east and north side of the WTC 1 core after aircraft impact for Case B.

The global analysis results showed that WTC 1 did not collapse following aircraft impact, as was observed, and had considerable reserve capacity. The core columns were loaded to approximately 50 percent of their capacity prior to impact, and the exterior columns were loaded to approximately 20 percent of their capacity. The exterior columns were capable of large load transfers from the core columns.

Gravity loads were redistributed to adjacent core columns and the exterior walls, primarily through the hat truss. Figures 8–9 and 8–10 show the demand-to-capacity ratios for the core columns before and after impact. The capacity of core and exterior columns was computed as the plastic (or inelastic) buckling load according the American Institute of Steel Construction (AISC) Load and Resistance Factor Design (LRFD) Specification procedures. Ratios less than 1.0 indicate that the column can carry additional gravity loads, whereas ratios greater than 1.0 indicate that the column is carrying more than its computed capacity and, therefore, has plastic strains. Figure 8–10 shows that only two columns had a demand-to-capacity ratio greater than 1.0, and they were adjacent to severed or heavily damaged core columns.

After the aircraft impact, gravity loads that were previously carried by severed columns were redistributed to other columns. Table 8–2 shows that the north wall at Floor 98 carried a total load of 10,974 kip before aircraft impact, and 10,137 kip after the impact. The total load lost due to aircraft impact was 837 kip, or about 7 percent of the total load. Table 8–3 shows that the north wall at Floor 105 lost 732 kip of axial force after impact. Therefore, most of the core loads (732 kip out of 837 kip) were transferred by the hat truss, and the rest were redistributed to the adjacent exterior walls by the spandrels. Due to the impact damage and the tilting of the building to the north after impact, the south wall also lost gravity loads, and about 7 percent (604 kip) was transferred by the hat truss. As a result, the east and west walls

each gained about 7 percent (466 kip and 472 kip, respectively) and the core gained about 1 percent (400 kip) through the hat truss.

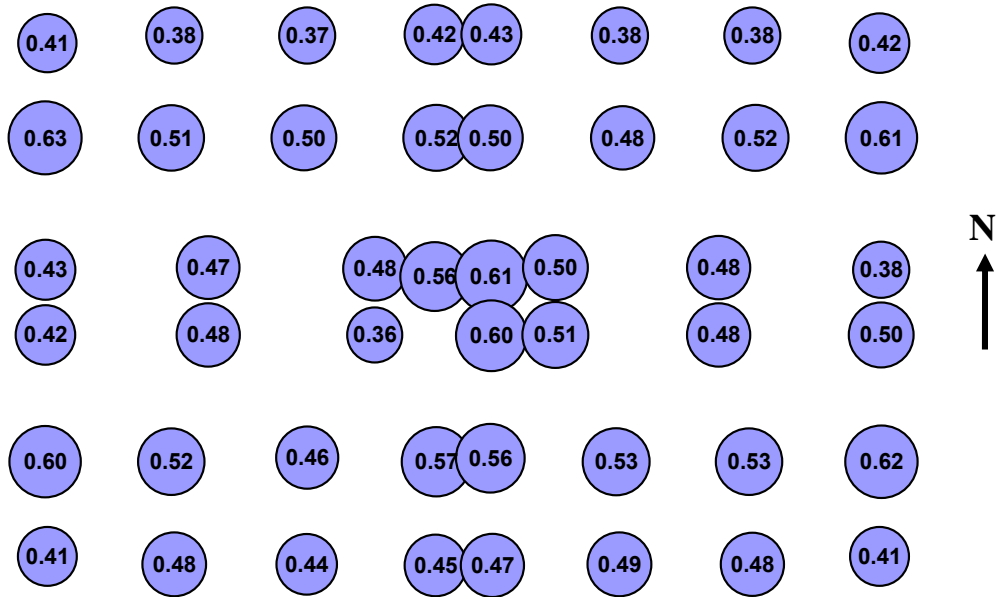


Figure 8–9. Maximum demand-to-capacity ratio for axial force in core columns between Floor 93 and Floor 99 of WTC 1 before aircraft impact.

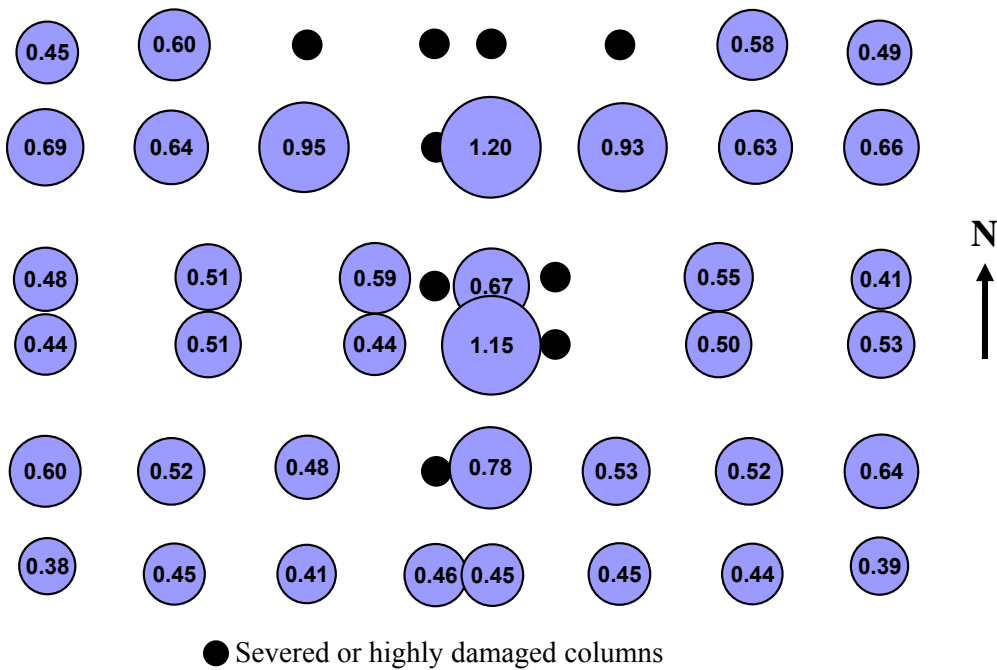


Figure 8–10. Maximum demand-to-capacity ratio for axial force in core columns between Floor 93 and Floor 99 of WTC 1 after aircraft impact for Case B.

Table 8–2. Total column loads at Floor 98 of WTC 1 for Case B conditions.

| | North | East | South | West | Core | Total |
|-------------------|--------|--------|--------|--------|--------|--------|
| (1) Before Impact | 10,974 | 8,545 | 11,025 | 8,572 | 34,029 | 73,144 |
| (2) After Impact | 10,137 | 9,071 | 10,356 | 9,146 | 34,429 | 73,139 |
| (3) 10 min | 9,796 | 8,490 | 9,848 | 8,536 | 36,473 | 73,143 |
| (4) 20 min | 10,437 | 9,108 | 9,900 | 9,202 | 34,495 | 73,143 |
| (5) 30 min | 10,913 | 10,034 | 10,420 | 9,715 | 32,060 | 73,142 |
| (6) 40 min | 11,068 | 10,599 | 11,004 | 10,178 | 30,294 | 73,142 |
| (7) 50 min | 11,149 | 10,908 | 11,192 | 10,458 | 29,435 | 73,141 |
| (8) 60 min | 11,205 | 11,168 | 11,285 | 10,716 | 28,766 | 73,141 |
| (9) 70 min | 11,286 | 11,366 | 11,343 | 10,939 | 28,205 | 73,138 |
| (10) 80 min | 11,376 | 11,555 | 11,409 | 11,119 | 27,681 | 73,140 |
| (11) 90 min | 10,916 | 11,991 | 9,949 | 11,657 | 28,587 | 73,099 |
| (12) 100 min | 10,828 | 12,249 | 9,638 | 11,905 | 28,478 | 73,098 |
| (13) (2) - (1) | -837 | 526 | -668 | 574 | 400 | -5 |
| (14) (10) - (2) | 1,239 | 2,484 | 1,052 | 1,973 | -6,748 | 1 |
| (15) (12) - (2) | 692 | 3,178 | -719 | 2,759 | -5,951 | -41 |
| (16) (12) - (10) | -548 | 694 | -1,771 | 786 | 797 | -42 |

Note: Compression is positive. Units are in kip.

Table 8–3. Total column loads at Floor 105 of WTC 1 for Case B conditions.

| | North | East | South | West | Core | Total |
|-------------------|-------|--------|--------|-------|--------|--------|
| (1) Before Impact | 8,026 | 6,562 | 8,092 | 6,604 | 20,361 | 49,645 |
| (2) After Impact | 7,294 | 7,028 | 7,488 | 7,076 | 20,761 | 49,646 |
| (3) 10 min | 6,944 | 6,461 | 6,981 | 6,469 | 22,790 | 49,646 |
| (4) 20 min | 7,551 | 7,075 | 7,057 | 7,158 | 20,806 | 49,647 |
| (5) 30 min | 8,020 | 7,998 | 7,569 | 7,685 | 18,377 | 49,648 |
| (6) 40 min | 8,193 | 8,571 | 8,129 | 8,147 | 16,608 | 49,649 |
| (7) 50 min | 8,285 | 8,878 | 8,315 | 8,428 | 15,743 | 49,650 |
| (8) 60 min | 8,351 | 9,130 | 8,414 | 8,687 | 15,069 | 49,650 |
| (9) 70 min | 8,435 | 9,319 | 8,481 | 8,914 | 14,502 | 49,651 |
| (10) 80 min | 8,528 | 9,497 | 8,551 | 9,097 | 13,978 | 49,651 |
| (11) 90 min | 8,096 | 9,847 | 7,327 | 9,506 | 14,876 | 49,652 |
| (12) 100 min | 8,023 | 10,076 | 7,066 | 9,720 | 14,767 | 49,653 |
| (13) (2) - (1) | -732 | 466 | -604 | 472 | 400 | 1 |
| (14) (10) - (2) | 1,234 | 2,470 | 1,063 | 2,021 | -6,783 | 5 |
| (15) (12) - (2) | 730 | 3,048 | -422 | 2,644 | -5,993 | 7 |
| (16) (12) - (10) | -504 | 579 | -1,485 | 623 | 790 | 2 |

Note: Compression is positive. Units are in kip.

8.4.2 WTC 1 Structural Response to Elevated Temperatures

In the early stages of the fire, temperatures of structural components in the core rose between 500 °C and 700 °C over a 10 min to 20 min time interval (where fireproofing was damaged), and the thermal expansion of the core was greater than the thermal expansion of the exterior walls. The difference in the thermal expansion between the core and the exterior walls increased the loads in the core columns at 20 min. After 20 min, the core continued to lose gravity loads due to thermal weakening and shortening until the south wall started to bow inward. By 50 min, the core had displaced downward by 1.6 in on average at Floor 99 due to creep and buckling of core columns. About 20 percent (6,748 kip) of the gravity load was transferred by the hat truss to the exterior walls due to thermal weakening of the core at 80 min, as shown in Table 8–2; the north and south walls each carried about 10 percent more loads (1,239 kip and 1,052 kip, respectively) and the east and west walls each carried about 25 percent more loads (2,484 kip and 1,973 kip, respectively). Since the hat truss outriggers to the east and west walls were stiffer than the outriggers to the north and south walls, they transferred greater loads to the east and west exterior walls. At 100 min, the core displaced downward at Floor 99 by 2.0 in. on the south side of the core. As the core was weakened by creep and plastic buckling, gravity loads in the core were transferred to the exterior walls.

The full floor analyses for WTC 1 Case B showed that the floors on the south side in the impact zone did not begin to sag and apply a pull-in force at the column connections until approximately 80 min after impact. Based upon the full floor and isolated south wall subsystem analyses, 5 kip of pull-in force was applied to all columns across Floors 95 to 99 beginning at 80 min, as shown in Fig. 7–30. Figures 8–11 and 8–12 show the out-of-plane displacement contours of the south wall at 80 min and 100 min, respectively. Figure 8–13 shows the time history of the inward bowing of the south wall. Until the 5 kip pull-in forces were applied, no inward bowing had occurred. With the application of the 5 kip pull-in force, the maximum inward bow increased to 15.5 in.

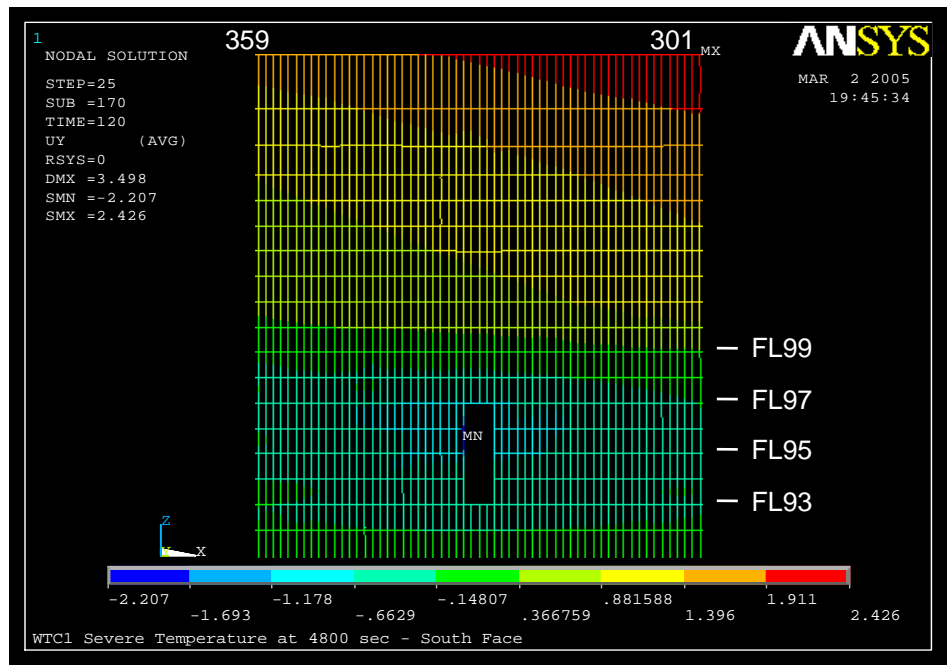


Figure 8–11. Out-of-plane displacement of south wall of WTC 1 at 80 min for Case B.

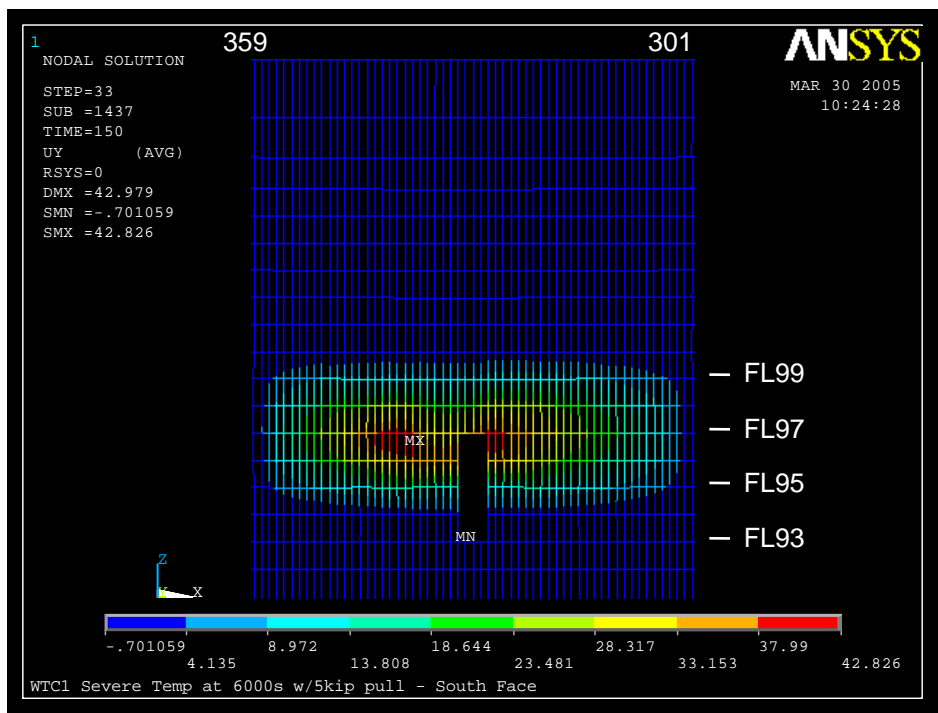


Figure 8–12. Out-of-plane displacement of south wall of WTC 1 at 100 min for Case B conditions with 5 kip pull-in forces.

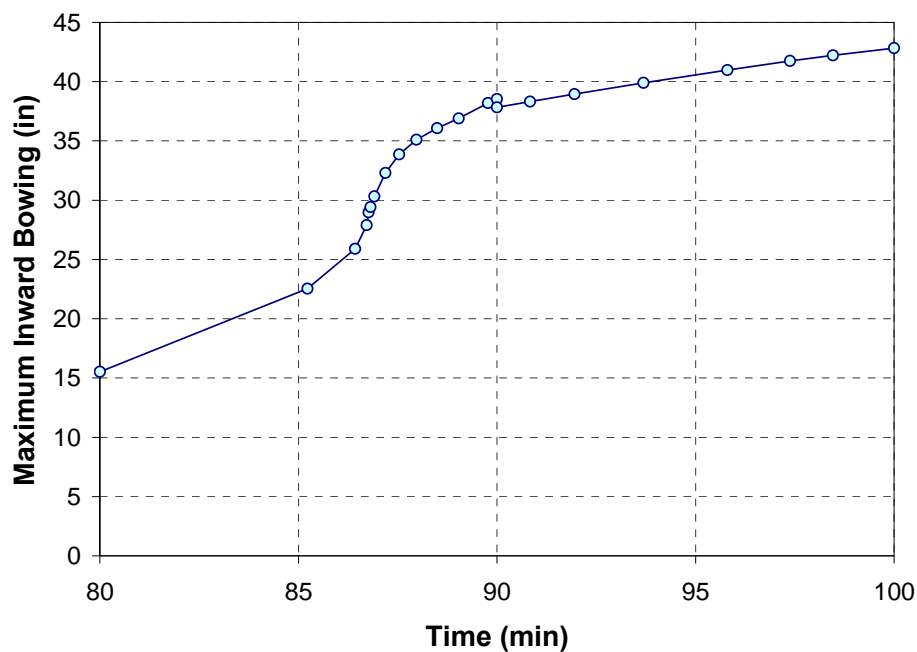


Figure 8–13. Time history of maximum out-of-plane displacement of WTC 1 south wall for Case B with 5 kip pull-in forces.

Figure 8–14 shows that Columns 318 to 346 on the south wall unloaded due to inward bowing after 80 min. The loads increased on the east and west walls. Figure 8–15 shows the load increase for the east

wall. Due to bowing of the south wall, the vertical displacement of the south wall increased as shown in Figs. 8–16 and 8–17, and the south wall lost about an additional 5 percent (1,771 kip) of load between 80 min and 100 min (see Table 8–2). As a result, the east and west walls and the core gained gravity loads.

By approximately 87 min, the inward bowing increased significantly. As the bowing of the south wall increased, a section of the south wall above the bowed-in area moved downward as can be seen in Fig. 8–18. By 90 min, the rate of increase in the inward bowing slowed down as the south wall redistributed the gravity loads to the east and west walls and to the core. The inward bowing increased to 42.8 in. at 100 min. However, the south wall remained stable (had not buckled) at 100 min.

Isolated exterior wall and global analyses showed that varying the inward pull force by a small amount caused a large difference in the amount of inward bowing. For a comparison, the inward bowing of the south wall at 100 min from the analysis with a 4 kip pull-in force was only 14.5 in. at 100 min. Given that the inward bowing increased from 14.5 in. to 42.8 in. when the inward pull force was increased from 4 kip to 5 kip, a slight increase in the pull-in force over 5 kip would have resulted in instability of the south wall.

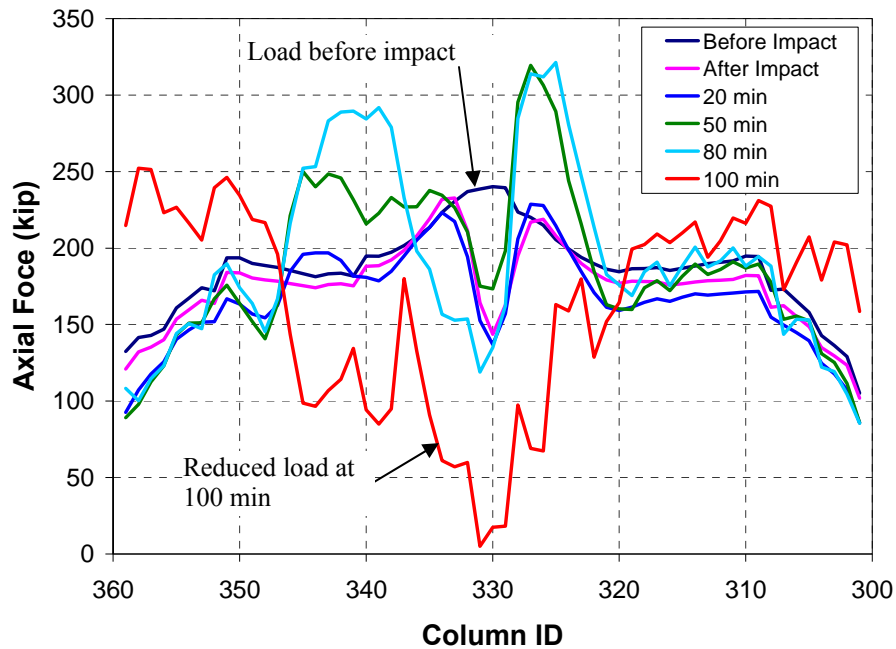


Figure 8–14. Distribution of axial force in exterior columns at Floor 98 of WTC 1 south wall for Case B with 5 kip pull-in forces.

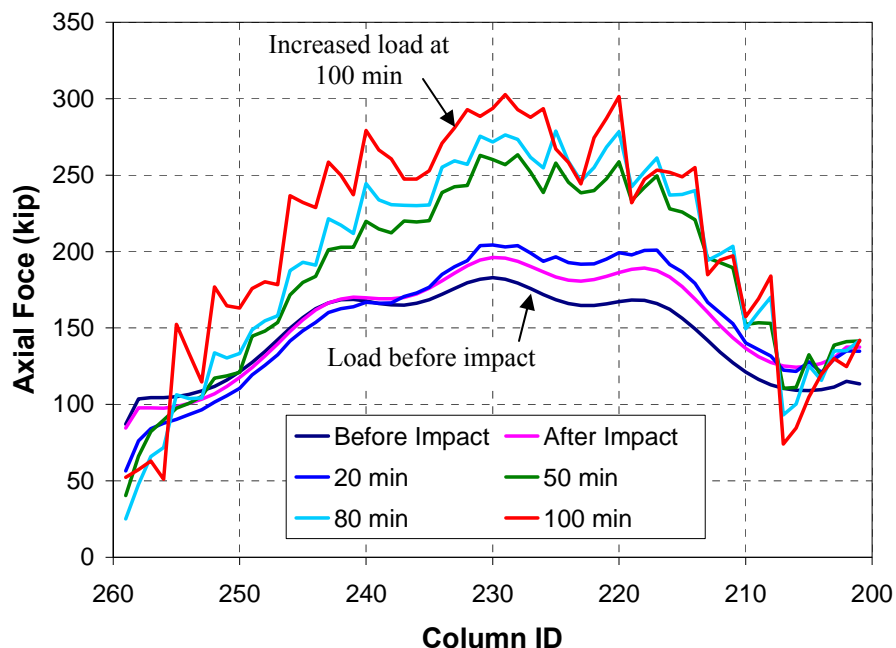


Figure 8–15. Distribution of axial force in exterior columns at Floor 98 of WTC 1 east wall for Case B with 5 kip pull-in forces.

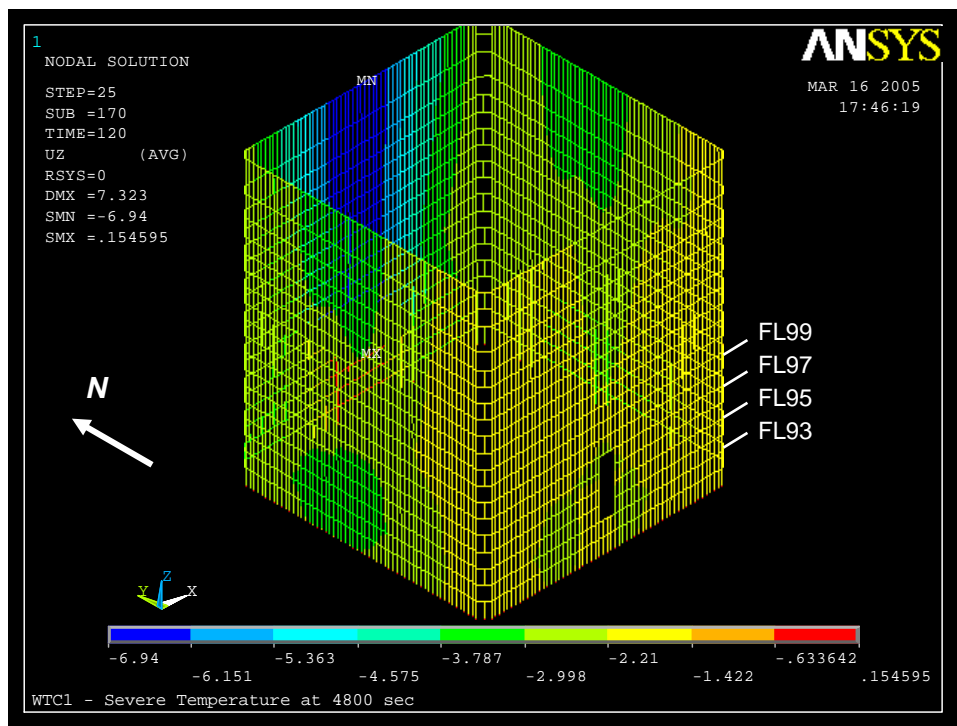


Figure 8–16. Vertical displacement of west and south exterior walls of WTC 1 at 80 min for Case B.

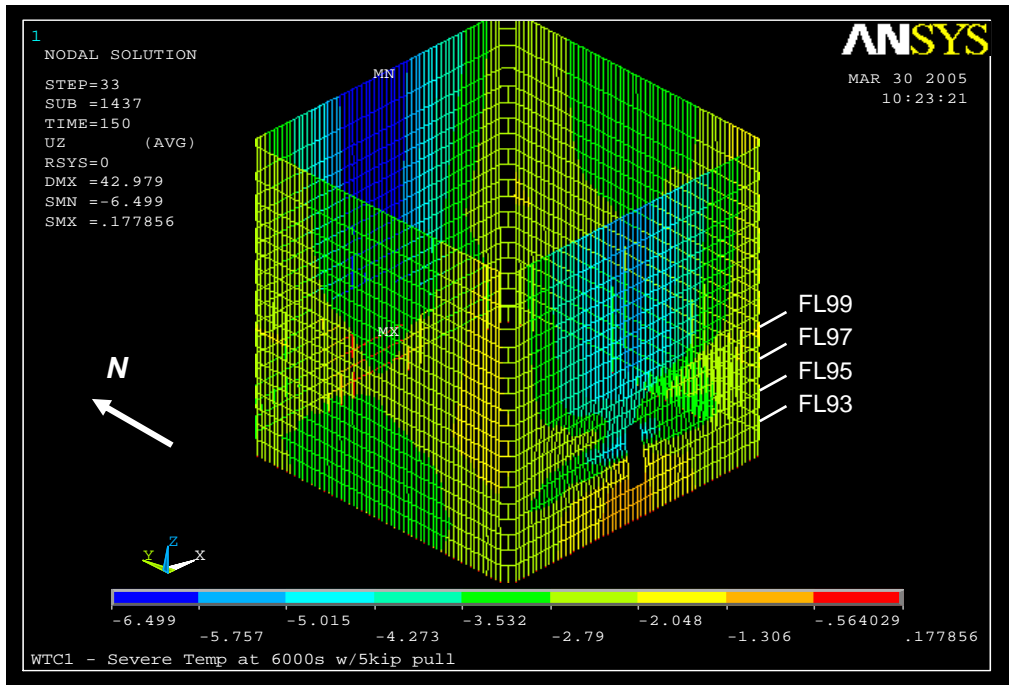
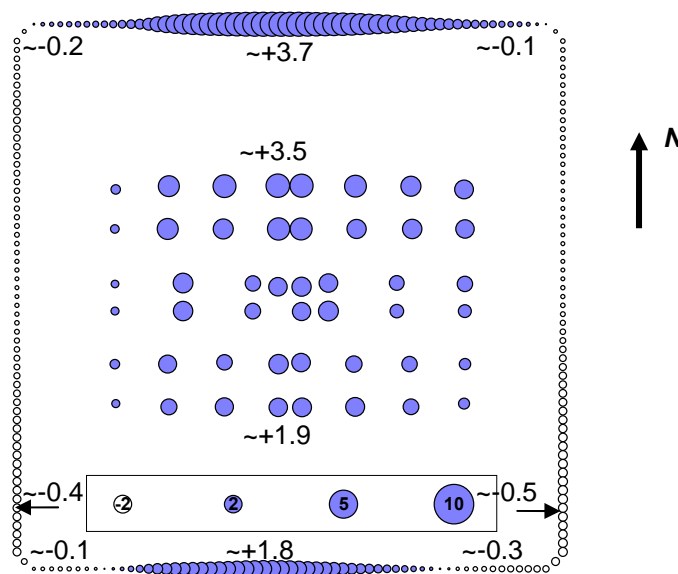


Figure 8–17. Vertical displacement of west and south exterior walls of WTC 1 at 100 min for Case B.



Note: downward displacement is shown as positive displacement

Figure 8–18. Change in vertical displacement at Floor 99 of WTC 1 from the state before impact to 100 min for Case B.

Plastic and creep strains played a significant role in the structural response of WTC 1 to the fires. Figures 8–19 to 8–21 show the maximum elastic-plus-plastic-plus-creep strain in each column between Floor 93 and Floor 99 at 10 min, 40 min, and 100 min, respectively. Before the aircraft impact, the columns had no plastic strain. After the aircraft impact, several columns that were close to severed and

highly damaged columns experienced plastic strains. Plastic strain of the core increased for the first 40 min, and then remained almost constant to 100 min. Plastic strain of the south exterior columns increased in almost all the bowed columns from 40 min to 100 min. However, creep strain was found to be far greater than plastic strain, especially in the core. At 40 min, 22 of 47 core columns had creep strain larger than 1.0 percent. After 40 min, creep strain in core columns on the south side had increased. The maximum elastic-plus-plastic-plus-creep strain at 100 min was 7.3 percent in Column 1006. As temperature increased on the south exterior wall in the later stages of the fire, creep strain also increased in about 20 columns on the south face. The maximum elastic-plus-plastic-plus-creep strain in the south exterior columns reached 2.9 percent.

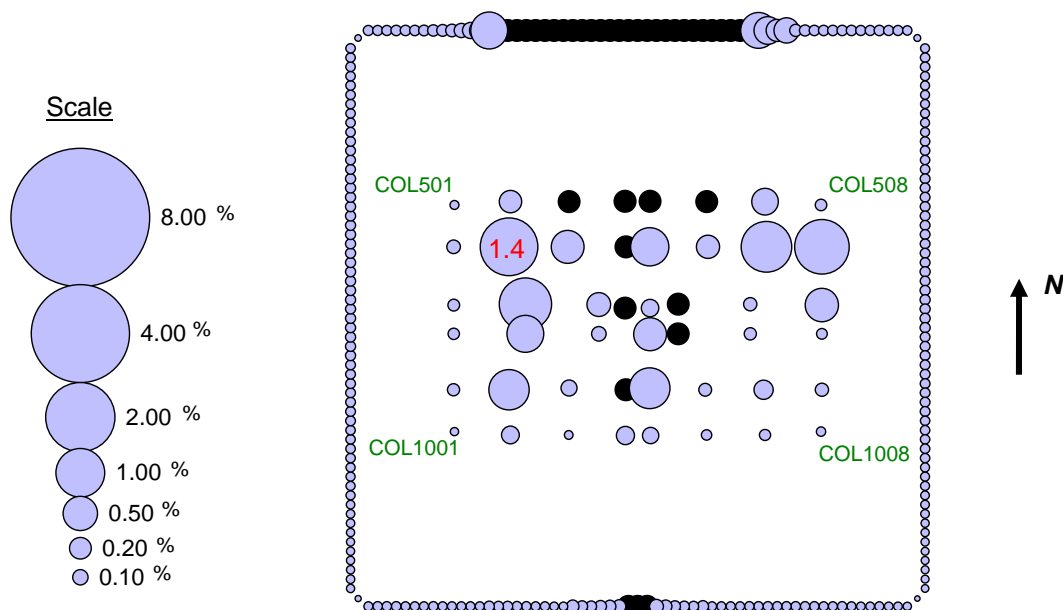


Figure 8–19. Maximum elastic-plus-plastic-plus-creep strain for columns between Floor 93 and Floor 99 of WTC 1 at 10 min for Case B (strain values are in percent).

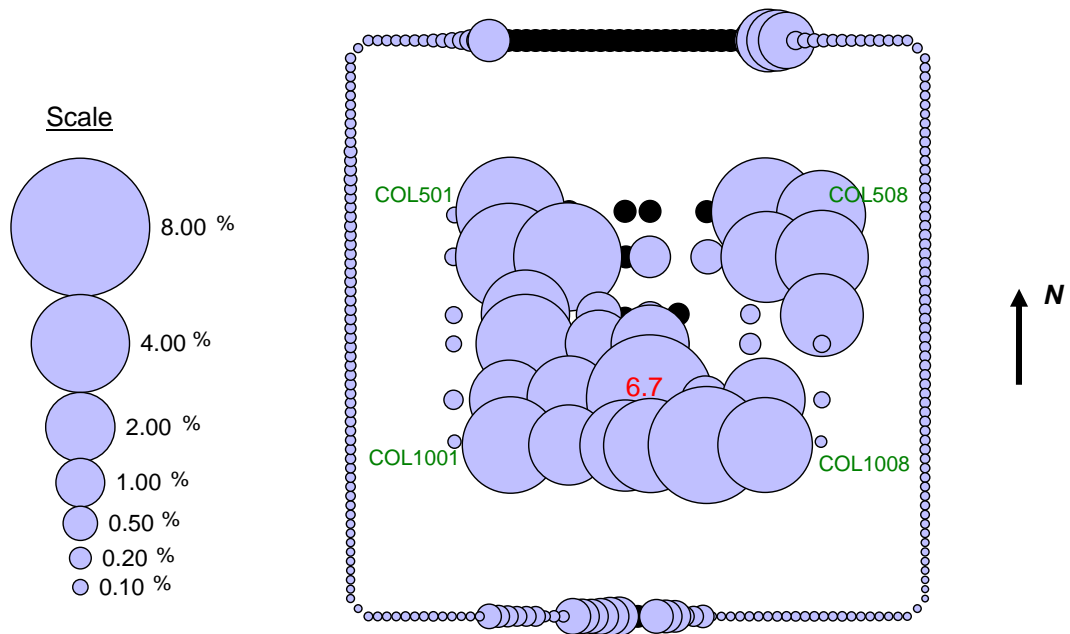


Figure 8–20. Maximum elastic-plus-plastic-plus-creep strain for columns between Floor 93 and Floor 99 of WTC 1 at 40 min for Case B (strain values are in percent).

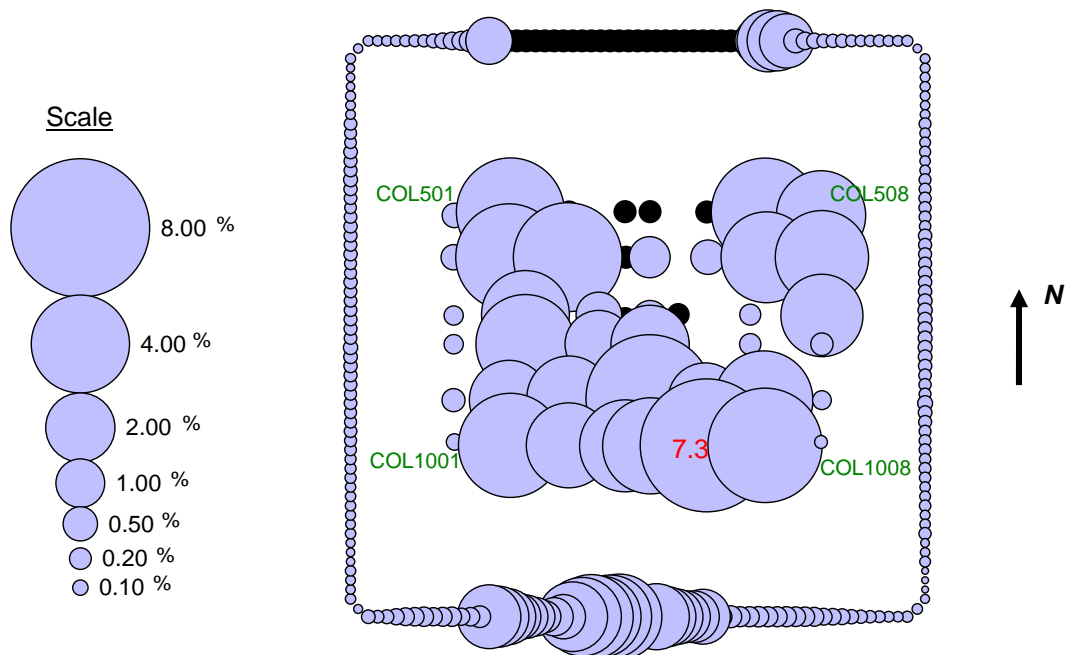


Figure 8–21. Maximum elastic-plus-plastic-plus-creep strain for columns between Floor 93 and Floor 99 of WTC 1 at 100 min for Case B with 5 kip pull-in forces (strain values are in percent).

Figures 8–22 and 8–23 show the axial force demand-to-capacity ratio for each core column at 80 min and 100 min, respectively. Compressive capacities of the core columns were calculated by AISC LRFD Eq. E2-1 for plastic buckling with effective length factor of K equal to 1.0 and a resistance factor of 1.0. Comparison of Figs. 8–10 and 8–23 shows that the demand-to-capacity ratio increased for core columns with relatively small elastic-plus-plastic-plus-creep strains and decreased for columns with high strains. Figure 8–21 shows that core columns with high creep strains had lower demand-to-capacity ratios. Columns with high compressive loads and large creep strains shortened and unloaded to stiffer columns with less creep.

At 100 min, the core had weakened on the south side and shortened by 1.6 in. The south wall had bowed inward approximately 43 in. and was unloading to the core and the adjacent east and west walls. As discussed previously, a small change in the magnitude of the inward pull force changed the rate at which the exterior wall bowed inward and reached a point of instability. Based upon observations and similar results for WTC 2 at collapse initiation (described in the next Section), the following sequence of events likely occurred as soon as the south wall reached instability and buckled.

The inward bowing of the south wall caused failure of exterior column splices and spandrels, and induced column instability. The instability progressed horizontally across the entire south face. The south wall unloaded and redistributed its gravity loads to the thermally weakened core through the hat truss and to the east and west walls through the spandrels. The beginning of this load redistribution is illustrated in Tables 8–1 and 8–2. The building section above the impact zone began tilting to the south as column instability progressed rapidly from the south wall along the adjacent east and west walls and increased the gravity load on the core columns. The change in potential energy due to downward movement of the building mass above the buckled columns exceeded the strain energy that could have been absorbed by the structure. Global collapse then ensued.

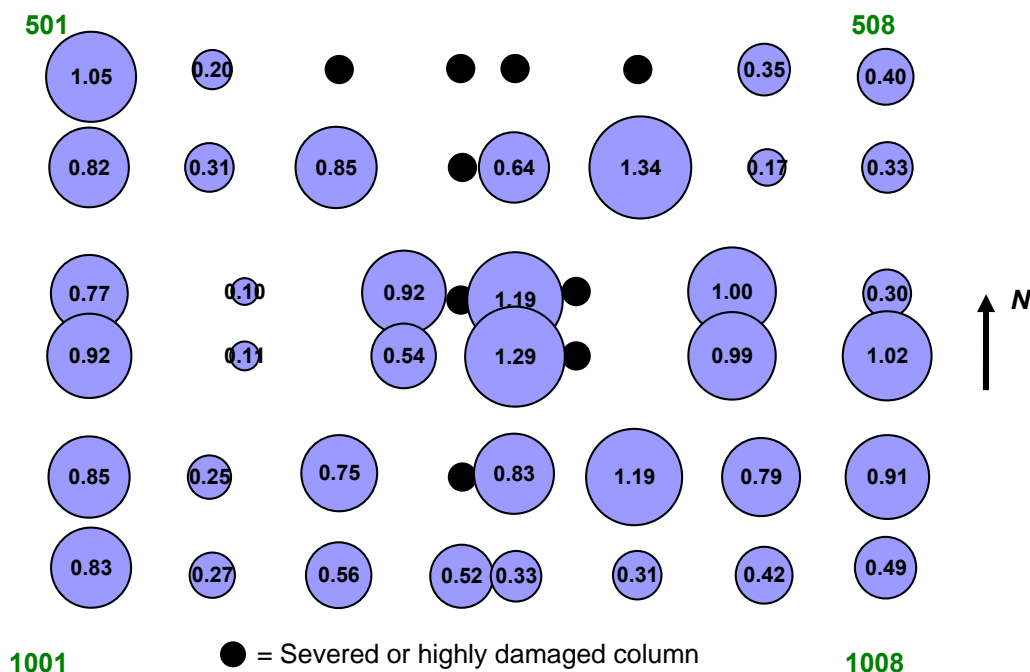


Figure 8–22. Maximum demand-to-capacity ratio for axial force in core columns between Floor 93 and Floor 99 of WTC 1 at 80 min for Case B conditions.

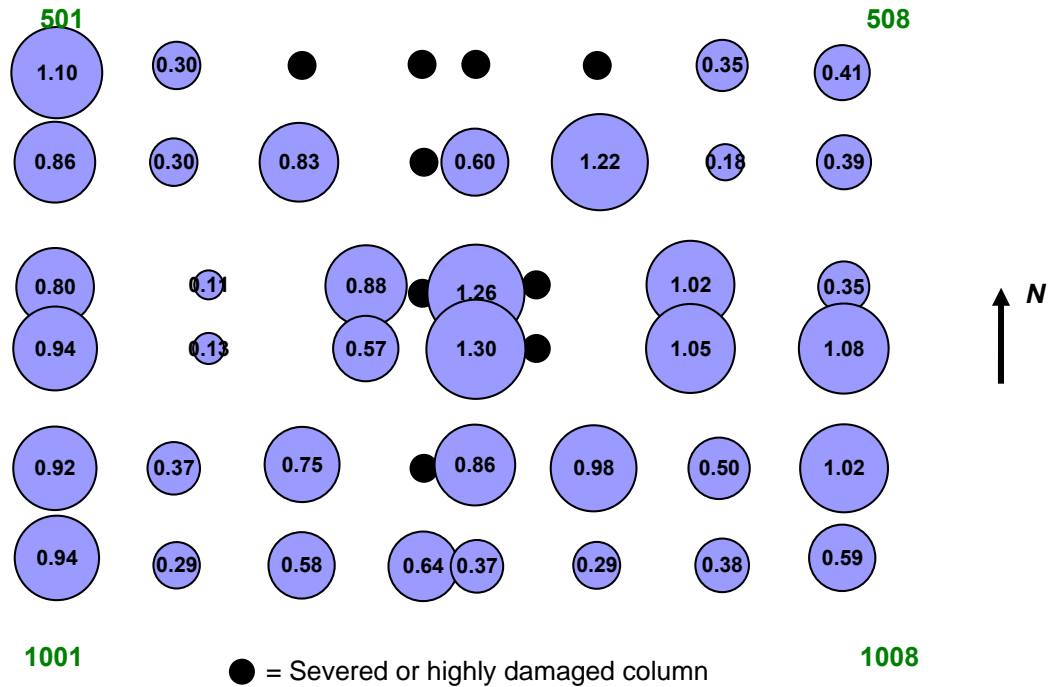


Figure 8–23. Maximum demand-to-capacity ratio for axial force in core columns between Floor 93 and Floor 99 of WTC 1 at 100 min for Case B with 5 kip pull-in forces.

8.4.3 WTC 1 Hat Truss Members and Connections

The state of the hat truss members and the connections were checked since the global model did not include break elements to capture column and hat truss splice failures or sufficient beam elements to capture buckling of the hat truss outriggers. The condition of the connections and the members in the primary load path of the hat truss was evaluated at various time intervals. The evaluation included the core column splices for tension, outriggers and supporting columns for compression, and the hat truss connections that were in the primary load path for tension.

Core column splices had compressive forces before the aircraft impact. With the aircraft impact damage and increasing plastic and creep strains, the core weakened and shortened, and some core columns were supported from the hat truss. At 100 min, nine core columns (503, 504, 505, 602, 603, 604, 605, 702, and 802) were in tension at Floor 105 as shown in Fig. 8–24. To evaluate the condition of the core column splices at Floor 106, the tension capacity of these splices was compared to the tensile forces developed during each 10 min time interval. To calculate the connection tensile capacity, AISC-LRFD procedures were used. It was found that tensile forces in the core columns were less than the capacities of the splices.

There were sixteen outriggers (four on each face), as shown in Fig. 8–25, that transferred gravity loads between the core and the exterior walls. In the global model, each of these outriggers was modeled by only one BEAM 24 element; therefore, buckling of the member was not captured although material nonlinearity was included. Table 8–4 lists demand-to-capacity ratios for the outrigger members over time. Capacities of the outriggers were calculated using AISC LRFD procedures for plastic (inelastic) buckling with effective length factor K equal to 0.75 (the outrigger end connections were different from those used for the core columns) and a resistance factor of 1.0. As the outrigger members were not

modeled with sufficient elements to capture plastic buckling, they yielded when the outrigger reached its compressive capacity; therefore, force redistribution to other outriggers was underestimated.

The hat truss connections within the hat truss itself were also checked. The hat truss connections in the primary load path were identified, and their capacities were compared to their forces. The primary load path was identified by selecting hat truss members with an absolute axial stress of 25 ksi or more at 80 min, as this was when maximum forces occurred. Only the connections that were transferring tensile forces were evaluated. In calculating the capacity of the connections, the AISC-LRFD procedures were used. None of the hat truss connection capacities were exceeded. It was concluded that the hat truss redistributed loads between the core and the exterior wall columns as modeled in the global analysis.

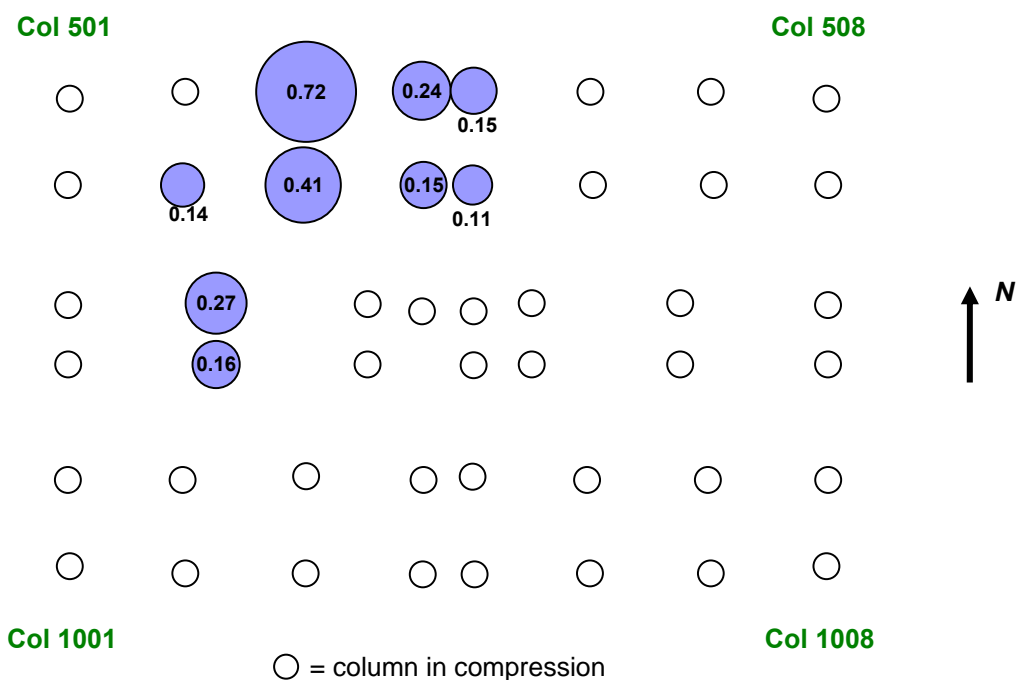


Figure 8–24. Tension demand-to-capacity ratio for core column splices at WTC 1 Floor 106 at 100 min for Case B with 5 kip pull-in forces.

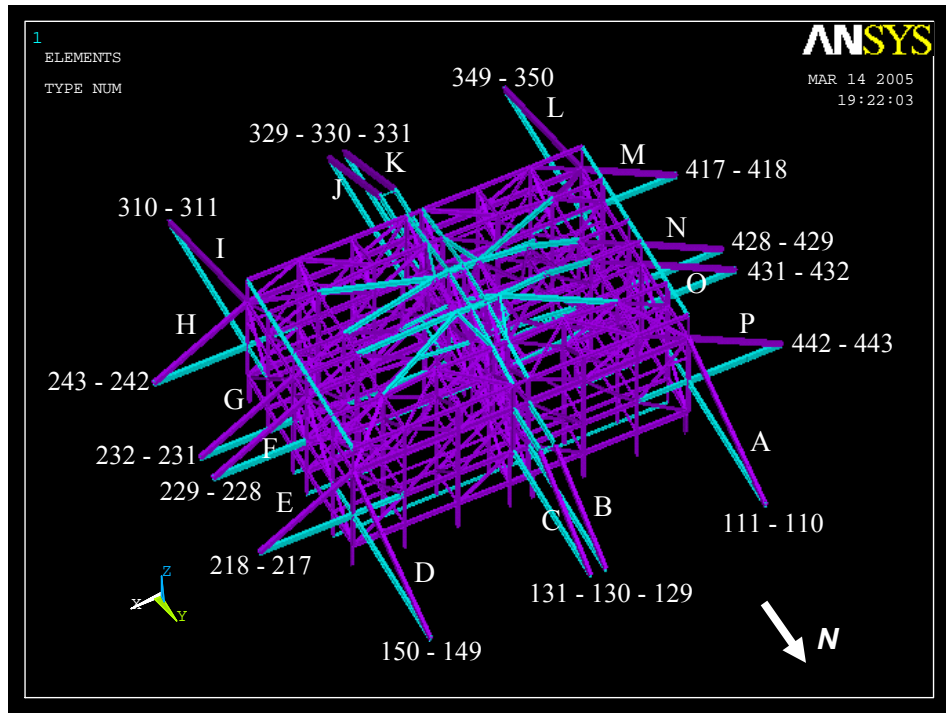


Figure 8–25. Location and label of outriggers and supporting columns for WTC 1.

Table 8–4. Demand-to-capacity ratio for axial force in outriggers of WTC 1 for Case B.

| Outrigger ID | Bfr Imp | Afr Imp | 10 min | 20 min | 30 min | 40 min | 50 min | 60 min | 70 min | 80 min | 90 min | 100 min |
|--------------|---------|---------|--------|--------|--------|--------|--------|--------|--------|--------|--------|---------|
| North | | | | | | | | | | | | |
| A | 0.26 | 0.35 | 0.26 | 0.40 | 0.49 | 0.53 | 0.56 | 0.59 | 0.62 | 0.65 | 0.54 | 0.52 |
| B | 0.22 | -0.07 | -0.13 | -0.04 | 0.02 | 0.04 | 0.06 | 0.07 | 0.08 | 0.09 | 0.03 | 0.03 |
| C | 0.21 | -0.05 | -0.11 | -0.02 | 0.04 | 0.06 | 0.08 | 0.08 | 0.09 | 0.11 | 0.05 | 0.04 |
| D | 0.25 | 0.35 | 0.29 | 0.45 | 0.61 | 0.67 | 0.70 | 0.72 | 0.73 | 0.75 | 0.65 | 0.63 |
| East | | | | | | | | | | | | |
| E | 0.32 | 0.48 | 0.38 | 0.56 | 0.75 | 0.83 | 0.88 | 0.92 | 0.94 | 0.97 | 0.95 | 0.96 |
| F | 0.23 | 0.28 | 0.21 | 0.30 | 0.41 | 0.48 | 0.52 | 0.55 | 0.57 | 0.59 | 0.62 | 0.64 |
| G | 0.23 | 0.26 | 0.20 | 0.26 | 0.35 | 0.42 | 0.46 | 0.49 | 0.51 | 0.54 | 0.58 | 0.61 |
| H | 0.33 | 0.31 | 0.23 | 0.25 | 0.36 | 0.46 | 0.51 | 0.55 | 0.58 | 0.60 | 0.72 | 0.77 |
| South | | | | | | | | | | | | |
| I | 0.25 | 0.12 | 0.04 | 0.03 | 0.12 | 0.20 | 0.23 | 0.26 | 0.27 | 0.28 | 0.28 | 0.28 |
| J | 0.21 | 0.10 | 0.01 | 0.03 | 0.13 | 0.24 | 0.28 | 0.29 | 0.30 | 0.31 | 0.04 | -0.02 |
| K | 0.21 | 0.10 | 0.01 | 0.03 | 0.13 | 0.24 | 0.27 | 0.28 | 0.30 | 0.31 | 0.02 | -0.04 |
| L | 0.26 | 0.12 | 0.02 | 0.05 | 0.11 | 0.20 | 0.24 | 0.27 | 0.29 | 0.31 | 0.19 | 0.18 |
| West | | | | | | | | | | | | |
| M | 0.33 | 0.33 | 0.22 | 0.29 | 0.36 | 0.44 | 0.49 | 0.53 | 0.56 | 0.58 | 0.69 | 0.73 |
| N | 0.24 | 0.27 | 0.20 | 0.28 | 0.34 | 0.40 | 0.44 | 0.47 | 0.50 | 0.52 | 0.56 | 0.58 |
| O | 0.24 | 0.29 | 0.22 | 0.31 | 0.38 | 0.43 | 0.47 | 0.50 | 0.53 | 0.55 | 0.59 | 0.61 |
| P | 0.33 | 0.48 | 0.39 | 0.54 | 0.64 | 0.71 | 0.75 | 0.79 | 0.83 | 0.87 | 0.88 | 0.90 |

8.5 RESULTS OF WTC 2 ANALYSIS

The global model of WTC 2 with creep, plastic buckling of columns, plasticity, and nonlinear geometry was analyzed with Case D structural damage and temperature histories.

8.5.1 WTC 2 Structural Response to Aircraft Impact Damage

Case D structural and passive fire protection damage after the aircraft impact was as follows:

- WTC 2 had 34 severed columns on the south wall (Columns 407 to 440) and 11 core columns on the south side of the core (Columns 701, 702, 801, 802, 803, 901, 903, 1001, 1002, 1003, and 1004) and 4 exterior columns on the north wall (Columns 253, 254, 257, and 258) that were severed or heavily damaged between Floors 78 to 84.
- Floor slabs and framing were severed or heavily damaged in the south office floor area through the east side of the core between Floors 78 and 84.
- WTC 2 fireproofing damage extended from the south exterior wall, through the east side of the core, to the east and north exterior walls between Floors 78 and 84.

The vertical displacements of the exterior wall before the aircraft impact were about 2.0 in. to 3.0 in. (Fig. 8–26). After aircraft impact, the vertical displacements increased to 7.4 in. on the south wall (Fig. 8–27). There was no horizontal (out-of-plane) displacement on the east wall before the aircraft impact. After aircraft impact, the south side of the east wall at Floor 86 displaced outward about 2.0 in.; whereas, the north side at the same floor did not displace.

In the core, the vertical displacements were about 3.5 in. to 4.2 in. before the aircraft impact, as shown in Fig. 8-28. After aircraft impact, the vertical displacements increased to 10 in. at the southeast corner of the core where the aircraft impact had severed columns, as shown in Fig. 8–29.

Figures 8–30 and 8-31 show the north-south and east-west lateral displacements of the exterior wall above Floor 86 after aircraft impact. Floor 110 moved toward the south about 5.1 in. and toward the east about 5.0 in. There was also a slight twist around the z-axis of the tower of about 0.07 percent at Floor 110. The twist around the z-axis was calculated by taking the difference between the average in-plane displacement of the two opposing exterior walls (such as the east and the west walls) at Floor 110 and dividing the result by the distance between these walls (~200 ft).

The global analysis showed that WTC 2 was stable following aircraft impact, as was observed, and had considerable reserve capacity. Similar to WTC 1, the core columns were loaded to approximately 50 percent of their capacity prior to impact, and the exterior columns were loaded to approximately 20 percent of their capacity. The exterior columns were capable of large load transfers from the core columns after impact.

The loads in the severed exterior columns were transferred to adjacent exterior columns through the spandrels and to the core through the hat truss. Several of the severed core columns at the southeast corner of the core were computed to have failed splice connections to the hat truss (discussed in Section 8.5.3). The loads from these columns were transferred through the core floors to adjacent core columns and then to the east and south exterior walls through the hat truss. Additionally, the severed core columns at the southeast corner resulted in the core leaning to the southeast. While the isolated WTC 2 core model was not stable with the structural impact damage, within the global system the core was supported by the floors and exterior walls.

The leaning of the core to the southeast contributed to the load redistribution in WTC 2, with a general pattern of increased loads on the south and east columns (core and exterior) and decreased loads on the north and west columns. Tables 8–5 and 8–6 show the total columns loads at Floors 83 and 105, respectively, for the analysis stages from before impact to collapse initiation at 43 min. After impact, as shown in Table 8–5, the core carried 6 percent less loads (4,007 kip), and the east wall carried 24 percent more gravity loads (4,368 kip). The north wall loads decreased by 10 percent (1,374 kip), and the south and west walls loads increased by 2 percent (227 kip) and 3 percent (604 kip), respectively.

The loads on the core columns before aircraft impact were distributed essentially symmetrically with respect to the center of the core. There was a slight difference between corner columns on the south side (501 and 1001) and north side (508 and 1008) due to slightly higher dead and live loads in the north side columns. Columns 506, 507, 508, and 1008 at the northeast and northwest corners unloaded; the other intact core columns increased in load (Figs. 8–32 and 8–33). The loads in Columns 904 and 1005, which were adjacent to the severed and heavily damaged columns, increased substantially at Floor 83 after impact. Column 904 increased from 660 kip to 1,506 kip and Column 1005 increased from 1,287 kip to 2,794 kip.

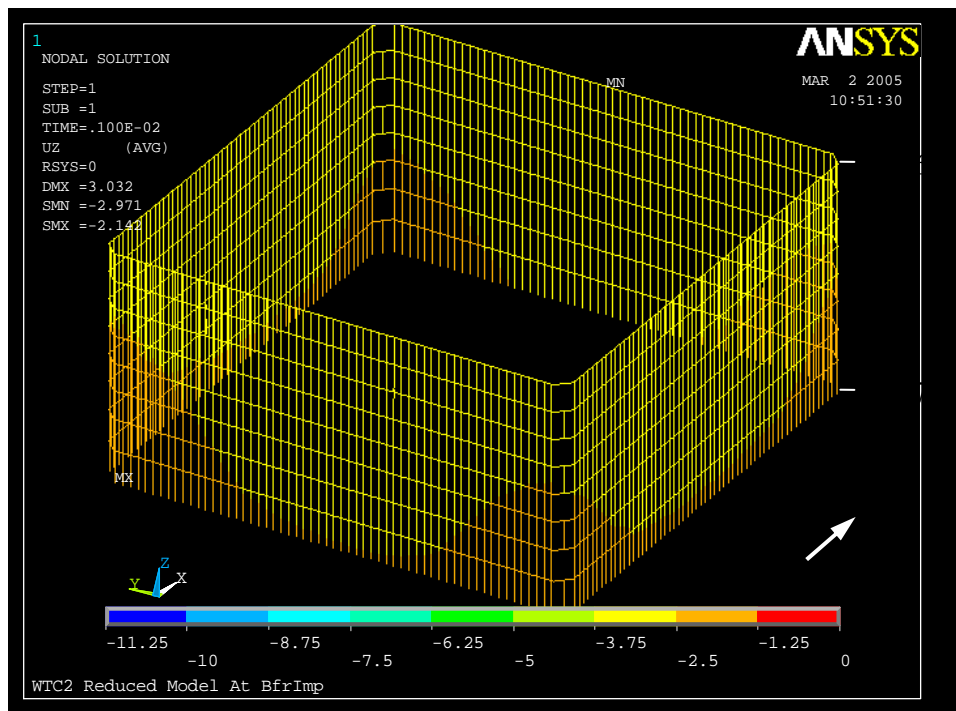


Figure 8–26. Vertical displacement before impact of WTC 2 exterior wall for Case D.

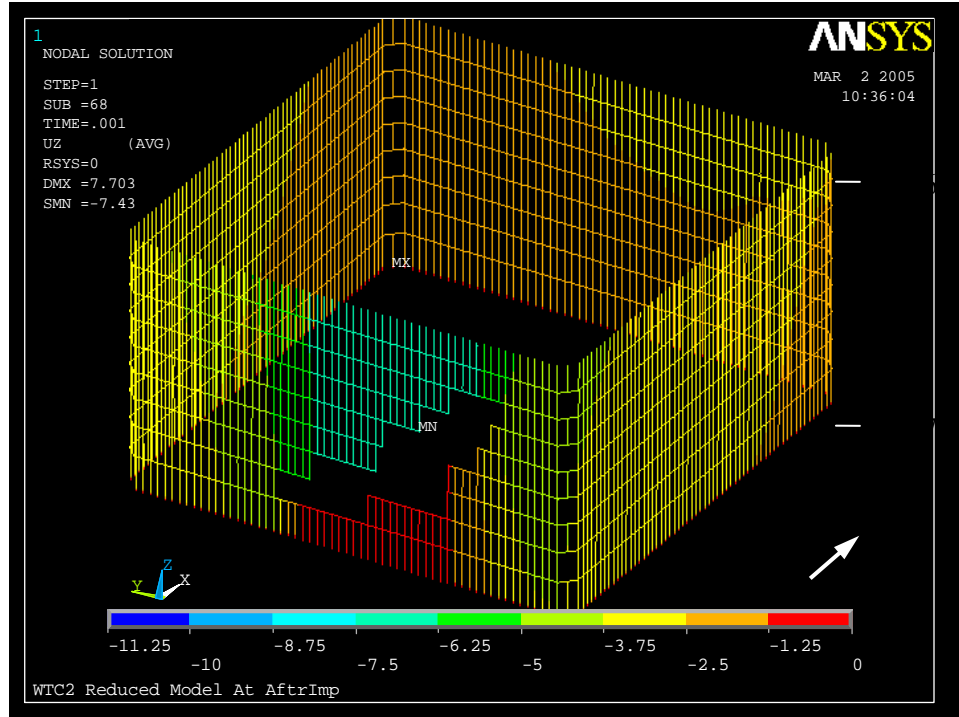


Figure 8–27. Vertical displacement after impact of WTC 2 exterior wall for Case D.

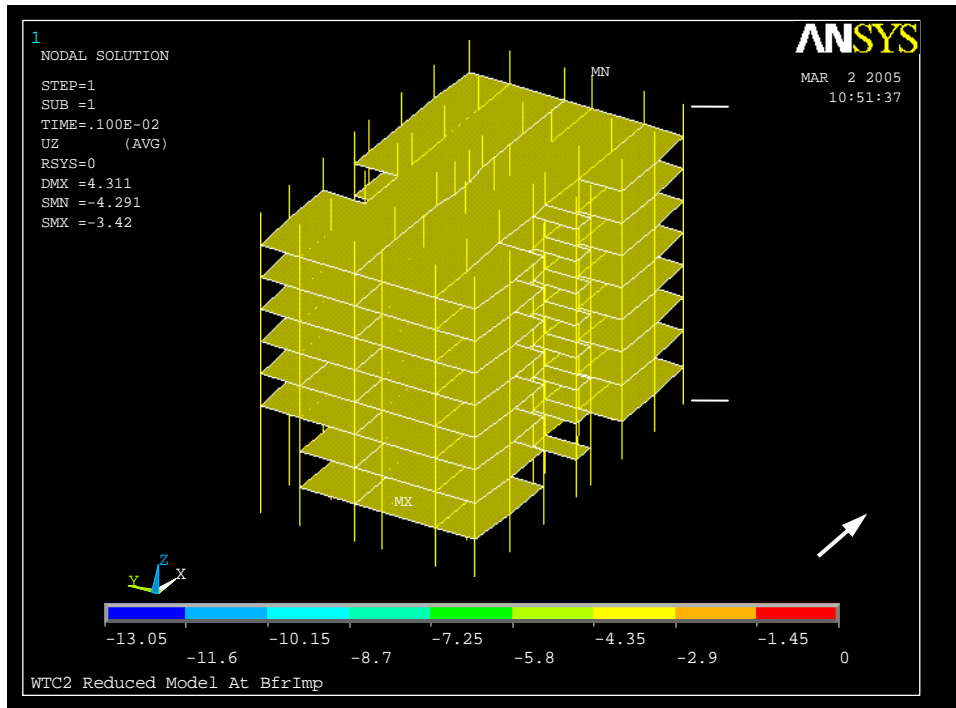


Figure 8–28. Vertical displacement before impact of WTC 2 core for Case D.

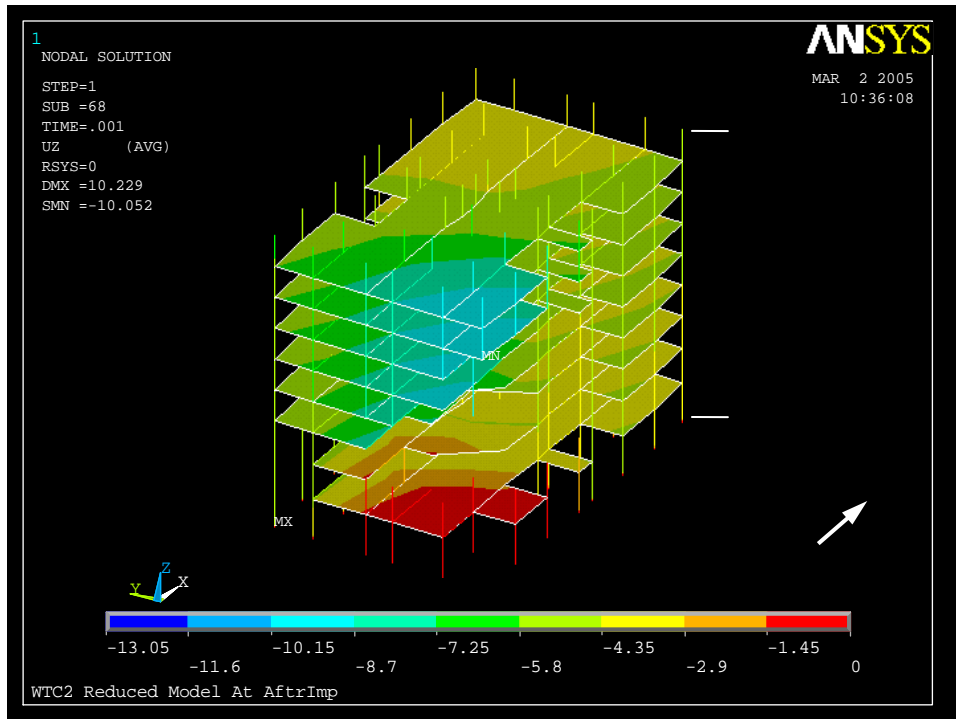


Figure 8–29. Vertical displacement after impact of WTC 2 core for Case D.

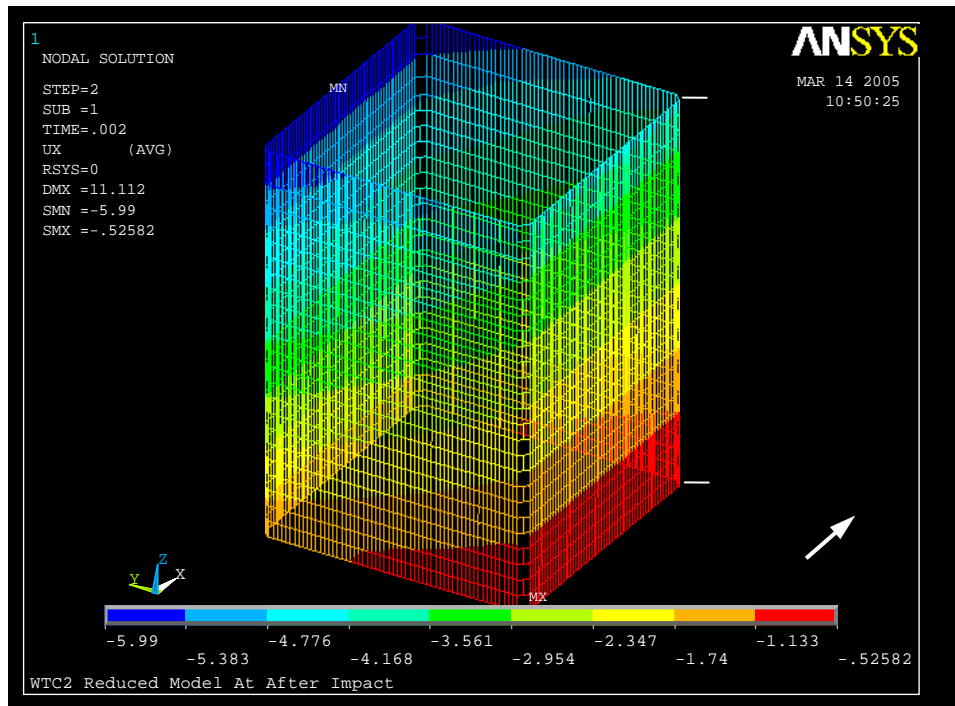


Figure 8–30. Lateral displacements after impact above WTC 2 Floor 86 in the x-direction (north-south) for Case D.

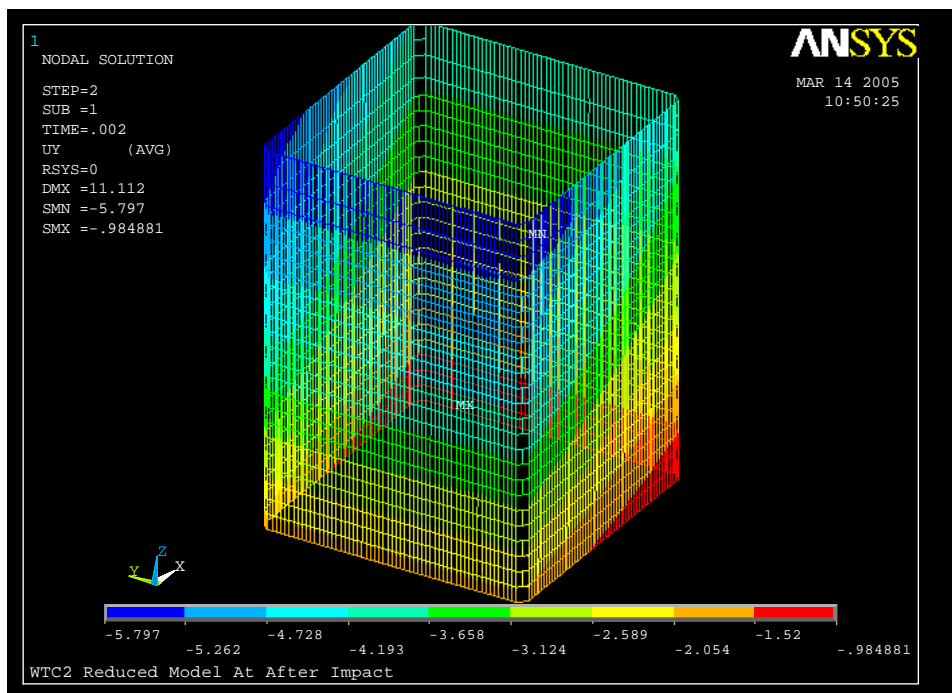


Figure 8–31. Lateral displacements after impact above WTC 2 Floor 86 in the y-direction (east-west) for Case D.

Table 8–5. Total column loads at WTC 2 Floor 83 for Case D (Compression is positive).

| Row | Analysis Stage | West | East | North | South | Core | Sum |
|------|----------------|-------|-------|-------|-------|-------|--------|
| (1) | Before Impact | 18065 | 18114 | 13567 | 13284 | 61828 | 124857 |
| (2) | After Impact | 18670 | 22481 | 12193 | 13511 | 57821 | 124676 |
| (3) | 10 min | 18728 | 22226 | 11896 | 13358 | 58413 | 124621 |
| (4) | 20 min | 18914 | 22208 | 12052 | 13318 | 58124 | 124616 |
| (5) | 30 min | 18876 | 23681 | 11770 | 13365 | 56967 | 124659 |
| (6) | 40 min | 18531 | 23682 | 11906 | 13473 | 56825 | 124418 |
| (7) | 43 min | 15667 | 15143 | 14215 | 16292 | 62422 | 123738 |
| (8) | (2)-(1) | 604 | 4368 | -1374 | 227 | -4007 | -181 |
| (9) | (3)-(1) | 662 | 4112 | -1670 | 74 | -3415 | -236 |
| (10) | (4)-(1) | 849 | 4094 | -1515 | 35 | -3704 | -241 |
| (11) | (5)-(1) | 811 | 5567 | -1797 | 81 | -4861 | -199 |
| (12) | (6)-(1) | 466 | 5568 | -1661 | 190 | -5003 | -439 |
| (13) | (7)-(1) | -2398 | -2971 | 648 | 3009 | 594 | -1119 |

Table 8–6. Total column loads at WTC 2 Floor 105 for Case D (Compression is positive).

| Row | Analysis Stage | West | East | North | South | Core | Sum |
|------|----------------|-------|-------|-------|-------|-------|-------|
| (1) | Before Impact | 8497 | 8572 | 7382 | 7169 | 17123 | 48742 |
| (2) | After Impact | 9170 | 11272 | 6487 | 8432 | 13382 | 48742 |
| (3) | 10 min | 9182 | 11061 | 6250 | 8275 | 13975 | 48742 |
| (4) | 20 min | 9279 | 11120 | 6311 | 8351 | 13682 | 48742 |
| (5) | 30 min | 9370 | 11859 | 6416 | 8553 | 12544 | 48742 |
| (6) | 40 min | 9198 | 11927 | 6524 | 8691 | 12402 | 48742 |
| (7) | 43 min | 7086 | 8026 | 6546 | 9169 | 17915 | 48742 |
| (8) | (2)-(1) | 674 | 2699 | -895 | 1263 | -3741 | 0 |
| (9) | (3)-(1) | 685 | 2489 | -1132 | 1106 | -3148 | 0 |
| (10) | (4)-(1) | 783 | 2547 | -1071 | 1182 | -3441 | 0 |
| (11) | (5)-(1) | 873 | 3287 | -965 | 1384 | -4579 | 0 |
| (12) | (6)-(1) | 702 | 3355 | -858 | 1522 | -4721 | 0 |
| (13) | (7)-(1) | -1411 | -547 | -835 | 2000 | 792 | 0 |

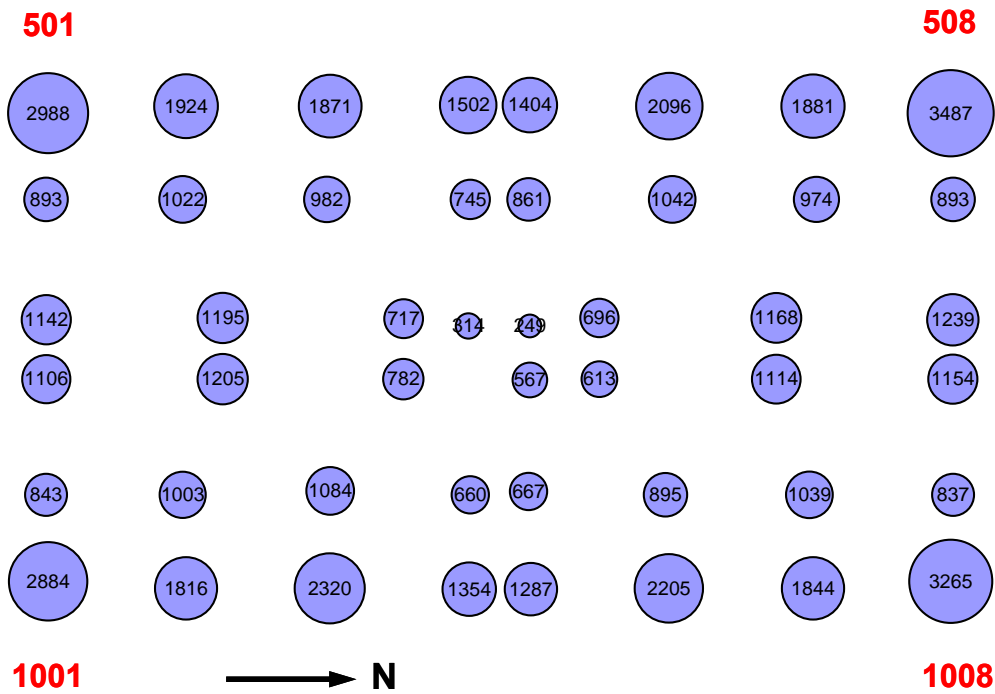


Figure 8–32. Core column loads (kip) before impact at WTC 2 Floor 83 for Case D (compression is positive).

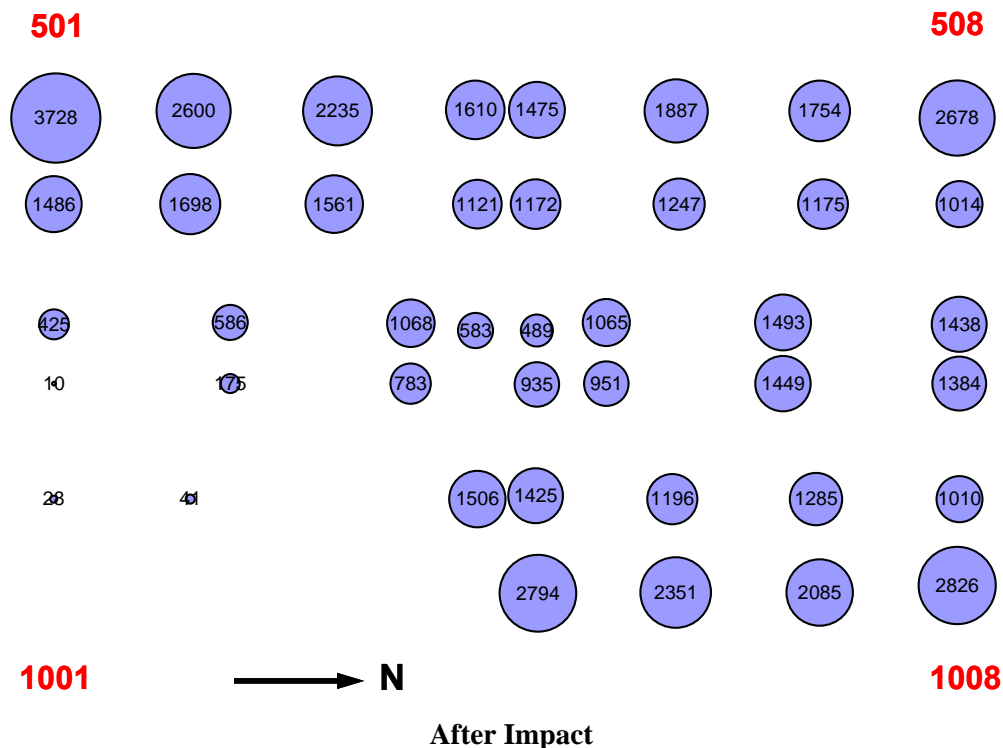


Figure 8–33. Core column loads (kip) after impact at WTC 2 Floor 83 for Case D (compression is positive).

8.5.2 WTC 2 Structural Response to Elevated Temperatures

In contrast to the fires in WTC 1, which generally progressed from the north side to the south side over approximately one hour, the fires in WTC 2 started and remained on the east side of the building until it collapsed, with the fires spreading from south to north. With fireproofing dislodged over much of the same area, the structural temperatures increased in the core, floors, and exterior walls at similar times. During the early stages of the fires, columns with dislodged fireproofing elongated due to thermal expansion. As the structural temperatures continued to rise beyond 500 °C, the thermal expansion was overcome by plastic and creep deformations under compressive loads.

Vertical displacement of the exterior walls before impact were 2.0 in. to 3.0 in. Vertical displacements of the south and east walls after impact were around 7.3 in. on the south face (over the severed columns) and about 3.5 in. on the east face, as shown in Figs. 8–34 and 8–35. These vertical displacements remained essentially constant after impact until the east wall became unstable at 43 min (Figs. 8–36 and 8–37).

After impact, the core and the north wall unloaded, and their load was redistributed to the south, west, and east walls. Table 8–7 shows that about 94 percent (3,740 kip/4,000 kip) of the load from the core was redistributed through the hat truss to the east, south, and west walls and 6 percent was redistributed through the floors to the east wall. A similar calculation for the east wall indicates that about 62 percent (2,699 kip/4,368 kip) of the load increase came through the hat truss and 38 percent was transferred through the spandrels to the north and south walls. Comparison of loads shown in Rows 8, 9, 10, and 11

in Tables 8–5 and 8–6 show that the column loads did not significantly change until the core unloaded at 30 min. Prior to this point, the thermal expansion of the core columns caused loads to increase. When the plastic and creep strains exceeded the thermal strains, the core columns shortened and unloaded. Loads in weakened core columns were redistributed to adjacent columns primarily through the hat truss.

Shortly after impact, Floors 79 to 83 began to sag and pull inward on the east wall (except where truss seat connections had failed). At 20 min, the east wall had bowed inward 9.5 in. near the center of the east wall, as shown in Fig. 8–38. The computed inward displacement agrees well with the observed inward displacement (~10 in.) that was measured from photographs at 9:21 a.m. (approximately 20 minutes after the aircraft impact). Inward displacements of the east wall steadily increased until collapse initiation.

At 30 min, the core unloaded about 850 kip (from 4,861 kip to 4,007 kip), the east wall increased about 1,200 kip (from 5,567 kip to 4,368 kip), and the north wall unloaded about 420 kip (from 1,797 kip to 1,374 kip) at Floor 83. Floor 105 column loads remained almost constant after aircraft impact until the east wall became unstable at 43 min. From 40 min to 43 min, the east wall suddenly unloaded about 8,540 kip, the west wall unloaded about 2,860 kip, the core load increased by about 5,600 kip, the north wall load increased by about 2,310 kip, and the south wall load increased about 2,820 kip at Floor 83 (Table 8–8). Comparison of the load redistribution that took place at Floor 105 with that at Floor 83 indicates that essentially all the additional core load from the east and west walls was transferred through the hat truss. For the east wall, about 46 percent (3,901 kip/8,539 kip) of the load shed was redistributed through the hat truss to the core and 54 percent was redistributed primarily through the spandrels to the south and north walls. After the load redistribution, the total load in the core columns increased to the same level as before the aircraft impact.

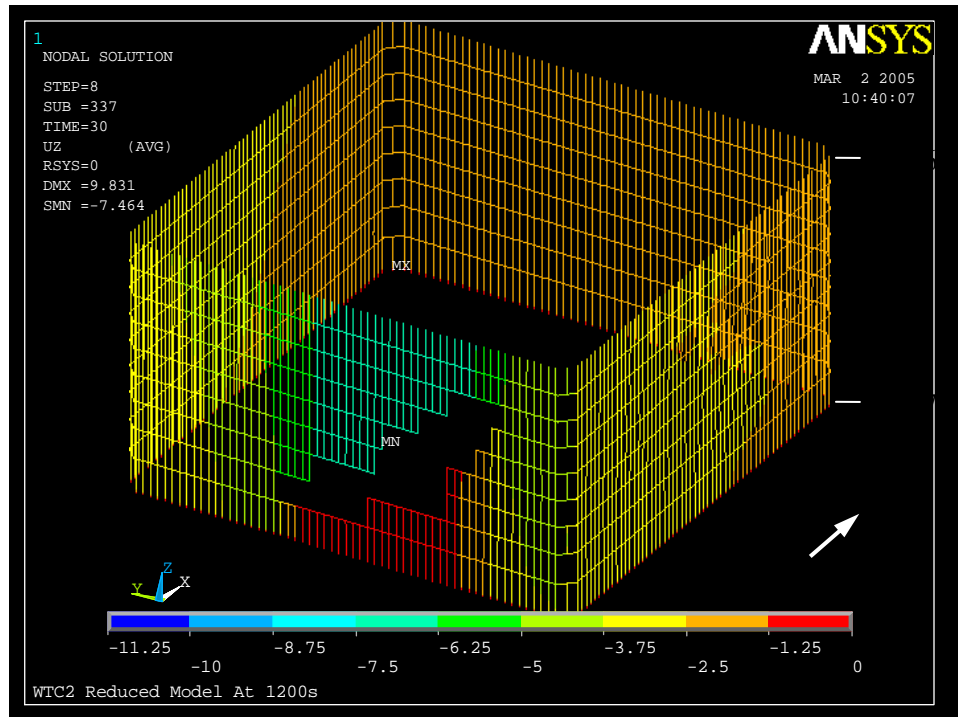


Figure 8–34. Vertical displacement of exterior wall of WTC 2 at 20 min for Case D.

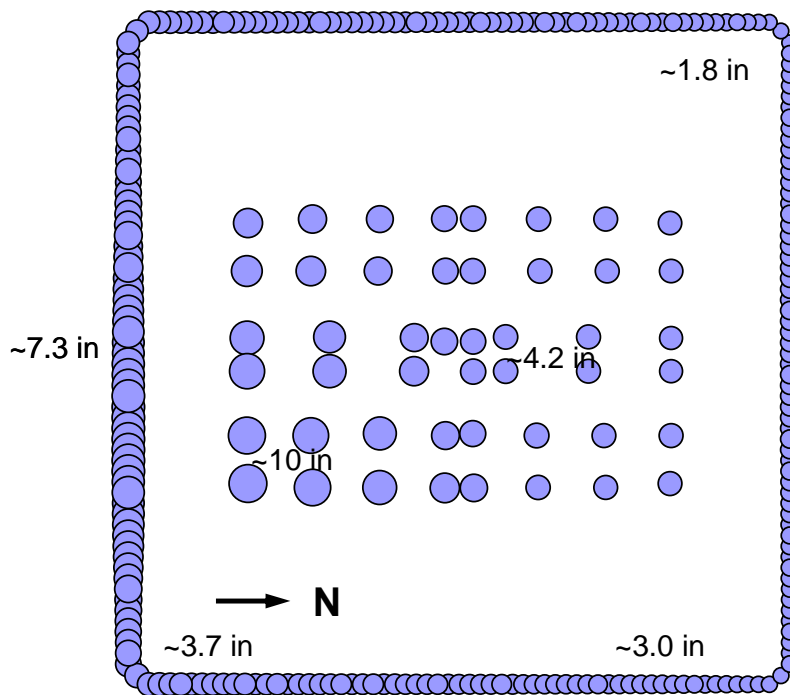


Figure 8–35. Vertical displacement at Floor 83 of WTC 2 at 20 min for Case D (note the tilt toward east and south).

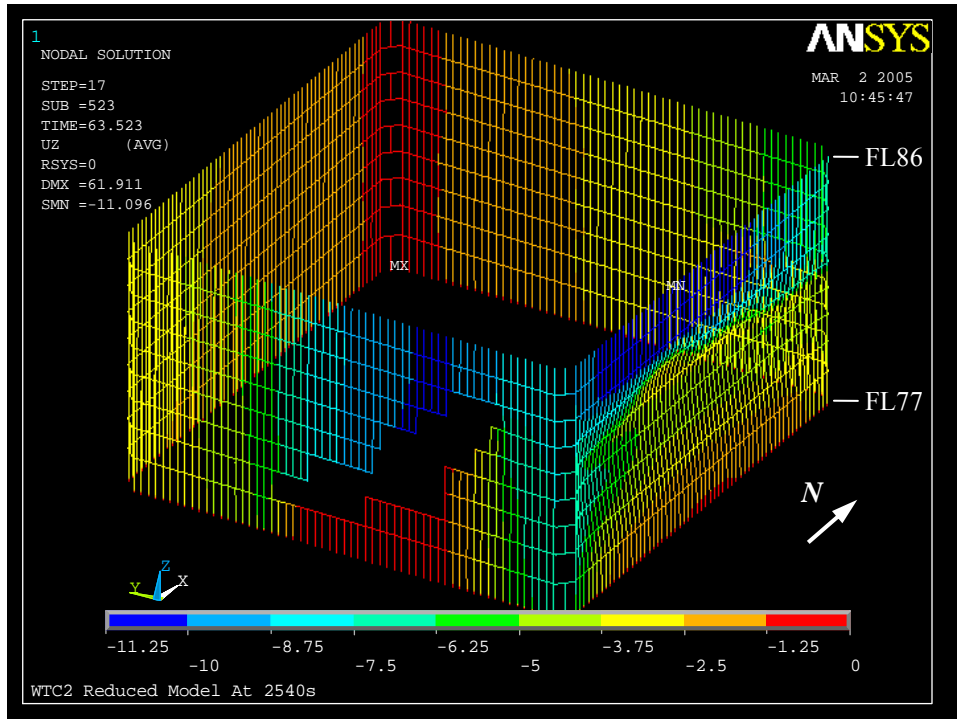


Figure 8–36. Vertical displacement of exterior wall of WTC 2 at 43 min for Case D.

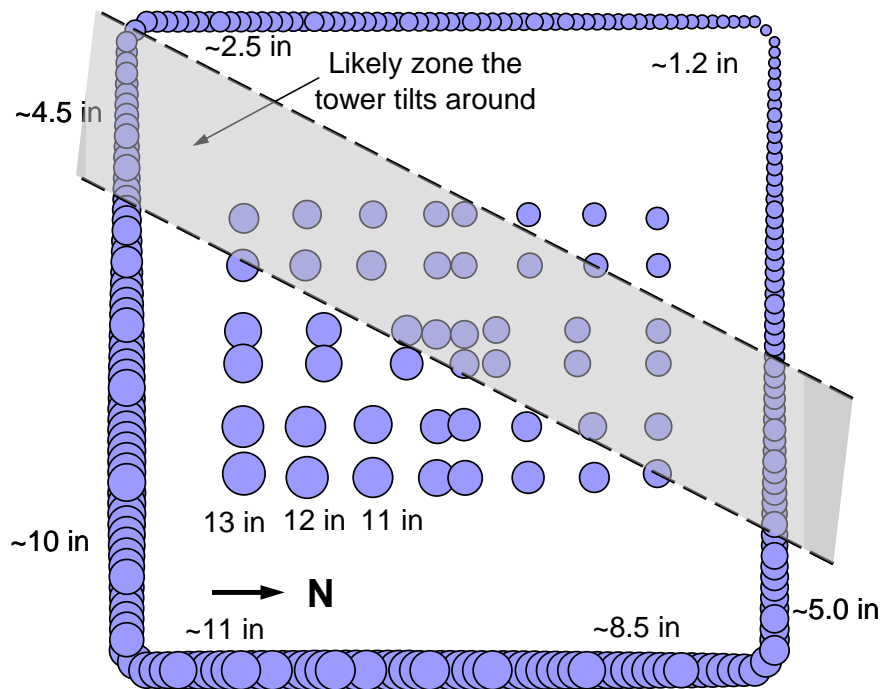


Figure 8–37. Vertical displacement at Floor 83 of WTC 2 at 43 min for Case D (note the tilt toward east and south).

**Table 8–7. Change in total column loads before and after aircraft impact.
(Loads After Impact) – (Loads Before Impact)
(Compression is positive).**

| Row | Floor | West | East | North | South | Core |
|-----|-----------|------|-------|-------|-------|-------|
| (1) | 83 | 604 | 4368 | -1374 | 227 | -4007 |
| (2) | 105 | 674 | 2699 | -895 | 1263 | -3741 |
| (3) | (2) - (1) | 69 | -1668 | 479 | 1035 | 266 |

**Table 8–8. Change in total column loads between 40 min and 43 min.
(Loads at 43 min) – (Loads at 40 min)
(Compression is positive).**

| Row | Floor | West | East | North | South | Core |
|-----|-----------|-------|-------|-------|-------|------|
| (1) | 83 | -2864 | -8539 | 2309 | 2819 | 5596 |
| (2) | 105 | -2112 | -3901 | 23 | 479 | 5513 |
| (3) | (2) - (1) | 752 | 4637 | -2286 | -2340 | -84 |

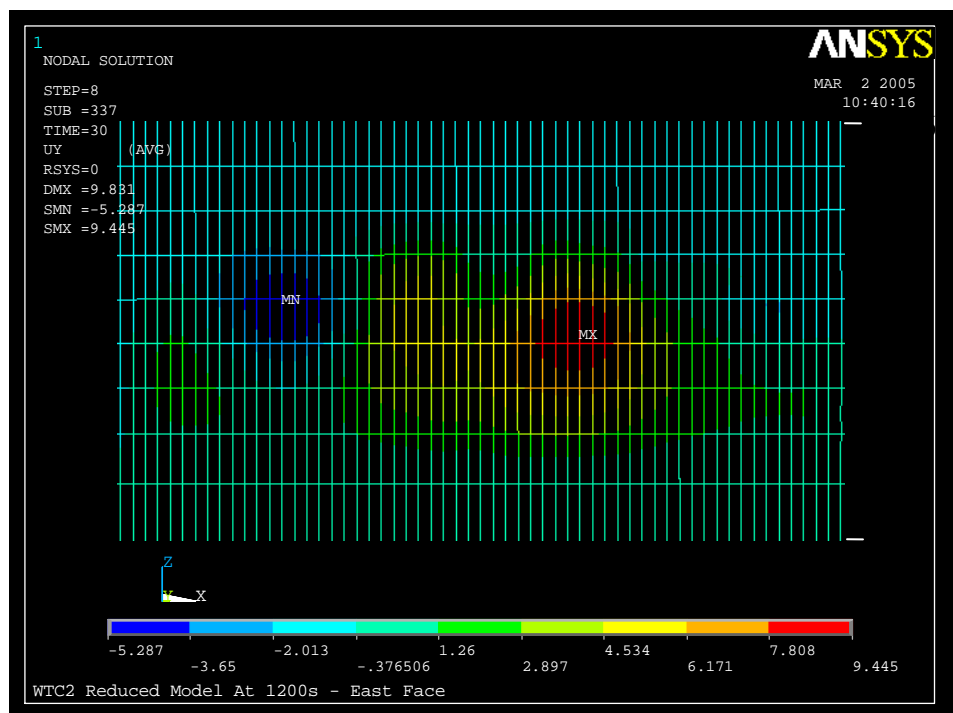


Figure 8–38. Out-of-plane displacement of the east wall of WTC 2 at 20 min for Case D.

At 43 min, the east wall became unstable and the inward displacement increased to 62 in., as shown in Figs. 8–39 and 8–40. The south and east wall vertical displacements increased to 11.3 in. The northwest corner of the exterior wall displaced upward about 1.0 in. to 2.0 in., as the tower tilted to the southeast around an axis passing through the southwest and northeast corners, as indicated in Fig. 8–37. The north exterior wall displaced laterally by an additional 15.2 in. to the east, and the south exterior wall displacement increased 6.7 in. to the south. The building section above the impact damage rotated about the tower axis an additional 0.10 percent at Floor 110.

The core displacements suddenly increased to 13 in. at the southeast corner of the core, as shown in Figs. 8–41 and 8–42. Loads on the core columns increased significantly, especially at the northeast corner. For instance, at Floor 83 the load in core column 1008 increased from 2,826 kip after aircraft impact (Figs. 8–33 and 8–43) to 5,317 kip at 43 min (Fig. 8–44), the load in core column 907 increased from 1,290 kip to 2,328 kip, the load in core column 805 increased from 950 kip to 1,483 kip.

Figure 8–45 shows the total displacements (deformed shape scaled by a factor of 20) above Floor 86 when the east wall buckled. The building section above the impact damage tilted to the southeast, and collapse initiated. For reference, the original undeformed tower is also shown.

When the east wall buckled, the load distribution changed significantly, due to the increased tilting of the building section above the impact damage towards the east. Figures 8–46 to 8–49 show how exterior columns loads changed in the exterior walls from before impact to when the east wall became unstable at 43 min. The exterior columns of the east wall unloaded about 200 kip on average at Floor 83. Similarly, the columns on the west face unloaded about 65 kip on average. Part of the load from the east and the west walls was redistributed to the east side of the south and the north walls. The column loads on the east side of the south wall increased from about 500 kip to 800 kip. The column loads on the east side of the north wall increased from about 250 kip to 400 kip.

Figures 8–50 and 8–51 illustrate the load redistribution among the exterior wall and core columns at Floor 83 before aircraft impact and at 43 min, respectively. The tilting of the building about an axis through the shaded area in Fig. 8–51 followed the buckling of the east wall and weakening of the core. Comparison of column loads before aircraft impact and when the east wall became unstable shows the columns unloading over the width of the east face and increasing at the east side of the south and north walls.

Figures 8–52 and 8–53 show the maximum elastic-plus-plastic-plus-creep strains in the columns between Floor 78 and Floor 83 at 20 min and 43 min, respectively. The elastic-plus-plastic strains, which were less than 0.05 percent before the aircraft impact, reached 0.60 percent in some exterior columns and 0.35 percent in some core columns after the aircraft impact, typically those adjacent to severed or heavily damaged columns. With increasing temperatures the plastic and creep strains increased, especially on the east wall and the east side of the core. When the east wall buckled, the elastic-plus-plastic strains reached their maximum of 2.2 percent in the east wall and 0.9 percent in the east side core columns. Creep strains were 1.0 percent to 2.0 percent in the east wall, about 2.0 percent to 6.0 percent in the core columns, and about 4.0 percent to 5.0 percent in the east side of the north wall.

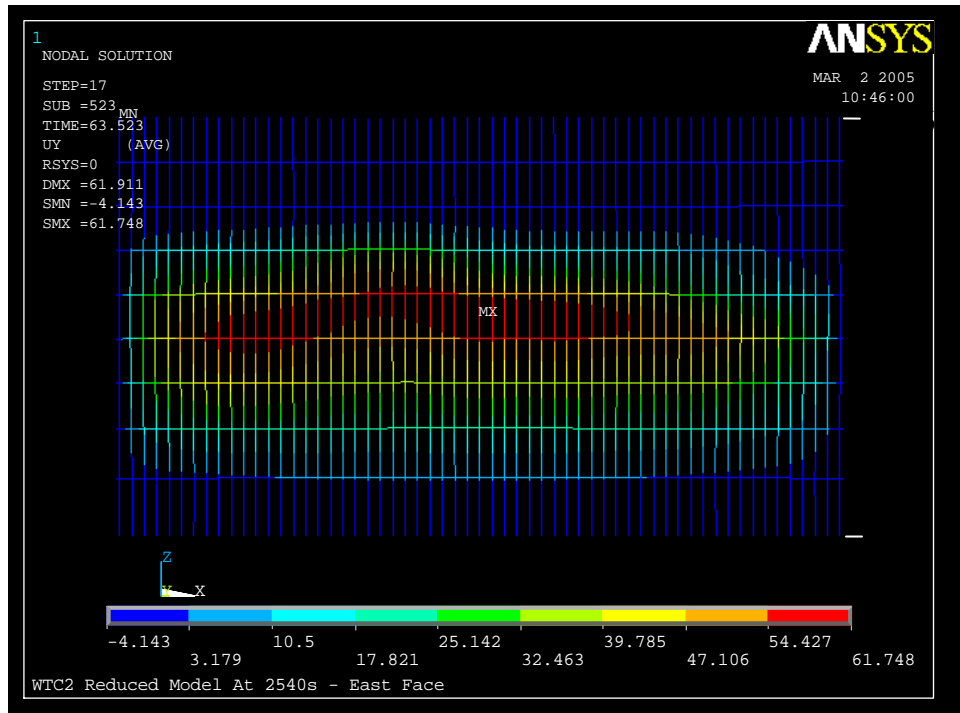


Figure 8–39. Out-of-plane displacement of the east wall of WTC 2 at 43 min for Case D.

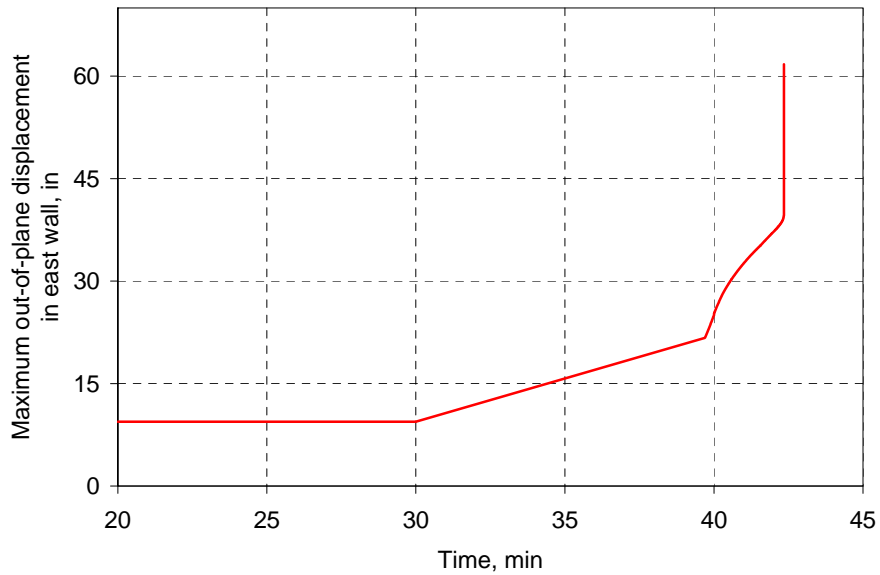


Figure 8–40. Variation of maximum out-of-plane displacement on the east wall of WTC 2 over time for Case D.

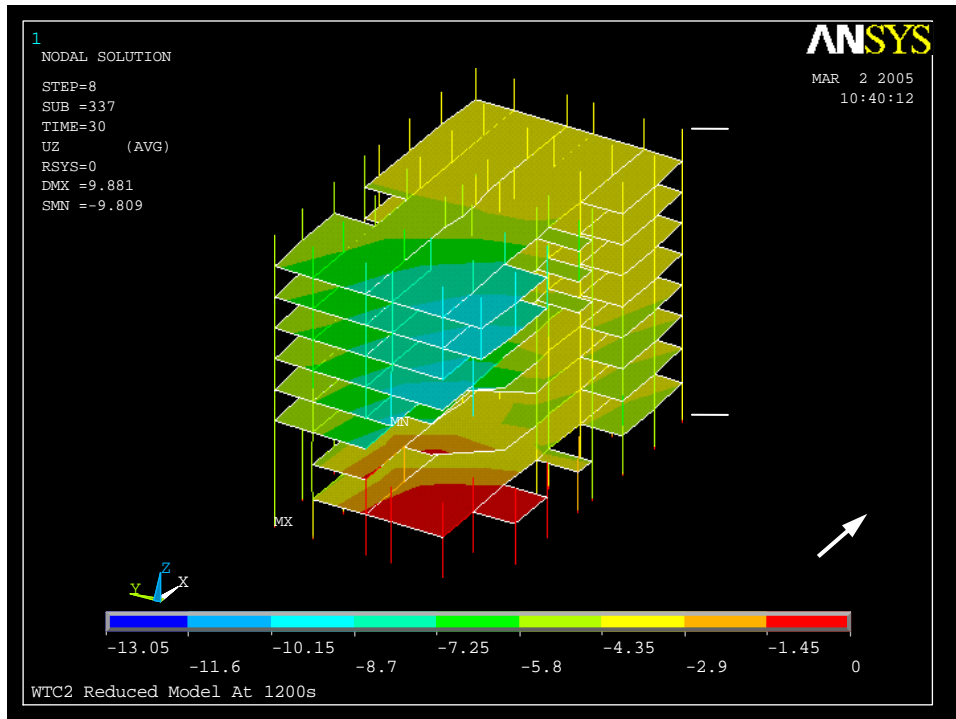


Figure 8–41. Vertical displacement of core of WTC 2 at 20 min for Case D.

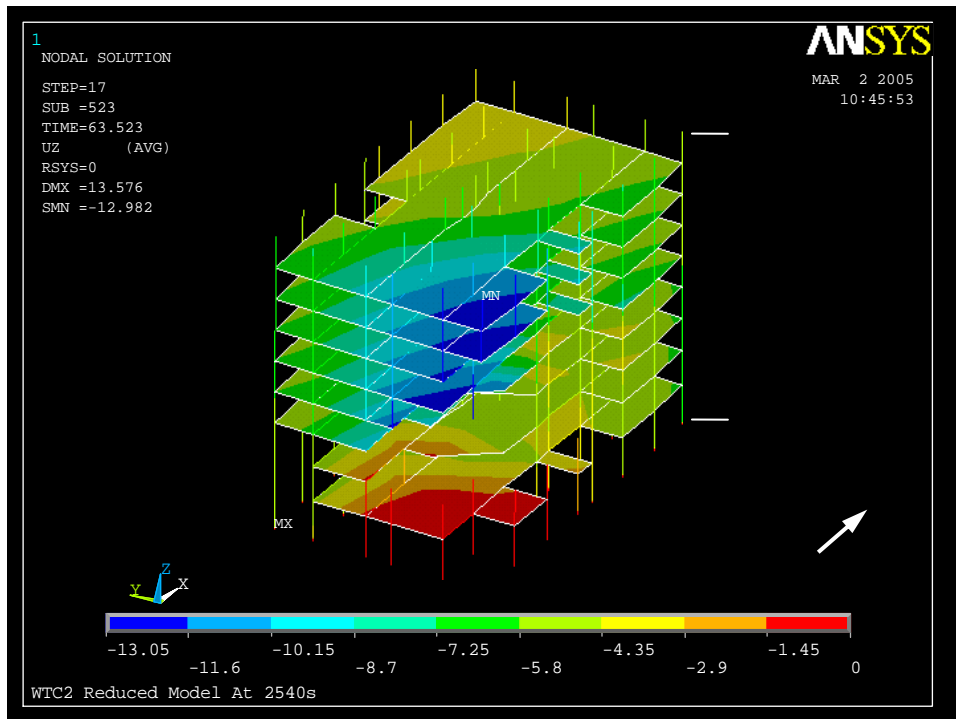


Figure 8–42. Vertical displacement of core of WTC 2 at 43 min for Case D.

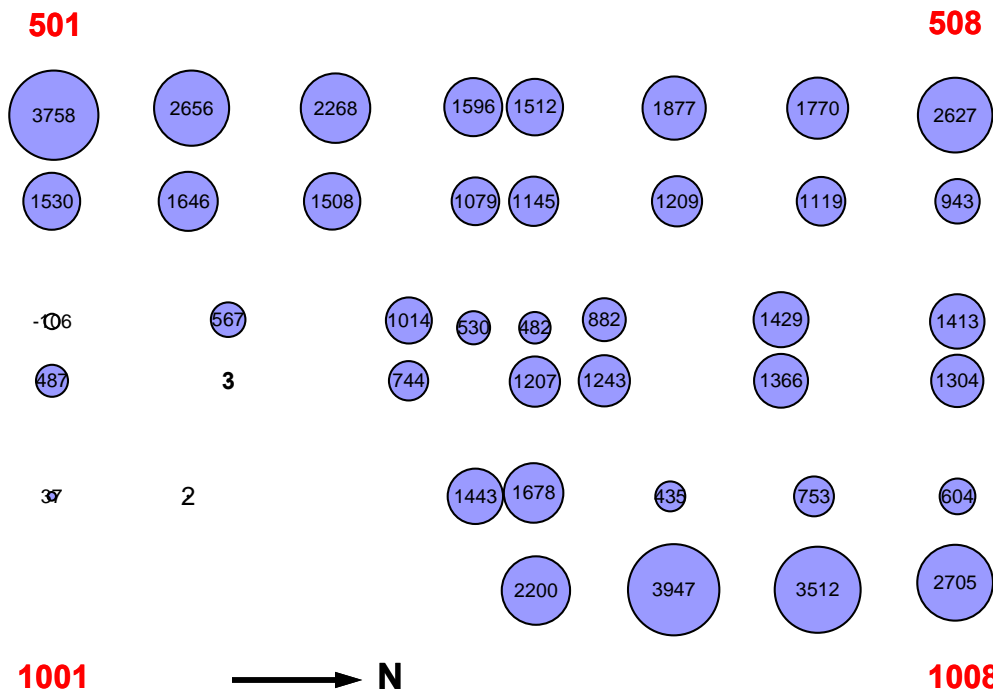


Figure 8-43. Core column loads (kip) at Floor 83 of WTC 2 at 20 min for Case D (compression is positive).

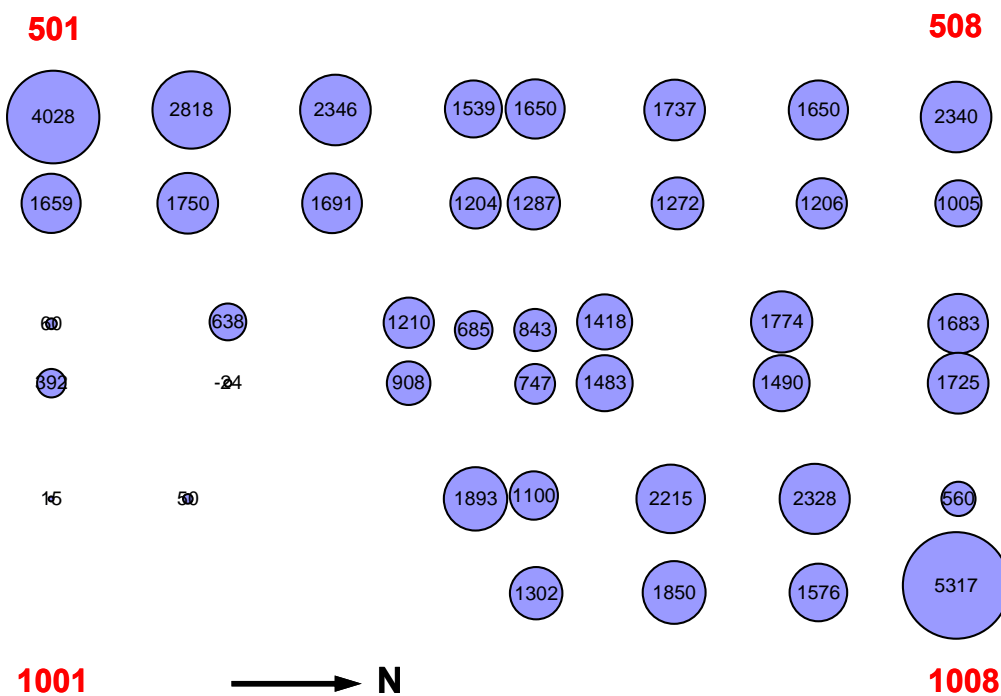


Figure 8-44. Core column loads (kip) at Floor 83 of WTC 2 at 43 min for Case D (compression is positive).

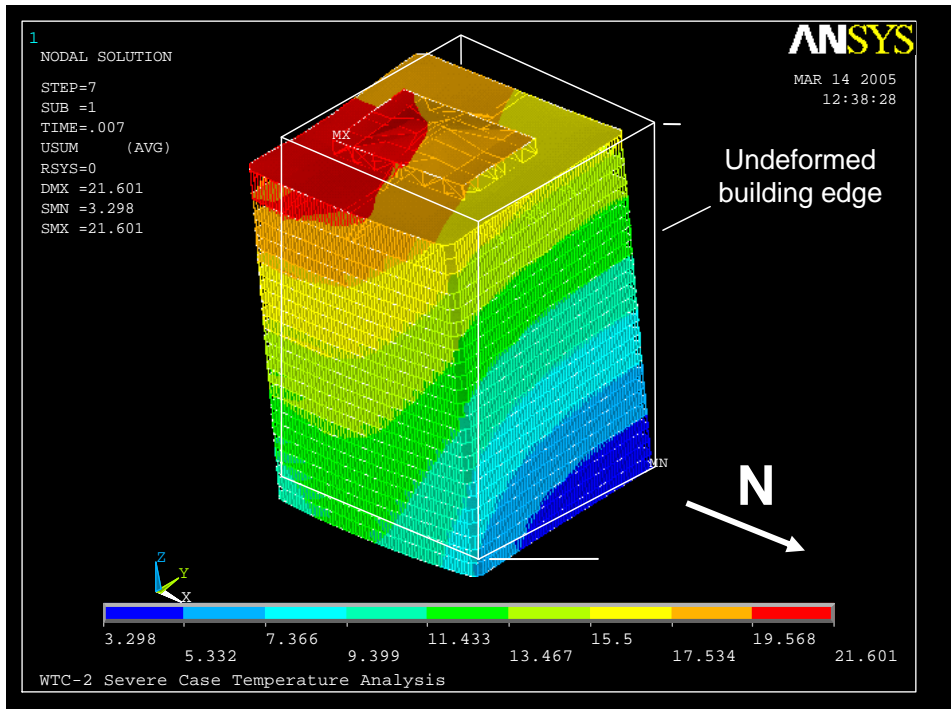


Figure 8–45. Total displacements of WTC 2 above Floor 86 at 43 min of Case D (deformed shape magnified 20 times). Note the tilt toward east and south.

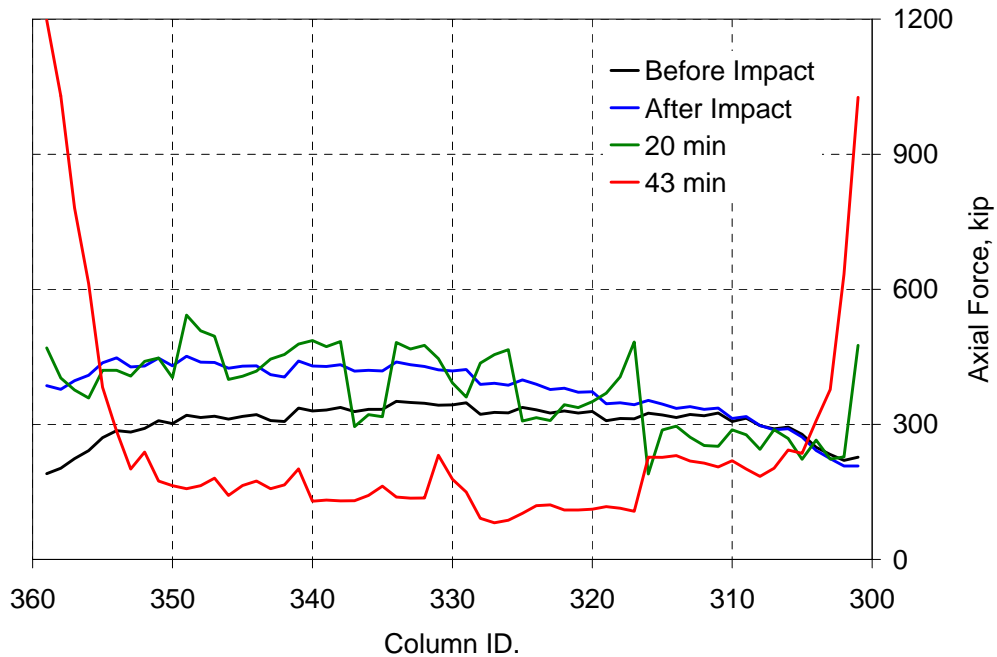


Figure 8–46. Axial force in the east wall columns at Floor 83 of WTC 2 for Case D (compression is positive).

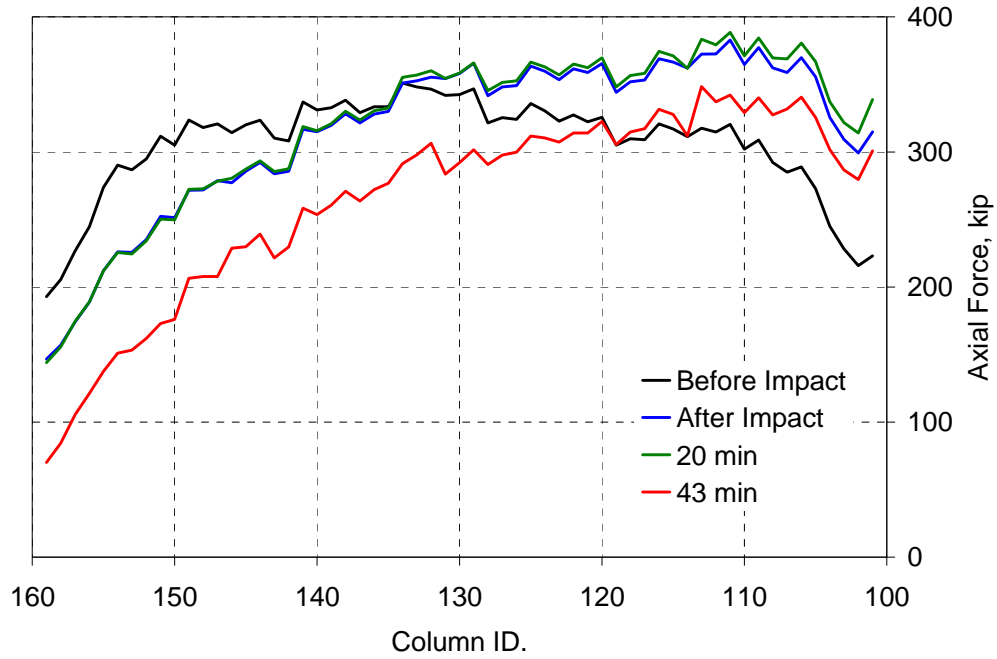


Figure 8–47. Axial force in the west wall columns at Floor 83 of WTC 2 for Case D (compression is positive).

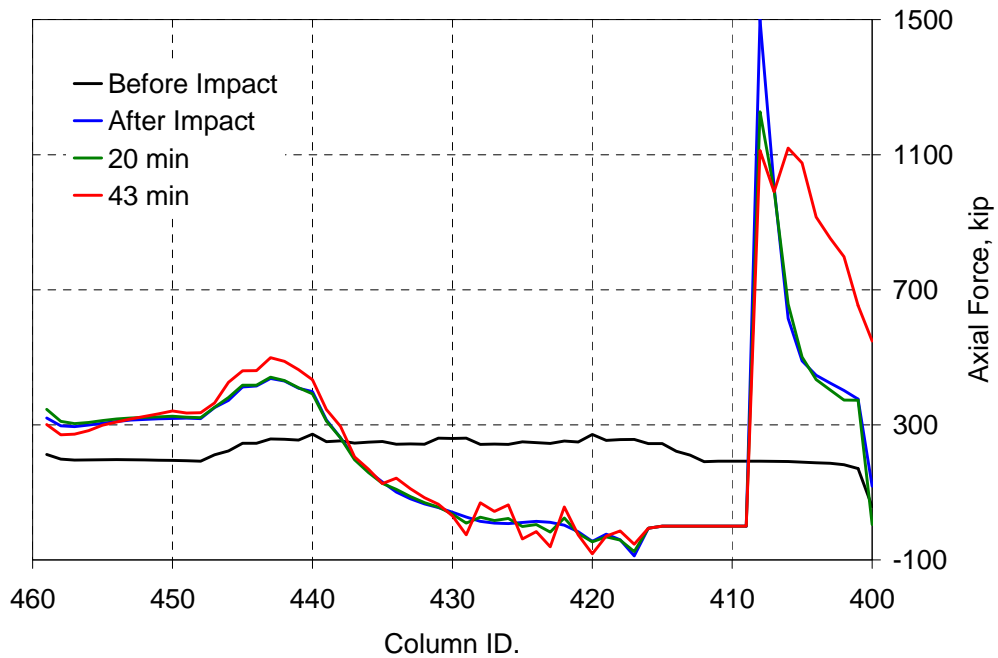


Figure 8–48. Axial force in the south wall columns at Floor 83 of WTC 2 for Case D (compression is positive).

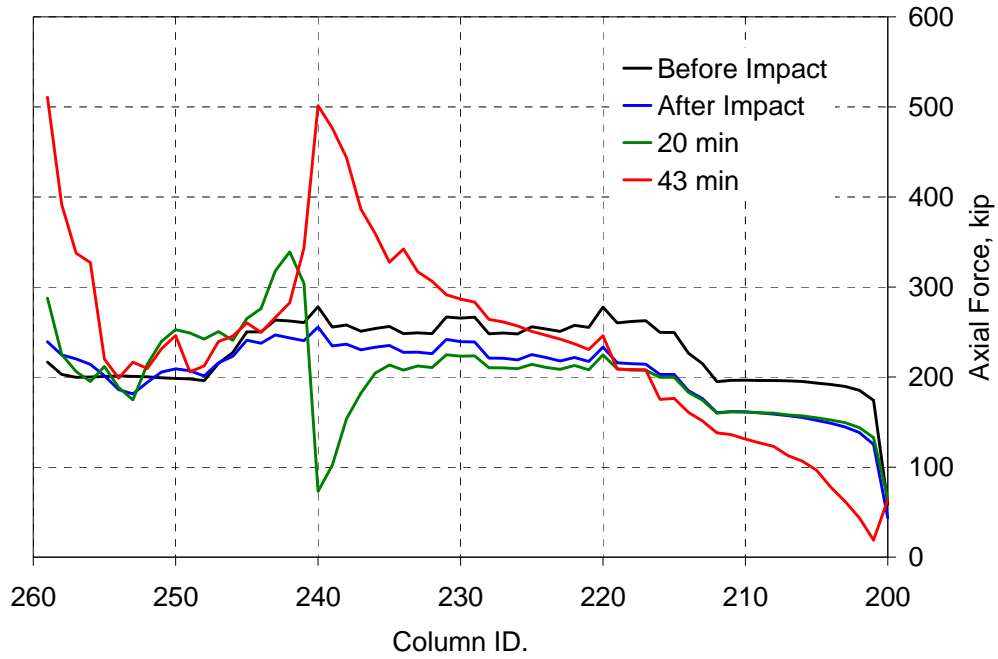


Figure 8–49. Axial force in the north wall columns at Floor 83 of WTC 2 for Case D (compression is positive).

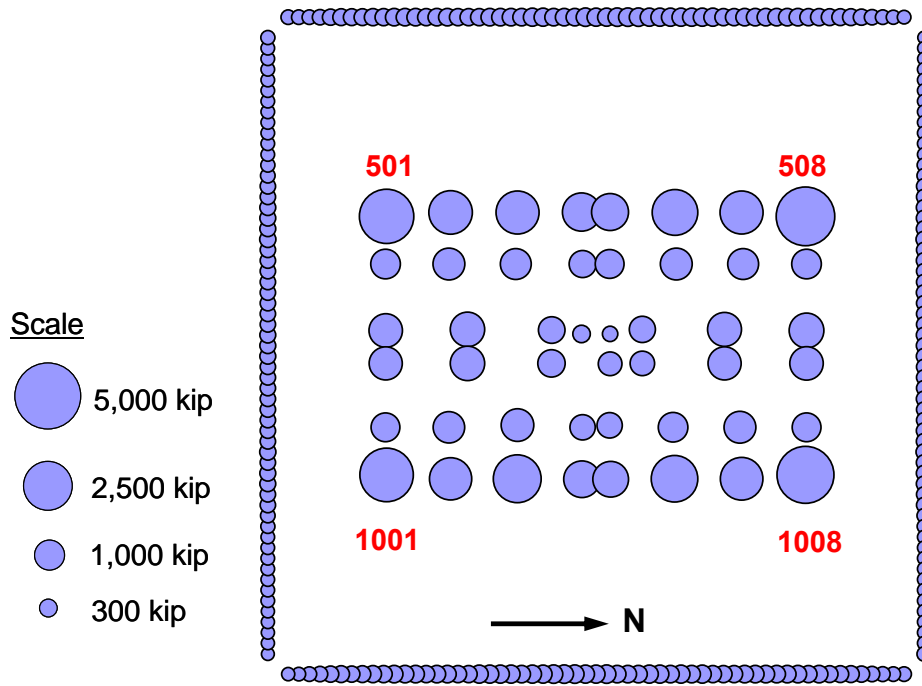


Figure 8–50. Axial force in Floor 83 columns of WTC 2 before impact for Case D (compression is positive).

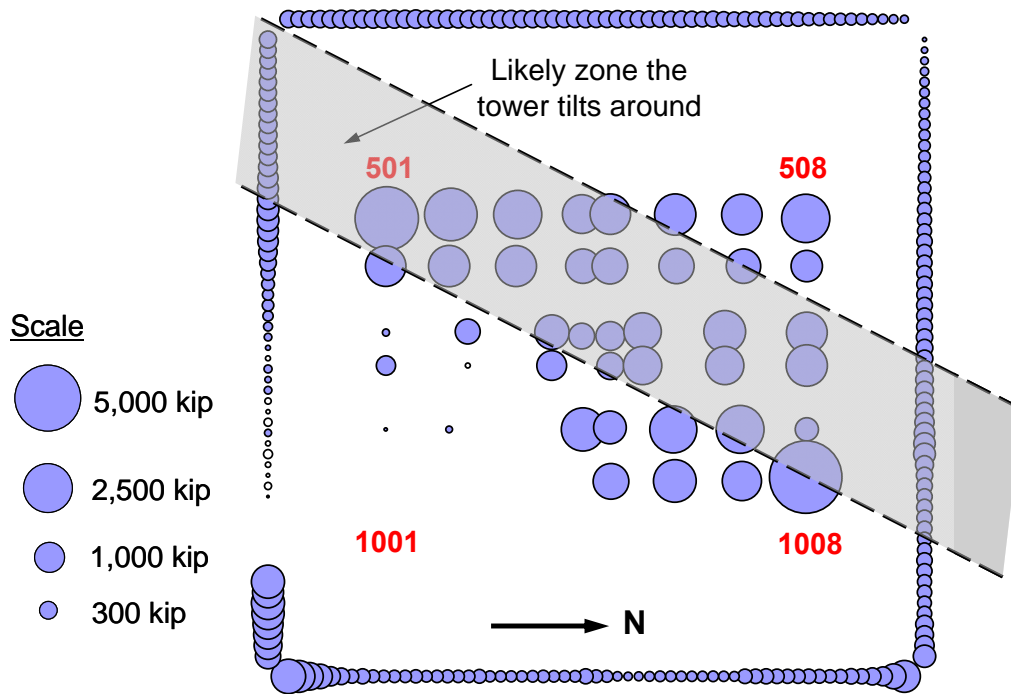


Figure 8-51. Axial force in Floor 83 columns of WTC 2 at 43 min for Case D (compression is positive).

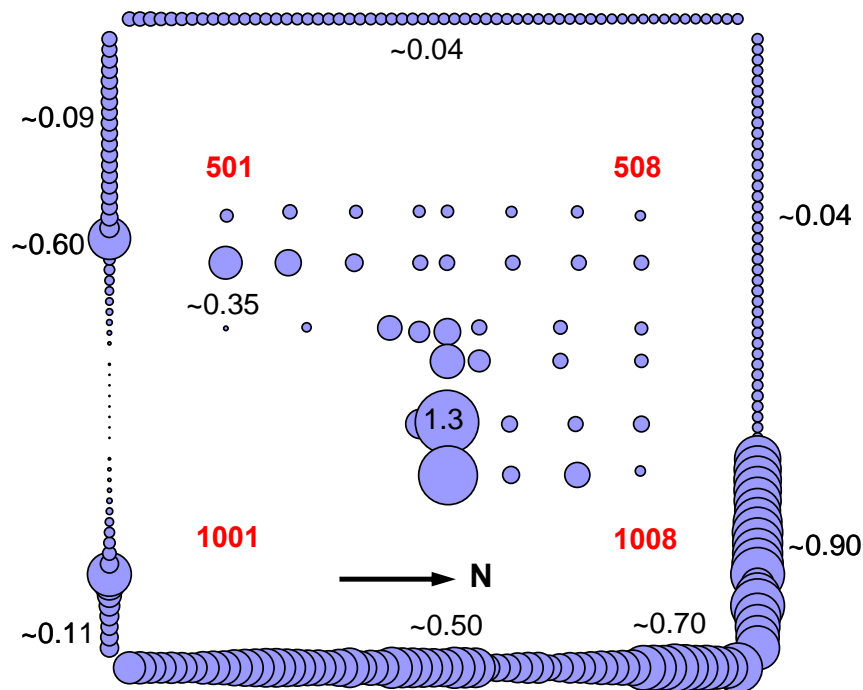


Figure 8-52. Maximum elastic-plus-plastic-plus-creep strains at 20 min for columns between Floor 78 and Floor 83 of WTC 2 for Case D (strain values are in percent).

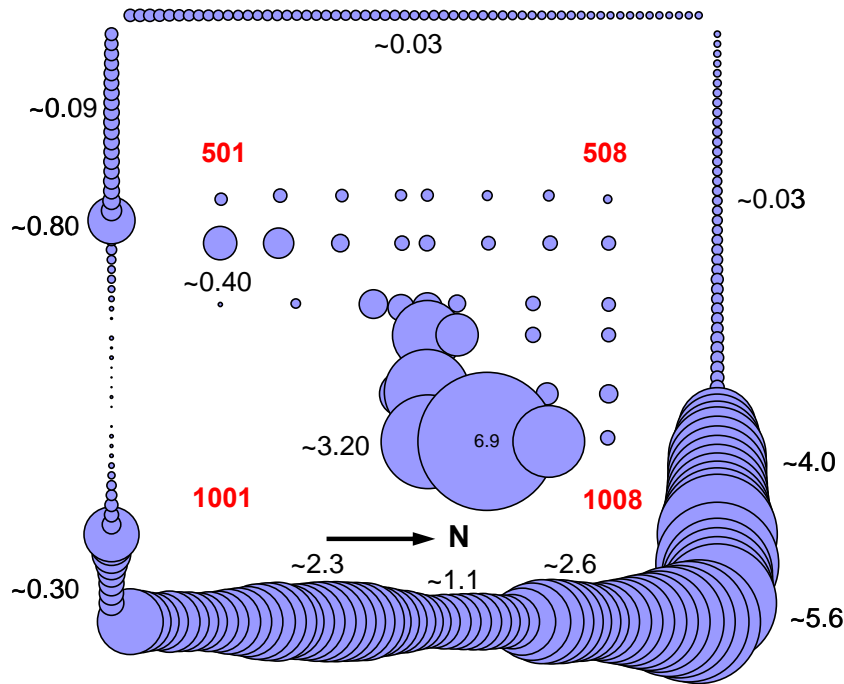


Figure 8–53. Maximum elastic-plus-plastic-plus-creep strains at 43 min for columns between Floor 78 and Floor 83 of WTC 2 for Case D (strain values are in percent).

At 43 min, the core had weakened on the east side and shortened by 3.0 in. at the southeast corner. The east wall had bowed inward approximately 62 in. and unloaded to the core and the adjacent north and south walls. The inward bowing of the east wall caused failure of exterior column splices and spandrels, and induced column instability. The instability progressed horizontally across the entire east face. The east wall unloaded and redistributed its loads to the thermally weakened core through the hat truss and to the east and west walls through the spandrels. This load redistribution is shown in Tables 8–5 and 8–6. The building section above the impact zone began tilting to the east (and to the south, although to a lesser extent) as column instability progressed rapidly from the east wall along the adjacent north and south walls, and increased the gravity load on the weakened east core columns. The change in potential energy due to downward movement of building mass above the buckled columns exceeded the strain energy that could have been absorbed by the structure. Global collapse then ensued.

8.5.3 WTC 2 Hat Truss Members and Connections

The state of the hat truss members and the connections were checked as the global model did not include break elements to capture column and hat truss splice failures or sufficient beam elements to capture buckling of hat truss outriggers. The condition of the connections and the members in the primary load path of the hat truss was evaluated at different time intervals. The evaluation included the core column splices for tension, outriggers and supporting columns for compression, and the hat truss connections that were in the primary load path for tension.

In the WTC 2 global model, the hat truss was part of the super-element above Floor 86. The elastic model that generated the stiffness matrix for the super-element, referred to as the “top model” hereinafter, was used to determine component forces. The displacements obtained at the interface nodes between the

super-element and the nonlinear portion of the building (Floor 86) were applied to the base of the top model for each analysis step.

Figures 8–54, 8–55, and 8–56 show the loads on the core column splices at the hat truss level at different steps of the analysis. Each splice was under compressive load before the aircraft impact. After the aircraft impact, the splices at severed core column lines started to carry tensile loads. The tensile capacity of the splices was compared to tensile forces at 40 min, which was when the maximum tensile forces occurred. In calculating the tensile capacity of the connections, AISC-LRFD procedures were used.

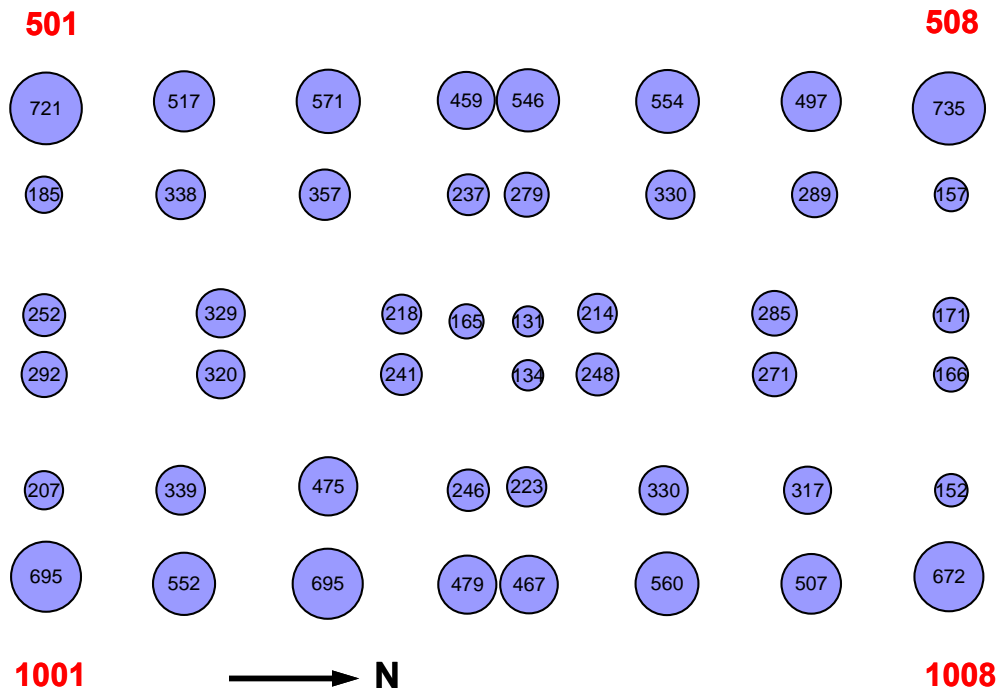


Figure 8–54. Axial force in core columns (kip) at WTC 2 Floor 105 (at hat truss level) before impact for Case D (compression is positive).

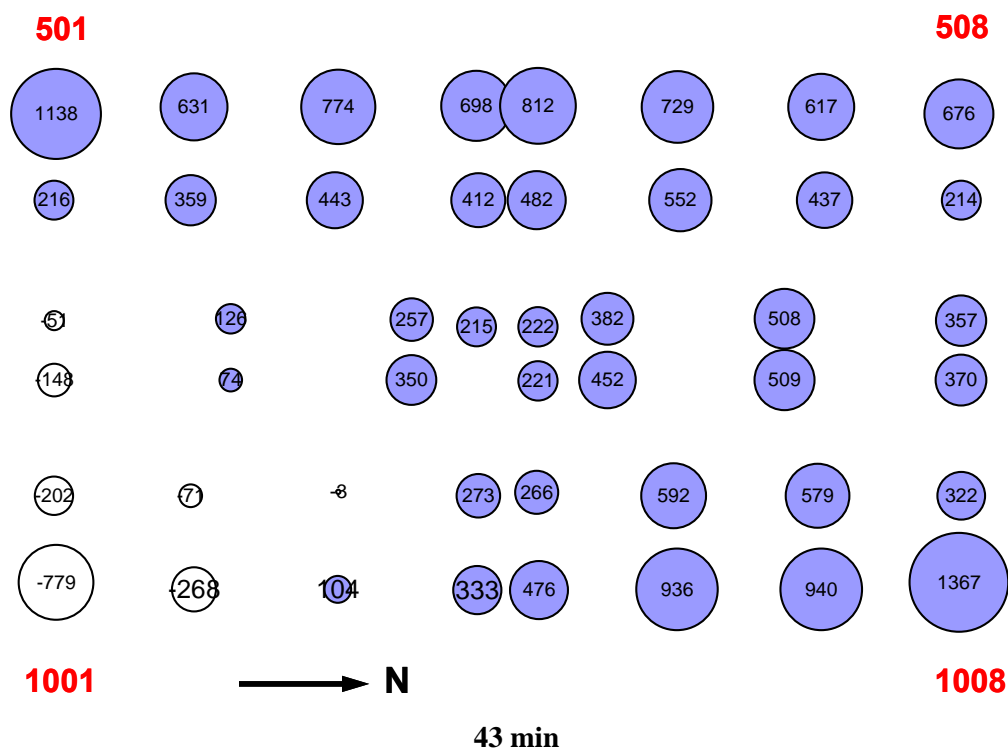


Figure 8–56. Axial force in core columns (kip) at Floor 105 (at hat truss level) of WTC 2 for Case D conditions (compression is positive).

The evaluation of core column splices required an iterative procedure as splice failures were not modeled in the top model. In the first iteration, the top model reached equilibrium using the interface node displacements at 40 min. Once equilibrium was reached, the columns exceeding their splice capacity were identified (in the first iteration columns 1001 and 1002 were identified) and removed from the top model. Before removing the columns, the displacement boundary conditions applied at the bottom of these column lines (at Floor 86) were replaced with the reaction forces that were obtained at the end of the first iteration. This conversion from displacement to force boundary condition allowed the remaining portion of the column lines to displace in the vertical direction when the columns were removed at Floor 105 to simulate splice failure. This iterative procedure was repeated until none of the remaining splices exceeded their tension capacity. A stable state was reached at the end of the fourth iteration. Fig. 8–57 shows the state of the core column splices at the end of the fourth iteration. Splices for columns 1001 and 1002 failed after impact, and splices for columns 701, 801, 901, 902, and 1003 failed either after impact or as the core responded to the fires.

In the global analyses, splice failures were not included in the super-element, which remained elastic throughout the analysis. However, based upon the analyses discussed below, it was concluded that the inclusion of splice failures would not have significantly affected the load redistribution in the global analysis. The core floors would have redistributed the loads in the failed columns to adjacent core columns, as occurred for columns with failed splice connections in the impact area. The adjacent columns would have then transferred the loads to the hat truss.

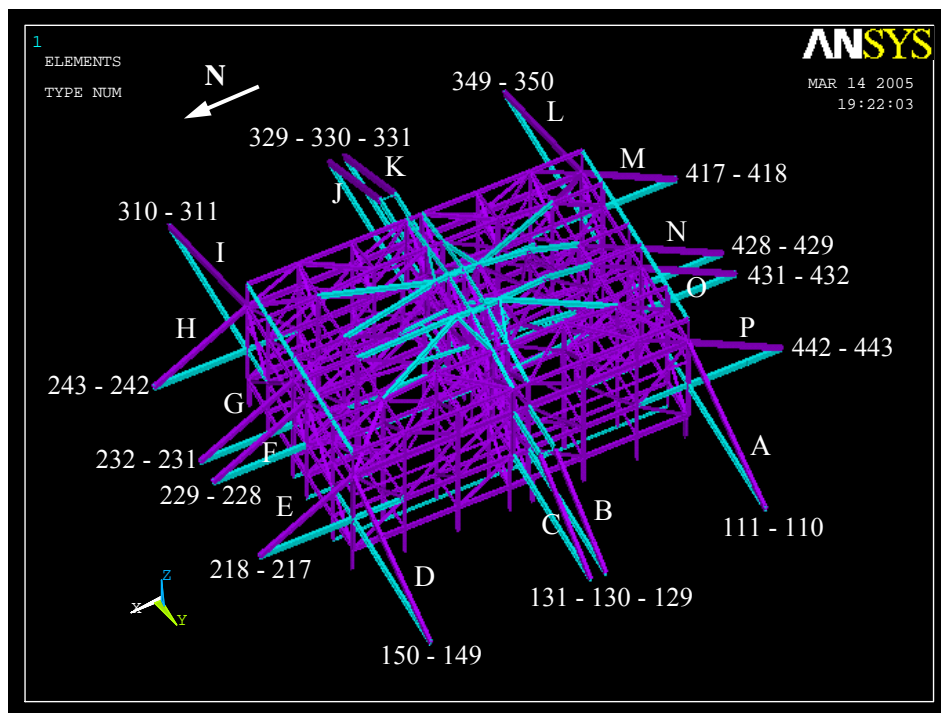


Figure 8–58. Location and IDs of outriggers and supporting columns

Table 8–9. Demand-to-capacity ratios for outriggers of WTC 2 for Case D conditions (outrigger IDs are shown in Fig. 8–3).

| Outrigger ID | Bfr. Imp. | Aftr. Imp. | 10 min | 20 min | 30 min | 40 min | 40* min | 40** min | 43 min |
|--------------|-----------|------------|--------|--------|--------|--------|---------|----------|----------|
| West | | | | | | | | | |
| A | 0.23 | 0.61 | 0.61 | 0.64 | 0.66 | 0.63 | 0.63 | 0.38 | 0.25 |
| B | 0.19 | 0.30 | 0.30 | 0.32 | 0.33 | 0.31 | 0.31 | 0.25 | -0.03*** |
| C | 0.19 | 0.27 | 0.27 | 0.28 | 0.30 | 0.27 | 0.28 | 0.22 | -0.07 |
| D | 0.21 | 0.18 | 0.18 | 0.19 | 0.21 | 0.18 | 0.20 | 0.19 | -0.29 |
| North | | | | | | | | | |
| E | 0.29 | 0.11 | 0.10 | 0.10 | 0.13 | 0.14 | 0.17 | 0.09 | -0.01 |
| F | 0.21 | 0.10 | 0.08 | 0.08 | 0.10 | 0.12 | 0.13 | 0.11 | 0.08 |
| G | 0.20 | 0.11 | 0.08 | 0.08 | 0.11 | 0.13 | 0.14 | 0.13 | 0.10 |
| H | 0.30 | 0.21 | 0.16 | 0.18 | 0.19 | 0.18 | 0.19 | 0.24 | 0.24 |
| East | | | | | | | | | |
| I | 0.22 | 0.39 | 0.35 | 0.34 | 0.45 | 0.43 | 0.42 | 0.41 | -0.18 |
| J | 0.18 | 0.56 | 0.52 | 0.53 | 0.66 | 0.65 | 0.61 | 0.71 | 0.02 |
| K | 0.18 | 0.62 | 0.58 | 0.59 | 0.72 | 0.72 | 0.66 | 0.79 | 0.09 |
| L | 0.22 | 1.12 | 1.09 | 1.12 | 1.24 | 1.30 | 1.11 | 0.00 | 0.72 |
| South | | | | | | | | | |
| M | 0.30 | 0.68 | 0.64 | 0.64 | 0.70 | 0.75 | 0.52 | 0.72 | 0.87 |
| N | 0.22 | 0.34 | 0.32 | 0.33 | 0.36 | 0.38 | 0.28 | 0.34 | 0.40 |
| O | 0.22 | 0.30 | 0.28 | 0.30 | 0.32 | 0.33 | 0.27 | 0.31 | 0.33 |
| P | 0.31 | 0.51 | 0.50 | 0.52 | 0.53 | 0.53 | 0.50 | 0.57 | 0.49 |

* After load redistribution due to core column splice failures.

** After Outrigger L was removed.

*** Negative value indicates tension

With the identified splice failures in Columns 1001 and 1002 and adjacent core columns, the load in this outrigger would have been redistributed to other outriggers. Based on the computed load redistribution after splice failures, the demand-to-capacity ratio on Outrigger L was estimated to be reduced from 1.3 to 1.1 (Column “40* min” in Table 8–9).

Outrigger L was removed from the top model after all the failed splices were removed to determine the effect on adjacent outriggers. Removal of the Outrigger L represented an upper bound solution as the load in the Outrigger would not have dropped down to zero. The adjacent outriggers increase in load; however, after the removal of the Outrigger L as presented in Column “40** min” of Table 8–9, none of the remaining outriggers exceeded their buckling or yield capacities.

The connections within the hat truss were also checked. The hat truss connections in the primary load path were identified, and their capacities were compared to their forces. The primary load path was identified by selecting hat truss members with an absolute axial stress of 25 ksi or more at 40 min, as this was when maximum forces occurred. Only the connections that transferred tensile forces were evaluated. In calculating the capacity of the connections, the AISC-LRFD procedures were used. None of the hat truss connection capacities were exceeded. Before redistribution of load due to the column-to-hat truss splice failure, none of the hat truss connections had exceeded their capacities except for the hat truss connections associated with the 1001 core column. After the load redistribution following the splice failure, the demand on the hat truss connections for the 1001 column was less than the yield capacities of all connections. It was concluded that the hat truss was capable of transferring loads from core columns to the outriggers.

Based on this discussion, it was concluded that the hat truss transferred the majority of the loads between core and exterior wall columns, even though some column splices may have failed and one outrigger may have buckled.

8.6 STRUCTURAL RESPONSE OF THE WTC TOWERS TO FIRE WITHOUT IMPACT DAMAGE

Whether the towers would have collapsed if subjected to an intense but conventional fire without aircraft impact was considered to better understand the relative roles of the impact damage and fires. This is not to imply that the fire growth and spread observed in the towers could be obtained without aircraft damage to the buildings and rapid ignition of multi-floor fires due to the dispersion of jet fuel. NIST used the observations, information, and analyses developed during the Investigation to enable the formulation of probable limits to the damage from such a fire. Since a complete analysis beyond the actual collapse times of the towers was not conducted, the findings in this section represent NIST’s best technical judgment based upon the available observations, information, and analyses.

In making the comparison, the following points were considered.

- Both WTC 1 and WTC 2 were stable after the aircraft impact. The global analyses showed that both towers had considerable reserve capacity after structural impact damage. For example, Figs. 8–9 and 8–10 show the core column demand-to-capacity ratios remained nearly the same before and after impact, except for a few columns adjacent to the severed columns. Global analysis produced similar trend for the exterior columns. This was confirmed by analysis of video footage of the post-impact vibration of WTC 2, the more

severely damaged of the two towers, which showed that the period of vibration of the building before and after impact were nearly the same, thus showing that the building had significant reserve capacity. WTC 2 oscillated with a peak amplitude that was between 30 percent and 40 percent of the tower sway under design winds and at periods nearly equal to the first two translation and torsion mode periods calculated for the undamaged structure (see NIST NCSTAR 1-2).

- Results of both the multi-workstation experiments and the simulations of the WTC fires showed that the combustibles in a given location, if undisturbed by the aircraft impact, would have been almost fully burned out in about 20 min. Note that, for the occupancies in the World Trade Center, the fuel load was estimated—and supported by fire dynamics calculations and visual observations—to be approximately 4 psf (see NIST NCSTAR 1-5).
- The fires used in the Investigation (Cases A through D), estimated from fire dynamics simulations, represented fires that were far more severe than an intense conventional fire (see NIST NCSTAR 1-5).
- In WTC 1, if fires had been allowed to continue past the time of building collapse, complete burnout would likely have occurred within a short time since the fires had already traversed around the entire floor and most of the combustibles would already have been consumed (see NIST NCSTAR 1-5). During the extended period from collapse to burnout, the steel temperatures would likely not have increased very much. The installed insulation in the fire-affected floors of this building had been upgraded to an average thickness of 2.5 in.
- In a fire simulation of WTC 2, that extended Case D for 2 hours with all windows broken during this period, the temperatures in the truss steel on the west side of the building (where the insulation was undamaged) increased for about 40 minutes before falling off rapidly as the combustibles were consumed. Results for a typical floor (floor 81) showed that temperatures of 700 °C to 760 °C were reached over approximately 15 percent of the west floor area for less than 10 minutes. Approximately 60 percent of the floor steel had temperatures between 600 °C and 700 °C for about 15 minutes. Approximately 70 percent of the floor steel had temperatures that exceeded 500 °C for about 45 min. At these temperatures, the floors would be expected to sag and then recover a portion of the sag as the steel began to cool. Based on results for Cases C and D, the temperatures of the insulated exterior and core columns would not have increased to the point where significant loss of strength or stiffness would occur during these additional 2 hours. With intact, cool core columns, any inward bowing of the west exterior wall that might occur would be readily supported by the adjacent exterior walls and core columns.
- In the simulations of Cases A through D, none of the columns and trusses for which the insulation was intact reached temperatures at which significant loss of strength occurred for the duration analyzed. The relative effects of the presence or absence of insulation on structural components, subjected to the same fire conditions, are shown in Fig. 8–59 (see NIST NCSTAR 1-5) for both adjacent trusses and exterior columns. As the plots indicate, the rate of heating was found to differ significantly depending on whether the insulation was intact or not.

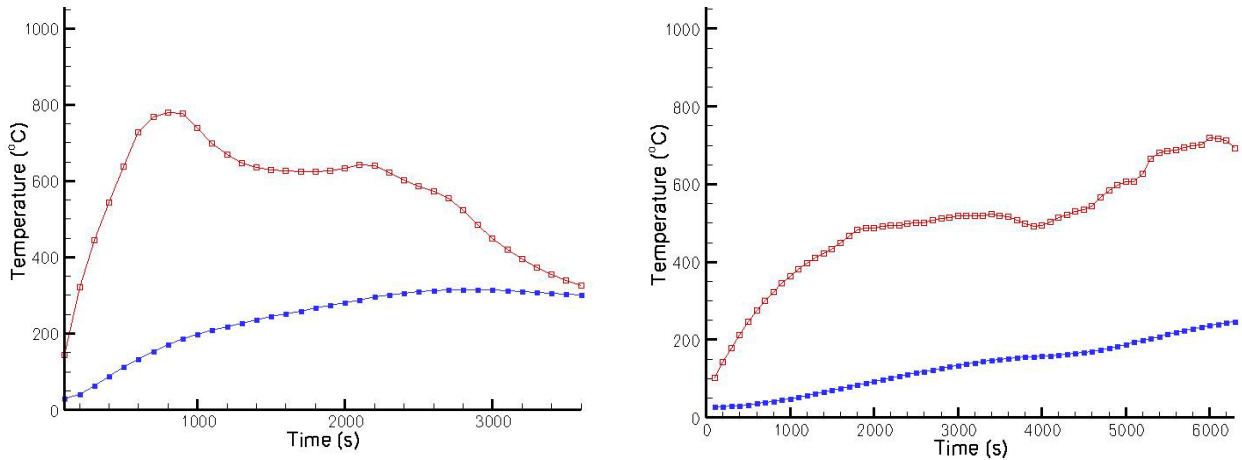


Figure 8–59. Temperatures of two adjacent trusses (left) and two adjacent perimeter columns (right) exposed to simulated fires in WTC 1. Data plotted in blue are for structural steel components with fireproofing; data in red are for steel components without fireproofing (from NIST NCSTAR 1-5).

- Structural computer simulations of the floor system (Chapter 7), supported by results of full-scale fire tests (NIST NCSTAR 1-5) and performance observed in standard fire tests (NIST NCSTAR 1-6B), showed that structural steel, insulated with $\frac{3}{4}$ in. thick fireproofing, would not have reached temperatures greater than 650 °C prior to burnout of the combustibles (20 min as noted above). Simulations also showed that variations in thickness resulting from normal application, even with occasional gaps in coverage, would not have changed this result.
- The structural temperatures of core columns in WTC 1 and WTC 2 did not exceed 300 °C where the fireproofing was intact. Thermal analysis of the WTC 1 and WTC 2 floors and exterior columns indicated that the steel temperatures were generally lower than 300 °C, with a few isolated members that rarely exceeded temperatures of 400 °C for WTC 1 and 500 °C for WTC 2 (NIST NCSTAR 1-5). Under these temperatures, reductions of stiffness and strength were small and creep effects and buckling were found not to be significant (Chapters 4 and 7). Insulated floors thermally expanded and pushed outward on the exterior columns as well as sag in the full floor analyses, but the floor sag was insufficient to exert an inward pull on the exterior columns.
- Inward bowing of the exterior walls in both WTC 1 and WTC 2 was observed only on the face with the long-span floor system. In WTC 1, this was found to be the case even though equally extensive fires were observed on all faces. The impact damage to the north face reduced the area over which pull-in could occur. In WTC 2, fires were not observed on the long-span west face and were less intense on the short-span faces than on the east face.

- Inward bowing was a necessary but not sufficient condition to initiate collapse. In both WTC 1 and WTC 2, significant weakening of the core due to aircraft impact damage and thermal effects was also necessary to initiate building collapse.
- The tower structures had significant capacity to redistribute loads (a) from bowed walls to adjacent exterior walls with short-span floors via the arch action of spandrels, and (b) between the core and exterior walls via the hat truss and, to a lesser extent, the floors.

In evaluating how the undamaged towers would have performed in an intense, conventional fire, NIST considered the following factors individually and in combination:

- The temperatures that would be reached in structural steel components with intact insulation.
- The extent of the area over which high temperatures (e.g., greater than 600 °C where significant thermal weakening of the steel occurs) would be reached at any given time.
- The duration over which the high temperatures would be sustained concurrently in any given area.
- The length of the floor span (long or short) where high temperatures would be reached.
- The number of floors with areas where high temperatures would be sustained concurrently in the long-span direction.
- The potential for inward bowing of exterior walls (i.e., magnitude and extent of bowing over the width of the face and the number of floors involved) due to thermally-induced floor sagging of long-span floors and associated inward pull forces.
- The capacity of the structure to redistribute loads (e.g., via the spandrels, hat truss, and floors) if the thermal conditions were sufficiently intense to cause inward bowing of the exterior walls.

In addition, NIST considered the following known facts about the performance of the WTC tower structures in fires:

- Historical fires also provided evidence that the towers would not collapse if subjected to a major fire without accompanying impact damage. WTC 1 did not collapse during the major fire in 1975, which engulfed about 9,000 ft² on the southeast quadrant of Floor 11. The fire spread mostly via utility closets to ten floors. At the time, office spaces in the WTC towers were not sprinklered. The fire caused minimal damage to the floor system with the ½ in. specified insulation thickness applied on the trusses (four trusses were slightly distorted) and at no time was the load carrying capacity of the floor system compromised. The fire “did not damage a single primary, fireproofed element. Some top chord members (not needed for structural integrity), some bridging members (used to reduce floor tremor and the like) and some deck support angles (used only as construction elements) were buckled in the fire—all were un-fireproofed steel.” (SCHR Letter Report 1975).

- Additionally, the four Standard Fire Tests (ASTM E 119) of floor assemblies like those in the WTC towers showed that the load carrying capacity of the short span 35 ft floor system with a 0.75 in. insulation thickness was not compromised by heating for two hours at furnace temperatures with applied loads that exceeded those on September 11, 2001 by a factor of two. It took about 90 minutes of sustained heating in the furnace for temperatures to exceed 600 °C on steel truss members with either ½ in. or ¾ in. insulation thickness. The high temperature conditions in the furnace tests were at least as severe and lasting as long as the WTC fires, although the top of the slab was not heated. Although some web members buckled and the floor test assembly sagged up to 14 in. during the tests, the insulation remained intact during the tests.

From these points and observed performance, NIST concluded:

- In the absence of structural and insulation damage, a conventional fire substantially similar to or less intense than the fires encountered on September 11, 2001 likely would not have led to the collapse of a WTC tower.
- The condition of the insulation prior to aircraft impact, which was found to be mostly intact, and the insulation thickness on the WTC floor system contributed to, but did not play a governing role, in initiating collapse of the towers.
- The towers likely would not have collapsed under the combined effects of aircraft impact and the subsequent multi-floor fires encountered on September 11, 2001 if the insulation had not been widely dislodged or had been only minimally dislodged by aircraft impact.

These conclusions apply to fires that are substantially similar to or less intense than those encountered on September 11, 2001. They do not apply to a standard fire exposure or an assumed fire exposure which has (a) uniform high temperatures over an entire floor or most of a floor (note that the WTC floors were extremely large) and concurrently over multiple floors and (b) high temperatures that are sustained indefinitely or for long periods of time (greater than about 20 min at any location), and (c) combusted fire loads that are significantly greater than those considered in the analyses. They also do not apply if the capacity of the undamaged structure to redistribute loads via the spandrels, hat truss, and floors were not accounted for adequately in a full 3-dimensional simulation model of the structure.

8.7 SUMMARY OF STRUCTURAL RESPONSE OF THE WTC TOWERS

The structural analyses conducted of floors, isolated exterior walls and cores, and global models of WTC 1 and WTC 2 found that the collapse of the towers was due to the combined effects of structural and insulation damage from aircraft impact and the subsequent fires.

Impact damage alone did not cause collapse of the towers, as they were stable after the aircraft impact and analyses showed that they had substantial reserve capacity. The fires alone also would not have caused collapse of the towers. Without impact damage, there would not have been extensive dislodging of insulation, and the structural steel temperatures would have been generally less than 300 °C, with a few steel temperatures reaching 400 °C in WTC 1 floors and 500 °C in WTC 2 floors. The core would not have weakened, the floor sag would have been insufficient to pull inward on the exterior columns, and as a consequence the exterior walls would not have bowed inward.

Collapse occurred after the fires weakened areas of the core, floors, and exterior walls that had dislodged insulation, and the core and exterior columns were unable to support the gravity loads with their reduced capacity.

The towers would likely not have collapsed under the combined effects of aircraft impact and the subsequent multi-floor fires if the insulation had not been dislodged or had been only minimally dislodged by aircraft impact. The existing condition of the insulation prior to aircraft impact and the insulation thickness on the WTC floor system did not play a significant role in initiating collapse of the towers.

8.8 REFERENCES

National Oceanic and Atmospheric Administration (NOAA)/National Climatic Data Center (NCDC), (NOAA 2001a)"Automated Surface Observing System Data; Unedited Surface Weather Observations - Hourly Data, LaGuardia Airport, September 11, 2001"

National Oceanic and Atmospheric Administration (NOAA)/National Climatic Data Center (NCDC), (NOAA 2001b)"Automated Surface Observing System Data; Unedited Surface Weather Observations - Hourly Data, John F. Kennedy Airport, September 11, 2001"

National Oceanic and Atmospheric Administration (NOAA)/National Climatic Data Center (NCDC), (NOAA 2001c)"Automated Surface Observing System Data; Unedited Surface Weather Observations - Hourly Data, Newark, NJ Airport, September 11, 2001"

Chapter 9

PROBABLE COLLAPSE SEQUENCES

9.1 INTRODUCTION

World Trade Center (WTC) 1 and WTC 2 were subjected to aircraft impact and uncontrolled fires and experienced a series of events that required complex analyses to determine their probable collapse sequences. The analysis of these events required a formal approach to integrate multiple disciplines effectively, to discern which parameters significantly influenced the analysis methods and results, and to determine the probable sequence of events leading to the initiation of structural collapse. These methods were applied as appropriate to different scales of modeling—component, subsystem, and global scales—for the aircraft impact damage, fire dynamics, thermal, and structural response analyses.

To identify the probable collapse sequences, National Institute of Standards and Technology (NIST) adopted an approach that combined mathematical modeling, statistical-based analysis methods, laboratory experiments, and analysis of photographs and videos. The approach accounted for variations in models, input parameters, analyses, and observed events. It included the evaluation and comparison of possible collapse hypotheses based on various damage states, fire paths, and structural responses to determine the following:

- The probable sequence of events from the moment of aircraft impact until the initiation of global building collapse;
- How and why WTC 1 stood nearly twice as long as WTC 2 before collapsing (102 min for WTC 1 versus 56 min for WTC 2), although they were hit by virtually identical aircraft (Boeing 767-200ER);
- What factors, if any, could have delayed or prevented the collapse of the WTC towers.

Section 9.2 describes the methodology used to conduct the aircraft impact, fire dynamics, thermal, and structural response analyses for determining the probable collapse sequence of each tower, which is presented in Section 9.3. Section 9.4 presents a discussion and summary of the collapse sequences.

9.2 METHODOLOGY

To determine the probable collapse sequence for each tower, the following steps were required:

- identification of key observables, primarily from photographs and videos
- development of collapse hypotheses, which were updated periodically through the course of the investigation with the acquisition of new data and analysis results

- sensitivity studies to identify influential parameters through the application of a formal statistical approach, orthogonal factorial design (OFD)
- development and refinement of mathematical modeling—finite element analyses and computational fluid dynamics
- evaluation of analysis results against observed and expected structural behavior, with adoption of the event tree technique, and pruning and updating of the tree branches based upon comparisons with observed data

These steps were applied to the degree needed in each phase of the analyses, from aircraft impact to fire spread, thermal loads, and structural response.

9.2.1 Key Observed Events and Conditions

Observations and data about the events following the aircraft impact were primarily obtained from three sources:

- Photographic and video records that had been catalogued and time stamped for the NIST Investigation (NIST NCSTAR 1-5A)
- Interviews of individuals in the towers during the event and those contacted by individuals in the towers during the event (NIST NCSTAR 1-7)
- Interviews of emergency response personnel and emergency communication records (NIST NCSTAR 1-8)

Observations were used to develop timelines and refine collapse hypotheses for each tower. Key observations were used to guide the towers' structural analysis and are summarized in the structural timelines (Chapter 6). Structural analyses were used to develop and refine understanding of the sequences of events, particularly events near or in the core that could not be observed.

Observations were classified into two groups: key observations and noted observations. Key observations were significant structural events that were explicitly addressed in or used to validate the structural analyses. Noted observations were events that may have been linked to a structural response, but their significance could not be conclusively assessed.

Observables were used in all the analyses in three ways: (1) to determine input parameters, such as the aircraft speed and direction at impact, (2) to impose time-related constraints on the analysis, such as imposing observed broken windows over time to constrain the spread of fire, or (3) to validate analysis results, such as global stability after impact and during thermal loading.

9.2.2 Collapse Hypotheses

Collapse hypotheses were developed over the course of the NIST Investigation. The first hypotheses were published in the May 2003 NIST Progress Report, and were updated in the June 2004 Progress Report and October 2004 Public Meeting at NIST. The Probable Collapse Sequence for each tower was

presented at the April 2005 Public Meeting in New York City. The stages of hypothesis development are summarized as follows:

- **Possible Collapse Hypotheses** (May 2003) – not building specific; key events not identified
- **Working Collapse Hypothesis** (June 2004) – single hypothesis for both WTC towers; identified chronological sequence of major events
- **Leading Collapse Hypotheses** (October 2004) – separate hypothesis for each WTC tower; identified building-specific load redistribution paths and damage scenarios in addition to chronological sequence of major events
- **Probable Collapse Sequences** (April 2005) – refined building-specific collapse sequences with chronological sequence of major events, load redistribution paths, and damage scenarios.

Over the course of the investigation, NIST continued to investigate technical issues and modify or refine the collapse hypotheses for each tower as needed. Technical issues that were analyzed and refined during the investigation included:

- Aircraft impact damage to structural components, insulation, and partition walls.
- Dispersion of aircraft debris and damage to building contents.
- Thermal effects on core columns and floors, especially extent and movement of fires.
- Thermal effects on exterior columns, especially temperature gradients in columns.
- Extent of load redistribution within and between core columns and exterior wall columns and their reserve capacity to accommodate added gravity loads with thermal effects.
- Capacity of hat truss to accommodate load redistribution from severed columns.
- Capacity of bolted splices in the severed core columns to carry tensile loads to the hat truss.
- Relative magnitude of the load redistribution provided by the hat truss, local core floor, and the truss floor system for each tower.
- Axial/shear/bending capacity of floor connections to core and exterior columns.
- Mechanisms to propagate instability laterally in the exterior columns
- Capacity of spandrels, including splices, to transfer shear in the exterior walls.
- Role of bolted splices in the instability of exterior columns.
- Comparison and reconciliation of hypotheses with observed facts (photographs and videos, eyewitness accounts, emergency communication records).

The possible collapse hypotheses published in May 2003 were developed by NIST and considered several leading hypotheses that had been postulated publicly by experts. These are summarized in Appendix C, Table C-1. One hypothesis suggested that the load carrying core columns were weakened by the fires and failed, initiating overall building collapse without the need for any weakening or failure of the steel truss floor system. Another hypothesis suggested that significant portions of one or more floor truss systems sagged, as they were weakened by fires, pulling the exterior columns inward via the connections to initiate overall building collapse through combined compression and bending failure of the exterior columns. A variation of this hypothesis suggested that the sagging floor system failed in shear at its connections to the columns, leading to overall building collapse initiation through buckling failure of the exterior columns. Load eccentricities introduced by partially damaged floor systems could also have contributed to buckling failure of the columns.

The working collapse hypothesis published in June 2004 was developed to explain the collapse initiation of the WTC towers. The working hypothesis (summarized in Appendix C, Table C-2) identified the chronological sequence of major events as the WTC tower structures redistributed loads from one structural element to another to accommodate the aircraft impact and subsequent fire damage until no further load redistribution was possible, thus, leading to collapse. The working hypothesis was based on analysis of the available evidence and data, consideration of a range of hypotheses (including those postulated publicly by experts), and the understanding of structural and fire behavior at that time. It allowed for multiple load redistribution paths and damage scenarios for each building.

The leading collapse hypotheses for WTC 1 and WTC 2 that were presented in October 2004 are shown in Appendix C, Figs. C-3 and C-4. A separate collapse hypothesis was developed for each tower that identified load redistribution paths and damage scenarios for each major event. The leading hypotheses accounted for the WTC structural system, aircraft impact and subsequent fires, post-impact condition of insulation, the quality and properties of the structural steel and concrete, and the relative roles of the exterior and core columns and the composite floor system, including connections. The hypotheses were consistent with evidence held by NIST (at that time). They were based on the subsystem analysis described in Chapter 7.

The Probable Collapse Sequences for WTC 1 and WTC 2 were presented in April 2005 following completion of global structural response analyses and are shown in Section 9.3. The structural sequences of events were consistent with evidence held by NIST.

9.2.3 Mathematical Modeling – Analysis Interdependencies

Events that played a significant role in the structural performance of the towers were the aircraft impact, rapid ignition of fire on multiple floors, and the growth and spread of fire in each tower. To determine the structural response, detailed information was required on the condition of the structural system and its passive fire protection system both before and after the aircraft impact and during the ensuing fires that elevated temperatures in the structural members.

The interdependence of the various analyses is illustrated in Fig. 9-1. Reference structural models were developed before other structural models to determine the baseline performance of each tower prior to September 11, 2001. The reference models were used as a basis for the aircraft impact damage models and the structural response and failure models to ensure consistency between structural models. The

aircraft impact analysis determined damage to the exterior and the interior of the building and included the structural system, insulation, partition walls, and furnishings for each tower. The analysis also provided an estimate of the fuel dispersion in the towers. These results provided initial conditions for the fire dynamics analysis, thermal analysis, and structural analysis. The fire dynamics analysis simulated the growth and spread of fires and produced gas temperature histories for each floor subjected to fire. The fire dynamics model accounted for damage to interior partition walls and floors (which affected ventilation conditions) and the distribution of debris and fuel.

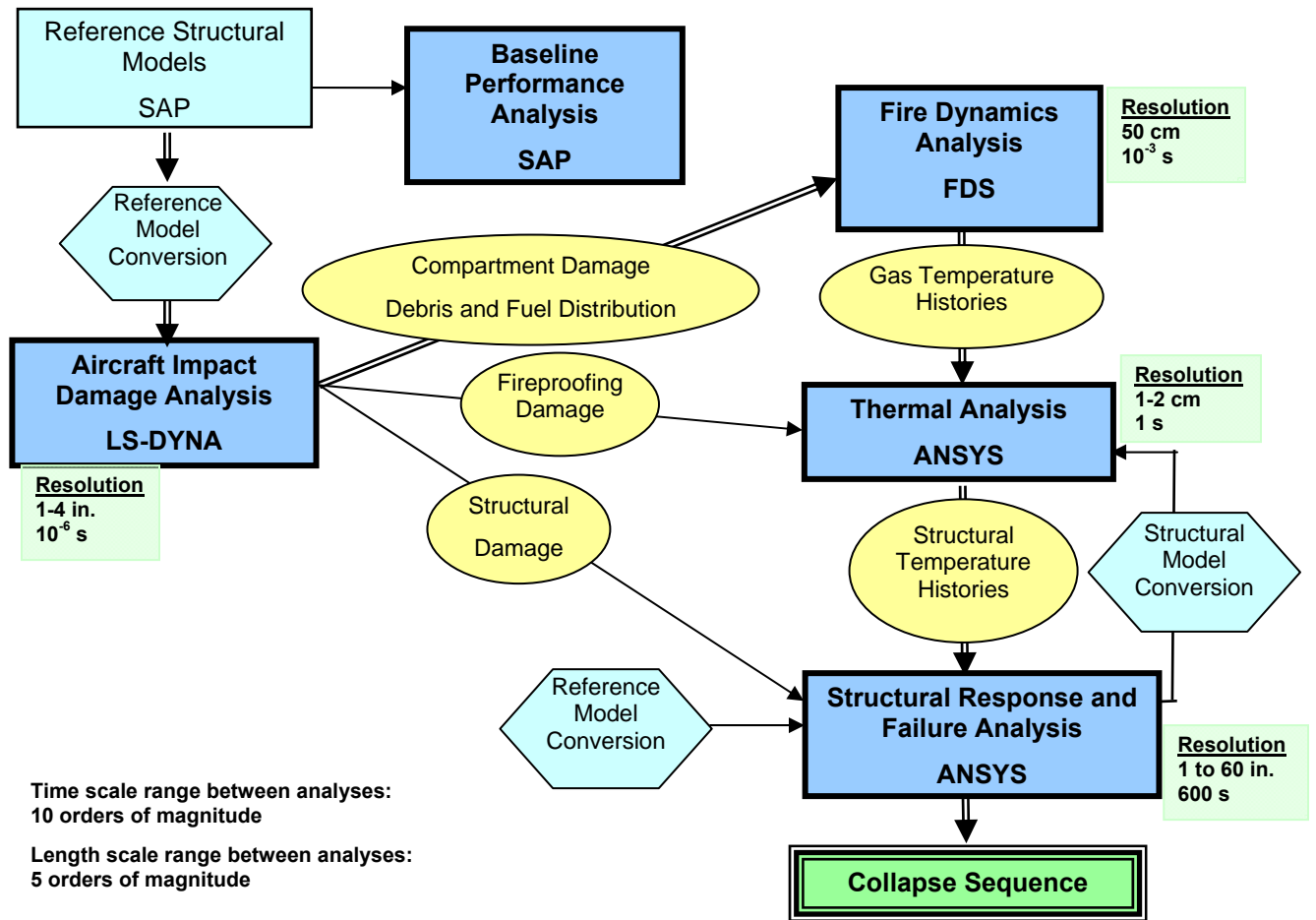


Figure 9–1. Critical analysis inter-dependencies.

The thermal analysis used a solid element heat transfer model to determine temperature histories for the various structural components accounting for the presence or dislodgement of insulation. The thermal analysis required input from the structural analysis model, fire dynamics analysis results, the analysis of damage to insulation, and temperature-dependent thermal material properties. The structural temperature histories, also referred to as thermal loads, were input to the structural analysis, along with the structural impact damage and temperature-dependent material properties, to determine the structural response of each tower.

9.2.4 Sensitivity Studies to Identify Influential Variables

Sensitivity studies were conducted for the aircraft impact, fire dynamics, and thermal analyses to identify the most influential parameters for component, connection, and subsystem behavior. To identify the most influential parameters, an orthogonal factorial design process was used to design analysis ‘experiments’ (Box, 1978). Numerical experiments with an orthogonal factorial design (OFD) method were conducted for detailed models of components and subsystems to identify parameters that strongly influenced the analysis results:

- Only parameters whose values were not accurately known were selected (parameters that were known with near certainty were set to the known values).
- Selected parameters were varied within a range of likely values, determined from available data and assigned three alternative values: lower value (-), central value (0), upper value (+).

The OFD approach allowed for identification of influential parameters that reduced the number of analysis runs at the global level. The influential parameters for the structural response analyses included the aircraft impact analyses through the impact damage and temperature histories that were part of the required input data. To determine structural response to damage and thermal loads, numerous component and subsystem studies were conducted that identified critical structural behavior and failure mechanisms and how they varied with temperature. Structural behaviors that were studied included restrained thermal expansion, thermal weakening of columns and floors, floor sagging and associated inward pull on exterior wall, and load redistribution through major structural subsystems. Failure mechanisms that were studied included, for example, tensile failure of core column splices and hat truss connections, column buckling, or loss of composite action in the floor system.

The influential parameters that were identified for each analysis, based on available information, were used to create three input data sets. Figure 9–2 illustrates the analysis tree with all influential parameter combinations resulting from this procedure for the three likely values, a lower value, a central value, and an upper value. It is apparent that analysis of all possible combinations required the number of analyses at each level to increase by a factor of three. The number of global structural response analyses was prohibitive with this approach.

However, computational analyses provided valuable insight into the relationship between input and output data for the aircraft impact, fire dynamics, thermal, and structural response analyses. These insights, along with the sensitivity studies, enabled significant reduction of the number of scenarios that were analyzed. Figure 9–3 shows the final pruned analysis tree, which was obtained as follows. After the aircraft impact analysis results were evaluated for the three sets of input parameters, the less severe damage case was discarded (pruned) as it did not reasonably match key observables. The base and more severe damage cases were each analyzed for fire growth and spread (FDS) and for the corresponding temperature histories of structural components (FSI). The linkage between the aircraft impact, fire dynamics, and thermal analyses for each damage case created highly correlated sets of input data and analysis results. For instance, the damage from the severe aircraft impact case provided input data for analysis of the fires corresponding to the severe impact damage, and both analyses provided input data for the thermal analysis of structural components subject to severe impact damage and the corresponding fires. The high level of correlation between the linked sets of aircraft impact, fire, and thermal analyses, as well as similar results for alternative fire conditions for the same impact damage, led to a single branch

at each successive analysis, as shown in Fig. 9–3. The temperature histories for the base and more severe cases (referred to as Case A and Case B for WTC 1 or Case C and Case D for WTC 2 elsewhere in this report) were used in the structural analysis of major subsystems—the isolated core, a full floor, and the exterior wall analyses. The results of the subsystem analyses showed that the more severe case impact damage results better matched key observables. The subsystem analysis results led to the pruning of the global structural analysis for the base case impact damage sub-tree, as shown in Fig. 9–3. Consequently, only the more severe cases (Cases B and D) were used in the global analysis of each tower.

Tables 9–1 to 9–4 list the observables used for the validation of analysis results, the significant input data, influential parameters, and significant output for each analysis.

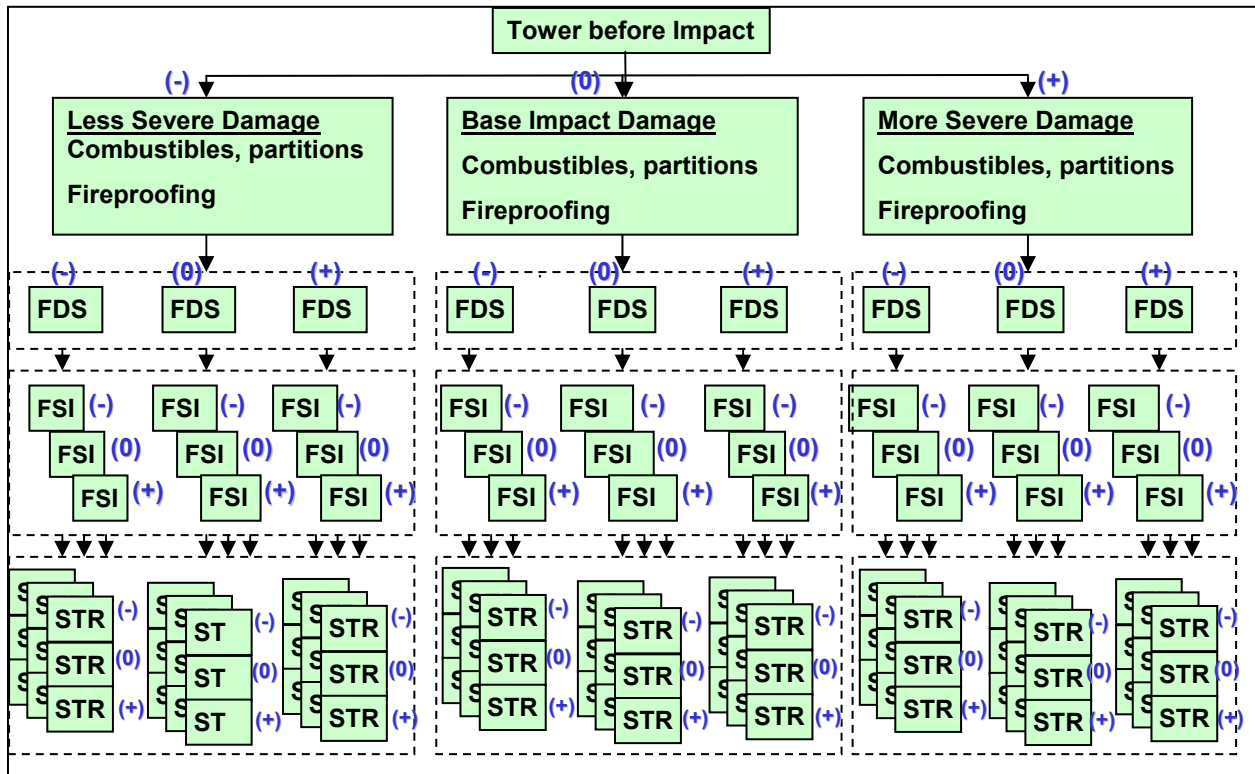


Figure 9–2. Full analysis tree for influential parameter effects.

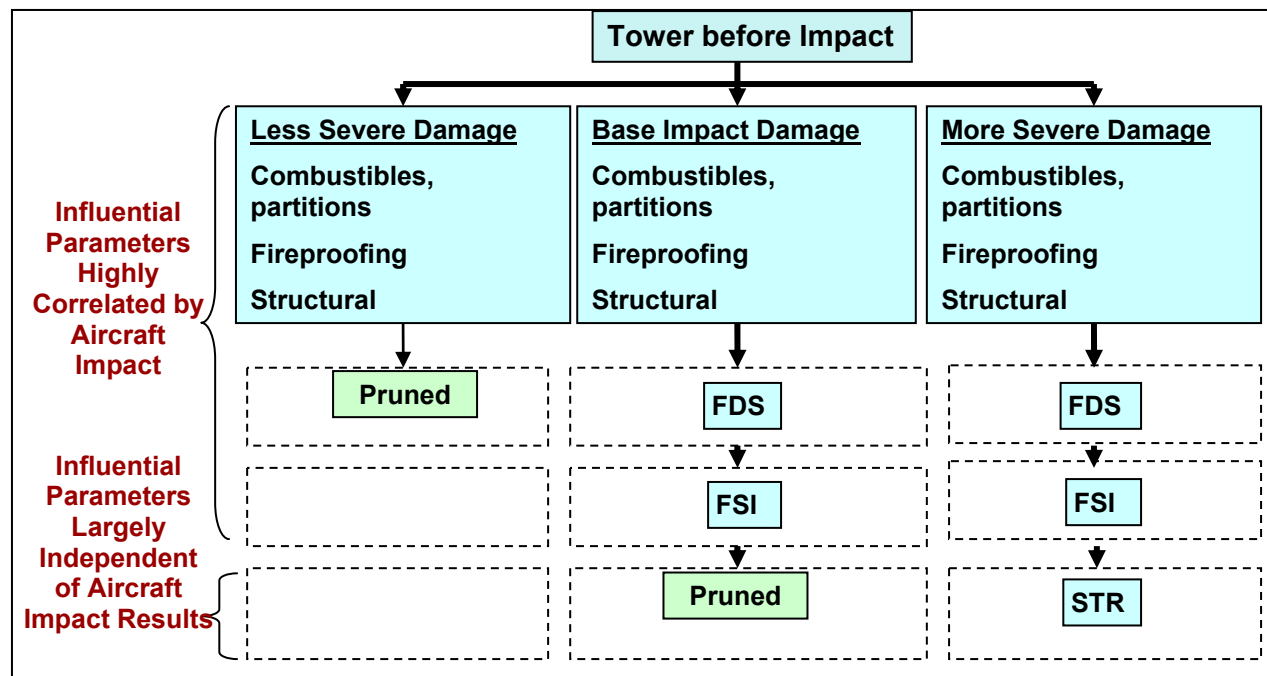


Figure 9–3. Pruned analysis tree for influential parameter effects.

Table 9–1. Aircraft impact analysis parameters.

| <i>Validation Data</i> | | <i>Model and Analysis</i> | | |
|--|------------------------------------|--|----------------------------------|---|
| Observables from Photo/Video | Observables from Interviews | Significant Input | Influential Parameters | Significant Output |
| Impact damage to exterior wall | Stairwell damage | Structural model with service loads | Aircraft velocity | Structural damage |
| Engine/landing gear exit location and speed | | Aircraft model with proper contents and mass | Aircraft pitch | Debris path (insulation and partition damage) |
| Aircraft impact conditions for model input (velocity, location, orientation to building) | | Floor content layout | Aircraft mass | Fuel path |
| | | Material properties for high strain rates | Aircraft material failure strain | |
| | | | Tower steel failure strain | |
| | | | Partition strength | |
| | | | Live load weight | |

Table 9–2. Fire dynamics analysis parameters.

| <i>Validation Data</i> | | <i>Model and Analysis</i> | | |
|--|------------------------------------|---|---|---------------------------|
| Observables from Photo/Video | Observables from Interviews | Significant Input | Influential Parameters | Significant Output |
| Fire near windows vs location and time | None | Ventilation sources from debris damage | Average fuel density | Gas temperature histories |
| Smoke out windows vs location and time | | Added fuel from aircraft | Distribution of intact contents vs rubble | |
| Window breakage vs location and time | | Fuel distribution after aircraft impact | Shaft ventilation in core | |
| | | Window openings vs time | Partition damage | |
| | | Floor content layout | | |

Table 9–3. Thermal analysis parameters.

| <i>Validation Data</i> | | <i>Model and Analysis</i> | | |
|-------------------------------------|------------------------------------|------------------------------|-------------------------------|----------------------------------|
| Observables from Photo/Video | Observables from Interviews | Significant Input | Influential Parameters | Significant Output |
| None | None | Thermal models of structure | Insulation initial condition | Structural temperature histories |
| | | Insulation initial condition | Estimated insulation damage | |
| | | Estimated insulation damage | | |
| | | Gas temperatures | | |

Table 9–4. Structural response analysis parameters.

| <i>Evidence/ Data</i> | | <i>Model and Analysis</i> | | |
|---|---|---|--------------------------------------|--|
| Observables from Photo/Video | Observables from Interviews and Recordings | Significant Input | Influential Parameters | Significant Output |
| Initial Stability | NYPD Aviation Unit first responder communications | Initial structural condition after impact | Pull-in force location and magnitude | Probable collapse sequence |
| Floors sagging at windows | | Structural temperature histories | Floor disconnections | Sequence of component and subsystem failures, including instability of exterior wall |
| Exterior wall inward bowing and instability | | Pull-in force location and magnitude | Creep strain | Global stability vs time |
| Tilt of building section above impact during collapse | | | | |

9.2.5 Evaluation of Collapse Hypotheses

Development and validation of the probable collapse sequence for each tower was shaped by evidence gathered in the investigation, including photographs and videos, design and maintenance documents, and eyewitness accounts. Photographs and videos provided knowledge about aircraft impact damage to the tower exterior walls, fire growth and spread at the building exterior, inward bowing of an exterior wall in each tower, and the direction of tilt for the building section above the impact zone as the towers collapsed. Eyewitness accounts provided some information about the interior conditions surrounding the impact areas, but the descriptions tended to be general in nature and often did not provide locations or specifics within a floor level. Figure 9–4 lists data (primarily based on photos and videos except for the metallurgical measurements) used to determine input data, impose time-related constraints, and validate analysis results for determining the probable collapse sequences.

The use of observables as a constraint had the important effect of reducing the uncertainty in the analysis results. The time and frequency of the applied constraints affected the degree to which the analysis uncertainty was reduced.

Figure 9–5 illustrates conceptually how the variance (or uncertainty) of the global stability of the towers (indicated here by the global reserve capacity RC) changed from the time of impact to the time of collapse. The shaded band qualitatively indicates the degree of uncertainty in RC at each time t after considering the analysis results and the observations made prior to t , except for collapse. The aircraft impact caused a reduction in the towers strength, but substantial reserve capacity remained afterward. The combined effect of the impact damage and fires caused a gradual reduction of the global capacity. The initial period of heating caused minimal changes in the structural capacity, but as time progressed,

various events occurred that caused a sudden or more rapid loss of global capacity. For instance, failure of critical columns from thermal weakening or inward bowing of an exterior wall may be events associated with a rapid loss of global capacity.

Based only on model predictions, the variance (or uncertainty) of the global reserve capacity grew with time. However, whenever an observable matched analysis results, it reduced the uncertainty in the analysis results. Alternatively, when the observables were used to constrain model parameters and adjust results to be consistent with observations, the variance of the global reserve capacity and the sequence of events that took place were reduced. As the structural analyses approached the time to collapse, the ability of the analyses to match the time to failure depended upon the variance in the analysis results. When considering the sequence of structural events and time to failure, it was more important to match the sequence of events as the time to collapse initiation was influenced by adjustments in influential parameters and imposition or matching of observables. As a result of using observables to constrain model parameters and analysis results, NIST believes that the probable collapse sequences that were determined are highly robust. The times to failure for the collapse sequences, however, are subject to considerable variability, particularly since they are sensitive to small changes in the magnitude of the pull-in forces.

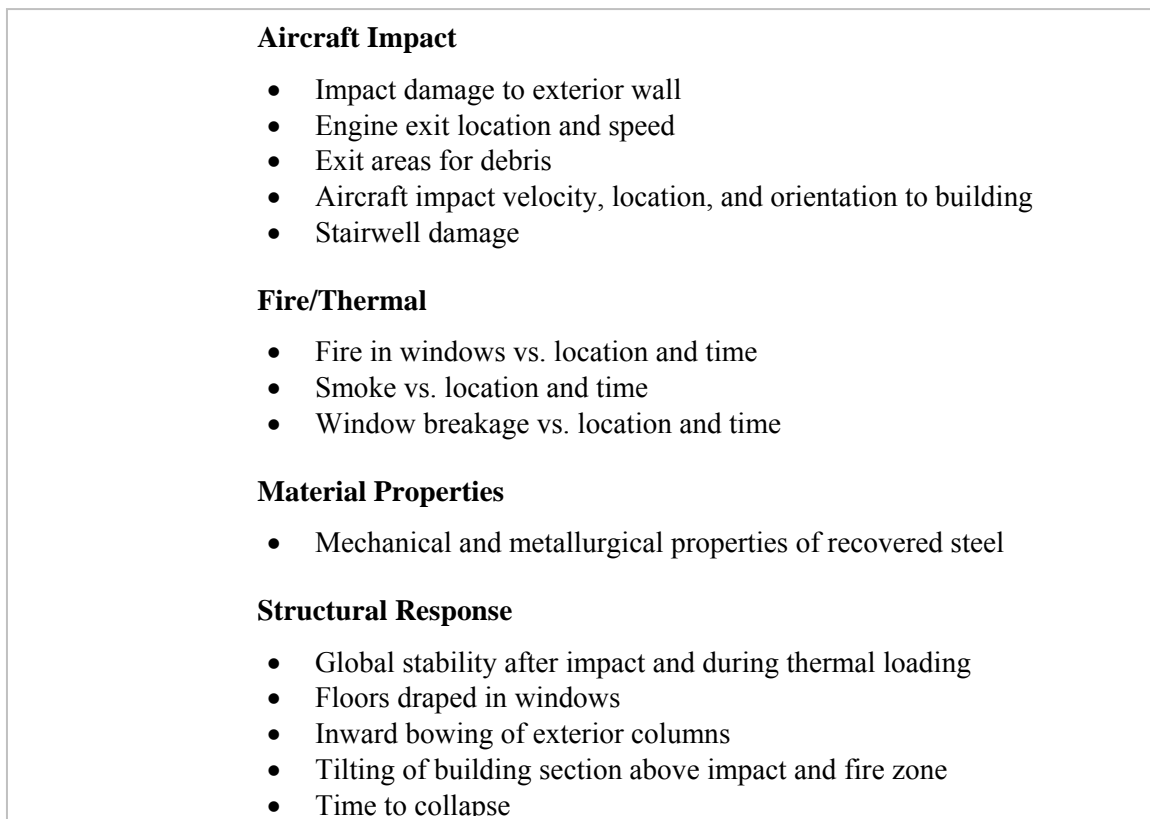


Figure 9–4. Data used for input, constraints, and validation of probable collapse sequences.

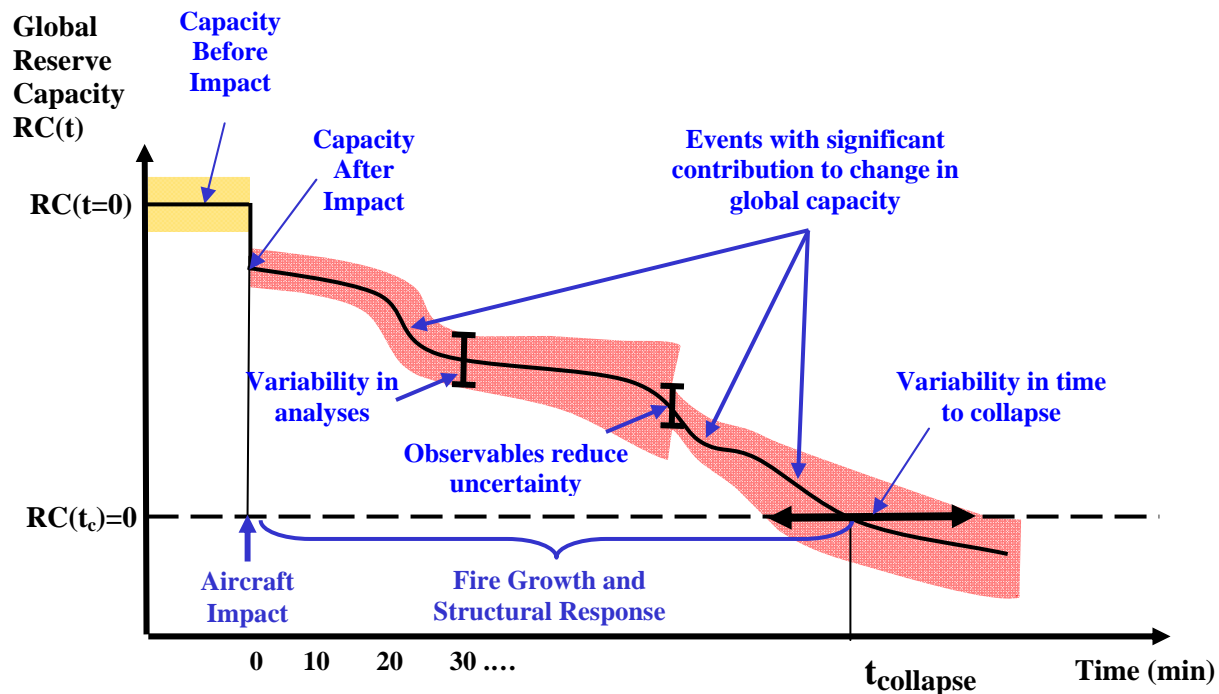


Figure 9–5. Variability in global reserve capacity using model predictions and observables for sequential analyses with imperfect information.

9.3 PROBABLE COLLAPSE SEQUENCES

The following four structural events that were common to both towers are part of the sequence of events described:

- **Floor sagging** was caused by elevated steel temperatures resulting from loss of insulation. Substantial sagging of the floor resulted in pull-in forces at column connections, and led to inward bowing of the exterior wall. Calculations, supported by the four Standard Fire Tests, showed that the most likely cause of floor sagging was buckling of the truss web diagonals, as shown in Fig. 9–6. In the figure, the left portion of the truss maintained flexural stiffness, but the right end lost some flexural stiffness as a result of extensive web buckling. The resultant sagging produced tensile forces in the floor system which was approximated by a combination of flexural and catenary behaviors as shown in Fig. 9–7. A floor system with tensile forces at its connections does not restrain the exterior wall from bowing inward.
- **Bowing and plastic buckling of an exterior wall** under the combined effects of elevated temperatures, redistributed gravity loads, pull-in forces from sagging floors, and loss of lateral support due to failure of truss seat connections.
- **Weakening of the core columns** (which was resisted by the hat truss) was caused by the combined effects of structural impact damage, redistributed gravity loads, elevated temperatures, plastic and creep strains, and plastic buckling of core columns.

- Redistribution of gravity loads** resulted from impact damage, restrained thermal expansion, core weakening, leaning of the tower section above the impact damage, and bowing and buckling of exterior walls. Redistribution of gravity loads between the core to the exterior walls occurred primarily through the hat truss, while load redistribution between adjacent exterior walls occurred primarily through the spandrels. Restrained thermal expansion occurred in the exterior wall when heated columns were restrained by adjacent cooler columns. Restrained thermal expansion also occurred when the core columns were restrained by the hat truss connection to the exterior wall; elongation of the core columns transferred loads from the exterior wall to the core.

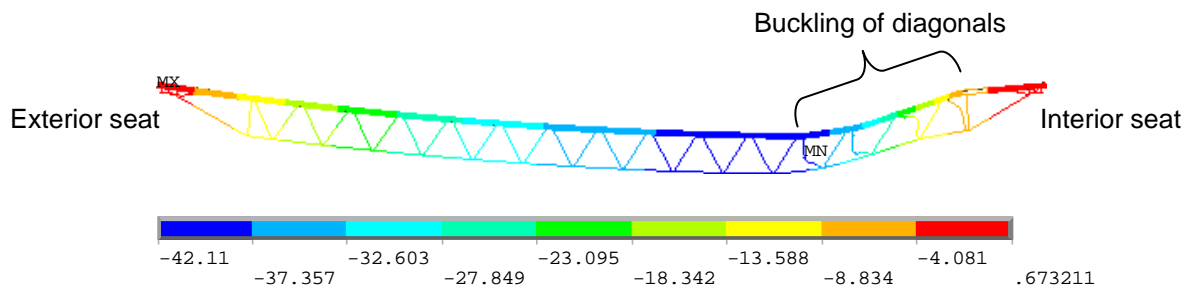


Figure 9–6. Vertical displacement contour of the detailed truss model under thermal loading.

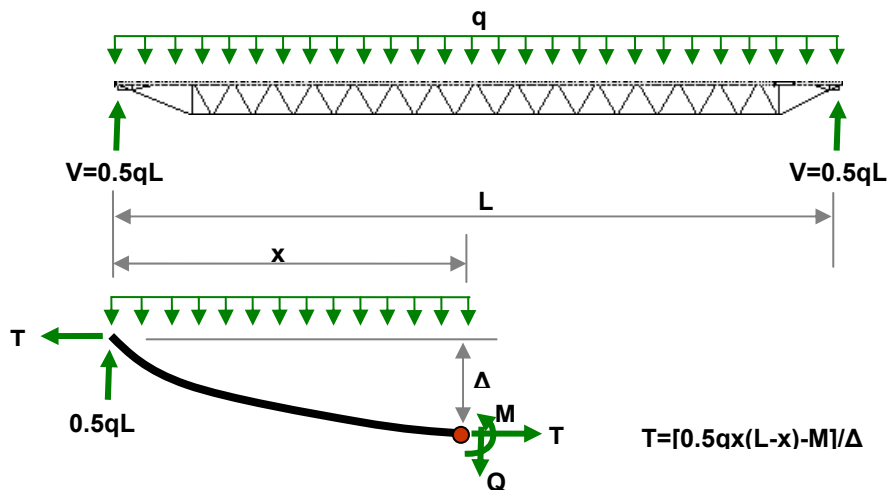


Figure 9–7. Combined flexural and catenary action in the floor system.

9.3.1 Probable Collapse Sequence of WTC 1

The aircraft impacted the north wall of WTC 1 at 8:46 a.m. The aircraft impact severed exterior columns and floors on the north side of the tower and into the core between Floors 93 and 98. The subsequent fires weakened structural subsystems, including the core, floors, and exterior walls. The core weakened, the floors sagged, and the south exterior wall bowed inward. At 10:28 a.m., about 102 min after the aircraft impact, WTC 1 began to collapse.

A sequence of main structural events that led to the collapse of WTC 1 starting from aircraft impact is discussed below. The WTC 1 collapse sequence consisted of five main events: aircraft impact, core weakening, floor sagging and disconnection, inward bowing of the south wall, and collapse initiation. Each event is discussed in terms of (1) the factors and sub-events that led to the event and (2) the consequential structural changes that were caused by the event. Observations for WTC 1 are presented again in Table 9–5. The probable collapse sequence is presented in Fig. 9–8.

Table 9–5. Observations for WTC 1.

| <i>Time</i> | <i>Time from Impact</i> | <i>Observation</i> |
|-------------|-------------------------|---|
| 8:46:26 | 0 min | WTC 1 was impacted by a Boeing 767 between Floors 93 and 99 and Columns 109 and 152. Fig 6–1 shows Columns 120 to 159. |
| 9:25:28 | 39 min | Fire on west side of south wall. |
| 9:40 | 69 min | No inward bowing of perimeter columns was visible |
| 10:22:59 | 97 min | Inward bowing of the south perimeter wall was visible from Floor 95 to about Floor 99, with a maximum inward bowing of ~ 55 in. at Column 315 and Floor 97. |
| 10:28:18 | 102 min | Smoke and debris clouds out of the north, east, and west walls on Floor 98. Fire out of windows on the north, east, west, and south walls between Floor 92 and Floor 98, and Floor 104. |
| 10:28:20 | 102 min | Tower began to collapse – first exterior sign of collapse was at Floor 98. Rotation of at least 8 degrees to the south occurred before the building section began to fall vertically under gravity. |
| 10:28:48 | 102 min | Remaining portion of core collapsed. |

1. Aircraft Impact Damage:

- Aircraft impact severed a number of exterior columns on the north wall from Floor 93 and Floor 98, and the wall section above the impact zone moved downward.
- After breaching the building's exterior, the aircraft continued to penetrate into the building, severing floor framing and core columns at the north side of the core. Core columns were also damaged toward the center of the core and, to a limited extent on the south side of the core. Fireproofing was damaged from the impact area to the south exterior wall, primarily through the center of WTC 1 and at least over a third to a half of the core width.
- Aircraft impact severed a single exterior panel at the center of the south wall between floors 94 and 96.
- The impact damage to the exterior walls and to the core resulted in redistribution of severed column loads, mostly to the columns adjacent to the impact zones. The hat truss resisted the downward movement of the north wall, and rotated about the east-west axis.
- As a result of the aircraft impact damage, the north and south walls each carried about 7 percent less gravity loads after impact, and the east and west walls each carried about 7 percent more loads. The core carried about 1 percent more gravity loads after impact.

2. Effects of Subsequent Fires and Impact Damaged Fireproofing:**A. Thermal Weakening of the Core:**

- The undamaged core columns developed high plastic and creep strains over the duration the building stood, since both temperatures and stresses were high in the core area. The plastic and creep strains exceeded thermal expansion in the core columns.
- The shortening of the core columns (due to plasticity and creep) was resisted by the hat truss, which unloaded the core over time and redistributed loads to exterior walls.
- As a result of the thermal weakening (and subsequent to impact and prior to inward bowing of the south wall), the north and south walls each carried about 10 percent more gravity loads, and the east and west walls each carried about 25 percent more loads. The core carried about 20 percent less gravity loads after thermal weakening.

B. Thermal Weakening of the Floors:

- Floors 95 to 99 weakened with increasing temperatures over time on the long-span floors and sagged. The floors sagged first and then contracted due to cooling on the north side; fires reached the south side later, the floors sagged, and the seat connections weakened.
- Floor sagging induced inward pull forces on the south wall columns.
- About 20 percent of the connections to the south exterior wall on floors 97 and 98 failed due to thermal weakening of the vertical supports.

C. Thermal Weakening of the South Wall:

- South wall columns bowed inward as they were subjected to high temperatures and inward pull forces in addition to axial loads.
- Inward bowing of the south wall columns increased with time.

Figure 9–8. WTC 1 probable collapse sequence.

3. Collapse Initiation

- The inward bowing of the south wall induced column instability, which progressed rapidly horizontally across the entire south face.
- The south wall unloaded and tried to redistribute the loads via the hat truss to the thermally weakened core and via the spandrels to the adjacent east and west walls.
- The entire section of the building above the impact zone began tilting as a rigid block (all four faces, not only the bowed and buckled south face) to the south (at least about 8°) as column instability progressed rapidly from the south wall along the adjacent east and west walls.
- The change in potential energy due to downward movement of building mass above the buckled columns exceeded the strain energy that could be absorbed by the structure. Global collapse then ensued.

Figure 9–8. WTC 1 probable collapse sequence (cont).

Aircraft Impact

WTC 1 was impacted by an aircraft on the north wall. Columns 112 to 151 between Floors 94 and 98 were severed or heavily damaged on the north wall. After breaching the building's perimeter, the aircraft continued to penetrate into the building. The north office area floor system sustained severe structural damage between Columns 112 and 145 at Floors 94 to 98. Core columns were severed or heavily damaged (nine were predicted) between Floor 92 and Floor 97. The aircraft impact also severed a single exterior panel at the center of the south wall from Columns 329 to 331 between Floor 93 and Floor 96. In addition, insulation on floor framings and columns were damaged from the impact area to the south perimeter wall, primarily through the center of WTC 1 and over one-third to one-half of the core width.

Gravity loads on severed columns were redistributed mostly to columns adjacent to the impact zone. Due to the severe impact damage to the north wall, the wall section above the impact zone moved downward. The hat truss resisted the downward movement of the north wall and rotated about its east-west axis, which reduced the load on the south wall. As a result, the north and south walls each carried about 7 percent less gravity loads at Floor 98 after impact, the east and west walls each carried about 7 percent more loads, and the core carried about 1 percent more gravity loads at Floor 98 after impact, as shown in Table 9–6.

Core Weakening

Temperatures in the core area rose quickly; therefore, the thermal expansion of the core was larger than the thermal expansion of the exterior walls in early stages of the fire, resulting in an increase in the gravity loads in the core columns until 10 min (8:56 a.m.), as shown in Table 9–6. The additional loads due to impact damage and high temperatures resulted in high plastic and creep strains in the core columns during early stages of the fire. Creep strain continued to increase until the collapse initiated. By 30 min (9:16 a.m.), the plastic-plus-creep strains exceeded thermal expansion strains. Due to high plastic and creep strains and plastic buckling of some core columns, at 100 min (10:26 a.m.), the core structure at Floor 99 had displaced downward 2.0 in. on average.

Table 9–6. Total column loads at Floor 98 and Floor 105 of WTC 1 for Case B.

| | | North | | East | | South | | West | | Core | |
|------|---------------|----------|-----------|----------|-----------|----------|-----------|----------|-----------|----------|-----------|
| | | Floor 98 | Floor 105 |
| (1) | Before Impact | 10,974 | 8,026 | 8,545 | 6,562 | 11,025 | 8,092 | 8,572 | 6,604 | 34,029 | 20,361 |
| (2) | After Impact | 10,137 | 7,294 | 9,071 | 7,028 | 10,356 | 7,488 | 9,146 | 7,076 | 34,429 | 20,761 |
| (3) | 10 min | 9,796 | 6,944 | 8,490 | 6,461 | 9,848 | 6,981 | 8,536 | 6,469 | 36,473 | 22,790 |
| (4) | 20 min | 10,437 | 7,551 | 9,108 | 7,075 | 9,900 | 7,057 | 9,202 | 7,158 | 34,495 | 20,806 |
| (5) | 30 min | 10,913 | 8,020 | 10,034 | 7,998 | 10,420 | 7,569 | 9,715 | 7,685 | 32,060 | 18,377 |
| (6) | 40 min | 11,068 | 8,193 | 10,599 | 8,571 | 11,004 | 8,129 | 10,178 | 8,147 | 30,294 | 16,608 |
| (7) | 50 min | 11,149 | 8,285 | 10,908 | 8,878 | 11,192 | 8,315 | 10,458 | 8,428 | 29,435 | 15,743 |
| (8) | 60 min | 11,205 | 8,351 | 11,168 | 9,130 | 11,285 | 8,414 | 10,716 | 8,687 | 28,766 | 15,069 |
| (9) | 70 min | 11,286 | 8,435 | 11,366 | 9,319 | 11,343 | 8,481 | 10,939 | 8,914 | 28,205 | 14,502 |
| (10) | 80 min | 11,376 | 8,528 | 11,555 | 9,497 | 11,409 | 8,551 | 11,119 | 9,097 | 27,681 | 13,978 |
| (11) | 90 min | 10,916 | 8,096 | 11,991 | 9,847 | 9,949 | 7,327 | 11,657 | 9,506 | 28,587 | 14,876 |
| (12) | 100 min | 10,828 | 8,023 | 12,249 | 10,076 | 9,638 | 7,066 | 11,905 | 9,720 | 28,478 | 14,767 |
| (13) | (2) - (1) | -837 | -732 | 526 | 466 | -668 | -604 | 574 | 472 | 400 | 400 |
| (14) | (10) - (2) | 1,239 | 1,234 | 2,484 | 2,470 | 1,052 | 1,063 | 1,973 | 2,021 | -6,748 | -6,783 |
| (15) | (12) - (2) | 692 | 730 | 3,178 | 3,048 | -719 | -422 | 2,759 | 2,644 | -5,951 | -5,993 |
| (16) | (12) - (10) | -548 | -504 | 694 | 579 | -1,771 | -1,485 | 786 | 623 | 797 | 790 |

Note : Compression is positive. Units are in kip.

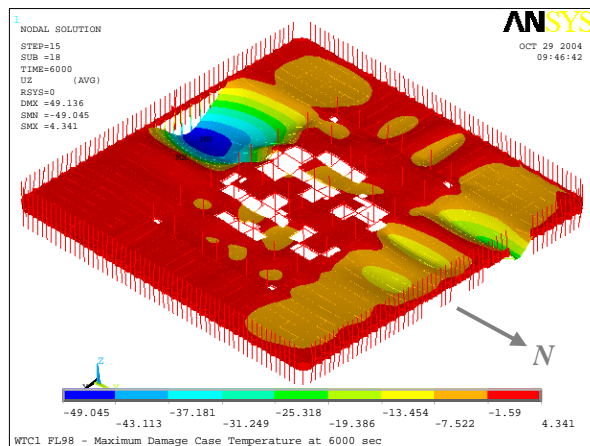
The shortening of core columns was resisted by the hat truss, which unloaded the core with time and redistributed the gravity loads from the core to the exterior walls, as can be seen in Table 9–6 at 80 min. As a result, the north, east, south, and west walls carried about 12 percent, 27 percent, 10 percent, and 22 percent more gravity loads, respectively, for Floor 98 at 80 min than the state after impact, and the core carried about 20 percent less loads. At 80 min, the unloading of the core columns was at its maximum.

Sagging of Floors and Floor/Wall Disconnections

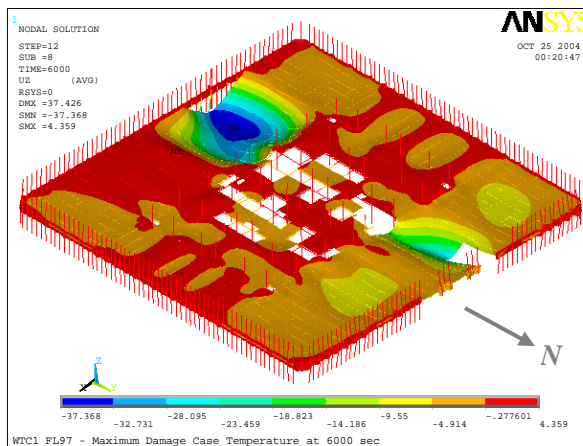
The floors thermally expanded in the early stages of the fires. However, the thermal expansion was overcome by the significant sagging of the floors, which then pulled inward on the exterior columns. Floor 95 to Floor 99 sagged due to elevated temperatures in the south floor areas with long-span trusses. While the north floors first sagged and then contracted due to cooling on the north side, the fires reached the south side later, and the south floors sagged. Figure 9–9 shows vertical displacement contours of Floor 95 to Floor 98 predicted by the full floor models at 100 min (10:26 a.m.). Floor sagging induced pull-in forces on the south wall columns over Floors 95 to 99. In addition, about 20 percent of the exterior seats of Floors 97 and 98 on the south wall failed due to their reduced vertical shear capacity, as shown in Fig. 9–10.

Bowing of South Wall

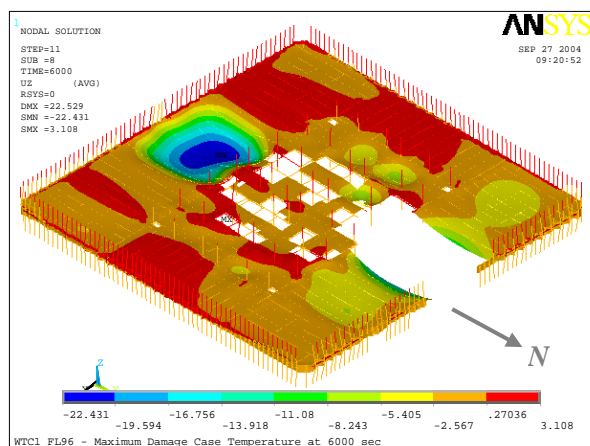
Exterior columns on the south wall bowed inward as they were subjected to high temperatures, pull-in forces from the floors (beginning at about 80 min), and additional loads redistributed from the core. The observed inward bowing of the south wall at 10:23 a.m. was 55 in. while the calculated inward bowing was 31 in., as shown in Figs. 9–11 and 9–12. Since no bowing was observed on the south wall at 9:55 a.m., the south wall was considered to begin bowing inward around 10:10 a.m. when the floors on the south side began to experience large sagging. The inward bowing of the south wall increased with time due to additional gravity loads caused by core weakening and increased temperatures on the south wall. As the floor applied inward pull to the south exterior wall at approximately 80 min, the south wall began to unload to adjacent walls and the core.



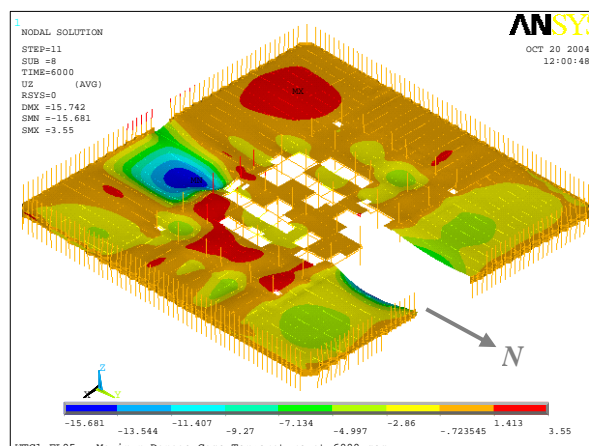
(a) Floor 98



(b) Floor 97

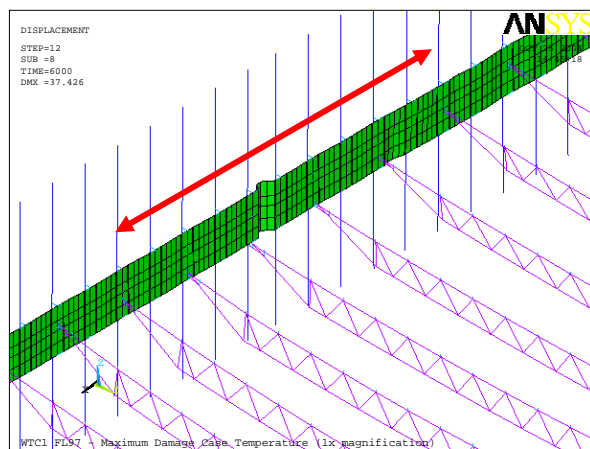


(c) Floor 96

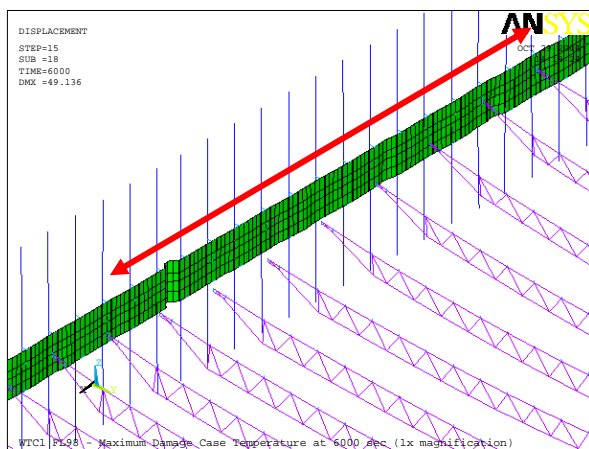


(d) Floor 95

Figure 9–9. Vertical displacement of Floors of WTC 1 for Case B' at 100 min.



(a) Floor 97



(b) Floor 98

Figure 9–10. Loss of vertical supports observed in Floor 97 and Floor 98 of WTC 1 for Case B' (1x displacement magnification).

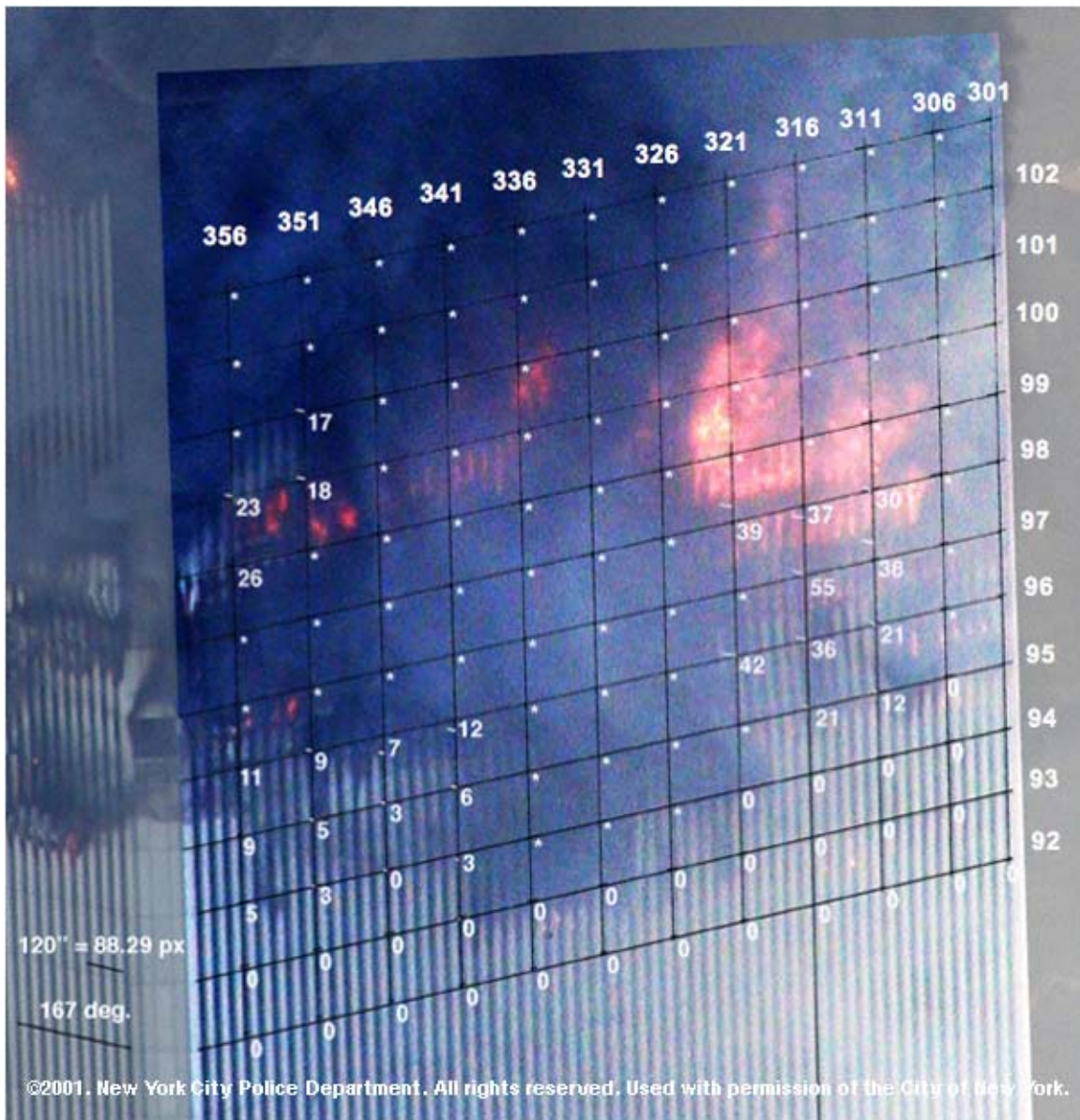


Figure 9–11. Inward bowing of the WTC 1 south wall of WTC 1 at 10:23 a.m.

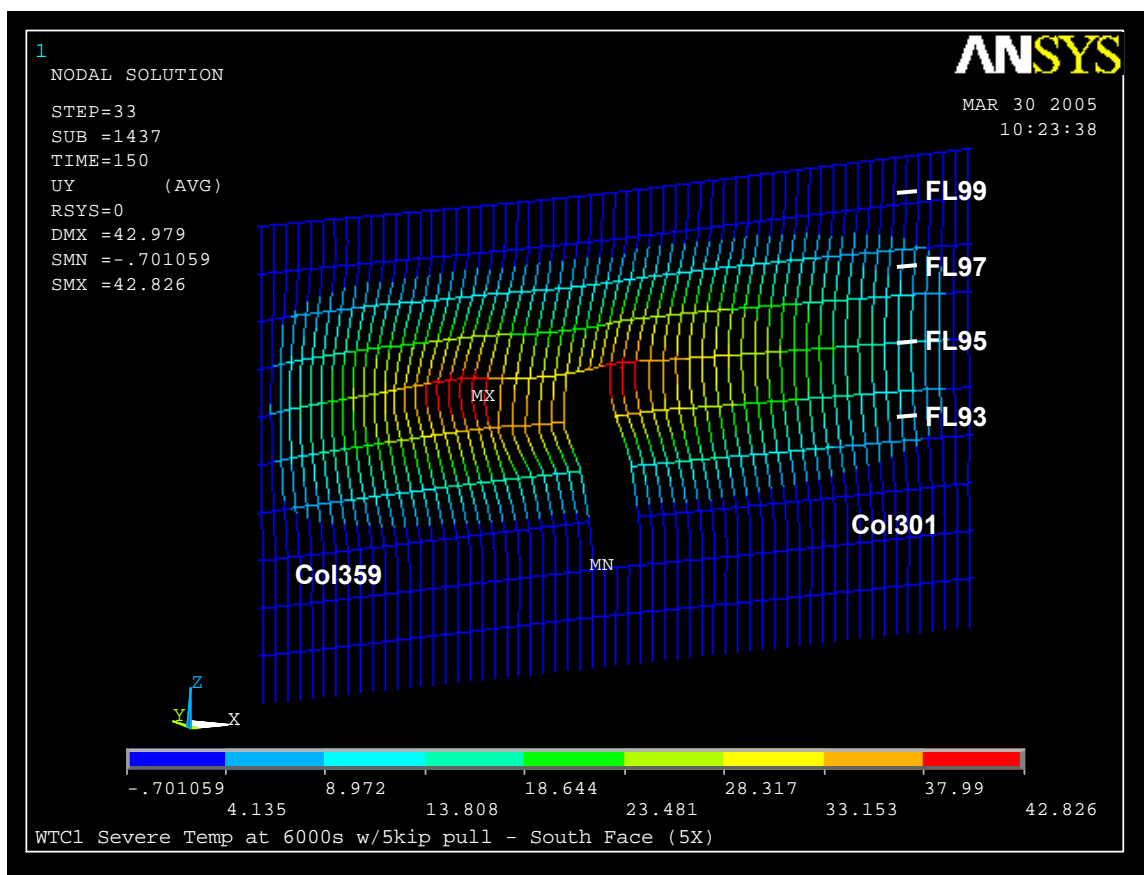


Figure 9–12. Inward bowing of south wall of WTC 1 global model with creep at 100 min for Case B with 5 kip pull-in forces (5x displacement magnification).

Buckling of South Wall and Collapse Initiation

The inward bowing of the south wall increased as the post-buckling strength of bowed columns continued to reduce. The bowed columns increased the loads on the unbuckled columns on the south wall by shear transfer through the spandrels. Consequently, instability progressed horizontally, and when it engulfed the entire south wall, it progressed along the east and west walls. Moreover, the unloading of the south wall resulted in further redistribution of gravity loads on the south wall to the east and west walls and to the thermally weakened core via the hat truss. At 100 min, the north, east, and west walls at Floor 98 carried about 7 percent, 35 percent, and 30 percent more gravity loads than the state after impact, and the south wall and the core carried about 7 percent and 20 percent less loads, respectively. The increased loads on the east and west walls were due to their relative higher stiffness compared to the impact damaged north wall and bowed south wall. The section of the building above the impact zone began tilting to the south at least about 8° as column instability progressed rapidly from the south wall along the adjacent east and west walls, as shown in Fig. 9–13. The gravity loads could no longer be redistributed, nor could the remaining core and perimeter columns support the gravity loads from the floors above. The change in potential energy due to downward movement of building mass above the buckled columns exceeded the strain energy that could have been absorbed by the structure. Global collapse ensued.



Fire expelled on east face

Smoke and debris expelled on north face at Floor 98



WTC 1 building section above impact damage zone tilts to the south



Figure 9–13. Expulsion of smoke and debris at WTC 1 Floor 98 on the east, north, and west faces.

9.3.2 Probable Collapse Sequence of WTC 2

The aircraft impacted the south wall of WTC 2 at 9:03 a.m. The impact mostly severed columns and floors that were toward the east side of the building between Floor 78 and Floor 84. The subsequent fires were also observed on the east side of the building. At 9:59 a.m., about 56 min after the aircraft impact, the building started to collapse, with the east wall buckling inward followed by tilting of the building portion above Floor 82 toward the east and south.

The section below discusses the sequence of main structural events that led to the collapse of WTC 2 starting from aircraft impact. Each event is discussed in terms of (1) the factors and sub-events that caused the event and (2) the structural changes that were caused by the event. The probable collapse sequence consists of five main structural events: aircraft impact, sagging and disconnections of floors, inward bowing of the east exterior wall, unloading and tilting of the core, and initiation of collapse. Observations for WTC 2 are presented in Table 9–7. The probable collapse sequence is presented in Fig. 9–14.

Table 9–7. Key observations on WTC 2.

| Time | Time from Impact (min) | Observation |
|---------|------------------------|---|
| 9:03 | 0 min | WTC 2 was impacted by a Boeing 767 between Floors 77 and 85 and Columns 404 and 443. |
| 9:23 | 20 min | Inward bowing of east face, maximum deflections of 10 in. at Floor 80. |
| 9:53 | 50 min | Bowing in of columns, maximum deflections of 20 in. at Floor 80. East side of Floor 83 draped between Columns 310 and 342. |
| 9:58:02 | | Perimeter columns bowing inward on east face. |
| 9:58:59 | | WTC 2 began to collapse. |
| 9:58:59 | 55 min – 56 min | Building section above the impact area tilted to the east and south. Tilting appears to take place around Floor 82. Rotation of approximately 4 to 5 deg to the south and 20 to 25 deg to the east occurred before the building section began to fall vertically. |

Aircraft Impact

The aircraft impacted the south wall of WTC 2 and severed a significant number of exterior columns on the south wall from Floor 78 to Floor 84. The floors on the south side sustained severe structural damage between Columns 410 and 436 from Floors 79 and 83. Core columns were severed or heavily damaged (11 were predicted) between Floor 77 and Floor 84. The aircraft impact also severed two columns in the north wall. The aircraft impact caused damage to the floor framing and core columns at the southeast corner of the core. Insulation was damaged from the impact area through the east half of the core to the north and east perimeter walls. The floor truss seat connections over about one-quarter to one-half of the east side of the core were predicted to be severed by the impact analysis on Floor 80 and Floor 81. Based on the hanging object in the photographs, about one-third of the east perimeter wall floor connections on Floor 83 were assumed to be severed.

1. Aircraft Impact Damage:

- Aircraft impact severed a number of exterior columns on the south wall from floors 78 to 84, and the wall section above the impact zone moved downward.
- After breaching the building's exterior, the aircraft continued to penetrate into the building, severing floor framing and core columns at the southeast corner of the core. Fireproofing was damaged from the impact area through the east half of the core up to the north and east exterior walls. The floor truss seat connections over about 1/4 to 1/2 of the east side of the core were severed on floors 80 and 81 and over about 1/3 of the east exterior wall on floor 83.
- Aircraft impact severed a few columns near the east corner of the north wall between floors 80 and 82.
- The impact damage to the exterior walls resulted in redistribution of severed column loads, mostly to the columns adjacent to the impact zones. The impact damage to the core columns resulted in redistribution of severed column loads mostly to other intact core columns and the east exterior wall. The hat truss resisted the downward movement of the south wall, and rotated about the east-west axis.
- As a result of the aircraft impact damage, the core carried 6 percent less gravity loads after impact and the north face carried 10 percent less loads. The east face carried 24 percent more gravity load, while the west face and the south face carried 3 percent and 2 percent more gravity load, respectively.
- After impact, the core was leaning toward the east and south exterior walls. The exterior walls acted to restrain the core structure.

2. Effects of Subsequent Fires and Impact Damaged Fireproofing:**A. Thermal Weakening of the Core:**

- Several of the undamaged core columns near the damaged and severed core columns developed high plastic and creep strains over the duration the building stood, since both temperatures and stresses were high in the core area. The plastic and creep strains exceeded thermal expansion in the core columns.
- The core continued to tilt toward the east and south due to the combination of column shortening (due to plasticity, creep, and buckling) and the failure of column splices at the hat truss in the southeast corner.
- As a result of thermal weakening (and subsequent to impact), the east wall carried about 5 percent more gravity loads and the core carried about 2 percent less loads. The other three walls carried between 0 and 3 percent less loads.

B. Thermal Weakening of the Floors:

- Floors 79 to 83 weakened with increasing temperatures over time on the long-span floors on the east side and sagged.
- Floor sagging induced inward pull forces on the east wall columns.
- About an additional 1/3 of the connections to the east exterior wall on floor 83 failed due to thermal weakening of the vertical supports.

C. Thermal weakening of the east wall:

- East wall columns bowed inward as they were subjected to high temperatures and inward pull forces in addition to axial loads.
- Inward bowing of the east wall columns increased with time.

Figure 9–14. WTC 2 probable collapse sequence.

3. Collapse Initiation

- The inward bowing of the east wall induced column instability, which progressed rapidly horizontally across the entire east face.
- The east wall unloaded and tried to redistribute the loads via the hat truss to the weakened core and via the spandrels to the adjacent north and south walls.
- The entire section of the building above the impact zone began tilting as a rigid block (all four faces; not only the bowed and buckled east face) to the east (about 7° to 8°) and south (about 3° to 4°) as column instability progressed rapidly from the east wall along the adjacent north and south walls. The building section above impact continued to rotate to the east as it began to fall downward, and rotated to at least 20 to 25 degrees.
- The change in potential energy due to downward movement of building mass above the buckled columns exceeded the strain energy that could be absorbed by the structure. Global collapse then ensued.

Figure 9–14. WTC 2 probable collapse sequence (cont).

As a result of the impact damage, dead and live loads carried by severed columns on the south wall and in the southeast corner of the core were redistributed to adjacent intact columns and also to the columns on the east wall (see Table 9–8). After redistribution, the total axial load on the core columns reduced by 6 percent, and the total axial load on the north wall columns reduced by 10 percent. The total axial load on the east wall columns, however, increased by 24 percent, and the total axial load on the west and south wall columns slightly increased by 2 percent to 3 percent.

Just below the hat truss level (Floor 105), analyses predicted that about seven column splices failed for columns at the southeast corner of the core. This increased the core tilting toward the southeast and also increased the vertical downward displacement of the core at the impact zone. After the failure of the core column splices, the remaining core columns transferred 73 percent of the loads released in the failing core columns to the exterior walls through the hat truss and 27 percent of the loads were transferred through the core floors.

Even though some column loads on the south wall were reduced after impact, the total load did not change, as some of the loads from the core area were redistributed to that wall through the hat truss (see Table 9–9). At the end of the load redistribution after impact, the core was leaning toward the east and south. The perimeter walls acted to restrain the core structure in the lateral direction.

Sagging of Floors and Floor/Wall Disconnections

Thermal expansion of the floors also occurred early in the fires, but as floor temperatures increased, the floor sagged and began to pull inward on the exterior columns. As a result of the aircraft impact damage and increasing temperatures due to subsequent fires, Floor 79 through Floor 83 sagged over time. The amount of sagging was more significant at Floor 80 and Floor 81 where the truss seats on the east side of the core were failed due to aircraft impact (see Fig. 9–15). Increased temperatures also weakened the truss seats on the east exterior wall and caused additional disconnections at Floor 82 and Floor 83, which further increased the floor sag (see Fig. 9–16). Floor sagging induced pull-in forces on the east wall columns, and started shortly after impact and grew with time.

Bowing of East Wall

The east wall columns bowed inward as a result of increasing temperatures (reduced strength and stiffness) and pull-in forces induced by sagging floors (see Figs. 9–17 and 9–18). The amount of inward bowing in the east wall steadily increased with time due to the combined effects of pull-in forces from sagging floors, increased axial loads, and a continuous increase in thermally induced plastic and creep strains (see Fig. 9–19). The load in bowed columns decreased, with some load transferring to adjacent unbowed columns, but the total column load on the east wall remained more or less constant for the duration after aircraft impact (see Fig. 9–20).

Unloading and Tilting of Core

With increasing time and temperatures, the core columns developed high compressive plastic and creep strains, especially on the east side of the core. Plastic and creep strains started to exceed the thermal expansion strains approximately 30 min after the aircraft impact (see Fig. 9–21). High plastic and creep strains caused unloading on the east side core columns. This increased the core tilt toward the southeast and transferred more loads to the east wall. As a result, at Floor 83, the total axial load carried by the core columns were reduced by 8 percent, the east wall loads increased by 29 percent, and the north wall loads decreased by 12 percent, relative to the total loads before aircraft impact. The total loads on the south and west walls did not change significantly (see Tables 9–8 and 9–9).

Buckling of East Wall and Collapse Initiation

With continuously increased bowing and axial loads, the east wall became unstable. The instability started at the center portion of the wall and rapidly progressed horizontally on both sides. As a result of buckling, the east wall significantly unloaded, redistributing its loads to the weakened core through the hat truss and to the east side of the south and north walls through the spandrels (see Figs. 9–22 through 9–24 and Table 9–10). Furthermore, the portion of the building above the buckled columns suddenly moved downward, and the building tilt towards the east increased.

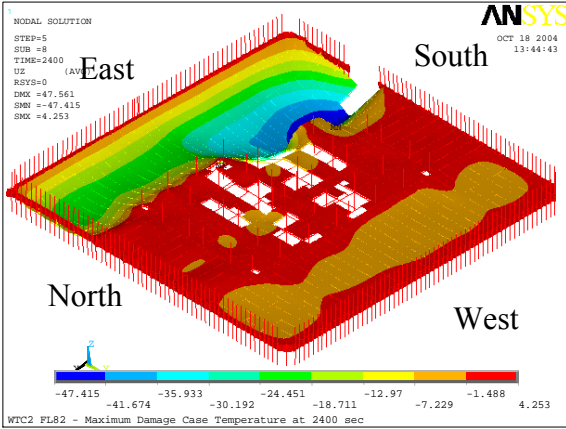
The section of the building above the impact zone began tilting to the east (about 7° to 8°) and south (about 3° to 4°) as column instability progressed from the east wall to the adjacent south and north walls. The building section above impact continued to rotate to the east as it began to fall downward, and rotated to at least 20 degrees to 25 degrees. The gravity loads could no longer be redistributed, nor could the remaining core and perimeter columns support the gravity loads from the floors above. The change in potential energy due to downward movement of the building mass above the buckled columns exceeded the strain energy that could be absorbed by the structure. The building portion above the impact zone became unstable, and building collapse ensued.

Table 9–8. Total column loads at Floor 83 of WTC 2 for Case D. Compression is positive.

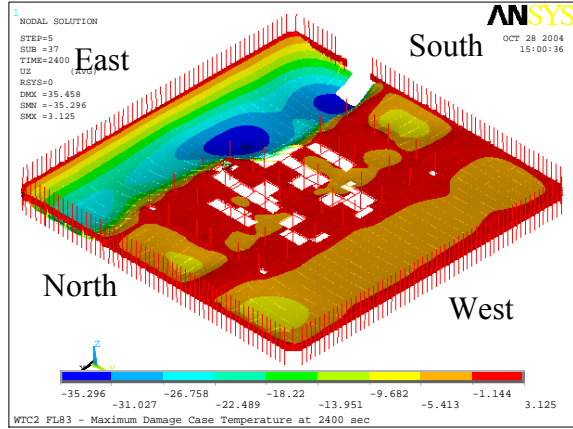
| Row | Analysis Stage | West | East | North | South | Core |
|------|----------------|-------|-------|-------|-------|-------|
| (1) | Before Impact | 18065 | 18114 | 13567 | 13284 | 61828 |
| (2) | After Impact | 18670 | 22481 | 12193 | 13511 | 57821 |
| (3) | 10 min | 18728 | 22226 | 11896 | 13358 | 58413 |
| (4) | 20 min | 18914 | 22208 | 12052 | 13318 | 58124 |
| (5) | 30 min | 18876 | 23681 | 11770 | 13365 | 56967 |
| (6) | 40 min | 18531 | 23682 | 11906 | 13473 | 56825 |
| (7) | 43 min | 15667 | 15143 | 14215 | 16292 | 62422 |
| (8) | (2)-(1) | 604 | 4368 | -1374 | 227 | -4007 |
| (9) | (6)-(2) | -138 | 1201 | -287 | -38 | -996 |
| (10) | (7)-(6) | -2864 | -8539 | 2309 | 2819 | 5596 |

Table 9–9. Total column loads at Floor 105 of WTC 2 for Case D. Compression is positive.

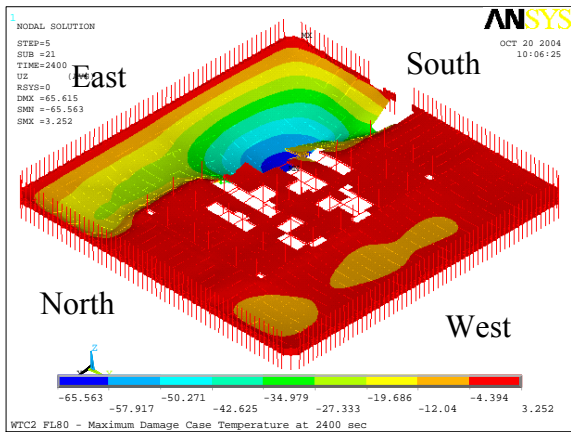
| Row | Analysis Stage | West | East | North | South | Core |
|------|----------------|-------|-------|-------|-------|-------|
| (1) | Before Impact | 8497 | 8572 | 7382 | 7169 | 17123 |
| (2) | After Impact | 9170 | 11272 | 6487 | 8432 | 13382 |
| (3) | 10 min | 9182 | 11061 | 6250 | 8275 | 13975 |
| (4) | 20 min | 9279 | 11120 | 6311 | 8351 | 13682 |
| (5) | 30 min | 9370 | 11859 | 6416 | 8553 | 12544 |
| (6) | 40 min | 9198 | 11927 | 6524 | 8691 | 12402 |
| (7) | 43 min | 7086 | 8026 | 6546 | 9169 | 17915 |
| (8) | (2)-(1) | 674 | 2699 | -895 | 1263 | -3741 |
| (9) | (6)-(2) | 28 | 656 | 37 | 259 | -980 |
| (10) | (7)-(6) | -2112 | -3901 | 23 | 479 | 5513 |



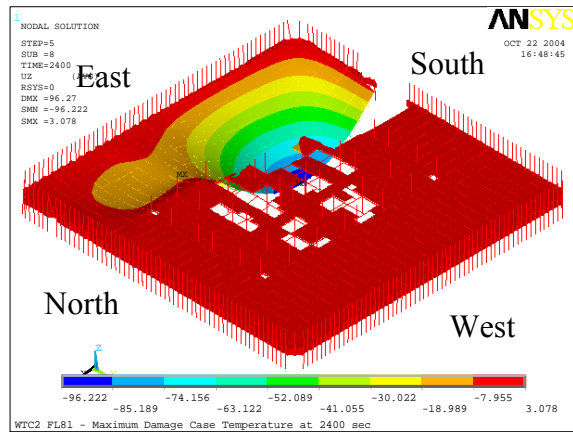
Floor 82



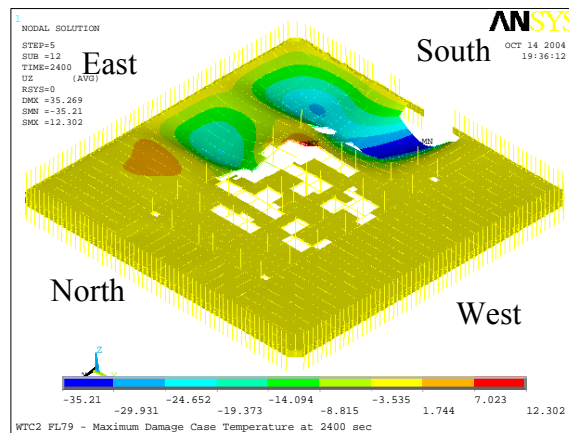
Floor 83



Floor 80

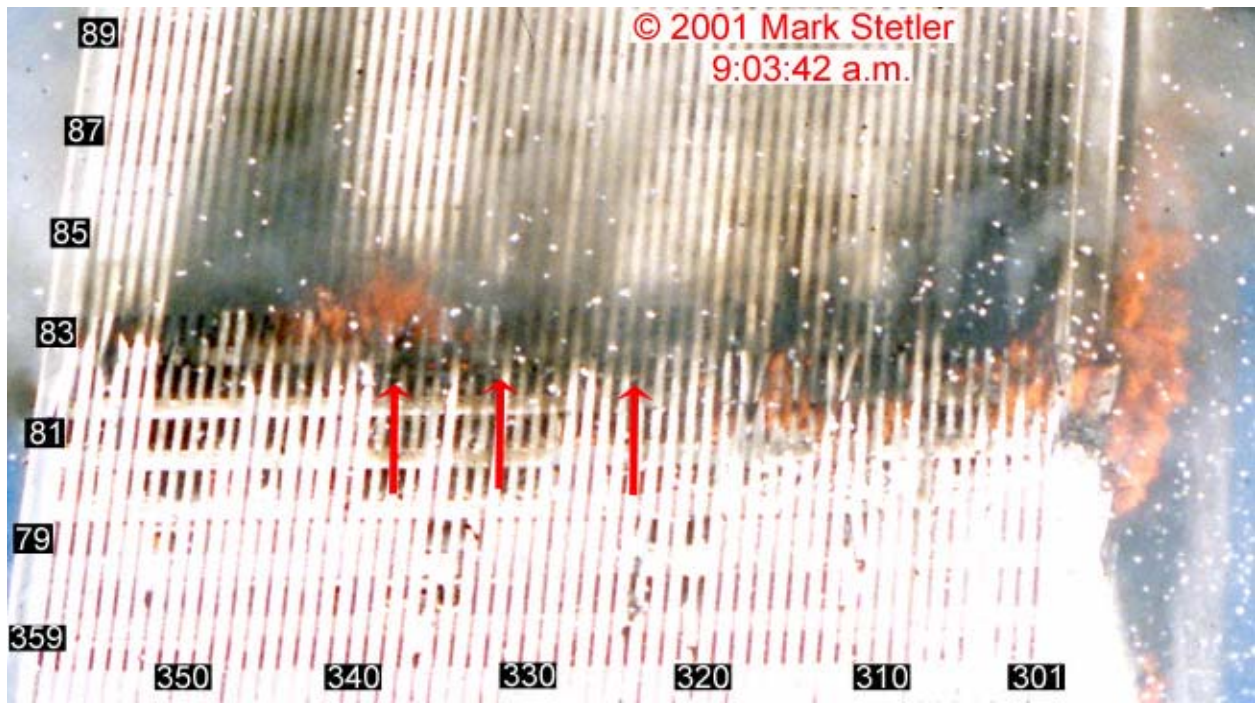


Floor 81

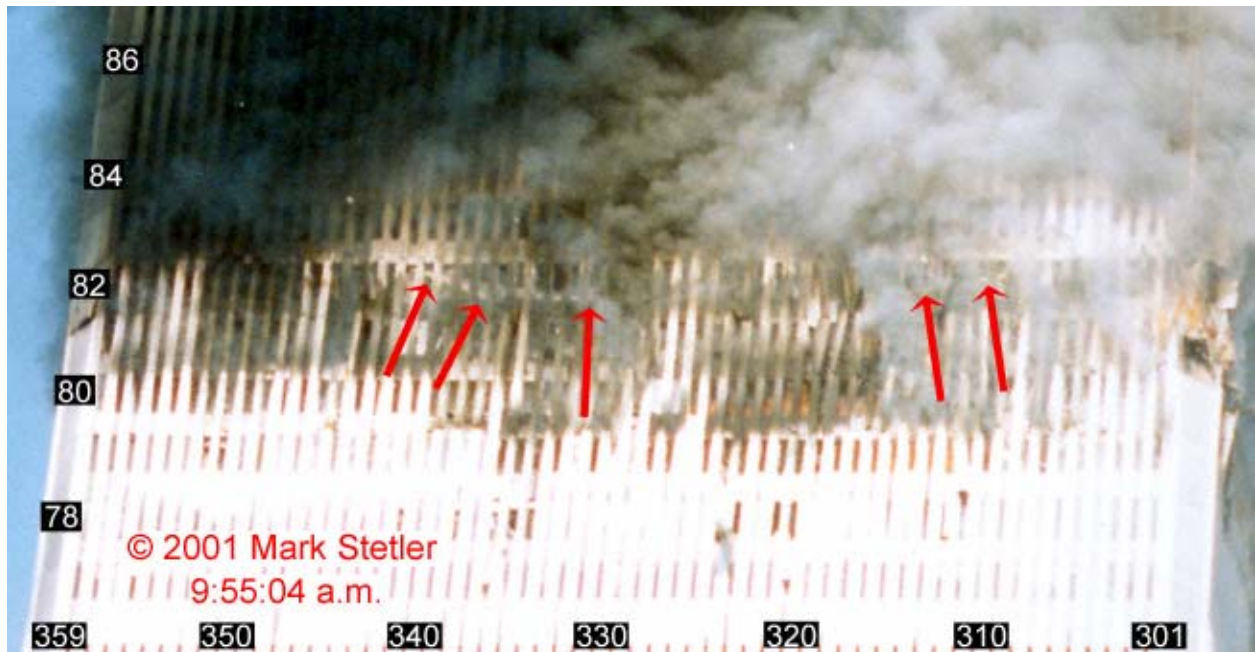


Floor 79

Figure 9–15. Vertical displacements of Floors 79 through Floor 88 of WTC 2 at 40 min (Case D).

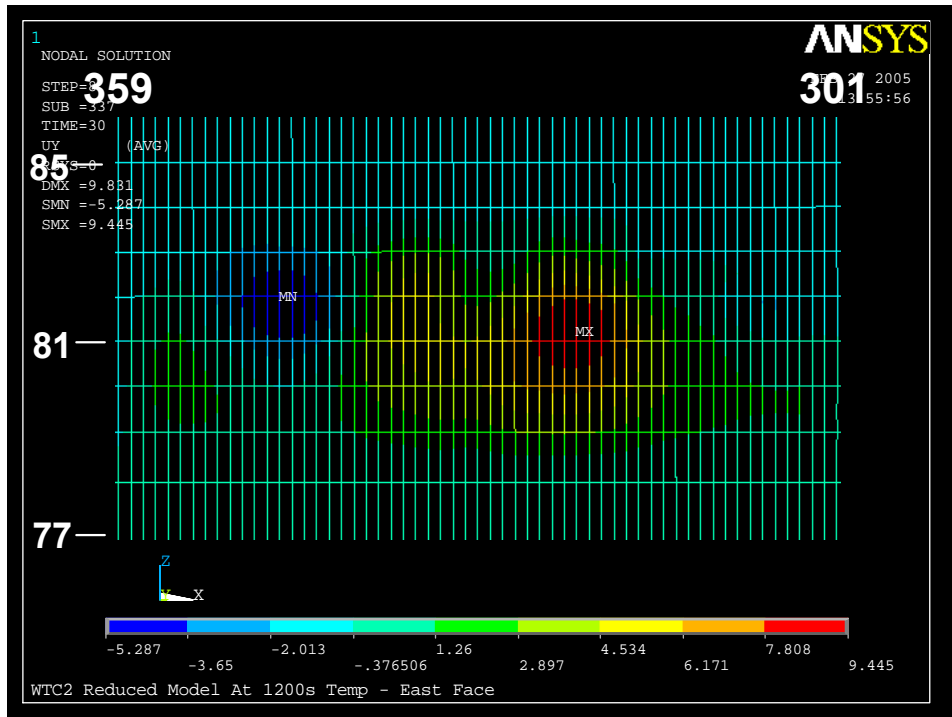


After impact damage

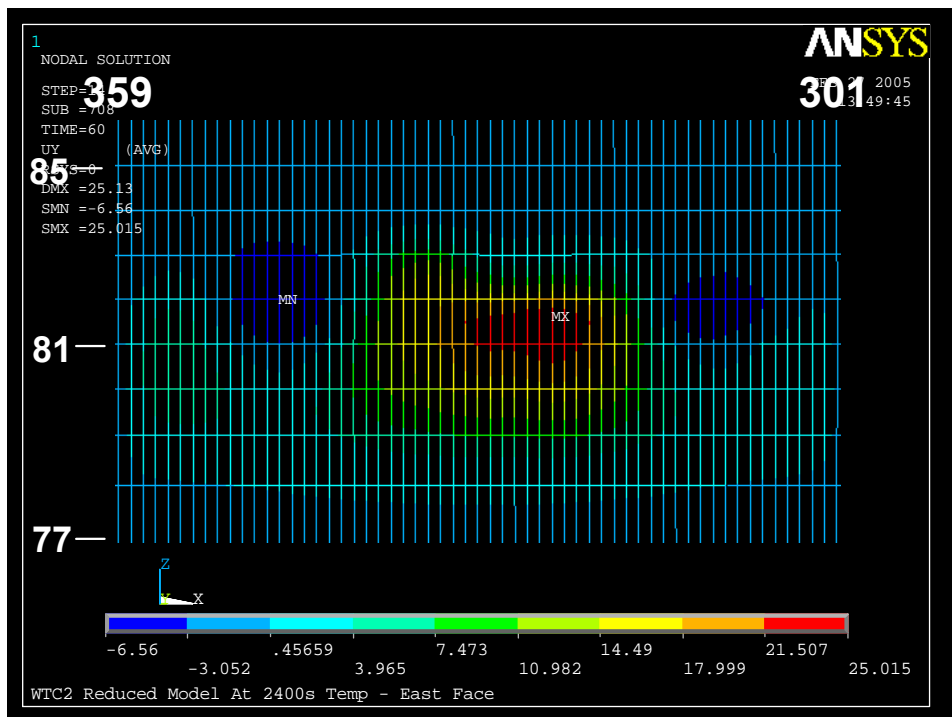


Damage a few minutes before collapse

Figure 9–16. Floor sagging observed on the east wall of WTC 2 at different stages.



At 20 minutes



At 40 minutes

Figure 9–17. Out-of-plane displacements on the east wall of WTC 2 (Case D).

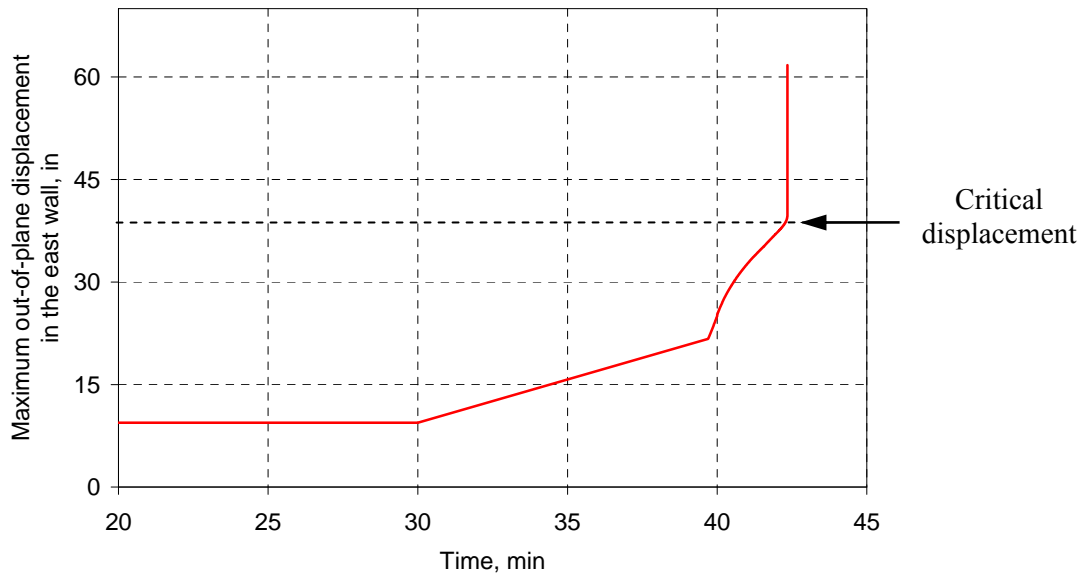


Figure 9–19. Variation of maximum out-of-plane displacement on the east wall of WTC 2 (Case D).

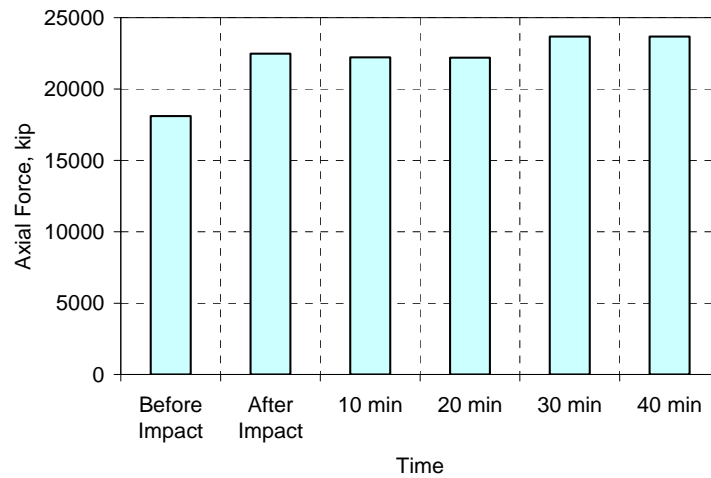


Figure 9–20. Total column loads at Floor 83 of the east wall of WTC 2 at different stages (Case D).

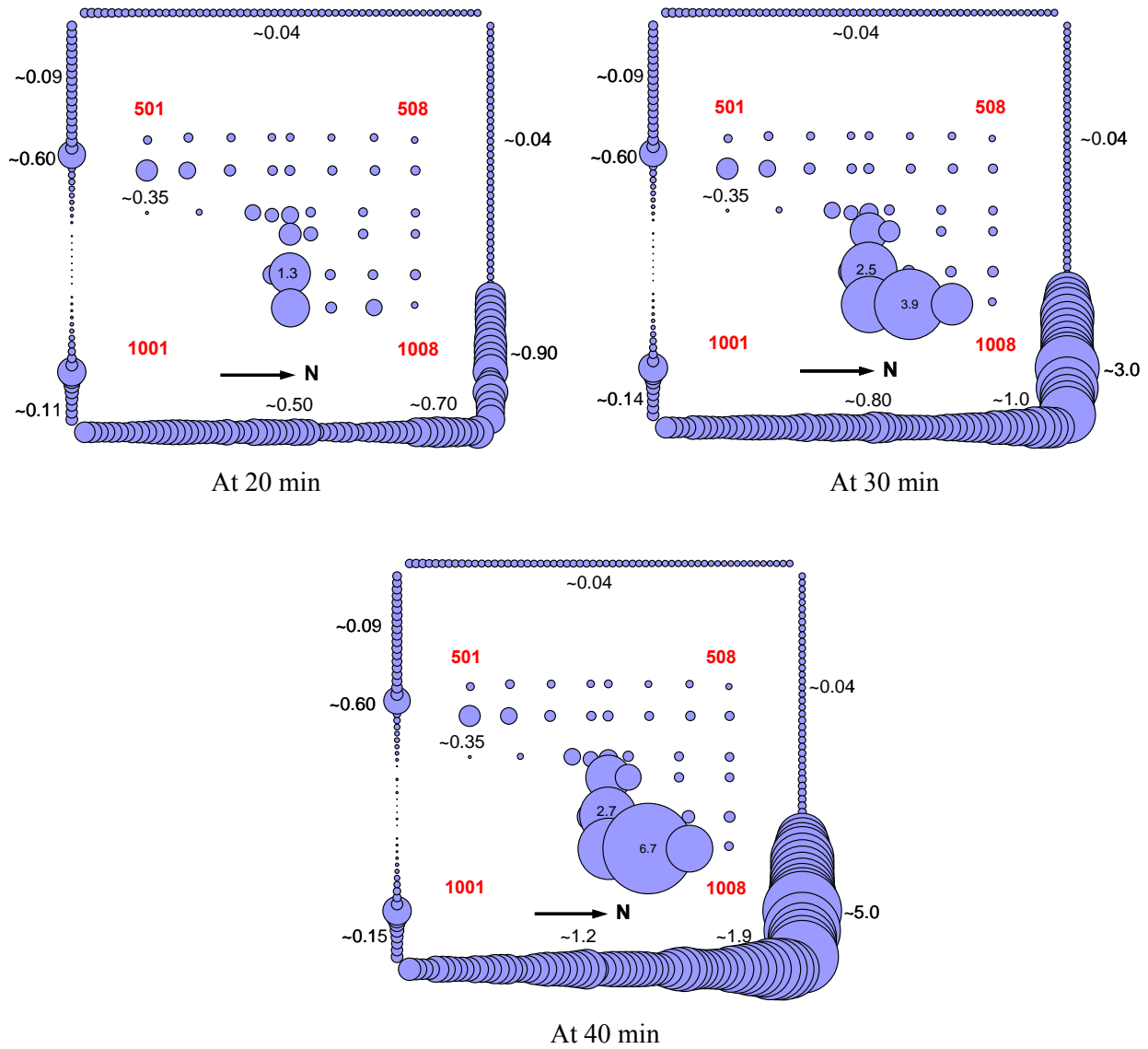


Figure 9–21. Maximum elastic + plastic + creep strains for columns between Floor 78 and Floor 83 of WTC 2 at different stages (Case D) (strain values are in percent).

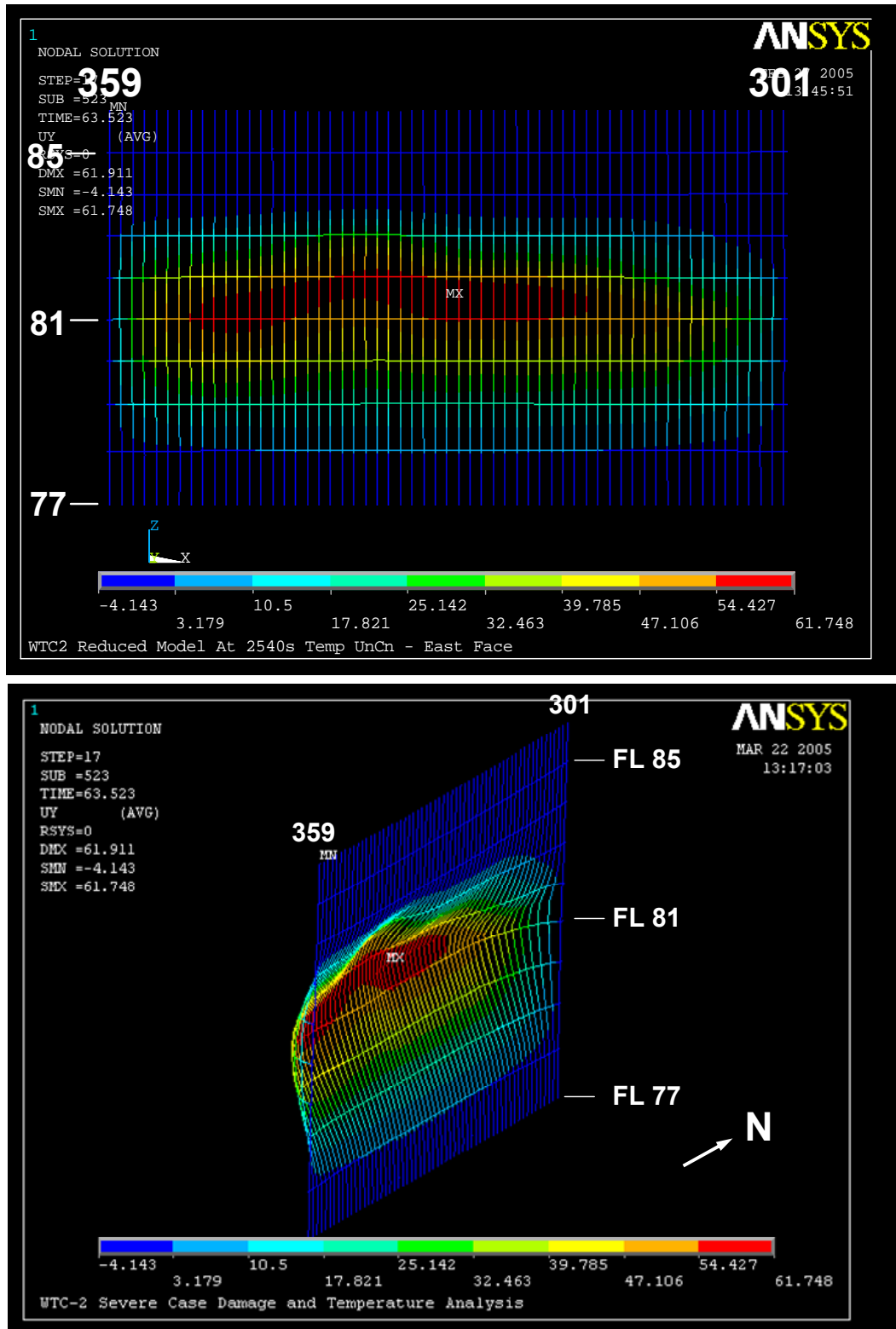


Figure 9–22. Inward bowing of the east wall of WTC 2 when buckled at 43 min for Case D (4x displacement magnification).

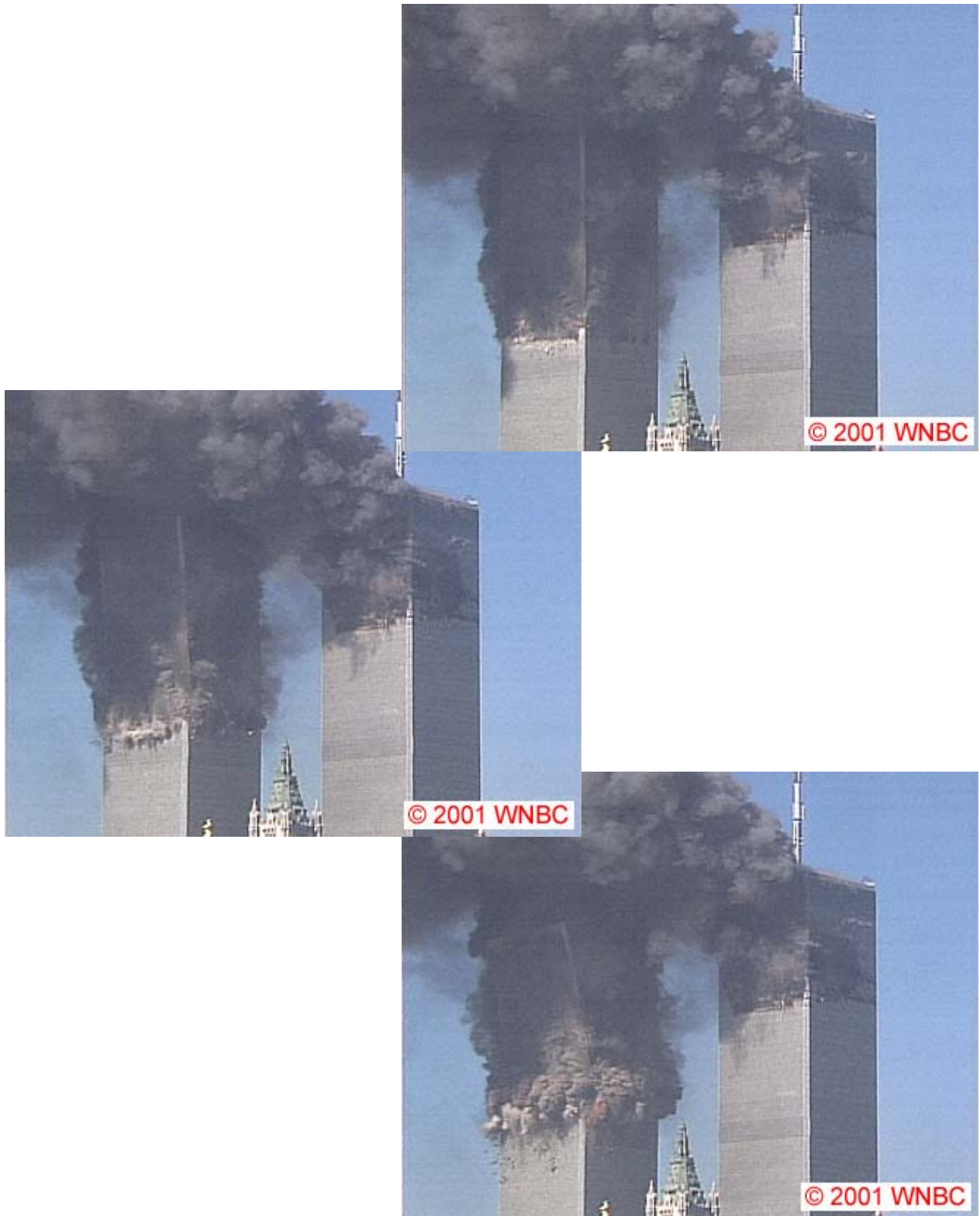


Figure 9–23. Inward bending of exterior columns of the west wall of WTC 2 just before collapse.

Table 9–10. Change in total column loads when the east wall of WTC 2 buckles (Case D, compression is positive).

| Row | Floor | West | East | North | South | Core |
|-----|-----------|-------|-------|-------|-------|------|
| (1) | 83 | -2864 | -8539 | 2309 | 2819 | 5596 |
| (2) | 105 | -2112 | -3901 | 23 | 479 | 5513 |
| (3) | (2) - (1) | 752 | 4637 | -2286 | -2340 | -84 |

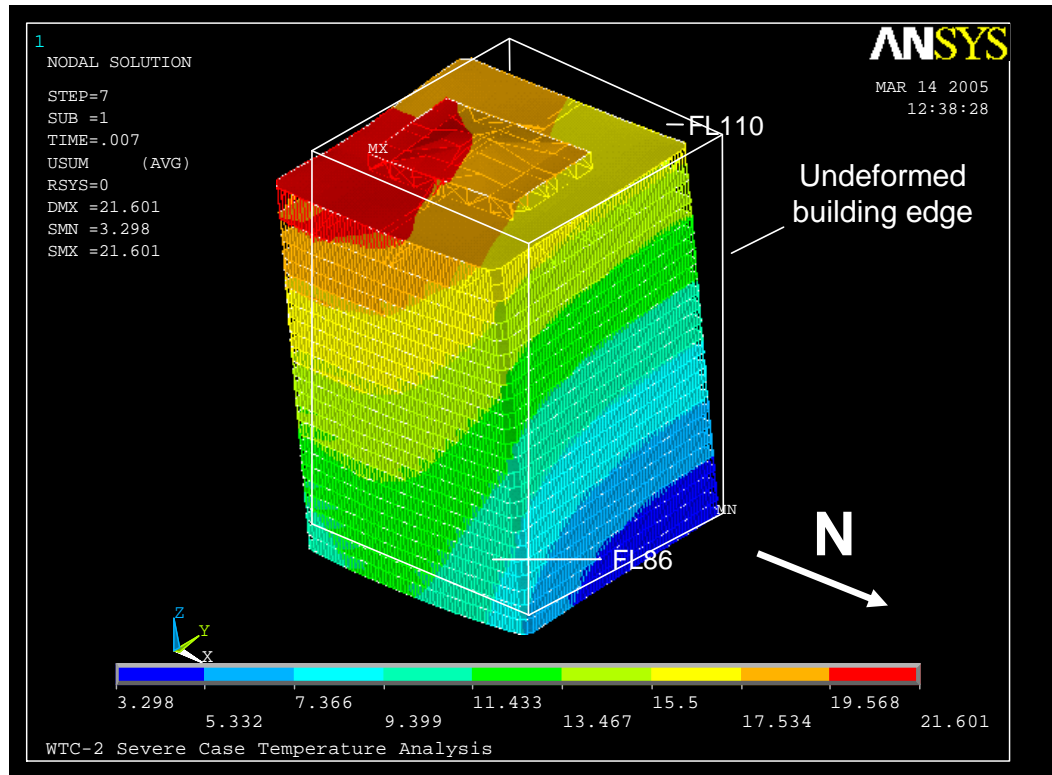


Figure 9–24. Total displacements of WTC 2 above Floor 86 at 43 min for Case D. Note tilt toward east and south (20x displacement magnification).

9.3.3 Events Following Collapse Initiation

Failure of the south wall in WTC 1 and east wall in WTC 2 caused the portion of the building above to tilt in the direction of the failed wall. The tilting was accompanied by a downward movement. The story immediately below the stories in which the columns failed was not able to arrest this initial movement as evidenced by videos from several vantage points.

The structure below the level of collapse initiation offered minimal resistance to the falling building mass at and above the impact zone. The potential energy released by the downward movement of the large building mass far exceeded the capacity of the intact structure below to absorb that through energy of deformation.

Since the stories below the level of collapse initiation provided little resistance to the tremendous energy released by the falling building mass, the building section above came down essentially in free fall, as seen in videos. As the stories below sequentially failed, the falling mass increased, further increasing the demand on the floors below, which were unable to arrest the moving mass.

The falling mass of the building compressed the air ahead of it, much like the action of a piston, forcing material, such as smoke and debris, out the windows as seen in several videos.

NIST found no corroborating evidence for alternative hypotheses suggesting that the WTC towers were brought down by controlled demolition using explosives planted prior to September 11, 2001. NIST also did not find any evidence that missiles were fired at or hit the towers. Instead, photographs and videos from several angles clearly showed that the collapse initiated at the fire and impact floors and that the collapse progressed from the initiating floors downward, until the dust clouds obscured the view.

9.4 DISCUSSION AND SUMMARY

The results of structural analyses conducted in this study on components, subsystems, isolated exterior walls and cores, and global models of WTC 1 and WTC 2 showed that the collapses of the towers were initiated by the combined effects of the structural and insulation damage from aircraft impact and the subsequent intense fires.

The impact damage alone did not cause collapse of the towers, as they stood for a period of time, and collapse occurred after the fire-induced weakening of core, floor systems and exterior walls. Global analyses showed that both towers had substantial reserve capacity after the aircraft impact.

Similarly, the fires alone did not cause the collapse of the towers. In the absence of insulation damage, the weakening of the core columns and sagging of the floors sufficient to pull in on the exterior walls would not have occurred.

9.4.1 Structural Response to Impact Damage and Fire

All three major subsystems played a role in the structural collapse sequence for WTC 1 and WTC 2 as described herein.

Role of the Building Core

The core columns were designed to carry the building gravity loads and were loaded to approximately 50 percent of their capacity before the aircraft impact.

The core columns were weakened significantly by the aircraft impact damage and thermal effects. Thermal effects dominated the weakening of WTC 1. As the fires moved from the north to the south side of the core, the core was weakened over time by significant creep strains on the south side of the core. Aircraft impact damage dominated the weakening of WTC 2. Immediately after impact, the vertical displacement at the southeast corner of the core increased 6 in. (from 4 in. to 10 in.). With the impact damage, the core subsystem leaned to the southeast and was supported by the south and east floors and exterior walls.

Gravity loads redistributed from the core to the exterior faces primarily through the hat truss due to aircraft impact and thermal effects. The WTC 1 core carried 1 percent less loads after impact but 20 percent less after thermal weakening. The WTC 2 core carried 6 percent less loads after impact and 2 percent less loads after thermal weakening.

Additional axial loads redistributed to the exterior columns from the core were not significant (only about 20 percent to 25 percent on average) as the exterior columns were loaded to approximately 20 percent of their capacity before the aircraft impact.

Role of the Building Floors

The floors were designed to support occupancy loads and transfer them to the core and perimeter columns. They were also designed to act as horizontal diaphragms when the buildings were subject to high winds. In the collapse of the towers, the primary role of the floors was to provide inward pull forces after sagging that induced inward bowing of exterior columns (South face of WTC 1; East face of WTC 2).

The floors provided inward pull forces as they sagged significantly under thermal loads. However, the sagging floors continued to support their floor loads despite the dislodged insulation and extensive fires. Some truss seat connections with dislodged insulation at the exterior columns did fail and disconnect from the exterior wall under thermal loads. Floor disconnections increased the unsupported length of the exterior columns and distributed floor loads to adjacent truss seats. There were no inward pull forces where the floors were disconnected.

Role of Exterior Walls

Column instability over an extended region of the exterior face ultimately triggered the global system collapse as the loads could not be redistributed through the hat truss to the already weakened building core. In the area of exterior column buckling, loads transferred through the spandrels to adjacent columns and adjacent exterior walls. As the exterior wall buckled (south face for WTC 1 and east face for WTC 2), the column instability propagated to adjacent faces and caused the initiation of the building collapse.

The exterior wall instability was induced by a combination of thermal weakening of the columns, inward pull forces from sagging floors, and to a much lesser degree, additional axial loads redistributed from the core.

9.4.2 Structural Response to Fire Without Impact Damage

Without insulation to delay the heating of steel components, steel temperatures began to rise upon exposure to fires. Thermal expansion occurred as temperatures increased; members restrained against thermal expansion increased in compressive load and may have caused a local or global load redistribution, depending upon the compressive load increase and extent of heating. Once steel temperatures exceeded 500 °C to 600 °C, the steel experienced significant reductions in stiffness and strength. The thermal analysis found that temperatures of floor trusses and columns with intact insulation rarely exceeded 400 °C during Case B fires (100 min long) for WTC 1 and 500 °C during Case D fires (60

min long) for WTC 2. Insulated floors thermally expanded, pushed outward on the exterior columns, and sagged in the full floor analyses, but the floor sag was insufficient to exert an inward pull on the exterior columns.

Steel members with dislodged insulation were found to have temperatures greater than 600 °C and often higher than 800 °C within 10 min to 15 min after exposure to a nearby fire. Fire exposures considerably longer than the 60 to 100 min exposure in WTC 2 and WTC 1, respectively, were required for insulated members to reach these temperatures. Reductions in modulus of elasticity, yield strength, and ultimate tensile strength of steel in the WTC towers were predicted to be 13 percent, 20 percent, and 10 percent, respectively, at 400 °C, and 35 percent, 92 percent, and 80 percent, respectively, at 700 °C. Steel loses its strength significantly at 700 °C. At these temperatures, the long-span floors were found to sag sufficiently to exert an inward pull on the exterior walls, primarily due to buckling of truss web diagonal members. In addition, creep in steel columns becomes significant when the steel temperatures are greater than 500 °C and subject to high stresses for a period of time.

Inward bowing of an exterior wall was a necessary but not sufficient condition to initiate collapse. In both WTC 1 and WTC 2, significant weakening of the core due to aircraft impact damage and thermal effects was also necessary to initiate building collapse. The tower structures had significant capacity to redistribute loads (a) from bowed walls to adjacent exterior walls with short-span floors via the arch action of spandrels, and (b) between the core and exterior walls via the hat truss and, to a lesser extent, the floors. Without the impact damage, the towers' capacity to redistribute loads would have been even greater.

As shown in the analysis results, the temperatures in steel components without insulation damage were lower for the same fire. Lower temperatures resulted in reduced creep, plasticity, and buckling. Without insulation damage, floor sagging was insufficient to exert pull-in forces on the exterior wall; the core columns maintained their stiffness and strength; and the exterior wall did not bow inward. The lack of thermally induced damage would result in negligible load redistributions, and the towers would have remained stable.

9.4.3 Time to collapse

The difference in the time it took for each WTC tower to collapse was due primarily to the differences in structural damage, the time it took the fires to travel from the impact area across the floors and core to critical locations, and the time it took to weaken the core and exterior columns. WTC 2 had asymmetric structural damage to the core, including the severing of a corner core column, and WTC 1 had more symmetrical damage. The fires in WTC 2 reached the east side of the building more quickly, within 10 to 20 minutes, than the 50 to 60 minutes it took the fires in WTC 1 to reach the south side.

9.4.4 Comparison with Other Collapse Hypotheses

Alternate analyses and collapse hypotheses were performed and reported by other studies. A comparison of NIST and other hypotheses is presented to review assumptions, methodologies, and results. The comparison includes analyses performed by

- Northwestern University,

- Weidlinger Associates, Inc. with Hughes Associates and ArupFire,
- University of Maryland at College Park and the Israel Institute of Technology,
- Edinburgh University, and
- Arup.

The NIST structural response analyses included the effects of aircraft impact damage to the structure and thermal insulation, fire growth and spread, the resulting time-varying temperatures of the structural components, and the progression of local structural failure leading up to collapse initiation. The analyses included the effects of construction sequence, thermal expansion, plastic and creep strains, temperature-dependent material properties, and relevant failure modes for structural members and connections.

With the exception of the Weidlinger-led study, the analyses for the other collapse hypotheses presented here ignored impact damage, assumed time-temperature curves for structural subsystems (i.e. floor trusses and exterior columns), and conducted analyses of components or subsystems but did not conduct global analyses of the entire structure (i.e., core, floors, exterior walls, and hat truss) that considered all of the load redistribution paths as local members and subsystems were thermally weakened over time. The Weidlinger study included impact damage and assumed time-temperature curves for structural subsystems for their global analyses of each tower.

Northwestern University

The study performed by Northwestern University (Bazant 2002) was a simplified approximate analysis of the overall collapse of the WTC towers which addressed the question of why a total collapse occurred. The analysis addressed the results of prolonged heating which would have caused the columns of a single floor to lose their load carrying capacity and initiated the collapse of the building. The analysis assumed loss of thermal insulation during impact, uniform temperatures of 800 °C for a uniform column size and load across a single floor, and creep buckling and loss of load carrying capacity in over half of the columns. The analysis included evaluation of the dynamic amplification of the loads and the ability of the columns in the lower floors to dissipate the kinetic energy of the falling upper building mass through formation of plastic hinge mechanisms. The analysis found that the ratio of the kinetic energy of the upper building section dropping one floor to the deformation energy of plastic hinge rotation in the lower building columns was approximately a factor of eight.

The study by Northwestern did not address the details of impact damage, fire dynamics, or structural response of the towers. Rather, a generalized condition was assumed of heated columns, and the question of why there was total collapse was addressed. NIST agrees with the assessment of the tower's required structural capacity to absorb the released energy of the upper building section as it began to fall as an approximate lower bound. The likelihood of the falling building section aligning vertically with the columns below was small, given the observed tilting, so that the required capacity would be greater if interaction with the floors was also considered, as pointed out in the study.

Weidlinger Associates, Inc. with Hughes Associates and ArupFire

The study led by Weidlinger Associates, Inc. (Abboud 2003, Post 2002a, Post 2002b, Glanz 2002) used the SAP2000 and FLEX finite element code to calculate the aircraft impact damage to both towers and their structural response to damage and elevated temperatures. FLEX is an explicit, nonlinear, large deformation transient analysis finite element code for the analysis of structures subject to blast, impact, and shock loads. The fires were evaluated by Hughes Associates and ArupFire Inc. The fires were found to be less than fully developed office fires, with gas temperatures ranging from 400 °C to 700 °C in the impact regions and well ventilated regions near the exterior walls; exterior locations with persistent fires were assumed to have 1000 °C temperatures. Based upon study of smoke plumes and fire spread, it was concluded that the floors did not fail or have a significant role in the collapse of the towers. The structural response analysis found that the impact debris dislodged thermal insulation and that the hat truss played a significant role in transferring loads between the core and exterior walls. The analysis identified the specific cause of each towers' collapse to be the failure of core columns that either lost insulation or were destroyed during the aircraft impact. WTC 2 exterior columns on the east side began to fail first and redistributed loads to the core columns until the loads could no longer be supported, due to successive failures of core columns. WTC 1 core columns began to fail first due to damage and thermal weakening and attempted to redistribute loads to the exterior walls through the hat truss. WTC 2 was found to collapse first primarily because the damage was off-center and compromised the southeast corner of the core.

NIST agrees with many of the findings by the Weidlinger Associates, Inc. led study. However, there were some differences in the modeling approach and assessment of contributing factors. The most significant difference was that the floors were not analyzed for their response to fire, so that the collapse hypothesis did not account for floor sag and its contribution to inward bowing of the exterior columns. The reason for WTC 2 collapsing before WTC 1 was attributed to the off-center damage, particularly the damage to the southeast corner core column. NIST found that in addition to the differences in impact damage between the two towers, the time it took the fires to travel from the impact area across floors and the core to critical areas, and the time it took for the core and exterior columns to become thermally weakened, also contributed to the difference in times to collapse initiation.

University of Maryland and Israel Institute of Technology

The study performed by the University of Maryland and the Israel Institute of Technology (Quintiere 2002) was based upon a thermal conduction analysis of truss web members subjected to a uniform gas temperature and a structural failure analysis based on buckling of the truss web member due to a temperature-induced reduction in stiffness. Gas temperatures were estimated to be approximately 900 °C for the duration of the fires in each tower. A thermal conduction analysis of web members was conducted to estimate the temperature of the web member as a function of time and insulation thicknesses (0.75 in. and 1.5 in.). A web member with an assumed load was calculated to buckle when temperatures of about 630 °C to 770 °C were reached, due to a reduced modulus of elasticity. The time at which the insulated members reached temperatures that met the buckling criteria fell within the observed collapse time of each tower. It was noted that a bare steel web member would fail by this criteria in 10 min to 15 min, and that this time did not match the observed time to collapse initiation. Given the failure of truss web members, it was postulated (not supported by calculations) that the floors would sag and fail at their connections to the columns and that progressive collapse would ensue as the floors below also failed.

NIST findings differed from those given in this study. NIST also found that web members in the floor trusses buckled when heated sufficiently, which led to sagging of the floor, but did not find appreciable floor sagging when the truss insulation remained intact. The Maryland study suggested that the sagging floors resulted in failure of the floor to column connections; NIST analyses found that the sagging floors did not cause floor connections to fail, except at a few isolated locations, but rather produced an inward pull on the exterior walls. An inward pull of exterior columns would not occur if floor to column connections had failed. To produce the inward bowing of the exterior walls that was observed, the floors had to sag and exert an inward pull well before collapse initiated, not at the time of collapse as proposed in the Maryland study. Additionally, analysis of a floor collapsing onto a floor below, which was unlikely given the required event of all floor connections failing nearly at the same time, was not found to result in failure of the impacted floor.

University of Edinburgh

The University of Edinburgh study (Usmani 2003, Usmani 2005) performed a nonlinear, large displacement finite analysis of a typical 2D slice of the tower structure that encompassed twelve floors around the impact level of WTC 1 using ABAQUS. However, there were also some simplifying assumptions to reduce the model complexity, such as restraining lateral movement of the floor at the core end and a pinned connection to the external columns at the other end. The truss diagonals were modeled with a single axial element and connections were not explicitly modeled. It was assumed that the core columns were relatively cool and that the collapse would initiate at the exterior columns. A generalized exponential curve represented the time-temperature relationship, and assumed temperature profiles were applied to the floors for various fire scenarios. The exterior columns were linearly ramped from ambient temperatures. The analysis found that the heated floors expanded and pushed the exterior columns outward and that the outward movement was resisted by tension in the cool floors above and below the fire floors. The analysis also found that a floor buckled at 400 °C, causing the exterior column to ‘rebound’, resulting in large compressive loads on the floors above and below, which in turn buckled. It was stated that the same mechanism propagated to adjacent floors until it was arrested or caused collapse. Consideration of the hat truss, its capacity for redistribution of loads between the exterior walls and core, and its role in delaying the collapse mechanism until the structure’s redistribution capacity was exhausted was discussed, but no supporting analyses were presented. These results were cited as a possible fire-induced collapse mechanism for a tower without impact damage that was based on thermal expansion rather than fire-induced loss of strength and stiffness.

NIST findings also differed from the findings of the University of Edinburgh study. NIST included thermal expansion in its detailed analyses of full floor systems, and did not find that buckling of any floor system occurred. Rather, as truss web members began to buckle, the floors began to sag, which increased over time. The sudden buckling of the first floor in the Edinburgh analysis, followed by the sudden subsequent failure of floors above and below, does not match the observed inward bowing of the exterior walls which increased over time. Further, NIST found that failure of an exterior wall was necessary but not sufficient to initiate the collapse of either tower. In both WTC 1 and WTC 2, significant weakening of the core due to aircraft impact damage and thermal effects was also necessary to initiate building collapse.

Arup

The study by Arup (Lane 2005) was conducted to determine if the WTC towers had any collapse mechanisms specific to their structural system features. Based upon information available through presentations, studies included 2D analysis of a twelve-floor slice of the exterior column and floors to the core, a twelve-floor slice across the entire tower (from exterior column to exterior columns), and 3D quarter floor, half floor, and quarter-floor seven-story section models. None of the models included the hat truss; all of the models included individual floor trusses and the floor slabs. Temperatures from the fires for structural members were assumed, where the floor trusses reached 800 °C in a “very short time”, the exterior columns and spandrels heated linearly to 400 °C by 3600 s. Slab temperatures were not reported. Three floors were heated to 800 °C, the floors sagged and the exterior wall section was pulled inward. The inward bowing of the exterior wall was considered to be a collapse mechanism for the towers. Arup stated that the behavior was calculated for the duration of the fire with no user intervention and without inclusion of any aircraft impact damage, including damage to thermal insulation.

The description of Arup analyses is based on presentations since no published reports by Arup were available prior to the release of this report. The study by Arup found that the composite truss floors sagged as they were heated and pulled inward on the exterior wall, similar to the findings by NIST. However, the NIST analyses did not find uniform temperatures across an entire floor nor simultaneously on multiple floors, as assumed in the Arup analyses. Further, NIST did not find any insulated truss members reaching temperatures of 800 °C prior to the collapse of either tower. NIST thermal analyses showed that steel temperatures in areas where the insulation remained intact rarely exceeded 400 °C in WTC 1 and 500 °C in WTC 2. The Arup 3D seven-floor model did not include load transfer mechanisms, including the hat truss, the core, and sufficient portions of the exterior wall to provide the arching action observed in the impact faces. NIST found that failure of an exterior wall was necessary but not sufficient to initiate the collapse of either tower. In both WTC 1 and WTC 2, significant weakening of the core due to aircraft impact damage and thermal effects and redistribution of loads between the core and exterior wall were found to be necessary to initiate building collapse.

9.4.5 Factors that Affected Performance

From the collective knowledge and insights gained through the Investigation of the collapse of the WTC towers, the following factors were identified that affected performance of both towers on September 11, 2001:

- The closely spaced columns, along with deep short spandrels, allowed a redistribution of loads as a result of aircraft impact damage to the exterior wall.
- Because there was effectively no wind on the morning of September 11, 2001, the capacity of the exterior wall provided to accommodate design wind loads was available to carry redistributed gravity loads.
- The large dimensional size of the WTC towers helped the buildings withstand the aircraft impact.
- The composite floor system with primary and bridging trusses forming a 2-way grid, and the two layers of welded wire fabric in the slab, acted to bridge over damaged areas without

propagation of collapse from areas of aircraft impact damage to other locations, thereby avoiding larger scale floor collapse upon impact.

- The hat truss played a major role in the post-impact performance of the building. This was accomplished through redistribution of the loads from the significant weakening of the core, due to aircraft impact damage and subsequent thermal effects, by redistributing loads from the damaged core columns to adjacent intact columns and, ultimately, by redistributing loads to the exterior walls from the thermally weakened core columns that lost their ability to support the buildings' weight.
- The buildings would likely not have collapsed under the combined effects of aircraft impact and the subsequent jet-fuel ignited multi-floor fires, if the insulation had not been dislodged or had been only minimally dislodged by aircraft impact. The existing condition of the insulation prior to aircraft impact and the insulation thickness on the WTC floor system did not play a significant role in initiating collapse on September 11, 2001.

9.5 REFERENCES

Zdenek Bazant and Yong Zhou (2002), *Why Did the World Trade Center Collapse?—Simple Analysis*, Journal of Engineering Mechanics, Vol. 128, No. 1

Abboud, Najib et.al., (2003), Anatomy of a disaster: A structural investigation of the World Trade Center collapses, Proceedings of the Third Congress Forensic Engineering, San Diego, CA, United States, Oct 19-21 2003, p 360-370

Nadine Post (2002a), Report Ties WTC Collapses to Column Failures, Engineering News Record, McGraw Hill Construction, 10/25/2002

Nadine Post (2002b), Study Absolves Twin Tower Trusses, Fireproofing, Engineering News Record, McGraw Hill Construction, 11/04/2002

James Glanz and Eric Lipton (2002), In Data Trove, A Graphic Look at Towers' Fall, The New York Times, October 29, 2002

J.G. Quintiere, M. di Marzio, and R. Becker (2002), A suggested cause of the fire-induced collapse of the World Trade Towers, Fire Safety Journal, Vol. 37, Issue 7, October 2002, p 707-716.

A.S. Usmani, Y.C. Chung, and J.L. Torero (2003), How did the WTC towers collapse: a new theory, Fire Safety Journal, vol 38, Issue 6, October 2003, p 501-533.

A.S. Usmani (2005), Stability of the World Trade Center Twin Towers Structural Frame in Multiple Floor Fires, Journal of Engineering Mechanics, Vol. 131, No. 6, Jun 2005, p 654-657.

B. Lane (2005), Comments on structural fire response and collapse analysis, Presentation given at the Technical Conference on the Federal Building and Fire Safety Investigation of the World Trade Center (WTC) Disaster, National Institute of Standards and Technology (NIST), Gaithersburg, Maryland, September 13-15, 2005, <http://wtc.nist.gov>

This page intentionally left blank.

Chapter 10

FINDINGS

There were many facets to the work reported herein. First, the thickness of the passive fire protection was established from recorded measurements and interpretation of photographs of the originally applied SFRM. This information was used, along with statistical analysis and thermal structural analyses, to establish the thickness of passive fire protection (insulation or fireproofing) to be used in finite element thermal analyses. Next, standard fire resistance tests were conducted to establish the appropriate classification (fire resistance rating) of the original design of the WTC floor system and structural performance of the floor system in standard fires for insight into performance in actual fires. Characterization of the temperatures of the structural components, determined from simulated WTC fires, allowed the calculation of the performance of major subsystems constituting the structural system of the towers. In turn, insights obtained from these analyses were used to formulate and execute global analyses to analyze the collapse sequence of each tower. The structural analyses results were guided, and where possible validated, by observations made from the review of thousands of photographs and video recordings. This chapter reports the findings resulting from these efforts to characterize the conditions of the WTC towers before the attacks, their weakening due to the aircraft impacts, their subsequent response to the growth and spread of fires, and the progression of local failure that ultimately led to the total collapse of both towers.

10.1 PASSIVE FIRE PROTECTION

The passive fire protection applied to the steel structural components in the WTC towers was investigated to provide information on the in-place condition of the thermal insulation before and after the aircraft impact. The specified and “as applied” thicknesses, the variability in thickness, the condition of the insulation over a 30-year service life, and the effects that the variability and condition have on the structural behavior of insulated steel members were studied. The rationale behind the selection of the effective thickness of thermal insulation for use in thermal analyses was presented. Additionally, the procedures and practices used to provide the passive fire protection for the floor system of the WTC tower structures was documented.

10.2 BUILDING CODE REQUIREMENTS FOR STRUCTURAL FIRE RESISTANCE

Finding 1: The WTC towers were classified as Class 1B, as defined by the 1968 New York City Building Code. This classification required a 3 h fire rating for columns and 2 h for floors. The towers could have been classified as Class 1A since both Class 1A and 1B permitted buildings of unlimited height. Class 1A required a 4 h fire resistance rating for columns and a 3 h rating for floors. In 1969, The Port Authority of New York and New Jersey (PANYNJ) specified 0.5 in. fireproofing for all beams, spandrels, and trusses, to maintain the Class 1-A Fire Rating of the New York City Building Code. A condition assessment conducted in 2000 reported that the WTC towers were classified as Class-1B—noncombustible, fire-protected, and retrofitted with sprinklers consistent with Local Law 5/1973.

10.2.1 Selection of Fire Resistive Materials

Finding 2: The passive fire protection for the floor trusses was specified to be 0.5 in. of BLAZE-SHIELD Type D, although the technical basis for the selection of this product and required thickness value is not known. After applying the Type D sprayed fire resistive materials to the lower 40 floors of WTC 1, the BLAZE-SHIELD insulating material was switched to Type D/CF (reported to meet or exceed the insulating properties of Type D) which did not contain asbestos. In 1995, the Port Authority conducted a study to establish the fireproofing requirements for the floor trusses in areas undergoing major tenant renovation. The thickness required to achieve a 2 h fire rating was determined to be 1.5 in. using the BLAZE-SHIELD II product. At the time of the WTC disaster, fireproofing had been upgraded on a number of floors in the WTC towers: 18 floors in WTC 1, including all of the floors affected by the aircraft impact and fires, and 13 floors in WTC 2, although none that were directly affected by the aircraft impact and fires.

10.2.2 Equivalent thickness of SFRM

Finding 3: Based on analyses of SFRM thickness measurements and interpretation of photographs showing the condition of the originally applied material, the average thickness of the original thermal insulation on the floor trusses was estimated to be 0.75 in. with a standard deviation of 0.3 in. (coefficient of variation of 0.40). The average thickness of the upgraded thermal insulation was estimated to be 2.5 in. with a standard deviation of 0.6 in. (coefficient of variation of 0.24). Based on finite-element simulations, it was concluded that the original passive fire protection on the floor trusses was thermally equivalent to a uniform thickness of 0.6 in., and the upgraded insulation was thermally equivalent to a uniform thickness of 2.2 in. These values were used in the thermal analyses for determining temperature histories of structural components.

Finding 4: No information was available on in-place conditions of the thermal protection on the exterior columns and spandrel beams, and little information was available on the conditions of fire resistive material on core beams and columns. For thermal analyses of the towers, the SFRM on these elements was taken to have uniform thicknesses equal to the specified thickness. This assumption was supported by the observation that measured average thickness tended to be *greater* than the specified thickness while, due to variability, the effective thickness tended to be *less* than the average uniform thickness. The specified thickness values were 0.5 in. for beams and spandrels, 2.06 in. (2 1/16 in.) for columns lighter than 14WF228, and 1.19 in. (1 3/16 in.) for columns equal to or heavier than 14WF228.

Finding 5: The adhesive strength of BLAZE-SHIELD DC/F to primed steel was found to be a third to a half of the adhesive strength to steel that had not been coated with primer paint. The SFRM products used in the WTC towers were applied to steel components with primer paint.

10.3 FIRE RESISTANCE TESTS

Four Standard Fire Tests (ASTM E 119) were conducted on floor assemblies constructed to duplicate, as closely as practical, the floor system used in the WTC towers. Full scale tests with a 35 ft span and having 3/4 in. thick SFRM were tested, one in the restrained test condition and the other in the unrestrained test condition. Tests of half-scale specimens, which spanned approximately 17 ft, were conducted using SFRM conditions simulating the “as specified” condition (0.5 in. thick SFRM) and the “as-applied”

condition (0.75 in. thick SFRM). The following findings are based on this series of four tests and a comparison of their results.

10.3.1 Structural Performance

Finding 6: Test assemblies, representative of the WTC floor system, exposed to the Standard Fire Test (ASTM E 119) conditions resulted in extensive spalling on the underside of the floor slab, thermal damage to the bridging trusses, and buckling of compression diagonals and vertical struts of the main trusses.

Finding 7: All four tests demonstrated that the floor assemblies were capable of sagging without failure. The unrestrained test, which had two 0.875 in. bolts fastening the main truss to the truss seats, did not sag sufficiently to bear on the bolts. In the three restrained tests the main truss ends were welded to the truss seats to provide the required restraint. The magnitude of the sagging observed in the tests was consistent with that computed from finite element structural analyses. No evidence of knuckle failure was seen in the tests.

Finding 8: All four test assemblies supported their full design load under standard fire conditions for two hours without failure.

10.3.2 Fire Resistance Ratings

Finding 9: The 1968 New York City (NYC) building code—the code that the WTC towers were intended but not required to meet when they were built—required a 2 h fire rating for the floor system.

Finding 10: The restrained duplicated floor system obtained a fire resistance rating of 1.5 h while the unrestrained floor system achieved a 2 h rating. This finding was unexpected since the unrestrained rating is typically less than the restrained rating.

Finding 11: The test of the 17 ft specimen with as-applied SFRM did not produce the same rating as the 35 ft test specimen, giving 2 h and 1.5 h, respectively. In both cases, the rating was established on the basis of temperatures of the unexposed surface (top of concrete slab) and not on the ability of the specimen to support the load.

Finding 12: The 45 min rating for the standard 17 ft test with the specified 0.5 in. SFRM did not meet the 2 h requirement of the 1968 NYC Building Code. This test had no SFRM on the bridging trusses nor on the underside of the metal deck.

Finding 13: The 2 h rating for the standard 17 ft test with the as-applied average 0.75 in. SFRM met the 2 h requirement of the 1968 NYC Building Code. This test had half the SFRM thickness on the bridging trusses (0.375 in.) and overspray on the underside of the metal deck.

Finding 14: The difference in test results for the two 17 ft specimens is due primarily to the concrete slab performance (spalling and cracking) and the presence or lack of SFRM overspray on the metal deck and not due to the SFRM thickness on the trusses. Differences in the degree of concrete spalling were possibly due to differences in moisture content and the slab cracking.

10.4 RESPONSE OF STRUCTURAL COMPONENTS

The response of the structural components and their connections for the tenant floors and exterior walls was examined with detailed structural models. Results of the floor and exterior wall component and connection analyses identified structural behaviors and failure modes that were required for inclusion in the global analyses.

10.4.1 Floor System

Finding 15: The interior truss seats had a greater vertical shear capacity than the exterior truss seats. The controlling failure mode for vertical shear was weld fracture. However, the vertical load at the truss connection of approximately 16 kip had to increase by a factor of two to six to reach failure (weld fracture) for temperatures near 600 °C to 700 °C.

Finding 16: Detailed structural analysis of a single truss section of the composite floor system subjected to elevated uniform temperatures was found to initially push out on the exterior columns as a result of the concrete slab thermal expansion and then pull inward as the web diagonals buckled and the truss sag increased. The magnitude of the pull-in force was found to depend highly on the stiffness of the exterior box column which, in turn, depended on expansion of floors above and below.

Finding 17: Detailed analysis of the knuckles (shear connectors in the floor system for composite action) through test simulation and detailed truss analysis found that failure of the knuckles in the floor system was unlikely. This finding was also supported by the lack of any knuckle failures in the four standard fire resistance tests (ASTM E 119) of the floor truss assemblies with twice the floor load that was on the WTC floors.

10.4.2 Exterior Wall System

Finding 18: Large inelastic deformations and buckling of the spandrels at elevated temperatures were predicted, but were found not to significantly affect the stability of the exterior columns. Partial separations of the spandrel splices were also predicted at elevated temperatures, but were found not to significantly affect the stability of the exterior columns.

Finding 19: Analyses of bolted splices in the exterior columns found that the splice may slide or open when the exterior columns are bowing and subject to large lateral deflections. No column splice bolts were predicted to have failed.

Finding 20: An exterior wall section (9 columns wide and 9 floors high) was found to bow inward when the floor connections applied an inward pull force. For the condition where three sequential floors were disconnected, there was no bowing of the columns for five different elevated temperature conditions. When the column section with three disconnected floors was subjected to increased axial column loads, the wall section bowed outward over the unsupported column length.

10.5 FIRE PROTECTION AND PARTITION DAMAGE DUE TO AIRCRAFT IMPACT

The aircraft impact of the WTC towers caused extensive damage to the buildings' exteriors, penetrated into the interiors causing further damage to the structural systems, dislodged insulation, and ignited multi-floor fires. The structural damage to each tower resulting from the aircraft impact was estimated using a transient finite element analysis. Results of this analysis were used to predict damage to the structure, fireproofing, and partition walls in the path of the debris field.

Finding 21: For WTC 1, partitions were damaged and fireproofing was dislodged by direct debris impact over five floors (Floors 94, 95, 96, 97, and 98) and included most of the north floor areas in front of the core, the core, and central regions of the south floor areas, and on some floors, extended to the south wall. For WTC 2, partitions were damaged and fireproofing was dislodged by direct debris impact over six floors (Floors 78, 79, 80, 81, 82, and 83) and included the south floor area in front of the core, the central and east regions of the core, and most of the east floor area, and extended to the north wall.

Finding 22: The fireproofing damage estimates were conservative as they ignored possibly damaged and dislodged fireproofing in a much larger region that was not in the direct path of the debris but was subject to strong vibrations during and after the aircraft impact. A robust criteria to generate a coherent pattern of vibration-induced dislodging could not be established to estimate the larger region of damaged fireproofing.

10.6 OBSERVATIONS AND TIMELINE

Thousands of photographs and hours of video records were reviewed for insights into the structural performance of the towers. A timeline of significant events that characterized the weakening and eventual collapse of the WTC towers was developed with the photographs and videos that were time-stamped. Quantitative information, such as the amount of inward bowing observed on the exterior walls of the buildings, was extracted from key photographs through image enhancement and scaled measurements. Key observations and the timelines were used to guide the global collapse analyses.

10.6.1 WTC 1

Finding 23: Inward bowing of the south exterior wall was first observed at 10:23 a.m. The bowing appeared to extend between Floors 94 and 100 and Columns 305 and 359. The maximum bowing was estimated from images to be 55 in.±6 in. at Floor 97 on the east side of the south face of WTC 1. The central area in available images was obscured by smoke. The extent of fires observed on all faces of WTC 1 was similar, although somewhat more extensive on the east and west faces (where short span floors were located) and similarly extensive on the north and south faces (where long span floors were located). Inward bowing was observed only on the south face. The north face had extensive aircraft impact damage, and the damaged floors were not capable of imposing inward pull forces on the north face.

Finding 24: The time to collapse initiation was 102 minutes from the aircraft impact (8:46:30 a.m. until 10:28:22 a.m.).

Finding 25: From exterior observations, tilting of the building section appeared to take place near Floor 98. Column buckling was then observed to progress rapidly across the east and west faces.

Finding 26: The WTC 1 building section above the impact and fire area tilted to the south as the structural collapse initiated. The tilt was toward the side of the building that had the long span floors. Video records taken from east and west viewpoints showed that the upper building section tilted to the south. Video records taken from a north viewpoint showed no discernable east or west component in the tilt. A tilt to the south of at least 8 degrees occurred before dust clouds obscured the view and the building section began to fall downward.

10.6.2 WTC 2

Finding 27: On the east face and north face of WTC 2, draped objects were observed through the windows of floor 82 on the east face and floors 81 to 83 on the north face near the northeast corner. The draped objects appeared to be hanging floors. The drape of these objects was observed to increase with time and extend across approximately half of the east face.

Finding 28: Inward bowing of the east wall was first observed at 9:21 a.m. The inward bowing was approximately 10 in.±1 in. at Floor 80 and extended between Floors 78 and 83 and Columns 304 and 344. The remaining portion of the face to the south of Column 344 was not included in the image. The bowing appeared to extend over a large fraction of the east face and to be greatest near the center of the face. Fires were more extensive along the east face (where long span floors were located) and at the east side of the north and south faces (where short span floors were located). Fires were not observed on the west face (where long span floors were located). Inward bowing was observed only on the east face. The south face had extensive aircraft impact damage, and the damaged floors were not capable of imposing inward pull forces on the south face. There was no impact damage or fire on the west floors to cause pull-in forces on the west face.

Finding 29: An increase of the inward bowing of the east wall was observed at 9:53 a.m. The inward bowing appeared to extend between Floors 78 and 84 and Columns 305 and 341. The remaining portion of the face to the south of Column 344 was not included in the image. The maximum bowing was estimated from images to be 20 in.±1 in. at Floor 80 on the east face of WTC 1.

Finding 30: The time to collapse initiation was 56 minutes after aircraft impact (9:02:59 a.m. to 9:58:59 a.m.).

Finding 31: From exterior observations, tilt of the building section above the impact and fire area appeared to take place near Floor 82. Column buckling was then seen to progress across the north face.

Finding 32: The building section above the impact and fire area tilted to the east and south at the onset of structural collapse. The tilt occurred toward the east side with the long span floors. Estimates made from photographs indicate that there was approximately a 3 degree to 4 degree tilt to the south and a 7 degree to 8 degree tilt to the east prior to significant downward movement of the upper portion of the building. The tilt to the south did not increase any further as the upper building section began to fall, but the tilt to the east continued, reaching 20 degrees to 25 degrees before dust clouds obscured the view.

10.7 STRUCTURAL RESPONSE OF MAJOR TOWER SUBSYSTEMS

Prior to conducting the analysis of the global structural response of each tower, major structural subsystems were analyzed to provide insight into their behavior within the WTC global system. The three major structural subsystems, the core framing, a single exterior wall, and full tenant floors, were analyzed separately for their response to impact damage and fire. The hat truss was not analyzed separately as its structural behavior did not require significant simplification in the global analysis. The component analyses provided a foundation for these large, nonlinear analyses with highly redundant load paths, and they enabled a significant reduction in finite element model complexity and size. The major subsystem models used final estimates of impact damage and elevated temperatures determined from the aircraft impact analysis and the fire dynamics and thermal analyses.

10.7.1 Isolated Core Subsystem

Finding 33: The WTC 1 isolated core subsystem analysis found that the core structure was most weakened from impact and thermal effects at the center of the south side of the core. Smaller displacements occurred in the global model due to the constraints of the hat truss and floors.

Finding 34: The WTC 2 isolated core subsystem analysis found that the core structure was unstable for the estimated structural damage to core columns. The core was most weakened from impact and thermal effects at the southeast corner and along the east side of the core. Larger displacements occurred in the global model as the isolated core model had lateral restraints imposed that were somewhat stiffer than in the global model.

10.7.2 Full Floor Subsystem

Finding 35: Floor sagging was caused primarily by either buckling of truss web diagonals or disconnection of truss seats at the exterior wall or the core perimeter. Except for the truss seat failures near the southeast corner of the core in WTC 2 following the aircraft impact, web buckling or truss seat failure was caused primarily by elevated temperatures of the structural components.

Finding 36: Analysis results from both the detailed truss model and the full floor models found that the floors began to exert inward pull forces when floor sagging exceeded approximately 25 in. for the 60 ft floor span.

Finding 37: Sagging at the floor edge was due to loss of vertical support at the truss seats. The loss of vertical support was caused in most cases by the reduction in vertical shear capacity of the truss seats due to elevated steel temperatures.

10.7.3 Isolated Exterior Wall Subsystem

Finding 38: Inward pull forces were required to produce inward bowing that was consistent with displacements measured from photographs. The inward pull was caused by sagging of the floors. Heating of the inside face of the exterior columns also contributed to inward bowing.

Finding 39: The observed inward bowing of the exterior wall indicated that most of the floor connections were intact to cause the observed bowing.

Finding 40: The floors that were identified through analysis to be affected by the fires and the dislodged insulation matched well with the floors that were observed to have participated in the inward bowing of the exterior walls.

Finding 41: The extent of floor sagging required at each floor was greater than that predicted by the full floor models. The estimates of the extent of sagging at each floor were governed by the combined effects of insulation damage and fire; insulation damage estimates were limited to areas subject to direct debris impact. Other sources of floor and insulation damage from the aircraft impact and fires (e.g., insulation damage due to shock and subsequent vibrations as a result of aircraft impact or concrete slab cracking and spalling as a result of thermal effects) were not included in the floor models.

10.8 STRUCTURAL RESPONSE TO AIRCRAFT IMPACT DAMAGE AND FIRE

Global analysis of WTC 1 and WTC 2 used final estimates of impact damage and elevated temperatures to determine the structural response and sequence of component and subsystem failures that led to collapse initiation.

10.8.1 General Findings

Finding 42: The structural analyses of WTC 1 and WTC 2 found that the collapse of the towers was due to the combined effects of structural and insulation damage from aircraft impact and the subsequent fires on the core, floor systems, and exterior walls. The towers collapsed when the weakened core and exterior columns could no longer redistribute or support the building loads with their reduced load carrying capacity.

Finding 43: Impact damage alone did not cause collapse of the towers, as they were stable after the aircraft impact. Global analyses showed that both towers had substantial reserve capacity after the aircraft impact.

Finding 44: The multi-floor fires alone did not cause collapse of the towers. Without impact damage to the insulation, the structural steel temperatures would have been generally less than 200 °C to 300 °C, with a few isolated locations of structural steel temperatures exceeding 400 °C in WTC 1 floors and 500 °C in WTC 2 floors. The core would not have weakened, the floor sag would have been insufficient to pull inward on the exterior columns, and the exterior walls would not have bowed inward.

Finding 45: The towers would likely not have collapsed under the combined effects of aircraft impact and the subsequent multi-floor fires if the insulation had not been dislodged or had been only minimally dislodged by aircraft impact. Had insulation not been dislodged by the debris field, temperature rise of structural components would likely have been insufficient to induce global collapse. Structural components that became thermally weakened were generally determined by impact of the debris field. The existing condition of the insulation prior to aircraft impact and the insulation thickness on the WTC floor system did not play a role in initiating collapse of the towers.

Finding 46: Creep strain was significant in the core and exterior columns over the 56 min to 102 min period of fire exposure in columns with temperatures greater than 500 °C to 600 °C and high stress. Columns with creep strains of sufficient magnitude to cause column shortening played a significant role in the collapse initiation.

Finding 47: The faces of the buildings that exhibited inward bowing were associated with the long span direction of the floor system. The primary direction of tilting at collapse initiation for WTC 1 and WTC 2 was in the direction of the bowed faces.

10.8.2 Performance with Intact Fire Protection

Finding 48: A detailed thermal-structural analysis, which did not include slab delamination/spalling effects, showed that a full collapse of the WTC floor system would not occur even with a number of failed trusses or connections.

Finding 49: Most of the horizontal and vertical capacity of the floor connections to the exterior and core columns significantly exceeded the demand under design load conditions.

10.9 PROBABLE COLLAPSE SEQUENCES

The results of structural analyses conducted in this study on components, subsystems, isolated exterior walls and cores, and global models of WTC 1 and WTC 2 showed that the collapses of the towers were initiated due to the combined effects of the structural and insulation damage from aircraft impact and the subsequent intense fires. The probable collapse sequences for WTC 1 and WTC 2 are based upon the collective consideration of structural analyses, statistical based methods, observations, and laboratory testing.

10.9.1 Role of the Building Core

Finding 50: The core columns were weakened significantly by the aircraft impact damage and thermal effects. Thermal effects dominated the weakening of WTC 1. As the fires moved from the north to the south side of the core, following the debris damage path, the core was weakened over time by significant creep strains on the south side of the core. Aircraft impact damage dominated the weakening of WTC 2. Immediately after impact, the vertical displacement at the southeast corner of the core increased 6 in. (from 4 in. to 10 in.). With the impact damage, the core subsystem leaned to the southeast and was supported by the south and east floors and exterior walls.

Finding 51: As the core was weakened from aircraft impact and thermal effects, it redistributed loads to the exterior walls primarily through the hat truss. Additional axial loads redistributed to the exterior columns from the core were not significant (only about 20 percent to 25 percent on average) as the exterior columns were loaded to approximately 20 percent of their capacity before the aircraft impact.

10.9.2 Role of the Building Floors

Finding 52: The primary role of the floors in the collapse of the towers was to provide inward pull forces that induced inward bowing of exterior columns (south face of WTC 1; east face of WTC 2).

Finding 53: Sagging floors continued to support floor loads as they pulled inward on the exterior columns. There would have been no inward pull forces if the floors truss seats had failed and disconnected.

10.9.3 Role of Exterior Frame-Tube

Finding 54: Column instability over an extended region of the exterior face ultimately triggered the global system failure as the loads could not be redistributed through the hat truss to the already weakened building core. In the area of exterior column buckling, load transferred through the spandrels to adjacent columns and adjacent exterior walls. As the exterior wall buckled (south face for WTC 1 and east face for WTC 2), the column instability propagated to adjacent faces and caused the initiation of the building collapse.

Finding 55: The exterior wall instability was induced by a combination of thermal weakening of the columns, inward pull forces from sagging floors, and to a lesser degree, additional axial loads redistributed from the core.

10.9.4 Probable Collapse Sequences

Finding 56: Although the north face of WTC 1 had extensive impact damage, thermal weakening of the core columns on the south side of the core and inward bowing of the south face caused the building to tilt to the south at collapse initiation. The extent of fires observed on all faces of WTC 1 was similar, although somewhat more extensive on the east and west faces (where short span floors were located) and somewhat less extensive on the north and south faces (where long span floors were located). Thermal weakening of exterior columns with floor sagging (which induced inward pull and occurred on the south side) caused inward bowing of the south face and tilting in the south direction.

Finding 57: Although the south face of WTC 2 had extensive impact damage, thermal weakening of the core columns on the east side of the core and inward bowing of the east face caused the building to tilt more to the east and less to the south at collapse initiation. Fires were more extensive along the east face and at the east side of the north and south faces. Thermal weakening of exterior columns with floor sagging (which induced inward pull and occurred on the east side) caused inward bowing of the east face and primary tilting in that direction (with additional southward tilting due to the aircraft impact damage).

Finding 58: The time it took for each WTC tower to collapse was due primarily to the differences in structural damage, the time it took the fires to travel from the impact area across the floors and core to critical locations, and the time it took to weaken the core and exterior columns. WTC 2 had asymmetric structural damage to the core, including the severing of a corner core column, and WTC 1 had more symmetrical damage. The fires in WTC 2 reached the east side of the building more quickly, within 10 min to 20 min, than the 50 min to 60 min it took the fires in WTC 1 to reach the south side.

Finding 59: NIST found no corroborating evidence for alternative hypotheses suggesting that the WTC towers were brought down by controlled demolition using explosives planted prior to September 11, 2001. NIST also did not find any evidence that missiles were fired at or hit the towers. Instead, photographs and videos from several angles clearly showed that the collapse initiated at the fire and

impact floors and that the collapse progressed from the initiating floors downward, until the dust clouds obscured the view.

This page intentionally left blank.

Appendix A

SUMMARY OF AIRCRAFT IMPACT DAMAGE FOR INITIAL CASES 1 TO 4

WTC 1 CASE A_i – THERMAL INSULATION AND PARTITION DAMAGE FOR OCCUPANCY FLOOR

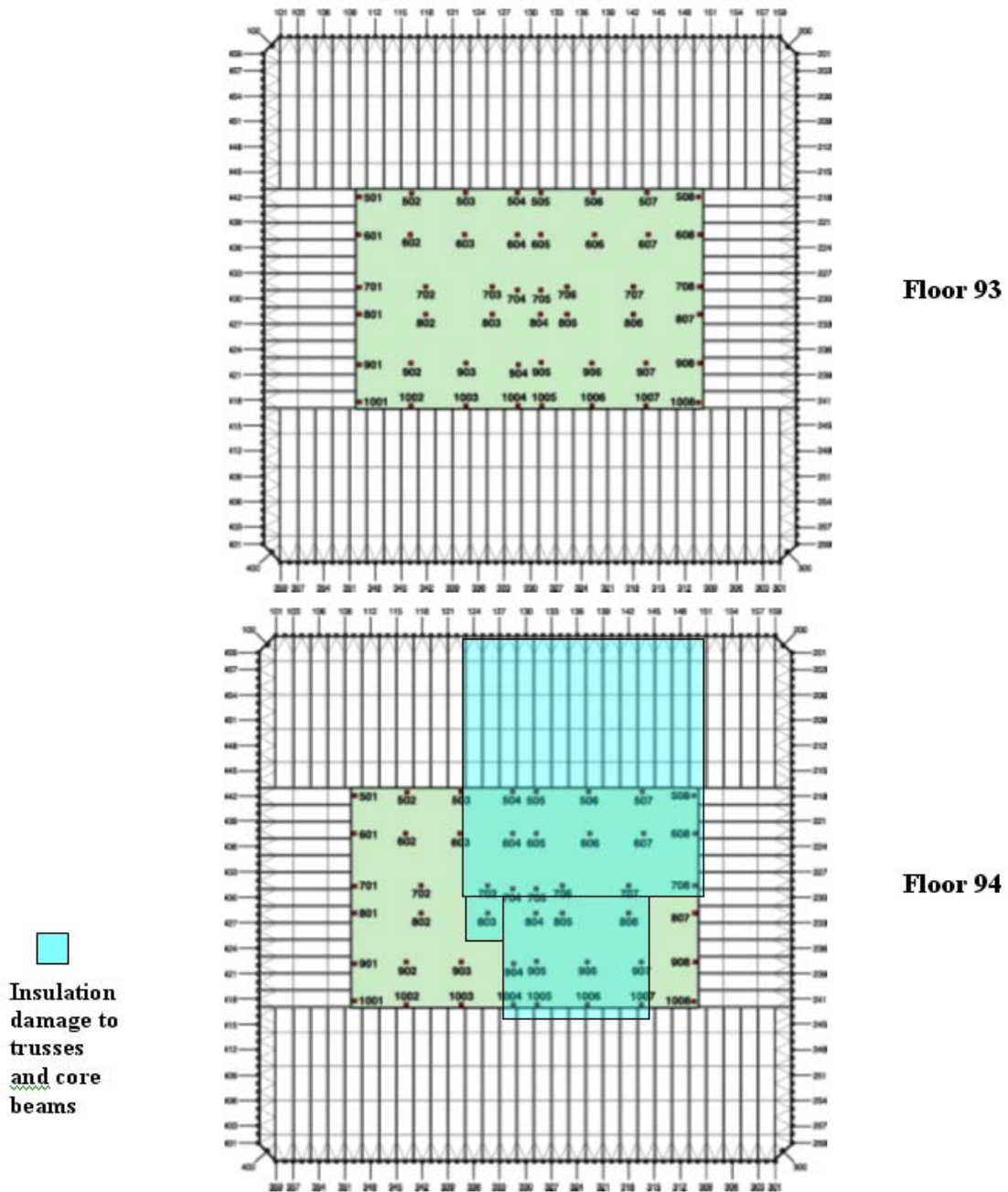


Figure A–1. WTC 1 Case A_i aircraft impact damage to Structural Floor 93 and 94.

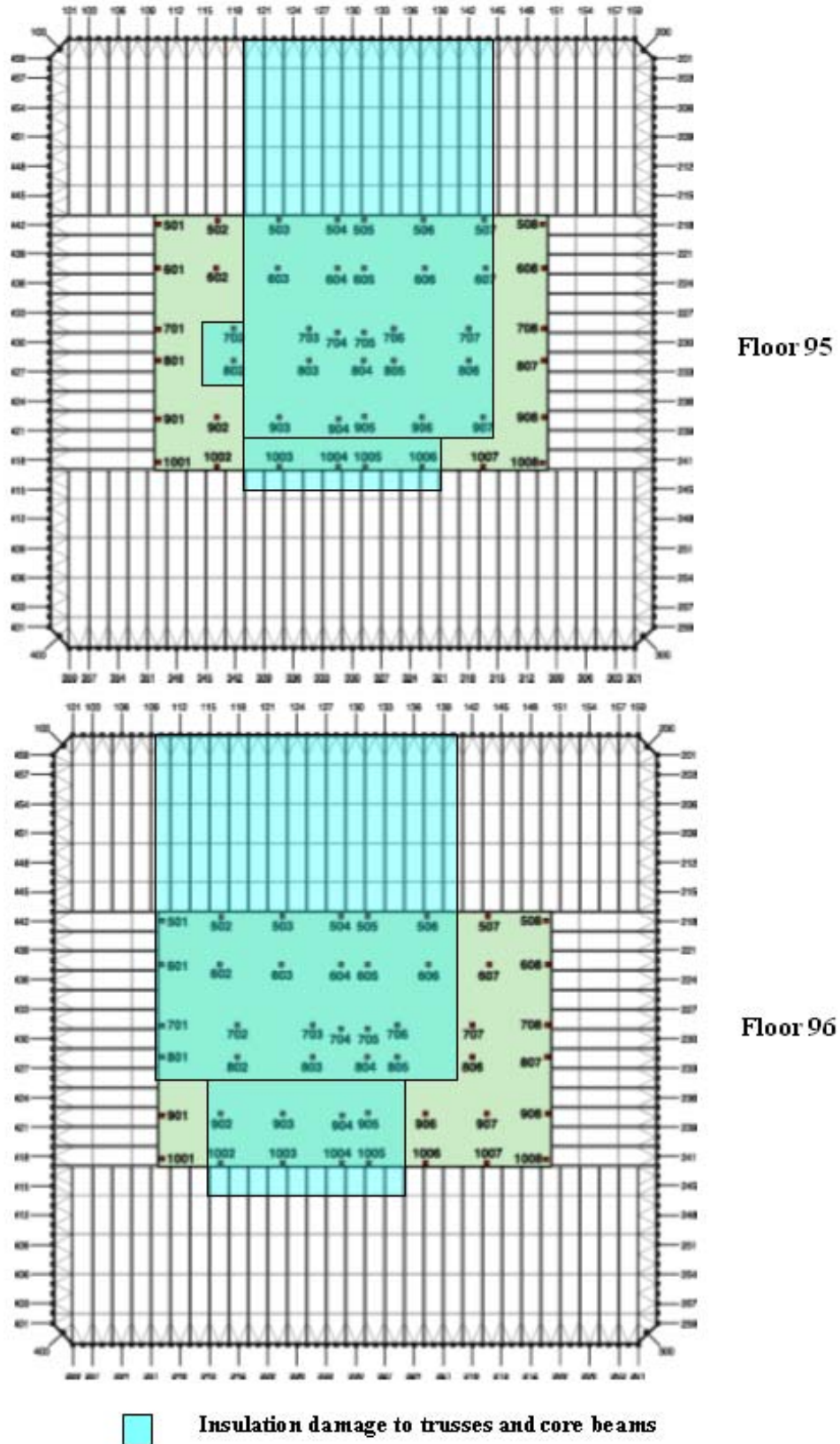


Figure A-2. WTC 1 Case A; aircraft impact damage to Structural Floors 95 and 96.

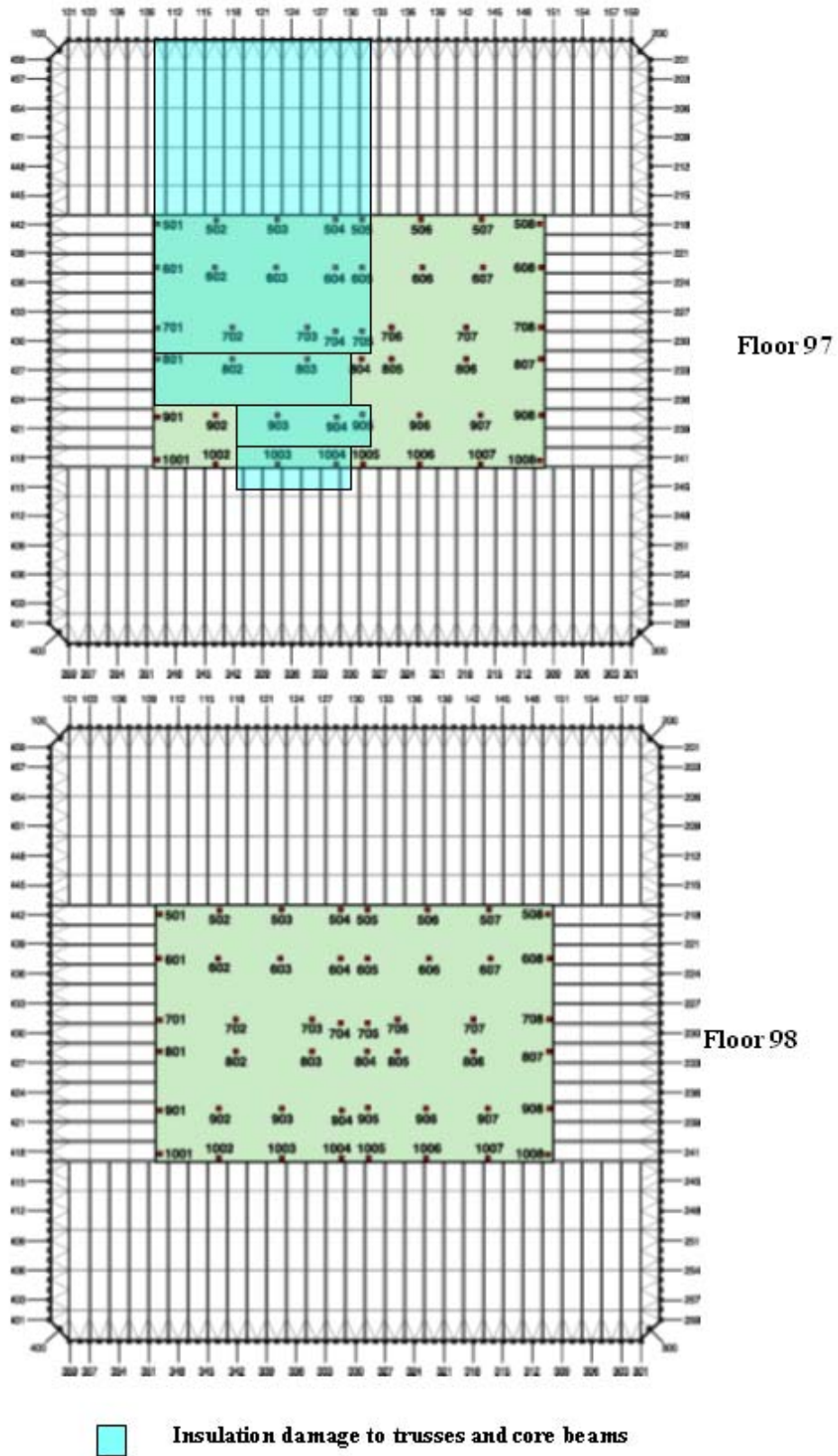


Figure A-3. WTC 1 Case A, aircraft impact damage to Structural Floors 97 and 98.

WTC 1 CASE A₁ – DAMAGE FOR STRUCTURAL FLOOR

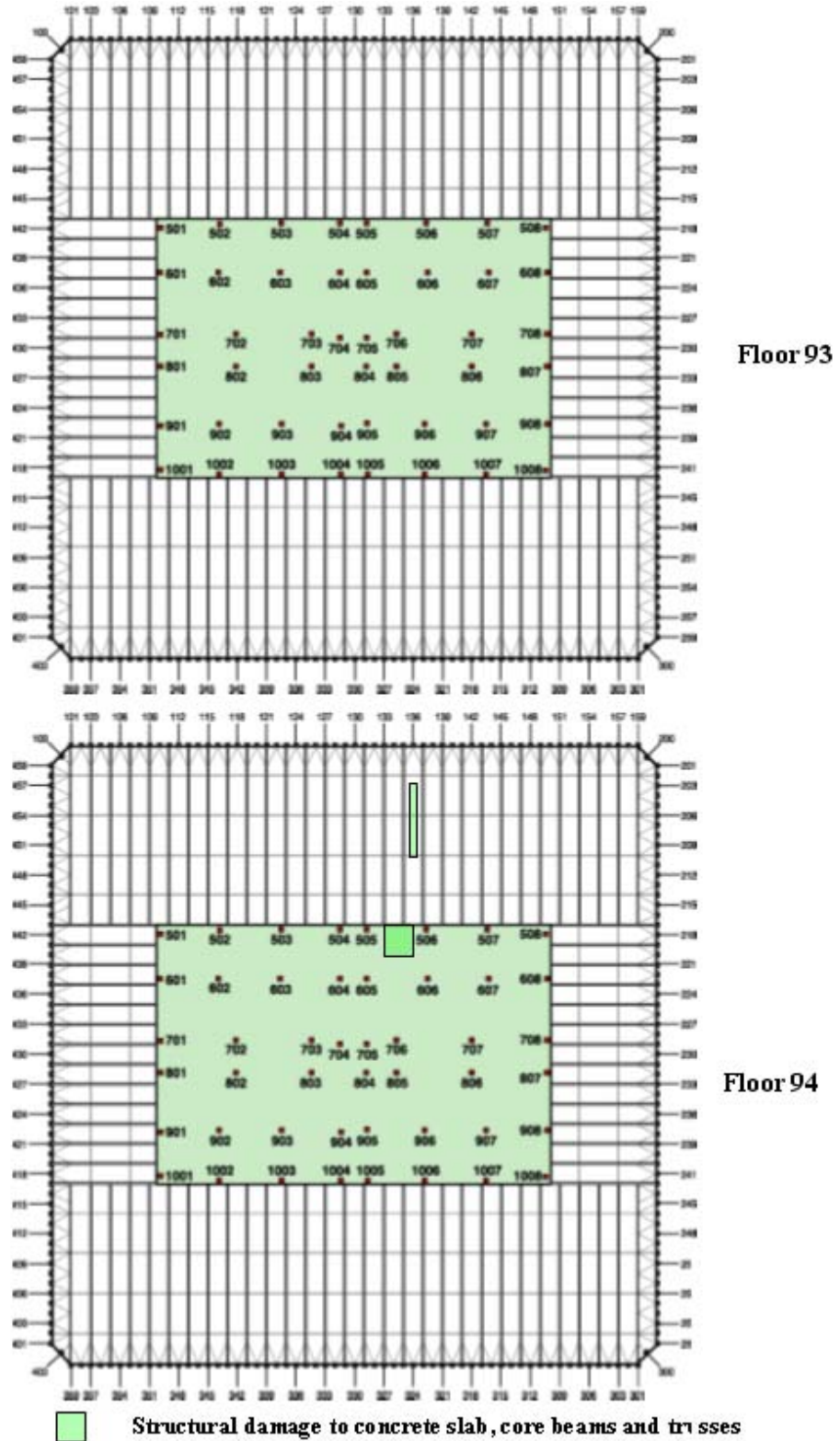


Figure A-4. WTC 1 Case A₁ aircraft impact damage to Structural Floor 93 and 94.

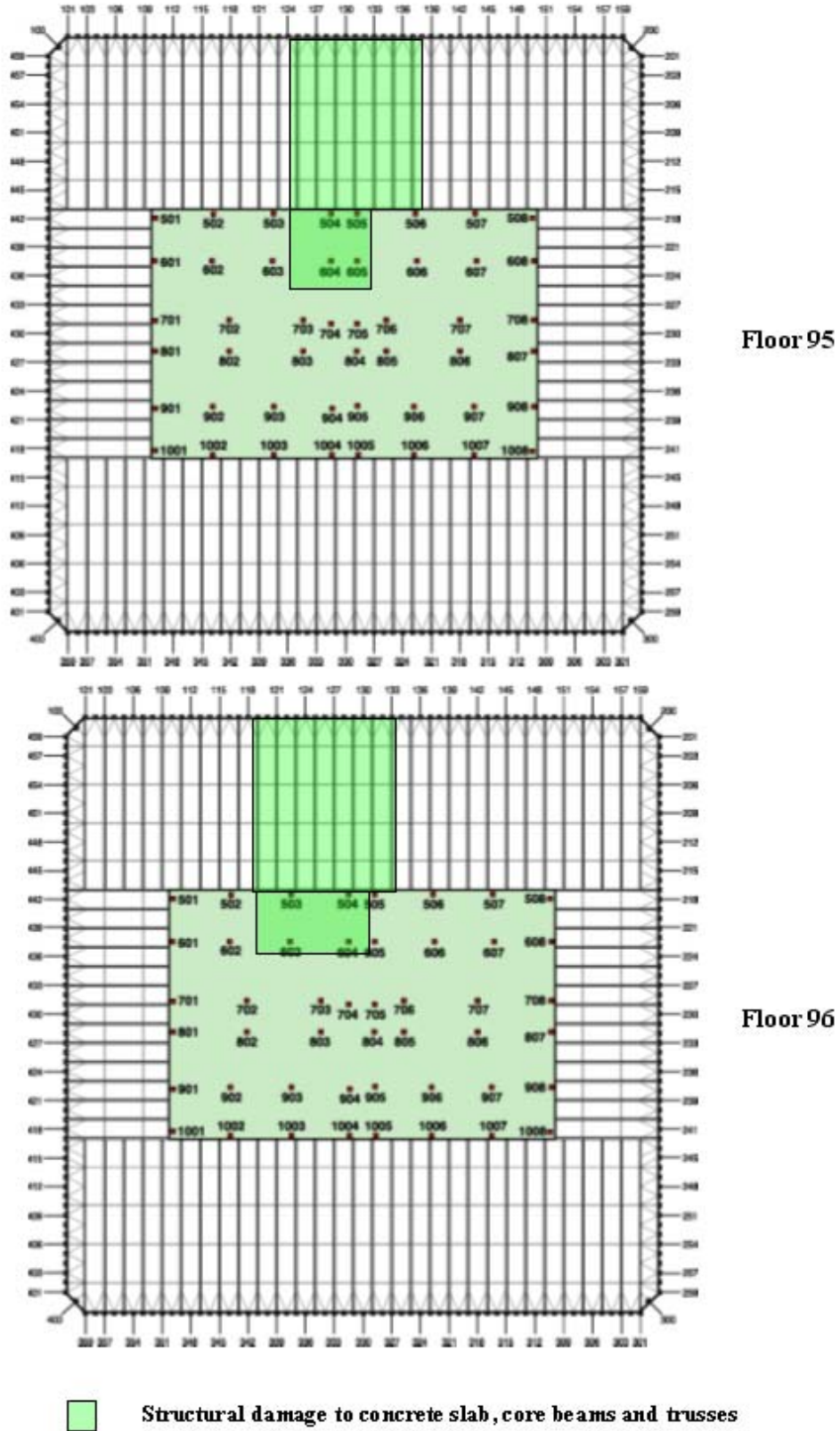


Figure A-5. WTC 1 Case A; aircraft impact damage to Structural Floors 95 and 96.

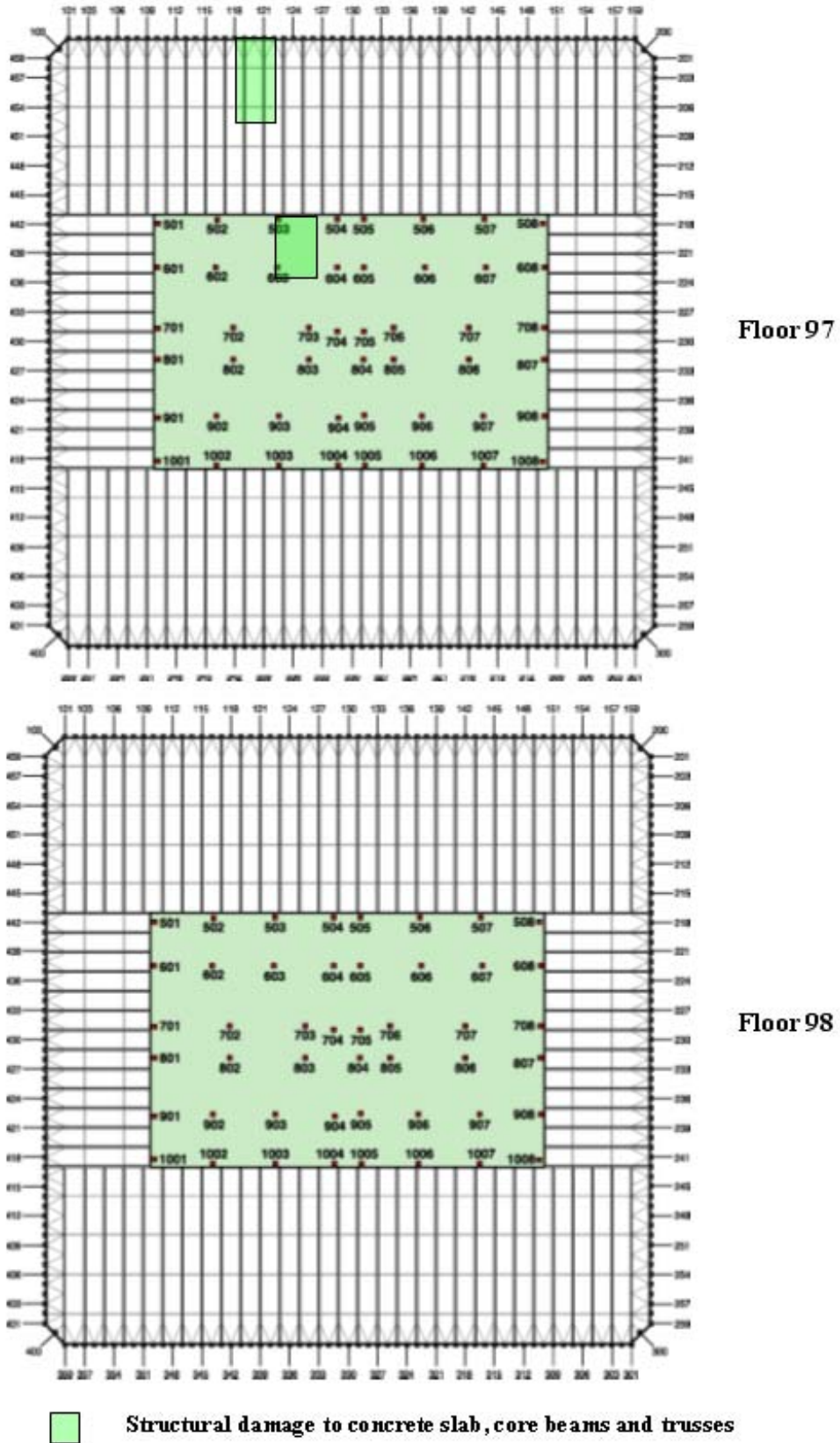


Figure A-6. WTC 1 Case A; aircraft impact damage to Structural Floors 97 and 98.

WTC 1 CASE B₁ – THERMAL INSULATION AND PARTITION DAMAGE FOR OCCUPANCY FLOOR

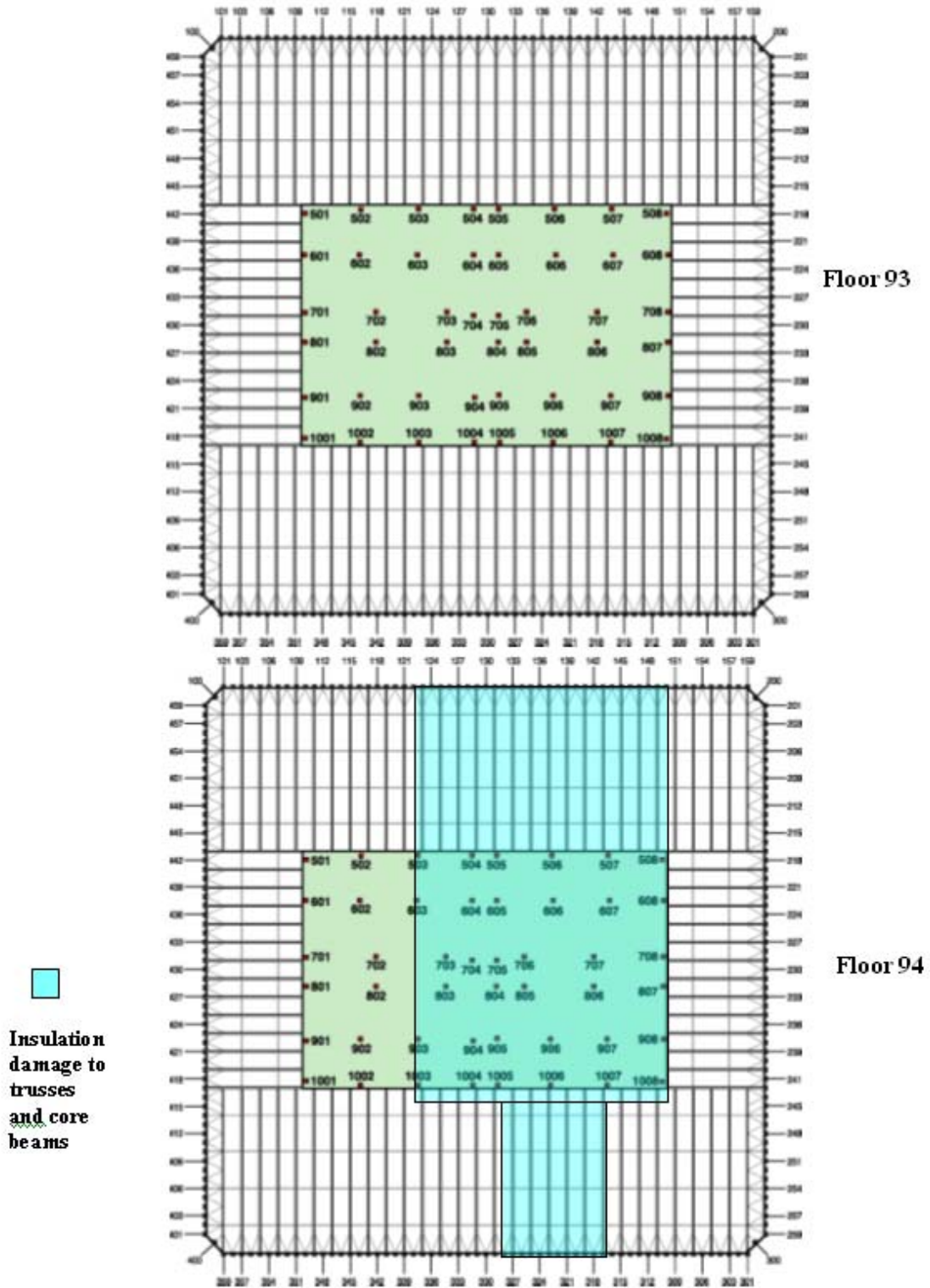


Figure A-7. WTC 1 Case B₁ aircraft impact damage to Structural Floor 93 and 94.

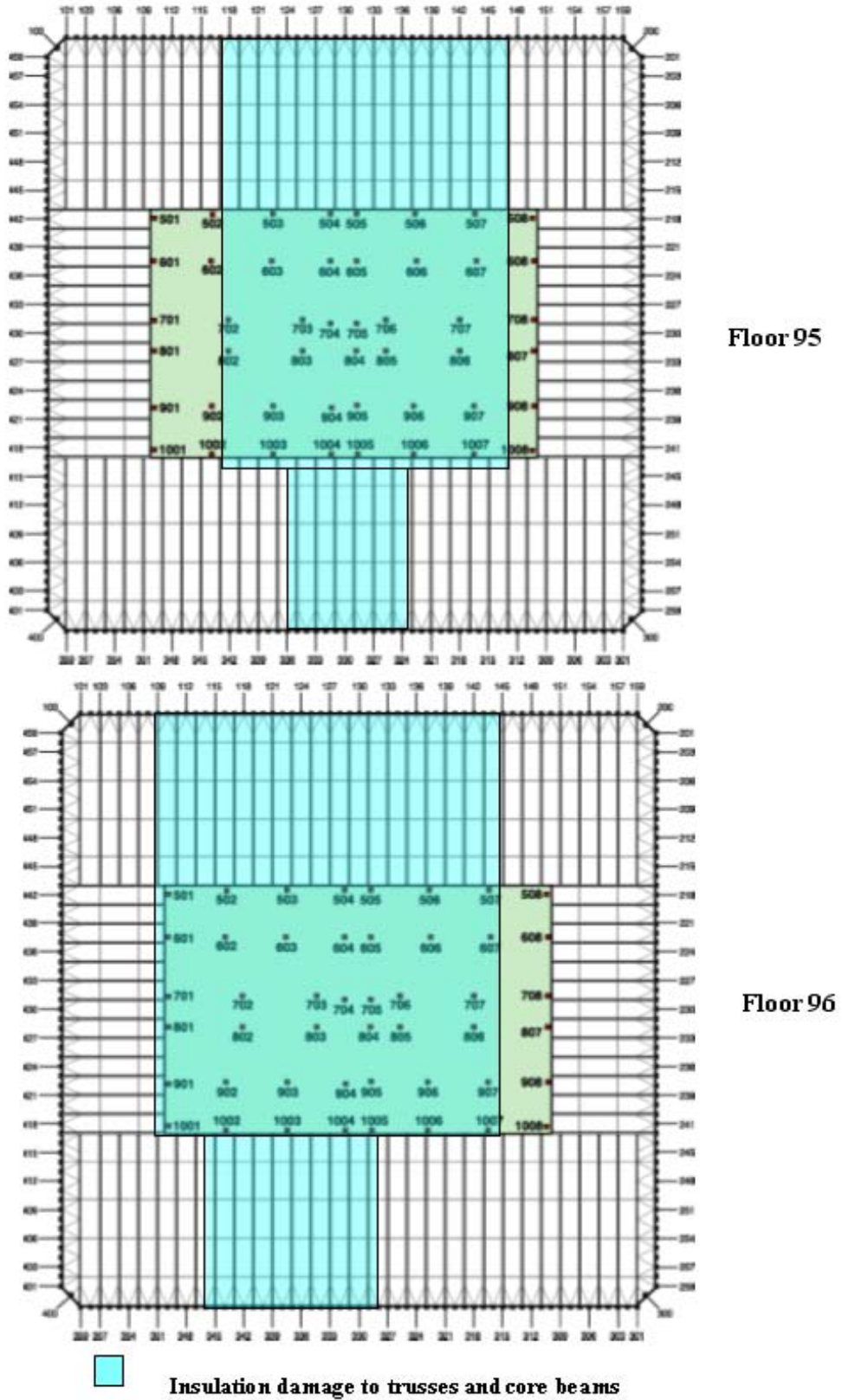


Figure A-8. WTC 1 Case B, aircraft impact damage to Structural Floors 95 and 96.

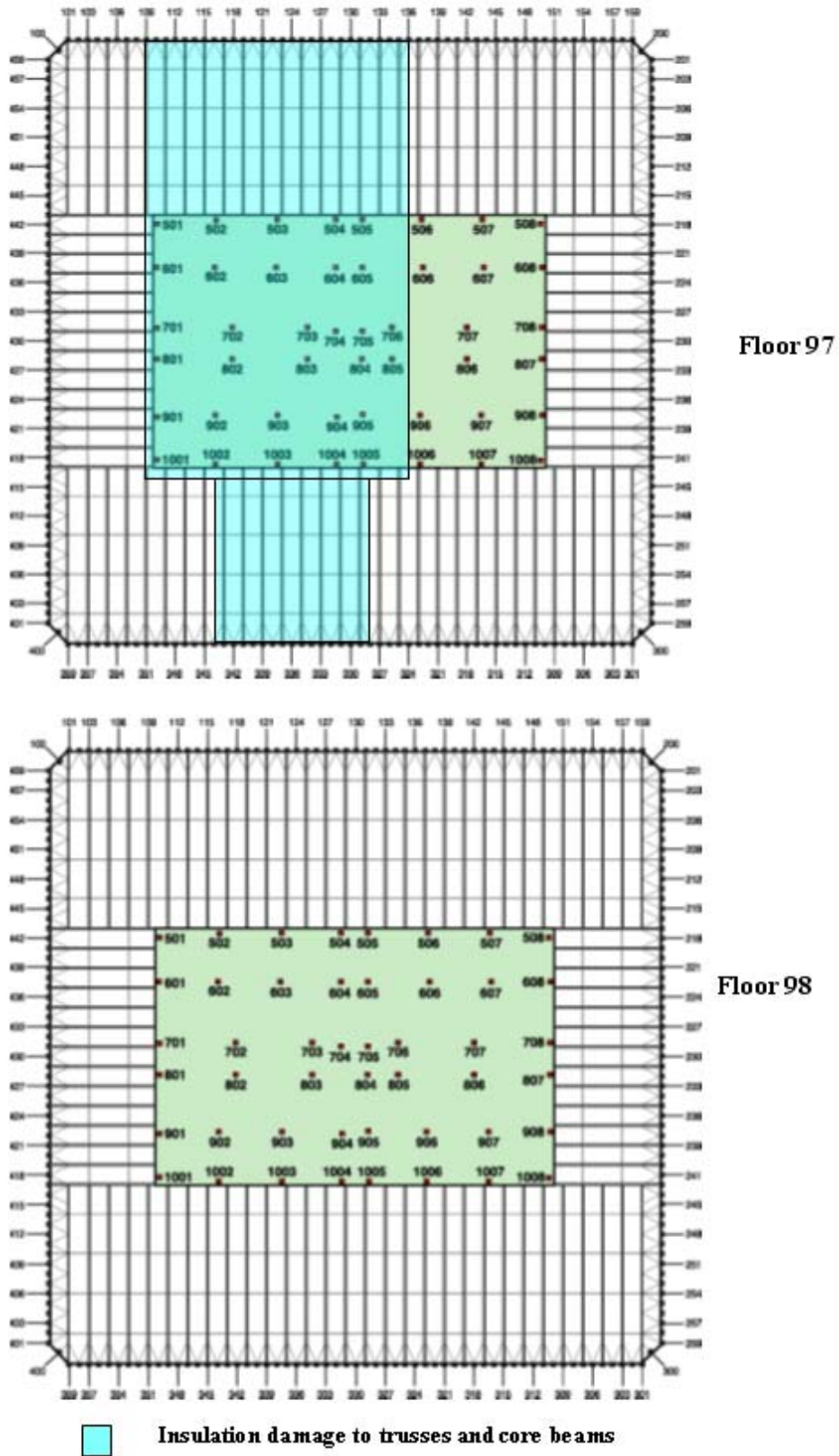


Figure A-9. WTC 1 Case B, aircraft impact damage to Structural Floors 97 and 98.

WTC 1 CASE B₁ – DAMAGE FOR STRUCTURAL FLOOR

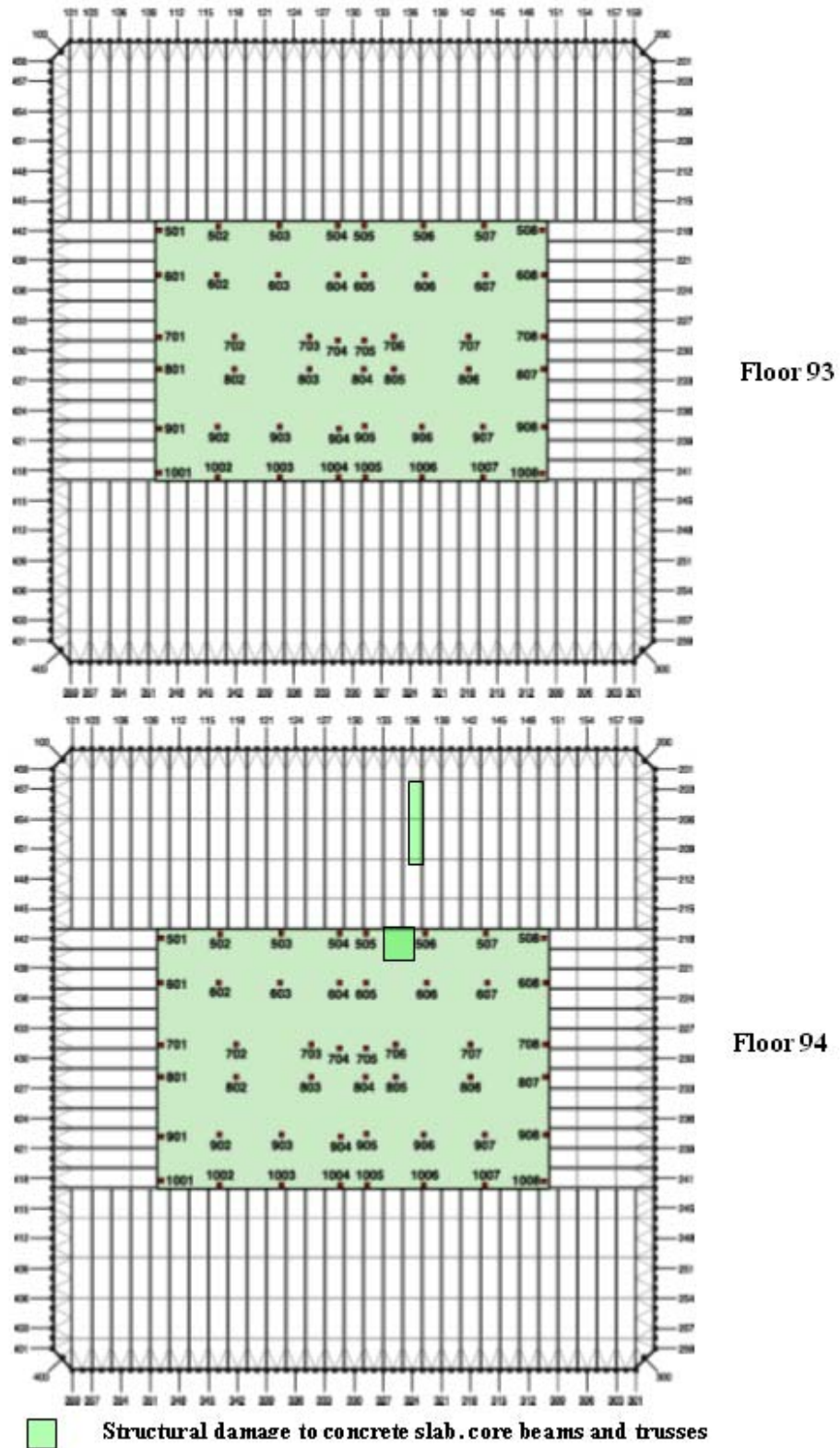
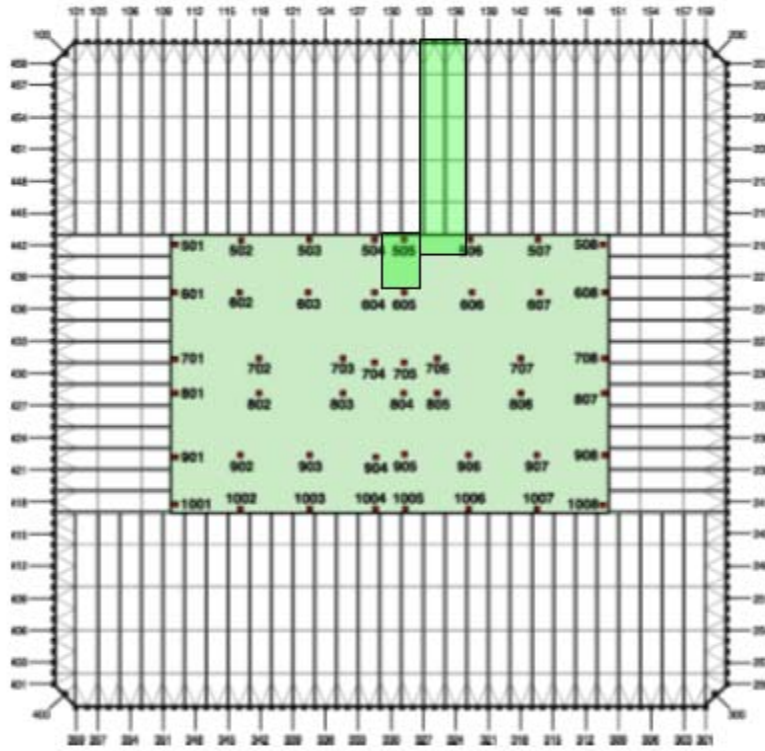
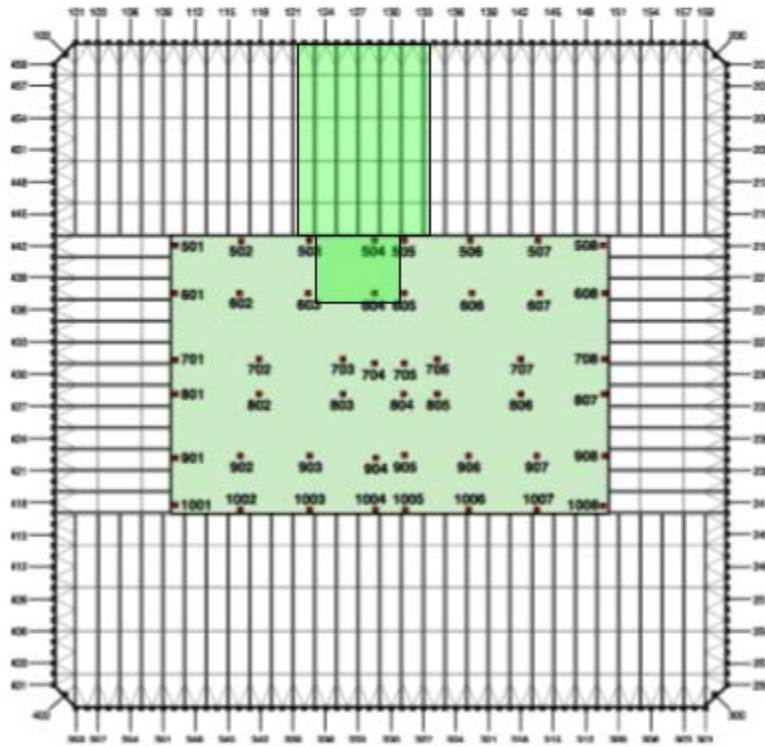


Figure A-10. WTC 1 Case B₁ aircraft impact damage to Structural Floor 93 and 94.



Floor 95



Floor 96

 Structural damage to concrete slab, core beams and trusses

Figure A-11. WTC 1 Case B_i; aircraft impact damage to Structural Floors 95 and 96.

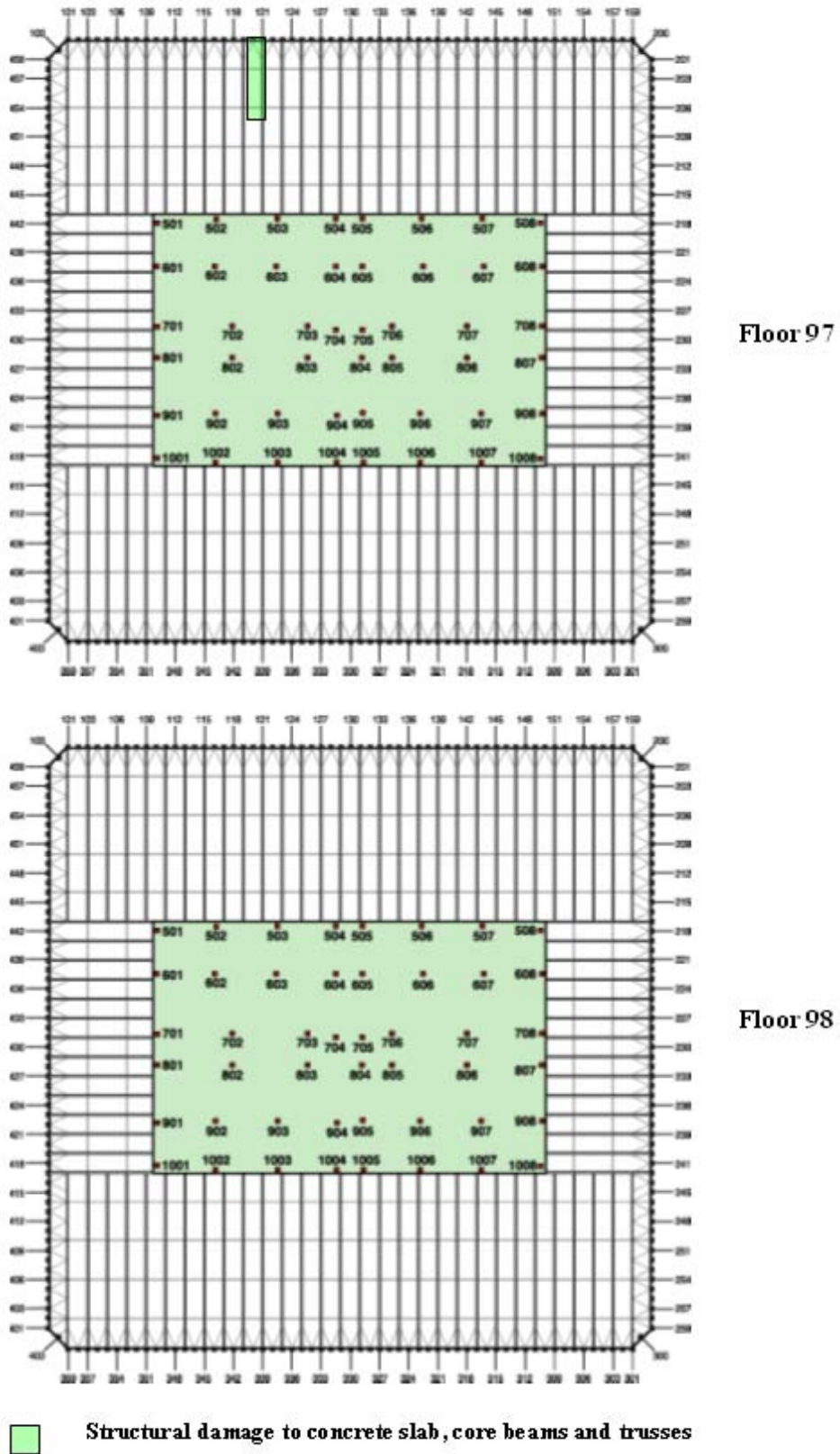


Figure A-12. WTC 1 Case B_i aircraft impact damage to Structural Floors 97 and 98.

WTC 2 CASE C₁ – THERMAL INSULATION AND OCCUPANCY DAMAGE FOR OCCUPANCY FLOOR

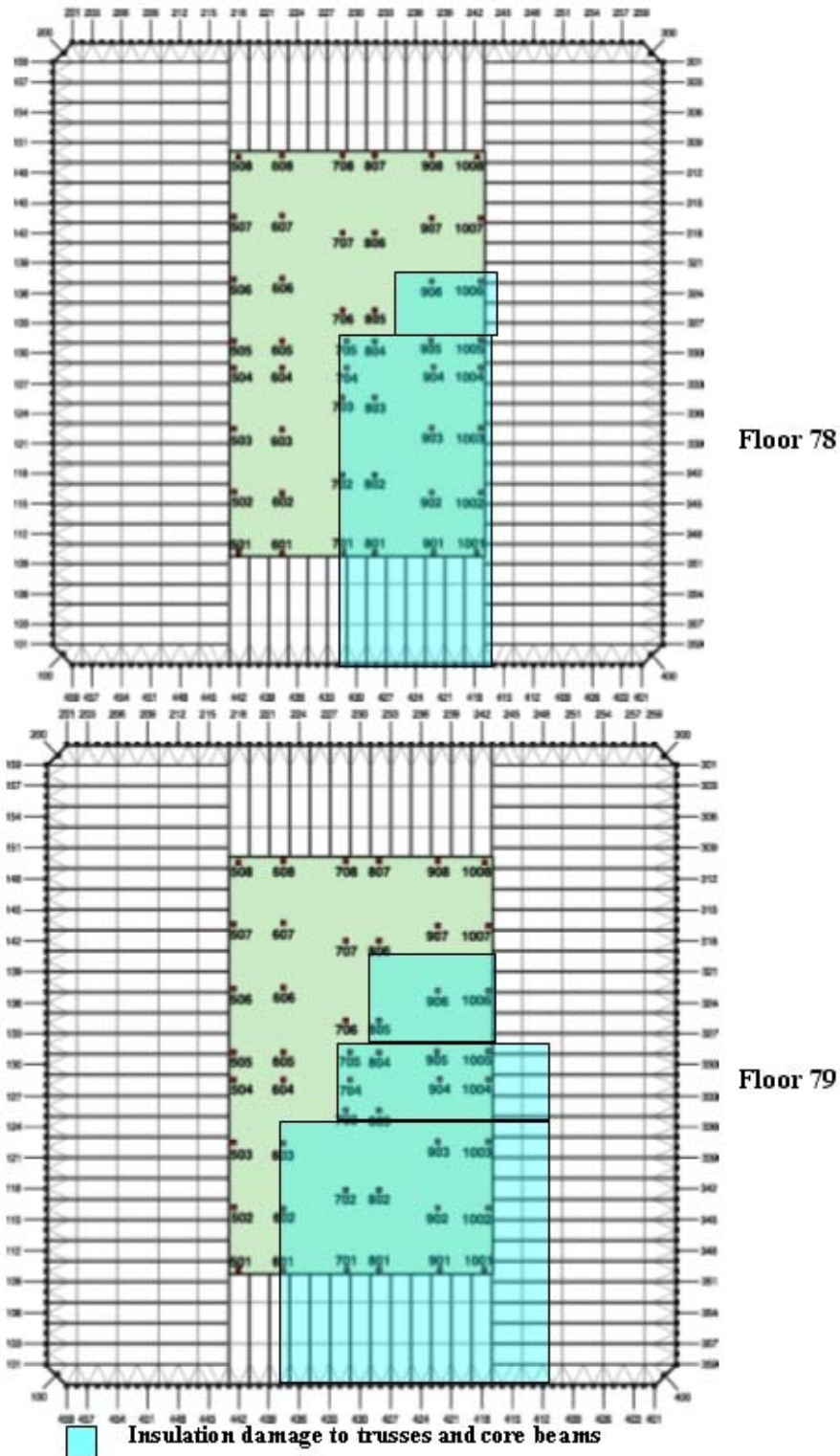


Figure A-13. WTC 2 Case C₁ aircraft impact damage to Structural Floors 78 and 79.

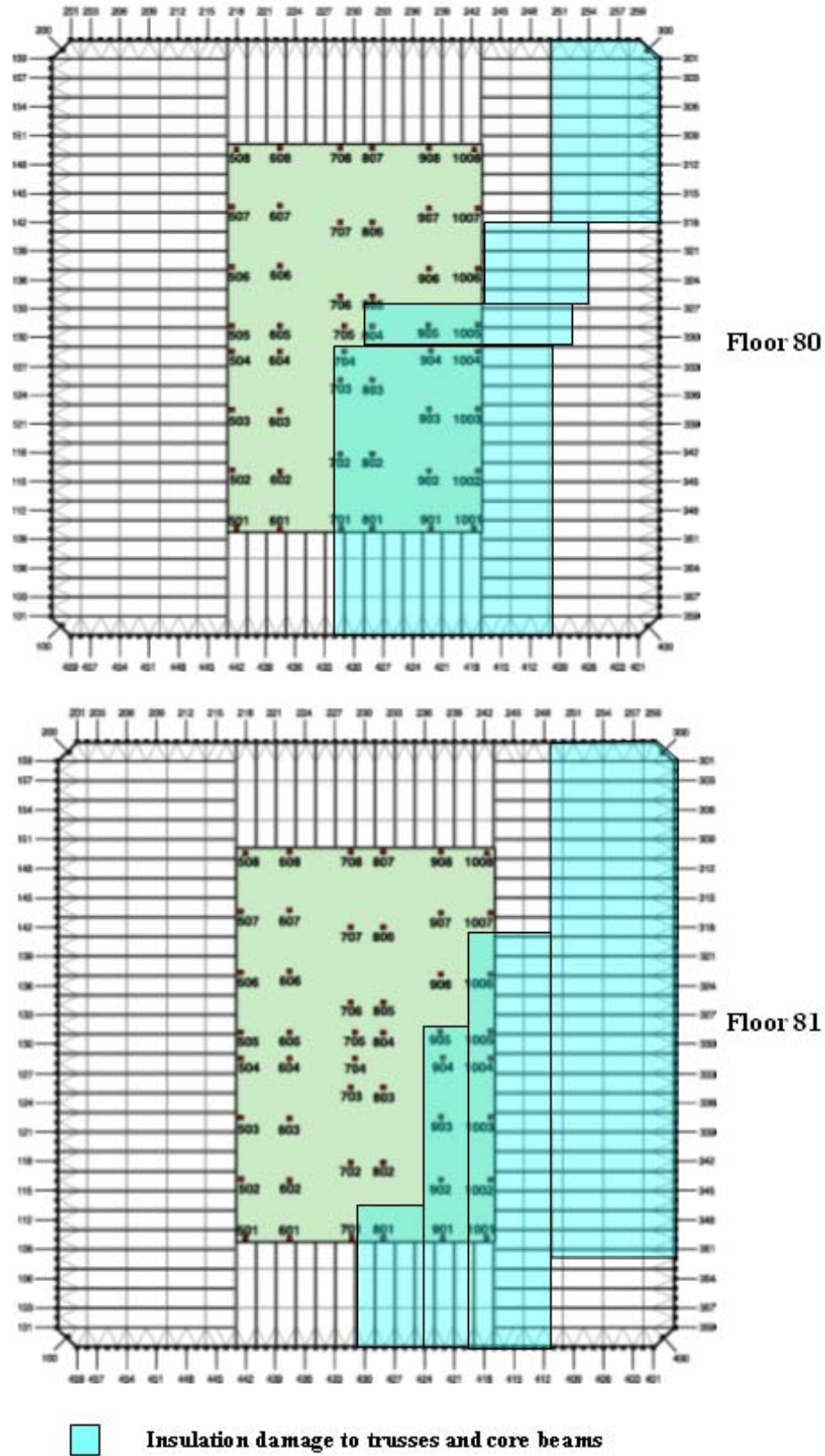


Figure A-14. WTC 2 Case C₁ aircraft impact damage to Structural Floors 80 and 81.

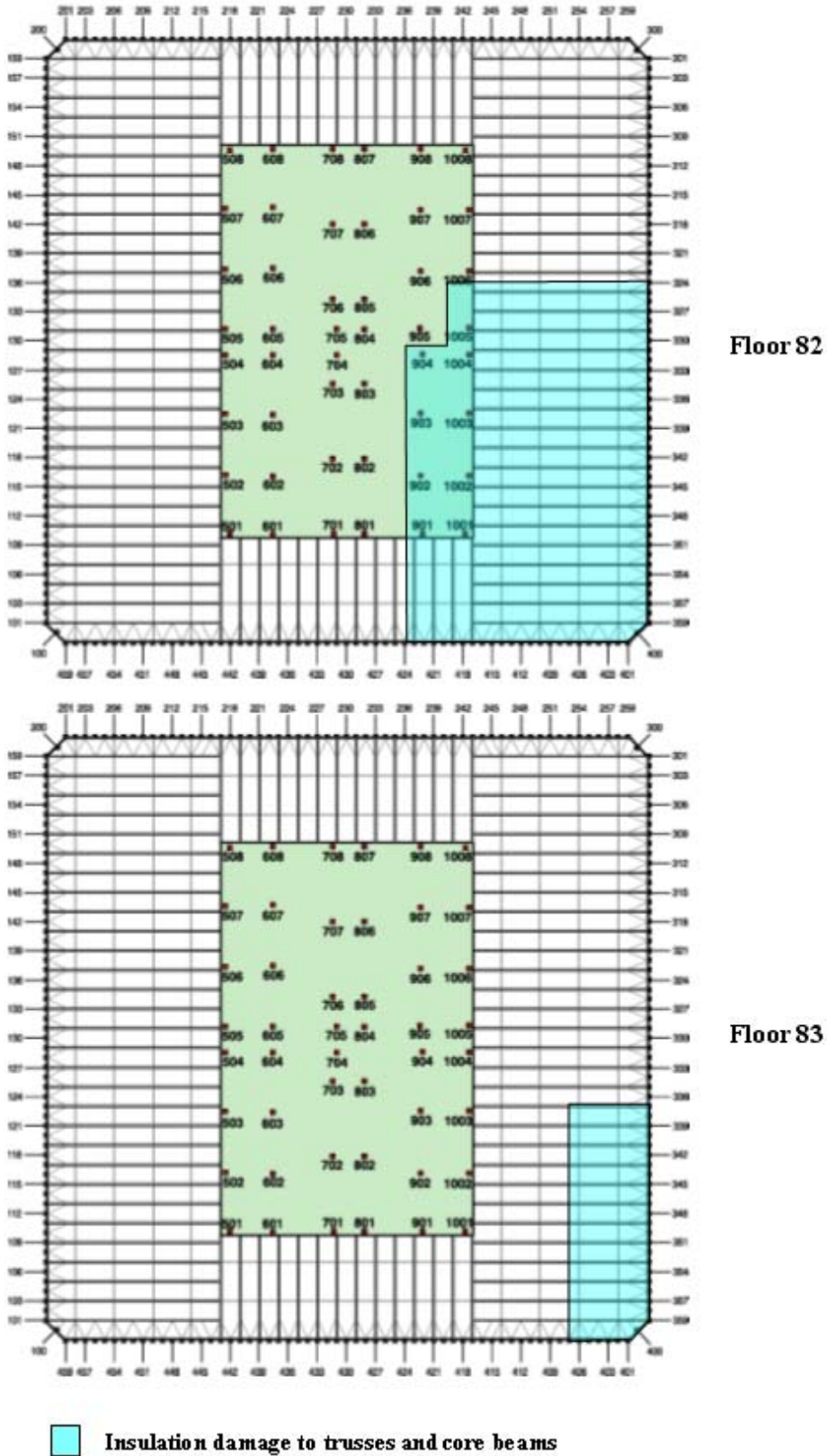


Figure A-15. WTC 2 Case C_i aircraft impact damage to Structural Floors 82 and 83.

WTC 2 CASE C₁ – DAMAGE FOR STRUCTURAL FLOOR

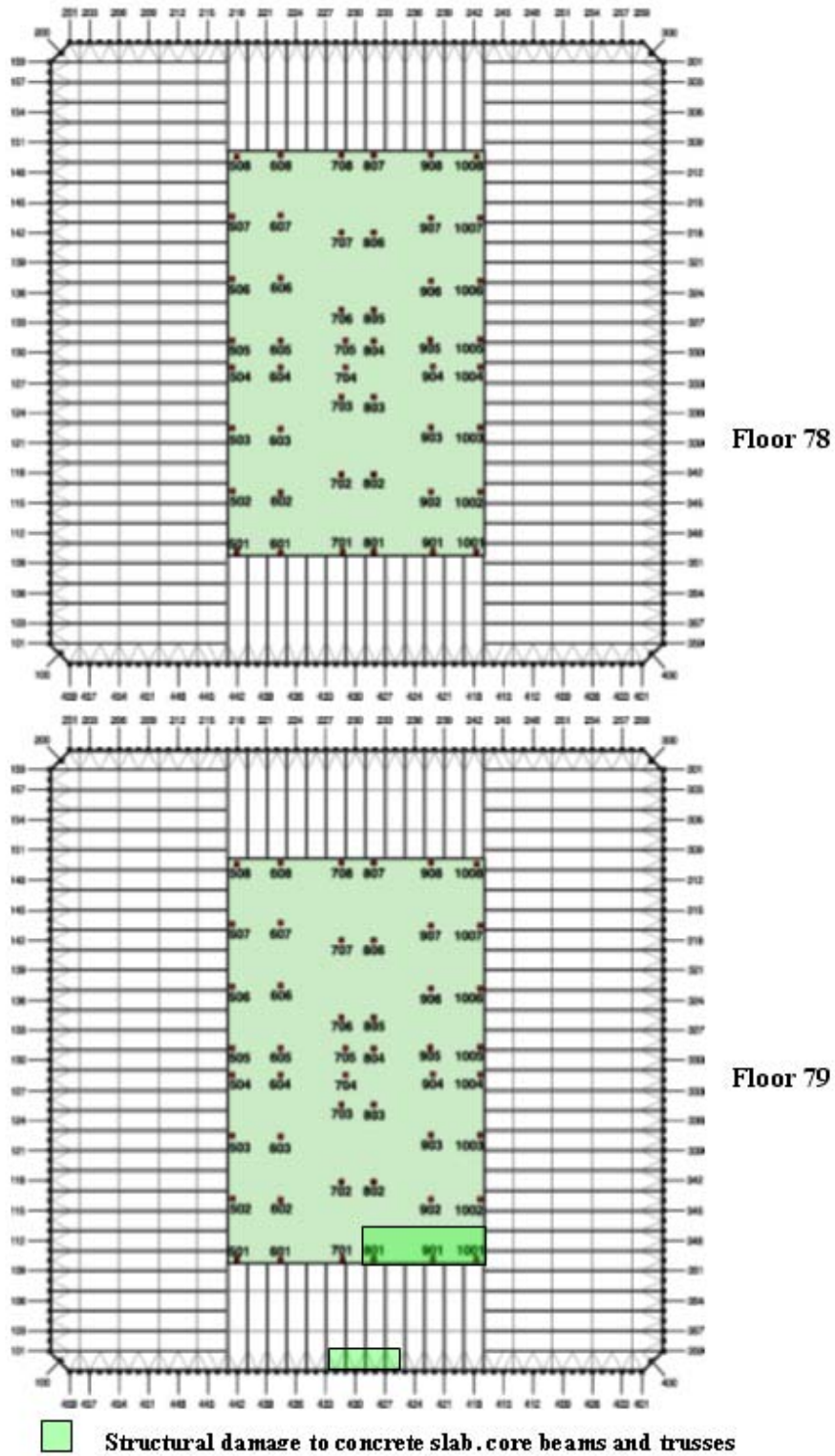
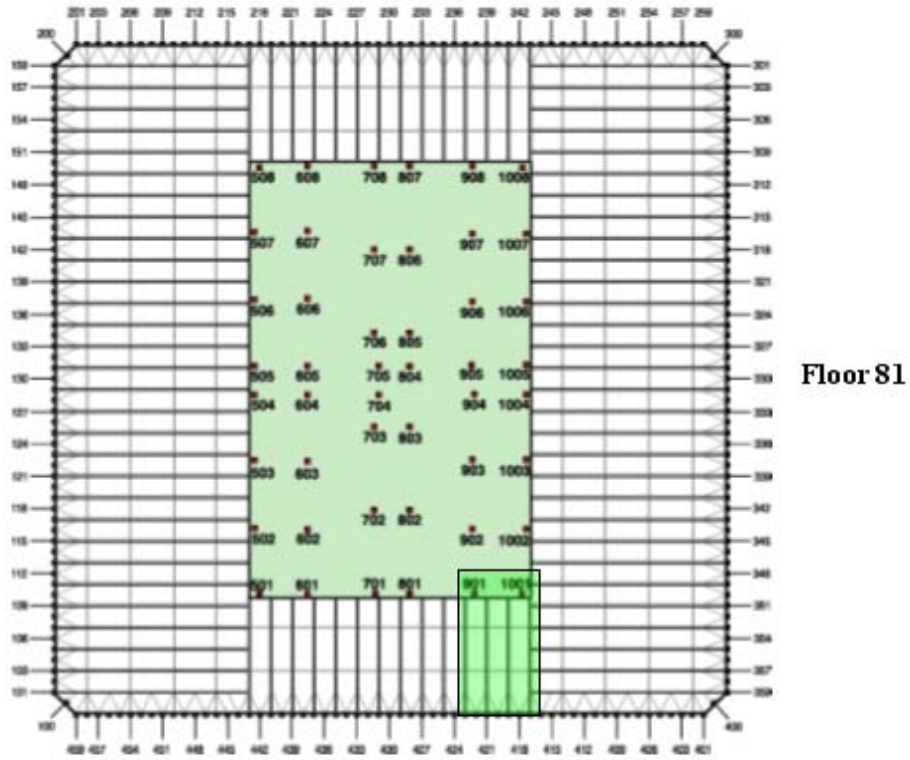
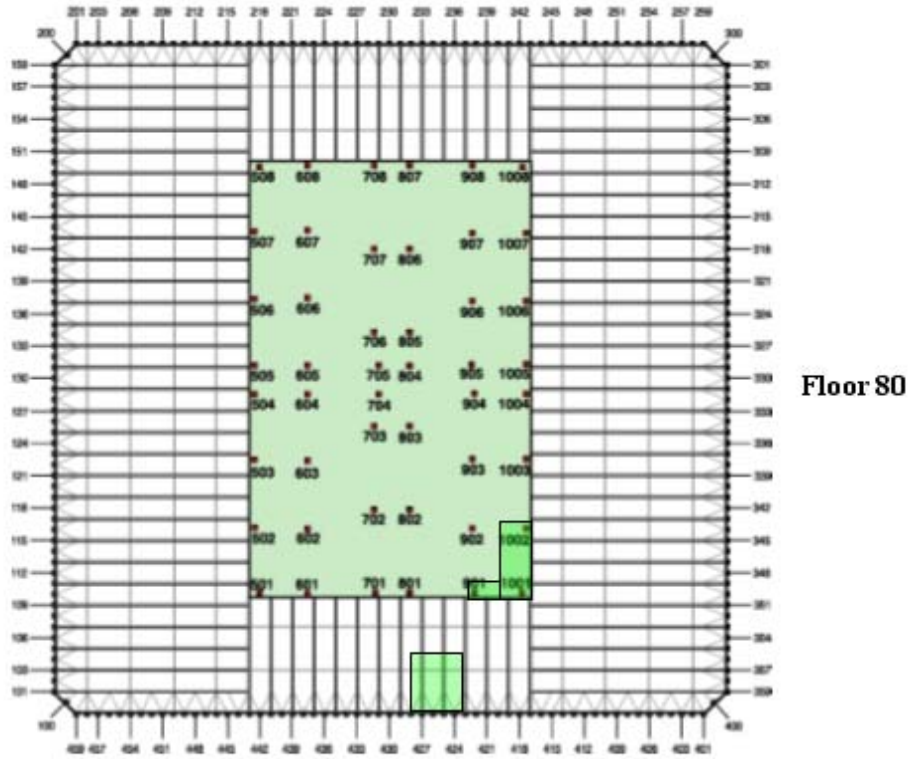
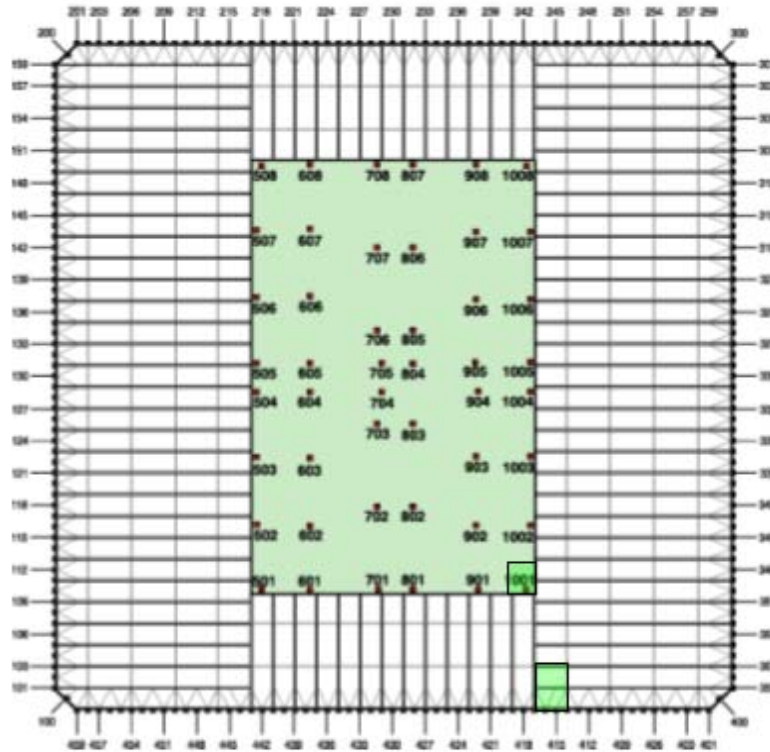


Figure A-16. WTC 2 Case C₁ aircraft impact damage to Structural Floors 78 and 79.

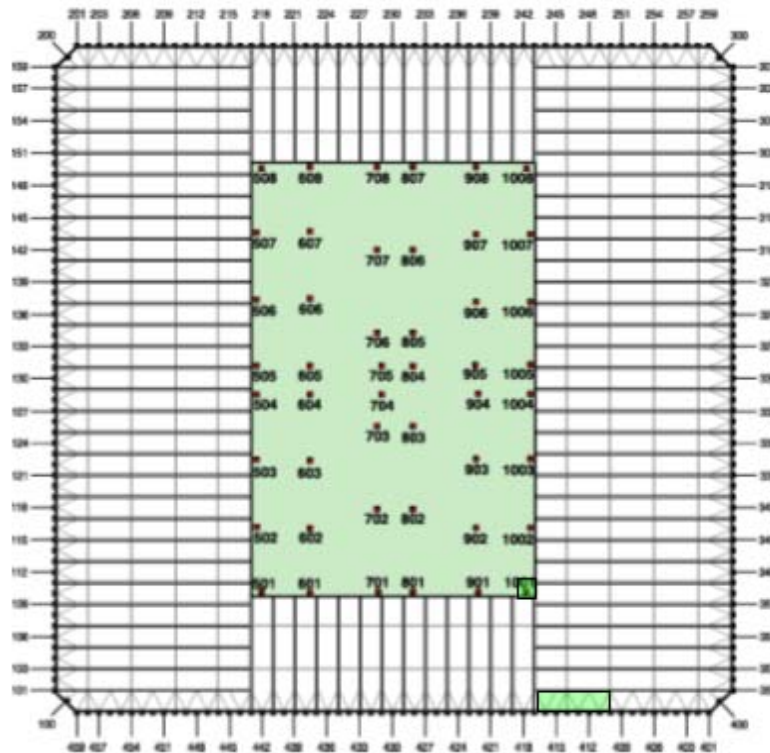


Structural damage to concrete slab, core beams and trusses

Figure A-17. WTC 2 Case C_i aircraft impact damage to Structural Floors 80 and 81.



Floor 82



Floor 83

 Structural damage to concrete slab, core beams and trusses

Figure A-18. WTC 2 Case C; aircraft impact damage to Structural Floors 82 and 83.

WTC 2 CASE D₁ – THERMAL INSULATION AND PARTITION DAMAGE FOR OCCUPANCY FLOOR

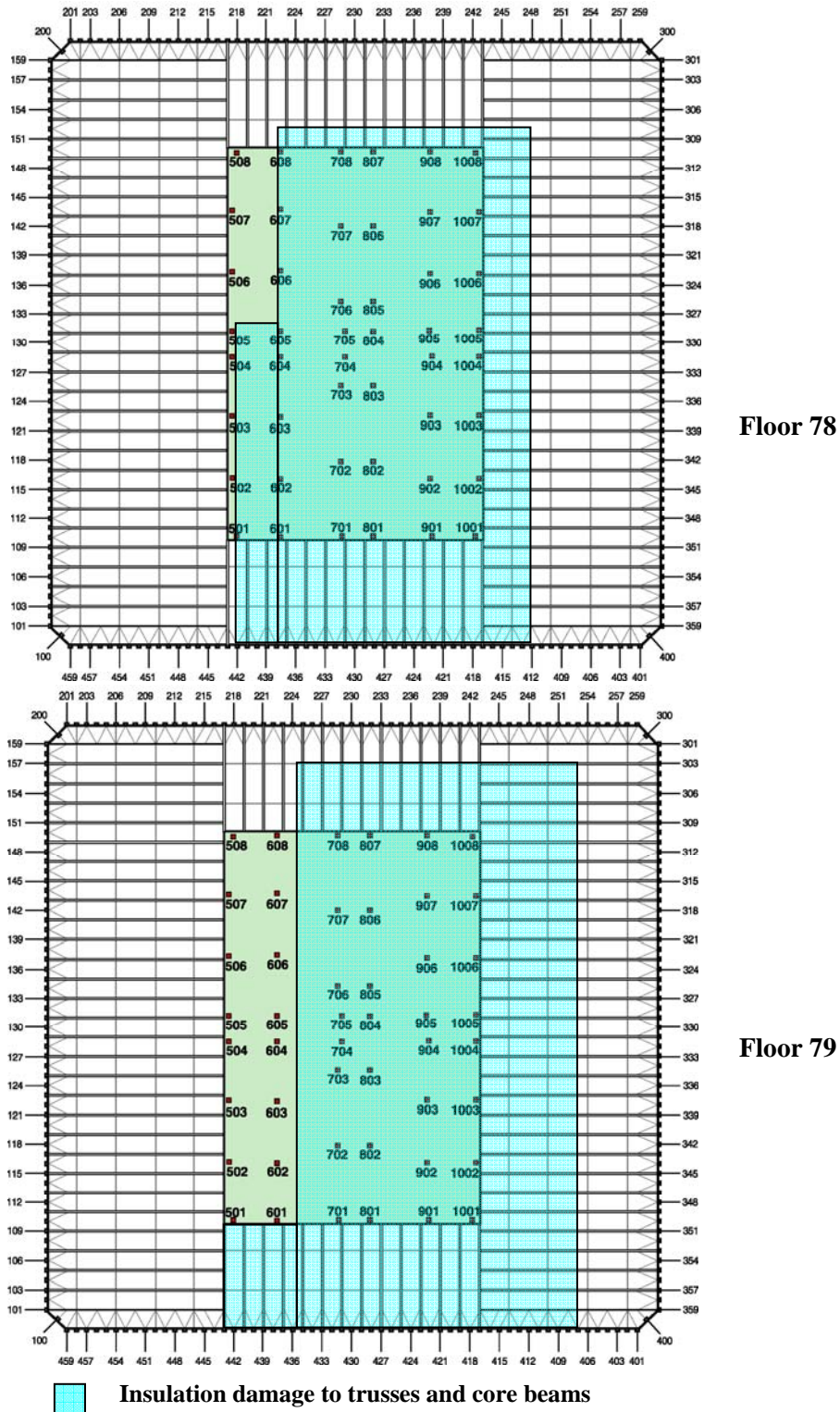


Figure A–19. WTC 2 Case D₁ aircraft impact damage to Structural Floors 78 and 79.

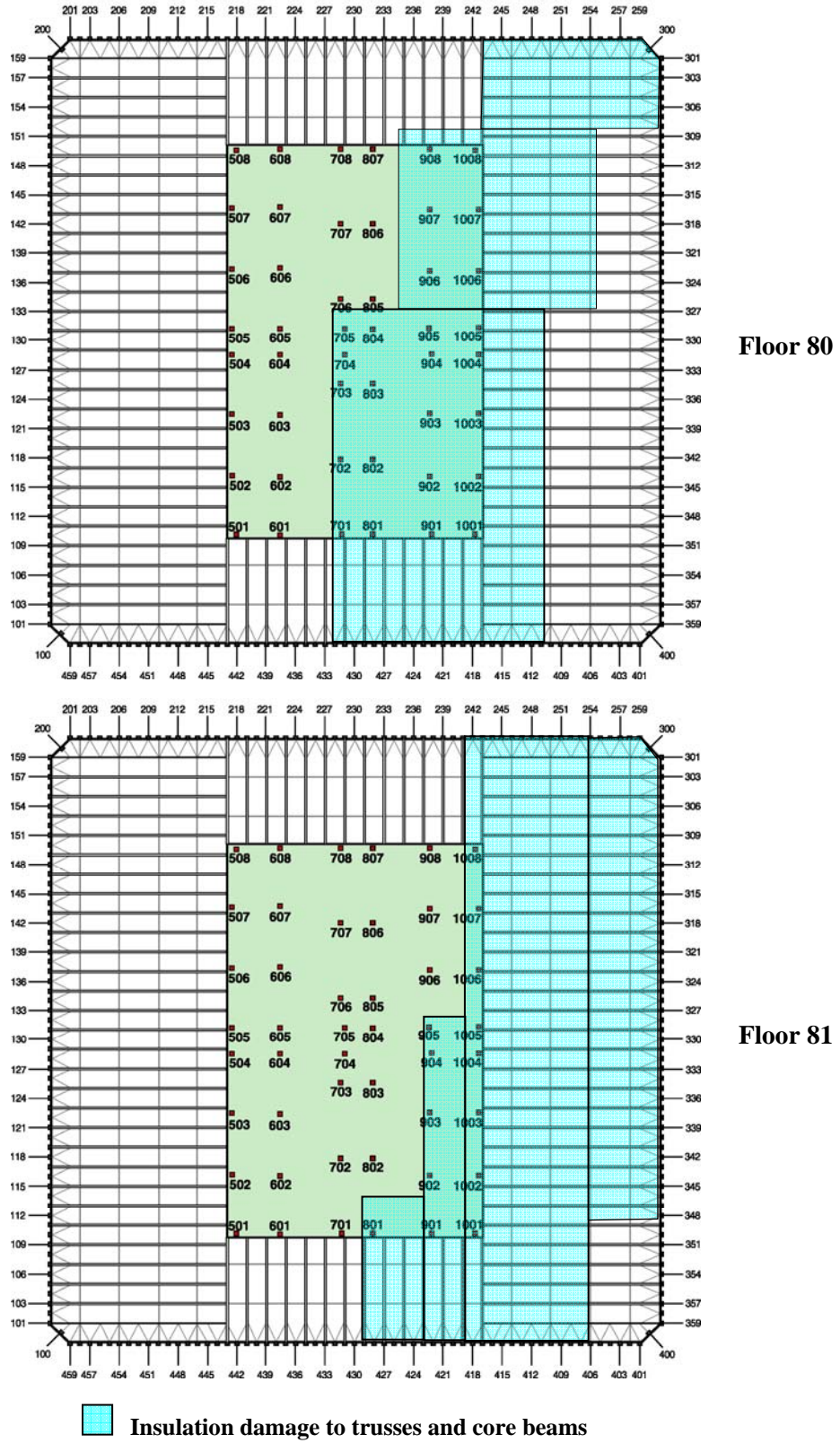


Figure A-20. WTC 2 Case D_i aircraft impact damage to Structural Floors 80 and 81.

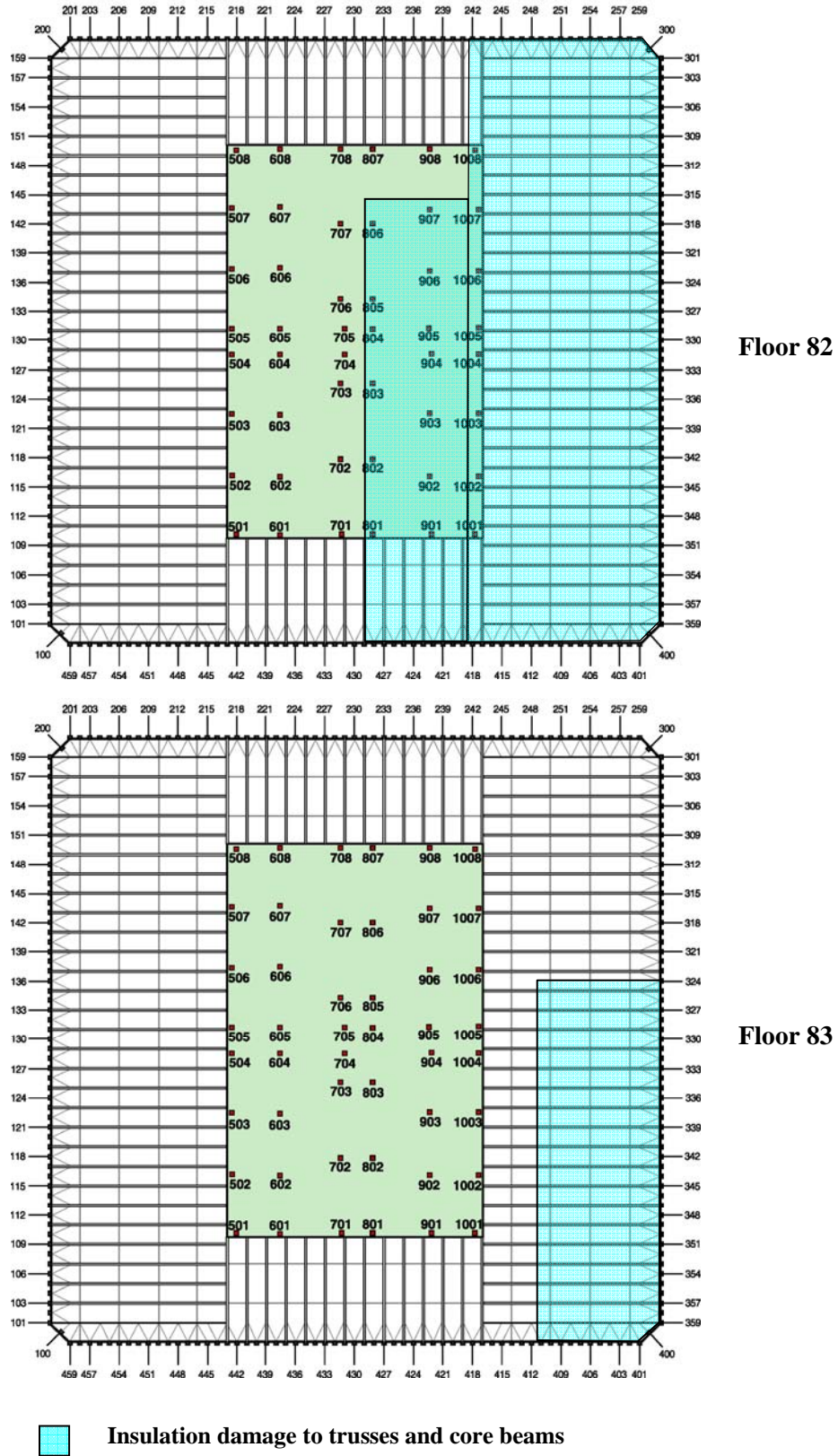


Figure A-21. WTC 2 Case D; aircraft impact damage to Structural Floors 82 and 83.

WTC 2 CASE D₁ – DAMAGE FOR STRUCTURAL FLOOR

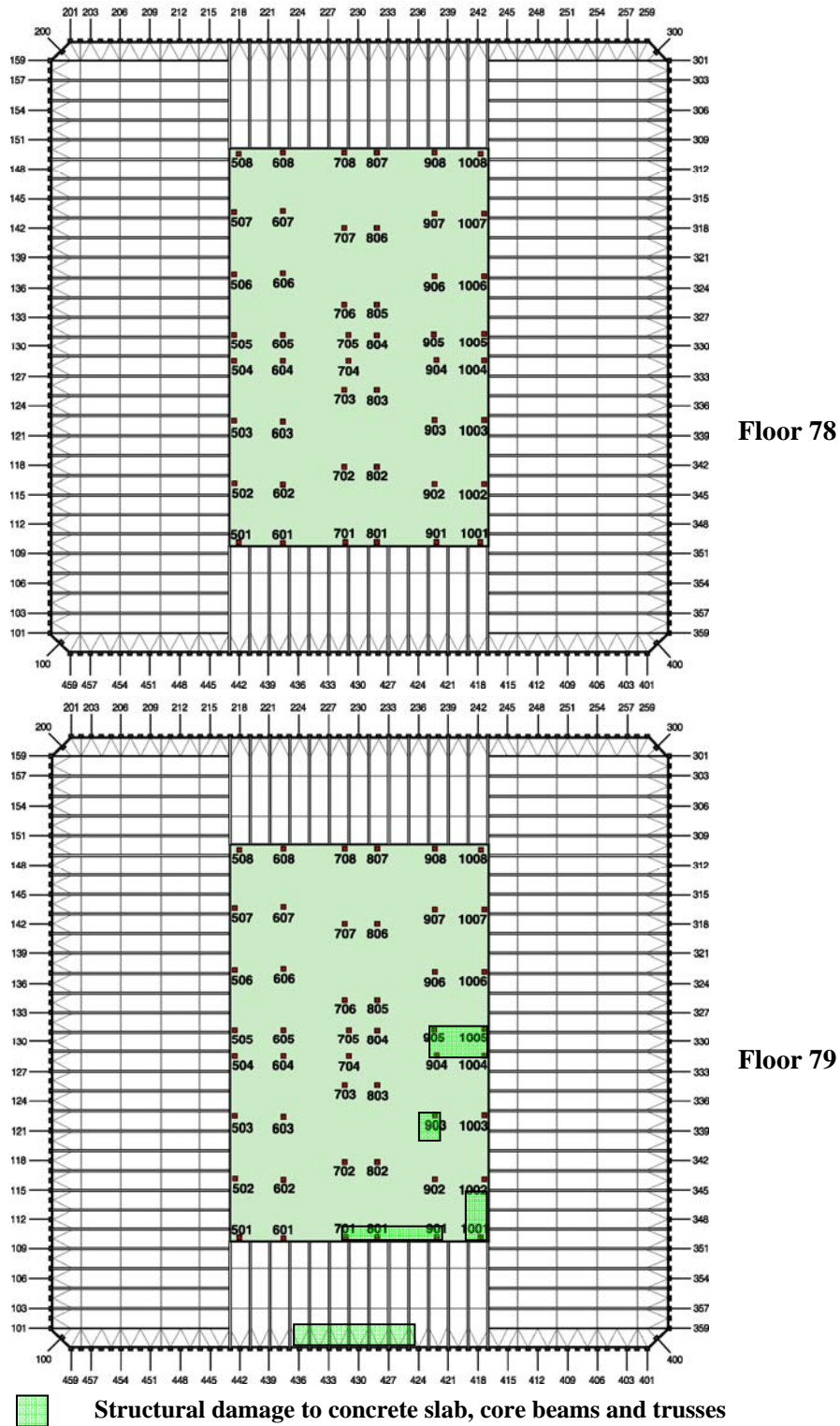


Figure A–22. WTC 2 Case D₁ aircraft impact damage to Structural Floors 78 and 79.

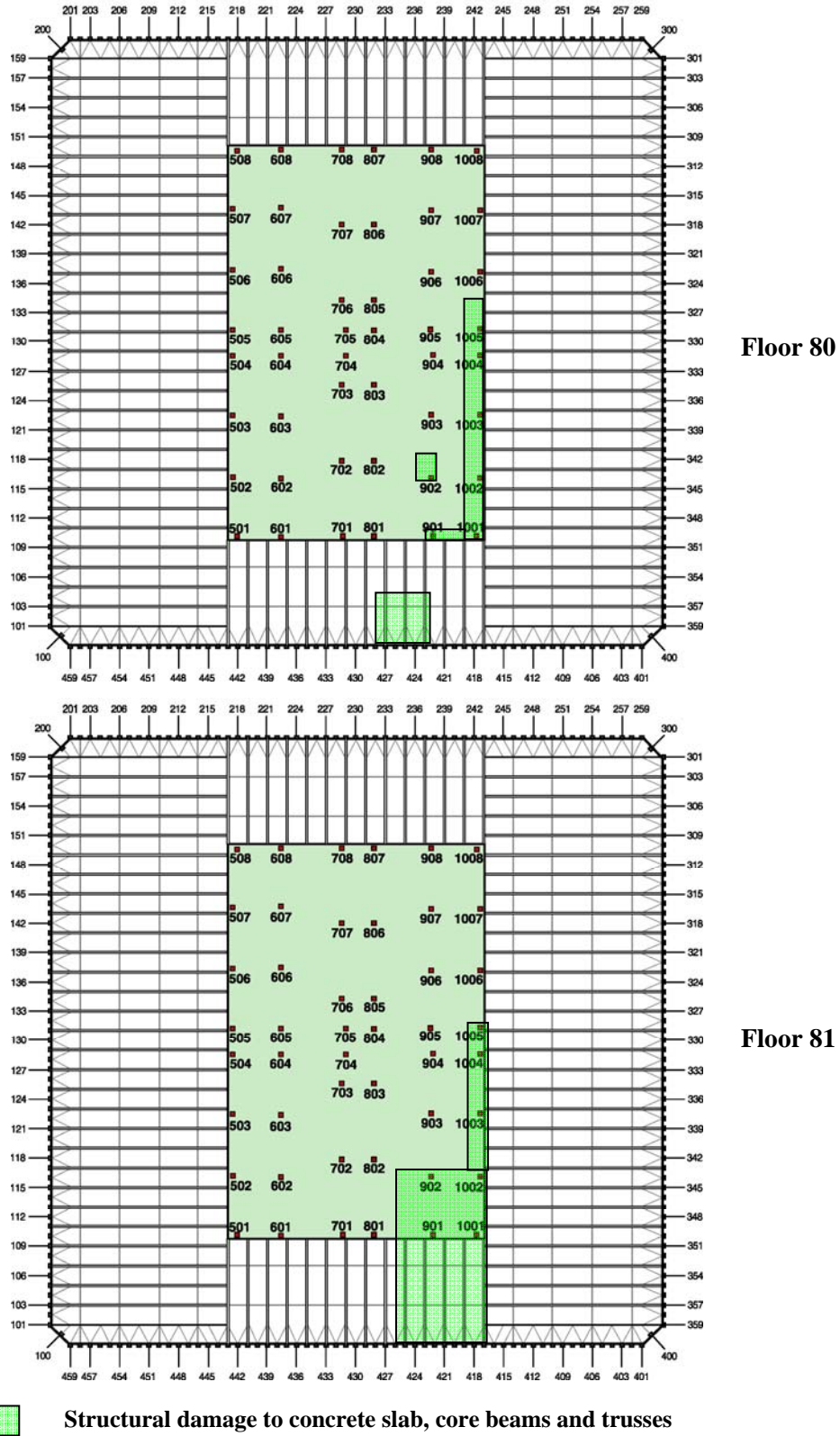
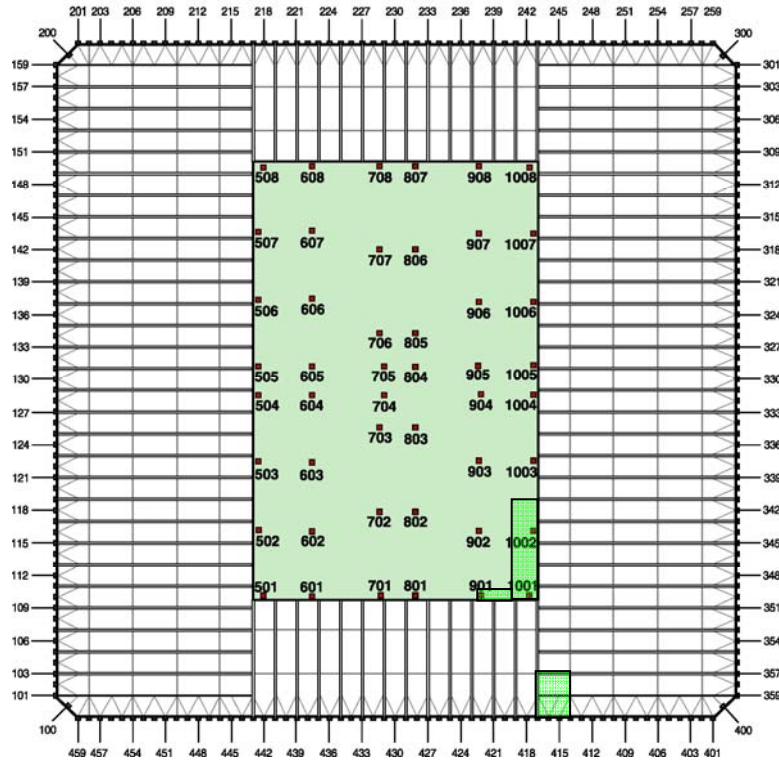
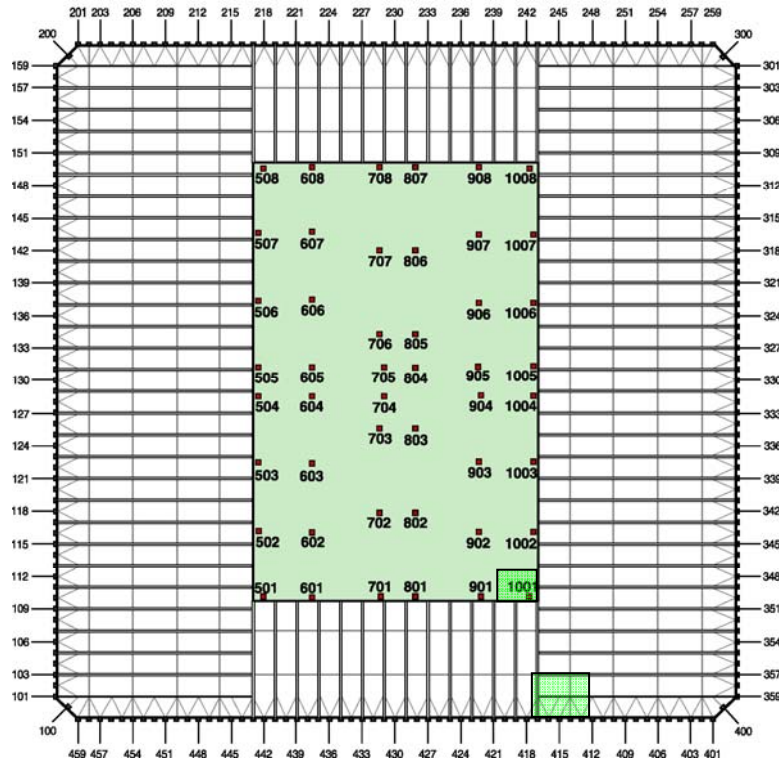


Figure A-23. WTC 2 Case D_i aircraft impact damage to Structural Floors 80 and 81.



Floor 82



Floor 83

 Structural damage to concrete slab, core beams and trusses

Figure A-24. WTC 2 Case D; aircraft impact damage to Structural Floors 82 and 83.

Appendix B

SUMMARY OF AIRCRAFT IMPACT DAMAGE FOR FINAL CASES A TO D

WTC 1 CASE A - OCCUPANCY FLOOR GRAPHICS

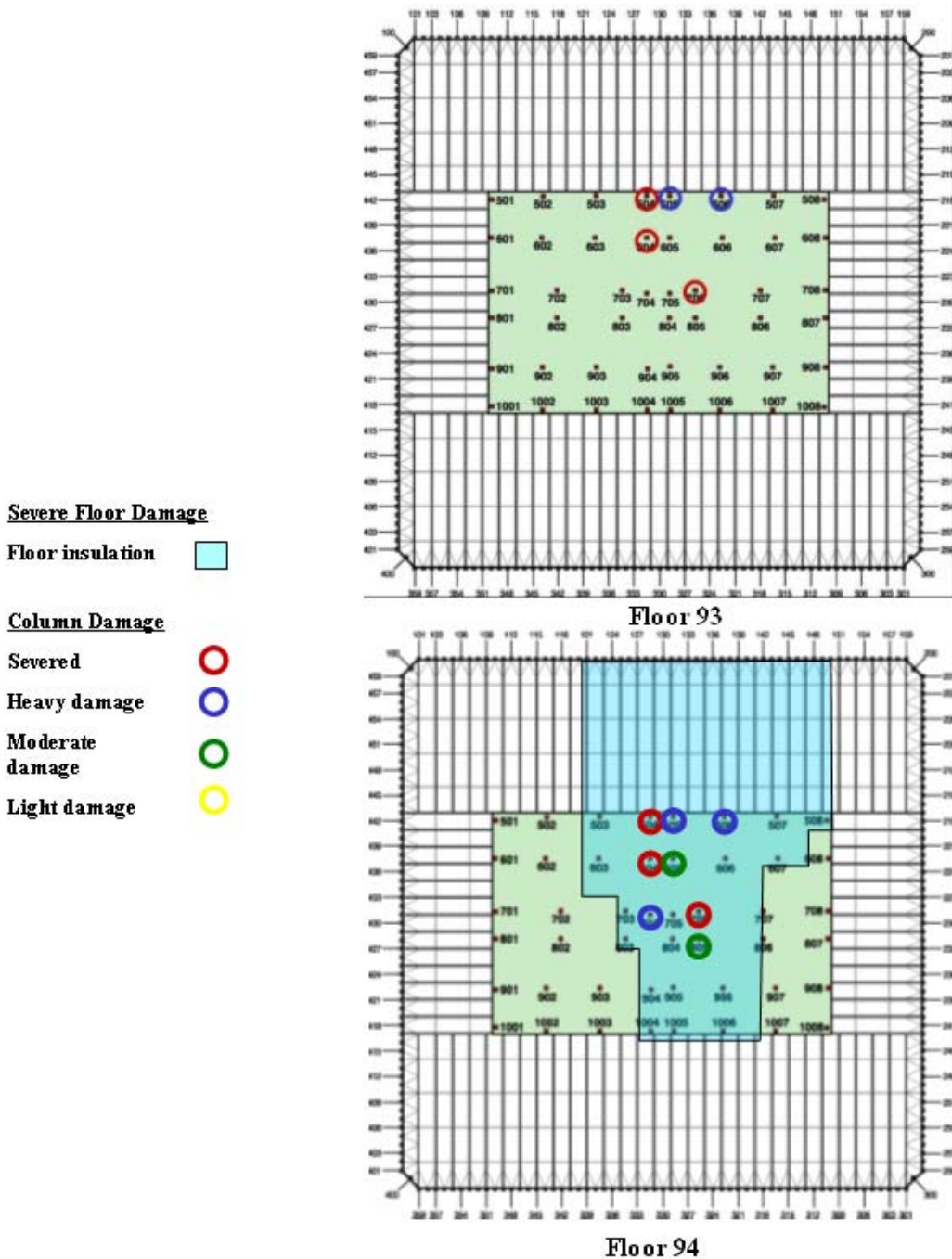


Figure B-1. WTC 1 Case A aircraft impact damage to Occupancy Floors 93 and 94.

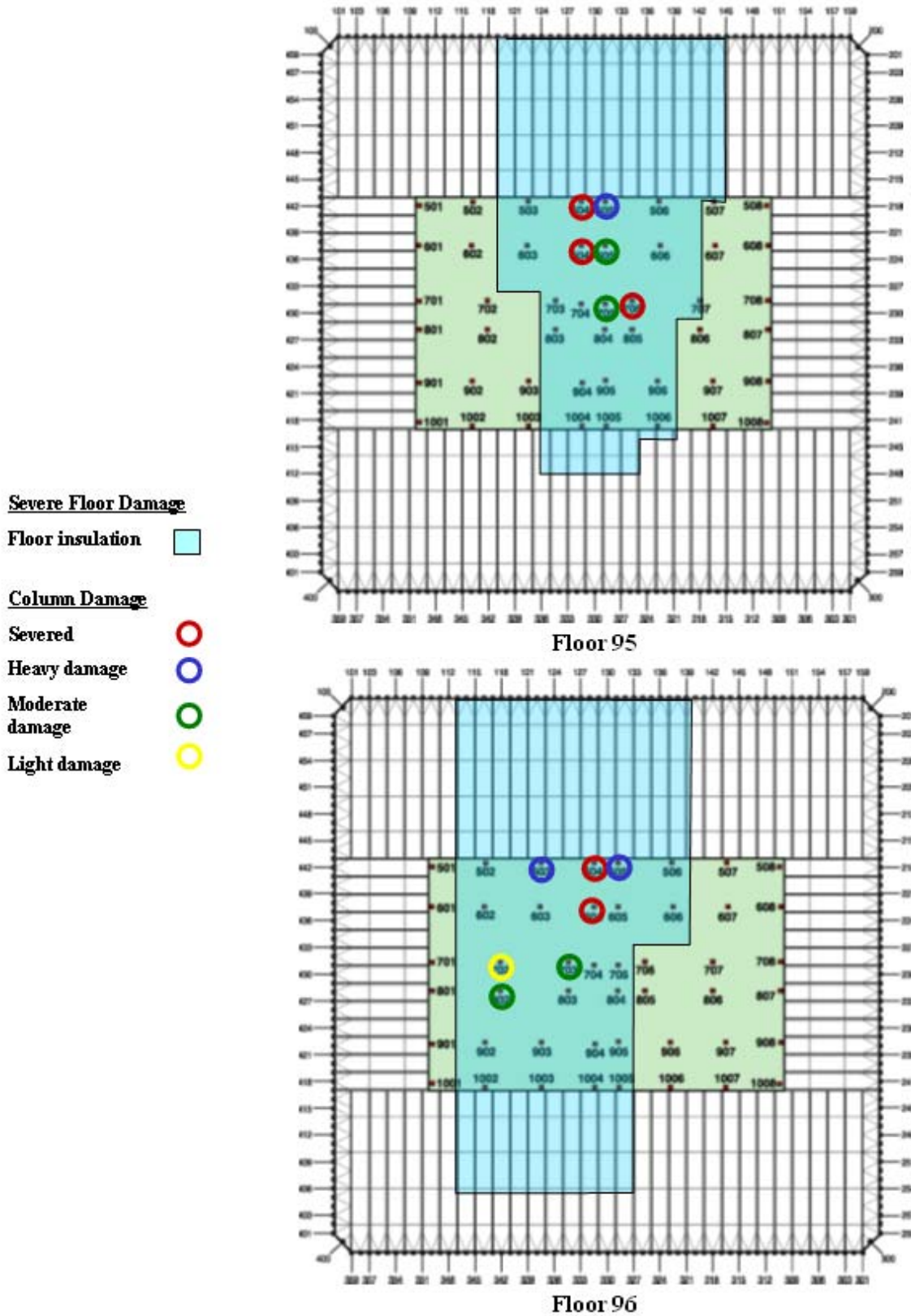


Figure B-2. WTC 1 Case A aircraft impact damage to Occupancy Floors 95 and 96.

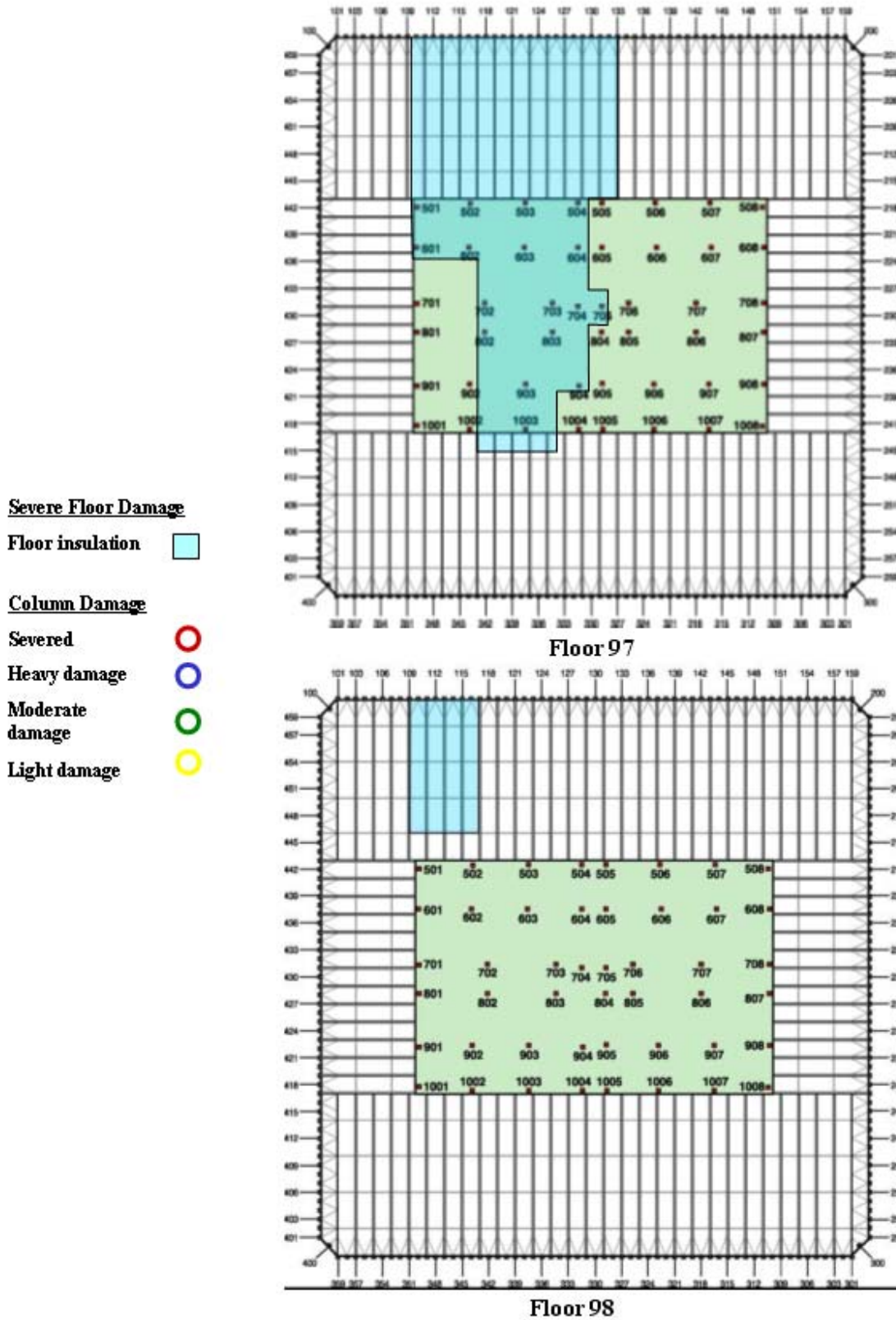


Figure B-3. WTC 1 Case A aircraft impact damage to Occupancy Floors 97 and 98.

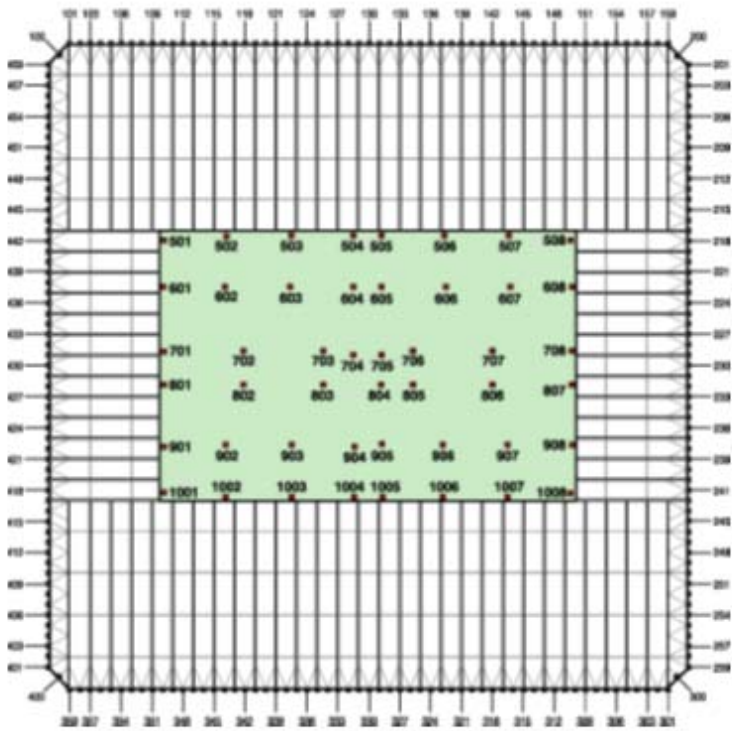
WTC 1 CASE A - STRUCTURAL FLOOR GRAPHICS

Severe Floor Damage

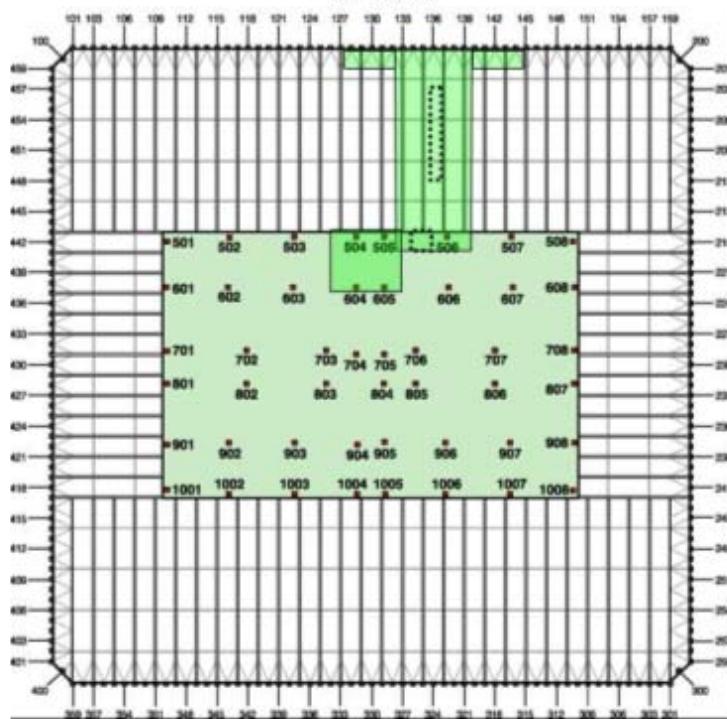
Floor system structural damage



Floor system removed



Floor 93



Floor 94

Figure B-4. WTC 1 Case A aircraft impact damage to Structural Floors 93 and 94.

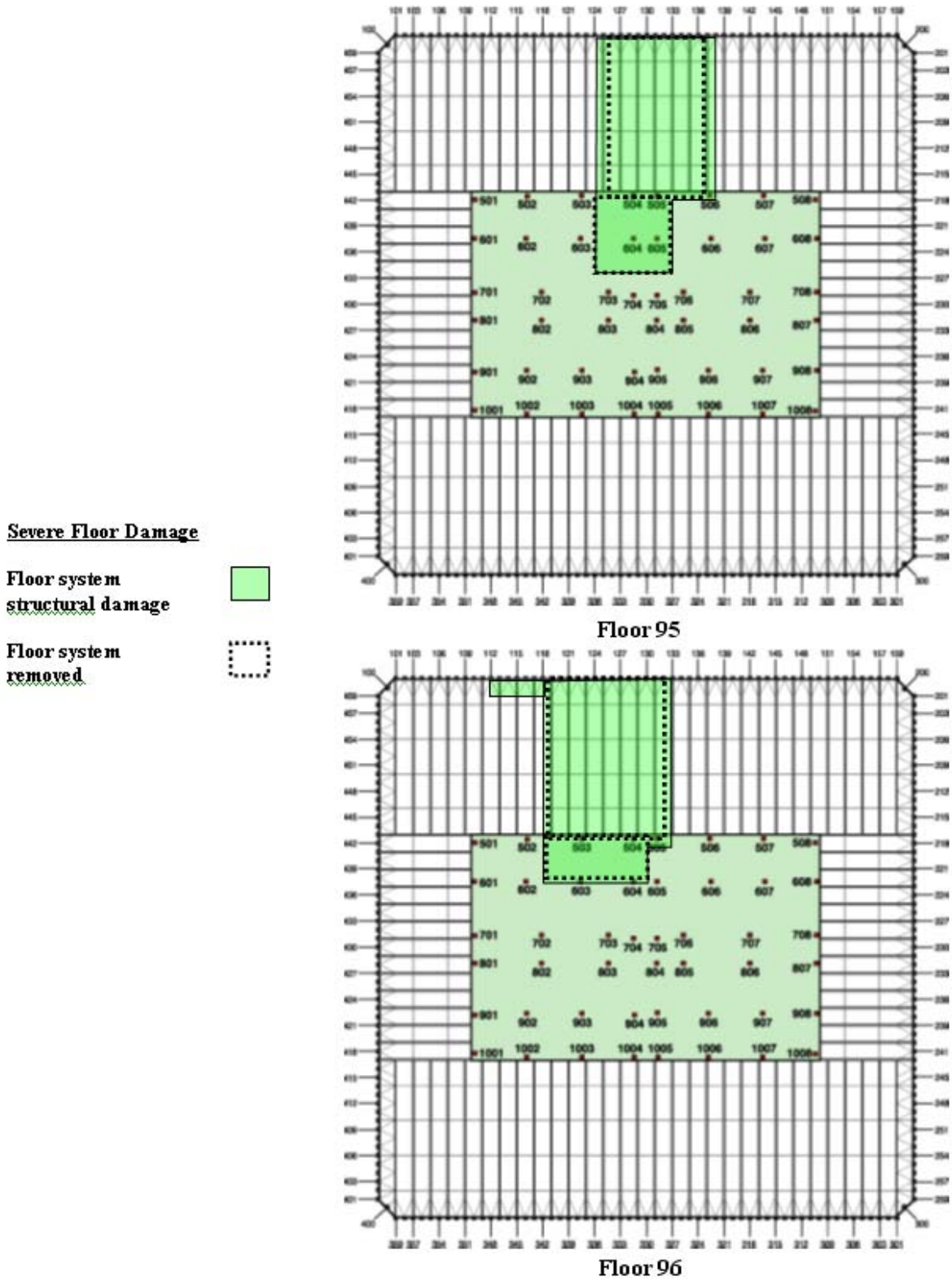
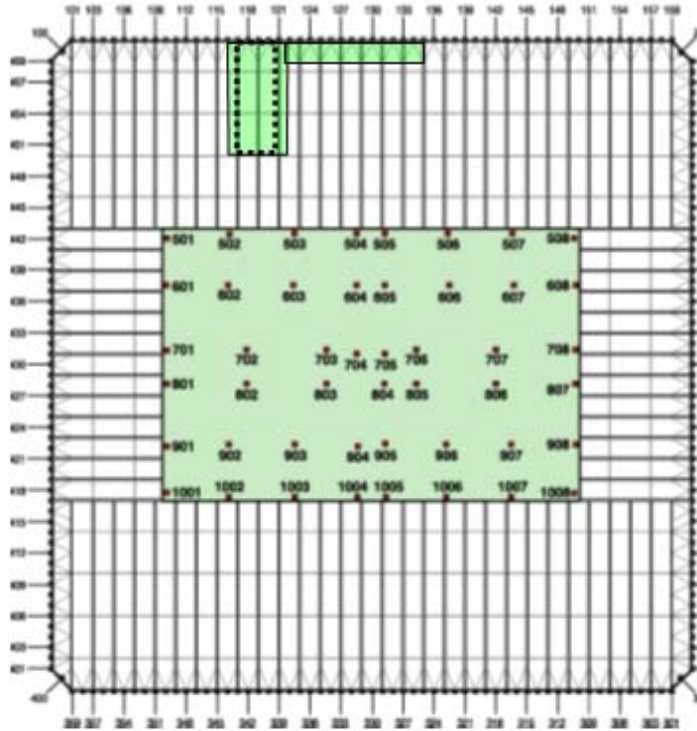


Figure B-5. WTC 1 Case A aircraft impact damage to Structural Floors 95 and 96.

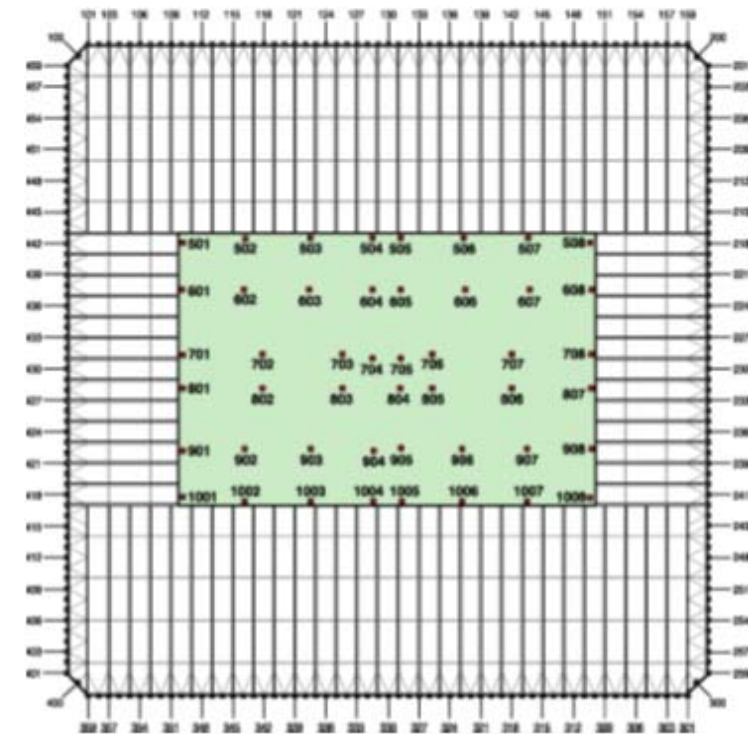
Severe Floor Damage

Floor system structural damage

Floor system removed



Floor 97



Floor 98

Figure B-6. WTC 1 Case A aircraft impact damage to Structural Floors 97 and 98.

WTC 1 CASE B - OCCUPANCY FLOOR GRAPHICS

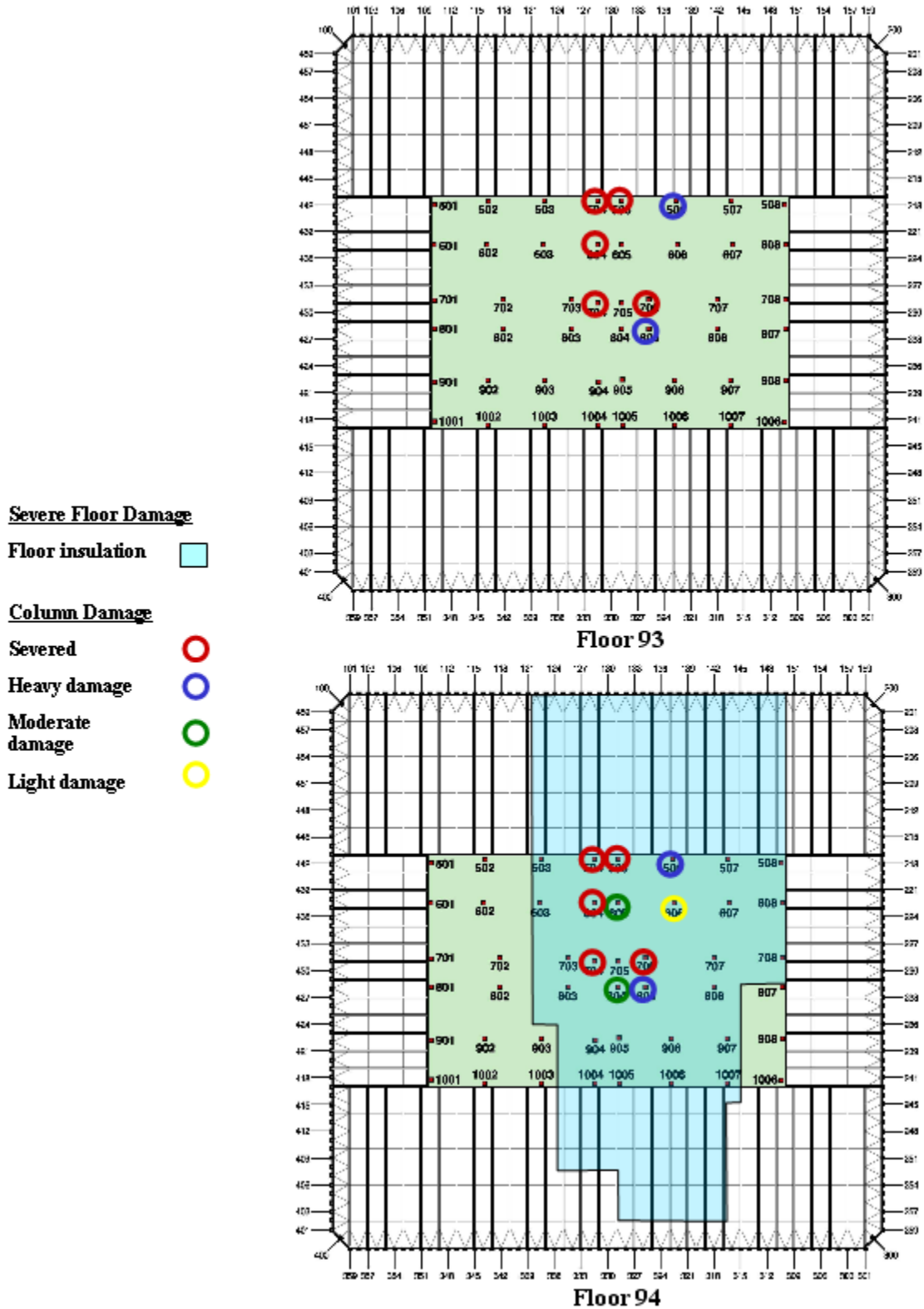


Figure B-7. WTC 1 Case B aircraft impact damage to Occupancy Floors 93 and 94.

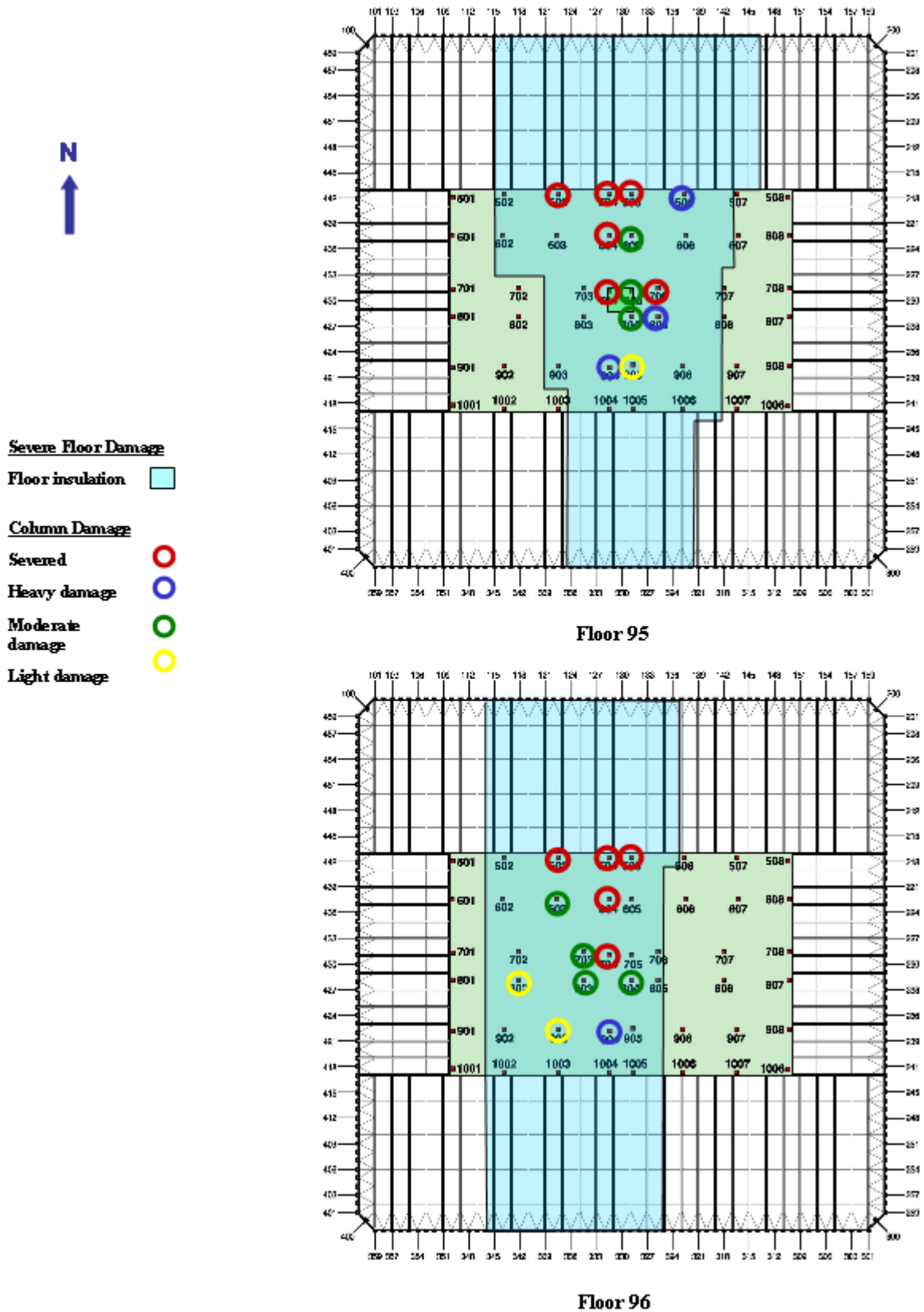


Figure B-8. WTC 1 Case B aircraft impact damage to Occupancy Floors 95 and 96.

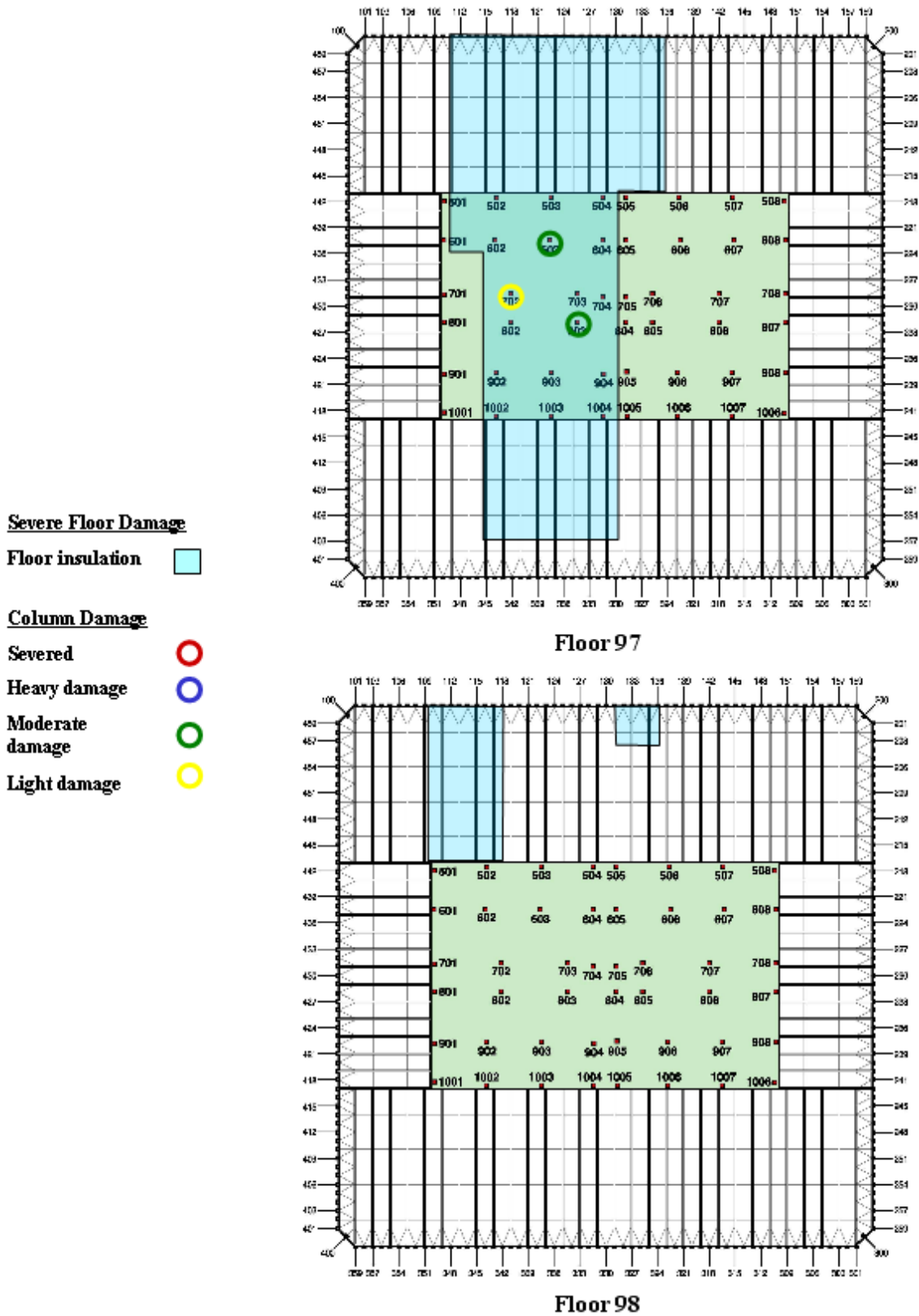


Figure B-9. WTC 1 Case B aircraft impact damage to Occupancy Floors 97 and 98.

WTC 1 CASE B - STRUCTURAL FLOOR GRAPHICS

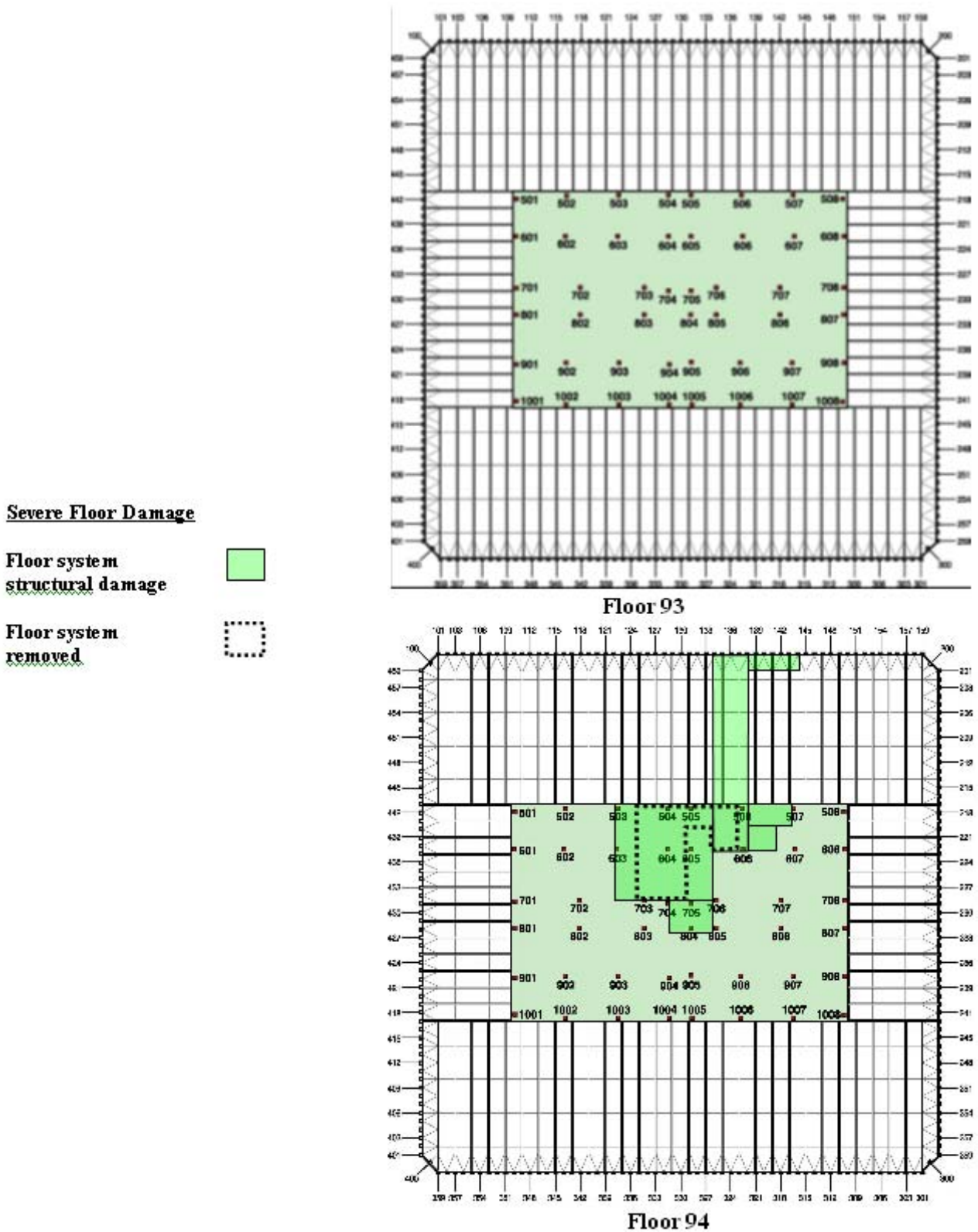


Figure B-10. WTC 1 Case B aircraft impact damage to Structural Floors 93 and 94.

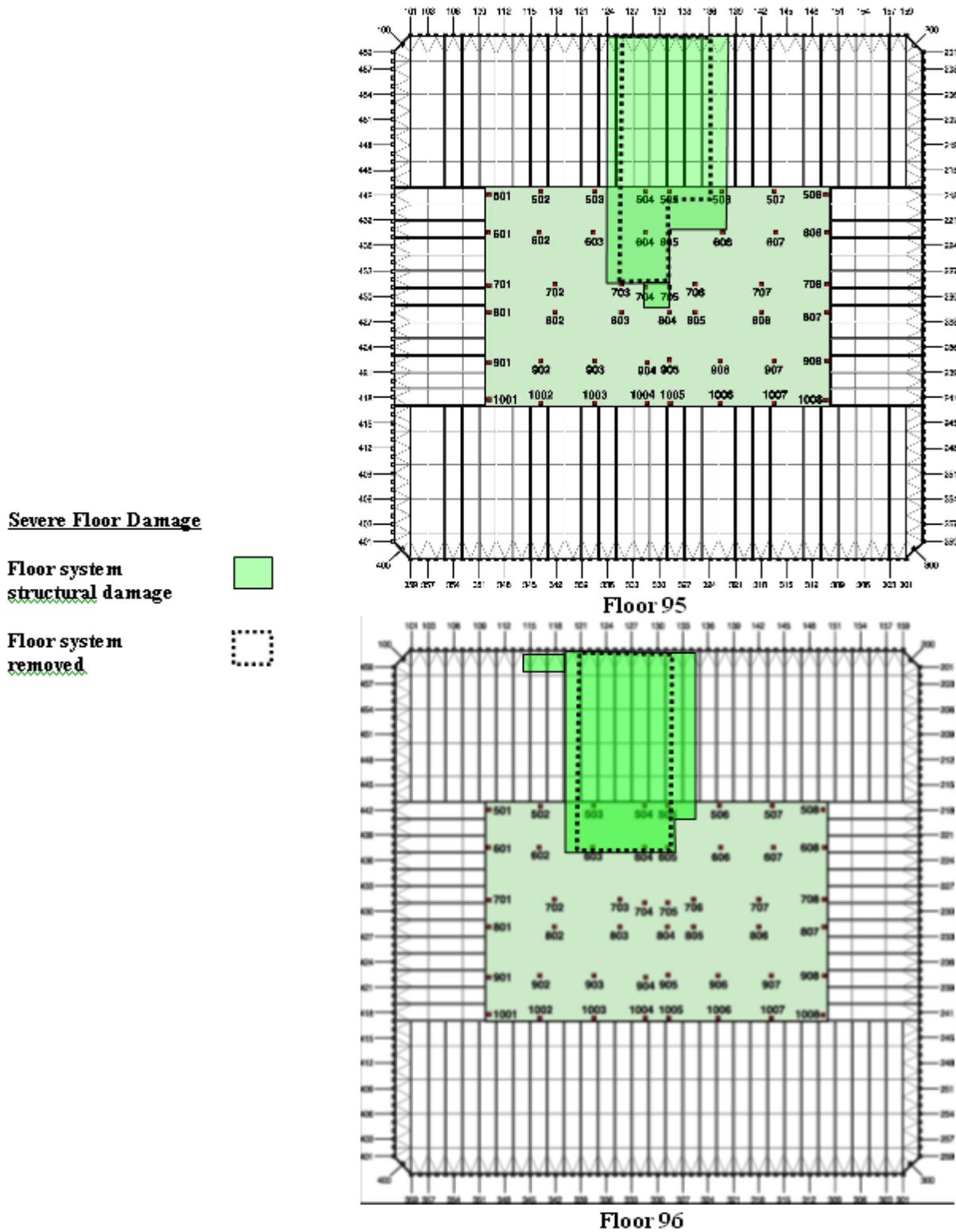
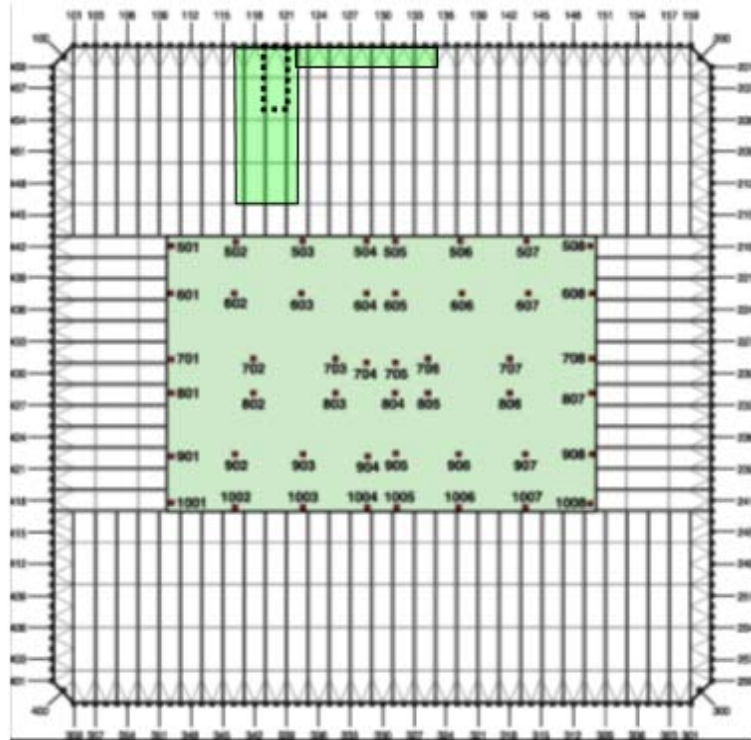


Figure B-11. WTC 1 Case B aircraft impact damage to Structural Floors 95 and 96.

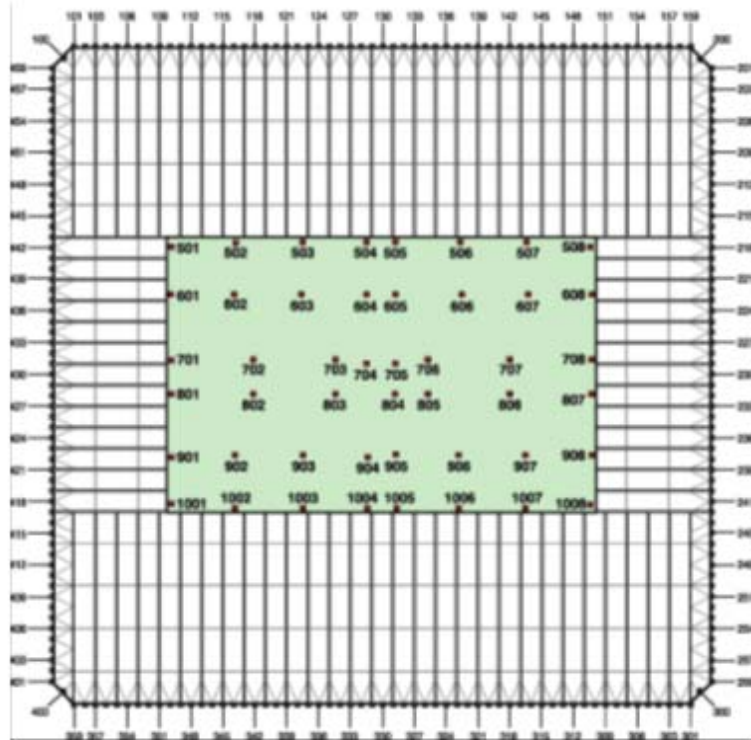
Severe Floor Damage

Floor system structural damage

Floor system removed



Floor 97



Floor 98

Figure B-12. WTC 1 Case B aircraft impact damage to Structural Floors 97 and 98.

WTC 2 CASE C – OCCUPANCY FLOOR GRAPHICS

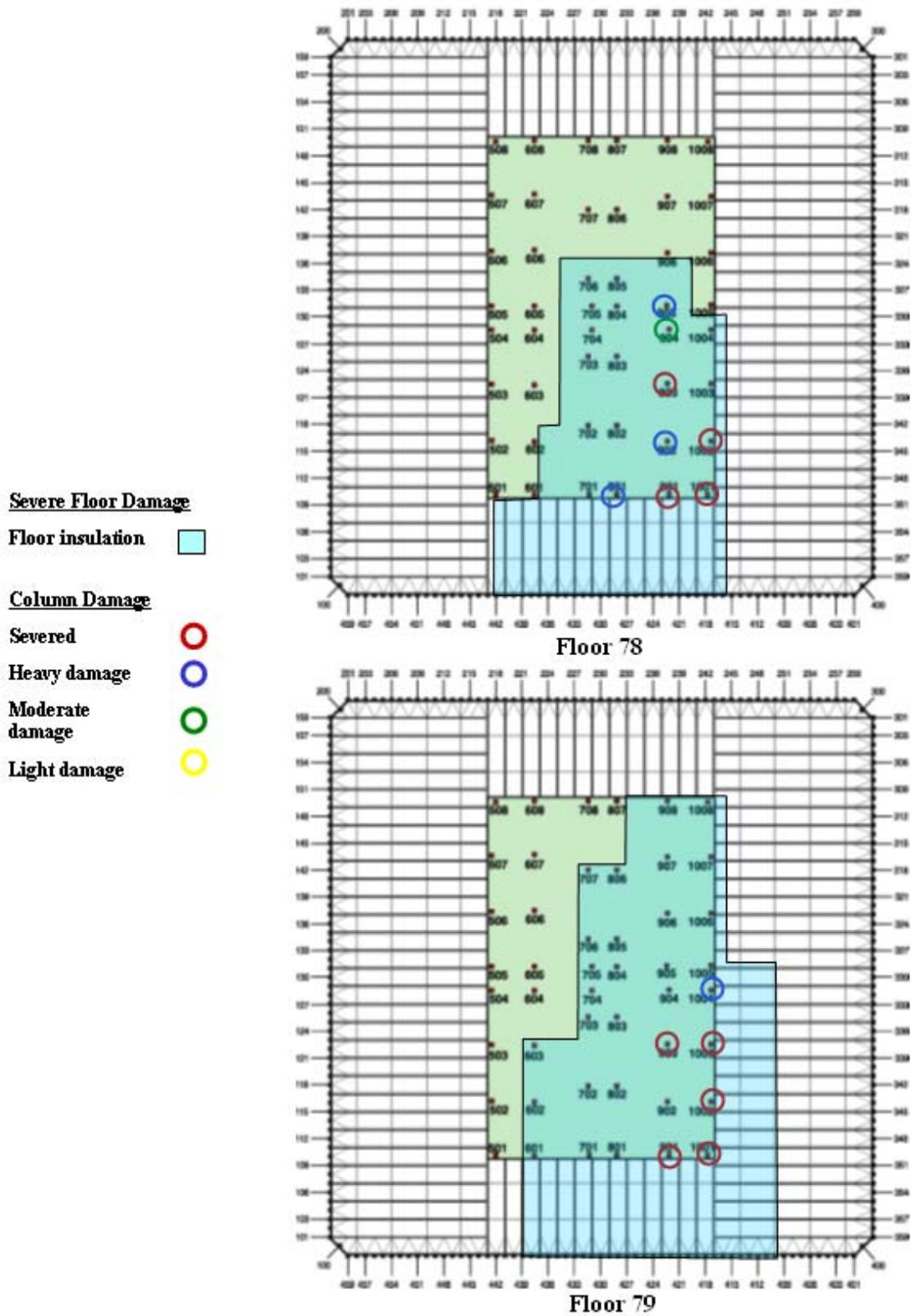


Figure B-13. WTC 2 Case C aircraft impact damage to Occupancy Floors 78 and 79.



Figure B-14. WTC 2 Case C aircraft impact damage to Occupancy Floors 80 and 81.

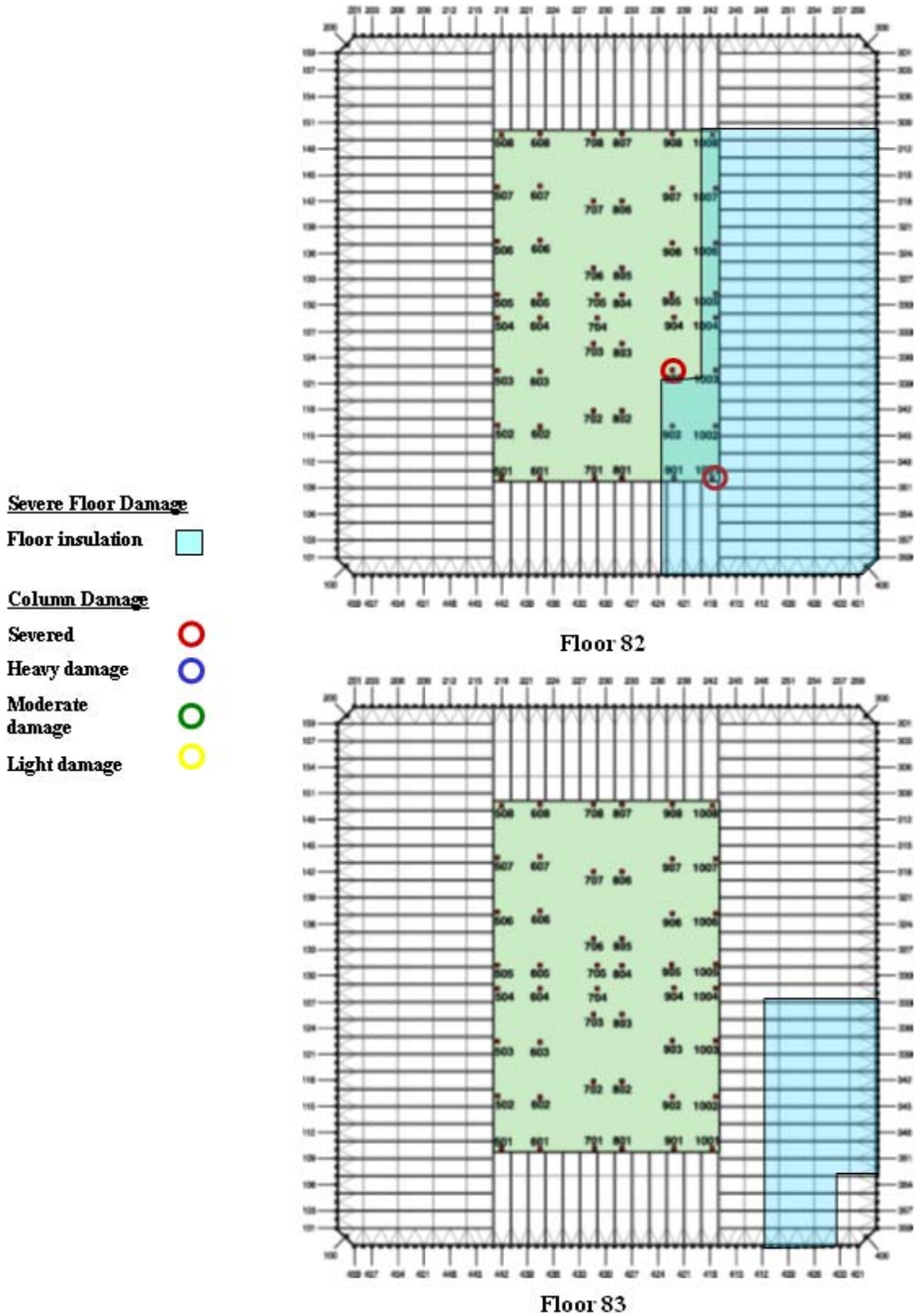


Figure B-15. WTC 2 Case C aircraft impact damage to Occupancy Floors 82 and 83.

WTC 2 CASE C – STRUCTURAL FLOOR GRAPHICS

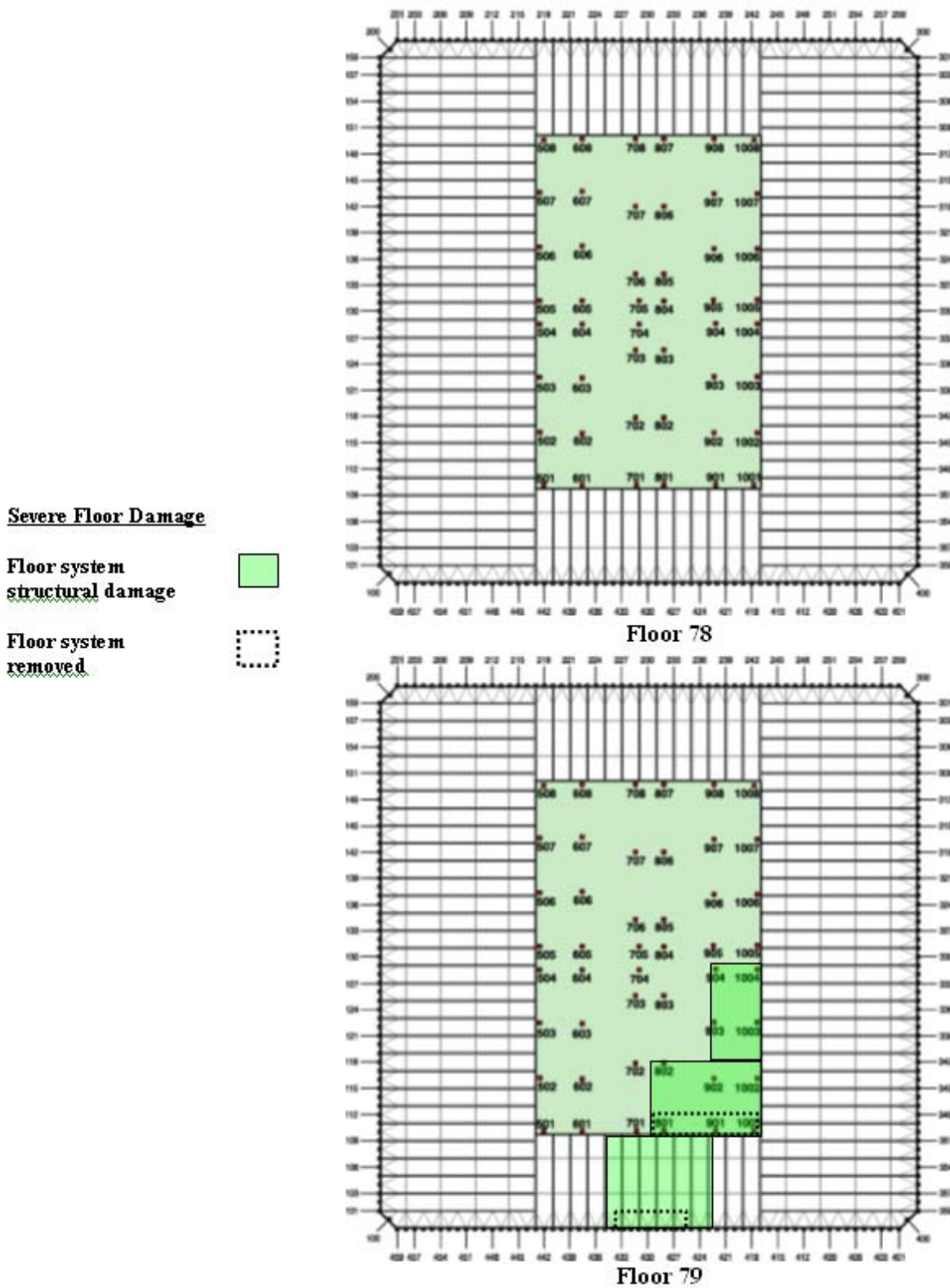


Figure B-16. WTC 2 Case C aircraft impact damage to Structural Floors 78 and 79.

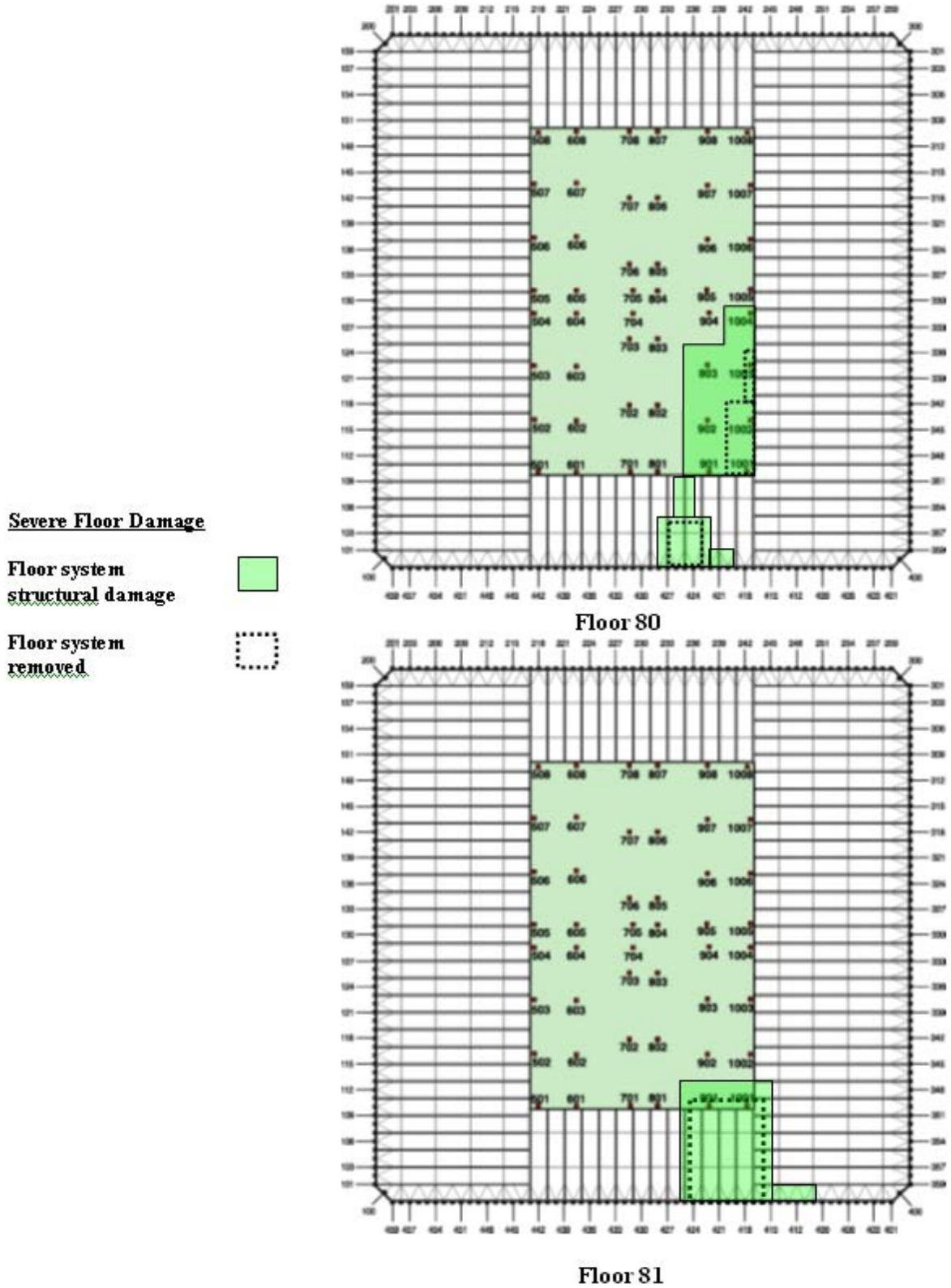


Figure B-17. WTC 2 Case C aircraft impact damage to Structural Floors 80 and 81.

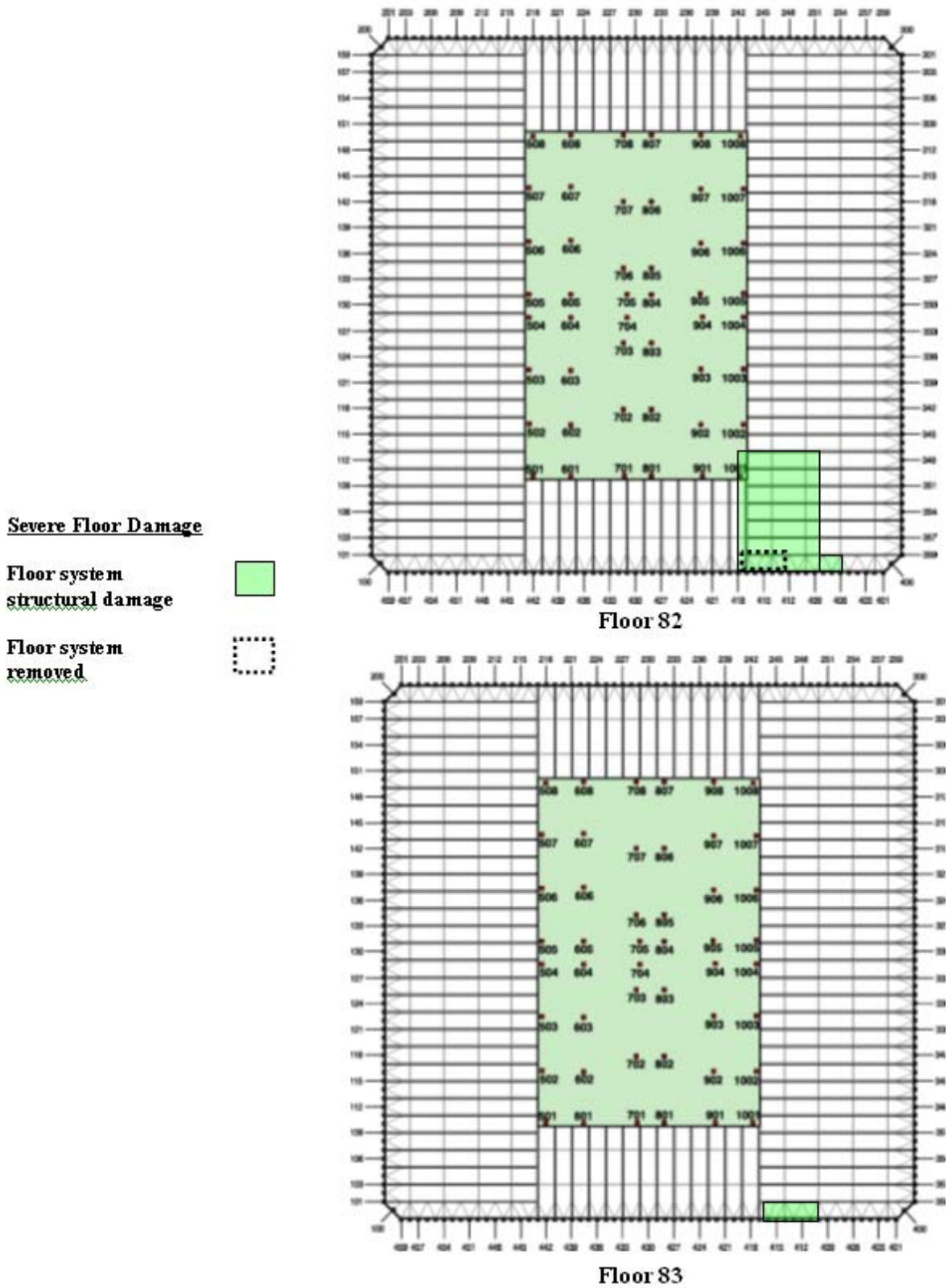


Figure B-18. WTC 2 Case C aircraft impact damage to Structural Floors 82 and 83.

WTC 2 CASE D – OCCUPANCY FLOOR GRAPHICS

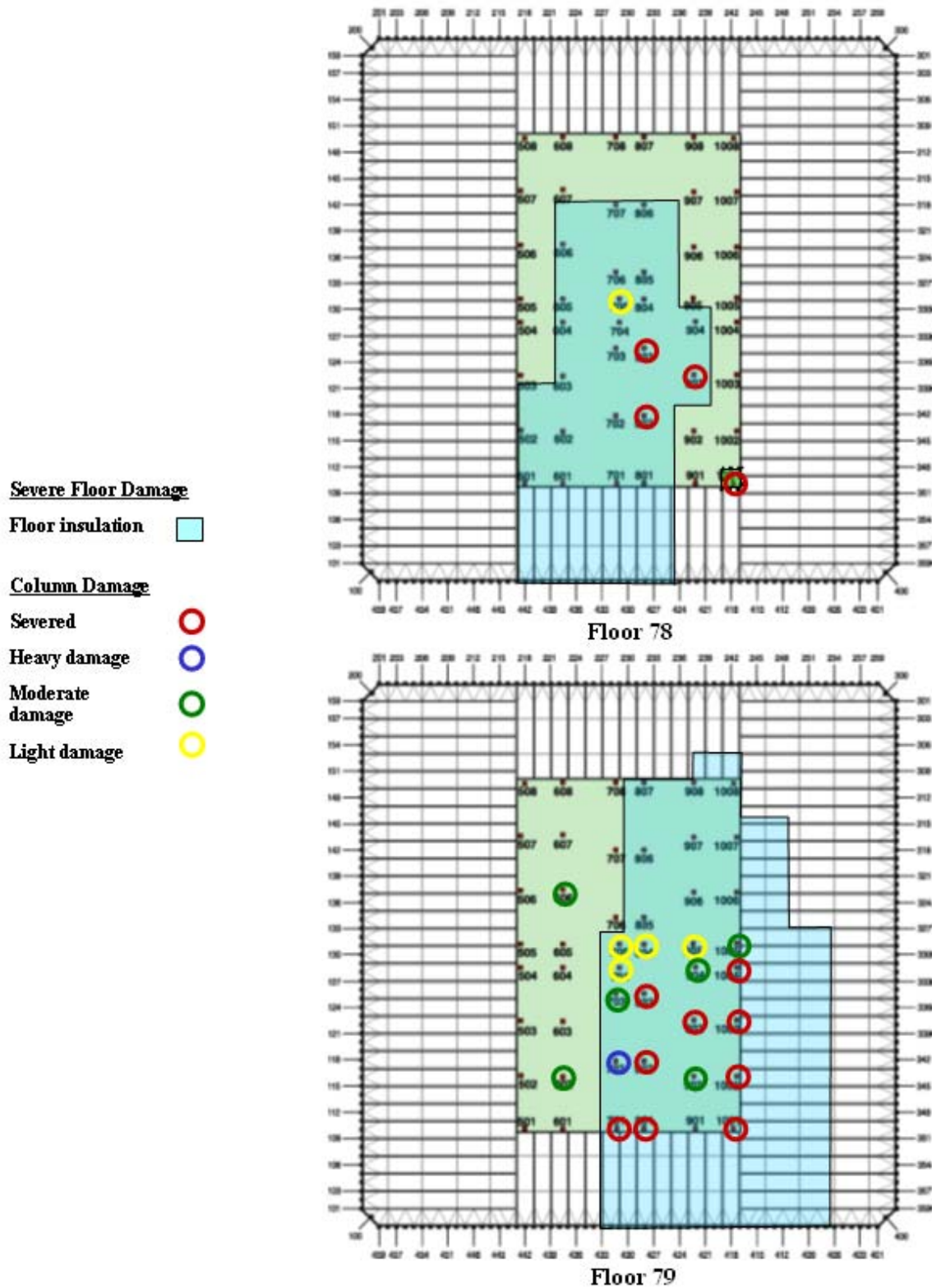


Figure B-19. WTC 2 Case D aircraft impact damage to Occupancy Floors 78 and 79.

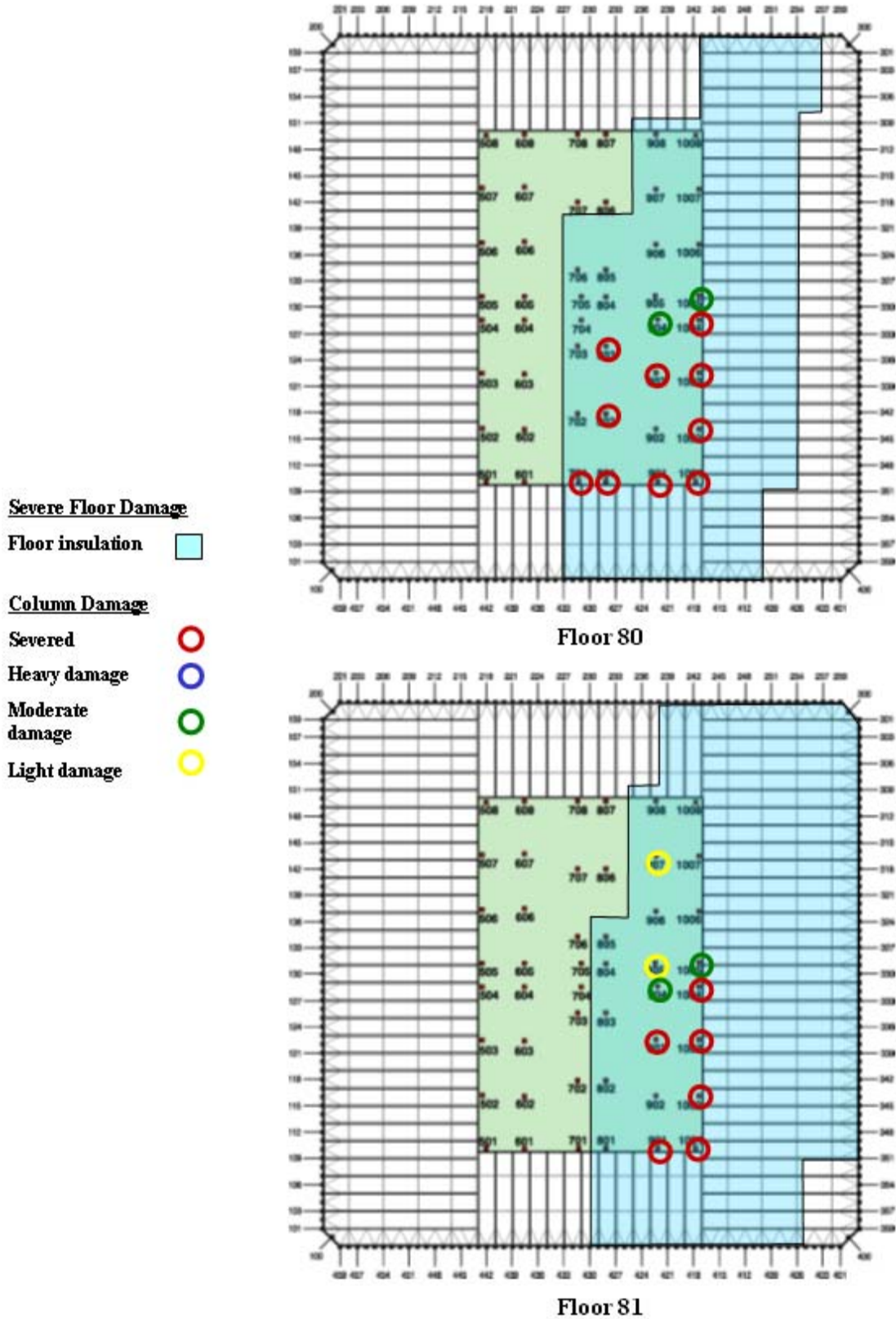


Figure B-20. WTC 2 Case D aircraft impact damage to Occupancy Floors 80 and 81.

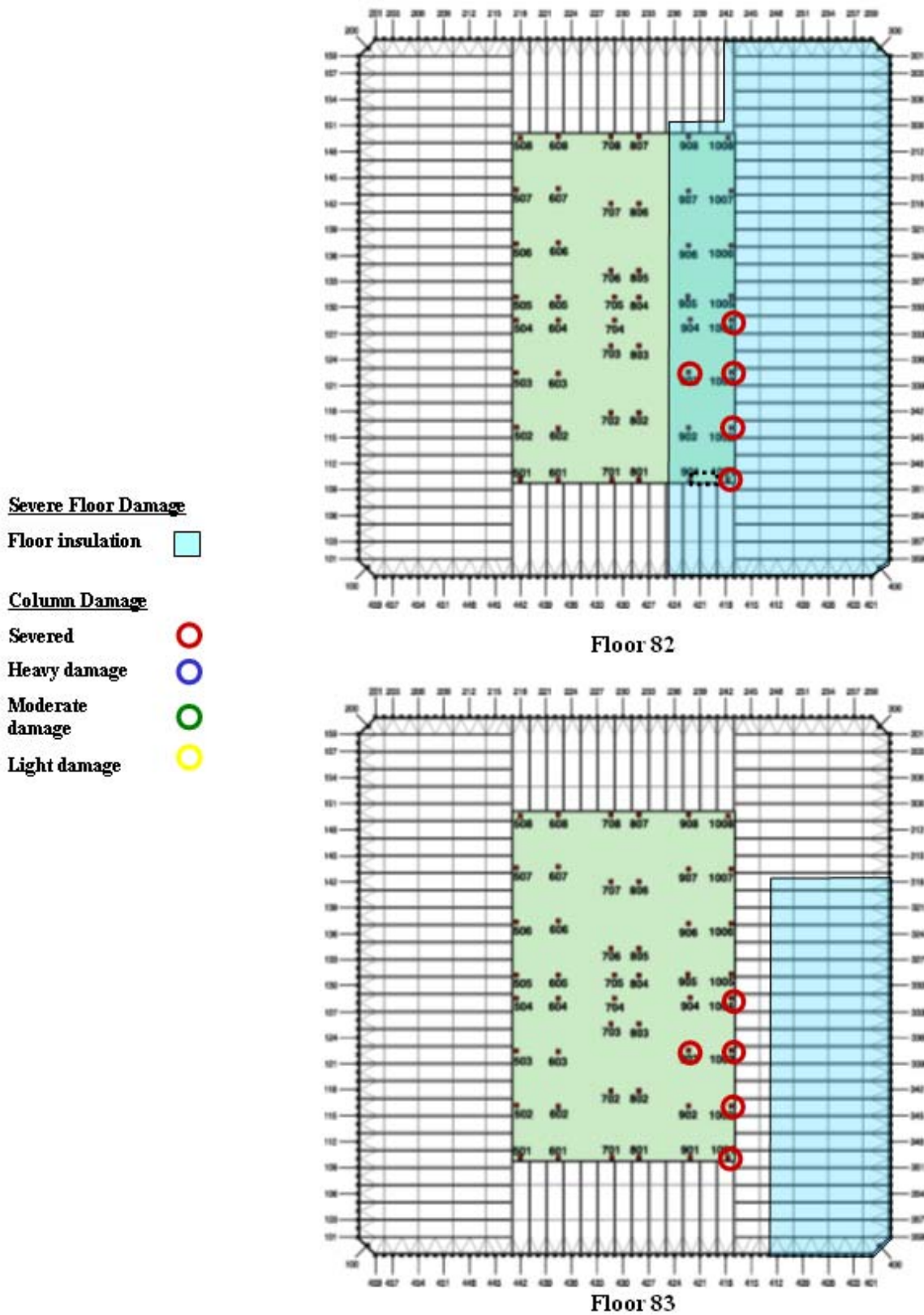


Figure B-21. WTC 2 Case D aircraft impact damage to Occupancy Floors 82 and 83.

WTC 2 CASE D – STRUCTURAL FLOOR GRAPHICS

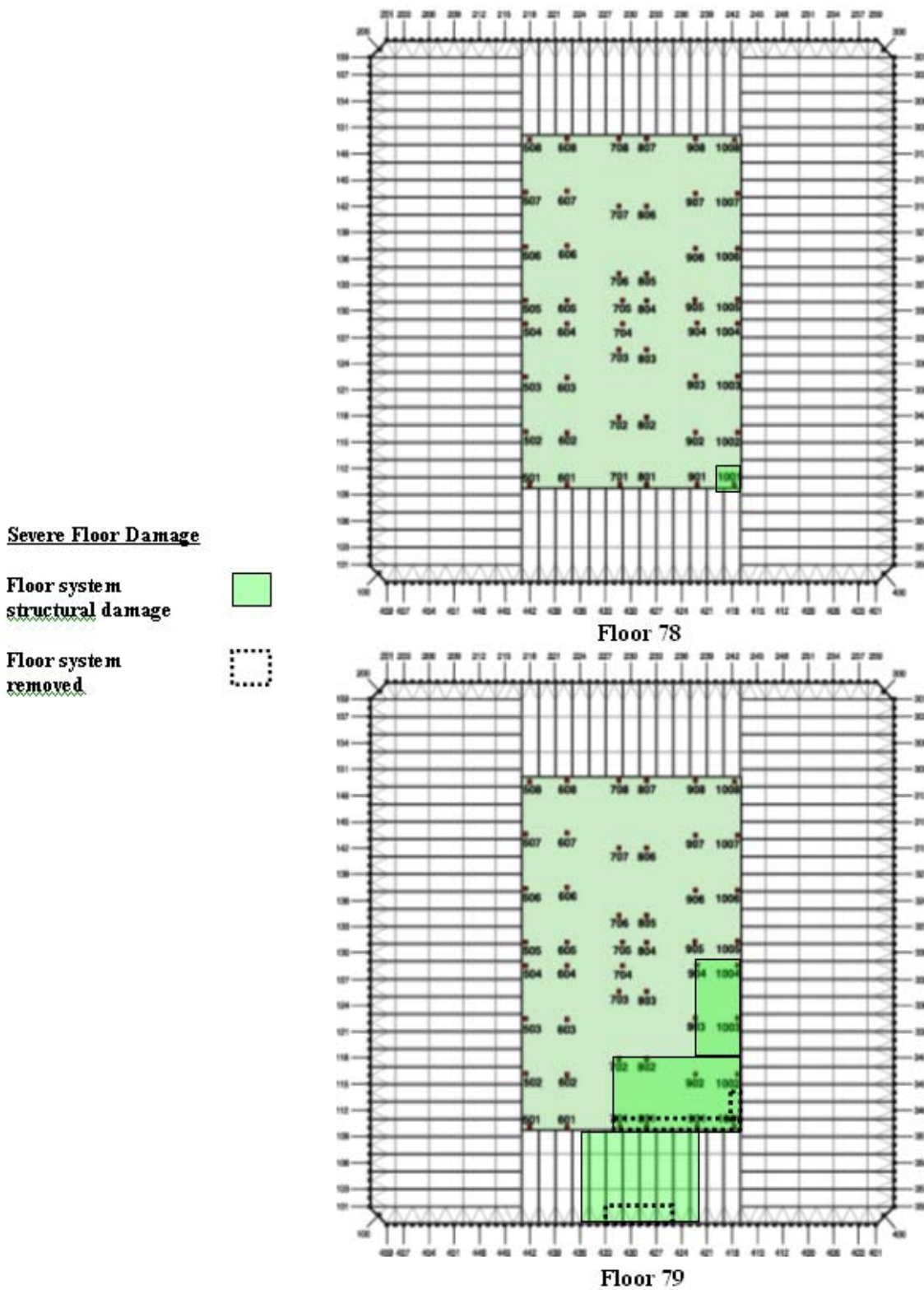


Figure B–22. WTC 2 Case D aircraft impact damage to Structural Floors 78 and 79.

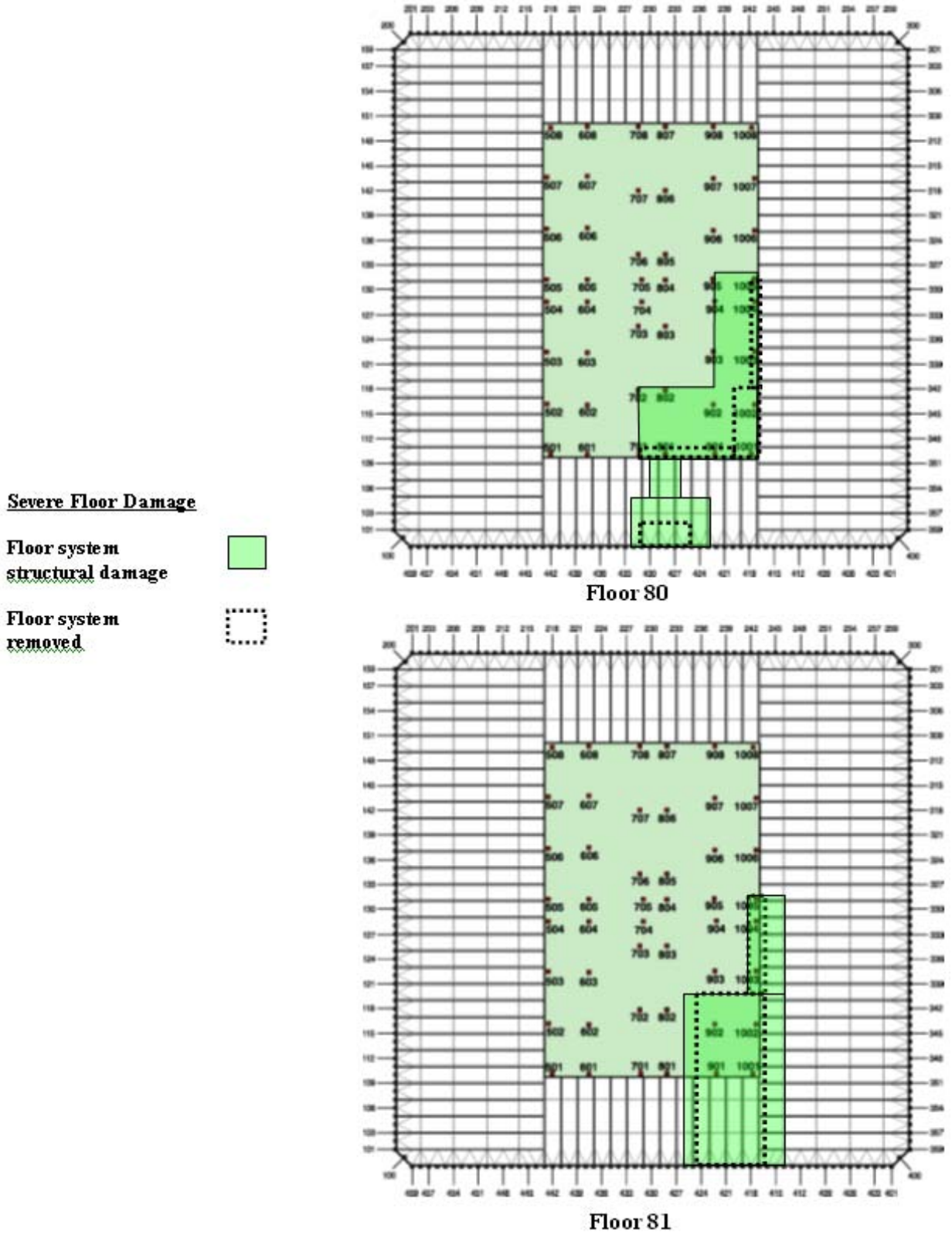


Figure B-23. WTC 2 Case D aircraft impact damage to Structural Floors 80 and 81.

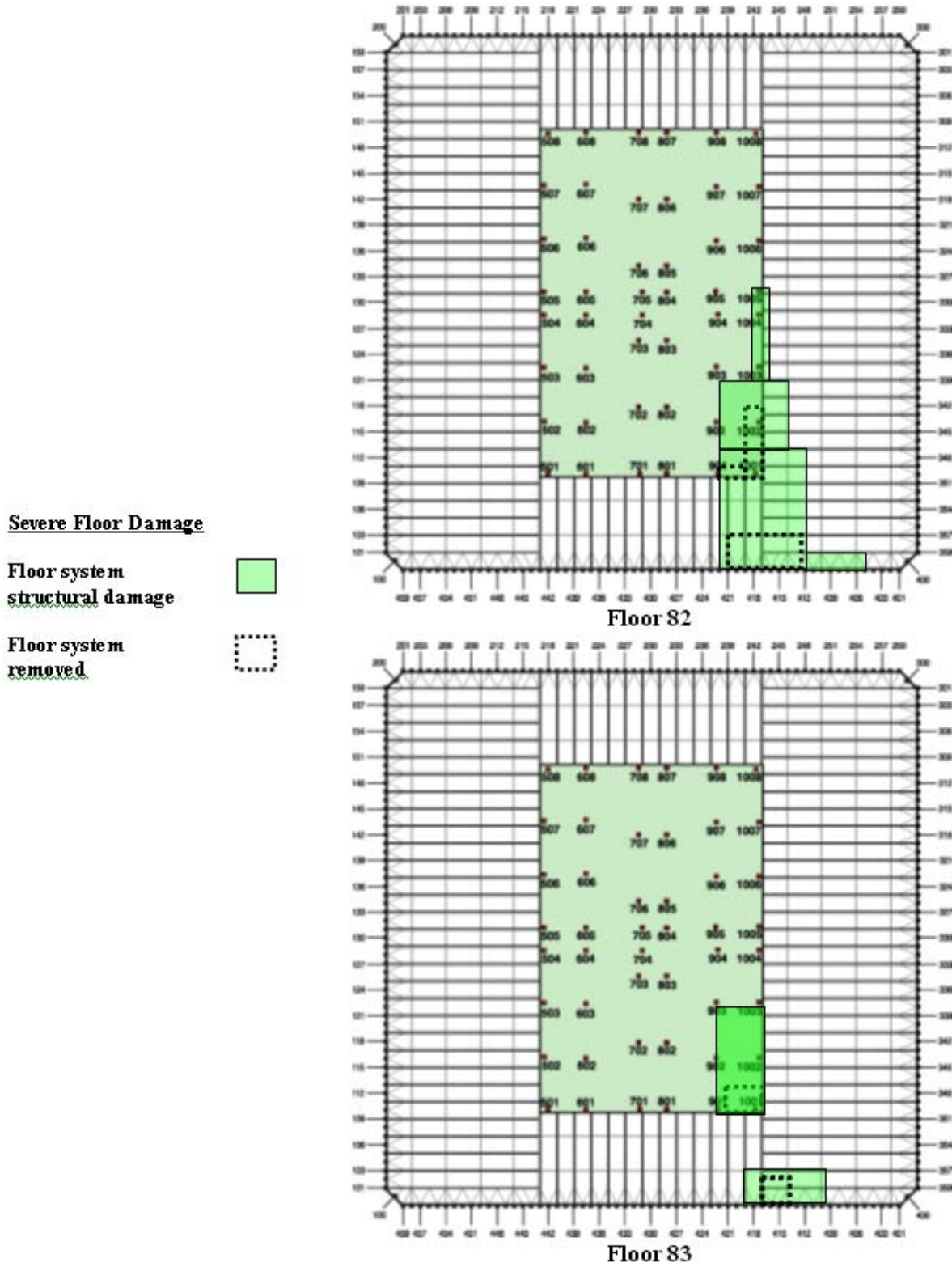


Figure B-24. WTC 2 Case D aircraft impact damage to Structural Floors 82 and 83.